Dottorato in Biotecnologie – XXXVII ciclo
Università degli Studi di Napoli Federico II

MOVING TOWARD HYDROGEN: THE MICROBIOLOGY OF UNDERGROUND HYDROGEN STORAGE

Dottorando: Martina Cascone

Relatore: Prof. Marco Moracci

Correlatore: Prof. Donato Giovannelli

Coordinatore: Prof. Marco Moracci

Settore Scientifico Disciplinare BIO/19

Table of Contents

Summary 2

Sommario 3

Chapter 1 - Hydrogenotrophic metabolisms in subsurface natural and engineered environments and implications for underground hydrogen storage 5

Chapter 2 - Microbial taxonomic and functional diversity of potential underground hydrogen storage sites 42

Chapter 3 - Exploring Microbial Dynamics in Underground Hydrogen Storage: Insights from Microcosm Experiments on Reservoir Brines Exposed to Hydrogen Atmosphere 67

Chapter 4 - Hydrogenotrophic metabolisms in the subsurface: insights from natural deeply-sourced seeps in diverse geological settings 96

Chapter 5 - Conclusions and future directions 124

Appendix I - Fundings, acknowledgements and ethics declarations 126

Appendix II - Internships 127

Appendix III - Sampling expeditions 128

Appendix IV - Contribution to conferences and workshops 131

Appendix V - Publications 135

Appendix VI - Hydrogen 2022: Sampling Natural Hydrogen Sites in Italy - Expedition Report 140

Unione europea
Fondo sociale europeo
Ministero dell'Università e della Ricerca
PON RICERCA E INNOVAZIONE 2014 - 2020

Summary

The global energy transition is at a pivotal juncture, with hydrogen emerging as a transformative, clean energy carrier capable of decarbonizing hard-to-abate sectors. Hydrogen's versatility as fuel, industrial feedstock, and energy storage medium, combined with its zero-emission potential, makes it a cornerstone of a sustainable energy future. However, realizing its full potential requires addressing cost, technological, and infrastructure challenges, particularly for Green Hydrogen production and Underground Hydrogen Storage (UHS). Storing hydrogen in subsurface reservoirs like aquifers or salt caverns can ensure energy reliability, but microbial interactions pose risks. Subsurface microbial communities, utilizing hydrogen in metabolic pathways like methanogenesis and sulfate reduction, can degrade hydrogen purity and infrastructure integrity. Understanding these interactions is crucial to mitigating risks and ensuring storage feasibility. This thesis investigates the intersection of microbiology and hydrogen storage, exploring microbial dynamics, geochemical transformations, and biogeochemical feedback in natural and engineered environments. **Chapter 1** Characterizes hydrogenases, enzymes central to microbial hydrogen metabolism, providing a database to predict microbial impacts in UHS. **Chapter 2** analyses microbial communities in prospective UHS sites using molecular techniques, revealing site-specific metabolic pathways influencing hydrogen stability. **Chapter 3** employs experimental microcosms to simulate hydrogen injection, showing microbial shifts under hydrogen-rich conditions. **Chapter 4** examines hydrogenase diversity in natural hydrogen springs, uncovering how geochemical conditions shape microbial adaptation and hydrogenotrophy. This work advances our understanding of microbial hydrogen cycling, with implications for optimizing UHS and prospecting natural hydrogen reservoirs. This contributes actionable insights for a hydrogen-based future, highlighting the need for interdisciplinary strategies to manage microbial risks and leverage natural resources sustainably.

Sommario

Il panorama energetico globale si trova in un punto in cui lavorare per un futuro sostenibile e a basse emissioni di carbonio è diventata una necessità piuttosto che una scelta. Poiché gli impatti dannosi della dipendenza dai combustibili fossili—che vanno dalle emissioni di gas serra al grave inquinamento ambientale—diventano sempre più evidenti, la transizione verso fonti di energia rinnovabili non è più un obiettivo lontano ma una priorità urgente. Tra il ventaglio di soluzioni, l'idrogeno emerge come un candidato convincente per guidare il passaggio verso un'economia a basse emissioni di carbonio. Con la sua capacità di fungere da vettore energetico pulito e versatile, una promettente risorsa naturale e un elemento cardine per la decarbonizzazione dei settori più difficili da trasformare, l'idrogeno offre un potenziale trasformativo. Tuttavia, realizzare questo potenziale richiede investimenti coordinati, uno sviluppo tecnologico innovativo e una comprensione più profonda delle sfide che devono essere affrontate.

L'idrogeno si distingue per la sua versatilità: può fungere da combustibile pulito per i trasporti, da materia prima per i processi industriali e da mezzo per immagazzinare l'energia in eccesso proveniente da fonti rinnovabili. Inoltre, l'idrogeno naturale offre la promessa di soddisfare la domanda energetica attuale con una risorsa naturale a basso impatto fornita dai processi geologici. Quando viene bruciato, l'idrogeno emette solo vapore acqueo, rendendolo un'alternativa a zero emissioni ai combustibili fossili. È importante sottolineare che l'idrogeno verde, prodotto tramite elettrolisi alimentata da energia rinnovabile, ha il potenziale di separare completamente la produzione di energia dalle emissioni di carbonio. Tuttavia, mentre la promessa dell'idrogeno è considerevole, la strada verso un'economia basata sull'idrogeno è piena di sfide tecniche, economiche e infrastrutturali che richiedono attenzione immediata e un impegno a lungo termine.

Una delle barriere centrali all'adozione diffusa dell'idrogeno risiede nella disparità dei costi tra le diverse vie di produzione. Mentre l'idrogeno grigio, derivato dal gas naturale, domina i mercati attuali grazie al suo basso costo, è associato a significative emissioni di carbonio. Al contrario, l'idrogeno verde rimane costoso, ostacolato dai costi elevati degli elettrolizzatori e dalla disponibilità limitata di

infrastrutture per le energie rinnovabili. Espandere la capacità produttiva e ridurre i costi attraverso ricerca, sviluppo e implementazione è essenziale per rendere competitivo l'idrogeno verde. Questo investimento deve inoltre estendersi allo sviluppo di sistemi di stoccaggio e trasporto dell'idrogeno, che rimangono colli di bottiglia critici per consentire all'idrogeno di svolgere un ruolo di vettore energetico globale.

Lo stoccaggio sotterraneo di idrogeno (UHS) è un aspetto fondamentale di questa transizione, offrendo una soluzione ai disallineamenti stagionali e giornalieri insiti nella generazione di energia rinnovabile. Stoccare idrogeno in giacimenti depleti, acquiferi o caverne saline fornisce un mezzo per bilanciare domanda e offerta, garantendo una fornitura energetica affidabile anche durante i periodi di bassa produzione di energia rinnovabile. Tuttavia, l'UHS introduce una serie di sfide proprie, in particolare le interazioni tra idrogeno, formazioni geologiche e comunità microbiche. Il sottosuolo non è un ambiente sterile. È abitato da comunità microbiche complesse che si sono evolute per sfruttare una varietà di substrati chimici come fonti di energia. Tra questi, l'idrogeno molecolare serve come donatore di elettroni critico in diversi percorsi metabolici, inclusi la metanogenesi, la riduzione dei solfati e l'acetogenesi. Sebbene questi metabolismi sostengono cicli biogeochimici vitali, pongono rischi significativi all'integrità e all'efficienza dell'UHS. Il consumo microbico di idrogeno può ridurre la purezza dell'idrogeno stoccato, comprometterne la disponibilità e persino portare al deterioramento delle infrastrutture attraverso processi come la corrosione indotta dai microbi. Inoltre, le interazioni tra comunità microbiche, oligoelementi e condizioni geochimiche nei serbatoi di stoccaggio sono poco comprese, limitando la nostra capacità di prevedere e gestire efficacemente questi rischi. Comprendere e mitigare queste interazioni è cruciale per garantire la stabilità e l'efficienza a lungo termine dei siti di stoccaggio, un aspetto che ha guidato gran parte del lavoro presentato in questa tesi. Inoltre, oltre allo studio della microbiologia dell'UHS, l'indagine sulla comunità microbica idrogenotrofa in sorgenti naturali caratterizzate da diversi contesti geologici e geochimici fornisce non solo informazioni sulle sfide e opportunità dell'idrogeno come vettore energetico, ma anche strumenti e framework preziosi per il prospecting dell'idrogeno naturale.

Chapter 1 - Hydrogenotrophic metabolisms in subsurface natural and engineered environments and implications for underground hydrogen storage

Abstract

Hydrogen is a fundamental electron donor in diverse microbial metabolisms and it is considered the energetic currency exchanged within microbial communities in anaerobic environments. Hydrogen is also the major actor in the transition to alternative and non-polluting energy sources, primarily due to its dual role as energy source and energy carrier and the production of water as a byproduct of combustion. Besides the technological efforts required for the transition to an hydrogen based economy, the geological storage of hydrogen gas, known also as Underground Hydrogen Storage (UHS), in a stable terrestrial reservoir for later use is a key prerequisite to decouple production from utilization. Medium to long-term targets for storage include depleted natural gas reservoirs, salt caverns and deep aquifers. Studies carried out in the past 30 years have unveiled a large subsurface ecosystem able to interact with the geochemical cycles and volatiles present in Earth's crust. When hydrogen is stored underground, the microbial communities present in situ can interact with it, consuming it as electron donor, potentially producing undesired metabolic byproducts capable of affecting the success of UHS operations. Here we review the current state of knowledge in hydrogenotrophic metabolisms capable of affecting UHS operations and discuss how the microbiology of natural hydrogen seeps can be used as analog to model the state space of UHS operations.

1.1 Introduction

Nowadays the negative effects of fossil fuels on the environmental and human health (*e.g.,* climate change, global warming, air pollution) are gaining more and more public attention, and new energy sources are investigated to guide the energy transition by reducing or replacing the use of fossil fuels (Tarhan and Çil 2021). The renewable energy sources (RES) such as wind, solar, tidal

and geothermal energies produce electricity without the emission of greenhouse gases. However there is a mismatch between energy generation and demand because these sources of energy are intermittent and seasonally-dependent (Thiyagarajan et al. 2022). When a large amount of energy is produced from RES, the energetic surplus can be converted into hydrogen, which can be safely stored in specific geological underground formations (Zivar, Kumar, and Foroozesh 2021; Matos, Carneiro, and Silva 2019; Takach et al. 2022). Precisely, the so-called "Green Hydrogen" is produced through the process of water electrolysis, splitting H_2O in $2H^+$ and O^{2-}. Hydrogen is considered the key to the energy transition also because it is a non-toxic gas, with the lowest molecular weight, a very poor solubility in water, a lower viscosity and a higher energy density per mass compared to CO_2 and CH_4 (Thiyagarajan et al. 2022; R. Tarkowski and Uliasz-Misiak 2022). Furthermore, hydrogen combustion only releases water as the final reaction product (Ishaq, Dincer, and Crawford 2022), resulting in zero carbon emissions.

Medium/long-term storage solutions for hydrogen include geological storage in depleted natural gas reservoirs and saline aquifers (Heinemann et al. 2021), also known as "Underground Hydrogen Storage" (UHS) technology. Compared to salt caverns, geological porous formations, such as deep saline aquifers and depleted oil and gas reservoirs, offer reasonably larger hydrogen storage capacities (several orders of magnitude) (Zivar, Kumar, and Foroozesh 2021b; Heinemann et al. 2021; Hassanpouryouzband et al. 2021). Additionally, previous experiences in gas storage operations in saline aquifers and gas/oil reservoirs provide significant hydrological and geological information required to evaluate the potential for UHS (Michael et al. 2010; 2009). This strategy makes hydrogen usable with the times and methods already developed for natural gas, ensuring high safety and versatility in energy production. On the other side, salt caverns storage are suggested to be more suitable for short-to medium-term hydrogen storage (Heinemann et al. 2021), mainly because of their lower working gas volume capacity, which is the amount of gas that can be withdrawn or injected with installed subsurface and surface facilities (Ozarslan 2012). These environments have been widely used for various industrial applications such as natural gas storage, crude oil storage, and

waste disposal (Firme, Roehl, and Romanel 2019). However, when hydrogen is stored underground, the microbial communities present *in situ* can interact with it, consuming it as electron donor, potentially producing undesired metabolic byproducts capable of affecting the success of UHS operations. This is the main reason to study in depth the hydrogenotrophic metabolic activities in these environments.

On the other hand, a noteworthy but relatively inconspicuous increase in research about the origins and destiny of naturally released hydrogen is occurring, sometimes referred to as 'gold' or 'white' hydrogen. Geological manifestations of hydrogen have been acknowledged for millennia (Zhao et al. 2023; SMITH et al. 2005; Dugamin, Truche, and Donze 2019). Hydrogen can be found in its molecular form (H_2) and frequently coexists with other gasses, including methane, helium, hydrogen sulfide and nitrogen. The fundamental questions revolve around its existence as a volumetrically significant, discoverable, predictable, and exploitable resource. Preliminary investigations indicate that we can initiate the characterization of potential hydrogen sources, the depths at which they are likely to be generated, the mechanisms governing their migration, and the factors influencing their retention or loss concerning the exploration and microbial utilization of this gas. While there have been an increasing number of reports of hydrogen-containing seeps (Prinzhofer, Tahara Cissé, and Diallo 2018; Frery et al. 2021; Etiope 2023; Larin et al. 2015; Milkov 2022), substantial discoveries and extensive analyses about the *in situ* microbiome remain conspicuously absent.

Microorganisms, the unseen architects of the microbial world, play a pivotal role in unlocking hydrogen's potential, integrating knowledge from diverse scientific disciplines to comprehend the intricate interplay between microorganisms and hydrogen. Hydrogenases, enzymes embedded in these microorganisms, act as molecular catalysts facilitating hydrogen conversion and evolution, depending on the thermodynamic circumstances. Aware of the extreme importance of such wide-range hydrogenase gene diversity, in this review we delve into the diverse array of hydrogenases (Figure 4) found across microbial taxa inhabiting diverse natural and engineered environments, highlighting potential hydrogenase gene diversity and distribution drivers, and their implications for Underground Hydrogen Storage. Sequences

similar to those of proteins corresponding to [NiFe]/[FeFe]/[Fe-only]-hydrogenases in Bacteria and Archaea were retrieved from the National Center for Biotechnology Information (NCBI) database (http://www.ncbi.nlm.nih.gov/) using the Basic Local Alignment Search Tool (Altschul et al. 1990). Aminoacidic sequences belonging to the different enzymatic subgroups were assembled into a manually curated database, including specific related information such as the accession numbers, PFAM ID, operone structure and others. Phylogenetic trees of amino acid sequences translated from the gene specifying the large subunit of [NiFe]-hydrogenases were constructed with neighbor-joining and maximum-parsimony algorithms by using MAFFT. This approach will allow future investigations of the hydrogenase gene diversity in specific environments of interest and preliminarily evaluations of potentially suitable hydrogen storage locations, where microbial activity is considered less dangerous in terms of hydrogen consumption and by-products release.

1.2 Hydrogen as a key resource for energy transition

As the world grapples with the urgency of addressing climate change and transitioning towards cleaner energy sources, hydrogen has surfaced as a versatile and environmentally friendly option for the urgently needed energy transition. Among other advantages, hydrogen has the highest gravimetric density of all known substances (120 kJ g^{-1}) and produces no contamination in the combustion process, since water is the only byproduct (Miocic et al. 2023; Lemmon et al., n.d.; Yue et al. 2021; (Ishaq, Dincer, and Crawford 2022)(Lemmon et al., n.d.).

The diverse landscape of hydrogen extends beyond its elemental simplicity, offering a spectrum of different types of production processes that result in varying degrees of environmental sustainability (Miocic et al. 2023). At the forefront there is "Green Hydrogen," a beacon of promise produced through electrolysis using surplus energy from renewable energy sources. This method ensures a zero-emission footprint, aligning seamlessly with the global agenda to reduce greenhouse gas emissions. As the energy transition gains momentum, the importance of understanding and optimizing the production of Green Hydrogen cannot be overstated. On the transitional front, "Blue Hydrogen"

emerges as a pragmatic solution. It is derived from fossil fuels, primarily natural gas, but incorporates carbon capture and storage (CCS) technologies to mitigate emissions. While not entirely emission-free, the implementation of CCS minimizes the environmental impact compared to conventional methods. "Gray Hydrogen," on the other hand, is the most common form of hydrogen production, involving the same pathway of the previous one but without implying carbon capture. “Pink Hydrogen” is produced through electrolysis powered by nuclear energy, and can also be referred to as “Purple” or “Red Hydrogen”. Additionally, the very high temperatures from nuclear reactors can be utilized in other hydrogen production methods. For example, nuclear reactors can generate steam for more efficient electrolysis or for steam methane reforming of fossil gas. “Turquoise Hydrogen” is an emerging type of hydrogen whose large-scale production is yet to be demonstrated. It is generated through methane pyrolysis, a process that produces hydrogen and solid carbon. This hydrogen type has the potential to be a low-emission hydrogen source, provided the thermal process is powered by renewable energy and the solid carbon byproduct is permanently stored or repurposed. “White Hydrogen” also known as “Golden Hydrogen” is naturally occurring geological hydrogen found in underground deposits and can also be created through fracking. Currently, there are no strategies in place to exploit this hydrogen source. Finally, the so-called “Black” and “Brown Hydrogen”, obtained from coal or lignite usage (the “brown coal”) in the hydrogen-making process, are at the opposite pole of Green Hydrogen in the hydrogen spectrum and the most environmentally polluting.

Comprehending the nuances of these hydrogen types is crucial for orchestrating a well-rounded strategy in the fight against climate change. The urgency to decarbonize various sectors, including transportation, industry, and power generation, highlights the need for scalable and sustainable hydrogen solutions. As the global community embraces the hydrogen revolution, recognizing the potential and limitations of each hydrogen type becomes paramount. Green and White Hydrogen stand as incredible opportunities for a sustainable future, while transitional solutions like Blue Hydrogen pave the way for realizable, immediate reductions in carbon emissions.

The nature of the hydrogen generation process as well as the geological nature of the reservoir may greatly impact the operational settings. The list of initiatives related to UHS has also been increasing in recent years, associated with the interest in these systems (Zivar, Kumar, and Foroozesh 2021; Miocic et al. 2023).

Besides, these subsurface systems may host rich and diverse microbial communities that not only consume the stored hydrogen, but can also produce harmful byproducts, such as hydrogen sulfide, thus leading to the metal infrastructure corrosion (see section "The microbiology of UHS") (Amils et al. 2023, Fullerton et al. 2021, Magnabosco et al. 2018, Gregory et al. 2019). Therefore, assessing the potential risks of these communities that can jeopardize the stability of the stored hydrogen gas and of the whole UHS process is of critical interest. The mentioned impact of microorganisms, as explored in this review, further accentuates the need for interdisciplinary collaboration, providing a bridge between scientific disciplines to ensure the effective implementation of hydrogen in our journey towards a carbon-free future.

In summary, both the hydrogen generation processes, the storage of the gas and its delivery issues expose the need for a comprehensive, end-to-end assessment of the whole pipeline: from the production of hydrogen gas to its final transformation into usable energy. It is precisely for these reasons and for hydrogen potential to facilitate the transition to a low carbon-emitting society that underground hydrogen storage (UHS) has been receiving increasing interest (Dopffel, Jansen, and Gerritse 2021; Miocic et al. 2023; Thaysen et al. 2023; Muhammed et al. 2022; Zivar, Kumar, and Foroozesh 2021).

1.3 Hydrogen as key energy source in microorganisms

Molecular hydrogen (H_2) is widespread in various environments, arising from biological, geothermal, and atmospheric sources. It presents desirable physical properties for biological systems, including its redox potential ($E^{\circ\prime}$=−0.42 V) and diffusion coefficient (4×10^{-9} $m^2 s^{-1}$). Microorganisms effectively leverage these properties through specialized metalloenzymes known as hydrogenases (Schwartz, Fritsch, and Friedrich 2013) and can respire it in diverse ecosystems, ranging from hypoxic H_2-enriched environments like animal guts and bog soils to aerated soils and

waters with trace H_2 concentrations (Greening et al. 2016a). Recent studies have highlighted the involvement of aerobic soil actinobacteria and acidobacteria in scavenging H_2 from the lower atmosphere, challenging the conventional notion that hydrogen metabolism is limited to environments with low O_2 and high H_2 concentrations (Greening and Cook 2014). These investigations have provided biochemical insights into mechanisms that enable certain hydrogenases to function in the presence of oxygen, which was traditionally considered an inhibitor of their active sites (Schwartz, Fritsch, and Friedrich 2013; Shomura et al. 2011; Horch et al. 2015). Minimalistic hydrogenase-containing respiratory chains have been identified in anaerobic systems, demonstrating their involvement in efficient energy generation within oligotrophic environments (Kim et al. 2010; Lim et al. 2014). Simultaneously, the knowledge of electron-bifurcating hydrogenases has advanced our understanding of energy conservation in anaerobic processes such as cellulolytic fermentation, acetogenesis, and methanogenesis (Schut and Adams 2009; Kaster et al. 2011; Buckel and Thauer 2013; Schuchmann and Müller 2014).

Hydrogenases catalyze the reversible conversion between H_2 and protons, making them essential players in H_2 oxidation and evolution (Mills et al. 2013; Volbeda et al. 1995). Understanding the diversity and distribution of these enzymes is crucial for unraveling ecological processes, reflecting non engineered environments and all the implications for underground hydrogen storage technology.

Hydrogenases are classified into three main groups based on their metal cofactors as [FeFe]-hydrogenases, [NiFe]-hydrogenases, and [Fe]-only hydrogenases. In [NiFe]-and [FeFe]-hydrogenases, hydrogen is the only substrate or product, according to the following reaction: $H_2 \leftrightarrow 2H^+ + 2e^-$. Here the electrons are transferred one by one to electron acceptors via the iron-sulfur clusters. One iron ion in both dinuclear centers is coordinated by sulfur, CO, and cyanide ligands, as supported by crystal structures of the [NiFe]-hydrogenase (Volbeda et al. 2005; 1995) and of the [FeFe]-hydrogenase (Nicolet et al. 2001; Bennett, Lemon, and Peters 2000; Nicolet et al. 1999; Peters et al. 1998). On the contrary, [Fe]-only hydrogenases do not catalyze *per se* the exchange of H_2 with protons of water or the conversion of para-H_2

to ortho-H_2, but hydrogen uptake is coupled to methenyl-tetrahydromethanopterin (methenyl-H_4MPT+) reduction (Lyon et al. 2004; Hartmann et al. 1996; Schwörer et al. 1993) and from this its systematic name, H_2-forming methylene-H_4MPT dehydrogenase (Hmd), derives. The latter is also named "FeS cluster-free hydrogenase" because, as opposed to the other two enzymes, it lacks FeS cubane centers (Korbas et al. 2006). [Fe]-only hydrogenases active site contains a labile light-sensitive cofactor (most likely Fe(II)) with a mononuclear low-spin iron that binds two CO ligands. The latter study demonstrates that in the active mHmd holoenzyme, the number of iron ligands increases by one in the presence of Hmd inhibitors (CO or KCN). This observation suggests that in active Hmd, the iron site contains an open coordination site, proposed to be the site of H_2 interaction.

All hydrogenases could be classified into eight previously described major lineages (Greening et al. 2016; Vignais and Billoud, 2007; Calusinska et al., 2010): groups 1 to 4 [NiFe]-hydrogenases, groups A to C [FeFe]-hydrogenases and [Fe]-hydrogenases. Among these, [NiFe]-hydrogenases are the most widespread and well-studied. They are further categorized into groups 1, 2, 3 and 4, each exhibiting unique structural and functional characteristics. Group 1 and 2 [NiFe]-hydrogenases are typically found in aerobic bacteria and some anaerobes, while Group 3 is prevalent in anaerobes. The Group 4 [NiFe]-hydrogenase enzymes are predicted to be the most abundant major type of hydrogenase on the planet, detected in both bacteria and archaea, which preferentially generates hydrogen exploiting various partner enzymes or ferredoxin, while in some cases translocating ions across biological membranes (Finney and Sargent 2019). [FeFe]-hydrogenases, primarily found in numerous anaerobic microorganisms, both prokaryotes and eukaryotes but not in archaea (Peters et al. 2015), possess a unique di-iron cofactor known as the H-cluster. These enzymes exhibit exceptional catalytic efficiency and are crucial for microbial communities thriving in anoxic environments. Despite similarities in structures and properties, [FeFe]- and [NiFe]-hydrogenases are phylogenetically not related. [Fe]-hydrogenases, although less common, are essential for certain anaerobic archaea, specifically called "methanogens". Although [Fe]-only hydrogenases do not show sequence similarity to [NiFe]- and [FeFe]-hydrogenases

(Thauer, Klein, and Hartmann 1996), they are able to substitute for [NiFe]-hydrogenases when the cells grow under nickel-limiting conditions (Afting, Hochheimer, and Thauer 1998).

The enzymes involved in the oxidation of H_2 produce electrons with low potential, which can either be directed through respiratory chains or utilized in fixing inorganic carbon. On the other hand, the process of H_2 evolution efficiently releases excess reducing agents as a diffusible gas during microbial fermentation and photobiological processes (Schwartz, Fritsch, and Friedrich 2013).

Despite significant progress, many aspects of microbial H_2 metabolism at both microscopic and macroscopic levels remain unexplored. Detailed phylogenetic and biochemical informations, and atomic-resolution structures are available for only a subset of hydrogenases (Volbeda et al., 1995; Peters et al., 1998; Shima et al., 2008; Fritsch et al., 2011; Mills et al., 2013). For example, thanks to recent advancements in sequencing technologies have expanded genome and metagenome sequence data, we got important insights into the phylogeny and diversity of hydrogenases (Wu and Mandrand, 1993; Vignais et al., 2001; Vignais and Billoud, 2007). Greening et al. (Greening et al. 2016a) analysis of publicly available genome and metagenome resources reveals that H_2 metabolism is more diverse and widespread at both taxonomic and community levels than previously recognized. Specifically this latter study shows that, among the enzymes, [NiFe]-hydrogenases exhibited the broadest distribution, being present in 36 bacterial and 6 archaeal phyla. These were consistently found in all classes of Proteobacteria, as well as in Firmicutes, Cyanobacteria, Aquificae, Euryarchaeota, and Crenarchaeota. Noteworthy occurrences of [NiFe]-hydrogenases were also noted in phyla lacking previous hydrogenase descriptions, including Bacteroidetes, Chlorobi, Chloroflexi, Planctomycetes, and Verrucomicrobia. Putative group A1 [FeFe]-hydrogenases were detected in anaerobic bacteria across 12 phyla, unicellular eukaryotes within 5 phyla, and surprisingly, in a single-amplified genome associated with the archaeal candidate phylum Diapherotrites (pMC2A384). Other [FeFe]-hydrogenase types, encompassing bifurcating, ancestral, and sensory variants, were exclusive to anaerobic bacteria such as Firmicutes, Bacteroidetes, Spirochaetes, Thermotogae, and Fusobacteria. Both [NiFe]- and [FeFe]-hydrogenase genes were identified in the

genomes of recently characterized phyla. In contrast, genes encoding the functionally restricted [Fe]-hydrogenases were exclusively found within the genomes of 25 methanogens. The phylogenetic distribution of hydrogenases correlated with oxygen preference: obligate anaerobes harbored O_2-sensitive [NiFe]- and [FeFe]-hydrogenases, obligate aerobes contained O_2-tolerant [NiFe]-hydrogenases (groups 1d, 1h, 2a, 3b, 3d), and genomes of facultative anaerobes exhibited a diverse range of them. Many hydrogenases displayed a mosaic distribution that deviated from 16S rRNA gene sequence phylogeny, exemplified by the widespread occurrence of group 1d and group 3b [NiFe]-hydrogenases, indicating significant pressure for lateral acquisition of these enzymes.

Surprisingly, metagenomic analyses on the hydrogenase distribution in the cold desert soils of continental Antarctica, showed that the most abundant and prevalent microorganisms are metabolically versatile aerobes that use atmospheric hydrogen to support aerobic respiration, through a phylogenetically and structurally distinct enzyme, the group 1l [NiFe]-hydrogenase, encoded by nine bacterial phyla (Ortiz et al. 2021).

Greening et al. 2016 (Greening et al. 2016b) additionally propose oxygen partial pressure (*p*O2) as a key driver in shaping the evolution and distribution of respiratory hydrogenases. Phylogenetic analysis indicates that the deepest-branching forms (groups 1a, 1b) are O_2-sensitive and involved in anaerobic respiration in strictly anaerobes, prevalent in hypoxic soils. Mid-branching heterotetrameric hydrogenases (groups 1c, 1e, 1g) show broader taxonomic dispersion, supporting roles in various metabolic processes across diverse taxa. Conversely, more recently branching lineages (groups 1d, 1h, and 2a) appear to be oxygen-tolerant enzymes involved in respiration in aerobes and facultative anaerobes. These subgroups were predominant in aerated samples, suggesting independent development of O_2 tolerance mechanisms after the emergence of oxygenic photosynthesis.

Although the importance of H_2 metabolism in certain environments is well recognized, the precise function of hydrogenases in overall soil and aquatic ecosystems remains largely unclear (Barz et al. 2010; Constant et al. 2011; Beimgraben et al. 2014; Greening et al. 2015).

Recent evidence suggests that H_2 serves as a crucial energy source for marine communities, even in oxic conditions (Lappan et al. 2023). Through a combination of biogeochemical, metagenomic, and thermodynamic modeling analyses, Lappan and colleagues demonstrated that a diverse yet limited subset of community members oxidize H_2 at rates conducive to lithotrophic growth. The findings underscore the role of these ubiquitously-distributed marine bacteria in mitigating atmospheric H_2 emissions and highlight H_2, alongside CO, as among the most reliable energy sources in the ocean due to their relatively high concentrations and energy yields, despite the sustained number of microbial groups capable of utilizing H_2. This scarcity may be attributed to the tradeoff between the significant resource investment required for synthesizing hydrogenases, even in iron and solar energy-limited oceanic regions, and the final energy concretely gained. Generally, in energy-limited waters, particularly in subantarctic regions with low primary production, the investment in iron for H_2 and CO consumption is likely to be justified. Notably, even in areas with higher iron availability, such as deeper circulating waters and continental shelves, elevated hydrogenase expression and activity have been detected. Specifically, groups 1d, 1l and 2a [NiFe]-hydrogenases, enabling cells to uptake electrons from H_2 into the aerobic respiratory chain (Ortiz et al. 2021; Islam et al. 2020; Podzuweit et al. 1986; Søndergaard, Pedersen, and Greening 2016), are by far the most abundant among the H_2-oxidizing enzymes detected in surface seawater samples (Lappan et al. 2023). Consequently, despite the significance of H_2 and CO as energy sources for marine bacteria, oceans remain a net source of these gases.

These evidences push the idea that investigating the influence of H_2 evolution and utilization on the microbial community shaping and global biogeochemical cycling is more than necessary (Greening et al. 2016a) both to achieve a deeper knowledge about our planet H_2 biogeochemical cycle and to access important biotechnological applications and innovative strategies.

1.4 The microbiology of potential UHS sites

The assessment of the risks associated with hydrogen loss requires the knowledge of biotic and abiotic processes occurring in storage sites, in order to estimate hydrogen production and

consumption rates (Gregory et al. 2019). When hydrogen is stored underground, the microbial communities present *in situ* can use it as an electron donor for anaerobic metabolisms, consuming important fractions of stored hydrogen (Hagemann et al. 2016). Research carried out in the past 30 years has unveiled a large subsurface ecosystem (Magnabosco et al. 2018) capable of interacting with the deep carbon cycle and volatiles present or recycled in Earth's crust (Fullerton et al. 2021). When there are suitable electron acceptors, hydrogen concentration can control the speed of microbial metabolic reactions occurring: this suggests that the high amount of hydrogen injected in a storage site could accelerate the metabolic reactions (Zivar, Kumar, and Foroozesh 2021b).

Very diverse microorganisms have been isolated and/or detected from oil fields, such as aerobic, microaerophilic and anaerobic microorganisms. Among the aerobic bacteria, *Pseudomonas* and *Acinetobacter* are known to be oil degraders (van Beilen, Wubbolts, and Witholt 1994; Bach, Berdichevsky, and Gutnick 2003). Bacteria related to the genera *Xanthobacter polyaromaticivorans* and *Stenotrophomonas sp.* are also detected in such environments and are known to be capable of growing in presence of molecular oxygen (Hirano et al. 2004; Yoshida et al. 2005). Another microbe that can grow using oxygen as an electron acceptor is *Shewanella putrefaciens*, isolated from an oil field site (Yusupova et al. 2020). Members of this species are defined as facultative anaerobic because of their additional sulfur- and iron-reducing properties (Nazina et al. 2007). Microaerophilic microorganisms belonging to the genera *Campylobacter*, *Oceanospirillum*, *Thiomicrospira* and *Geobacillus* are also known to inhabit petroleum reservoirs (N. K. Singh and Choudhary 2021; Magot, Ollivier, and Patel 2000). In particular *Geobacillus* is a microaerophilic thermophile able to degrade alkanes under strict oxic conditions, but there are some strains known as nitrate reducers under anoxic conditions. The great majority of the oil field microbial community is dominated by strictly anaerobic microorganisms such as *Methanolobus*, *Archaeoglobus*, *Desulfosarcina*, *Deferribacter*, *Oceanospirillum* and *Thiomicrospira* (Greene, Patel, and Sheehy 1997; Hubert et al. 2003; Voordouw et al. 1996; Li et al. 2017).

Although we know that these microbial groups mainly include fermentative bacteria, sulfate reducing bacteria (SRB), iron reducing bacteria, syntrophic bacteria and methanogens (Beeder et al. 1994; Orphan et al. 2001; Dopffel, Jansen, and Gerritse 2021), detailed reports about their *in situ* metabolic activities are currently missing. Microbial activity can cause the formation of biofilms, which may affect the porosity and permeability of the storage formation. Mineral precipitation or dissolution caused both by abiotic and biotic processes may have the same effect (Zivar, Kumar, and Foroozesh 2021b; Truche et al. 2010; Etiope, Schoell, and Hosgörmez 2011). The possible negative implications are hydrogen flow path blockage, pores clogging, corrosion of the infrastructures by H_2S, losing caprock integrity, and the subsequent hydrogen leakage from the caprock (Heinemann et al. 2021; Zivar, Kumar, and Foroozesh 2021b; Dopffel, Jansen, and Gerritse 2021; Thaysen et al. 2021). Despite many studies have reported alterations in gas composition, microbial diversity, and biotic/abiotic clogging affecting injection wells, very few have presented quantitative data on microbial growth or permeability modifications during time (Shafahi and Vafai 2009; G. Haddad et al. 2022).

Moreover, the lack of a definite description of the adopted sampling strategy makes it impossible to be sure that the detected microbiome is really 'indigenous' or it is the result of the outcoming contaminations. Indeed there is the probability that microorganisms could have been introduced into the reservoir by waterflooding (Matz et al. 1992). To date, available data suggest that especially the strict anaerobes could be considered as indigenous of oil reservoirs since the analysis of the genome of some isolates confirms their adaptation to those peculiar conditions (Magot 2005; Bernard and Connan 1992). In addition, the detection of taxonomically close microorganisms in similar oil fields (Grassia et al. 1996; Magot 1996) supports the existence of a widespread anaerobic microbial community in such environments. To confirm this data, still a significant amount of similar studies need to be carried out.

Aquifers are considered the second-most economically-attractive option for geological hydrogen storage after depleted oil and gas reservoirs (Jafari Raad, Leonenko, and Hassanzadeh 2022). An aquifer storage operation involves neither freshwater injection nor

the disposal of brine. It's also true that, even if the risk of stored hydrogen contamination is very low in aquifer storage operations, it exists, and also in this case the microbial community plays a critical role in influencing the efficiency of the storage technology. Depending on storage formation and physico-chemical properties such as temperature, pressure, pH, and salinity, different groups of microorganisms (e.g., methanogens, sulfate-reducers, homo-acetogens, and iron-reducing bacteria) (Heinemann et al. 2021; Thaysen et al. 2021; G. Haddad et al. 2022) in common with the natural gas reservoirs, could be activated in storage aquifers leading to hydrogen consumption and the subsequent release of byproducts, among which the H_2S is the more dangerous one.

On the other hand, salt caverns are thought to be the best solution for short and medium-term hydrogen storage (Heinemann et al. 2021; Böttcher et al. 2017). Salt crystals are formed when saline water evaporates and since microorganisms can be included in these geological formations (Park et al. 2009; R. H. Vreeland et al. 1998), it is relatively easy to detect them during the process of solution mining. The sulfate minerals in Permian salts are potential electron acceptors for microbial energy generation, while the presence of carbonate rock may provide an inorganic carbon source for anabolism and cell growth. This allows the assumption that autotrophic microbial life is feasible under certain circumstances, given the presence of a potent electron donor such as the H_2. Microbial groups such as *Halobacteria*, *Halanaerobiales*, *Balneolales, Halanaerobiaeota, Proteobacteria*, *Halobacterota*, *Bacteroidota*, *Firmicutes*, *Actinobacteriota*, and *Desulfobacterota* have been detected in these environments (Schwab et al. 2022). They are able to live at high salt concentration conditions (Oren 2014) and/or saturated solutions (Fendrihan et al. 2006). Some of them are homo-acetogenic microorganisms and strict anaerobes able to grow autotrophically on H_2/CO_2 or CO, and heterotrophically on a wide range of sugars, alcohols, methoxylated aromatic compounds and one carbon compounds, yielding acetate as their sole metabolic end-product. Their presence in the salt caverns might promote H_2 oxidation by halophilic sulfate reducers. Hydrogenotrophic methanogens may also compete for H_2, since to date they have been detected in hypersaline environments such as solar salterns, soda and salt lakes (Mcgenity and Sorokin 2018; Foti et al. 2007; Pal et al. 2020)

and deep-sea salt-saturated formation (Yakimov et al. 2013). This suggests that, even at salinities approaching to saturation, the reduction of sulfur species is possible, and anaerobic microorganisms, including methanogens and also sulfate reducers (Foti et al. 2007), can be enriched from such environments (Blum et al. 2012; D. Y. Sorokin et al. 2017; D. Sorokin 2011). Coherently with these previous studies, a 250 million-year-old halotolerant bacterium has been isolated for the first time from a salt mine constructed 650 meters below the ground surface in the geologically stable Permian age Salado salt formation (Russell H. Vreeland, Rosenzweig, and Powers 2000). This finding invokes many intriguing questions, regarding how long microorganisms can survive and specifically, how halophiles could stay alive for 250 million years in their small, saline "cages". These observations do indeed imply that some microorganisms may have eternal life, at least in relation to the brief lifetime of most plants and animals.

Considering that several physiologically and taxonomically different halophilic microorganisms are able to utilize H_2 as energy source, the long-term storage of this gas in oil reservoirs, deep aquifers and salt caverns should be accompanied by metagenomic and geochemical monitoring to detect unwanted microbial reactions in time.

Hydrogen holds a pivotal role in the energy metabolism of underground life forms (Colman et al. 2017). However, the utilization of H_2 by deep microbial metabolisms of specific H_2 storage sites such as salt caverns, gas and oil reservoirs and deep aquifers remains largely unexplored (Zgonnik 2020). Recent studies show that in underground H_2 storage reservoirs, the predominant H_2-consuming metabolisms belong to hydrogenotrophic sulfate reducing bacteria (SRB) that couple H_2 oxidation to sulfate reduction, resulting in hydrogen sulfide production (Dopffel, Jansen, and Gerritse 2021). Additionally, hydrogenotrophic methanogens reduce carbon dioxide to methane through H_2 oxidation, while homoacetogens couple H_2 oxidation to carbon dioxide reduction, producing acetate (Dopffel, Jansen, and Gerritse 2021; Pannekens et al. 2019; Gregory et al. 2019). The same three groups of microorganisms are additionally involved in subsurface corrosion (Loto 2017; Skovhus, Enning, and Lee 2017).

Numerous recent reviews have pointed out the relevant role of microbial activity in geological H_2 storage sites (Gregory et al. 2019; Dopffel, Jansen, and Gerritse 2021; Strobel et al. 2020; Aftab et al. 2022; G. Haddad et al. 2022; Ranchou-Peyruse et al. 2019). Gregory et al. (Gregory et al. 2019) explored different abiotic and biotic H_2-producing and H_2-consuming processes in the subsurface. In the same year, Ranchou-Peyruse et al. (Ranchou-Peyruse et al. 2019) investigated how gas storage can shape deep life, referring particularly to sulfate reducing and methanogenic microorganisms, by using high-throughput sequencing. Dopffel et al. (Dopffel, Jansen, and Gerritse 2021) provided insights into different microbially driven scenarios, offering key indicators for processes and recommending strategies for monitoring and managing microbial activity in subsurface H_2 storage. Strobel et al. (Strobel et al. 2020) enlightened the powerful concept of underground methanation using data from the Sun Storage project (Bauer and Pichler 2017), focusing on methanogen growth and changes in gas composition due to methanogenesis. Aftab et al. (Aftab et al. 2022) highlights the microbial consumption of H_2, leading to pore-network precipitation, plugging, and partial permeability impairment, all processes discussed in association with diverse geological settings constraints. There are not many studies like the one of G. Haddad et al. (G. Haddad et al. 2022) where an experimental reactor mimicking the storage site (in this case an aquifer) has been employed. They show that as soon as H_2 was injected, formate was produced in the aqueous phase and CO_2 was consumed from the gas phase. After CO_2 complete depletion, microbial activities cease, and a substantial portion of injected H_2 transforms into H_2S, formate, and methane. The findings underscore the significant influence of microbial life in deep storage sites, particularly affecting sulfate, CO_2, calcite, and H_2 concentrations in the system.

Currently, it remains uncertain the potential physiologic response of subsurface microorganisms to various H_2 concentrations (N. Liu et al. 2023; Osman et al. 2022), both in engineered and in natural subsurface environments. A range of studies investigated the metabolism of methanogens at excess H_2 concentrations and ambient pressure, with contrasting results. Conrad et al. (Conrad, Schütz, and Babbel 1987) demonstrated that excess H_2 stimulated methanogenesis and growth rates in anoxic paddy soil. On the

contrary, results by Topcuoglu et al. (Topçuoğlu et al. 2019) and Stewart et al. (Stewart et al. 2019) suggest an inhibitory effect of high partial pressures of H_2. Similar observations were made for Methanothermobacter thermoautotrophicus using comparative proteomic analysis (Enoki et al. 2011). Members of the order Thermotogales have often been detected both in potential hydrogen storage sites such as aquifers and depleted gas reservoirs (Ben Hania et al. 2013; Bassani et al. 2023) and in natural gas field (Dohrmann and Krüger 2023). Several studies demonstrate that Thermotogales tolerance to H_2 differ greatly between species depending on H_2 partial pressure and hydrogen excess can inhibit the growth of most of them, with few exceptions such as *Mesotoga spp*. (Huber and Stetter 2001; Dohrmann and Krüger 2023).

The majority of available data on microbial H_2 turnover rates derive from batch cultures under selected growth conditions (Esquivel-Elizondo et al. 2017; de Poorter, Geerts, and Keltjens 2007), where environmental variables affecting the *in situ* microbial metabolisms, may strongly differ from the subsurface (Hoehler and Jørgensen 2013). Further complicating matters is the fact that many microorganisms in the deep subsurface are not culturable and are possible to study only through metagenomics (Long et al. 2016; Soares et al. 2023; Xie et al. 2021).

Hydrogenotrophs, aside from requiring fitting thermodynamic conditions to be metabolically active, depend on H_2 as an electron source for energy, an electron acceptor such as sulfate, elementar sulfur, pyrite, iron (III), and a inorganic/organic carbon source for cell division. Besides carbon, nutritional requirements include macro elements such as N, P, Ca, Mg, S, and Fe, and trace elements like Co, Mn, Ni, Mo, Cu, Zn. Additionally, S and W are particularly important for acetogens and hydrogenotrophic methanogens due to their role in the function of hydrogenases and formate dehydrogenase, converting formate to CO_2 and H_2 (Mares, Moreno-Andrade, and Quijano 2023; Biswas et al. 2009; Šafarič et al. 2020). Optimal growth often demands additional components like vitamins, yeast extract, coenzyme M, aromatic acids, or combinations thereof (Demirel and Scherer 2011; Scherer and Sahm 1981; Shima et al. 2020; Nobu et al. 2017; SCHNÜRER, SCHINK, and SVENSSON 1996).

Despite the potential hydrogen storage sites could correspond to extreme environments where microbial life is not highly favored, metabolic key elements like carbon, sulfur, phosphorus, and iron, can be potentially released by mineral weathering (Berthelin 1988). For example, sulfur-oxidizing bacteria known as *Thiobacilli*, widely detected in potential UHS sites like petroleum reservoirs (Tian et al. 2017; Al-Khazaali and Ataei 2023), play a significant role in the production of sulfuric acid through the oxidation of various sulfur compounds, including sulfide, sulfur, sulfite, and thiosulfate (Ehrlich, 1981). Thiosulfate reduction is an important step for sulfur cycling not only in oil reservoirs but also in anaerobic thermal environments such as the slightly acidic and neutral-pH volcanic geothermal springs (Xu et al. 1998; Ravot et al. 1995; Zhou et al. 2018). Some species demonstrate the ability to grow in absence of oxygen, utilizing nitrate as an electron acceptor during anaerobic respiration and releasing nitric acid as a byproduct. The resulting acidity (H+) is recognized as a key factor in the solubilization of carbonates in soils (Dommergues and Mangenot, 1970; Duchaufour, 1982), in the weathering of limestone (Kauffmann, 1960; Jaton, 1972) and serpentinized ultrabasic rocks (Lebedeva et al., 1978). In soils, over 50 % of 1100 microbial strains are capable of mineral weathering, as demonstrated by their ability to mineralize biotite (Huang et al. 2014).

It's noteworthy to know that also the a-biotic interactions of hydrogen with the rock minerals available in a reservoir rock and caprock can cause mineral dissolution (e.g., carbonate, sulfate, feldspars, clay) and precipitation (e.g., illite, sulfide, pyrrhotite) (Perera 2023). Mineral dissolution can also determine changes in the rock structure, activating faults and causing a mechanical weakening of the reservoir rocks (Ciantia et al. 2015; Ciantia, Castellanza, and di Prisco 2015; Zhang et al. 2023). Because of the thermodynamically unstable nature of pyrite in the presence of hydrogen (Ebrahimiyekta 2017), pyrite dissolution is considered the major abiotic process that can happen in a reservoir during hydrogen storage.

Thaysen et al. (Thaysen et al. 2021) describes an extensive inventory of microbial metabolisms that occur in subsurface environments. Since sulfur oxidizers can potentially use the same substrates as sulfur reducers (i.e. sulfide and thiosulfate) (Porter,

Roychoudhury, and Cowan 2007), they are collectively defined as sulfur species reducing microorganisms (SSRM). Sulfate reduction is specifically addressed due to its associated high risks for hydrogen storage operations. Indeed, SSRM release toxic and corrosive hydrogen sulfide which is inflammable and corrosive for the *in situ* installed infrastructures. SSRM require sulfate and/or other sulfur compounds to produce H_2S and typically dominate in environments rich in these electron acceptors, probably due to a generally higher affinity for hydrogen compared to homoacetogens and methanogens (Thaysen et al. 2021). Only in certain low temperature and/or low salinity environments, homoacetogens outcompete SSRM (Thaysen et al. 2021). Sulfur respiration is constrained by low solubility, requiring cell attachment to sulfur particles (Hedderich et al. 1998), but it can form easily metabolizable polysulphides reacting with potentially present sulfide. However, sulfur readily reacts with sulfide formed during the reduction of sulfate to form easily metabolizable polysulphides (Rickard and Luther 2007).

Iron (III) reduction is among the typical biotic processes that can transpire in underground gas storage sites. This reaction is performed by heterotroph dissimilatory iron reducing bacteria (DIRB), and relies on iron oxides and minerals such as smectite and chlorite, as well as on the presence of organic carbon (Hernsdorf et al. 2017). In natural environments rich in Fe oxides and organic carbon, DIRB may have a great advantage over SSRM, methanogens and homoacetogens, due to a very high affinity for H_2 (Thaysen et al. 2021). Contrary to many sediments and aquifers, in carbon-rich oil fields iron oxides are poorly present and dissimilatory iron reduction may be less relevant (Juergen Wiegel, Hanel, and Aygen 2003). Oxygen, nitrate, and aerobic processes become significant only with aquifer contamination, while halogenated compound concentrations are generally too low to impact hydrogen storage (Thaysen et al. 2021). Additionally, fumarate may be used as an alternative electron acceptor by SSRM (Muyzer and Stams 2008) and homoacetogens (Bengelsdorf et al. 2018; Schuchmann and Müller 2016) but the relevance of anaerobic fumarate respiration using hydrogen is considered low due to the rarity of readily metabolizable organic matter both in engineered and not engineered subsurface

environments (Ghiorse and Wilson 1988; Dassonville and Renault 2002).

Microorganisms carry out carbon assimilation through autotrophy or heterotrophy (Schönheit, Buckel, and Martin 2016). Some of the main subsurface microbial groups such as methanogens, homoacetogens and a portion of SSRM are flexibly able to grow autotrophically, heterotrophically, or mixotrophically (Debabov 2021; Yin et al. 2013; Kuenen et al. 1997). The assimilation of nitrogen encompasses the utilization of ammonia, nitrate, or nitrogen fixation (diazotrophy) and is prevalent in SSRM, methanogens, and homoacetogens (Whitman, Bowen, and Boone 1992). Storage temperatures for hydrogen in depleted oil/gas fields and saline aquifers and caverns range from about 20 to 100 °C, within a depth range of 500 to 2000 m (Matos, Carneiro, and Silva 2019; Shi, Jessen, and Tsotsis 2020; Hassanpouryouzband et al. 2020). At elevated temperatures, thermophiles and hyperthermophiles face challenges associated with increased reaction rates. The rapid abiotic reactions may negate any benefits to microorganisms catalyzing the reactions, prompting high-temperature-adapted microorganisms to produce enzymes with faster reaction rates (Steinweg et al. 2013). While most cultivated hydrogenotrophic methanogens are mesophiles (range temperature from 30 to 40 °C) (Nozhevnikova et al. 2001), especially metagenomic and metaproteomic analyses suggest their optimal growth temperatures span in a thermophilic regime from 15 to 98 °C (Y. Liu and Whitman 2008), with a notable proportion favoring temperatures above 60 °C (Y. Liu and Whitman 2008; Bu et al. 2018; Holden and Sistu 2023; Hagen et al. 2016; Maus et al. 2016). Exceptionally, *Methanopyrus kandleri* was found to grow at a hyperthermophilic range between 84 and 122 °C (Kurr et al. 1991; Takai et al. 2008).

Similarly, homoacetogens show optimum growth temperatures between 20 and 30 °C, except in a few cases. The upper limits for their growth correspond to 70–72 °C (Basen and Müller 2017; Leigh, Mayer, and Wolfe 1981; Basen et al. 2018). Cultivated sulfur species-reducing microorganisms (SSRM) typically exhibit optimum growth temperatures of 20–30 °C or 50–70 °C, with sulfur reducing archaea having higher optimum growth temperatures than sulfur and sulfate reducing bacteria. The full range for optimum growth of SSRM spans 10–106 °C, and the critical

temperature for the growth of cultivated SSRM is 113 °C (*Pyrolobus fumarii*) (Thaysen et al. 2021).

On the other hand, a net upper salinity limit to microbial activity has not been established (Yakimov et al. 2015; Merino et al. 2019). It appears to be the brine composition, rather than the salinity alone, that puts a hard limit on microbial growth (Payler et al. 2019; K. Singh 2016) and this is particularly true speaking of salt caverns. During the water evaporation process, small parts of the brine become trapped in the salt and end up as fluid inclusions. Any halophilic microorganisms present in the fluid will be trapped as well and subsequently freed during the process of solution mining. For example, the sulfate minerals in Permian salts are potential electron acceptors for microbial energy generation, while the presence of carbonate rock may provide an inorganic carbon source for anabolism and cell growth (Russell H. Vreeland, Rosenzweig, and Powers 2000). This suggests that autotrophic microbial life is feasible under certain circumstances, given the presence of a suitable electron donor (like injected H_2) and electron acceptor(s).

The typical salt concentration in hydrogen storage sites, such as depleted gas/oil reservoirs and deep aquifers, ranges from 0 to 3 M NaCl (Buttinelli et al. 2011; Delshad et al. 2023; Shi, Jessen, and Tsotsis 2020), at which highly diverse microbial communities can live (Rothschild and Mancinelli 2001; Merino et al. 2019; Telesh, Schubert, and Skarlato 2013). Hydrogenotrophic methanogens cultivated in these conditions generally prefer salt concentrations up to 0.77 M NaCl, very close to the salinity of seawater. However, few strains demonstrate resilience under more halophilic conditions, of which two correspond to extremely halophilic mesophilic hydrogenotrophic methanogens, tolerating salt concentrations of approximately 3.3–3.4 M (Ollivier et al. 1998; T. N. Zhilina et al. 2013). The majority of cultivated single-strain sulfate-reducing mesophiles (SSRM) thrive optimally at low salinities between 0 and 0.4 M NaCl. Nonetheless, some SSRM strains, including thirty-four mesophiles, exhibit the capability to grow at NaCl concentrations up to 1.7 M (OLLIVIER et al. 1991; Krekeler et al. 1997; Jakobsen, Kjeldsen, and Ingvorsen 2006). Studies on the salt tolerance of homoacetogens are limited, with cultivated strains showing low optimum salinities of 0–0.4 M NaCl

and upper growth temperatures of 42 and 47 °C, respectively (T. N. Zhilina et al. 1996; Tatyana N. Zhilina and Zavarzin 1990).

Additionally, the pH of the brine determines the *in situ* environmental redox conditions, with an important outcome on the microbial growth and metabolic activity. Most methanogens, homoacetogens, and SSRM are adapted to a pH range of 6.5–7.5, with the inability to grow outside the pH range of 4–9.5 for most methanogens and SSRM. Only few (seven) known methanogens can withstand a critical pH of 10, and only nine known methanogens can withstand acidic conditions of pH <5 (Stewart et al. 2015; Takai, Inoue, and Horikoshi 2002; Ganzert et al. 2014; Bräuer et al. 2011). Generally, pH values below 7 favor the growth of methanogens over sulfate reducers, whereas above pH 7.5, sulfate reducers tend to outcompete methanogens (O'Flaherty et al. 1998). Among SSRM, there are known strains adapted to both highly alkaline environments above pH 10, and acidic habitats down to a pH <5. Rarer are the sulfur reducers that can grow down to a pH of 1. Among known homoacetogenic strains, some of them exhibit high critical pH values of 10.0–10.7, and a lower number of strains can tolerate pH values as low as 3.6–4.5 (Jürgen Wiegel, Braun, and Gottschalk 1981; Tanner, Miller, and Yang 1993; Kaneuchi, Benno, and Mitsuoka 1976; Küsel et al. 2000; Gössner et al. 2008).

Reported pressure conditions for H_2 storage range from 5–20 MPa (Matos, Carneiro, and Silva 2019) to 1–50 MPa (Shi, Jessen, and Tsotsis 2020). On Earth's surface, pressure spans from 0.1 to 112 MPa, with elevated pressures documented in subsurface settings, where it has been estimated that microbial life could thrive at pressures around 340 MPa (Merino et al. 2019). While an upper pressure limit for H_2 storage microbial life has not been established (Merino et al. 2019; Dopffel, Jansen, and Gerritse 2021), studies indicate that high pressures in crustal pore spaces are generally less inhibitory to microbial cellular activity than high temperatures (Yernazarova et al. 2016). Growth of various mesophilic microorganisms adapted to atmospheric pressure is inhibited at 30–50 MPa, whereas pressure effects are favorable for hyperthermophiles. Microorganisms thriving optimally at 10 MPa or above are obligate and facultative piezophiles (Merino et al. 2019; Rothschild and Mancinelli 2001). Most mesophiles and thermophiles from habitats with pressures <50 MPa can grow in

enrichment cultures at atmospheric pressure (Payler et al. 2019). The majority of identified cultivated piezophiles are psychrophiles, with limited relevance to our study. Only four mesophilic strains, three of them hydrogenotrophic sulfate reducers, were reported, growing optimally at 10–40 MPa. Thermophiles such as the hydrogenotrophic methanogen *Methanococcus thermolithrophicus*, were identified, with optimal growth at 50 MPa. The hyperthermophilic group includes hydrogenotrophic *Methanopyrus kandleri* and *Methanocaldococcus jannaschii*, growing optimally at 20–75 MPa, respectively. A temperature-dependent pressure response was reported for the SSRM *Desulfovibrio indonesiensis*, exhibiting similar growth rates at high and ambient pressure (45 °C) but reducing growth rate at 20 °C and 30 MPa compared to 0.1 MPa (Fichtel et al. 2015). Pressures above 1 bar of carbon dioxide can be toxic for some microorganisms, including SSRM and methanogens (Dupraz et al. 2013). Oxygen is also toxic for many anaerobic methanogens and homoacetogens (such as members belonging to the genus Clostridium) (Lu and Imlay 2021).

Syntrophic interactions, involving the cooperative relationship between different microbial groups where metabolic byproducts of one group serve as substrates for another, are common in hydrogen storage sites. For instance, SSRM and homoacetogens collaboratively participate in microbial-induced corrosion of steel, where SSRM grow on acetate produced by homoacetogenesis (Usher et al. 2015). Syntrophy explains the co-occurrence of sulfate-reducing *Desulfovibrio* and homoacetogens like *Acetobacterium* in environments such as petroleum and subsurface CO_2 reservoirs (Grabowski et al. 2005; Freedman, Tan, and Thompson 2017). Similarly, H_2-producing heterotrophs coexist with methanogens in petroleum reservoirs, where the former facilitate H_2 transfer to the latter (Topçuoğlu et al. 2019). Special habitats for syntrophic growth of methane-producing Archaea are found in depleted oil reservoirs during oil biodegradation processes, where sulfate reduction and methanogenesis dominate, influenced by sulfate concentrations exceeding 50 µM (Porter, Roychoudhury, and Cowan 2007) as observed in studies by Jiménez et al. (Jiménez et al. 2016).

All these hydrogenotrophic metabolisms are able to consume and convert hydrogen in other chemical compounds, parallelly resulting

in a substantial loss of energy (Reitenbach et al. 2015). Among the chemical bioproducts, there are: Methane (CH_4), Hydrogen sulfide (H_2S), Ferrous-ferric oxide (Fe_3O_4) and Acetate.

Microbially driven methanogenesis can enhance reservoir storage capacity, utilizing H_2 and CO_2 to produce methane. This biogenic gas potentially serves as an additional energy resource, contributing to the overall energy output from storage reservoirs. Hydrogen sulfide, a toxic gas produced by sulfate-reducing bacteria (SRB), is highly inflammable and corrodes steel infrastructures in a process called Microbial Induced Corrosion (MIC) causing economic damages (Hemme and van Berk 2017; Dopffel, Jansen, and Gerritse 2021). Exposure to H_2S, and its bisulfide ion, HS^-, induces damage to microbial proteins and coenzymes (Chen, Cheng, and Creamer 2008; Ntagia et al. 2020). At 5.0–6.3 mM H2S, SSRM growth is completely inhibited, although metabolic activity persists under these conditions (Kushkevych, Dordević, and Vítězová 2019; Choi and Rim 1991). For methanogens and homoacetogens 3.8–7.5 mM H_2S and total sulfide concentrations of 3.3 mM, respectively, stop the growth (Choi and Rim 1991; Ntagia et al. 2020). In systems characterized by circumneutral pH and ferric ion concentrations surpassing 1 mM, the precipitation of H_2S in mackinawite is predicted to maintain concentrations below toxic levels (Rickard and Luther 2007). Ferrous-ferric oxide (also called “magnetite”) produced in the iron-reduction carried out by iron-reducing bacteria (IRB), can react with hydrogen sulfide leading to precipitation of iron sulfide (FeS) which causes clogging events affecting permeability and fluid flow. Moreover, if magnetite formation occurs near wellbores or within infrastructure, it may pose challenges related to wellbore stability, casing integrity, and the following loss of H_2 reservoir injectivity (Enning and Garrelfs 2014). The major organic acid produced in fuel-oil/aqueous systems is acetic acid (Loto 2017). Acid-producing bacteria have been described to be mainly responsible for the corrosion problems (Thaysen et al. 2021)

In general, unveiling the microbial intricacies of hydrogen storage environments highlights the importance of microbial monitoring in this field, implying proactive strategies to enhance the safety and efficiency of hydrogen storage technologies.

1.5 The microbiology of natural hydrogen seeps

The so-called white or gold H_2 primarily originates from the Earth's core and mantle. However, the suite of biotic processes and water-rock reactions that take place within the mantle and the crust represent a secondary source of natural H_2 (Langhi and Strand 2023; Klein, Tarnas, and Bach 2020a). H_2 formation can be the result of microbial energetic metabolism and thermogenesis (Langhi and Strand 2023). On the other hand, the main geological processes leading to H_2 formation include H_2O reduction during Fe oxidation in minerals (*i.e.* serpentinization of ultramafic rocks), H_2S oxidation coupled with low-pressure magma degassing, K-, Th-, and U-bearing minerals decay leading to H_2O radiolysis, and H_2O reaction with surface radicals during the mechanical break of the rock Si-O bond (Langhi and Strand 2023; Klein, Tarnas, and Bach 2020a).

On Earth's surface, one of the main H_2-releasing microbial processes is photosynthesis, as H_2 evolves from NADH (Nandi and Sengupta 1998). Furthermore, microbial metabolism plays a crucial role in the transition of organic matter (and thus H_2) from the biosphere to the geosphere taking place in the first few meters of the lithosphere. In fact, microbes take part in the first step of diagenesis, through which sedimentary biopolymers are converted into geopolymers. Either aerobic respiration or anaerobic fermentation allow the degradation of biotic macromolecules that serve as an energy source in such a light-deprived environment (Tissot and Welte 1984; Suzuki et al. 2024). In both metabolic pathways, excess electrons are disposed through the catalytic activity of the hydrogenases, resulting in H_2 production (Nandi and Sengupta 1998). The remaining catabolism residues are polycondensed into insoluble organic matter, namely *kerogen*, which is rich in H_2. The ongoing sediment burial results in a progressive increase in the heat and pressure to which it is subjected. In the temperature range from 100°C to 350 °C kerogen is exposed to thermal cleavage, eventually leading to the formation of oil, gas, hydrocarbons (mostly methane) and H_2 - a process termed "catagenesis" (Tissot and Welte 1984; Hanson and Hanson 2024).

Among the geological processes crucial to the formation of natural H_2, serpentinization plays a pivotal role. The latter is a H_2-releasing

geological process associated with ultramafic rocks, which contain in total less than about 45 wt % SiO2 and elevated amounts of ferromagnesian minerals such as olivines and pyroxenes. When H_2O enters in contact with Fe^{2+} and Mg^{2+}, these latter are oxidized thanks to H_2O hydrolysis, which in turn releases H_2 (Holm et al. 2015; Russell, Hall, and Martin 2010). Ultramafic rocks are hosted by mid-ocean ridges, forearc systems, and terrestrial ophiolites. While geophysical evidence suggests serpentinization is limited to the uppermost 2 km of ridge crests, subduction zone represent a major geological setting where H_2O derived from sediments and subducting igneous rocks can infiltrate and serpentinize the overriding forearc mantle up to more than 10 km deep (Skelton et al. 2005; Fryer 2012). The production of H_2-CH_4 fluids through serpentinization has been observed at mid-ocean ridges (Konn et al. 2015; Kelley et al. 2005), on land (Etiope and Sherwood Lollar 2013), and in the shallow forearc of subduction zones (Mottl et al. 2003; Kelley et al. 2005). As a consequence, ultramafic rocks-hosted hydrothermal vents can discharge large amounts of H_2. There is compelling evidence that deep microbial communities utilize H_2-CH_4 sourced from serpentinite. Furthermore, the discovery of essential building blocks of life in serpentinized ultramafic rocks supports the hypothesis that these environments may have been sites for the emergence of life on Earth (Sleep, Bird, and Pope 2011; Russell, Hall, and Martin 2010; Müntener 2010). Considering how widespread the geological settings where serpentinization occurs are and that these processes have been going on throughout most of Earth's history, the amount of the hypothesized naturally-generated H_2 is enormous (Vitale Brovarone et al. 2020; Merdith et al. 2023).

Additionally, H_2 is one of the main trace elements released both in the hydrothermal fluids and in the volcanic plumes due to magmatic degassing. Its abundance reflects the degassing pressure and the SO_2-H_2S equilibrium, which in turn controls magma redox conditions and hence H_2/H_2O ratios (A. Aiuppa and Moussallam 2024; A. Aiuppa et al. 2011; Giggenbach 1987). Another highly H_2 yielding process is H_2O radiolysis: the decay of K, Th, and U included in minerals releases α, β, and γ radiations that cleave H-O bonds, thus generating reactive hydrogen radicals that form H_2 molecules (Spinks and Woods 1990). This reaction occurs at all pressure and temperature values at which H_2O is

stable. Since it only requires H_2O and radionuclides to take place, radiolytic H_2 production is a relatively ubiquitous process throughout Earth's crust (Klein, Tarnas, and Bach 2020b). Lastly, natural H_2 can be a result of mechanical forces acting on silica-containing rocks and producing reactive radicals, a process hence termed mechanoradical H_2 generation. It takes place in active fault zones, where the mechanical stress exerted on silicate minerals breaks the covalent Si-O bond, thus creating Si-bearing radicals that can react with H_2O and release H_2 as a by-product (Klein, Tarnas, and Bach 2020b). Not only faults are ubiquitous geologic features, but they also represent key paths for hydrothermal fluids, thus likely enhancing the amount of natural H_2 these latter transport. Besides, mechanoradical H_2 can be released wherever the shattering of silicate minerals occurs (*i.e.*, due to frost wedging, rock abrasion, and even the bedrock comminution beneath glaciers) (Telling et al. 2015).

All of the above points to H_2 representing the major electron donor available for microbial metabolism in subsurface environments (Gregory et al. 2019). In fact, hydrogenase gene abundance is almost an order of magnitude higher in subsurface environments, compared to surface environments (Löffler, Tiedje, and Sanford 1999). Despite determining to what extent each H_2-generating geological process supports microbial communities is not trivial, evidence is growing (Gregory et al. 2019). For instance, in radiolytic environments, measured H_2 concentrations are significantly lower than expected, and this discrepancy suggests that radiolytic H_2 production almost equals its consumption (Lin, Hall, et al. 2005; Blair et al. 2007; Sauvage et al. 2021). One plausible explanation is that the redox disequilibria generated via radiolysis supports chemolithoautotrophic microbial communities (Türke, Nakamura, and Bach 2015; Dzaugis et al. 2016). In particular, the *in situ* microorganisms are believed to be capable of autotrophic acetogenesis and methanogenesis of acetoclastic methanogenesis, while abundant H_2 thermodynamically inhibits H_2 producing microbes (*i.e.*, anaerobic fermenters) (Pedersen 2000; Lin, Hall, et al. 2005; Lin, Slater, et al. 2005). Furthermore, Vitale Brovarone et al. (2020) present findings from exhumed subduction zone high-pressure rocks and thermodynamic modeling, demonstrating that deep serpentinization at depths of 40-80 km produces substantial quantities of H_2 and abiotic CH_4, as well as

H_2S and NH_3. These findings clearly indicate that subduction zones could globally harbor significant sources of deep H_2 and abiotic CH_4, thereby supplying energy to the subsurface biosphere in the forearc regions of convergent margins.

Finally, The above mentioned findings point to the widespread availability of differently-originated natural-H_2 and to the opportunity for this energetic currency to be exploited by chemolithoautotrophic microorganisms as an electron donor, thus suggesting that H_2 may have contributed to the origin of life on Earth and could constantly support diverse ecosystems (Milkov 2022).

1.6 Conclusions

The role of hydrogenotrophic microorganisms and their associated hydrogenase enzymes in underground hydrogen storage (UHS) presents both challenges and opportunities for the future of energy storage. As the global community seeks to reduce reliance on fossil fuels and transition towards sustainable energy solutions, hydrogen stands out as a promising alternative, offering high energy density and the potential for carbon-free energy. However, the success of UHS depends on a comprehensive understanding of the microbial processes that can affect hydrogen storage.

This review highlights the diversity of hydrogenases, which are enzymes that catalyze the oxidation and evolution of hydrogen. These enzymes, found across various domains of life, reflect the adaptability and resilience of microbial life in diverse environments, including those that may be encountered in engineered Underground Hydrogen Storage sites. The presence of hydrogenotrophic microorganisms in subsurface environments, where UHS is likely to occur, poses significant risks to storage efficiency. These microorganisms can consume stored hydrogen, reducing the available energy content, and potentially produce by-products such as methane or hydrogen sulfide, which could compromise the integrity of storage facilities and the purity of the stored hydrogen.

Understanding these microbial communities and their metabolisms using natural hydrogen seeps as paradigms also opens up avenues for managing and mitigating these risks. Advances in molecular biology, metagenomics, and bioinformatics have provided tools to identify and characterize the microbial

populations present in potential UHS sites. By mapping the diversity of hydrogenase genes and understanding the environmental conditions that favor hydrogenotrophic activity, it may be possible to design strategies that either inhibit microbial hydrogen consumption or utilize microbial processes to enhance storage stability. Moreover, the study of hydrogenotrophic metabolisms and hydrogenase diversity has broader implications beyond UHS. It contributes to our understanding of subsurface microbial ecology, biogeochemical cycling, and the evolutionary history of life on Earth. The insights gained from studying these microorganisms in the context of UHS can inform other areas of biotechnology, such as bioremediation, microbial fuel cells, and the development of bio-inspired catalysts.

In conclusion, while the microbial consumption of hydrogen in UHS presents a significant challenge, it is not insurmountable. Through continued research and collaboration across disciplines, it is possible to develop strategies that mitigate the risks while harnessing the potential of these microorganisms for innovative energy solutions. The future of UHS as a viable energy storage technology will depend not only on advances in engineering and materials science but also on a deep understanding of the microbial world that interacts with stored hydrogen. By integrating knowledge from microbiology, geochemistry, and engineering, we could ensure that UHS plays a vital role in the transition to a sustainable energy future. As research progresses, exploring the yet uncultivated microbial majority through metagenomics and metatranscriptomics will likely unveil additional insights into the vast diversity of hydrogenases and their roles in biogeochemical cycles. Integrating phylogenetic approaches with functional studies will further enhance our understanding of the ecological significance of hydrogenases in microbial communities.

1.7 Reference

Aftab et al. *Industrial & Engineering Chemistry Research* 61 (9):
Afting et al. *Archives of Microbiology* 169 (3): 206–10.
Altschul et al. *Journal of Molecular Biology* 215 (3): 403–10.
Bach et al. *Appl. and Env. Microbiol.* 69 (5): 2608–15.
Barz et al. *PLOS ONE* 5 (11): e13846.
Basen et al. *Appl. and Env. Microbiol.* 84 (3): e02210-17.

Basen et al. *Extremophiles* 21 (1): 15–26.
Bassani et al. *Environmental Microbiology* 25 (12): 3683–3702.
Bauer et al. *Energ. Wasser-Prax* 8:64–69.
Beimgraben et al. *Appl. and Env. Microbiol.* 80 (12): 3776–82.
Ben Hania et al. *IIJSEM,* 63 (Pt_8): 3003–8.
Bengelsdor et al. In *Adv. in Applied Microbiol.*, 103:143–221.
Bennett et al. *Biochemistry* 39 (25): 7455–60.
Berthelin et al. NATO ASI Series. Dordrecht: Springer
Biswas et al. *BioMetals* 22 (1): 131–39.
Blair et al. *Astrobiology* 7 (6): 951–70.
Blum et al. *Extremophiles* 16:727–42.
Böttcher et al. *Environmental Earth Sciences* 76 (3): 98.
Bräuer et al. *IJSEM* 61 (Pt 1): 45–52.
Brazelton et al. *Frontiers in Microbiology* 2 (January).
Bu et al. *Bioresource Technology* 266 (October):364–73.
Bucke et al. *Bioenergetics*, 1827 (2): 94–113.
Buttinelli et al. *Energy* 36 (5): 2968–83.
Cerqueira et al. *Microbial Ecology* 74 (2): 332–49.
Chen et al. *Bioresource Technology* 99 (10): 4044–64.
Choi et al. *Water Science and Technology* 23 (7–9): 1259–64.
Colman et al. *PNMAS* 114 (27): 6895–6903.
Conrad et al. *FEMS Microbiology Ecology* 3 (5): 281–89.
Constant et al. *Applied and Environmental Microbiology* 77 (17):
Dassonville et al. *Agronomie* 22 (1): 51–68.
Debabov et al. *Microbiology* 90 (3): 273–97.
Delshad et al. *SPE Journal* 28 (05): 2547–65.
Demirel et al. *Biomass and Bioenergy* 35 (3): 992–98.
Dohrmann et al. *Env. Science & Technol.* 57 (2): 1092–1102
Dopffel et al. 2021. *Int. J. of Hydrogen Energy* 46 (12): 8594–8606.
Dupraz et al. 2013. *Geochimica et Cosmochimica Acta* 119
Dzaugis et al. 2016. *Frontiers in Microbiology* 7 (February).
Ebrahimiyekta. 2017. Université d'Orléans, Thesis.
Enning et al. 2014. *Appl. and Env. Microbiol.* 80 (4): 1226–36.
Enoki et al. 2011. *PLOS ONE* 6 (8): e24309.
Esquivel-Elizondo et al. 2017. *Biotech. for Biofuels* 10 (1): 220.
Etiope. 2023. *Int. J. of Hydrogen Energy* 48 (25): 9172–84.
Etiope et al. 2011. *Earth and Planet. Sci. Lett.* 310 (1–2): 96–104.
Fendrihan et al. 2006. *Rev. in Env. Sci. Biotech.* 5 (2–3): 203–18.
Fichtel et al. 2015. *Frontiers in Microbiology* 6.
Finney et al. *Advances in Microbial Physiology* 74:465–86.

Firme et al. 2019. *J. of Natural Gas Sci. and Eng.* 72:103006.
Foti et al. 2007. *Appl. and Env. Microbiol.* 73 (7): 2093–2100.
Freedman et al. 2017.. *Env. Microbiology* 19 (6): 2228–45.
Frery et al. 2021. *Int. J. of Hydrogen Energy* 46 (61): 31158–73.
Fullerton et al. 2021. *Nature Geoscience* 14 (5): 301–6.
Ganzert et al. 2014.. *IJSEM* 64 (Pt 10): 3478–84.
Greene et al. 1997. *IJSEM* 47 (2): 505–9.
Greening et al. 2016a. *The ISME Journal* 10 (3): 761–77.
Greening et al. 2014. *Current Opinion in Microbiology*, 18:30–38.
Gregory et al. 2019. *Microorganisms* 7 (2): 53.
Haddad et al. 2022. *Energy & Env. Sci.* 15 (8): 3400–3415.
Hagemann et al. 2016. *Comp. Geosci.* 20 (3): 595–606.
Hanson et al. 2024. *Unconventional Resources* 4:100057.
Hartmann et al. 1996. *JBIC J. of Biol. Inorg. Chem.*1 (5): 446–50.
Hassanpouryouzband et al. 2021. *ACS En. Letters* 6 (6): 2181–86.
Hedderich et al. 1998.*FEMS Microbiol. Rev.* 22 (5): 353–81.
Heinemann et al. 2021. *Energy & Env. Science* 14 (2): 853–64.
Hemme et al. 2017. *J.of Nat. Gas Sci. and Eng.* 47:114–23.
Hoehler et al. 2013. *Nature Reviews Microbiology* 11 (2): 83–94.
Holden et al. 2023. *Frontiers in Microbiology* 14.
Holm et al. 2015. *Astrobiology* 15 (7): 587–600.
Horch et al. 2015. *J. of the Am.Chem. Soc.* 137 (7): 2555–64.
Huang et al. 2014. *App.and Env. Microbiol.* 80 (1): 29–42.
Huber et al. 2001. 'Thermotogales'. *E LS*.
Hubert et al. 2003. *Biotechnology Progress* 19 (2): 338–45.
Ishaq et al. 2022. *Int. J; of Hydrogen Energy*, 47 (62): 26238–64.
Islam et al. 2020.*The ISME Journal* 14 (11): 2649–58.
Jafari et al. 2022. *Renew. and Sust. En. Rev.* 168:112846.
Jakobsen et al. 2006. *IJSEM*, 56 (Pt 9): 2063–69.
Jiménez et al. 2016.*Microbial Physiology* 26 (1–3): 227–42.
Kaneuchi et al. 1976. *IJSEM* 26 (4): 482–86.
Kaster et al. 2011. *PNAS* 108 (7): 2981–86.
Kelley et al. 2005. *Science*, March.
Kim et al. 2010. *Nature* 467 (7313): 352–55.
Klein et al. 2020a. *Elements* 16 (1): 19–24.
Konn, C. et al. 2015. *Astrobiology* 15 (5): 381–99.
Korbas et al. 2006. *Journal of Biological Chemistry* 281 (41):
Krekeler et al. 1997. *Archives of Microbiology* 167 (6): 369–75.
Kuenen et al. 1997. *Phil. Trans. Royal Soc. of London.* 298 (1093):
Kurret et al. 1991. *Archives of Microbiology* 156 (4): 239–47.

Küselet al.2000. *IJSEM,* 50 Pt 2 (March):537–46.
Kushkevychet al. 2019. *Archives of Microbiology* 201 (3): 389–97.
Langhi et al. 2023. *Geoenergy* 1 (1): geoenergy2023-014.
Lappan et al. 2023. *Nature Microbiology* 8 (4): 581–95.
Larinet al. 2015. *Natural Resources Research* 24 (3): 369–83.
Leighet al. 1981. *Archives of Microbiology* 129:275–80.
Lemmonet al. *NIST Standard Reference Database Number 69*.
Liet al. 2017. *Frontiers in Microbiology* 8:1011.
Lim et al. 2014. *Proceedings of the National Academy of Sciences*
Liu et al. 2023. *Frontiers in Energy Research* 11.
Longet et al. 2016. *Trends in Microbiology* 24 (8): 600–610.
Lyonet et al. 2004. *Journal of the American Chemical Society* 126
Magnaboscoet et al. 2018. *Nature Geoscience* 11 (10): 707–17.
Magotet et al. 2005. 21–33. John Wiley & Sons, Ltd.
Mares, et al. 2023. *J. of Env. Chem. Eng.* 11 (2): 109528.
Matos et al. 2019. *Journal of Energy Storage* 21
Matz et al. 1992.. In . OnePetro.
Maus et al. 2016. *Biotechnology for Biofuels* 9 (1): 171.
Mcgenity et al. 2018. In Methanogens, 1–27.
Merdith et al. et al. 2023. *Geochemistry, Geophysics, Geosystems*
Merino et al. 2019. *Frontiers in Microbiology*
Michael et al. 2009, *Energy Procedia*, 9, 1 (1): 1973–80.
Michael et al. 2010. *Int. J. of Greenh.Gas Control* 4 (4): 659–67.
Milkov, Alexei V. 2022. *Earth-Science Reviews* 230 (July):104063.
Mills et al. 2013. *eLife* 2 (March):e00218.
Miocic et al. 2023. *Geological Society, London,* 528 (1): 73–86.
Mottl et al. 2003. *Geochemistry, Geophysics, Geosystems* 4 (11).
Nandi et al. 1998. *Critical Reviews in Microbiology*
Nazina et al. 2007. *Microbiology* 76 (3): 287–96.
Nicolet et al. 2001. *Journal of the American Chemical Society* 123
Nobu et al. 2017. *Environmental Microbiology* 19 (11): 4576–86.
Nozhevnikova et al. 2001. *Water Science and Technology* 44 (8):
Ntagia et al. 2020. *Microbial Biotechnology* 13 (4): 1026–38.
O'Flaherty et al. 1998.*Process Biochemistry* 33 (January).
Ollivier et al. 1998. *Int. J. of Syst. Bact.* 48:821–28.
Oren et al. 2014. 153–77. Berlin, Heidelberg: Springer.
Orphan et al. 2001. *Applied and Environmental Microbiology* 67
Ortiz et al. 2021. *PNAS* 118 (45): e2025322118.
Osman et al. 2022. *Environmental Chemistry Letters* 20 (1):
Ozarslan, Ahmet. 2012. *International Journal of Hydrogen Energy*

Pal et al. 2020. *Extremophiles* 24 (6): 875–85.
Pannekens et al. 2019. *New Biotechnology* 49:1–9.
Park et al. 2009. *Geobiology* 7 (5): 515–23.
Payler et al. 2019. *Frontiers in Microbiology* 10.
Pedersen, K. 2000. *FEMS Microbiology Letters* 185 (1): 9–16.
Perera, M. S. A. 2023. *Fuel* 334 (February):126677.
Perner et al. 2007. *FEMS Microbiology Ecology* 61 (1): 97–109.
Peters et al. 1998. *Science* 282 (5395): 1853–58.
Podzuweit et al.1986. *Biochimie* 68 (1): 103–11.
Poorter et al. 2007. *Applied and Environmental Microbiology* 73
Porter et al. 2007. *Geochimica et Cosmochimica Acta* 71 (21):
Prinzhofer et al. 2018. *International Journal of Hydrogen Energy*
Ranchou-Peyruse et al. 2019. *Environmental Microbiology* 21 (10):
Ravot et al. 1995. *Applied and Environmental Microbiology* 61 (5):
Rickard et al. 2007. *Chemical Reviews* 107 (2): 514–62.
Rothschild et al. 2001. *Nature* 409 (6823): 1092–1101.
Russell et al. 2010. *Geobiology* 8 (5): 355–71.
Šafarič et al. 2020. *Microorganisms* 8 (4): 598.
Sauvage et al. 2021. *Nature Communications* 12 (1): 1297.
Scherer et al. 1981. *Acta Biotechnologica* 1 (1): 57–65.
Schönheit et al. 2016. *Trends in Microbiology* 24 (1): 12–25.
Schuchmann et al. 2014. *Nature Reviews Microbiology* 12 (12):
Schut et al. 2009. *Journal of Bacteriology* 191 (13): 4451–57.
Schwab et al. 2022. *International Journal of Hydrogen Energy* 47
Schwartz et al. et al. 2013. Springer.
Schwörer et al. *European Journal of Biochemistry* 212 (1): 255–61.
Shafahi et al. 2009. *Int. J. of Heat and Mass Transf.* 52: 574–81.
Shi et al. 2020. *International Journal of Hydrogen Energy* 45 (15):
Shima et al. 2020. *Annual Review of Microbiology* 74:713–33.
Shomura, et al. 2011. *Nature* 479 (7372): 253–56.
Singh Kripal. 2016. *Land Degradation & Development* 27 (3):
Skelton, et al. 2005. *Geofluids* 5 (3): 153–64.
Skovhus, et al. 2017. *Microbiol. Infl. Cor. in Oil and Gas Industry*.
Sleep et al. 2011.. *Phil.Trans. of the Royal Soc.,* 366: 2857–69.
Smith et al. 2005. *Geological Society, London,* 6 (1): 349–58.
Soares, et al. 2023. *Microbiology* 169 (1): 001172.
Søndergaard et al. 2016. *Scientific Reports* 6 (1): 34212.
Sorokin et al. 2011. *Frontiers in Microbiology* 2.
Sorokin et al. 2017. *The ISME Journal* 11 (5): 1245–60.
Spinks et al. 1990. January. https://www.osti.gov/biblio/5851776.

Steinweg et al. 2013. *Frontiers in Microbiology*
Stewart et al. 2015. *IJSEM* 65 (Pt 4): 1280–83.
Strobel et al. 2020. *Renewable and Sustainable Energy Reviews*
Suzuki et al. 2024. *Communications Earth & Environment* 5
Takach, et al. 2022. *Energies* 15 (4): 1415.
Takai et al. 2008. *PNAS* 105 (31): 10949–54.
Tanner et al. 1993. *Int. J. of Syst. Bact.* 43 (2): 232–36.
Tarhan et al. 2021. *Journal of Energy Storage* 40
Tarkowski et al. 2022. *Ren. and Sust. Energy Reviews* 162
Telesh et al. 2013. *Estuarine, Coastal and Shelf Science* 135
Telling et al. 2015. *Nature Geoscience* 8 (October):851–54.
Thauer et al. 1996. *Chemical Reviews* 96 (7): 3031–42.
Thaysen et al. 2021. *Renewable and Sustainable Energy Reviews*
Thiyagarajan et al. 2022. *Journal of Energy Storage* 51
Tian et al. 2017. *Frontiers in Microbiology* 8 (February).
Topçuoğlu et al.2019. *Applied and Environmental Microbiology* 85
Truche et al. 2010. *Geochimica et Cosmochimica Acta* 74
Türke et al. 2015. *Astrobiology* 15 (10): 793–803.
Usher et al. 2015.*Corrosion Science* 98 (June).
Vitale et al. 2020. *Nature Communications* 11 (1): 3880.
Volbeda et al. 1995. *Nature* 373 (6515): 580–87.
Vreeland et al 1998. *Extremophiles* 2 (3): 321–31.
Vreeland et al. 2000. *Nature* 407 (6806): 897–900.
Whitman et al. 1992. *The Prokaryotes, Vol.I.*, no. Ed. 2, 719–67.
Wiegel et al. 1981. *Current Microbiology* 5 (4): 255–60.
Xie et al. 2021. *Frontiers in Microbiology* 12.
Xu et al. 1998. *Geochi. et Cosmochi. Acta* 62 (23): 3729–43.
Yakimov et al. 2015. *Environmental Microbiology* 17 (2): 364–82.
Yernazarova et al. 2016. Chemical Enhanced Oil Recovery
Yin et al. 2013. *Advanced Materials Research* 716:470–74.
Yoshida et al. 2005. *Jou. of Biosci. and Bioeng.* 99 (2): 143–49.
Yusupova et al. 2020. *Petroleum Chemistry* 60 (11): 1216–25.
Zgonnik et al. 2020. *Earth-Science Reviews* 203 (April):103140.
Zhao et al. 2023. In OnePetro.
Zhilina et al. 1996. *Current Microbiology* 32 (6): 320–26.
Zhilina et al. 1990. *FEMS Microbiology Letters* 87 (3): 315–21.
Zhou et al. 2018. *Extremophiles* 22 (6): 983–91.
Zivar et al. 2021a. *Int. Jou. of Hydrogen Energy*, 46(45):23436–62.
Zivar et al. 2021b. *Int. Jou. of Hydrogen Energy,* 46(45):23436–62.

1.8 Figures

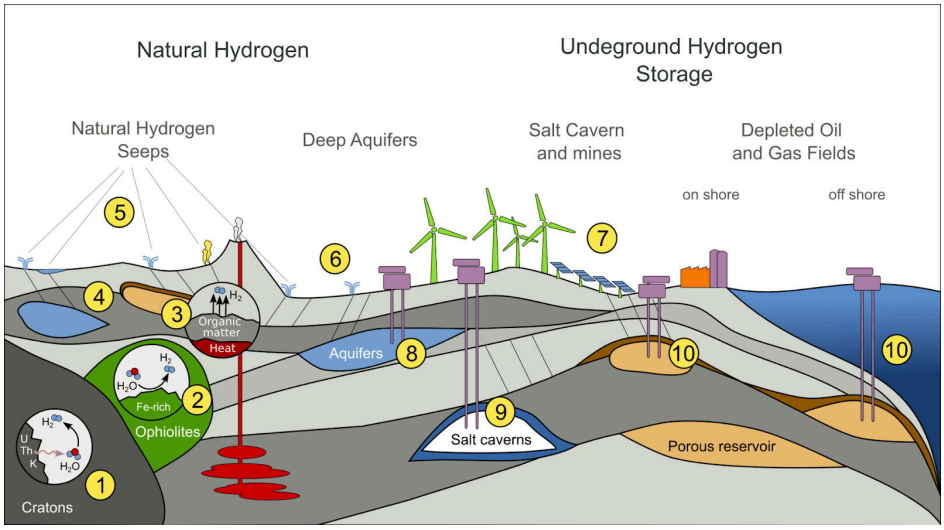

Figure 1. Summary of the natural processes contributing to natural hydrogen in the environments and target storage sites for Green Hydrogen. 1. radiolytic H_2 production in stable cratons; 2. serpentinization reaction in Fe-Rich mantle rocks; 3. Thermogenic and biogenic production of hydrogen in organic rich basins; 4. Natural hydrogen produced through a variety of processes can accumulate in deep aquifers and porous reservoirs similar to those targeted for UHS; 5. Natural hydrogen deeply-sourced seeps can be used to research and explore the interaction of subsurface microbes with hydrogen as well as enable natural hydrogen prospecting; 6. Deeply-sourced seeps can also be used to monitor potential leakages from UHS sites; 7. Renewable energy production facilities are used to electrolyze water and produce hydrogen during peak production times. Produced hydrogen can then be stored in: 8. Deep aquifers; 9. Salt caverns and mines; and 10. onshore and offshore depleted oil and gas reservoirs.

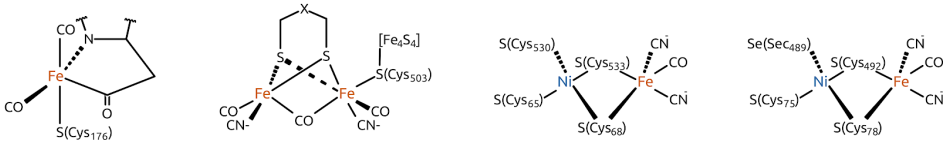

Figure 2. Cofactor diversity in the 4 main types of hydrogenases: [Fe] (A), [FeFe] (B), [NiFe] (C) and [NiFeSe] (D).

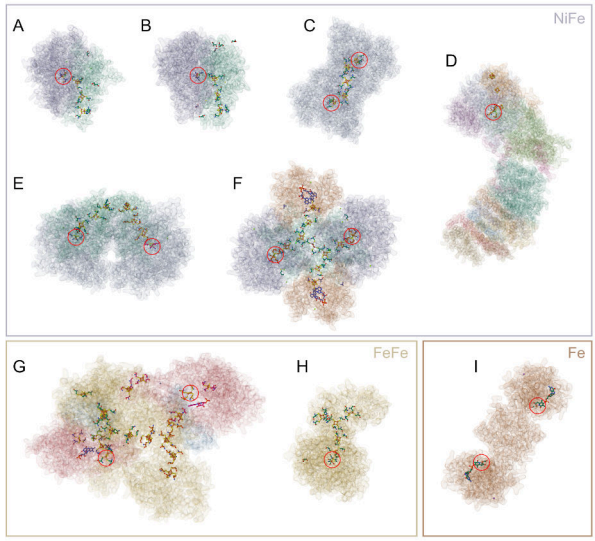

Figure 3. Structural diversity of selected hydrogenase groups from. Representative NiFe, FeFe and Fe structures are drawn with the catalytic site highlighted with a red circle. A. the O2-tolerant respiratory NiFeSe]-hydrogenase from *Desulfomicrobium baculatum* (PDB 4KL8); B. the prototypical respiratory O2-sensitive [NiFe]-hydrogenase from *Megalodesulfovibrio gigas* (PDB 1YQ9); C. 3B52; D. 6CFW; E. 6EHQ; F. 4OMF; G. 7P8N; H. 6N59; I. 3F47

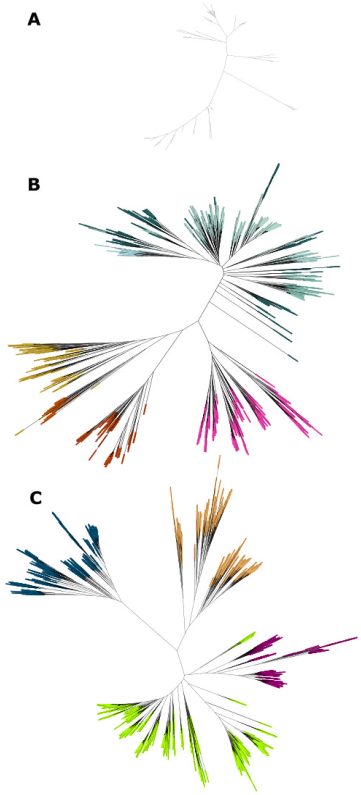

Figure 4. Phylogenetic trees for Fe (A), FeFe (B) and NiFe (C) hydrogenases. The color in the trees indicates the subgroup: in the FeFe tree (B), group A is colored in blues, group B in fuchsia, group C in orange/yellow; in the NiFe tree, group 1 is colored in green, group 2 in purple, group 3 in yellow and group 4 in blue. Group 1k appears inserted between groups 1 and 2.

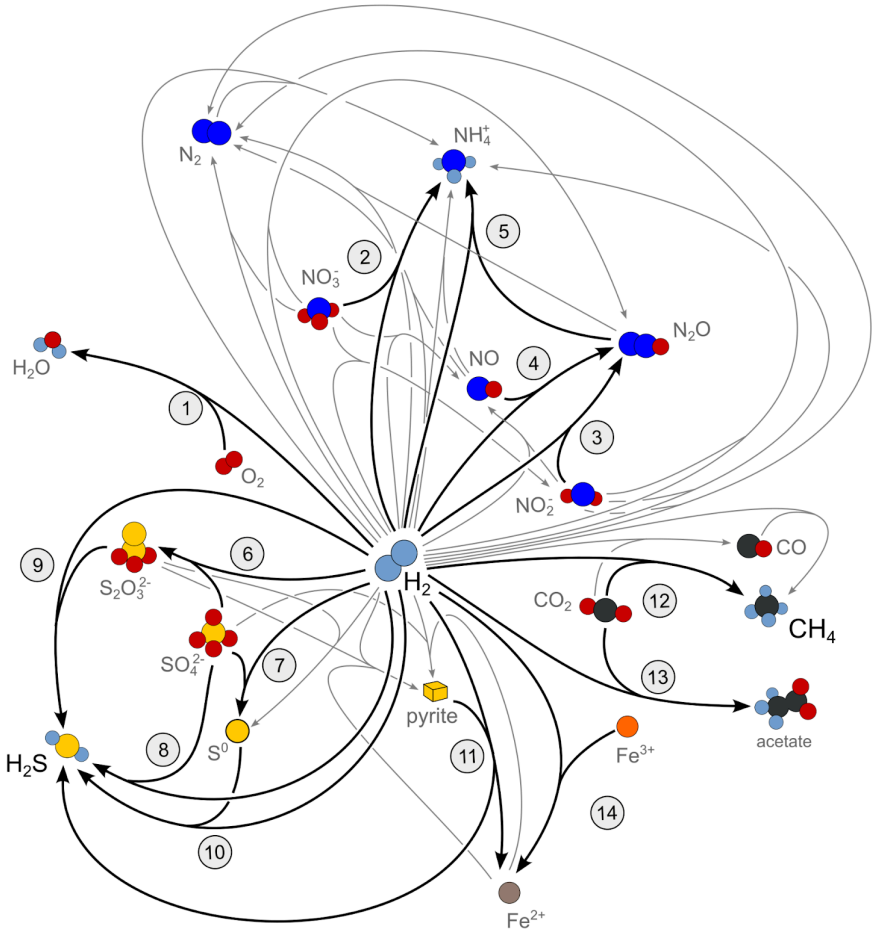

Figura 5. Hydrogenotrophic metabolism of interest in underground hydrogen storage sites and in natural hydrogen reservoirs. Lines for exemplificative reactions of relevance for each principal electron acceptors are in bold and numbered. The other reactions are marked with light gray lines. Reactions using minerals as electron acceptors are omitted, with the exception of pyrite. Key compounds of interest (H_2, H_2S and CH_4) are highlighted.

Chapter 5 - Conclusions and future directions

The research presented in this thesis provides a comprehensive exploration of the interactions between microbial communities, geochemical conditions, and hydrogen in the context of underground hydrogen storage (UHS). Through a combination of field studies, laboratory experiments, and advanced molecular approaches, this work has elucidated critical aspects of hydrogenotrophic metabolisms, hydrogenase diversity, and the biogeochemical dynamics of hydrogen-rich environments. The findings underscore the complexity of subsurface microbial ecosystems, highlighting their resilience and adaptability in natural hydrogen seep environments as well as in simulated UHS conditions. By bridging the gap between fundamental microbial ecology and applied geochemistry, this thesis lays a foundation for advancing our understanding of the risks and opportunities associated with UHS.

Key insights emerged from the investigation of natural hydrogen seeps, which revealed a diverse array of hydrogenotrophic microorganisms and their metabolic pathways. These natural systems served as valuable analogs for hydrogen storage environments, offering a glimpse into the ecological strategies that microbial communities employ to exploit hydrogen as an energy source. The study of hydrogenase gene diversity provided a deeper understanding of the evolutionary and functional adaptations of microbes to different geochemical landscapes, identifying key drivers such as temperature, pH, and trace element availability. The controlled microcosm experiments extended this knowledge to engineered environments, demonstrating how microbial communities from depleted reservoirs respond to hydrogen injection and highlighting the challenges posed by microbial hydrogen consumption and infrastructure corrosion. These experiments emphasized the intricate balance between microbial activity, geochemical conditions, and hydrogen availability, showcasing the need for site-specific strategies to mitigate microbial impacts on storage efficiency.

Despite these advances, this thesis also highlighted significant knowledge gaps and challenges that warrant further investigation. One critical area is the integration of microbial, fluid, rock, and gas interactions in the context of UHS. The interplay between microbial

activity and geochemical transformations, such as mineral dissolution and precipitation, has profound implications for reservoir stability and hydrogen retention. Future research should aim to develop holistic models that incorporate the dynamic feedbacks between hydrogen, fluids, rock matrices, and microbial communities under various geological conditions. Such models would enable more accurate predictions of hydrogen utilization rates and the long-term sustainability of storage operations. In situ studies that directly measure hydrogen consumption and microbial activity in operational reservoirs are essential for validating these models and refining our understanding of the mechanisms driving hydrogen loss and biogeochemical transformations.

Moreover, there is a pressing need to constrain hydrogen utilization rates under a wider range of conditions and geological settings. The diversity of reservoir types, from porous sandstones to salt caverns, introduces variability in microbial community composition, geochemical parameters, and storage dynamics. Comparative studies across these settings will help identify universal patterns and context-specific factors influencing microbial behavior. These efforts should be complemented by the exploration of strategies to control microbial activity, such as the use of biocides, competitive inhibitors, or trace element manipulation, while balancing these interventions with the preservation of reservoir integrity and environmental sustainability.

In conclusion, this thesis underscores the central role of microbiology in the success and sustainability of UHS. By advancing our understanding of hydrogenotrophic metabolisms and their interactions with geochemical environments, it provides critical insights for mitigating risks and enhancing the efficiency of hydrogen storage operations. Looking forward, a multidisciplinary approach that integrates microbiology, geochemistry, and reservoir engineering will be essential for addressing the complex challenges of UHS. Such efforts will not only enable the safe and efficient storage of hydrogen but also contribute to the broader transition toward a sustainable energy future. The findings and perspectives presented here serve as a foundation for future research, driving innovation and collaboration in the pursuit of a hydrogen-based society.

Appendix I - Fundings, acknowledgements and ethics declarations

This PhD was supported by a Programma Operativo Nazionale (PON) fellowship Action IV.5 - PhDs on Green themes (Azione IV.5 on green technologies from Asse IV of PON Ricerca e Innovazione 2014-2020 “Istruzione e ricerca per il recupero – FSE REACT-EU”) from the Ministry of University and research (MUR).

This work received additional work from funding from the European Research Council (ERC) under the European Union’s Horizon 2020 research and innovation program Grant Agreement No. 948972—COEVOLVE—ERC-2020-STG. Additional individual funding to coauthors have been acknowledged in the respective publications submitted or in preparation.

The coauthors Paola Panfili, Lucilla Del Gaudio, Elisabetta Franchi, Ilaria Pietrini, Giovanna Carpani, Delfina Bersano are employed by ENI, which is a company working on hydrogen storage. All the authors declare no competing interests.

Appendix II - Internships

During the PhD I visited one international laboratory (Prof. Katriona Edlmann, University of Edinburgh) for a period of 3 months and the ENI S.p.A. R&D laboratories for a period of 6 months. The full contacts are reported below.

Prof. Katriona Edlmann
School of Geosciences
University of Edinburgh
Edinburgh - UK
katriona.edlmann@ed.ac.uk

Dr. Ilaria Petrini
Dr. Olga Shafran
ENI S.p.A.
Centro Ricerche di San Donato Milanese
R&D Environmental & Biological Laboratories
San Donato Milanese
Milano - Italy
Ilaria.Pietrini@eni.com

Appendix III - Sampling expeditions

2024. Aeolian Island expedition AEO24

16 June 2024 - 27 June 2024

I participated in the sampling expedition “AEO24” organized by Prof. Donato Giovannelli (donato.giovannelli@unina.it) in the framework of the ERC CoEvolve project. The expedition sampled several gas emissions sites particularly in Vulcano island but also in Panarea, Stromboli and Lipari, including both terrestrial and submarine locations. Sampled matrices included fluids, sediments, biofilms and gas that will be used for the characterization of the geochemistry and microbiology of the sites. I was involved in sample collection, sample processing and preservation in the field and additionally in lab processing protocols.

2023. Iceland expedition ISL23

25 August 2023 - 15 September 2023

I participated in the sampling expedition “ISL23” organized by Prof. Donato Giovannelli (donato.giovannelli@unina.it) in the framework of the ERC CoEvolve project. The expedition sampled the deeply-sourced springs in Island, including both terrestrial and submarine locations. Sampled matrices included fluids, sediments and biofilms that will be used for the characterization of the geochemistry and microbiology of the sites. I was involved in sample collection, sample processing and preservation in the field.

2023. CN5 expedition – Shallow-water hydrothermal vents

2023 June - 2023 July

I participated in the sampling expedition “CN5” organized by Prof. Donato Giovannelli (donato.giovannelli@unina.it). The focus was on shallow-water hydrothermal vents in the Gulf of Pozzuoli, to analyze their microbial taxonomic and functional diversity and to unveil their impact on the surrounding ecosystem. Sampled matrices included fluids and biofilms that will be used for the characterization of the geochemistry and microbiology of the sites. I was involved in sample collection, sample processing and preservation in the field.

2022. AT50-06 Expedition - Cruise on the East Pacific Rise

01 December 2022 - 04 January 2023

I participated in the sampling expedition "AT50-06" organized by Prof. Shawn M. Arellano (arellas@wwu.edu) (Biology Department of the Western Washington University) and Prof. Costantino Vetriani (vetriani@marine.rutgers.edu). The aim of the expedition is to understand the interplay between geology, microbes, and animals at these dynamic deep-sea oases. During this expedition a submarine called "Alvin" was used, in order to collect samples at a depth about 2500 km on the ocean floor, including fluids, rocks and marine organisms. I was involved in a dive (Alvin-D5139) to 2,500 metres depth to collect samples, and in performing on board experiments and sample processing such as high temperature fluid filtration, microbial incubation in selective anaerobic media, and sulfide/ferrozine/alkalinity measurements of the filtered fluids.

2022. Salt Cavern Realmonte expedition

22 November 2022 - 25 Novembre 2022

I participated in the sampling expedition "RLM22" organised by Giusy Anzelmo (giuseppa.anzelmo@unina.it) and Prof. David Iacopini (david.iacopini@unina.it) . We sampled the salt cavern in Realmonte, Agrigento. Sampled matrices included salt cores and fluids that will be used for the characterization of the geochemistry and microbiology of the sites. I was also involved in sample collection, sample processing and preservation in the field, DNA extraction, metagenomic and geochemical analysis.

2022. Hydrogen expedition HYD22

17 October 2022 - 24 October 2022

I have co-organized, together with Prof. Donato Giovannelli (donato.giovannelli@unina.it), the expedition "HYD22". We sampled the deeply-sourced springs in the italian territory, including the areas of Larderello, Orvieto, Viterbo, Pomezia, Roccamonfina, Ischia and Caserta. Sampled matrices included fluids, sediments and biofilms that will be used for the characterization of the geochemistry and microbiology of the sites. I was also involved in sample collection, sample processing and

preservation in the field, DNA extraction, metagenomic and geochemical analysis.

2022. International Continental Drilling Program Drilling into the Ivrea-Verbano Zone

09 October 2022 - 19 October 2022

I participated in the expedition "ICP-DIVE" where the focus was sampling rock cores from the area of Ivrea-Verbano. I was involved in sample collection, sample processing and preservation in the field.

2022. Aeolian expedition AEO22

26 August 2022 - 04 September 2022

I have co-organized, together with Prof. Donato Giovannelli (donato.giovannelli@unina.it), the expedition "AEO22". We sampled the deeply-sourced springs in the Aeolian Islands. Sampled matrices included fluids, sediments and biofilms that will be used for the characterization of the geochemistry and microbiology of the sites. I was also involved in sample collection, sample processing and preservation in the field, DNA extraction, metagenomic and geochemical analysis.

2022. Svalbard expedition SVA22

19 February 2022 - 09 March 2022

I participated in the expedition "SVA22" organized by Prof. Donato Giovannelli (donato.giovannelli@unina.it). We sampled permafrost and methane emissions from different sites along a transect that flanks the Bayelva river, with the exception of a site located in the forefield of the Midtre Lovénbreen glacier. At each location a snowpit of about 2×3 m was dug and the coring of the permafrost was performed using a portable driller. I was involved in collecting sample data, sample collection, sample processing and preservation in the field.

Appendix IV - Contribution to conferences and workshops

a. As first author and /or speaker

2024 November 25-26: Contributed to the H-NAT 2024 Conference – Poster presentation entitled "Hydrogenotrophic metabolisms in the subsurface: insights from natural hydrogen seeps in diverse geological settings".

2024 June 26-29: Contributed to the CORTONA PROCARIOTI CONFERENCE 2024 – Oral Talk entitled "Hydrogenotrophic metabolisms in the subsurface: insights from natural hydrogen seeps in diverse geological settings".

2023 September 21-24: Contributed to the XXXIV SIMGBM CONGRESS - MICROBIOLOGY 2023, Cagliari – Poster entitled "Hydrogenotrophic metabolisms in the subsurface: insights from natural hydrogen seeps in diverse geological settings".

2023 July 7-14: Contributed to the VII Goldschmidt Conference, Lyon – Oral Talk entitled "Hydrogenotrophic metabolisms in the subsurface: insights from natural hydrogen seeps in diverse geological settings".

2023 June 12-15: Contributed to the VII Congresso della Società Italiana di Astrobiologia, Rome– Poster with Oral Flash Talk entitled "Hydrogenotrophs diversity and distribution in subsurface extreme environments, with implications for Underground Hydrogen Storage".

2023 May 21: Organized and Contributed to the Cassini Hydrogen Workshop, University of Naples Federico II – Chair and Oral Talk entitled "Microbial hydrogenase diversity, distribution and implication for Underground Hydrogen Storage".

2023 May 18: Contributed to the Geoenergy meeting, University of Edinburgh – Oral Talk entitled "Moving toward hydrogen: the key role of subsurface microbiology".

2023 May 4: Contributed to the Living on Hydrogen webinar – Oral Talk entitled "Hydrogen utilization in microorganisms: hydrogenase diversity, distribution and implication for Underground Hydrogen Storage".

2022 September 14-16: XVI Congresso FISV" in Portici (NA) – Poster with Oral Flash Talk entitled "Hydrogenotrophic

metabolisms in the subsurface: ecological and biotechnological applications".

2022 September 5-9: Contributed to the fO2 School, Trieste – Oral Talk entitled "Hydrogenotrophic metabolisms in the subsurface: Utilizing reducing power from the deep Earth".

2022 June 22-24: Contributed to the Climate Change And Carbon Cycle (C4) Workshop, CNR Research Area in Pisa (Italy) – Oral Talk entitled "Deeply-sourced seeps of the Argentina backarc as windows into the subsurface".

2021 September 13-17: Contributed to the 3rd IBBR Memorial Workshop in loving memory of Maria Ciaramella, Naples (Italy) – Poster entitled "Hydrogenotrophic metabolisms in the subsurface: ecological and biotechnological applications".

2021 September 13-17: Contributed to the online 90° Congresso della Società Geologica Italiana – Oral Talk entitled "Deeply-sourced springs microbial diversity: a window into the deep Earth" (online).

2021 July 4-9: Contributed to the Goldschmidt Virtual Conference – Poster and Flash Talk entitled "Microbial diversity in the backarc hot springs of Argentina and its role in biogeochemical cycles" (online).

2021 June: Contributed the BVCN online conference "Holistic Bioinformatic Approaches used in Microbiome Re- search" – Poster and Flash Talk entitled "Deeply-sourced springs microbial diversity: a window into the deep of the Earth" (online).

b. As co-author

2024 November 25-26: Contributed to the H-NAT 2024 Conference. Coauthor of the oral presentation entitled "The microbiology of natural hydrogen and underground hydrogen storage". First author D Giovannelli (University of Naples Federico II).

2024 September 18-20: XLII European Culture Collections' Organisation (ECCO) meeting in Bari (Italy). Coauthor of the poster entitled "From microbial diversity of Campania thermal springs of their maintenance and preservation". First author F Oliva (University of Naples Federico II).

2024 September 18-20: XLII European Culture Collections' Organisation (ECCO) meeting in Bari (Italy). Coauthor of the poster entitled "The influence of prokaryote communities on Galdieria sulphuraria strain maintenance and cultivation". First author N Nappi (University of Naples Federico II).

2024 April 14-19: The General Assembly 2024 of the European Geosciences Union (EGU) in Vienna, Austria. Coauthor of the oral talk "Integrated approach for hydrogen storage in a salt mine: the case of Realmonte, Sicily (Italy)". First author G Anzelmo (Earth Science Department, University of Naples Federico II).

2024 January 13-14: The General Assembly 2024 of the Geobiology GRS Conference, Galveston, Texas, United States. Coauthor of the poster entitled "Microbial metabolic potential and the geochemical landscape across the Andean Southern Volcanic Zone". First author G. Hessen (Instituto de Ciencias Marinas y Limnológicas, Universidad Austral de Chile, Valdivia, Chile).

2023 November 14-17: 2023 Evolmar Virtual Congress on Marine Evolution (online). Coauthor of the oral presentation entitled "Environmental diversity, distribution and evolution of microbial metal ion transport systems". First author F Migliaccio (University of Naples Federico II).

2023 November 08-12: GSA 2023 Annual Scientific Meeting (online). Coauthor of the oral presentation entitled "Origin and fate of methane in the Central American convergent margin". First author M Selci (University of Naples Federico II).

2023 October 03-06: BeGEO Scientists 2023, Università di Napoli Federico II, Napoli. Coauthor of the poster entitled "Abiotic Leaching and Trace Metal Concentration of East Pacific Rise Hydrothermal Vents as a Window for the In-Situ Resource Utilization on Mars". First author L Tonietti (University Parthenope, Naples).

2022 December 12-16: AGU Fall Meeting 2022 (online). Coauthor of the poster entitled "Subseafloor Microbial Diversity of the Ross Sea, Antarctica (IODP 374), is Linked to Differences in Depositional Regimes". First author J Biddle (University of Delaware).

2022 July 7-14: VII Goldschmidt Conference, Lyon (France). Coauthor of the poster entitled "Origin and fate of methane in the

Central American convergent margin". First author M Selci (University of Naples Federico II).

2022 July 7-14: VII Goldschmidt Conference, Lyon (France). Coauthor of the poster entitled "Environmental availability of Copper in deeply sourced seeps and its influence on Copper binding proteins distribution". First author F Montemagno (University of Naples Federico II).

2022 July 7-14: VII Goldschmidt Conference, Lyon (France). Coauthor of the poster entitled "Ironborn: Fe distribution in geothermal fluids and its influence on the biosphere". First author B Barosa (University of Naples Federico II).

2022 July 7-14: VII Goldschmidt Conference, Lyon (France). Coauthor of the oral presentation entitled "Metal cofactor microbial usage across convergent margins". First author D Bastoni (University of Naples Federico II).

2022 July 7-14: VII Goldschmidt Conference, Lyon (France). Coauthor of the oral presentation entitled "Complex organic matter degradation by secondary consumers in chemolithoautotrophy-based subsurface geothermal ecosystems". First author K Lloyd (University of Tennessee, Knoxville, TN, USA).

2022 July 7-14: VII Goldschmidt Conference, Lyon (France). Coauthor of the oral presentation entitled "Linking microbial metabolic diversity with geochemical characteristics of Campania Region hot springs". First author A Bastianoni (University of Naples Federico II).

WORKSHOP AND MEETINGS ORGANIZATION

2023 May 25: Cassini Hydrogen Workshop, University of Naples Federico II and online (youtube recording: https://www.youtube.com/watch?v=BBvC2Ddr8Xw). I won the grant "Cassini Junior" (https://tinyurl.com/BandoCassini2022) for the theme "Fight against climate change and protection of biodiversity" (https://tinyurl.com/CassiniHydrogen). The title of this event was 'Hydrogen for a greener energetic future: crossing disciplines and joint research'. We had international invited speakers such as the Professor Isabelle Moretti (isabelle.moretti@univ-pau.fr) (Pau university (UPPA), Dan LÉVY, post doctoral researcher (dlevy@ipgp.fr) (Institut de Physique du

Globe de Paris), Professor David Iacopini (david.iacopini@unina.it) (Dept. of Earth Science, University of Naples Federico II, Italy), Professor Alberto Vitale Brovarone (alberto.vitaleb@unibo.it) (BiGeA, Alma Mater Studiorum Università di Bologna, Italy). The session programme aimed to offer many opportunities for interaction across different disciplines such as microbiology, geology and geochemistry, all converging towards the same goal: a new hydrogen economy.

Appendix V - Publications

A complete list of publications is present on Google Scholar https://scholar.google.com/citations?user=yFPgZaYAAAAJ

a. Peer review publications

9 – Barry PH, de Moor JM, Broadley MW, Seltzer AM, Bekaert DV, Patil K, Bartels CGE, Young ED, Longworth BE, Barosa B, Bastianoni A, Bastoni D, **Cascone M**, Turner SJ, Tyne RL, Anderson M, Li K, Curtice J, Kumar N, Jessen GL, Blamey JM, Ramírez CJ, Chiodi A, Aguilera F, Layana S, González C, Aguilera M, Masías Alvarez GPJ, Marty B, Lloyd KG, and Giovannelli D. 2025. Carbon, nitrogen, and noble gas isotopes reveal deep volatile signatures in thermal springs in the Central Volcanic Zone (CVZ) of the Andes, *Earth and Planetary Science Letter*, 2025, Doi: 10.1016/j.epsl.2024.119169

8 – Tonietti L, Esposito M, **Cascone M**, Barosa B, Fiscale S, Muscari Tomajoli MT, Sbaffi T, Santomartino R, Covone G, Cordone A, Giovannelli D, Rotundi A. 2024. Unveiling the bioleaching versatility of *Acidithiobacillus ferrooxidans*. *Microorganisms*, 2024, 12(12), 2407. Doi: 10.3390/microorganisms12122407

7 – Montemagno F, **Cascone M**, Cardellini C, Pasotti J, Manini E, Baldrighi E, Maiero E, Segato D, Cerrato R, Mazzola M, Vardè M, Cordone A, Caliro S, Rudnik I, Cramm M, Bradley J, Giovannelli D. 2024. PRA Melting-ICE Project: Svalbard 2022 Expeditions Report. *Open Research Europe*, 4:257

6 – Salzano A, Saggese A, Martino E, Neglia G, **Cascone M**, Selci M, Baccigalupi L, D'Onofrio N, Giovannelli D, Bifulco G, Ricca E, Balestrieri ML, D'Occhio M, Campanile G. 2024. Ruminal microbiota, carbohydrate-active enzymes and milk bioactive compounds in Italian Mediterranean dairy buffaloes fed total mixed ration with or without green forage. *Italian Journal of Animal Science*, 23 (1): 1681-1694

5 – Barosa B, Ferrillo A, Selci M, Giardina M, Bastianoni A, Correggia M, Di Iorio L, Bernardi G, **Cascone M**, Capuozzo R, Intoccia M, Price RE, Vetriani C, Cordone A, Giovannelli D. 2023. Mapping the microbial diversity associated with different geochemical regimes in the shallow-water hydrothermal vents of the Aeolian Archipelago, Italy. *Frontiers in Microbiology*, 14. Doi: 10.3389/fmicb.2023.1134114

4 – Paul R, Rogers TJ, Fullerton KM, Selci M, **Cascone M**, Stokes MH, Steen AD, de Moor JM, Chiodi A, Stefánsson A, Halldórsson SA, Ramirez CJ, Jessen GL, Barry PH, Cordone A, Giovannelli D, Karen Lloyd. 2023. Complex organic matter degradation by secondary consumers in chemolithoautotrophy-based subsurface geothermal ecosystems. *PLOS One*, doi: 10.1371/journal.pone.0281277

3 – Hay Mele B, Monticelli M, Leone S, Bastoni D, Barosa B, **Cascone M**, Migliaccio F, Montemagno F, Ricciardelli A, Tonietti L, Rotundi A, Cordone A, Giovannelli D. 2023. Oxidoreductases and metal cofactors in the functioning of the earth. *Essays in Biochemistry*, EBC20230012. doi:

10.1042/EBC20230012 NB. The article was accompanied by the cover of the issue.

2 – Cordone A, Selci M, Barosa B, Bastianoni A, Bastoni D, Bolinesi F, Capuozzo R, **Cascone M**, Correggia M, Corso D, Di Iorio L, Misic C, Montemagno F, Ricciardelli A, Saggiomo M, Tonietti L, Mangoni O, Giovannelli D*. 2023. Surface Bacterioplankton Community Structure Crossing the Antarctic Circumpolar Current Fronts. *Microorganisms*, 11(3):702. doi: 10.3390/microorganisms11030702

1 – Barry P, De Moor JM, A Chiodi, F Aguilera, MR Hudak, DV Bekaert, S J Turner, J Curtice, AM Seltzer, G L Jessen, E Osses, JM Blamey, M Amenabar, M Selci, **Cascone M**, A Bastianoni, M Nakagawa, R Filipovich, E Bustos, M Schrenk, J Buongiorno, CJ Ramírez, TJ Rogers, KG Lloyd and D Giovannelli. 2022. The helium and carbon isotope characteristics of the Andean Convergent Margin. *Frontiers in Earth Sciences*, 10. doi: 10.3389/feart.2022.897267

b. Book chapters

2 – Giovannelli D, **Cascone M**, Gallo G, Migliaccio F, Barosa B, Bastoni D, Brusca J, Longo A, Tonietti L, Cordone A. 2025. Trace metals as redox cofactors and their role in controlling microbial diversity and evolution. In: *Metal ions in Life*. Editer: Sigel A, Sigel H, Sigel RKO. Springer. *Expected in Spring 2025*

1 – Vilhelmsson O., Sigurbjornsdottir MA., Thorsteinsdottir GV., **Cascone M**, Corso D., Tonietti L., Migliaccio F., Nappi N., Ricciardelli A., Selci M, Montemagno F., Barosa B., Bastoni D., Bastianoni A., Cordone A., Giovannelli D. 2024. Diversity of Thermophilic Prokaryotes. In: *Thermophilic Anaerobes: Phylogeny, Physiology and Biotechnological Applications*. pp. 21-90. Springer. Doi: https://doi.org/10.1007/978-3-031-41720-7_2

c. Preprints

5 – Tonietti L, Esposito M, **Cascone M**, Barosa B, Fiscale S, Muscari Tomajoli MT, Sbaffi T, Santomartino R, Covone G, Cordone A, Giovannelli D, Rotundi A. 2024. Unveiling the bioleaching versatility of *Acidithiobacillus ferrooxidans*. *EarthArXiv*, 7142. Doi: https://doi.org/10.31223/X51D64

4 – Bastianoni A., **Cascone M**., de Moor M., Barry P. H., Price R., Cordone A., Aiuppa A., Fischer T., Marty B., Giovannelli D. The missing carbon budget puzzle piece: shallow-water hydrothermal vents contribution to global CO2 fluxes. *EarthArXiv*, doi: https://doi.org/10.31223/X52W81

3 – Mele BH., Monticelli M., Leone S., Bastoni D., Barosa B., **Cascone M.**, Migliaccio F., Montemagno F., Ricciardelli A., Tonietti L., Rotundi A., Cordone A., Giovannelli D*. 2023. Oxidoreductases and metal cofactors in the functioning of Earth. *EarthArXiv*, 5392. Doi: 10.31223/X58H36

2 – Cordone A., Selci M., Barosa B., Bastianoni A., Bastoni D., Bolinesi F., Capuozzo R., **Cascone M**, Correggia M., Corso D., Di Iorio L., Misic C., Montemagno F., Ricciardelli A., Saggiomo M., Tonietti L., Mangoni O., Giovannelli D*. 2022. Surface Bacterioplankton Community Structure

Crossing the Antarctic Circumpolar Current Fronts. *EarthArXiv*, doi: 10.31223/X58Q04

1 – Cordone, A., Coppola, A., Severino, A., Correggia, M., Selci, **Cascone M.**, A., Vetriani C, Giovannelli D*. (2021). From sequences to enzymes: comparative genomics to study evolutionary conserved protein functions in marine microbes. *OSF preprints*, doi:10.31219/osf.io/yacvr

d. In preparation

6 – **Cascone M.**, Migliaccio F., Corso D., Gargallo G. C., Cordone A., Franchi E., Pietrini I., Carpani G., Bersano D., Del Gaudio L., Shapran O., De Simoni M., di Benedetto A., Luciani G., Anzelmo G., Iacopini D., Parente M., Moracci M*, Giovannelli D*. Hydrogen utilization in microorganisms: hydrogenase diversity, distribution and implication for Underground Hydrogen Storage. *In prep*

5 – **Cascone M.**, Corso D., Selci M., Gallo G., Migliaccio F., Bastianoni A., di Iorio L., Correggia M., Cordone A., Bekaert D.V., Tyne R. L., Barry P. H., Lloyd K., Jessen G., Chiodi A., de Moor M. Ramirez C., Brovarone A. V., Moracci M., Giovannelli D*. Hydrogenotrophic metabolisms in the subsurface: insights from natural hydrogen seeps in diverse geological settings. *In prep*

4 – **Cascone M.**, Gallo G., Migliaccio F., di Iorio L., Correggia M., Cordone A., Tyne R. L., Barry P. H., Brovarone A. V., Moracci M., Giovannelli D*. A comprehensive census of microbial diversity in Italian deeply-sourced seeps using 16S rRNA gene Illumina sequencing. *In prep*

3 – **Cascone M.**, Gallo G., Corso D., Migliaccio F., di Iorio L., Correggia M., Cordone A., Tyne R. L., Barry P. H., Brovarone A. V., Moracci M., Giovannelli D*. Unveiling the microbial diversity and functional dynamics of Italian natural seeps, through a shotgun metagenomics approach. *In prep*

2 – Selci M., **Cascone M.**, Rogers T., Brovarone A.V., Ramirez C., Ono S., Yucel M., Jessen G., Schrenk M., De Moor J.M., Barry P.H., Cordone A., Lloyd K.G., Giovannelli, D., 2024. Origin and fate of methane in the Central American convergent margin. *In prep*

1 – **Cascone, M.**, Bastianoni, A., Selci, M., Correggia, M., di Iorio, L., Cordone, A., Manini, E., Barry, P., Lloyd, K.G., Jessen, G., Chiodi, A., De Moor, J.M., Schrenk, M., Ramirez, C., Nakagawa, M., Giovannelli, D. (2024). Deeply-sourced springs of the Argentina backarc as windows into the subsurface. *In Prep*

Unione europea
Fondo sociale europeo

Ministero dell'Università e della Ricerca

PON RICERCA E INNOVAZIONE 2014 - 2020

Appendix VI - Hydrogen 2022: Sampling Natural Hydrogen Sites in Italy - Expedition Report

Martina Cascone[1], Gabriella Gallo[1], Valentina Marcheselli[2], Peter H. Barry[3], Rebecca Tyne[4], Carlo Cardellini[5], J. Maarten de Moor[6,7], Angelina Cordone[1], Stefano Caliro[8], Donato Giovannelli[1,4,9,10]

1- Department of Biology, University of Naples Federico II, Naples, Italy

2- Department of Philosophy and Cultural Heritage, Ca' Foscari University of Venice, Venice, Italy

3- Marine Chemistry and Geochemistry Department, Woods Hole Oceanographic Institution, Woods Hole, MA, USA

4- University of Manchester, UK

5- Department of Physics and Geology, University of Perugia, Perugia, Italy

6- Observatorio Volcanológico y Sismológico de Costa Rica (OVSICORI), Universidad Nacional, Heredia, Costa Rica

7- Department of Earth and Planetary Sciences, University of New Mexico, Albuquerque, NM, USA

8- Italian National Institute of Geophysics and Volcanology, INGV, Section of Naples, Naples, Italy

9- Institute for Marine Biological Resources and Biotechnologies, Italian National Research Council, CNR-IRBIM, Ancona, Italy

10- Earth-Life Science Institute, ELSI, Tokyo Institute of Technology, Tokyo, Japan

Abstract

This report describes the HYD22 expedition along the central Italian Apennines to sample naturally leaking hydrogen seeps. Despite the large number of springs present in the area, our knowledge of the microbiology of these seeps and how they influence the Earth biogeochemical cycling is limited. The aim of the project is to understand the diversity of microbial communities brought to the surface by the seeps fluids, in order to give an insight on their role in biogeochemical cycling. The long term goal of the project is to focus particularly on natural hydrogen leaking seeps present in the entire italian territory, in order to study the hydrogenotrophic microbial community and their physiology connected to the different geochemistry and the geology settings. This approach will allow us to deepen our knowledge about the microbial hydrogen utilization in the subsurface, aiding both natural hydrogen exploitation and geological hydrogen storage. This leg of the expedition took place between 18 and 23 October 2022, 10 distinct sites were sampled for microbiology and geochemistry, while other 3 samples were collected mainly for microbial culture experiments.

1 Introduction

The current need of clean and sustainable energetic resources encouraged an increasing interest to native hydrogen, known as "gold hydrogen". Mainly, natural hydrogen is produced in the serpentinization process, based on the interaction between water and olivine-rich ultramafic rocks leading to the oxidation of water and the reduction of iron (Arrouvel and Prinzhofer, 2021), and in the subsurface radiolysis process in which the water is subjected to ionizing radiation with the consequent generation of byproducts like hydrogen (Bao et al., 2022). As a consequence of these processes, hydrogen can be trapped in the geological bodies over geological times, fueling microbial metabolisms, thus shaping the abundance and diversity of subsurface life (Warr et al., 2019; Gaucher, 2020; Jackson et al., 2024). Hydrogen, together other compounds like methane, carbon dioxide and water, returns to the surface, through tectonic discontinuities, resulting in geothermal manifestations such as hot springs, fumaroles, and geysers (Bekaert et al., 2021, Zheng et al., 2016; Zheng and Zhao, 2017; Zheng, 2019; Ochieng, n.d.). Overall, tectonically active regions, where Earth's crust is subjected to faults, are usually associated with hot springs and fumarolic field, offering the opportunity to have a small window in deep conduits of Earth (Aragno, 1992; Scott et al., 2020), through the study of microbial community and geochemical composition of deep fluids coming out (Falkowski et al., 2008).

Central-Southern Italy (Figure 1), the environmental background of this expedition, is characterized by rich geothermal springs with the production of gases like carbon dioxide and methane, but also hydrogen, mainly in the Larderello-Travale field (Minissale et al., 1997; Leila et al., 2021). These geothermal emanations are related to the Tyrrhenian pre-Apennine belt, an active geological system constantly monitored for its probable thermal anomalies and for the production of geothermal energy, exploited for sustainable energy sources by private companies (Vignaroli et al., 2013). In fact, the region of Larderello in Tuscany is well known for one of the biggest geothermal plants of a private company, making Italy one of the first producers of geothermal energy in the world (Manzella et al., 2018; Silvestri et al., 2020). The natural springs present in Central Italy are also exploited to provide pool systems attended by visitors and locals that use these thermal waters for

the belief of their beneficial health effects, especially in the city of Viterbo (Valeriani et al., 2018).

A complete study of these geological active areas, integrating microbiological and geochemical approaches, allows to get an enriched overview about the geochemical cycles, strongly shaped by microbial machines (Falkowski et al., 2008), and to better understand the correlation between the surface geothermal activities and the consequent greenhouse gas emissions (Venturi et al., 2019). The knowledge of geo-component of Central Italy is well studied (Minissale et al., 1997; Scrocca et al., 2003; Cosentino et al., 2010; Vitale and Ciarcia, 2018; Peccerillo, 2020), while its microbiology is less explored and the currently available information are mainly focused on the microbial activity linked to the presence of heavy metals like arsenic and mercury (Cuebas et al., 2011; Crognale et al., 2017; Cabassi et al., 2021a) or associated with the recreational purpose of the thermal waters (Valeriani et al., 2020, n.d.; Venturi et al., 2022). Concerning the microbiology of the Campania region, the predominant data are correlated to the Pisciarelli spring in the Campi Flegrei (Crognale et al., 2018; Iacono et al., 2020; Strazzulli et al., 2020). This project aims to explore the springs present in the Central Italy area, particularly selected from the MaGa database (http://www.magadb.net/) as springs where natural hydrogen gas was already detected. Additionally, springs never sampled before are included in this expedition, with the aim of characterizing them both geochemically and microbiologically. The final objective is to increase our knowledge on the microbial hydrogen utilization by subsurface communities, in order to build a strong bridge between the natural hydrogen exploitation strategies and the underground hydrogen reservoirs technologies, both relying on the subsurface hydrogenotrophic metabolic activities.

2 Expedition team and logistics

The project team is composed of interdisciplinary scientists spanning the fields of microbiology, biogeochemistry, microbial ecology and gas geochemistry. The expedition covered 10 sites in different regions in the central part of Italy, such as Tuscany, Latium and Campania.. The Field Science Party was responsible for sample collection and the field measurements. The Onshore Science Party was responsible for supporting the logistics and

preparation of the expedition as well as collaborating on sample processing and analysis. The expedition team was the object of a sociological study carried out by Valentina Marcheselli.

Field Science Party composition: Donato Giovannelli (Expedition Leader and PI of the project), Martina Cascone, Gabriella Gallo, Peter H. Barry, Rebecca Tyne, Valentina Marcheselli.

Support Science Party composition: Angelina Cordone, Luciano di Iorio, Monica Correggia, Carlo Cardellini, J. Maarten de Moor, Stefano Caliro.

3 Geological and environmental settings

The italian peninsula is situated in the middle of the Mediterranean Sea, subjected to the progression of two megaplates: Eurasia, to the North, and Africa to the South (Figure 2). In the peninsula, there are two mountain chairs: the Alps, which are the result of the convergence and collision of the European and African continental margins (occurring between the Middle Cretaceous, about from 145 to 66 million years ago, and the Late Eocene, from about 56 to 33.9 million years ago), and the Apennines, which are resulted both by the opening of Tyrrhenian Sea and the collision of Adria microplate, belonging to the African promontory, with Sardinia-Corsica block, during Miocene–Pliocene time, from 23 to 2.6 millions of years ago (Faccenna et al., 2001; Cosentino et al., 2010; Bosellini, 2017). Overall, the Italian arc-tectonic association of collision and extension is a consequence of subduction of the Apulian micro-plate beneath the European plate (Rouchon et al., 2008). The Northern-Western Apennines is characterised by many grabens resulted after the collapse of the western part of the chain as a consequence of the opening of the Tyrrhenian Sea while the Southern Apennines are defined by the presence of large carbonate platforms of Jurassic-Cretaceous (Bosellini, 2017). The Southern and Northern Apennine arcs are linked in central Italy along a marked feature, called the Ortona-Roccamonfina Line (Italiano et al., 2000). This entire geological system, recognized as TAS (Tyrrhenian-Apenninic System), is the result of the various tectonic phases occurring in the Late Miocene (Gambardella et al., 2004).

The active geothermal systems and the post-volcanism, characterising the Central Italy regions, are expressed through the presence of the thermal springs (Viviano et al., 2022), especially in

Tuscany, Latium and Campania, the most active regions. In Tuscany, laminated anhydrite layers between the carbonate series and the crystalline basement affect the composition of thermal springs located at the boundaries of Mesozoic carbonate formation, enriching them in Ca–SO_4 (Minissale et al., 2000). The Latium platform unit, shaped on the base of tectonics events occurring in the early Miocene (the contractional deformation caused by Alpine orogeny and an extensional phase caused by Tyrrhenian back arc extension) includes the belt of potassium-rich volcanoes present in the region between Southern Tuscany and the city of Rome, along the western side of the Italian peninsula (Buonasorte et al., 1991; Peccerillo, 2005, Petracchini et al., 2015). The Ernici-Roccamonfina volcanic province lies between the orogenic belt of the Apennines and the slow spreading center of the Tyrrhenian Sea. Campania province, situated between the Southern Apennines and the Tyrrhenians sea, is formed by the volcanoes of Somma-Vesuvio, the large volcanic complex of Campi Flegrei and the island of Procida. The mafic products show a moderately potassic alkaline affinity and degree of silica undersaturation, different from the ultrapotassic-undersaturated compositions present in the Roman Province (Peccerillo, 2020). The Campanian province also includes Ischia Island, area of still active residence and characterised by a high hydrothermal activities with hot spring and fumaroles. In particular, the sector more active is represented by the Monte Epomeo, on the west side of the island (Galvani et al., 2021a).

4 Sampling methodologies

Sample selection and environmental parameters

Fluids, sediments, background soils and gases were collected from 10 locations identified based on the literature. The springs show characteristics compatible with the definition of deeply-sourced seeps (Giovannelli et al., 2022). At each sampling site, the main seep outlet was identified using a combination of previous data from literature, field observation, pH, conductivity and temperature measurement. The objective was to sample the pristine gases and fluids as they emerged from the subsurface, minimizing their mixing and interaction with the surface and the atmosphere. Background soil samples from the nearby area do not show geothermal alterations. The rationale behind this type of

sampling approach is to maximize the subsurface information that can be extrapolated from the data. Temperature, conductivity, pH, redox potential, total suspended solids and dissolved oxygen were measured directly in the field using a Hanna Multiparameter WP probe, regularly calibrated. Alkalinity, dissolved hydrogen sulfide, ferrous iron were also measured in the field as described below.

Geochemistry samples acquisition

Dissolved gas geochemistry

Fluids for dissolved gas analysis were collected both for gas composition analysis and noble gas isotope systematics. Fluid samples for noble gas analysis were first flushed through silicone tubing and into 3/8-inch copper tubes. After ample flushing (*i.e.*, approximately 10x the volume of the tubing), stainless steel clamps were closed on each end of the copper tubes, trapping the sample inside of the copper tubing, between the clamps (Barry et al., 2022). Fluids for dissolved gas composition were collected in pre-evacuated 250 ml Giggenbach bottles as previously described (Barry et al., 2019).

Aqueous and Sediment Geochemistry

For the characterization of the major dissolved ions, 0.22 µm filtered fluids were collected in a 50 ml conical tube. The sulfide determination and the ferrous iron (Fe^{2+}) determination are carried out by a field spectrophotometer, using filtered fluids (0.22 µm). A duplicate sample was collected in acid-washed tubes and acidified with nitric acid (2 % final concentration) for the analysis of trace elements. Filtered fluids (0.22 µm) were also collected in a 10 ml penicillin vial air-free for dissolved inorganic carbon isotope composition. Sediment samples as close as possible to the fluid outlet point were collected into 50 ml acid-washed conical tubes.

Biological samples acquisition

At each site, sediments and fluid samples were collected aseptically for molecular analysis, with a sampling approach described in (Fullerton et al., 2021). Fluids for DNA extraction (2 L) were filtered in triplicate 0.22 µm Sterivex filter cartridges (MilliporeSigma). Filtration was achieved using a 3D-printed custom designed peristaltic pump (https://github.com/giovannellilab/Field_3D-printed_peristaltic_pump) connected to a battery powered portable drill. Sediments and

background solid were collected in sterile 50 ml conical tubes. Sediments, background soils and filters were immediately frozen. Fluids were also collected in 2 ml cryovial preserved in 3 % paraformaldehyde for cell counts. Penicillin vials (120 ml) were filled with biofilms and fluids for culturing and isolation purposes.

5 Sites and samples log

The description of each sampled location follows together with pictures useful for future identification of the site. A .kmz file containing the exact location of the sampled location is available on the online GitHub repository associated with this report (https://github.com/giovannellilab/HYD22_project) permanently stored on Zenodo with DOI 10.5281/zenodo.12206958.

Sorgente di Chiorba (CB)

Sorgente di Chiorba (43.1527486 °N, 10.853645 °E, series 1) is located in Biancane natural park, belonging to the geothermal field of Larderello, north of Monterotondo Marittimo town and 12 km south of Larderello, near Grosseto, in southern Tuscany (Figure 4). With an elevation of 614 m above sea level, this is the highest site of the entire expedition. This site, present in the MaGa database, was already studied, together with other thermal springs in the same area, from the geochemical point of view (Duchi et al., 1992a). This thermal spring emerges from an opening located in a stone made structure, where whitish and gelly biofilm has been collected. With a value of 18 mg/L, the spring has the highest sulfide concentration in the expedition, as expected from the literature data about the thermal springs of the park (Cabassi et al., 2021b).

Sasso Pisano (SP)

Sasso Pisano (43.1676069 °N, 10.8667609 E°, series 2) is a degassing site located in Castelnuovo Val di Cecina, in the central part of the Larderello field (Figure 5), approximately 8.0 km north of the Biancane natural park, previously described in this report. This site lies close to a camping area, behind a tennis groundfield (just as indicated in the MaGa database), in a place characterized by uncultivated plants, reachable by foot through a small street.

Soffioni Boraciferi San Federigo (SF)

Soffioni Boraciferi (43.1435272 °N, 10.8153437 E°, series 3) is a site in Monterotondo Marittimo (Colline Metallifere area), in the

south-western sector of Larderello field, where a large hot bubbling pool, similar to a geyser, is situated in an area poor in vegetation (Figure 6). This bubbling pool is located in the same area of Lake Boracifero, present in MaGa database, whose hot water and gases are exploited by industry activities. In the entire region, there are other geothermal manifestations but in most cases their access is limited for the presence of fences or for the need of specific permits. This site is easily accessible through an open gate.

Torre Alfina (TA)

Torre Alfina (42.747778 °N, 11.948202 E°, series 4) is a pool of meteoric water in patches of diffuse degassing within a farmed field in Orvieto, located to the north of the Vulsini calderas (Figure 7). The site is located in a big farmland without fences, reachable on foot from the street. The Torre Alfina area is already known in literature for its low temperature, very low pH and for the presence of sulphur springs (Duchi et al., 1992b; Vignaroli et al., 2013; Lisi et al., 2019), thus confirmed by the parameters recorded during this field campaign (T=14.5 °C; pH=1.76; H_2S=20 mg/L).

Solfatara di Ferento (FR)

Solfatara di Ferento (42.504311 °N, 12.1371561 °E, series 5) is a site characterised by a diffuse degassing in the side of a river within a large canyon, located 8 km far from Viterbo town (Figure 8). In this site, high concentration of hydrogen sulphide was detected, as demonstrated by the strong smell of rotten egg from the entire area. Additionally,high carbon dioxide concentrations are expected to be detected, making the entire area dangerous, as demonstrated by a warning sign, completely damaged.

Terme di Bullicame (BU)

Terme di Bullicame (42.420498 °N, 12.0732516 °E) is the most known system of bubbling pools in Viterbo (Figure 9), used for recreational purposes, whose waters are rich in a Ca-SO_4-HCO_3 composition for the presence of mesozoic carbonate structure in the Northern Latium (Valeriani et al., n.d.). This area, present in MaGa database, is well known since the Etruscan age and is visited daily by thousands of people who use the thermal waters even though high levels of arsenic in a range from 80 to 100 % are detected from previous studies (Rimondi et al., 2022). In this site, the primary hot spring feeding a water pools system was

surrounded by a glass structure. The sampling was not carried out because the municipal permits were required; only biofilm (yellow-green color) samples were collected.

Piscine Carletti (PC)

Piscine Carletti (42.4219036 °N, 12.0647823 °E) is a site close to "Terme di Bullicame", in which gas bubbling occurs in a constructed pool (Figure 10), where people exploit the hot thermal waters for recreational use. This zone has many characteristics similar to "Terme di Bullicame" but the soil is poorer in calcite, involving a minor level of arsenic content (6-63 %) (Rimondi et al., 2022). Also in this case, only biofilm samples (with colors from Green to Pink) were collected for the presence of a fence surrounding the site.

San Cristoforo (SC)

San Cristoforo (42.3984606 °N, 12.0592911 °E, series 6) is a pool of hot water carved in a carbonate mound, located in Viterbo, not far away from Terme di Bullicame and Piscine Carletti sites (Figure 11). This site is located in a big countryside, close to the road, reachable traveling a brief path on foot and going up stairs. This place is known for promiscous orgies and gay hookups. In this site, the highest value of the alkalinity (110 mg/L $CaCO_3$) of the expedition was detected, coherently with the carbonate rock featuring the pool.

Stagno Bianco (SB)

Stagno Bianco (41.7045854 °N, 12.5365787 °E, series 7) is a spring in a small canyon located in a degassing area, called "Solforata di Pomezia" within the "Riserva Naturale Decima Malafede", in the south of Rome (Figure 12). This area is known in the literature and present in the MaGa database for its strong gaseous manifestations such as CO_2 and H_2S related to the activity of the volcanic system of Colli Albani (Chiodini and Frondini, 2001). The area has no fencing and is easily reachable from the road. The site was characterised by intense greenish-blue color, probably linked to the high presence of silica (Wibowo et al., 1997). In these acidic waters, one of the highest sulfide concentrations of the expedition are detected (2.056 mg/L), coherently with gaseous manifestation, previously described.

Piccolo Inferno (PI)

Piccolo Inferno (41.314487 °N, 13.894006 °E, series 8) is a strong degassing site in the western foot of Roccamonfina Volcano, in Suio, in Northwestern Campania (Figure 13). The geothermal manifestations in Suio does not seem to be correlated to the volcanic activity of the Roccamonfina system but they are likely resulted from the vertical movement through a graben-boundary fault (Watts, 1987). This is a site difficult to sample because of its high H_2S, CO_2 and hydrocarbon gas content, as reported in literature (cit). The sampling procedure mandatorily required the use of a gas mask. The fluid of the spring is very acidic and rich in reduced iron, as demonstrated by the rather low pH value (2.13) and high Fe^{2+} content (3.356 mg/L). Despite the presence of fluids, it was clear that their origin was not deeply sourced but meteoric. Since the fluid flow was not intense enough for the filtration, only gas and sediment samples were collected from this site.

Bocca di Tifeo (TF)

Bocca di Tifeo (40.720034 °N, 13.879809 °E) is a site on the western side of Monte Epomeo in Ischia, the largest island sited in the Gulf of Naples, in the Ischia-Procida-Phlegrean volcanic complex (Figure 14). This area is known to have a temperature of 50 °C (Piochi et al., 2019). The geothermal manifestation of this site emerges as hot vapor, with the highest value of the expedition (90 °C), from a small opening under a boulder. Any kind of sample was collected from this site because of the absence of fluids and the scarce gas flow emissions.

Crateca wineyard (CW)

As reported by (Galvani et al., 2021b), the gas manifestations present in Crateca, such as Crateca wineyard (40.7370474 °N, 13.8860548 °E, series 9) fumarole, are related to Mt. Epomeo faults, in the central sector of Ischia island (Figure 15). This small fumarole field is on the flank of Ischia Volcano, reachable through a private property in which a winery is located. As at the “Bocca di Tifeo” site,, the only in situ detected physico-chemical parameter is the temperature but both gas and sediment samples were collected. There is an evident yellow-green precipitate around the vent, attributable to acicular crystals that are sulfur minerals typical of fumarolic gas sites (Piochi et al., 2015).

Ferrata Cardarelle (FC)

Ferrata Cardarelle (41.2622044 °N, 14.0615298 °E, series 10) is a degassing spring with copious amounts of iron mats on the side of a river in Teano, standing at the southeast foot of the extinct volcano of Roccamonfina, in the province of Caserta, in Campania region (Figure 16). In this area is present for the water company "Ferrarelle" whose name derives from the plausible presence of iron-minerals. Indeed, this site is characterised by the highest value in ferrous iron (25.653 mg/L) of the entire expedition. To access the site, it was necessary to enter a private property, and pass through a Mediterranean forest, mostly populated by Quercus ilex L. (Catalano et al., 2016), and during the expedition period it was infested by vipers. The presence of infesting plants and an unbeaten path caused some problems to reach the spring and to collect and process the samples.

6 Summary

The expedition successfully sampled 10 seeps, including springs, fumaroles and bubbling pools. Some other promising springs need specific licenses for easy access, and will eventually require a dedicated project, with the additional aim to research new spring sites. All the collected samples were brought back to our home laboratories in Italy and the USA for analysis. The data obtained will be made public according to the FAIR Principles for scientific data management.

7 References

Aragno, M. (1992). *The Prokaryotes*, 3917–3933.
Arrouvel ety al. (2021). *Int. J. Hydrog. Energy* 46, 18780–18794.
Bao, Q., et al. (2022). *Chem. Eng. J.* 446, 136964.
Barry, et al. (2022). *Front. Earth Sci.* 10.
Barry, et al. (2019). *Sci. Data* 6, 1–8.
Bekaert, et al. (2021). *Annu. Rev. Earth Planet. Sci.* 49, 37–70.
Bosellini, A. (2017). Cham: Springer International Publishing
Buonasorte, et al. (1991). *Geomorphol. Suppl.* 82, 59–71.
Cabassi, et al. (2021a). *J. Geochem. Explor.* 228, 106824.
Cabassi, et al. (2021b). *J. Geochem. Explor.* 228, 106824.
Catalano, et al. (2016). *Nova Hedwig.* 103, 95–116.
Chiodini, G., and Frondini, F. (2001). *Chem. Geol.* 177, 67–83.
Cosentino, et al. (2010). *J. Virtual Explor.* 36.
Crognale, et al. (2018). *FEMS Microbiol. Ecol.* 94, fiy190.

Crognale, et al. (2017). *Front. Microbiol.* 8.
Cuebas, et al. (2011). *J. Basic Microbiol.* 51, 364–371.
Duchi, et al. (1992a). *J. Volcanol. Geotherm. Res.* 49, 313–328.
Duchi, et al. (1992b). *Geothermics* 21, 401–413.
Faccenna, et al. (2001). *Geophys. J. Int.* 145, 809–820.
Falkowski, et al. (2008). *Science* 320, 1034–1039.
Fullerton, et al. (2021). *Nat. Geosci.* 14, 301–306.
Funch, P.,et al. (2001), Springer, 273–282.
Galvani, A., et al. (2021a). *Remote Sens.* 13, 4648.
Galvani, A. et al. (2021b).*Remote Sens.* 13, 4648.
Gambardella et al. (2004).. *J. Vol. Geotherm. Res.* 136, 31–52.
Gaucher. (2020). *Elements* 16, 8–9
Giovannelli (2022). *Nat. Rev. Env and Evol*
Hjartarson et al. (2010). in *Proc. World Geoth. Cong.*, 1–8.
Iacono et al. (2020).. *Molecules* 25, 4023
Italiano et al. 2000. *J. Geoph. Res. Solid Earth* 105, 13569–13578.
Jackson et al. (2024). *Geoenergy* 2, geoenergy2024.
Kristensen. (1987). *Ber. Über Grönl. Inst. Für Polar. Vom* 2, 25.
Leila et al. (2021).*Chem. Geol.* 585, 120564.
Lisi et al. (2019). *J. Seismol.* 23, 1279–1298.
Manzella et al. (2018). *Geothermics* 72, 232–248.
Minissale et al. (1997).*Chem. Geol.* 142, 175–192.
Minissale et al. (2000). *Tectonophysics* 319, 199–222.
Ochieng, L. (n.d.). Ov. Geotherm. Surf. Explor. Meth.
Peccerillo. (2005). *in Italy: Petrology, Geochemistry, Geodynamics*, 69–107.
Peccerillo. (2020). in *Vesuvius, Campi Flegrei, and Campanian Volcanism*, 79–120.
Petracchini et al. (2015). *in the Latium Region (Central Italy)*.
Piochi et al. (2019). *J. Volcanol. Geotherm. Res.* 376, 104–124.
Piochi et al. (2015).*J. Volcanol. Geotherm. Res.* 304, 180–193.
Rimondi et al. (2022). *Environ. Geochem. Health* 44, 465–485.
Rouchon et al. 2008. *J. Volcanol. Geotherm. Res.* 177, 500–514
Scott et al. (2020). *Geochem. Geophys. Geosystems* 21, e2020GC008919.
Scrocca et al. (2003). https://arpi.unipi.it/handle/11568/78760.
Silvestri et al. (2020). *Remote Sens.* 12, 2018.
Strazzulli et al. (2020). *FEBS J.* 287, 1116–1137.
Valeriani et al. (n.d.).
Valeriani et al. (2020). *Environ. Int.* 137, 105595.

Valeriani. *Int. J. Environ. Res. Public. Health* 15, 2675.
Venturi, S. et al. (2019). *Sci. Total Environ.* 655, 887–898.
Vignaroli, G. et al. (2013). *Tectonophysics* 608, 482–498.
Vitale, S. et al.(2018). *J. Maps* 14, 9–21.
Viviano, A., et al. (2022). *J. Integr. Biogeogr.* 37.
Warr, O. et al. (2019). *Chem. Geol.* 530, 119322.
Watts, M. D. (1987). *Geothermics* 16, 517–528.
Wibowo, J. et al. (1997). *MICRO* 15.
Zheng, Y. et al. (2016). *Sci. China Earth Sci.* 59, 651–682.
Zheng, Y.-F. (2019). Subduction zone geochemistry. *Geosci. Front.* 10, 1223–1254. doi: 10.1016/j.gsf.2019.02.003
Zheng et al. (2017). *J. Asian Earth Sci.* 145, 1–15.

8 Figures

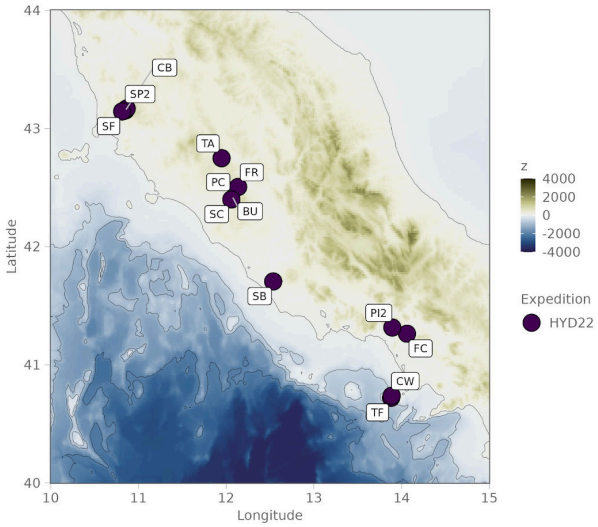

Figure 1. Map showing the sampled Italian natural hydrogen seeps in Central-Southern Italy. The dark violet markers represent sampled springs during the HYD22 expedition.

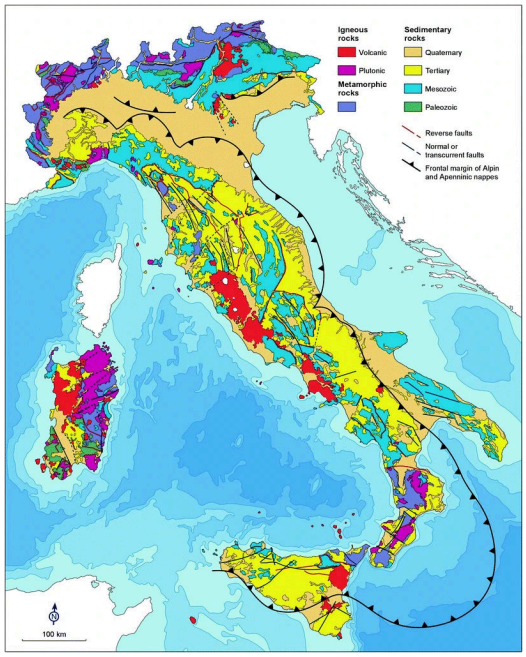

Figure 2. Geological map of Italy (Bosellini, A. (2017). Outline of the Geology of Italy. In: Soldati, M., Marchetti, M. (eds) Landscapes and Landforms of Italy. World Geomorphological Landscapes. Springer, Cham. https://doi.org/10.1007/978-3-319-26194-2_3).

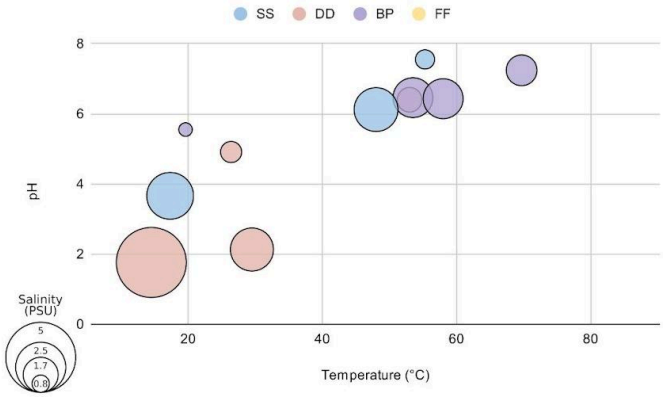

Figure 3. Graph showing the temperature (°C), pH, and salinity (proportional to the size of the circles in PSU) of the sampled locations. SS=Spring; DD=Diffuse degassing; BP=Bubbling pool; FF=Fumarole.

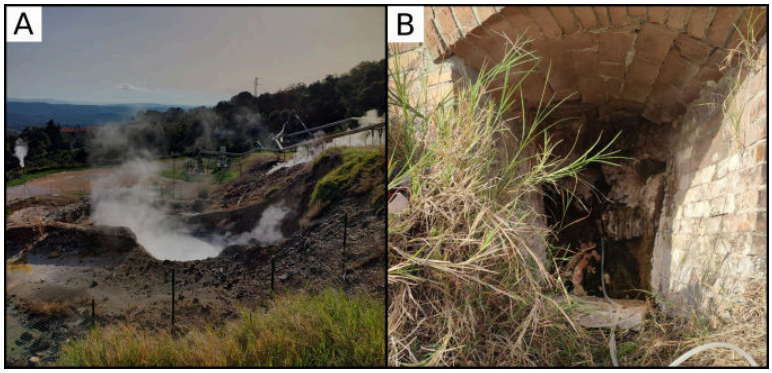

Figure 4. A. Large view of the Sorgente di Chiorba site in Biancane natural park. B. Detail of the sampling location where the fluid and biofilm samples were collected.

Figure 5. A. Large view of Sasso Pisano sampling site in Castelnuovo Val di Cecina, about 8.0 km north of the Biancane natural park. B. Detail of the sampling location where the fluid, sediment and gas samples were collected.

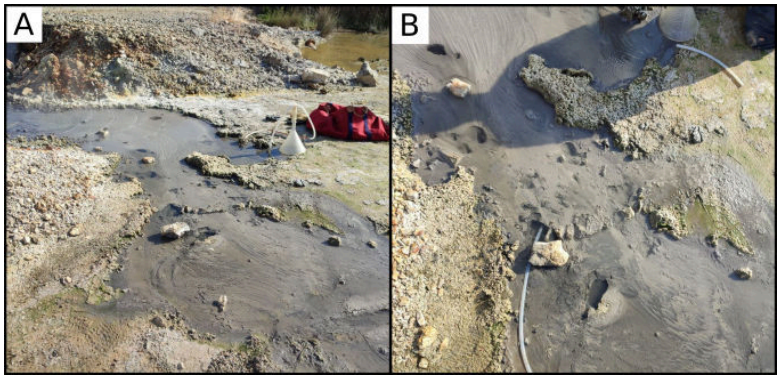

Figure 6. A. Large view of the Soffioni Boraciferi site in Monterotondo Marittimo, in the Colline Metallifere area. B. Detail of the sampling location where the fluid, sediment, biofilm and gas samples were collected.

Figure 7. A. Large view of the Torre Alfina site within a farmed field in Orvieto, located to the north of the Vulsini calderas. B. Detail of the sampling location where the fluid, sediment, biofilm and gas samples were collected.

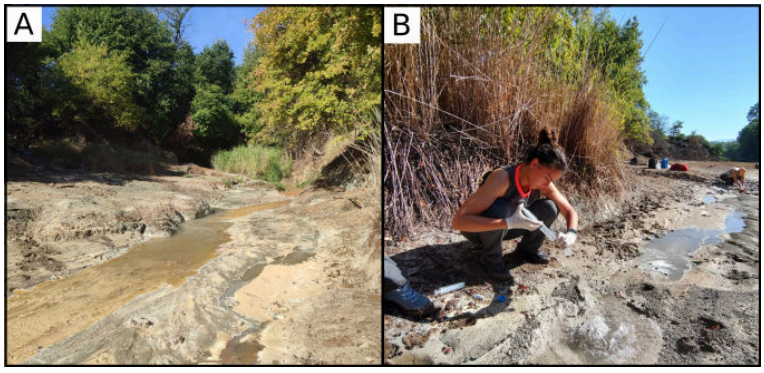

Figure 8. A. Large view of the Solfatara di Ferento site located 8 km far from Viterbo town. B. Detail of the sampling location where the fluid, sediment and gas samples were collected.

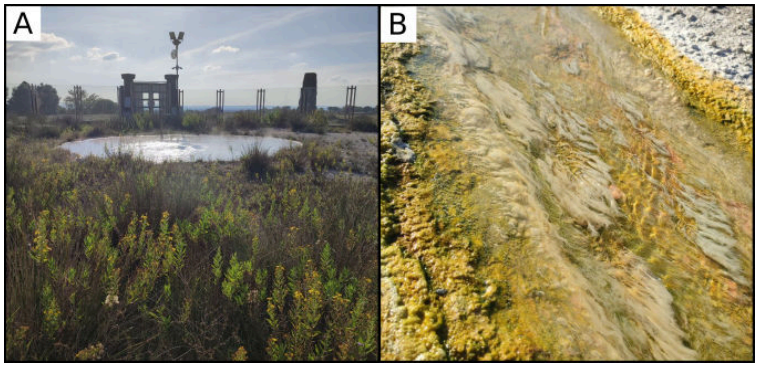

Figure 9. A. Large view of the Terme di Bullicame site in Viterbo. B. Detail of the sampling location where the biofilm samples were collected.

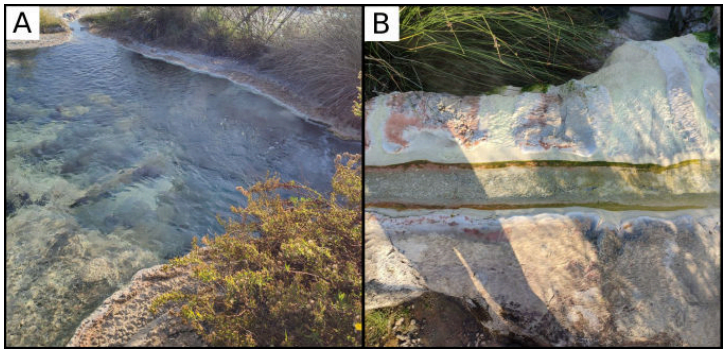

Figure 10. A. Large view of the Piscine Carletti site at about 1.2 km from the Terme di Bullicame site in Viterbo. B. Detail of the sampling location where the biofilm samples were collected.

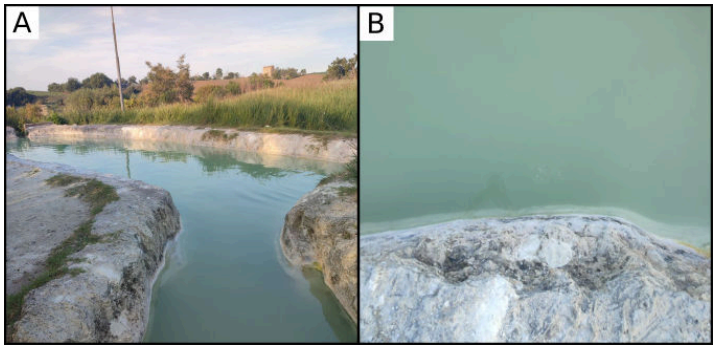

Figure 11. A. Large view of the San Cristoforo site in Viterbo. B. Detail of the sampling location where the fluid and gas samples were collected.

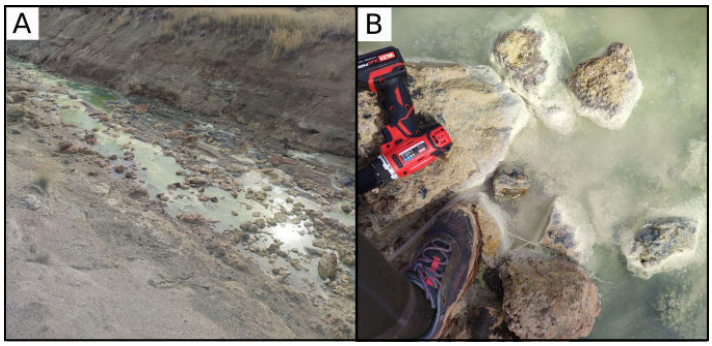

Figure 12. A. Large view of the Stagno Bianco site in the "Solforata di Pomezia" area located within the "Riserva Naturale Decima Malafede", in the south of Rome. B. Detail of the sampling location where the fluid, sediment, biofilm and gas samples were collected.

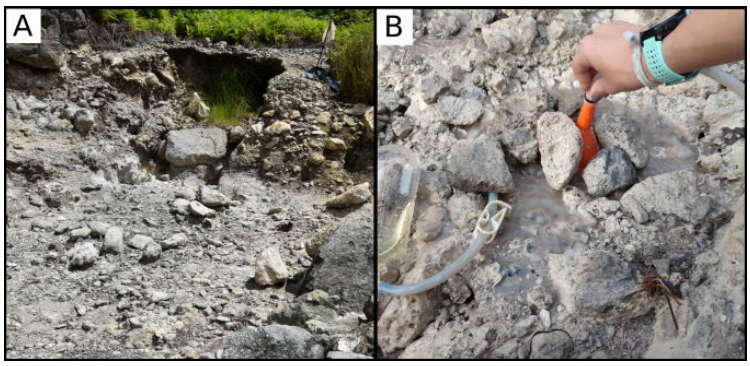

Figure 13. A. Large view of the Piccolo Inferno site in the western foot of Roccamonfina Volcano, Northwestern Campania. B. Detail of the sampling location where the gas samples were collected.

Figure 14. A. Large view of the Bocca di Tifeo site on the western side of Monte Epomeo in Ischia, in the Gulf of Naples. B. Detail of the sampling location where the physico-chemical variables were measured but it was impossible to collect samples. Photograph A taken from the internet (https://www.ischiaprenotazioni.it/blog/Luoghi-Di-Ischia/bocca-di-tifeo-ischia).

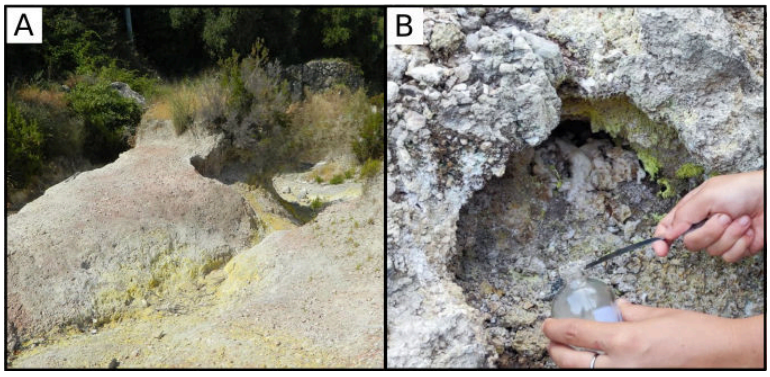

Figure 15. A. Large view of the Crateca wineyard site, inside a private wineyard in the central part of Ischia island. B. Detail of the sampling location where the gas and sediment samples were collected.

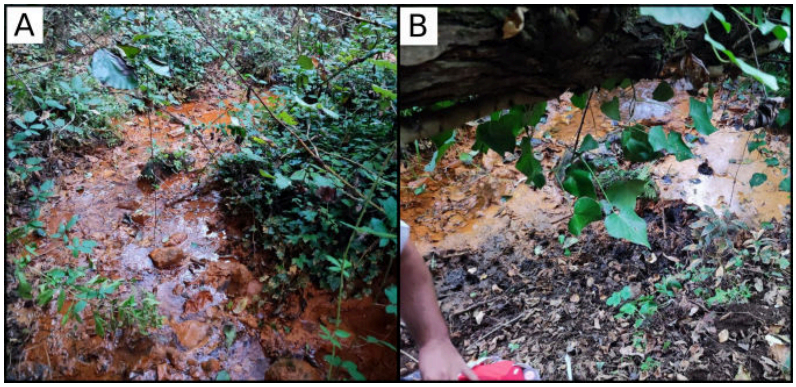

Figure 16. A. Large view of the Ferrata Cardarelle site in Teano, in the Campania region. B. Detail of the sampling location where the fluid, sediment, biofilm and gas samples were collected.

microorganisms

MDPI

Article

Surface Bacterioplankton Community Structure Crossing the Antarctic Circumpolar Current Fronts

Angelina Cordone [1,*,†], Matteo Selci [1,†], Bernardo Barosa [1], Alessia Bastianoni [1], Deborah Bastoni [1], Francesco Bolinesi [1], Rosaria Capuozzo [1], Martina Cascone [1], Monica Correggia [1], Davide Corso [1], Luciano Di Iorio [1], Cristina Misic [2], Francesco Montemagno [1], Annarita Ricciardelli [1], Maria Saggiomo [3], Luca Tonietti [1,4], Olga Mangoni [1,5] and Donato Giovannelli [1,6,7,8,9]

1 Department of Biology, University of Naples Federico II, 80126 Naples, Italy
2 Dipartimento di Scienze della Terra, Dell'Ambiente e della Vita, Universitá di Genova, 16132 Genova, Italy
3 Stazione Zoologica Anton Dohrn, 80121 Naples, Italy
4 Department of Science and Technology, University of Naples Parthenope, 80143 Naples, Italy
5 Consorzio Nazionale Interuniversitario delle Scienze del Mare (CoNISMa), 00196 Rome, Italy
6 Institute of Marine Biological Resources and Biotechnologies, National Research Council, 60125 Ancona, Italy
7 Earth-Life Science Institute, Tokyo Institute for Technology, Tokyo 152-8552, Japan
8 Department of Marine and Coastal Science, Rutgers University, New Brunswick, NJ 08901, USA
9 Marine Chemistry and Geology Department, Woods Hole Oceanographic Institution, Woods Hole, MA 02540, USA
* Correspondence: angelina.cordone@unina.it
† These authors contributed equally to this work.

Abstract: The Antarctic Circumpolar Current (ACC) is the major current in the Southern Ocean, isolating the warm stratified subtropical waters from the more homogeneous cold polar waters. The ACC flows from west to east around Antarctica and generates an overturning circulation by fostering deep-cold water upwelling and the formation of new water masses, thus affecting the Earth's heat balance and the global distribution of carbon. The ACC is characterized by several water mass boundaries or fronts, known as the Subtropical Front (STF), Subantarctic Front (SAF), Polar Front (PF), and South Antarctic Circumpolar Current Front (SACCF), identified by typical physical and chemical properties. While the physical characteristics of these fronts have been characterized, there is still poor information regarding the microbial diversity of this area. Here we present the surface water bacterioplankton community structure based on 16S rRNA sequencing from 13 stations sampled in 2017 between New Zealand to the Ross Sea crossing the ACC Fronts. Our results show a distinct succession in the dominant bacterial phylotypes present in the different water masses and suggest a strong role of sea surface temperatures and the availability of Carbon and Nitrogen in controlling community composition. This work represents an important baseline for future studies on the response of Southern Ocean epipelagic microbial communities to climate change.

Keywords: bacterioplankton diversity; Southern Ocean; 16S rRNA sequencing; primary productivity

check for updates

Citation: Cordone, A.; Selci, M.; Barosa, B.; Bastianoni, A.; Bastoni, D.; Bolinesi, F.; Capuozzo, R.; Cascone, M.; Correggia, M.; Corso, D.; et al. Surface Bacterioplankton Community Structure Crossing the Antarctic Circumpolar Current Fronts. *Microorganisms* **2023**, *11*, 702. https://doi.org/10.3390/microorganisms11030702

Academic Editors: Angelina Lo Giudice and Amedea Perfumo

Received: 31 January 2023
Revised: 28 February 2023
Accepted: 7 March 2023
Published: 9 March 2023

Copyright: © 2023 by the authors. Licensee MDPI, Basel, Switzerland. This article is an open access article distributed under the terms and conditions of the Creative Commons Attribution (CC BY) license (https://creativecommons.org/licenses/by/4.0/).

1. Introduction

Oceans cover more than 70% of Earth's surface, driving almost half of the global net primary production [1–3]. The Southern Ocean, in particular, is thought to contribute to nearly 15% of the oceanic primary production [4], and it is generally defined as the global ocean south of 60° S surrounding the Antarctic continent [5]. Due to the upwelling of nutrient-rich Circumpolar Deep Waters (CDW), as well as the presence of water masses with different physicochemical properties, the Southern Ocean plays an important role in the ocean ecosystem's functioning and composition [5,6].

The Southern Ocean is home to the world's strongest and deepest currents that control thermohaline circulation across the entire world's oceans. It connects the three main ocean

basins (Atlantic, Pacific and Indian) and creates a global circulation system that is largely driven by the Antarctic Circumpolar Current (ACC). The ACC flows from west to east around Antarctica, and it is considered the major water exchange driver between the world's oceans, being the only current that flows entirely around the globe. The ACC consists of a number of full-depth fronts, defined by changes in water properties that occur in a short distance, characterized by high velocities and separated by relatively quiescent zones [7]. These frontal regions also represent a strong exchange between waters, enabling the upwelling of deep nutrient-rich waters and the downwelling of less enriched surface waters. Hence, ACC fronts are considered to play an important role in the global distribution of nutrients (i.e., nitrate) due to the vertical exchange within fronts and the "mixing barrier" effect across fronts [5].

Traditionally, the Southern Ocean has been divided into three main fronts (from north to south): the Subantarctic Front (SAF), the Polar Front (PF), and the Southern ACC Front (sACCF). The northern and southern limits of the ACC are marked by the Subtropical Front (STF) and the Southern Boundary Front (SBDY) [5,8,9], respectively. Both fronts have very distinct dynamics with respect to the main ACC fronts, leading some authors to not consider them as part of the main ACC [7,10]. The ACC fronts are at their narrowest meridional constriction at the Drake Passage and diverge as the ACC flows downstream into the Scotia Sea. The island of South Georgia lies on the northeastern side of the Scotia Sea. It is south of the PF but is strongly influenced by the SACCF that loops anti-cyclonically around the island's shelf from the south before retroflecting to the east. Before reaching South Georgia, the SACCF runs through the southern half of the Scotia Sea, and although the island itself lies in the polar open ocean zone, the waters that lie off the north coast may have been seasonally influenced by the presence of ice cover.

Despite the persisting high nutrient and low chlorophyll (HNLC) conditions [11], primary productivity within the ACC is highly variable. Maximum phytoplankton growth rates are relatively low due to a combination of low temperatures, micronutrient availability, and high wind stress leading to a strong mixing over the region. However, the frontal zones' primary production generally results elevated compared to surrounding oceanic areas [12–14] and can be spatially extensive. Different studies show that the enhanced production in these regions is correlated to increased supplies of iron derived from shelf sediments, which are available within frontal jets [12,15]. In contrast, oceanic areas to the north and south of the fronts are iron-limited, and the low chlorophyll levels have a negative impact on export production [16,17].

The microbial diversity of such environments is shaped by both geography and environmental variables [18]. Physical barriers in marine environments are less evident compared to those in terrestrial settings (such as mountains, oceans, and islands) but are still remarkable [19]. The Antarctic Polar front (APF) [20,21], for instance, can create an open ocean dispersal barrier due to intense currents and a 3–4 °C horizontal thermocline [22,23]. The presence of fronts, such as the APF, has been shown to influence the genetic flow for larger eukaryotes such as Echinoderms, Annelids, and Chordates (e.g., brittle stars, worms, and toothfish) [22,24,25]. Prokaryote communities also appear to be separately shaped by ocean fronts [6,23,26], and the spatial distribution of phytoplankton groups seems to be highly correlated to ocean surface thermal gradients across the ACC [27].

Marine microorganisms, especially Bacteria and Archaea, are fundamental for the functioning of the world's oceans as they are the main players in the biogeochemical cycling of the elements. Their diversity and abundance have been extensively studied during the last decades thanks to different oceanographic campaigns that allowed for the collection of several seawater and sediment samples. For instance, the Tara Ocean Expedition, started in 2009, has allowed for more than 30,000 samples to be collected in more than 200 stations distributed throughout the world's oceans [28].

16S rRNA sequencing and shotgun metagenomic analysis from these samples revealed that the bacterial community of the world's oceans is dominated by Proteobacteria, like clades SAR11 and SAR86, both in terms of relative abundance and taxonomic richness,

followed by Cyanobacteria, Deferribacteres, and Thaumarcheaota [29]. Despite the great effort in analyzing the ocean's microbiome, the microbial diversity of the Southern Ocean, especially related to the water masses crossing this region, is still poorly characterized.

The rapid warming of the Southern Ocean could influence species turnover in the microbial community with widespread consequences for the global climate [6]. In this context, our study aims to characterize the bacterioplankton community of surface waters crossing the Antarctic Circumpolar Current Fronts from New Zealand to the Ross Sea and to investigate the effect of physicochemical changes of these fronts on the bacterial community structure.

2. Materials and Methods

2.1. Sampling Procedure and Study Site

Sampling activities were carried out on the R/V Italica during the austral summer of 2017 in the framework of a plankton biodiversity and functioning of the Ross Sea ecosystems in a changing Southern Ocean (P-ROSE) project funded by the Ministry of Education, University and Research (MIUR). Surface water samples (approximate depth of 5 m) were collected along the transect New Zealand–Ross Sea every 8 h using a plastic tube pumping water on board (Figure 1a,b). Seawater aliquots of 500 mL were filtered (Whatman 0.22 µm) and kept frozen (between −20 and −80 °C) on board. Of the 24 samples recovered, high-quality 16S rRNA libraries were obtained only for 13 stations and were used for downstream analysis.

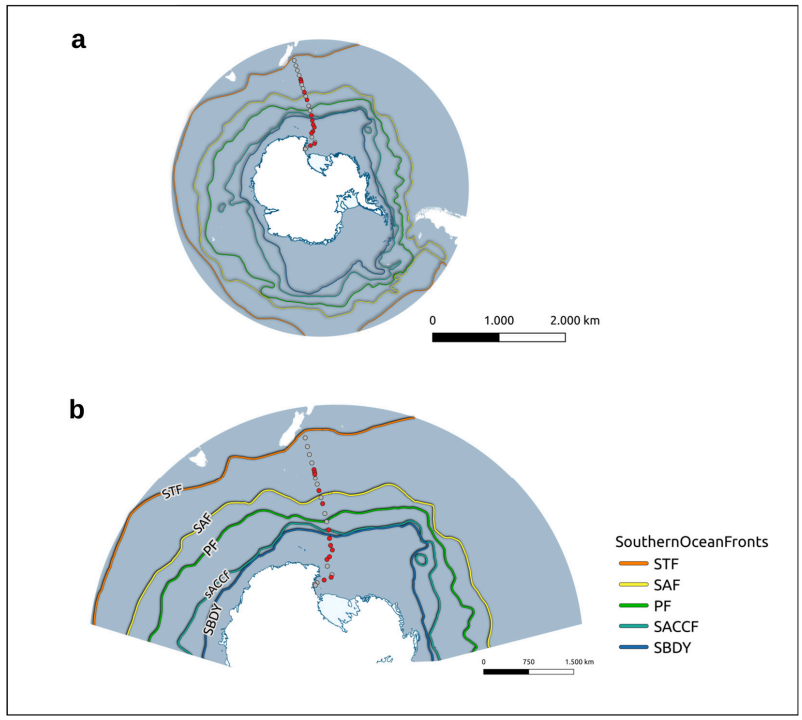

Figure 1. Transect between New Zealand and the Ross Sea sampled during the oceanographic campaign: (**a**) Distribution of the sampled stations (gray dots) and of the stations for which 16S rRNA libraries were obtained (red dots). In the figure are also reported the current fronts crossing the transect: STF—Sub-Tropical front; SAF—Sub-Antarctic Front; PF—Polar Front; SACCF—Southern Antarctic Circumpolar Current front; SBDY—Southern Boundary of the ACC; (**b**) Zoomed view of the stations covered within the transect with their name.

Further samples were collected for the biochemical measurements of particulate organic matter. Water (at least 1000 mL in duplicate for each analysis) was filtered through Whatman GFF filters (glass fiber, nominal porosity 0.45 μm), and stored at −20 °C until analysis.

2.2. Environmental Parameters

For each sampling station, data for Surface Primary Productivity (SPP) were obtained from the Ocean Productivity Database [30], based on the generalized vertical production model developed by [31]. Sea Surface Temperature (SST), Sea Surface Temperature Anomalies (SSTA), and Wind Speed (WS) data were obtained from the National Oceanic and Atmospheric Administration database [32], while data for the Current Speed (CS) were obtained from the NASA-funded research project, Ocean Surface Current Analysis Real-Time (OSCAR) [33]. Sea Surface Salinity (SSS) data were obtained from the Physical Oceanography Distributed Active Archive Center [34].

2.3. Community DNA Extraction

DNA extraction was carried out according to Giovannelli et al. (2016) with minor modifications (extra elution steps). Briefly, each filter was soaked in a saline lysing solution (100 mM NaCl (pH 8.0), 20 mM EDTA, 50 mM Tris-HCl (pH 8.0)) to which 50 μL of lysozyme (100 mg/mL) was added. The resulting solution was incubated at 37 °C for 1 h and treated with 50 μL of Proteinase K (20 mg/mL), followed by an incubation step at 37 °C for 1 h with shaking every 15 min. Subsequently, 1 mL of 20% sodium dodecyl sulfate (SDS) was added to the resulting solution, and the sample was incubated at 65 °C for 1 h. Afterward, samples were centrifuged at 13.000 rpm × 15 min. The supernatant was transferred in a sterile 2 mL Eppendorf tube. Nucleic acids were separated from the other cellular components by performing two consecutive liquid:liquid extractions with phenol:chloroform:isoamylic alcohol (25:24:1), each followed by a centrifugation step of 15 min at room temperature. After obtaining a phase separation, DNA was precipitated by adding 0.7 volumes of isopropanol (100%) and 0.1 volumes of sodium acetate and incubated overnight at room temperature. Finally, samples were centrifuged at 13.000 rpm × 30 min. The resulting pellet was washed with ethanol and re-precipitated by centrifuging at 13.000 rpm × 5 min. After drying the pellet at room temperature, the obtained DNA was resuspended with 50 μL of Tris-HCl (50 mM, pH 8.0). The effectiveness of the extraction was evaluated after performing runs on the electrophoresis cell, using 1% agarose gel stained with ethidium bromide, and visualizing the gel at the UV transilluminator [35–37]. The DNA integrity was checked spectrophotometrically and by PCR amplification. Briefly, a 500 bp fragment of the 16S rRNA gene was PCR amplified with MyTaq DNA Polymerase (Bioline) by using total DNA from each sample as a template and the oligo Ribo-For (5′-AGTTTGATCCTGGCTCAG-3′) and Ribo-rev (5′-ACCTACGTATTACCGCGGC-3′) as primers. PCR conditions were: 5 min at 95 °C, followed by 30 cycles of 95 °C for 30 s, 50 °C for 30 s, 72 °C for 30 s, concluding with an extension at 72 °C for 5 min. The PCR products were analyzed as previously reported [38,39].

2.4. 16S rRNA Gene Sequencing

The obtained DNA was sequenced at the Integrated Microbiome Resource (IMR, [40]) using primers targeting the V4-V5 of the 16S rRNA (515FB = GTGYCAGCMGCCGCGGTAA 926R = CCGYCAATTYMTTTRAGTTT), using Illumina MiSeq technology.

2.5. Biochemical Measurements

Particulate Organic Carbon (POC) and Particulate Nitrogen (PN) were analyzed as previously reported [41]. Briefly, filters were exposed to fumes of HCl for 4 h to remove inorganic carbon [41]. After drying (60 °C), filters were placed into tin capsules and analyzed using a Carlo Erba Mod. 1110 CHN Elemental Analyzer (dynamic flash combustion). Cyclohexanone 2–4-dinitrophenyl hydrazone (purchased from Sigma-Aldrich, Steinheim,

Germany) was used as a reference standard. For the determination of fractionated Chlorophyll, a protocol of serial filtration was followed, as reported by Mangoni et al. [42]. Frozen filters were processed in Italy for the determination of Chl a and phaeopigments (phaeo) content, using a solution of 90% acetone according to [43,44], with a spectrofluorometer (Shimadzu, Mod. RF–6000; Shimadzu Corporation-Japan) checked daily with a Chl a standard solution (Sigma-Aldrich). Particulate carbohydrate and protein concentrations were determined following [45,46], respectively. The method for carbohydrate determination is based on the reaction of the carbohydrates to phenol (5% in water solution) in an acid medium (sulfuric acid). For protein determination, copper sulfate pentahydrate was added to the samples, leading to the bond of Cu to amino acids. The Folin–Ciocalteu's phenol reagent completes the reaction with the development of a blue coloration. A Jasco V-530 spectrophotometer was calibrated with D-glucose solutions for carbohydrates (absorbance 490 nm) and with bovine serum albumin solutions for proteins (absorbance 650 nm). All materials were purchased from Sigma-Aldrich (Steinheim, Germany).

2.6. Bioinformatics and Statistical Analyses

Raw reads received from the sequencing center were processed using the DADA2 package [47]. Primers and adapters were trimmed, followed by a quality profile step, where only sequences with a call quality for each base between 20 and 40, were kept for further analysis. Amplicon sequence variants (ASVs) were estimated through the error profile and assigned taxonomy with the SILVA database (release 138) [48]. The resulting taxonomic assignments, in combination with variant abundance tables, were used to create a phyloseq object with the phyloseq package [49], as previously described in [38]. Subsequently, sequences related to Chloroplasts, Mitochondria, and Eukaryotes, as well as groups related to human pathogens and common DNA extraction contaminants [50], were removed from the dataset. The remaining reads represented 53.4% of the original raw reads with 535 ASVs. Alpha diversity was investigated using the Observed, Shannon, and Chao1 diversity indexes, while beta diversity was investigated using the Jaccard diversity index. Additionally, correlations between measured environmental variables and the resulting ordination were achieved using environmental fitting (env_fit function in vegan). The statistical analysis conducted, as well as data processing and visualization, was carried out in R software, version 4.1.2 [51], using the vegan [52] and ggplot2 [53] packages. The sequences analyzed in the present study are publicly available through the European Nucleotide Archive (ENA) with a bioproject accession number PRJEB45048. A complete R script describing the analysis can be found in the GitHub repository https://github.com/giovannellilab/Cordone_et_al_Southern_Ocean_microbial_diversity, accessed on 30 January 2023 and released with Zenodo with https://doi.org/10.5281/zenodo.7584581, accessed on 30 January 2023.

3. Results

3.1. Environmental and Biogeochemical Parameters

The coordinates of the sampled points and the respective environmental parameters, such as sea surface temperature (SST), sea surface temperature anomaly (SSTA), sea surface salinity (SSS), current speed (CS), and wind speed (WS), are listed in Table 1. There is a steep reduction in sea surface temperature when moving from New Zealand (7.9 °C) to the Antarctic region (−1.8 °C), showing a clear trend with the changes in latitude (Figure S1a). As for the sea surface salinity, it decreases moving towards the Antarctic region and then increases again once within the Ross Sea area (Figure S1b).

Table 1. Coordinates and environmental parameters of sequenced stations. SST—Sea Surface Temperature; SSTA—Sea Surface Temperature Anomaly; SSS—Sea Surface Salinity; CS—Current Speed; WS—Wind Speed; NSAF—North Sub-Antarctic Front; SSAF—South Sub-Antarctic Front; PF—Polar Front; SACCF—Southern Antarctic Circumpolar Current Front; RSCS—Ross Sea Continental shelf; STF—Sub-Tropical Front; SAF—Sub-Antarctic Front; sBdy—Southern Boundary Front.

Station	Latitude [°N]	Longitude [°E]	SST [°C]	SSTA [°C]	SSS [PSU]	cs [m/s]	ws [km/h]	Antarctic Current	Oceanic Front
5	−51.8092	175.0061	7.9	−0.8	34.4	0.32	62	NSAF	STF
6	−52.3100	175.0749	7.5	−0.7	34.3	0.29	14	NSAF	STF
7	−52.7343	175.0708	7.5	−0.7	34.3	0.24	15	NSAF	STF
10	−56.1723	175.8037	6.9	0	33.9	0.1	26	SSAF	STF
12	−58.8349	176.6923	4.9	−0.3	34	0.06	37	SSAF	SAF
15	−64.2124	178.3410	1.7	0.6	33.8	0.24	39	PF	PF
16	−65.9702	178.5408	−0.4	0	33.6	0.01	30	SACCF	SACCF
17	−67.4229	178.9109	−1.3	−0.3	33	0.01	13	SACCF	sBdy
18	−68.3780	179.7789	−1.6	−0.5	33.2	0.02	16	SACCF	sBdy
19	−69.7571	177.9027	−1.8	−0.6	33.8	0.03	17	SACCF	sBdy
20	−70.2680	176.2240	−1.8	−0.7	34.3	0.03	7	SACCF	sBdy
23	−74.0641	178.1007	−1.8	−1.5	34.5	0.05	17	RSCS	RSCS
24	−74.4742	172.4104	−1.8	−1.7	35.2	0.03	23	RSCS	RSCS

The biogeochemical parameters determined for all sequenced stations are shown in Table 2. Among the biogeochemical parameters analyzed, only the C fraction of dissolved organic matter (C-DOM), total carbohydrates (cho_tot) and particulate nitrogen (PN) showed significant correlations with the geographical location (latitude) of the sequenced stations. As expected, Particulate Organic Carbon (POC) was significantly correlated to PN and total protein content (pr_tot), while pr_tot was also significantly correlated to surface primary productivity (spp), and pn was also correlated to dissolved organic carbon (C-DOM) (Table S1).

Table 2. Biogeochemical parameters determined for the sequenced stations. spp—surface primary productivity; prt_tot—total proteins; cho_tot—total carbohydrates; PN—Particulate Nitrogen; POC—Particulate Organic Carbon; C-DOM—C fraction of Dissolved Organic Matter; Chl-a—Chlorophyll-a; Micro-chla—Microfraction of chlorophyll-a; Nano-chla—Nanofraction of chlorophyll-a; Pico-chla—Picofraction of chlorophyll-a.

Station	ssp [mg C/m^2 Day]	prt_tot [µg/L]	cho_tot [µg/L]	PN [µg/L]	POC [µg/L]	C-DOM [µg/L]	Chl-a [µg/L]	Micro-Chla [%]	Nano-Chla [%]	Pico-Chla [%]
5	398.14	66.84	41.60	9.00	69.77	11.11	0.32	12.98	30.81	56.20
6	323.15	56.58	35.98	6.71	57.22	8.12	0.41	1.63	54.14	44.23
7	290.04	48.64	33.71	4.91	52.76	8.70	0.58	12.66	40.06	47.28
10	282.89	46.76	18.05	7.38	46.41	8.49	0.69	14.22	64.64	21.14
12	265.15	56.56	34.37	14.87	90.08	11.72	1.44	15.28	56.38	28.33
15	211.15	56.81	58.67	17.94	97.71	16.74	1.56	23.13	62.66	14.21
16	275.82	98.02	63.21	28.90	216.08	17.41	1.06	24.51	56.68	18.81
17	285.45	49.86	59.06	16.59	79.81	14.90	0.55	31.24	51.44	17.32
18	249.01	53.63	54.32	22.27	106.55	12.12	1.44	21.42	55.29	23.29
19	244.42	36.57	43.70	10.49	50.87	10.08	0.63	19.80	51.32	28.88
20	103.30	23.87	31.64	8.92	45.32	10.25	0.55	14.85	54.89	30.26
23	475.60	71.14	64.82	20.80	116.38	18.08	0.99	20.91	53.31	25.78
24	943.99	124.22	34.73	54.01	274.66	19.13	2.47	3.15	49.46	47.39

3.2. Diversity of Bacterial Communities

Bacterial diversity along the transect New Zealand–Ross Sea was evaluated using the 16S rRNA gene sequence as reported in the materials and methods section. A total of

130,906 reads were obtained after quality check and data filtering and were used to identify 535 unique ASVs. The number of reads, ASVs, phyla, classes, orders, families, and genera per station has been reported in Table S2.

The rarefaction curves for the total reads–ASVs relationship were created to calculate the coverage of retrieved ASVs over the predicted ASVs obtained using the value of the Chao1 alpha diversity index (Figure S2). The coverages for all the sampled stations (Table S3) show that the sequencing depth reached in our study is adequate to analyze and characterize the bacterioplankton community structure crossing the ACCF, ranging from 83% and 96%. The alpha diversity evidenced a decreasing trend from the stations belonging to STF until SACCF, which sharply increased towards the southernmost part of the transect (Figure S3, Table S3).

As shown in Figure 2, in the station belonging to STF (stations 5, 6, 7, and 10), we mainly found Proteobacteria (recently reclassified as Pseudomonadota), Bacteroidota, and Cyanobacteria with an average of 44.78%, 40.94%, and 9.64% of reads assigned, respectively. Station 12, present on the SAF, had a similar distribution, with Proteobacteria (67.43%) and Bacteroidota (27.36%) being the two most abundant phyla, followed by Myxococcota (0.35%). Reads from the only station influenced by the PF (station 15) were also assigned to Proteobacteria (58.85%), Bacteroidota (38.92%), and Cyanobacteria (0.57%). In the case of station 16, associated with the SACCF, 57.16% of the reads were assigned to Bacteroidota, while 41.10% corresponded to Proteobacteria. In stations 17, 18, 19, and 20, all influenced by the SBDY, we mainly found Proteobacteria (50.90%) and Bacteroidota (47.84%), with Verrucomicrobiota having assigned just 0.12% of the reads. Finally, the two stations (23 and 24) belonging to the RSCS were also characterized by a predominance of Bacteroidota (49.57%) and Proteobacteria (46.69%), with nearly 0.1% of the reads (0.06%) assigned to the SAR324 clade (Marine group B).

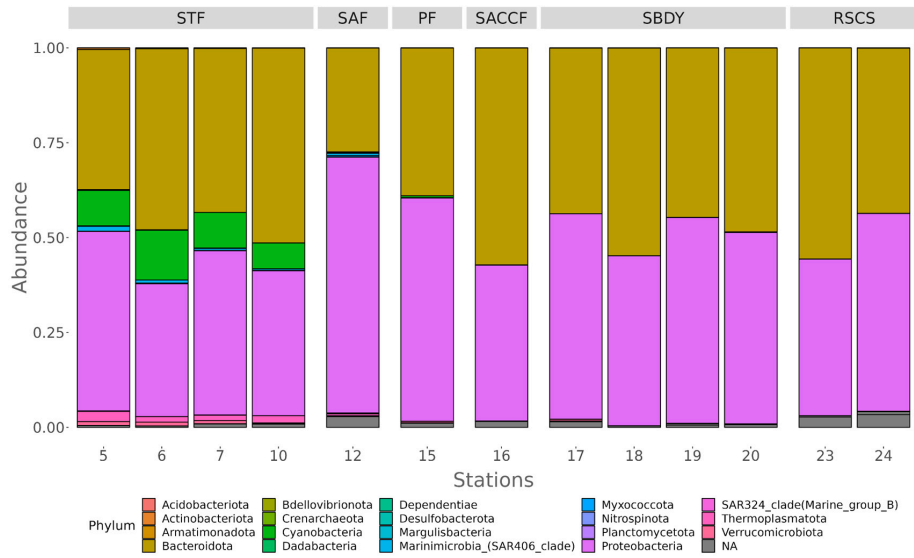

Figure 2. Diversity at the phylum level for all the stations considered. On top of the figure are the fronts to which each sampling station can be assigned. STF—South Tropical Front; SAF—Sub-Antarctic Front; PF—Polar Front; SACCF—Southern ACC Front; SBDY—Southern Boundary Front; RSCS—Ross Sea Continental Shelf.

Within the Bacteroidota, the Bacteroidia class was the most abundant among the stations influenced by the STF, SACCF, and RSCS, with average reads assigned of 36.91%, 57.16%, and 55.64%, respectively, while the stations influenced by the SAF, SPF, and SBDY,

had an average of reads assigned equal to 27.36%, 38.92%, and 33.80%, respectively. At the order level, Flavobacteriales represent the most abundant order, similarly distributed in all stations (Figure 3A), with the exception of station 12 (influenced by the SAF front), with an average of reads assigned of 44.43%, 38.66%, 55.06%, 46.59%, 45.91%, and 24.36% to the stations influenced by STF, SPF, SACCF, SBDY, RSCS, and SAF, respectively.

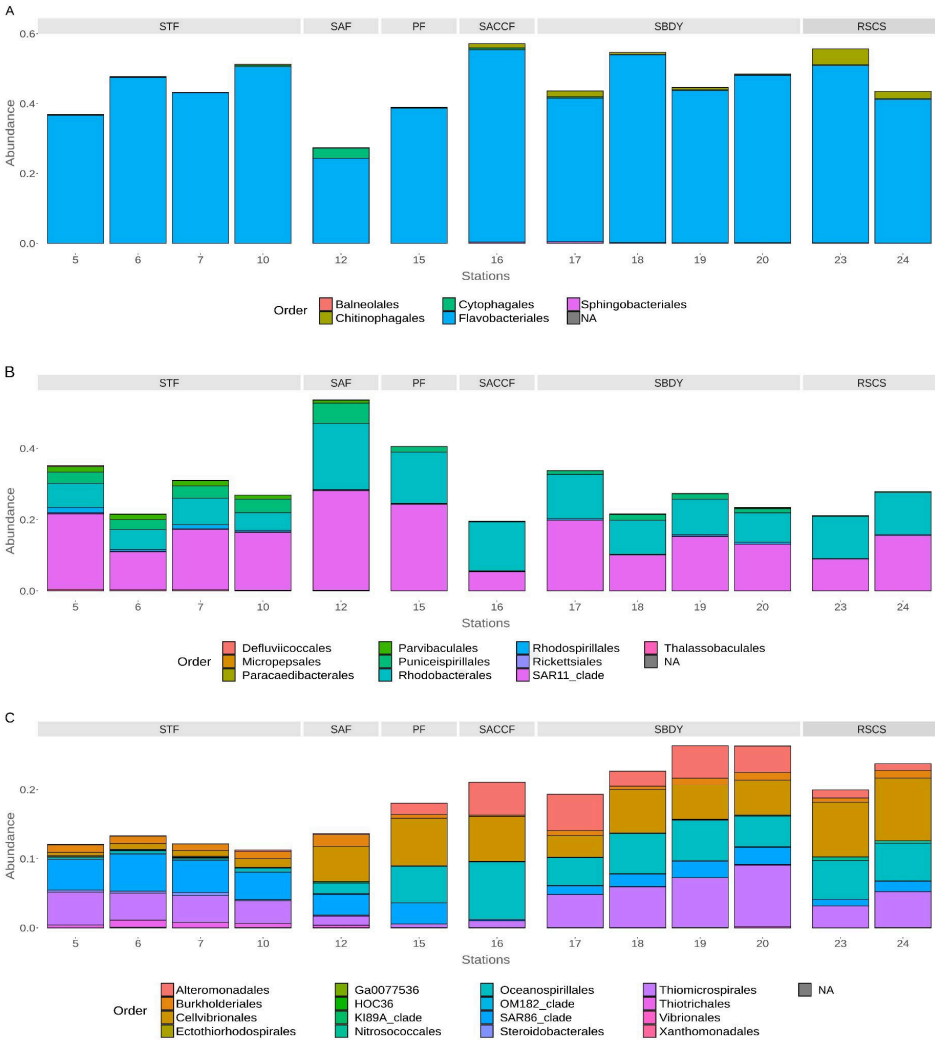

Figure 3. Order level distribution of the 16S rRNA diversity within the classes Bacteroidia (**A**), Alphaproteobacteria (**B**) and Gammaproteobacteria (**C**) for the stations.

A different distribution is observed for the Cytophagales and Chitinophagales orders, with the Cytophagales mainly detected in station 12 (2.86%) localized in the Sub-Antarctic front, and the Chitinophagales mainly present in the southern area of the transect—on average 3.31% for stations within the RSCS. Among the Flavobacteriales, different genera can be distinguished. The stations in the south are dominated by sequences assigned to the genera *Polaribacter* (40.78% in station 16 and 26% in the RSCS stations) and *Aurantivirga* (5.78% in the RSCS stations), while the stations in the north, influenced by STF, SAF, and

SPF, are dominated by sequences assigned to the genera *Formosa*, with an average read assigned equal to 4%, 4.20%, and 2.12%, respectively. The NS2b marine group is present in all the stations analyzed (Figure S4).

Within the Proteobacteria, most sequences are affiliated with the classes Alphaproteobacteria and Gammaproteobacteria. Among Alphaproteobacteria, SAR11 clade (STF = 16.25%, SAF = 27.95%, PF = 24.27%, SACCF = 5.39%, SBDY = 14.56%, RSCS = 12.26%) and Rhodobacterales (STF = 6.22%, SAF = 18.54%, PF = 14.42%, SACCF = 13.78%, SBDY = 10.05%, RSCS = 11.8%) represent the most abundant orders in all the stations, whereas Puniceispirillales are mainly present in the northern part of the transect, with a maximum of 5.68% in station 12 (SAF front) and a minimum of 1.55% in the PF (Figure 3B). Gammaproteobacteria are mainly represented by the orders SAR86 clade (STF = 4.63%, SAF = 2.99%, PF = 3.06%, SACCF = 0.20%, SBDY = 1.99%, RSCS = 1.25%) more abundant in the northernmost part of the transect, and Cellvibionales (STF = 0.85%, SAF = 5.09%, PF = 6.88%, SACCF = 6.51%, SBDY = 4.93%, RSCS = 8.59%), which instead are mainly distributed in the southernmost part. The order Thiomicrorpirales is detected in all the stations, with average reads assigned varying from 0.51% in station 15 (within PF) to 6.70% for stations 17, 18, 19, and 20 (SBDY). Stations within the STF had an average of 3.96%, while station 12 (SAF) had 1.33%, station 16 (SACCF) 1.01%, and stations 23 and 24 (RSCS) had an average of 4.18%. The orders Oceanospirillales and Alteromonadales are mainly detected in the southernmost stations (Figure 3C), with the highest percentage of average reads assigned to Oceanospirillales (8.28%) to the station within the SACCF (station 16) and the lowest (0.39%) to the stations belonging to the STF (stations 5, 6, 7 and 10); while Alteromonadales where mostly assigned to the reads from the SACCF and the SBDY stations (4.87% and 4.03%, respectively) (Figure 3C) with stations from the STF, SAF, PF, and RSCS having lower averages of assigned reads (0.09%, 0.12%, 1.64%, and 1.07%, respectively).

As mentioned before, sequences belonging to the phylum Cyanobacteria were detected mainly in the four northern stations of the transect (9.6% relative abundance), all influenced by the STF. In particular, within this phylum, most sequences are affiliated with the Synechococcales order (Figure 4).

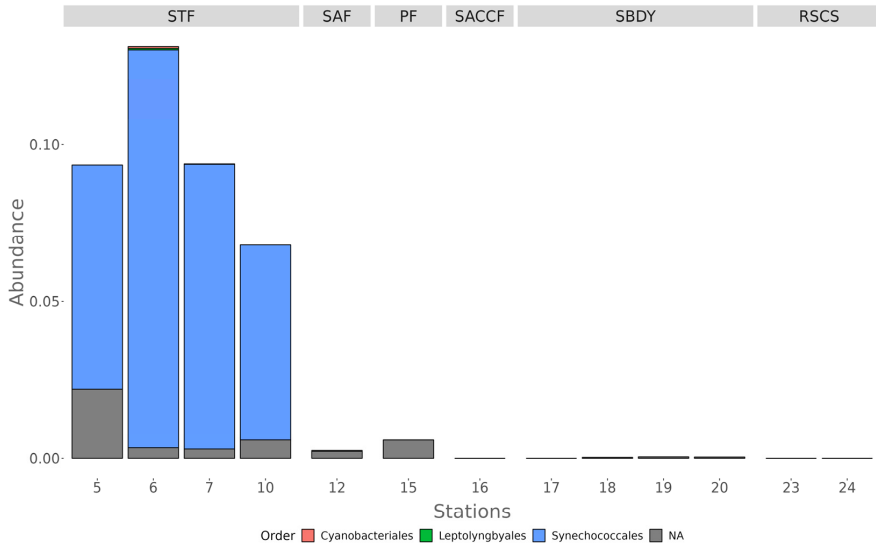

Figure 4. Order level distribution of the 16S rRNA diversity within the phylum Cyanobacteria.

To explain the bacterial community structure across the different fronts, we performed a principal coordinate analysis (PCoA) based on the relative abundance of the assigned

ASVs to each station and generated using a weighted Jaccard similarity distance. The first two axes of the PCoA were able to explain about 63% of the variance. As shown in Figure 5, there is a "U" pattern along Axis 1, also known as a "horseshoe" effect. This pattern has been associated with species turnover along an environmental gradient [54]. The site distribution follows a latitudinal trend, from north to south, with the only exception of station 16. The ASVs that mainly contribute to the distribution of our samples within the PCoA ordination are shown in Figure 6. Bacteroidota and Proteobacteria are distributed within the whole ordination, together with Cyanobacteria, Verrucomicrobia and Actinobacteriota, while the left part of the ordination is more characterized by Marinimicrobia, Thermoplasmatota, and Bdellovibrionota.

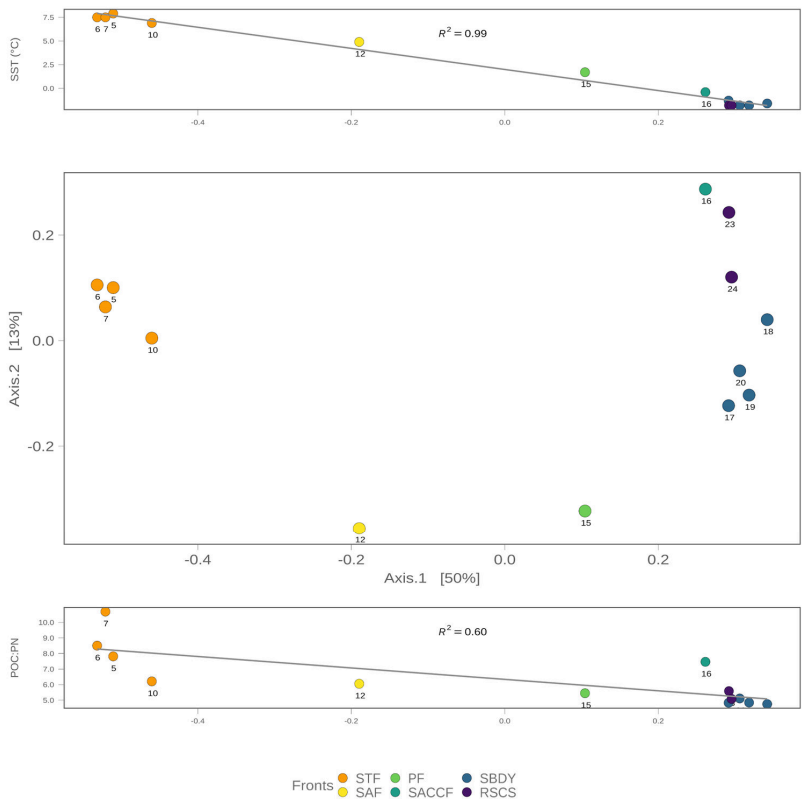

Figure 5. Principal Coordinate Analysis using a weighted Jaccard similarity distance illustrating the shifts in the community structure according to Southern Ocean waterfronts. SST—Sea Surface Temperature; POC:PN—Ratio between Particulate Organic Carbon and Particulate Nitrogen; STF—Sub-Tropical Front; SAF: Sub-Antarctic Front; PF—Polar Front; SACCF—Southern Antarctic Circumpolar Current Front; SBDY—Southern Boundary Front; RSCS—Ross Sea Continental Shelf. The amount of variance explained by each axis is reported within square brackets.

To further investigate the differences between the sampling sites and to discern the influence of the biogeochemical parameters on the community structure, we performed a principal component analysis (PCA). The PCA was able to explain 77.2% of the total variance associated with our community. A bi-plot of the PCA obtained is shown in Figure 7 and confirms the presence of a gradient between the different sites. In particular, samples associated with the STF (northern sampling sites) are influenced by sea surface temperature (sst), latitude (lat), and the chlorophyll-a picofraction (pico_chla). On the other hand,

samples associated with the most southern fronts (PF, SBDY, and RSCS) seem to be more influenced by variables such as the carbon fraction of dissolved organic matter (C-DOM) and total carbohydrates (cho_tot). Only the sample from station 24 and associated with the RSCS is more influenced by parameters like particulate nitrogen (PN), total protein content (prt_tot), sea primary productivity (spp), and particulate organic carbon (POC) contents of the seawater.

Figure 6. Phylum level load of the ASVs that mainly contribute to the distribution of the sampled stations within the PCoA ordination.

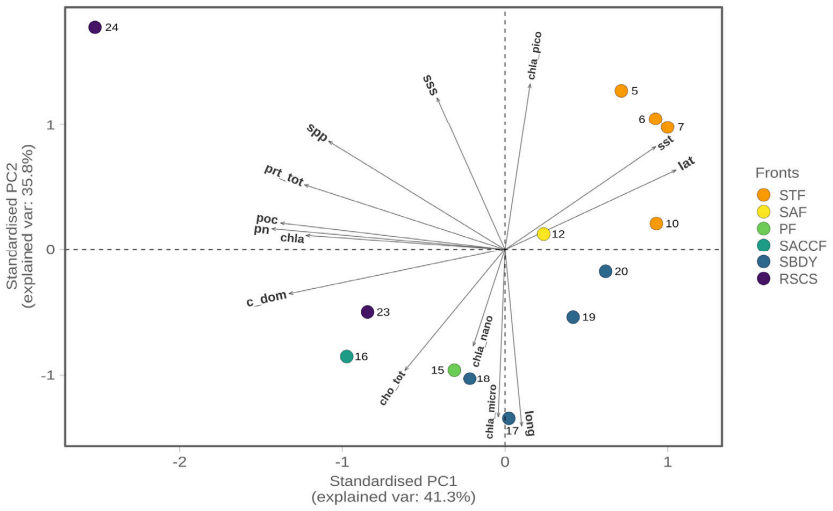

Figure 7. Principal Component Analysis biplot with each individual sample colored by front. STF—Sub=Tropical Front; SAF—Sub-Antarctic Front; PF—Polar Front; SACCF—Southern Antarctic Circumpolar Current Front; SBDY—Southern Boundary Front; RSCS—Ross Sea Continental Shelf. Lat—latitude; sst—sea surface temperature; sss—sea surface salinity; spp—surface primary productivity; prt_tot—total proteins; poc—particulate organic carbon; cho_tot—total carbohydrates; pn—particulate nitrogen; c-dom—carbon fraction of dissolved organic matter; chl-a—chlorophyll-a; chla-micro—microfraction of chlorophyll-a; chla-nano—nanofraction of chlorophyll-a; chla-pico—picofraction of chlorophyll-a.

4. Discussion

The Southern Ocean is the least studied oceanic region of the world, mainly as a consequence of its harsh climate and remoteness, making systematic sampling campaigns both difficult and expensive to conduct [5,55]. Water masses characterizing the Southern Ocean have different physicochemical properties, particularly surface temperature and salinity, which allow for their division into fronts [5,8,9]. These differences have led researchers to hypothesize the establishment of a zonation within the distribution of the microbial communities, with fronts playing a key role in structuring the microbial ecosystem. Our results supported this idea as the PCoA analysis shows a horseshoe pattern usually associated with species turnover over environmental gradients. The environmental gradients recovered by the PCA analysis follow the same general trend as the PCoA, suggesting a tight coupling between environmental variations across the transect and species turnover. In fact, stations that fall under the influence of the same front were clustered together and influenced by the same set of environmental variables, with sea surface temperature being among the strongest drivers and having a significant correlation with the PCoA axis 1 ($p < 0.005$).

We also observed a significant change in the phyla present as we moved further south and away from the influence of the SubTropical Front (STF), where warmer waters favor the presence of Cyanobacteria alongside members of the Proteobacteria and Bacteroidota phyla. Proteobacteria are mainly represented by Alphaproteobacteria and Gammaproteobacteria, while within Bacteroidota, the Flavobacteriales order was detected in all the stations with higher abundance. The presence of these phyla is consistent with previously reported results [6,56,57]. Additionally, the stations under the influence of the STF current are the only ones where the Cyanobacteria phylum is present, with an average abundance of 9.6% in stations 5, 6, 7, and 10

Among Alphaproteobacteria, SAR11 is thought to be the dominant bacterial group in Southern Ocean waters regardless of depth and distance from shore; however, it appears to be more abundant in the epipelagic zone [6]. Our results are in agreement with the biogeographic partitioning reported by several authors [6,58], where the abundance of SAR11 is higher near the Sub-Artic Front (SAF) and the Polar Front (PF) and decreases towards the Antarctic zones. According to Wilkins and coauthors [6], this behavior could be a consequence of the oligotrophic nature of SAR11, which gives it a competitive advantage in a High Nutrient–Low Chlorophyll (HNLC) environment compared to the Antarctic zone where phytoplankton blooms increase the concentration of high molecular weight dissolved organic matter and organic particulates. Among Gammaproteobacteria, the SAR86 clade follows the same trend as SAR11, as its presence is generally detected in HNLC waters [59], while Alteromonadales and Oceanospirillales, comprising heterotrophic cold-adapted bacteria, were mainly detected at the stations between the Southern ACC front and the Ross Sea continental shelf, where the concentration of particulate organic carbon was higher. This result is consistent with other reports suggesting that these taxa are major players in the POC remineralization process [60]. Bacteroidota were mainly represented by members of the Flavobacteriales order, which includes members capable of degrading High Molecular Weight (HMW) DOM and whose presence is generally associated with the phytoplankton blooms in such an area [6,61,62]. In particular, within Flavobacteriales, members belonging to *Polaribacter* and *Formosa* genus showed an interesting trend with an increase in the relative abundance of ASVs assigned to *Polaribacter* when approaching the RSCS and a concomitant decrease in the relative abundance of ASVs assigned to the *Formosa* genus. Abell and Bowman [63] hinted at a possible influence of water temperature over the diversity of the Flavobacteria clades in the Southern Ocean, showing that samples from the temperate zone and the Sub-Antarctic zone had relatively lower Flavobacteria diversity than samples from the Polar Front zone and the Antarctic zone. We also observed that there was a higher relative abundance of Flavobacteria in stations where the Alphaproteobacteria clade was at its lowest abundance. According to the literature [63–67], this trend could be a consequence of the differential degradation of organic matter capacity exhibited

by both groups of organisms, where Flavobacteria are able to produce proteins used to degrade complex organic substrates while Alphaproteobacteria SAR11 have the capability of synthesizing high-affinity uptake systems that allow the utilization of simpler byproducts of algal polymer degradation (i.e., sugars, acetate, ammonia), as metaproteomic assessments showed [67].

Recent evidence has shown an increase in cyanobacterial communities in response to increasing seawater temperatures [68]. Our results further support this trend since we are detecting Cyanobacteria only in the stations with higher temperatures and under the influence of the STF. Given the increase in Antarctic seawater temperatures [69], we could expect a future species turnover in the microbial communities inhabiting the different Antarctic current fronts, similar to what we found in this study. However, the consequences of this turnover in the overall community structure and trophic levels are still not known.

Taken together, our results show a clear ecological succession of bacterial taxa linked to the oceanic fronts crossing the Southern Ocean during the austral summer of 2017 and suggest a key role of microdiversity in separating the different water masses. Further metagenomic analysis, as well as a temporal re-sampling of the same area (seasonally or annually), will better clarify the specific functions of the dominant taxa living there.

Supplementary Materials: The following supporting information can be downloaded at: https://www.mdpi.com/article/10.3390/microorganisms11030702/s1, Figure S1: Trend of sea surface temperature (**a**) and salinity (**b**) against the latitude of the collected samples. Each individual sample is colored by front; Figure S2: Rarefaction curves based on the numbers of reads and ASVs for all the sampled stations; Figure S3: Alpha diversity metrics across the ACCF using the Observed and Shannon Indexes; Figure S4: Genus-level diversity of Flavobacteriales along the transect; Table S1: Pearson's correlation table among the environmental variables; Table S2: Numbers of total reads, retrieved ASVs and annotated taxa in each sample and the corresponding overall total numbers; Table S3: Alpha diversity indices (Observed, Shannon, Chao1) for the ASVs for all the sampled stations and coverage of retrieved ASVs over the predicted ASVs obtained using the value of the Chao1 alpha diversity index.

Author Contributions: Conceptualization, A.C., O.M. and D.G.; methodology, M.S. (Matteo Selci), A.C., C.M., F.B. and R.C.; software, M.S. (Maria Saggiomo), D.C. and L.D.I.; validation, A.B., A.R., D.B., M.C. (Monica Correggia) and B.B.; formal analysis, M.S. (Matteo Selci), A.C., A.B., A.R., D.B., M.C. (Martina Cascone), M.C. (Monica Correggia), F.M., D.C. and B.B.; investigation, M.S. (Matteo Selci), A.C., O.M. and D.G.; data curation, L.D.I., D.B., A.B., D.C., A.R. and B.B.; writing—original draft preparation, M.S. (Matteo Selci), A.C., A.B., A.R., D.B., M.C. (Martina Cascone), M.C. (Monica Correggia), R.C., F.M., L.T., M.S., F.B., C.M., O.M., D.C., B.B. and D.G. writing—review and editing, A.C., M.S. (Maria Saggiomo), C.M., O.M. and D.G.; visualization, M.S. (Matteo Selci) and A.C.; supervision, O.M. and D.G. All authors have read and agreed to the published version of the manuscript.

Funding: This research was funded by Ministero dell'Istruzione, dell'Università e della Ricerca (MUR), Italy, grant number PNRA16_00239.

Data Availability Statement: The sequences analyzed in the present study are publicly available through the European Nucleotide Archive (ENA) with bioproject accession number PRJEB45048. A complete R script describing the analysis can be found in the GitHub repository https://github.com/giovannellilab/Cordone_et_al_Southern_Ocean_microbial_diversity, accessed on 30 January 2023 and released with Zenodo with https://doi.org/10.5281/zenodo.7584581, accessed on 30 January 2023.

Acknowledgments: We acknowledge the Italian Antarctic National Program (PNRA) and the scientific personnel and crew of the research vessel Italica for logistical support.

Conflicts of Interest: The authors declare no conflict of interest. The funders had no role in the design of the study; in the collection, analyses, or interpretation of data; in the writing of the manuscript; or in the decision to publish the results.

References

1. Azam, F.; Fenchel, T.; Field, J.G.; Gray, J.S.; Meyer-Reil, L.A.; Thingstad, F. The Ecological Role of Water-Column Microbes in the Sea. *Mar. Ecol. Prog. Ser.* **1983**, *10*, 257–263. [CrossRef]
2. Cho, B.; Azam, F. Biogeochemical significance of bacterial biomass in the ocean's euphotic zone. *Mar. Ecol. Prog. Ser. Oldendorf* **1990**, *63*, 253–259. [CrossRef]
3. Field, C.B.; Behrenfeld, M.J.; Randerson, J.T.; Falkowski, P. Primary Production of the Biosphere: Integrating Terrestrial and Oceanic Components. *Science* **1998**, *281*, 237–240. [CrossRef]
4. Huntley, M.E.; Lopez, M.D.; Karl, D.M. Top Predators in the Southern Ocean: A Major Leak in the Biological Carbon Pump. *Science* **1991**, *253*, 64–66. [CrossRef] [PubMed]
5. Chapman, C.C.; Lea, M.-A.; Meyer, A.; Sallée, J.-B.; Hindell, M. Defining Southern Ocean fronts and their influence on biological and physical processes in a changing climate. *Nat. Clim. Chang.* **2020**, *10*, 209–219. [CrossRef]
6. Wilkins, D.; Lauro, F.M.; Williams, T.J.; DeMaere, M.; Brown, M.V.; Hoffman, J.M.; Andrews-Pfannkoch, C.; McQuaid, J.; Riddle, M.J.; Rintoul, S.R.; et al. Biogeographic partitioning of Southern Ocean microorganisms revealed by metagenomics. *Environ. Microbiol.* **2013**, *15*, 1318–1333. [CrossRef]
7. Park, Y.; Park, T.; Kim, T.; Lee, S.; Hong, C.; Rio, M.; Pujol, M.; Ballarotta, M.; Durand, I.; Provost, C. Observations of the Antarctic Circumpolar Current over the Udintsev Fracture Zone, the Narrowest Choke Point in the Southern Ocean. *J. Geophys. Res. Oceans* **2019**, *124*, 4511–4528. [CrossRef]
8. Orsi, A.H.; Whitworth, T., III; Nowlin, W.D., Jr. On the Meridional Extent and Fronts of the Antarctic Circumpolar Current. *Deep Sea Res. Part Oceanogr. Res. Pap.* **1995**, *42*, 641–673. [CrossRef]
9. Orsi, A.H.; Wiederwohl, C.L. A recount of Ross Sea waters. *Deep. Sea Res. Part II Top. Stud. Oceanogr.* **2009**, *56*, 778–795. [CrossRef]
10. Graham, R.M.; De Boer, A.M. The Dynamical Subtropical Front. *J. Geophys. Res. Oceans* **2013**, *118*, 5676–5685. [CrossRef]
11. Jacques, G. Dynamics of nutrients and phytoplankton, and fluxes of carbon, nitrogen and silicon in the Antarctic Ocean. *Polar Biol.* **1992**, *12*, 149–162. [CrossRef]
12. Boyd, P.; Robinson, C.; Savidge, G.; Williams, P. Water column and sea-ice primary production during Austral spring in the Bellingshausen Sea. *Deep. Sea Res. Part II Top. Stud. Oceanogr.* **1995**, *42*, 1177–1200. [CrossRef]
13. Van Leeuwe, M.; Scharek, R.; De Baar, H.; De Jong, J.; Goeyens, L. Iron enrichment experiments in the Southern Ocean: Physiological responses of plankton communities. *Deep. Sea Res. Part II Top. Stud. Oceanogr.* **1997**, *44*, 189–207. [CrossRef]
14. van Leeuwe, M.A.; de Baar, H.J.W.; Veldhuis, M.J.W. Pigment distribution in the Pacific region of the Southern Ocean (autumn 1995). *Polar Biol.* **1998**, *19*, 348–353. [CrossRef]
15. De Baar, H.J.W.; de Jong, J.; Bakker, D.; Löscher, B.M.; Veth, C.; Bathmann, U.; Smetacek, V. Importance of iron for plankton blooms and carbon dioxide drawdown in the Southern Ocean. *Nature* **1995**, *373*, 412–415. [CrossRef]
16. Abraham, E.R.; Law, C.S.; Boyd, P.W.; Lavender, S.J.; Maldonado, M.T.; Bowie, A.R. Importance of stirring in the development of an iron-fertilized phytoplankton bloom. *Nature* **2000**, *407*, 727–730. [CrossRef] [PubMed]
17. Ward, P.; Whitehouse, M.; Meredith, M.; Murphy, E.; Shreeve, R.; Korb, R.; Watkins, J.; Thorpe, S.; Woodd-Walker, R.; Brierley, A.; et al. The Southern Antarctic Circumpolar Current Front: Physical and biological coupling at South Georgia. *Deep. Sea Res. Part I Oceanogr. Res. Pap.* **2002**, *49*, 2183–2202. [CrossRef]
18. Green, J.; Bohannan, B.J. Spatial scaling of microbial biodiversity. *Trends Ecol. Evol.* **2006**, *21*, 501–507. [CrossRef]
19. Palumbi, S.R. Genetic Divergence, Reproductive Isolation, and Marine Speciation. *Annu. Rev. Ecol. Syst.* **1994**, *25*, 547–572. [CrossRef]
20. Belkin, I.M.; Gordon, A.L. Southern Ocean fronts from the Greenwich meridian to Tasmania. *J. Geophys. Res. Oceans* **1996**, *101*, 3675–3696. [CrossRef]
21. Ikeda, Y.; Siedler, G.; Zwierz, M. On the variability of Southern Ocean front locations between southern Brazil and the Antarctic Peninsula. *J. Geophys. Res. Ocean.* **1989**, *94*, 4757. [CrossRef]
22. Thornhill, D.J.; Mahon, A.R.; Norenburg, J.L.; Halanych, K.M. Open-ocean barriers to dispersal: A test case with the Antarctic Polar Front and the ribbon worm *Parborlasia corrugatus* (Nemertea: Lineidae). *Mol. Ecol.* **2008**, *17*, 5104–5117. [CrossRef] [PubMed]
23. Baltar, F.; Currie, K.; Stuck, E.; Roosa, S.; Morales, S.E. Oceanic fronts: Transition zones for bacterioplankton community composition. *Environ. Microbiol. Rep.* **2016**, *8*, 132–138. [CrossRef] [PubMed]
24. Hunter, R.L.; Halanych, K.M. Evaluating Connectivity in the Brooding Brittle Star Astrotoma agassizii across the Drake Passage in the Southern Ocean. *J. Hered.* **2008**, *99*, 137–148. [CrossRef]
25. Shaw, P.; Arkhipkin, A.I.; Al-Khairulla, H. Genetic structuring of Patagonian toothfish populations in the Southwest Atlantic Ocean: The effect of the Antarctic Polar Front and deep-water troughs as barriers to genetic exchange. *Mol. Ecol.* **2004**, *13*, 3293–3303. [CrossRef]
26. Milici, M.; Vital, M.; Tomasch, J.; Badewien, T.H.; Giebel, H.-A.; Plumeier, I.; Wang, H.; Pieper, D.H.; Wagner-Döbler, I.; Simon, M. Diversity and Community Composition of Particle-associated and Free-living Bacteria in Mesopelagic and Bathypelagic Southern Ocean Water Masses: Evidence of Dispersal Limitation in the Bransfield Strait. *Limnol. Oceanogr.* **2017**, *62*, 1080–1095. [CrossRef]
27. Mendes, C.R.B.; Kerr, R.; Tavano, V.M.; Cavalheiro, F.A.; Garcia, C.A.E.; Dessai, D.R.G.; Anilkumar, N. Cross-front phytoplankton pigments and chemotaxonomic groups in the Indian sector of the Southern Ocean. *Deep. Sea Res. Part II Top. Stud. Oceanogr.* **2015**, *118*, 221–232. [CrossRef]

28. Studying the Biodiversity of Marine Plankton | Tara Oceans. Available online: https://fondationtaraocean.org/en/expedition/tara-oceans/ (accessed on 20 February 2023).
29. Sunagawa, S.; Coelho, L.P.; Chaffron, S.; Kultima, J.R.; Labadie, K.; Salazar, G.; Djahanschiri, B.; Zeller, G.; Mende, D.R.; Alberti, A.; et al. Structure and function of the global ocean microbiome. *Science* **2015**, *348*, 1261359. [CrossRef]
30. Ocean Productivity: Online Vgpm Data. Available online: http://orca.science.oregonstate.edu/1080.by.2160.monthly.hdf.vgpm.s.chl.a.sst.php (accessed on 26 January 2023).
31. Behrenfeld, M.J.; Falkowski, P.G. Photosynthetic rates derived from satellite-based chlorophyll concentration. *Limnol. Oceanogr.* **1997**, *42*, 1–20. [CrossRef]
32. AVHRR Pathfinder SST. Available online: https://www.ncei.noaa.gov/products/avhrr-pathfinder-sst (accessed on 26 January 2023).
33. OSCAR—Earth and Space Research. Available online: https://www.esr.org/research/oscar/ (accessed on 26 January 2023).
34. RSS SMAP Level 3 Sea Surface Salinity Standard Mapped Image Monthly V4.0 Validated Dataset. Available online: https://podaac.jpl.nasa.gov/dataset/SMAP_RSS_L3_SSS_SMI_MONTHLY_V4 (accessed on 26 January 2023).
35. Cordone, A.; Lucchini, S.; De Felice, M.; Ricca, E. Direct and indirect control of Lrp on LEE pathogenicity genes of Citrobacter rodentium. *FEMS Microbiol. Lett.* **2011**, *325*, 64–70. [CrossRef]
36. Zanfardino, A.; Migliardi, A.; D'Alonzo, D.; Lombardi, A.; Varcamonti, M.; Cordone, A. Inactivation of MSMEG_0412 gene drastically affects surface related properties of Mycobacterium smegmatis. *BMC Microbiol.* **2016**, *16*, 267. [CrossRef] [PubMed]
37. Cordone, A.; Mauriello, E.M.F.; Pickard, D.J.; Dougan, G.; De Felice, M.; Ricca, E. The *lrp* Gene and Its Role in Type I Fimbriation in *Citrobacter rodentium*. *J. Bacteriol.* **2005**, *187*, 7009–7017. [CrossRef]
38. Cordone, A.; D'Errico, G.; Magliulo, M.; Bolinesi, F.; Selci, M.; Basili, M.; de Marco, R.; Saggiomo, M.; Rivaro, P.; Giovannelli, D.; et al. Bacterioplankton Diversity and Distribution in Relation to Phytoplankton Community Structure in the Ross Sea Surface Waters. *Front. Microbiol.* **2022**, *13*, 39. [CrossRef]
39. Buglione, M.; Ricca, E.; Petrelli, S.; Baccigalupi, L.; Troiano, C.; Saggese, A.; Rivieccio, E.; Fulgione, D. Gut microbiota plasticity in insular lizards under reversed island syndrome. *Sci. Rep.* **2022**, *12*, 12682. [CrossRef]
40. Integrated Microbiome Resource (IMR). Available online: https://imr.bio/ (accessed on 30 January 2023).
41. Hedges, J.I.; Stern, J.H. Carbon and nitrogen determinations of carbonate-containing solids1. *Limnol. Oceanogr.* **1984**, *29*, 657–663. [CrossRef]
42. Mangoni, O.; Saggiomo, V.; Bolinesi, F.; Margiotta, F.; Budillon, G.; Cotroneo, Y.; Misic, C.; Rivaro, P.; Saggiomo, M. Phytoplankton blooms during austral summer in the Ross Sea, Antarctica: Driving factors and trophic implications. *PLoS ONE* **2017**, *12*, e0176033. [CrossRef] [PubMed]
43. Holm-Hansen, O.; Lorenzen, C.J.; Holmes, R.W.; Strickland, J.D.H. Fluorometric Determination of Chlorophyll. *ICES J. Mar. Sci.* **1965**, *30*, 3–15. [CrossRef]
44. Manini, E.; Baldrighi, E.; Ricci, F.; Grilli, F.; Giovannelli, D.; Intoccia, M.; Casabianca, S.; Capellacci, S.; Marinchel, N.; Penna, P.; et al. Assessment of Spatio-Temporal Variability of Faecal Pollution along Coastal Waters during and after Rainfall Events. *Water* **2022**, *14*, 502. [CrossRef]
45. DuBois, M.; Gilles, K.A.; Hamilton, J.K.; Rebers, P.A.; Smith, F. Colorimetric method for determination of sugars and related substances. *Anal. Chem.* **1956**, *28*, 350–356. [CrossRef]
46. Hartree, E. Determination of protein: A modification of the lowry method that gives a linear photometric response. *Anal. Biochem.* **1972**, *48*, 422–427. [CrossRef] [PubMed]
47. Callahan, B.J.; McMurdie, P.J.; Holmes, S.P. Exact sequence variants should replace operational taxonomic units in marker-gene data analysis. *ISME J.* **2017**, *11*, 2639–2643. [CrossRef]
48. Quast, C.; Pruesse, E.; Yilmaz, P.; Gerken, J.; Schweer, T.; Yarza, P.; Peplies, J.; Glöckner, F.O. The SILVA Ribosomal RNA Gene Database Project: Improved Data Processing and Web-Based Tools. *Nucleic Acids Res.* **2012**, *41*, D590–D596. [CrossRef] [PubMed]
49. McMurdie, P.J.; Holmes, S. Phyloseq: An R package for reproducible interactive analysis and graphics of microbiome census data. *PLoS ONE* **2013**, *8*, e61217. [CrossRef]
50. Sheik, C.S.; Reese, B.K.; Twing, K.I.; Sylvan, J.B.; Grim, S.L.; Schrenk, M.O.; Sogin, M.L.; Colwell, F.S. Identification and Removal of Contaminant Sequences from Ribosomal Gene Databases: Lessons From the Census of Deep Life. *Front. Microbiol.* **2018**, *9*, 840. [CrossRef] [PubMed]
51. R Core Team. *R: A Language and Environment for Statistical Computing*; R Foundation for Statistical Computing: Vienna, Austria, 2020.
52. Oksanen, J.; Simpson, G.; Blanchet, F.; Kindt, R.; Legendre, P.; Minchin, P.; O'Hara, R.; Solymos, P.; Stevens, M.; Szoecs, E.; et al. Vegan: Community Ecology Package 2022. Available online: https://github.com/vegandevs/vegan (accessed on 12 October 2022).
53. Wickham, H. Ggplot2. *WIREs Comput. Stat.* **2011**, *3*, 180–185. [CrossRef]
54. Morton, J.T.; Toran, L.; Edlund, A.; Metcalf, J.L.; Lauber, C.; Knight, R. Uncovering the Horseshoe Effect in Microbial Analyses. *Msystems* **2017**, *2*, e00166-16. [CrossRef] [PubMed]
55. Danis, B.; Van De Putte, A.; Convey, P.; Griffiths, H.; Linse, K.; Murray, A.E. Editorial: Antarctic Biology: Scale Matters. *Front. Ecol. Evol.* **2020**, *8*, 91. [CrossRef]

56. Lim, Y.; Kang, I.; Cho, J.-C. Genome characteristics of Kordia antarctica IMCC3317T and comparative genome analysis of the genus Kordia. *Sci. Rep.* **2020**, *10*, 14715. [CrossRef]
57. Sadaiappan, B.; Kannan, S.; Palaniappan, S.; Manikkam, R.; Ramasamy, B.; Anilkumar, N.; Subramanian, M. Metagenomic 16S rDNA amplicon data of microbial diversity and its predicted metabolic functions in the Southern Ocean (Antarctic). *Data Brief* **2020**, *28*, 104876. [CrossRef]
58. Giebel, H.-A.; Brinkhoff, T.; Zwisler, W.; Selje, N.; Simon, M. Distribution of *Roseobacter* RCA and SAR11 lineages and distinct bacterial communities from the subtropics to the Southern Ocean. *Environ. Microbiol.* **2009**, *11*, 2164–2178. [CrossRef]
59. Obernosterer, I.; Catala, P.; Lebaron, P.; West, N.J. Distinct bacterial groups contribute to carbon cycling during a naturally iron fertilized phytoplankton bloom in the Southern Ocean. *Limnol. Oceanogr.* **2011**, *56*, 2391–2401. [CrossRef]
60. Kong, L.-F.; He, Y.-B.; Xie, Z.-X.; Luo, X.; Zhang, H.; Yi, S.-H.; Lin, Z.-L.; Zhang, S.-F.; Yan, K.-Q.; Xu, H.-K.; et al. Illuminating Key Microbial Players and Metabolic Processes Involved in the Remineralization of Particulate Organic Carbon in the Ocean's Twilight Zone by Metaproteomics. *Environ. Microbiol.* **2021**, *87*, e00986-21. [CrossRef] [PubMed]
61. Kirchman, D.L. The Ecology of Cytophaga–Flavobacteria in aquatic environments. *FEMS Microbiol. Ecol.* **2002**, *39*, 91–100. [CrossRef] [PubMed]
62. Pinhassi, J.; Sala, M.M.; Havskum, H.; Peters, F.; Guadayol, O.; Malits, A.; Marrase, C. Changes in Bacterioplankton Composition under Different Phytoplankton Regimens. *Appl. Environ. Microbiol.* **2004**, *70*, 6753–6766. [CrossRef]
63. Abell, G.C.; Bowman, J.P. Ecological and biogeographic relationships of class Flavobacteria in the Southern Ocean. *FEMS Microbiol. Ecol.* **2005**, *51*, 265–277. [CrossRef]
64. Abell, G.; Bowman, J.P. Colonization and community dynamics of class Flavobacteria on diatom detritus in experimental mesocosms based on Southern Ocean Seawater. *FEMS Microbiol. Ecol.* **2005**, *53*, 379–391. [CrossRef]
65. Williams, T.J.; Long, E.; Evans, F.; DeMaere, M.; Lauro, F.M.; Raftery, M.J.; Ducklow, H.; Grzymski, J.J.; Murray, A.E.; Cavicchioli, R. A metaproteomic assessment of winter and summer bacterioplankton from Antarctic Peninsula coastal surface waters. *ISME J.* **2012**, *6*, 1883–1900. [CrossRef]
66. West, N.J.; Obernosterer, I.; Zemb, O.; Lebaron, P. Major differences of bacterial diversity and activity inside and outside of a natural iron-fertilized phytoplankton bloom in the Southern Ocean. *Environ. Microbiol.* **2008**, *10*, 738–756. [CrossRef]
67. Williams, T.J.; Wilkins, D.; Long, E.; Evans, F.; DeMaere, M.Z.; Raftery, M.J.; Cavicchioli, R. The role of planktonic *Flavobacteria* in processing algal organic matter in coastal East Antarctica revealed using metagenomics and metaproteomics. *Environ. Microbiol.* **2013**, *15*, 1302–1317. [CrossRef] [PubMed]
68. Berner, C.; Bertos-Fortis, M.; Pinhassi, J.; Legrand, C. Response of Microbial Communities to Changing Climate Conditions During Summer Cyanobacterial Blooms in the Baltic Sea. *Front. Microbiol.* **2018**, *9*, 1562. [CrossRef]
69. Auger, M.; Morrow, R.; Kestenare, E.; Sallée, J.-B.; Cowley, R. Southern Ocean in-situ temperature trends over 25 years emerge from interannual variability. *Nat. Commun.* **2021**, *12*, 514. [CrossRef]

Disclaimer/Publisher's Note: The statements, opinions and data contained in all publications are solely those of the individual author(s) and contributor(s) and not of MDPI and/or the editor(s). MDPI and/or the editor(s) disclaim responsibility for any injury to people or property resulting from any ideas, methods, instructions or products referred to in the content.

frontiers | Frontiers in Earth Science

ORIGINAL RESEARCH
published: 13 June 2022
doi: 10.3389/feart.2022.897267

The Helium and Carbon Isotope Characteristics of the Andean Convergent Margin

P. H. Barry[1], J. M. De Moor[2,3], A. Chiodi[4], F. Aguilera[5,6], M. R. Hudak[1], D. V. Bekaert[1], S. J. Turner[7], J. Curtice[1], A. M. Seltzer[1], G. L. Jessen[8,9], E. Osses[8], J. M. Blamey[10], M. J. Amenábar[10], M. Selci[11], M. Cascone[11], A. Bastianoni[11], M. Nakagawa[12], R. Filipovich[4], E. Bustos[4], M. O. Schrenk[13], J. Buongiorno[14], C. J. Ramírez[15], T. J. Rogers[16], K. G. Lloyd[16] and D. Giovannelli[1,11,12,17]*

[1]Marine Chemistry and Geochemistry Department, Woods Hole Oceanographic Institution, Woods Hole, MA, United States, [2]Observatorio Vulcanológico y Sismológico de Costa Rica (OVSICORI), Universidad Nacional, San Jose, Costa Rica, [3]Department of Earth and Planetary Sciences, University of New Mexico, Albuquerque, NM, United States, [4]Instituto de Bio y Geociencias del NOA (IBIGEO, UNSa-CONICET), Salta, Argentina, [5]Millennium Institute on Volcanic Risk Research—Ckelar Volcanoes, Antofagasta, Chile, [6]Departamento de Ciencias Geológicas, Universidad Católica del Norte, Antofagasta, Chile, [7]Department of Geosciences, University of Massachusetts Amherst, Amherst, MA, United States, [8]Instituto de Ciencias Marinas y Limnológicas, Universidad Austral de Chile, Valdivia, Chile, [9]Centro de Investigación Oceanográfica COPAS COASTAL, Universidad de Concepción, Concepción, Chile, [10]Fundación Biociencia, Universidad de Santiago de Chile, Santiago, Chile, [11]Department of Biology, University of Naples "Federico II", Naples, Italy, [12]Earth-Life Science Institute, Tokyo Institute of Technology, Tokyo, Japan, [13]Department of Earth and Environmental Sciences, Michigan State University, East Lansing, MI, United States, [14]Division of Natural Sciences, Maryville College, Maryville, TN, United States, [15]Servicio Geológico Ambiental (SeGeoAm), Heredia, Costa Rica, [16]Department of Microbiology, University of Tennessee, Knoxville, TN, United States, [17]National Research Council, Institute of Marine Biological Resources and Biotechnologies—CNR-IRBIM, Ancona, Italy

OPEN ACCESS

Edited by:
Franco Tassi, University of Florence, Italy

Reviewed by:
Walter D'Alessandro, National Institute of Geophysics and Volcanology, Italy
Dario Tedesco, Biologiche e Farmaceutiche, Italy
Mariano Agusto, University of Buenos Aires, Argentina

***Correspondence:**
P. H. Barry
pbarry@whoi.edu

Specialty section:
This article was submitted to Volcanology, a section of the journal Frontiers in Earth Science

Received: *15 March 2022*
Accepted: *19 May 2022*
Published: *13 June 2022*

Citation:
Barry PH, De Moor JM, Chiodi A, Aguilera F, Hudak MR, Bekaert DV, Turner SJ, Curtice J, Seltzer AM, Jessen GL, Osses E, Blamey J, Amenábar MJ, Selci M, Cascone M, Bastianoni A, Nakagawa M, Filipovich R, Bustos E, Schrenk MO, Buongiorno J, Ramírez CJ, Rogers TJ, Lloyd KG and Giovannelli D (2022) The Helium and Carbon Isotope Characteristics of the Andean Convergent Margin. Front. Earth Sci. 10:897267. doi: 10.3389/feart.2022.897267

Subduction zones represent the interface between Earth's interior (crust and mantle) and exterior (atmosphere and oceans), where carbon and other volatile elements are actively cycled between Earth reservoirs by plate tectonics. Helium is a sensitive tracer of volatile sources and can be used to deconvolute mantle and crustal sources in arcs; however it is not thought to be recycled into the mantle by subduction processes. In contrast, carbon is readily recycled, mostly in the form of carbon-rich sediments, and can thus be used to understand volatile delivery *via* subduction. Further, carbon is chemically-reactive and isotope fractionation can be used to determine the main processes controlling volatile movements within arc systems. Here, we report helium isotope and abundance data for 42 deeply-sourced fluid and gas samples from the Central Volcanic Zone (CVZ) and Southern Volcanic Zone (SVZ) of the Andean Convergent Margin (ACM). Data are used to assess the influence of subduction parameters (e.g., crustal thickness, subduction inputs, and convergence rate) on the composition of volatiles in surface volcanic fluid and gas emissions. He isotopes from the CVZ backarc range from 0.1 to 2.6 R_A (n = 23), with the highest values in the Puna and the lowest in the Sub-Andean foreland fold-and-thrust belt. Atmosphere-corrected He isotopes from the SVZ range from 0.7 to 5.0 R_A (n = 19). Taken together, these data reveal a clear southeastward increase in $^3He/^4He$, with the highest values (in the SVZ) falling below the nominal range associated with pure upper mantle helium (8 ± 1 R_A), approaching the mean He isotope value for arc gases of (5.4 ± 1.9 R_A). Notably, the lowest values are found in the CVZ, suggesting more significant crustal inputs (i.e., assimilation of ^4He) to the helium budget. The crustal thickness in the CVZ (up to

70 km) is significantly larger than in the SVZ, where it is just ~40 km. We suggest that crustal thickness exerts a primary control on the extent of fluid-crust interaction, as helium and other volatiles rise through the upper plate in the ACM. We also report carbon isotopes from (n = 11) sites in the CVZ, where $\delta^{13}C$ varies between −15.3‰ and −1.2‰ [vs. Vienna Pee Dee Belemnite (VPDB)] and $CO_2/^3He$ values that vary by over two orders of magnitude (6.9×10^8–1.7×10^{11}). In the SVZ, carbon isotope ratios are also reported from (n = 13) sites and vary between −17.2‰ and −4.1‰. $CO_2/^3He$ values vary by over four orders of magnitude (4.7×10^7–1.7×10^{12}). Low $\delta^{13}C$ and $CO_2/^3He$ values are consistent with CO_2 removal (e.g., calcite precipitation and gas dissolution) in shallow hydrothermal systems. Carbon isotope fractionation modeling suggests that calcite precipitation occurs at temperatures coincident with the upper temperature limit for life (122°C), suggesting that biology may play a role in C-He systematics of arc-related volcanic fluid and gas emissions.

Keywords: helium, carbon, SVZ, CVZ, Andes (Argentina and Chile)

1 INTRODUCTION

Helium has two stable isotopes: ^3He and ^4He. ^3He is primordial and has been stored in the mantle since Earth's accretion, whereas ^4He is continuously produced in Earth's crust due to the radioactive decay of U and Th. Earth reservoirs have characteristic $^3He/^4He$ values (typically reported relative to air; R_A = air $^3He/^4He = 1.382 \times 10^{-6}$; Clarke et al., 1976; Mabry et al., 2013). For example, the upper mantle typically has a $^3He/^4He$ value that is ~8 ± 1 times the atmospheric ratio (R_A; Graham, 2002). The continental lithospheric mantle has lower $^3He/^4He$, approximately 6.1 ± 2.1 R_A (Dunai and Baur, 1995; Gautheron and Moreira, 2002; Day et al., 2015), presumably due to radiogenic addition from the U and Th rich lithosphere. Crustal material is dominated by radiogenic ^4He production and has a $^3He/^4He$ = 0.05 R_A (Andrews, 1985). The mean He isotope ratio for arc gases is ~5.4 ± 1.9 R_A (Hilton et al., 2002), likely reflecting radiogenic additions from the surrounding crust. As a result, the $^3He/^4He$ in geothermal fluids provides information about the origin of volatiles (i.e., mantle vs. crust derived).

High CO_2 concentrations have been observed in volcanic arcs as well as in other volcanic regions with high heat flow and mantle partial melting (e.g., Hilton and Porcelli, 2003). Typically, C isotopes of CO_2 in volcanic arcs are interpreted to be an admixture between magmatic sources [mantle $\delta^{13}C$ is between −5‰ and −8‰ vs. Vienna Pee Dee Belemnite (VPDB); Javoy et al., 1986] and subduction inputs (Sano and Marty, 1995), which can vary from 0‰ in marine carbonates down to ~−30‰ in organic carbon-rich sediments (Hayes et al., 1999; Plank and Manning, 2019). Together, $^3He/^4He$, $CO_2/^3He$, and C isotopes of CO_2 can be used to determine the volatile provenance of gas and fluid emissions (Sano and Marty, 1995), as well as secondary processes that affect emissions (e.g., Barry et al., 2019a).

Several prior studies have characterized He-C isotope systematics in volcanic and geothermal systems in the Andes (**Figure 1**; e.g., Hilton et al., 1993; Hoke et al., 1994; Varekamp et al., 2006; Sepúlveda et al., 2007; Aguilera, 2008; Ray et al., 2009; Tassi et al., 2009; Tassi et al., 2010; Capaccioni et al., 2011; Tassi et al., 2011; Aguilera et al., 2012; Agusto et al., 2013; Benavente et al., 2013; Chiodi et al., 2015; Aguilera et al., 2016; Benavente et al., 2016; Roulleau et al., 2016; Tardani et al., 2016; Tassi et al., 2016; Arnold et al., 2017; Tassi et al., 2017; Lopez et al., 2018; Chiodi et al., 2019; Arnold et al., 2020; Inostroza et al., 2020; Robidoux et al., 2020; Lages et al., 2021; Tardani et al., 2021; Filipovich et al., 2022) to understand the source of the volcanic fluid and gas emissions. These studies demonstrate the co-occurrence of mantle ($^3He/^4He$ up to ~8 R_A) and crustal ($^3He/^4He$ ~0.05 R_A) He sources. In this contribution, we report new fluid and gas He-C isotope and relative abundance data, which we combine with previously published data to determine the extent of magmatic vs. crustal contributions across the Andean Convergent Margin (ACM). One of the main objectives of this study is to compare He-C systematics in the Central Volcanic Zone (CVZ) and the Southern Volcanic Zone (SVZ) regions in order to assess the influence of subduction parameters (e.g., crustal thickness, subduction inputs, convergence rate) on the composition of volatiles emitted at the surface. Determining volatile pathways is fundamental for ascertaining the dominant processes in each volcanic region as well as for differentiating volcanic source features from secondary modification processes (e.g., gas dissolution, calcite precipitation and/or crustal assimilation).

2 GEOLOGICAL BACKGROUND

Subduction of the Nazca Plate beneath the South America Plate resulted in the formation of the ACM and the South American Volcanic Arc (Dewey and Bird, 1970; James, 1971; Jordan et al., 1983). The ACM accounts for about 17% of the total length of the "Ring of Fire" and active volcanism occurs within three main segments: 1) the Northern Volcanic Zone (5°N–2°S), 2) Central Volcanic Zone (20°S–27°S), and 3) Southern Volcanic Zone (33°S–39°S) (Thorpe and Francis, 1979; Thorpe, 1982; Harmon et al., 1984; Ray et al., 2009). A fourth segment (Austral Volcanic

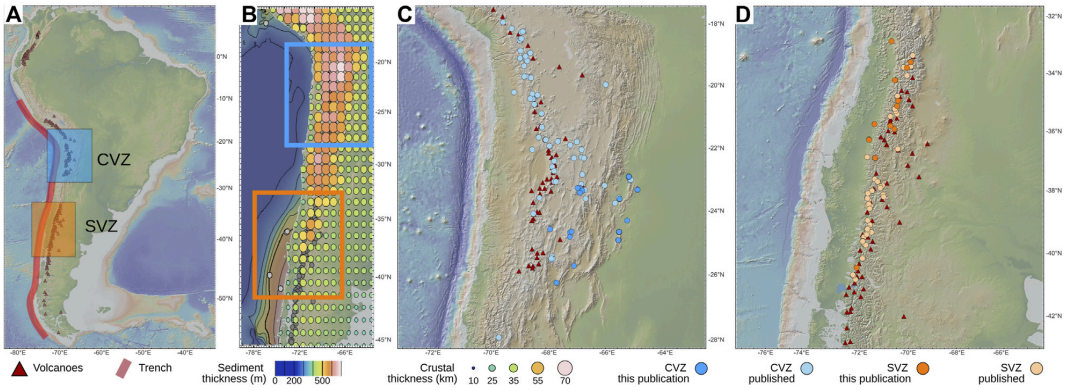

FIGURE 1 | Map sampling locations and subduction parameters. **(A)** Map of South America showing the relative location of the two sampling locations: the Central Volcanic Zone (CVZ) and the Southern Volcanic Zone (SVZ), which span across the ACM in Chile and Argentina. **(B)** Map showing offshore sediment thickness (see color bar) and crustal thickness (dot sizes) in the overriding plate. **(C)** Zoomed in view of the CVZ, with the location of all samples from this study (bright blue circles) and previously published studies (light blue circles) as well as the location of volcanic centers (red triangles). **(D)** Zoomed in view of the SVZ, with the location of all samples from this study (bright orange circles) and previously published studies (light orange circles) as well as the location of volcanic centers (red triangles). Published data are from Hilton et al. (1993), Hoke et al. (1994), Varekamp et al. (2006), Sepúlveda et al. (2007), Aguilera (2008), Ray et al. (2009), Tassi et al. (2009), Tassi et al. (2010), Capaccioni et al. (2011), Tassi et al. (2011), Aguilera et al. (2012), Agusto et al. (2013), Benavente et al. (2013), Chiodi et al. (2015), Aguilera et al. (2016), Benavente et al. (2016), Roulleau et al. (2016), Tardani et al. (2016), Tassi et al. (2016), Arnold et al. (2017), Tassi et al. (2017), Lopez et al. (2018), Chiodi et al. (2019), Arnold et al. (2020), Inostroza et al. (2020), Robidoux et al. (2020), Lages et al. (2021), Tardani et al. (2021), Filipovich et al. (2022) in this figure, as well as in subsequent figures.

Zone; 49°S–55°S) is located in the southernmost part of South America, and is related to the subduction of the Antarctica plate under the South American Plate (Stern, 2004). These are separated by gaps in magmatism associated with ridge subduction (the Nazca Ridge, to the north of the CVZ, and the Juan Fernandez Ridge, to the south) and shallow slab angles (e.g., Kay and Mpodozis, 2002; Newell et al., 2015). The current phase of subduction of the Nazca plate beneath the northern Andes began about 80 Myr ago (Ma) and propagated southwards reaching the SVZ about 55 Myr ago (Chen et al., 2019). The subducting plate is slightly older in the CVZ compared with the SVZ region (~45 Ma vs. 30 Ma; Syracuse and Abers, 2006), whereas the angle of subduction is slightly shallower (24° in the CVZ vs. 28° in the SVZ).

The CVZ is primarily composed of andesitic stratovolcanoes, which erupted from the Neogene until historic times (Robidoux et al., 2020). Crustal thickness varies drastically along this north to south transect, from ~30 to 70 km. The depth of the Benioff zone beneath the arc front varies from 80 to 120 km. Convergence rates are 7–9 cm/year on average (DeMets et al., 2010). Sediments are delivered to the arc at the trench and sediment thickness also varies significantly from north to south, with the CVZ being sediment-poor compared to the SVZ (**Figure 1B**) (Völker et al., 2013; Clift, 2017; Lages et al., 2021).

Volcanic activity in the CVZ consist mostly of andesites and dacites which have trace element and radiogenic isotope compositions (e.g., $^{87}Sr/^{86}Sr$ and $^{143}Nd/^{144}Nd$) consistent with nearly ubiquitous contamination during their prolonged ascent through the thick (~70 km; Thorpe, 1982) continental crust (De Silva, 1989; Mamani et al., 2010; Godoy et al., 2019). Hydrothermal activity occurs throughout the CVZ, expressed as major geothermal fields and intermittent thermal springs, particularly in the vicinity of volcanic centers such as Taapaca, Guallatiri, Isluga, and Putana (Tassi et al., 2010).

The SVZ extends from central to southern Chile-Argentina. It is composed of numerous stratovolcanoes and monogenetic cones (López-Escobar et al., 1995). The crust is significantly thinner in the SVZ compared to the CVZ, increasing from only ~30 km in the southernmost region to ~50 km near the northern segment terminus (Tassara and Echaurren, 2012), however there are several carbon-rich sedimentary basins (e.g., Neuquén Basin) adjacent to the SVZ (Howell et al., 2005). SVZ volcanic compositions consist mostly of basalts and andesites, though basaltic compositions become less common as crustal thickness increases (Tormey et al., 1991). Radiogenic isotope compositions of SVZ volcanics are variable and have been largely attributed to variations in mantle components where the crust is thin, with both mantle and crustal contributions apparent among more differentiated lavas in the north, where the crust is thicker (Jacques et al., 2014; Turner et al., 2017; Wieser et al., 2019). Hydrothermal activity is widespread in the SVZ due to high geothermal gradients, ongoing magmatic activity, permeable host rocks and abundant recharge (Ray et al., 2009).

3 MATERIALS AND METHODS

3.1 Sample Collection

Gas and water samples in this study were collected at subaerial hot and warm springs, natural gas seeps and fumaroles using

TABLE 1 | Helium and carbon isotope and abundance ratios for newly reported data (this study). 1-sigma uncertainties are less than 5% for $^4He/^{20}Ne$, R/R_A, R_C/R_A, $\delta^{13}C$, and $CO_2/^3He$. The abbreviation n.a., not available.

Sample name	Sample ID	Volcanic zone	Lat. °N	Long. °E	$^4He/^{20}Ne$	$\delta^{13}CO_2$	R/Ra	Rc/Ra	$CO_2/^3He$	Phase	pH	Temp. °C	Salinity g/L
Galan Fumarole	AR-GF190226-1	CVZ	−25.86	−66.99	197.9	n.a.	1.77	1.77	4.18E + 09	G	7.75	80	0.19
Galan Fumarole	AR-GF190226-2	CVZ	−25.86	−66.99	217.7	−6.2	1.79	1.79	4.13E + 09	G	7.75	80	0.19
Incachule	AR-IN190223	CVZ	−24.28	−66.47	106.7	−12	1.97	1.97	n.a.	G	6.52	46.9	1.54
La Colcha	AR-LC190226	CVZ	−26.03	−66.99	333.3	−7.5	1.45	1.45	2.22E + 10	G	6.94	84	6.1
La Colcha	AR-LC190226	CVZ	−26.03	−66.99	545.6	−7.5	2.58	2.58	6.86E + 08	G	6.94	84	6.1
Pio Perez	AR-PP190301	CVZ	−25.41	−64.59	1.7	−1.2	0.36	0.21	3.72E + 10	G	8.47	54.3	1.81
Tocomar	AR-TM190224	CVZ	−24.19	−66.55	72.3	−11.7	2.47	2.48	1.68E + 11	G	7.13	69.2	3.93
Fiambalá	FB210806	CVZ	−27.74	−67.548	215.3	n.a.	0.24	0.24	n.a.	G	n.a.	n.a.	n.a.
El Ceibal	EC-211106	CVZ	−26.149	−64.955	1.2	n.a.	0.71	0.63	n.a.	G	n.a.	n.a.	n.a.
Baños de Fleming	BF211031	CVZ	−24.592	−64.909	n.a.	n.a.	0.82	n.a.	n.a.	G	n.a.	n.a.	n.a.
Pizarro	PZ211029	CVZ	−24.237	−64.157	25.4	n.a.	0.51	0.51	n.a.	G	n.a.	n.a.	n.a.
Caimancito 1	CA211030-1	CVZ	−23.745	−64.518	1.4	n.a.	0.59	0.5	n.a.	G	n.a.	n.a.	n.a.
Caimancito 2	CA211030-2	CVZ	−23.744	−64.519	n.a.	n.a.	0.48	n.a.	n.a.	G	n.a.	n.a.	n.a.
Antuco	AR-AO190224	CVZ	−24.18	−66.67	99.8	−7.66	1.96	1.96	6.67E + 09	W	6.25	27.8	21.21
Botijuela Vista	AR-BJ190222	CVZ	−25.74	−67.82	64.5	n.a.	1.24	1.24	8.21E + 10	W	6.44	40	8.65
Aguas Calientes Galan	AR-GA190226	CVZ	−25.83	−66.92	177.3	−1.5	1.56	1.56	8.78E + 10	W	6.7	67	3.28
Incachule	AR-IN190223	CVZ	−24.28	−66.47	12.7	n.a.	1.77	1.79	1.97E + 10	W	6.52	46.9	1.54
Incachule	AR-IN190223	CVZ	−24.28	−66.47	8.8	n.a.	1.68	1.71	1.59E + 11	W	6.52	46.9	1.54
Pastos Grande	AR-PG190225	CVZ	−24.36	−66.57	107.7	−15.33	1.34	1.34	n.a.	W	8.74	44.9	0.61
Pio Perez	AR-PP190301	CVZ	−25.41	−64.59	1.4	−10.67	0.33	0.14	2.17E + 10	W	8.47	54.3	1.81
Pio Perez	AR-PP190301	CVZ	−25.41	−64.59	1.1	−10.67	0.36	0.11	4.86E + 09	W	8.47	54.3	1.81
Rosario de la Frontera	AR-RF190301	CVZ	−25.84	−64.93	6	−8.28	0.36	0.33	9.58E + 10	W	8.23	82	1.57
Villa Vil	AR-VV190228	CVZ	−27.11	−66.82	79.5	−13.28	0.9	0.89	8.83E + 09	W	9.09	38.2	0.4
Termas de Catillo	CH-CT200308	SVZ	−36.29	−71.65	0.3	n.a.	1.1	n.a.	n.a.	G	9.49	37.5	3
Campanario	CH-CP200307	SVZ	−35.93	−70.59	64.2	−8.72	5.01	5.03	1.00E + 10	G	5.89	53.2	25
Panamavida	CH-PM200308	SVZ	−35.76	−71.42	0.4	n.a.	1.12	1.43	n.a.	G	9.91	32.45	4
San Pedro baños termales	CH-SP200302-2	SVZ	−35.14	−70.48	40	−12.56	2.46	2.47	1.20E + 08	G	6.19	21.98	46.5
San Pedro baños termales	CH-SP200302-2	SVZ	−35.14	−70.48	59.5	−12.56	2.4	2.4	4.70E + 07	G	6.19	21.98	46.5
Termas del Flaco	CH-TF-200303	SVZ	−34.96	−70.43	4	−11.15	1.44	1.48	2.20E + 09	G	6.24	68.4	5
Termas del Flaco	CH-TF-200303	SVZ	−34.96	−70.43	0.6	−11.15	1.13	1.27	3.90E + 10	G	6.24	68.4	5
Termas de Cauquenes	CH-CQ200301	SVZ	−34.25	−70.56	68.9	−15.9	1.67	1.68	n.a.	G	8.47	47.67	7.72
Baño Morales	CH-BM-200312	SVZ	−33.82	−70.06	8.1	−8.64	1.61	1.63	n.a.	G	6.07	27.2	20
Termas del Plomo	CH-TP-200304	SVZ	−33.62	−69.91	9.2	n.a.	2.52	2.58	2.00E + 08	G	6.43	36.8	19
Termas del Plomo	CH-TP200304	SVZ	−33.62	−69.91	21.1	n.a.	2.32	2.34	1.20E + 08	G	6.43	36.8	19
Chillan	CH5	SVZ	−36.9	−71.4	n.a.	−8.5	6.32	n.a.	5.00E + 10	G	n.a.	n.a.	n.a.
Chillan	CH6	SVZ	−36.9	−71.4	n.a.	−8.3	6.23	n.a.	5.30E + 10	G	n.a.	n.a.	n.a.
Cordon Caulle	Las Sopas	SVZ	−40.49	−72.17	n.a.	−4.1	6.6	n.a.		G	n.a.	n.a.	n.a.

(Continued on following page)

TABLE 1 | (*Continued*) Helium and carbon isotope and abundance ratios for newly reported data (this study). 1-sigma uncertainties are less than 5% for $^{4}He/^{20}Ne$, R/R_A, R_C/R_A, $\delta^{13}C$, and $CO_2/^{3}He$. The abbreviation n.a., not available.

Sample name	Sample ID	Volcanic zone	Lat. °N	Long. °E	$^{4}He/^{20}Ne$	$\delta^{13}CO_2$	R/Ra	Rc/Ra	$CO_2/^{3}He$	Phase	pH	Temp. °C	Salinity g/L
									7.10E + 10				
Chillan	CH1	SVZ	–36.9	–71.4	n.a.	–7.9	n.a.	n.a.	n.a.	G	n.a.	n.a.	n.a.
Chillan	CH3	SVZ	–36.9	–71.4	n.a.	–7.9	n.a.	n.a.	n.a.	G	n.a.	n.a.	n.a.
Termas de Catillo	CH-CT200308	SVZ	–36.29	–71.65	25.3	–17.17	0.65	0.65	3.69E + 09	W	9.49	37.5	3
El Medano	CH-EM-200301	SVZ	–35.82	–70.76	0.4	–10.19	0.94	0.74	3.43E + 10	W	7.22	37.5	3.5
Panamavida	CH-PM200308	SVZ	–35.76	–71.42	0.4	–15.34	0.97	0.89	2.27E + 10	W	9.91	32.45	4
Termas del Flaco	CH-TF200303	SVZ	–34.96	–70.43	2.5	n.a.	1.35	1.4	1.37E + 11	W	6.24	68.4	5
Auco	CH-AU200310	SVZ	–32.89	–70.71	n.a.	–12.15	0.96	n.a.	1.71E + 12	W	8.09	20.2	3

standard inverted funnel sampling techniques (e.g., Hilton et al., 2002; Barry et al., 2013). Gases and fluids were first flushed through silicone tubing and into 3/8-inch copper tubes (Weiss, 1968). After ample flushing (i.e., approximately 10x the volume of the tubing), stainless steel clamps were closed on each end of the copper tubes, trapping the sample inside of the copper tubing, between the clamps (e.g., Barry et al., 2016). Gas seeps with low flow rates required >1 h of flushing to effectively remove any air from the system. To ensure no back flow of air into the sampling apparatus, the outflow portion of the silicon tubing was submerged in a bottle of water, allowing gas to flow only in one direction (i.e., through the sampling apparatus).

Gases from bubbling springs were also collected using the water-displacement method (e.g., Craig, 1953; Mazor and Wasserburg, 1965). In brief, a funnel was submerged in a spring and the entire sampling apparatus (i.e., funnel, silicone tubing and copper tube) was initially filled with spring water. The funnel was then inverted and placed over the rising gas bubbles. As the bubbles of gas were captured, they slowly displaced the water in the copper tube. Once all water was displaced by sample gas, the stainless steel clamps were closed in the same way as described above. This technique is particularly useful in low flow gas seeps, where prohibitively long flushing times would be required (e.g., Kimani et al., 2021; Mtili et al., 2021). Water samples require minimal flushing and can often be collected in a matter of minutes. Gas samples were also collected using standard Giggenbach bottle methods (Giggenbach et al., 1989) for C isotope analysis and $CO_2/^{3}He$ determination. Giggenbach bottles were collected from the same tubing used for Cu-tubes and thus flushed in the same way as described above. Giggenbach bottle samples were not collected in the SVZ and samples for C isotopes and CO_2 concentrations were instead collected by injecting gas into previously evacuated 120 ml septum vials using a three-way valve and 60 ml syringe.

Geothermal samples were collected from 33 geographically distinct localities (**Table 1**) in the SVZ and CVZ between 2019–2021. A total of 44 samples (29 gas, 15 water) were analyzed for He and/or C isotopes and abundances, 23 from the CVZ and 21 from the SVZ, including duplicates and triplicates. The temperature, pH, and salinity of each sampling site were obtained using a portable YSI Plus 6-Series Sonde Multimeter (YSI Incorporated, Yellow Springs, OH, United States) and are reported alongside He-C data in **Table 1**.

3.2 Analytical Techniques

Noble gas analyses were conducted in the Barry Lab at Woods Hole Oceanographic Institution (WHOI) using a Nu Instruments multi-collector Noblesse HR mass spectrometer. The Noblesse has the capability to determine the isotope ratios of all 26 stable noble gases, with mass separation between all carbon-based interferences and Ar, as well as $^{40}Ar^{++}$ interferences with $^{20}Ne^{+}$. It has a unique zoom optics system that allows for instantaneous switching between different isotope sets. The zoom optics permit the detectors to be fixed, greatly enhancing stability. The sensitivity and resolving power are also adjusted without the complexity of a movable source slit. The instrument is interfaced to a noble gas processing and purification inlet system that is fully automated and allows all of the noble gases to be isolated prior to their inlet into the mass spectrometer.

Carbon isotopes were measured in three laboratories in total: Observatorio Vulcanológico y Sismológico de Costa Rica (OVSICORI) at Universidad Nacional, Costa Rica, University of Naples "Federico II," Naples, Italy and the Earth-Life Science Institute, Tokyo Institute for Technology, Tokyo, Japan. Details are in **Section 3.2.3**.

3.2.1 Gas Sample Noble Gas Purification

Copper tube samples were connected to the extraction line using an O-ring connection and ~5 cm^3 of gas was expanded into the cleanup line. The pressure was measured using a capacitance manometer and then a small aliquot of gas was expanded into the cleanup portion of the line. Reactive gases were chemically removed by exposing gases to a titanium sponge held at 650°C. The titanium sponge was then cooled for 10 min to room temperature in order to getter hydrogen before gases

were expanded to a dual hot (SAES ST707) and cold (SAES ST707) getter system, held at 250°C and room temperature, respectively. Another small aliquot of gas was then segregated for preliminary analysis on a quadrupole mass spectrometer (QMS). Noble gases were separated using a series of cryogenic traps, cooled using helium compressors. The heavy noble gases (Ar–Kr–Xe) were adsorbed at 30 K onto a nude stainless steel trap and He and Ne were adsorbed at 10 K on a charcoal trap. The temperature of the charcoal trap was then raised to 30 K, releasing only He, which was then inlet into the Noblesse mass spectrometer. Following He abundance and isotope determination, the temperature on the charcoal cryogenic trap was raised to 80 K for 15 min to release Ne, which was inlet into the Noblesse mass spectrometer. Following Ne isotope measurement, the nude and charcoal cryogenic traps were raised to 300 K for cleanup. Air-standards were analyzed daily from an air cylinder collected on the roof of the Clark Laboratory building on WHOI's Quissett campus on 15 September 2020. Air-standards are fully automated and run overnight, following sample analysis during the day. Air-standards were run for He and Ne using an identical method to the one employed for samples. Air-standards were measured over a concentration range which spanned two orders of magnitude, to account for any non-linearity of the system. Full procedural blanks were run weekly; average (mean) ^{4}He blanks and ^{20}Ne blanks were less than 5% of the sample size. Doubly-charged $^{40}Ar^{++}$ was monitored but because it can be resolved from ^{20}Ne, no correction was applied. Likewise, no CO_2^{++} correction was applied to ^{22}Ne, because CO_2 backgrounds were at the detection limit and thus corrections were considered insignificant.

3.2.2 Water Sample Noble Gas Purification Protocol

Water samples were processed on the same extraction line as gas samples; however the inlet procedure was slightly different. Cu tube samples were interfaced to the extraction system in an identical fashion. Approximately 13 ml of water was inlet and then degassed under vacuum using a magnetic stirrer in a glass bulb beneath the Cu tube inlet area. Noble gases were then quantitatively transferred into a smaller volume using the capillary method (Beyerle et al., 2000; Hunt, 2015; Tyne et al., 2019). Water vapor in the extraction line was cryogenically drawn across a capillary towards a stainless-steel cold trap cooled to liquid nitrogen temperature (−196°C). The consistent flow of water vapor towards the colder water trap effectively entrains the noble gases and quantitatively draws them into the cold trap, along with a small portion of the water vapor. The consistency of this flow prevents any backflow of noble gases, such that they are quantitatively transferred into this cold trap volume (Beyerle et al., 2000). He and Ne were then inlet into the purification portion of the line (i.e., with Ti and SAES getters) for cleanup and noble gas separation in an analogous fashion to what is described above for gas samples.

3.2.3 Carbon Isotope Analysis

Carbon isotope compositions of gas samples were analyzed at OVSICORI (Universidad Nacional, Heredia, Costa Rica) on a Picarro G2201-i. The 2019 samples were analyzed by the same methodology as that described in Barry et al. (2019a) on oxidized NaOH solution from Giggenbach bottles. The samples from 2020 were analyzed as gas phase samples collected in previously evacuated 120 ml septum vials and analyzed using methodology similar to that described in Malowany et al. (2017). Samples and gas phase standards were quantitatively diluted in ultra-high purity (UHP) N_2 using a 2 L gas syringe and transferred into a 2 L flexfoil bag which was then attached to the inlet of the Picarro. A 20 cm copper tube filled with copper wire was placed in line between the bag and the inlet of the Picarro to remove H_2S, which can create significant interference on the carbon isotope measurements of CO_2 (Malowany et al., 2015). δ^{13}C (vs. VPDB) values were calibrated against a set of in house gas standards with δ^{13}C values of −15.6‰, −3.8‰, and −8.3‰. Repeat analyses of standards yielded uncertainties of <0.3‰.

Carbon isotopes on dissolved inorganic carbon (DIC) were analyzed at the Giovannelli Lab at the University of Naples "Federico II" (Naples, Italy) and at the Earth-Life Science Institute (Tokyo, Japan). Fluid samples were collected at the spring source in the field using sterile 50 ml syringes. Samples were filtered through a 0.22 μm filter (Millipore) and directly injected into a pre-vacuumed 50 ml serum bottle sealed with butyl rubber septa and an aluminum crimp. DIC concentrations and δ^{13}C values were measured using CO_2 in the headspace of glass vials after a 3 h reaction with injected 0.5 ml H_3PO_4. The amount of CO_2 and the isotopic values were measured using an Elementar IsoFlow attached to a PrecisION IRMS (at the University of Naples Federico II) and using an Agilent 6890N gas chromatograph attached to a Thermo-Finnigan Delta XP^{Plus} (at the Earth-Life Science Institute). Two international standards (δ^{13}C = −13.90‰ and 2.52‰) were used for standardization, and the standard deviations were obtained from more than three measurements. To ensure comparable results, three calibrated internal laboratory standards were run independently, and their results were within the standard error of the standard ± 0.1‰.

3.2.4 Data Analysis and Visualization

Data were plotted using the R Statistical software (R 4.1.2, https://www.r-project.org/) and the ggplot2 (Wickham, 2016) and ggtern package (Hamilton and Ferry, 2018). The dataset composed of both the newly obtained measurements and the compilation from the literature together with the R code to reproduce the plots have been permanently archived on Zenodo at DOI: 10.5281/zenodo.6360624 (https://doi.org/10.5281/zenodo.6360624). The remaining figures have been produced using GeoMapApp (http://www.geomapapp.org, Ryan et al., 2009) and Inkscape (https://inkscape.org/).

4 RESULTS

Helium (**Figure 2**) and carbon isotopic and relative abundance ratios (**Figure 3**) are reported in **Table 1**. For comparison, we also

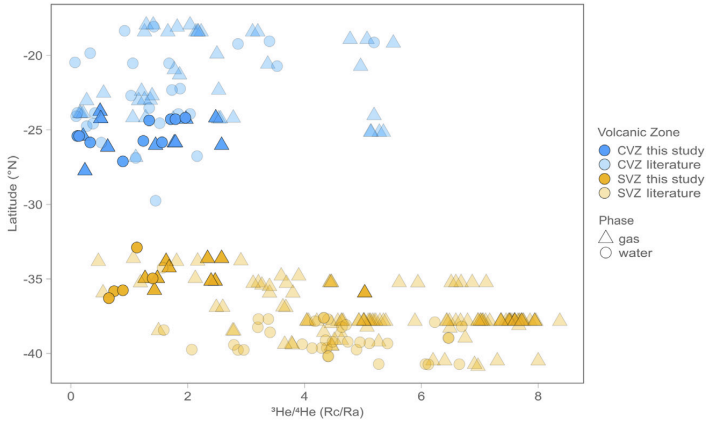

FIGURE 2 | Latitude versus air-corrected $^{3}He/^{4}He$ (R_C/R_A) values for gas (triangles) and water (circles) phase samples. Data from this study are shown as bright symbols, whereas data from previously published studies are represented by lighter colored symbols. On average CVZ samples have lower $^{3}He/^{4}He$ than SVZ samples, suggesting a larger crustal assimilation signature in the CVZ and a more pristine mantle signature in the SVZ.

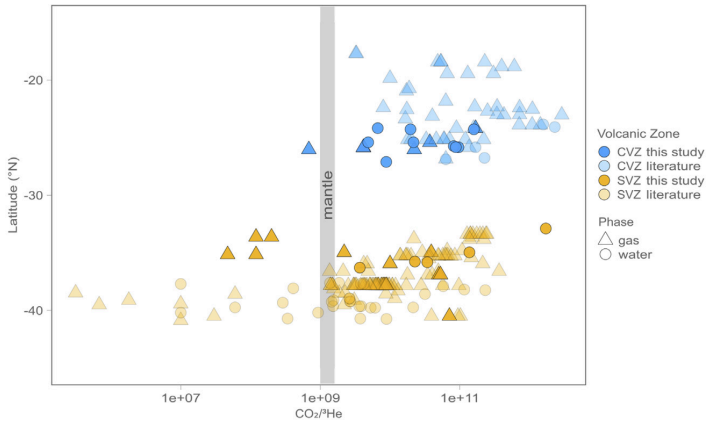

FIGURE 3 | Latitude versus $CO_2/^{3}He$ for gas (triangles) and water (circles) phase samples. Data from this study are shown in bright colors, whereas data from previously published studies are lighter in color. On average CVZ samples have higher $CO_2/^{3}He$ than SVZ samples, suggesting a larger subduction derived and/or crustal assimilation signature in the CVZ, and a more pristine mantle signature in the SVZ.

compile data from a number of previous studies (Hilton et al., 1993; Hoke et al., 1994; Varekamp et al., 2006; Sepúlveda et al., 2007; Aguilera, 2008; Ray et al., 2009; Tassi et al., 2009; Tassi et al., 2010; Tassi et al., 2011; Capaccioni et al., 2011; Aguilera et al., 2012; Agusto et al., 2013; Benavente et al., 2013; Chiodi et al., 2015; Aguilera et al., 2016; Benavente et al., 2016; Roulleau et al., 2016; Tardani et al., 2016; Tassi et al., 2016; Tassi et al., 2017; Arnold et al., 2017; Lopez et al., 2018; Chiodi et al., 2019; Arnold et al., 2020; Inostroza et al., 2020; Robidoux et al., 2020; Tardani et al., 2021; Lages et al., 2021; Filipovich et al., 2022; **Supplementary Table S1**). We also compute and report estimates of subduction and mantle derived inputs, after Sano and Marty (1995) (**Table 2**).

4.1 Helium Isotope ($^{3}He/^{4}He$)

Helium isotope results ($^{3}He/^{4}He$ of sample = R) from this study are reported relative to air (R_A), corrected for the occurrence of atmospheric He (to R_C/R_A) and blank contributions, which are consistently less than 5%. The $^{4}He/^{20}Ne$ value is used to apply an atmospheric correction to all samples, assuming ^{20}Ne is derived from air ($^{4}He/^{20}Ne = 0.32$) or air saturated water ($^{4}He/^{20}Ne = 0.26$ at 15°C; Ozima and Podosek, 2002; Hilton, 1996). As such,

TABLE 2 | Average carbon source (LSM) estimations from **Eqs 5**, **6**, **7**. Calculations were done for all gas samples compiled here as well as for samples with high He isotopes only (>5R_A). These calculations assume He–CO_2 characteristics (relative abundances and $\delta^{13}C$ systematics) can be used to resolve CO_2 contribution from three distinct sources: limestone (L) from subducted sediment and mineralized within slab basement, sedimentary (organic) carbon (S) from subducted sediment, and the mantle wedge (M). Each source is assumed to have a distinctive $CO_2/^3He$ (M = 2×10^9; L = 1×10^{13}; S = 1×10^{13}) and $\delta^{13}C$ (M = –5‰; L = 0‰; S = –30‰) signature. For reference, we also show the Clift (2017) estimates for inorganic to organic (L/S) carbon ratios in the bottom two rows.

Volcanic zone	N. samples	% L	% S	% M	L/S	(L/S)/M	Input/Output
CVZ (All)	46	70%	22%	8%	3.2	11.9	Output
SVZ (All)	107	55%	24%	21%	2.3	3.7	Output
CVZ (>5 RA)	12	73%	10%	17%	7.0	5.1	Output
SVZ (>5 RA)	28	54%	22%	24%	2.5	3.2	Output
CVZ Clift (2017)	—	—	—	—	5.0	—	Input
SVZ Clift (2017)	—	—	—	—	1.0	—	Input

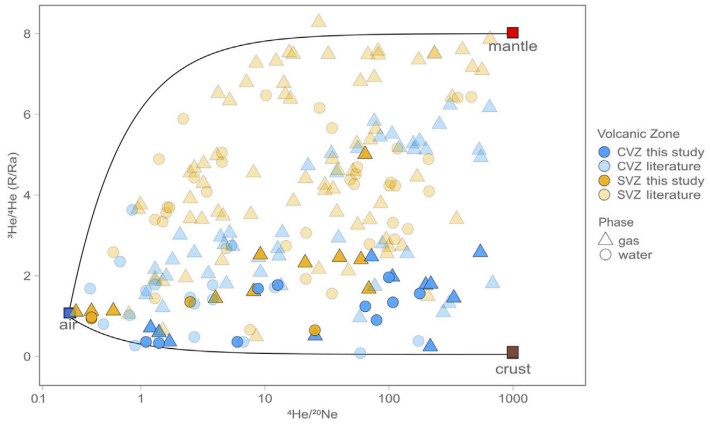

FIGURE 4 | Helium isotopes (^{3}He/^{4}He) vs. ^{4}He/^{20}Ne for gas (triangles) and water (circles) phase samples. Nearly all samples can be explained by three component mixing between air (blue square), mantle (red square) and crust (brown square). On average SVZ samples require more mantle contributions than CVZ samples, which display more radiogenic/crustal features.

the atmospheric He contribution can be calculated and then subtracted from the measured value (details and equations are given in **Section 5.1**). Notably, air corrections are small due to the fact that air contains only trace amounts of helium. ^{4}He/^{20}Ne values from this study are overlapping and vary by over four orders of magnitude in CVZ samples (**Table 1**; **Figure 4**) and by nearly three orders of magnitude in SVZ samples, with the highest values occurring in gas-phase samples. SVZ samples have the largest mantle contribution, whereas CVZ samples are dominated by radiogenic helium. We note duplicate sample analyses (i.e., same phase and locality) are in good agreement with respect to He isotopes; they deviate by less than 0.5 R_A for all samples except La Colcha, where duplicates vary by 1.13 R_A. In cases where there is a significant difference between He isotopes in duplicates we take the value with the highest ^{4}He/^{20}Ne to be most robust, because it indicates the lowest level of air contamination which is likely the culprit of any disagreement.

Across the CVZ, air-corrected helium isotope ratios range from 0.1 R_A to 2.6 R_A, and are slightly lower (more radiogenic) than recent reports of He isotopes from fluids and gases within the region (which range from 0.1 R_A to 5.5 R_A; Supplementary Table S1). Across the SVZ, air-corrected helium isotope ratios range from 0.7 R_A to 5.0 R_A, and are also generally lower (more radiogenic) than recent reports of He isotopes from the region (Agusto et al., 2013; Benavente et al., 2013; Roulleau et al., 2016; Tardani et al., 2016; Tassi et al., 2017; Lages et al., 2021; Tardani et al., 2021) which range from 0.5 R_A to 8.4 R_A (Supplementary Table S1).

Variations in He isotope (R_C/R_A) values are apparent between the CZV and SVZ, as well as within each region. These variations are most apparent when plotted against Lithosphere Asthenosphere Boundary (LAB) depths at each sample site (**Figure 5**), according to the model of Tassara and Echaurren (2012). High He isotope (R_C/R_A) values in each region occur where LAB depths are lowest. Though this result may in part reflect thin LAB model anomalies along the arc axis that arise due to high heat flow in regions of active volcanism, the correlation also persists across the entire data range. In summary, the most prominent characteristic of CVZ and SVZ helium isotope results is that all samples are characterized by an admixture of mantle

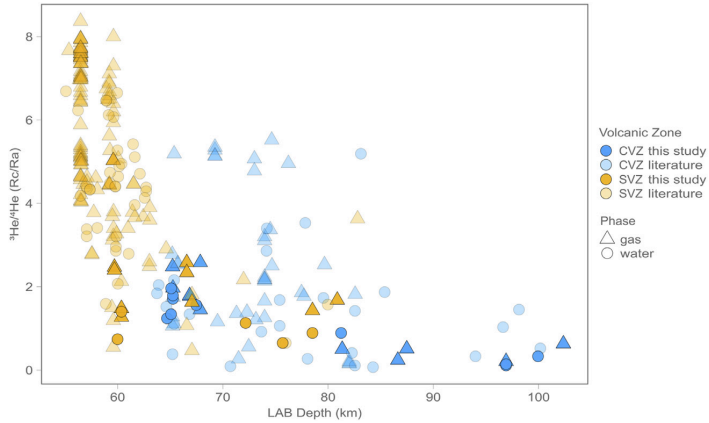

FIGURE 5 | Helium isotopes vs. Lithosphere Asthenosphere Boundary (LAB) depths according to the model of Tassara and Echaurren (2012) for gas (triangles) and water (circles) phase samples. Notably there is a negative correlation between He isotopes (R_C/R_A)and LAB depth.

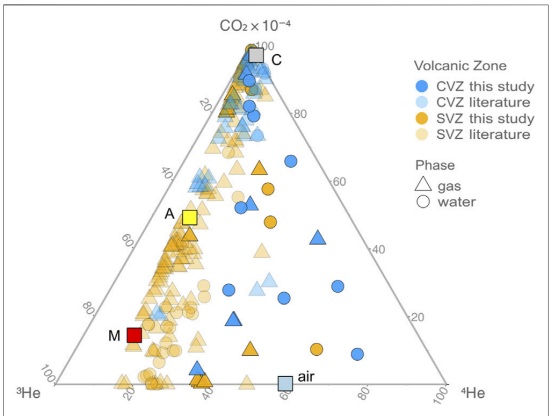

FIGURE 6 | Ternary plot of CO_2, ^{3}He, and ^{4}He for gas (triangles) and water (circles) phase samples from the CVZ and SVZ, illustrating the effects of crustal and radiogenic contamination of mantle-like volatiles. For reference, we plot "mantle" (^{3}He/^{4}He = 8 ± 1 R_A; $CO_2/^3$He = 2 × 10^9) with a red square (M) (Marty and Jambon, 1987), average arc mantle (^{3}He/^{4}He = 5.4 ± 1.9 R_A; $CO_2/^3$He = 1.2 × 10^{10}) with a yellow square (A) (Hilton et al., 2002), air (^{3}He/^{4}He = 1 R_A; $CO_2/^3$He = 5.5 × 10^7) with a blue square (air) and crust (^{3}He/^{4}He = 0.05 R_A; $CO_2/^3$He = 1 × 10^{13}) (Shaw et al., 2003; Barry et al., 2013) with a gray square (C). All gas samples fall on or are close to a binary mixing trajectory between mantle helium and variable amounts of crustal contamination. Fluid samples display lower $CO_2/^3$He and helium isotope values, suggesting carbon removal (calcite precipitation). There is no evidence for degassing induced fractionation, as this would drive water samples in the opposite direction as observed trends.

and radiogenic (i.e., crustal) contributions. The highest values from this study plot well below the nominal range of values associated with upper mantle helium (8 ± 1 R_A) whereas the lowest ratios are approaching the radiogenic He production ratio (0.05 R_A) (e.g., Morrison and Pine, 1955). Lages et al. (2021) recently pointed out that He isotopes from fluid inclusion lava data retain higher He isotope values on average compared to the gas and water phase data presented here.

4.2 Carbon Isotopes [δ^{13}C (CO_2)]

C-isotope ratios (δ^{13}C) range from −15.3‰ to −1.2‰ (versus VPDB) within CVZ samples, and from −17.2‰ to −4.1‰ (versus VPDB) within SVZ samples. On average, CVZ samples have higher δ^{13}C values (average = −8.7‰) compared to SVZ samples (average = −10.8‰).

4.3 $CO_2/^3$He Values

$CO_2/^3$He values vary over two orders of magnitude in CVZ samples, from ~6.9 × 10^8 (below MORB-like at 2 × 10^9) to higher values (~1.7 × 10^{11}) typically associated with input from crustal lithologies (e.g., O'nions and Oxburgh, 1988). The high $CO_2/^3$He values are consistent with either subducted carbon contributions and/or crustal assimilation upon fluid ascent and storage in the crust (**Figure 6**). $CO_2/^3$He varies by nearly five orders of magnitude in SVZ samples, from ~4.7 × 10^7 (well below MORB-like) to higher values (~1.7 × 10^{12}), well above the MORB range. The low $CO_2/^3$He values in the SVZ suggest that carbon may be preferentially removed in the crustal system (see **Section 5.3.3** for details).

5 DISCUSSION

A number of processes can affect regional geothermal ^{3}He/^{4}He ratios, δ^{13}C values and associated He–CO_2 characteristics. Here we aim to determine which samples have ^{3}He/^{4}He, $CO_2/^3$He, and δ^{13}C values most representative of the mantle source composition versus those that have been modified by secondary processes (e.g., carbon addition/loss, hydrothermal-related fractionation, and calcite precipitation) (**Figure 6**). Using such an approach, we

are able to elucidate the sources and sinks of volatiles, as well as their pathways from the mantle/crustal source to the surface. Ultimately the goal is to understand how large-scale (i.e., margin-wide) tectonic processes control the stark He-C geochemical variability that we observe between the CVZ and the SVZ.

5.1 Helium

5.1.1 Helium Sources

Helium can be derived from the mantle, crust, and/or atmosphere, and the relative contributions of these different sources will ultimately control the $^3He/^4He$ of a given sample. When considering all geothermal data [i.e., our data (**Table 1**) and literature data (Supplementary Table S1)], we show that uncorrected He isotope (R/R_A) values range from 0.1 to 7.3 R_A in the CVZ (n = 191) and from 0.5 to 8.3 R_A in the SVZ (n = 226), which is consistent with previous findings (e.g., Lages et al., 2021). Air-corrected $^3He/^4He$ is much lower on average in the CVZ (R_C/R_A = 1.8 R_A; 1-sigma standard deviation = 1.4 R_A) relative to the SVZ (R_C/R_A = 5.0 R_A; 1 sigma S.D. = 2.1 R_A). Nearly all samples have $^4He/^{20}Ne$ values that are significantly higher than air (= 0.32) or air-saturated water (ASW) (= 0.26 at 15°C; **Figure 4**), suggesting negligible atmospheric contributions. For our data, we adopt the methods of Hilton, (1996) and use "*X*-values" to correct He isotope ratios for atmospheric contribution. For gas samples, the *X*-value is defined using **Eq. 1**:

$$(X)_{gas} = (^4He/^{20}Ne)_{measured}/(^4He/^{20}Ne)_{air} \quad (1)$$

Where $(^4He/^{20}Ne)_{measured}$ is the measured ratio and $(^4He/^{20}Ne)_{air}$ is the value of air.

For water samples, measured $^4He/^{20}Ne$ values are converted to *X* values using temperature-dependent Bunsen solubility coefficients (β; Weiss, 1971), following **Eq. 2**:

$$(X)_{fluid} = (^4He/^{20}Ne)_{measured}/(^4He/^{20}Ne)_{air} \times (\beta_{Ne}/\beta_{He}) \quad (2)$$

For pure fresh water at 15°C, β_{Ne}/β_{He} = 1.22 (Weiss, 1971).

The *X*-value can then be combined with measured He isotope values (R/R_A) to calculate a corrected He isotope value (R_C/R_A):

$$R_C/R_A = ((R/R_A \times X) - 1)/(X - 1) \quad (3)$$

Where R/R_A is the measured He isotope value, reported relative to air, and X is calculated using **Eqs 1**, **2**.

5.1.2 Helium Mantle-Crust Mixing

Once air contributions are quantified and corrected for, we use air-corrected He isotope (R_C/R_A) values to calculate the fraction of mantle-derived He, assuming a binary mixture between mantle and crustal endmembers (e.g., Barry et al., 2013):

$$\%\,\text{Mantle He} = (R_C/R_A - {}^3He/^4He_{Crust})/(^3He/^4He_{Mantle} - {}^3He/^4He_{Crust}) \quad (4)$$

where, $^3He/^4He_{Mantle}$ = 8 R_A (Graham, 2002; Lages et al., 2021), and $^3He/^4He_{Crust}$ = 0.05 R_A (Morrison and Pine, 1955).

Using **Eq. 4**, we calculate that the CVZ is characterized by 21% mantle He and 79% crustal He on average. In contrast, we find that the SVZ is characterized by 62% mantle He and 38% crustal He on average. The extent of mixing between air, crustal and mantle components is most likely controlled by the thickness of the crust. We note that in the CVZ, where the crust is ~70 km thick on average, the $^3He/^4He$ is much lower (average (mean) R_C/R_A = 1.8 R_A) than in the SVZ (average (mean) R_C/R_A = 5.0 R_A), where the crust is only ~40 km thick on average. We hypothesize that, as fluids and gases migrate through thicker sections of crust in the overriding plate, they incorporate radiogenic ^4He due to interaction with the U- and Th-rich country rock (e.g., Hilton et al., 1993). This broad trend was recently pointed out by Lages et al., 2021, who presented a comprehensive He isotope compilation that included fluid and gas data as well as newly-reported He isotope data from fluid inclusions in minerals from lavas (mostly from the Northern Volcanic Zone). In total, the Lages et al. (2021) He isotope compilation reports 261 gas and water He isotope data points from the literature (spanning the NVZ, CVZ, and SVZ). Many of these data overlap with the compilation presented here, which focuses only on the CVZ and the SVZ, but contains (He and/or C isotope) data for 417 samples in total. The addition of C isotope data allows for interrogation of sources and processes affecting C cycling.

Several previous studies focused on He isotopes throughout the ACM (e.g., Hilton et al., 1993; Lages et al., 2021). Using fluid inclusion data, Lages et al., 2021 demonstrated that lavas retain mantle source signals (i.e., high $^3He/^4He$) more effectively than fluid and gas samples, with the most pristine lava samples yielding a He isotope endmember value of 8.0 R_A in the CVZ and 7.9 R_A in the SVZ. However, fresh lavas are only accessible in the volcanic arc, whereas geothermal fluids and gases provide a window into volatile cycling across the entire arc (forearc, arc, backarc). We thus adopt a mantle endmembers of 8.0 R_A for the above mixing calculation (**Eq. 4**). Notably, observed He isotope values below 8 R_A cannot be due to subduction of U- and Th-rich material, because radiogenic He-rich sediments would need to be far too old (i.e., >1890 Myr) to explain the observed data (Hilton et al., 1993; Lages et al., 2021). Instead, low He isotopes in the ACM are likely the result of either: 1) magma aging, or 2) fluid interaction/assimilation with the country rock. Hilton et al. (1993) showed that the latter scenario could explain He isotope trends if just 1% of country rock was assimilated from 10 million year old country rock. This would also satisfy observations in Sr and Pb isotope systematics (Hilton et al., 1993; Scott et al., 2018). An assimilation mechanism is preferred over magma aging, because in this scenario He isotope variability would be coupled with the age of the lowermost crust, thus predicting that SVZ samples would retain higher $^3He/^4He$ than CVZ samples, due to the relative thickness and antiquity of the crust.

5.2 Carbon

5.2.1 Carbon Sources

Carbon in geothermal samples can be derived from the mantle, the overlying crust, or introduced through subduction of carbon-laden sediments, which are released at depth and migrate to surface manifestations across the volcanic arc (e.g., Sano and Marty, 1995). $CO_2/^3He$ and $\delta^{13}C$ data can be used to differentiate between various carbon sources; however it is often difficult to definitively differentiate between the latter two processes. Here,

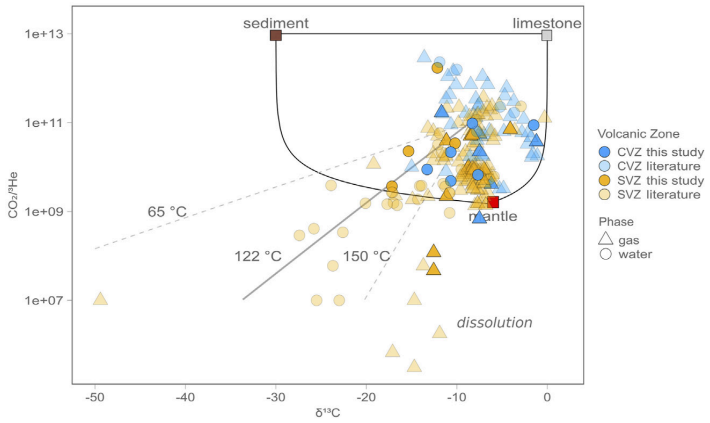

FIGURE 7 | $CO_2/^3He$ vs. $\delta^{13}CO_2$ for all gas (triangles) and water (circles) samples from this study (bright symbols) as well as from published studies (light symbols). Also plotted are subduction-related source end-member compositions for mantle (M), limestone (L), and sediment (S) for reference, along with mixing lines, after Sano and Marty (1995). Solid mixing lines represent binary mixtures between the three endmember values. The uncertainties on the $CO_2/^3He$ vs. $\delta^{13}CO_2$ data are lower than given by the size of the symbols. Predicted calcite fractionation model trends at 65°C, 122°C, and 150°C are also shown for fluid samples, assuming an initial $\delta^{13}C_i$ composition of −8.4‰ and $CO_2/^3He = 1.0 \times 10^{11}$, which are the average values from all gas samples. In contrast, gas samples with isotopically low $CO_2/^3He$ are likely affected by dissolution, which will drive $CO_2/^3He$ values down in gas samples.

we model $CO_2/^3He$ and $\delta^{13}C$ data for a total of 172 gas samples. These are mostly published data (n = 158) (Hilton et al., 1993; Hoke et al., 1994; Varekamp et al., 2006; Sepúlveda et al., 2007; Aguilera, 2008; Ray et al., 2009; Tassi et al., 2009; Tassi et al., 2010; Capaccioni et al., 2011; Tassi et al., 2011; Aguilera et al., 2012; Agusto et al., 2013; Benavente et al., 2013; Chiodi et al., 2015; Aguilera et al., 2016; Benavente et al., 2016; Roulleau et al., 2016; Tardani et al., 2016; Tassi et al., 2016; Arnold et al., 2017; Tassi et al., 2017; Lopez et al., 2018; Chiodi et al., 2019; Arnold et al., 2020; Inostroza et al., 2020; Robidoux et al., 2020; Lages et al., 2021; Tardani et al., 2021; Filipovich et al., 2022) and samples from this study (n = 14). We focus on gas samples in order to understand sources, as gases are less susceptible to fractionation processes than water phase samples. He–C isotope characteristics are similar to observations in other arcs worldwide (Sano and Marty, 1995; Sano and Williams, 1996), suggesting a prominent role of the subducting slab in supplying carbon to gas manifestations in both the CVZ and SVZ.

5.2.2 Subduction-Derived Carbon

Previous studies in the ACM have noted the role of sediment-derived fluids in melting the Sub-Andean mantle (e.g., Stern, 2007) and supplying volatiles to volcanically-derived samples (Ray et al., 2009). To quantify the extent of slab-derived CO_2, we adopt the approach of Marty et al. (1989), Varekamp et al. (1992), Sano and Marty (1995) which uses observed He-CO_2 characteristics to deconvolute mantle- versus subduction-derived (i.e., organic sediments and inorganic limestones) components. Specifically, this approach assumes that all deviations of volcanic gases from the mantle composition are subduction/mantle derived and that there is no crustal input from the overriding slab. Given these assumptions, He–CO_2 characteristics (relative abundances and $\delta^{13}C$ systematics) can be used to resolve CO_2 contribution from three distinct sources: limestone (L) from subducted sediment and mineralized within slab basement, sedimentary (organic) carbon (S) from subducted sediment, and the mantle wedge (M). Each endmember source component is assumed to have a distinctive $CO_2/^3He$ (M = 2×10^9; L = 1×10^{13}; S = 1×10^{13}) and $\delta^{13}C$ (M = −5‰; L = 0‰; S = −30‰) signature. In **Figure 7**, we plot the $CO_2/^3He$ ratios as a function of $\delta^{13}C$ for all gas samples, together with binary mixing trajectories. In order to quantify the relative proportions of CO_2 derived from each respective endmember component, mass fractions of three major sources of carbon are quantitatively calculated with **Eqs 5–7** below (Sano and Marty, 1995):

$$(^{13}C/^{12}C)_O = f_M(^{13}C/^{12}C)_M + f_L(^{13}C/^{12}C)_L + f_S(^{13}C/^{12}C)_S \quad (5)$$

$$1/(^{12C}/^3He)_O = f_M/(^{12}C/^3He)_M + f_L/(^{12}C/^3He)_L + f_S/(^{12}C/^3He)_S \quad (6)$$

$$f_M + f_L + f_S = 1 \quad (7)$$

where subscripts L, S and M correspond to the end members limestone, sediment and mantle (**Table 2**) and subscript O = observed.

In this way we calculate that the average CO_2 provenance in the CVZ to be L:S:M = 70:22:8, whereas the average CO_2 provenance in the SVZ is L:S:M = 55:24:21 (**Table 2**). This suggests more significant mantle contributions to gases in the SVZ, which is consistent with the observation of higher $^3He/^4He$. These calculations equate to an average L/S of 3.2 and an average (L + S)/M of 11.9 for the CVZ, and an average L/S of 2.3 and an average (L + S)/M of 3.7 for the SVZ (**Table 2**). This estimate for

the SVZ is broadly consistent with previous estimates by Ray et al. (2009) and findings at other arc-related geothermal systems (e.g., Sano and Marty, 1995).

If only gas samples with $^3He/^4He$ above 5 R_A are considered, the calculated L:S:M ratios change to 73:10:17 and 54:22:24 for the CVZ and SVZ, respectively. In this scenario, the mantle contribution is in better agreement between the two regions, which is not surprising considering that only high $^3He/^4He$ samples are being considered. Notably, slab-derived contributions dominate the CO_2 budget in both regions, irrespective of whether all samples or only those with high He isotope ratios are considered. Considering only samples with He isotopes >5 R_A, the average L/S is 7.0 and the average (L + S)/M is = 5.1 in the CVZ, and the average L/S is 2.5 and the average (L + S)/M is 3.2 in the SVZ. All L, S, M calculations are reported in **Table 2**.

We can directly compare estimates of L:S:M (**Table 2**) with input estimates of carbon concentrations in subducting lithologies (e.g., Clift, 2017). Carbon input estimates are compiled from scientific ocean drilling studies, which document the amount of carbonate and organic carbon subducted at convergent margins. Notably, the carbon input estimates from Clift (2017) factor in the erosional or accretionary nature of each margin when estimating how much carbon is delivered to the subduction zone. However, CVZ estimates remain poorly constrained due to lack of drill cores offshore of the CVZ. As noted above, the average output L/S in the CVZ and SVZ are 3.2 and 2.3, respectively. However, Clift (2017)'s L/S input estimates are 5.0 in the CVZ and 1.0 in the SVZ. Notably, if only samples with high He isotopes (>5 R_A) are considered (which equates to filtering out samples with a significant crustal contribution), then the L/S ratios increase from 3.2 to 7.0 and from 2.3 to 2.5 in the CVZ and SVZ, respectively (**Table 2**). In the CVZ, where crustal assimilation is more prevalent due to the exceedingly thick crust, this filtering exercise increases output L/S estimates by over a factor of two, presumably to a more representative input value [above estimates from Clift (2017)]. This suggests that the C contribution from the CVZ overriding plate is dominantly from organic rich sediments. In the SVZ, there is not a significant shift in L/S when a filter for only high He isotope samples is applied, due to the fact that the (thinner) crust does not have a significant impact on the L/S ratio.

In either scenario (with and without filtering), there is broad agreement between input L/S (Clift, 2017) and output estimates (this study) (**Table 2**). The fact that input and output estimates do not match perfectly may suggest that subducted C is actually being released over a much wider area than previously thought. We know from other studies (e.g., Barry et al., 2019a) that subducted carbon is likely released across the entire convergent margin (outer forearc, forearc, arc, backarc) and that adopting such a narrow view of where it could be released (i.e., only in the high He isotope arc) is likely an oversimplification. It is therefore important to sample across the entire arc system, so that carbon output estimates can be more systematically compared with input estimates. Additionally, the discrepancy between L/S inputs and outputs may suggest that C-bearing fluids are preferentially released from different slab lithologies at different subduction depths, similar to the process recently proposed for subducted sulfur by de Moor et al. (2022). Hence, one possible explanation for the difference between L/S inputs and outputs is that limestone-derived and organic sediment-derived C are not released in the same regions of the arc. The implication is that C isotope compositions of primary subduction-related fluids could vary significantly across the arc.

Similar disparities between input and output estimates have been observed at other arc-related localities, e.g., the Central America Volcanic Arc (CAVA), where output L/S estimates (3.8–5.6) were significantly lower than sedimentary input L/S estimates (11.5–13.6) (De Leeuw et al., 2007). The sense of the inputs-outputs discrepancy in the SVZ is in the opposite direction to CAVA [i.e., L/S output estimates (this study) are significantly higher (L/S = 2.3–2.5) than input estimates (L/S = 1.0; Clift, 2017) (**Table 2**)]. However, when only high (>5 R_A) samples are considered from the CVZ, the inputs-outputs discrepancy trends in the same direction as the SVZ (**Table 2**). The fact that L/S output estimates are lower than inputs in the CVZ suggests that there are relatively more organic contributions than what would be expected if all the C were quantitatively/proportionally released from the slab beneath the arc front. This could mean that limestone carbon is either preferentially 1) released in the forearc or 2) recycled to the deep mantle, whereas organic C is preferentially released beneath the volcanic arc. Notably, the latter scenario was recently suggested by Bouilhol et al. (2022), who noted decoupling of inorganic and organic carbon during subduction. Though speculative at this point, this topic may be of interest for future investigations. An alternative explanation for the general lack of agreement between carbon input and output estimates is that subducted sediment-derived C may not be entirely responsible for the observed variations in the gas chemistry data. In the following sections we explore alternative explanations for the variations in He-C characteristics.

5.2.3 Assimilation of Carbon From the Overriding Plate

The Sano and Marty (1995) approach assumes all He-C characteristics are controlled by subduction and mantle inputs and that there is no significant input of assimilated crustal CO_2. This assumption may be valid for high temperature arc samples marked by high $^3He/^4He$, but here we report and compile data from across the entire arc system (i.e., forearc, arc, backarc). In such diverse tectonic settings He isotope ratios are highly variable (**Figure 8**) and often much lower, suggesting significant interaction with the crust. In **Section 5.1** we suggested that He isotope variations are primarily controlled by the thickness of the crust, with lower He-isotope values on average in the CVZ versus the SVZ. We surmise that similar processes could affect the carbon systematics, as $CO_2/^3He$ is higher (2.9×10^{11}) on average in the CVZ (1-sigma standard deviation = 5.4×10^{11}) and lower (4.4×10^{10}) on average in the SVZ (1-sigma standard deviation = 1.4×10^{11}) (**Figure 8**). Additionally, $\delta^{13}C$ is −8.7‰ (1-sigma standard deviation = 4.5‰) on average in the CVZ and −10.8‰ (1-sigma standard deviation = 3.7‰) on average in the SVZ. Broadly speaking, the average $CO_2/^3He$ in the SVZ is closer to the mantle range (vs. the CVZ), whereas the average carbon

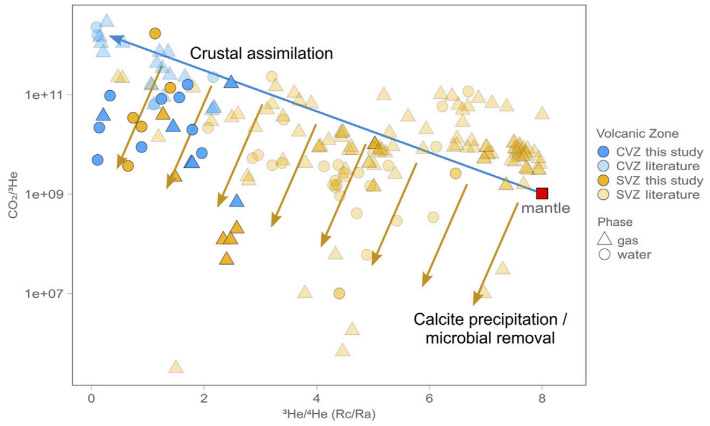

FIGURE 8 | $CO_2/^3He$ vs. He isotopes (R_C/R_A) for all samples. There is a notable trend (blue arrow) from the SVZ to the CVZ whereby samples range from nearly mantle-like to crustal (low He isotopes and higher $CO_2/^3He$). Yellow arrows indicate the effect of calcite precipitation and microbial removal. The fact that these arrows do not point straight down suggest that the residence time in the crust required for calcite removal is concomitant with time required to moderately lower He isotopes through ^4He addition.

isotope signature is farther from the canonical mantle range (vs. the CVZ). In **Section 5.3** we explore additional fractionation processes that could explain this apparent dichotomy.

5.3 Crustal Processes Acting to Modify He-C Characteristics

Carbon recycling and release from the subducted slab into volcanic fluids has been proposed to control the carbon isotope systematics across the ACM (Hilton et al., 1993; Ray et al., 2009). However, water samples suggest that secondary crustal processes are also at work in the region. This section therefore focuses on the additional processes that can modify the He–CO_2 of geothermal fluids, with the aim of determining if we can differentiate between source features (see **Sections 5.1**, **5.2**; mixing of mantle and slab-derived components) and secondary processes such as crustal overprinting (e.g., Mason et al., 2017; Karolytė et al., 2019), phase fractionation (e.g., Ray et al., 2009; Barry et al., 2013), gas dissolution and/or precipitation of calcite (Ray et al., 2009; Newell et al., 2015; Barry et al., 2019b). Likely, all of these processes exert some control on the observed He-C features.

5.3.1 Crustal Overprinting and Assimilation

As discussed in **Sections 5.1.2**, **5.2.3**, crustal overprinting appears to be pervasive in fluid and gas samples, particularly in lower temperature samples from the CVZ. He isotopes are highly variable, suggesting different amounts of assimilation with U- and Th- (and hence ^4He-) rich crust, consistent with radiogenic (i.e., Sr and Nd) observations (Hilton et al., 1993; Scott et al., 2018). Carbon appears to be similarly affected by interaction with the crust. Higher carbon isotope values on average in the CVZ indicate that isotopically heavy (i.e., inorganic) carbon is being preferentially assimilated in the CVZ versus the SVZ (**Figure 7**), suggesting that CVZ samples may be influenced by isotopically-heavy crustal/carbonate CO_2 dissolution (e.g., Mason et al., 2017; Karolytė et al., 2019) in addition to slab/MORB-like starting values. Notably, several previous He-C studies in acidic volcanic arc settings have suggested the release of previously sequestered CO_2 (Wehrmann et al., 2011; Dawson et al., 2016; de Moor et al., 2016; Mason et al., 2017). For example, Mason et al. (2017) attributed isotopically high C isotope values in mature continental arcs with accreted carbonate platforms (i.e., the CVZ) to the reworking of crustal limestone, effectively superimposing this signature on top of volcanic/subduction source features. Assimilation of carbon rich crustal material likely also occurs in the SVZ, but to a lesser extent. Alternatively, the elevated $CO_2/^3He$ (**Figure 6**) and non-mantle-like $\delta^{13}C$ values (**Figure 7**) could be entirely explained by subduction features as suggested in **Section 5.2**, but this would indicate that the much thicker crust in the CVZ versus the SVZ is not affecting the samples, which seems unlikely. A third explanation is that the carbon isotopes are controlled by additional secondary processes that induce fractionation, as is discussed in the following sections. We hypothesize that these competing processes together act to control volatile budgets not only in the Andes, but likely in arcs globally.

5.3.2 Degassing, Phase Fractionation, and Gas Dissolution

During degassing or boiling, a free gas phase separates from the fluid phase within the hydrothermal system. Helium partitions preferentially into the vapor phase relative to CO_2 as a consequence of its lower solubility in aqueous fluids (Ellis and Golding, 1963; Vogel et al., 1970; Ozima and Podosek, 1983; Ray et al., 2009; Barry et al., 2013).

For this reason, gas samples are often considered more representative of source features than water samples, as they are not subject to this additional fractionation mechanism. Accordingly, degassing and phase fractionation drive water $CO_2/^3He$ towards higher values (**Figure 6**) because CO_2 is more soluble in water than He. However, the opposite trend is observed in a subset of our data, as well as in the compiled literature data (i.e., we observe lower $CO_2/^3He$ in water samples versus gas samples on average; **Figure 6**). This strongly suggests that hydrothermal phase separation following degassing is not the dominant mechanism controlling He-C systematics between water and gas phase in the CVZ and SVZ, and that carbon is actively being removed from water samples. Low $\delta^{13}C$ values in the lowest $CO_2/^3He$ samples corroborate this explanation and we surmise that this is the result of calcite precipitation (see **Section 5.3.3** below; **Figure 7**).

Similarly, Gilfillan et al. (2009) and Güleç and Hilton (2016) showed that gas loss by dissolution in water can also result in $CO_2/^3He$ fractionation trends in both gas and water phase samples. Notably, the predicted fractionation gas trends are broadly similar to anticipated calcite precipitation trends (e.g., Güleç and Hilton, 2016). As gases ascend through bubbling springs towards the surface, they likely intersect one or more gas-undersaturated aquifers. When a gas phase comes into contact with such an aquifer, it preferentially loses the more soluble gas species (i.e., C) relative to the less soluble gas species (i.e., He), resulting in lower $CO_2/^3He$ in the gas phase which ultimately manifests at the surface (**Figure 7**). We surmise that this may have affected several of the gas samples in the SVZ (as noted on **Figure 7**). The opposite is true of water phase samples, which are ultimately left with elevated $CO_2/^3He$. Notably, a concomitate fractionation occurs in C-isotope of CO_2, resulting in a isotopically lower $\delta^{13}C$ values in residual gas phase sample. Such fractionation can sometimes be difficult to distinguish from that caused by calcite precipitation (e.g., Güleç and Hilton, 2016). The low $CO_2/^3He$ values observed in SVZ water samples suggests that carbon is actively being removed from the water and thus we attribute these signals to calcite precipitation (see **Section 5.3.3**).

5.3.3 Precipitation of Calcite

Secondary processes can be assessed using a CO_2-^3He-^4He ternary diagram (**Figure 6**), including the effects of carbon removal due to carbonate mineral formation in the crust. In **Figure 7**, $CO_2/^3He$ vs. $\delta^{13}C$ is plotted for all samples and it is clear that, on average, water and gas phase samples have broadly overlapping $CO_2/^3He$. However, we surmise that fluid samples in both regions may have experienced CO_2 loss by calcite precipitation at depth. In such a scenario, gases are dissolved in deep fluids that interact with country rock during transport through the hydrothermal system toward the surface. This migration results in the fluids becoming enriched in cations (e.g., Ca^{2+}, Mg^{2+}) (Spane and Webber, 1995; McLing and Johnson, 2002), especially where mafic rocks are prevalent. The CO_2-rich fluids emanating from the slab/mantle then react with these cations to precipitate carbonate minerals such as calcite or aragonite. During this reaction, CO_2 is retained in the carbonate mineral (e.g., $CaCO_3$, $MgCO_3$), resulting in lower $CO_2/^3He$ and more negative $\delta^{13}C$ in residual fluids as the heavier isotope of C is preferentially partitioned into the solid (carbonate) phase. Notably, this process is highly temperature-dependent, so by assuming a constant geothermal gradient, the extent of carbon isotope fractionation can be used to constrain the temperature (and depth) at which this process occurs. When considering data from this study together with published water data, we note that CVZ water samples exhibit higher $CO_2/^3He$ values on average, as well as the higher $\delta^{13}C$ values, only extending down to −18.7‰, whereas SVZ water samples exhibit the lower $CO_2/^3He$ values on average and $\delta^{13}C$ values as low as −27.4‰. Thus, the first order observation is that some samples in the SVZ, with very low $CO_2/^3He$ and $\delta^{13}C$, may reflect extreme carbon removal due to calcite precipitation (**Figure 8**).

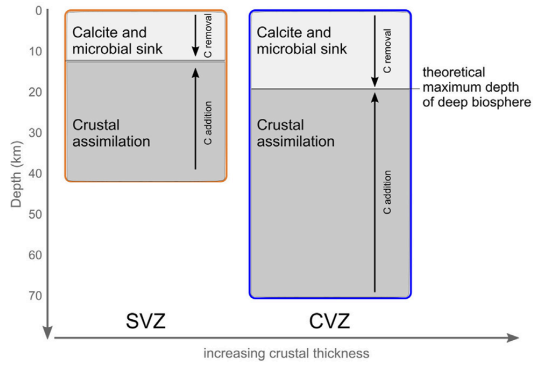

FIGURE 9 | Cartoon showing crustal thickness and the relative proportions of C removal (as calcite precipitation and potential microbial sink) vs. C addition (crustal assimilation) in the two volcanic zones. As the thickness of the crust increases from ~40 km in the SVZ to ~70 km in the CVZ, the depth to which biologically mediated calcite precipitation can occur, increases only marginally compared to crustal thickness. This disparity in crustal thickness results in different contributions of these competing processes. We hypothesize that these various processes each contribute to various extents to shape the volatile budget not just in the Andes, but likely in arcs globally.

In **Figure 7**, samples are plotted along with Rayleigh distillation fractionation lines for calcite precipitation at 65°C, 122°C, and 150°C. Notably, 65°C is the temperature at which calcite fractionation was proposed to occur in the Costa Rica forearc (Barry et al., 2019a). However, in the ACM, it appears that calcite precipitation occurs at higher temperatures, extending to temperatures as high as 150°C, which are consistent with observations from Baja, Mexico (Barry et al., 2020). Notably, 122°C is the estimated maximum temperature of cultured microorganisms (Takai et al., 2008), while 150°C has long been considered the theoretical upper limit for Life (Merino et al., 2019). The upper temperature limit of 150°C corresponds to a depth of ~6.8 km if a uniform geothermal gradient of ~22°C/km (Rothstein and Manning, 2003) is assumed. However, the actual depth for these temperatures might change in response to local heat flow, the type of rocks present, and the tectonic setting. For example, previous work has

suggested a shallower geothermal gradient in the forearc of cold subduction zones, such that the 122°C isotherm might reach ~15 km or deeper (Plümper, et al., 2017). Fullerton et al. (2021) used a depth of 15 km to calculate the total biomass present in the Costa Rican Forearc crust. The CVZ and SVZ have different average heat flows and large heterogeneities (Hamza et al., 2005). Taking this into account, and using rock compositions ranging from andesite to rhyolite, the theoretical depths to the 150°C isotherms are 12 and 20 km for the SVZ and CSZ, respectively (**Figure 9**). Within this area, low temperature processes like calcite precipitation and microbial metabolism might remove significant amounts of carbon (Barry et al., 2019a; Fullerton et al., 2021). Previously, microbes have been shown to serve as nucleation sites for the precipitation of carbonate minerals across a wide range of temperatures (e.g., Fouke et al., 2000; Tsesarsky et al., 2016). The agreement between the best fit calcite precipitation temperature and the upper temperature limit for life (~122°C) is consistent with biological nucleation potentially being important for overcoming kinetic limitations on calcite precipitation (**Figure 9**), but could also simply be a coincidence.

In order to estimate how much carbon has potentially been removed due to calcite precipitation, we construct a simple model (after Ray et al., 2009; Barry et al., 2019a; Barry et al., 2020) assuming that CO_2 is released from the slab/mantle mixture and reacts with groundwater to form 1) an initial DIC pool (dissolved CO_2) and 2) a free CO_2 gas pool. The fractionation factor (α) at isotopic equilibrium for CO_2-HCO_3^--$CaCO_3$ is temperature dependent (**Eq. 8**) and can be derived from the empirically determined fractionation between DIC and calcite (Ohmoto and Rye, 1979).

$$\alpha = \mathrm{Exp}\left(\left(-8.914 \times 108/T^3 + 8.557 \times 10^6/T^2 - 18.11 \times 10^3/T + 8.27\right)/1000\right) \quad (8)$$

where T is the temperature in Kelvin.

In **Figure 7**, the initial $\delta^{13}C_i$ input is assumed to be homogenous at −8.4‰, which corresponds to the average value of all gas samples (Supplementary Table S1). The starting $CO_2/^3He$ is assumed to be 1.0×10^{11}, which is the average for all gas samples compiled here. We emphasize that assuming a single starting point is likely an oversimplification as we are dealing with a very large variety of thermal manifestations; however these assumptions are made for the purposes of presenting a unified model for all data. The fraction (f) of carbon loss can be calculated for any observed $\delta^{13}C_o$ value can be calculated using **Eq. 9** (Holloway and Blank, 1994; Barry et al., 2021).

$$f = 1 - \left[\left(\mathrm{Exp}\left(\mathrm{Ln}\left(\left(\delta^{13}C_o + 1000\right)/\left(\delta^{13}C_i + 1000\right)\right)/(\alpha - 1)\right)\right)\right] \quad (9)$$

Likewise the $CO_2/^3He$ can be calculated by accounting for the amount of carbon removed, assuming that no ^3He is lost, due to its inert nature (**Figure 7**). The fraction (f) of carbon loss increases as calcite forms and the residual DIC $\delta^{13}CO_2$ and $CO_2/^3He$ decrease. Given these assumptions (calcite precipitation temperature = 122°C; $\delta^{13}C_i$ = −8.4‰; $CO_2/^3He_i$ = 1.0×10^{11}), the model predicts that >99% of the original carbon must be lost from the most highly fractionated water samples in the SVZ, and >97% in the CVZ, resulting in low $CO_2/^3He$ and $\delta^{13}C$. On average, 90% of carbon was removed from water samples in the SVZ and 40% was removed from water samples in the CVZ. Notably, our assumed starting compositions are non-unique and if mantle-like starting values are assumed instead, a slightly different amount of fractionation would be required to explain the data (**Figure 7**). The fact that the signal associated with calcite precipitation appears to be stronger in the SVZ compared to the CVZ suggests that this process is most prominent in regions with thinner crust, and/or more mafic rocks, providing cations that promote calcite precipitation (**Figure 9**). Notably, in the CVZ, there is also significant calcite precipitation, but the overall prevalence of this process is not as apparent, perhaps due to greater contributions of crustal carbon from the overriding plate to hot spring emissions (i.e., higher starting $CO_2/^3He$ due to assimilation), which appears to be pervasive throughout the CVZ (**Figure 8**).

5.4 He-C and Along-Arc Properties

Large scale subduction-related parameters vary significantly along-strike, likely affecting surface volatile characteristics. Below, we briefly discuss how these large scale features may affect the He-C signatures that are observed across the CVZ and SVZ.

5.4.1 Sediment Composition and Thickness

The results from **Section 5.2.2** suggest that subduction of inorganic and organic carbon likely impact gas and fluid emissions across the arc. However, deciphering source features from secondary fractionation effects in the overriding plate remains somewhat enigmatic. Higher precipitation in the southern Andes leads to higher sedimentation rates offshore of the SVZ (**Figure 1A**). The physical barrier of the Juan Fernandez Ridge at ~32 °S inhibits northward sedimentary transport along the trench, resulting in a sediment-starved incoming plate and trench at the CVZ and a sediment-flooded trench offshore of the SVZ [offshore sediment thickness is ~150 m in the CVZ vs. ~500 m in the SVZ (Contreras-Reyes, 2008; Contreras-Reyes, 2010; Völker et al., 2013; **Figure 1B**)]. Because sediments contain structurally bound carbon, the amount of incoming carbon is likely much higher in the SVZ than in the CVZ; however there are no drill cores that are directly relevant to the CVZ. In the absence of significant sediments, altered oceanic crust (AOC) could deliver significant amounts of carbon to the margins, respectively (e.g., Bekaert et al., 2021).

While carbon L/S output estimates (this study) do not perfectly match L/S input estimates (Clift, 2017) (**Table 2**), we note that the trend is in the corresponding direction, suggesting more inorganic L relative to organic S in the CVZ versus the SVZ. The fact that the CVZ retains higher $CO_2/^3He$ (**Figure 8**) despite receiving an order of magnitude less C is critically important, because this suggests that He-C cannot be solely explained by mixing between subducted components and carbon from the mantle wedge. Instead the

crust must be the source of a significant proportion of the carbon in the CVZ (**Figure 9**) through assimilation, which is supported by pervasively low He isotope ratios.

5.4.2 Slab Age, Subduction Rate and Angle

Along the Chile trench, the incoming plate is younger in the SVZ (~30 Ma) than in the CVZ (~45 Ma) (Syracuse and Abers, 2006); however convergence rates are steady between 7–9 cm/yr in each region. Because the amount of carbon delivered to the trench and the ratio of inorganic (L) to organic (S) carbon are almost entirely sediment-controlled, this moderate difference in slab age is not expected to make a significant difference to the budget of subducted C. However, the age difference between these two slabs may result in an initially warmer plate in the SVZ compared to the CVZ, which may promote melting at shallower depths. We surmise above that the disparity between our L/S estimates and the Clift (2017) estimates could be related to C being preferentially released in the forearc of SVZ, which in turn resulted in more calcite precipitation at lower temperatures in the overriding plate (e.g., Barry et al., 2019b). Furthermore, the subduction dip angle is steeper in the SVZ (28°) vs. the CVZ (24°), which likely affects carbon release depths. However, there is not sufficient resolution in the C isotope data to definitively postulate that subduction angle or slab age are primary drivers of He-C features in gas and fluid manifestations across the arc. Notably, previous studies have also estimated that the magmatic CO_2 flux from the CVZ is lower than in the SVZ (Aiuppa et al., 2019), which is broadly consistent with our findings. However, our results indicate that the total carbon flux (magmatic + crustal) may actually be higher in the CVZ, as an additional carbon pool is being mobilized in the CVZ.

6 SUMMARY

Carbon and other volatile elements are actively cycled between Earth reservoirs by plate tectonics at subduction zones, which has major implications for Earth's climate and habitability over geologic timescales. Here, we report He isotope ratios and abundance data for 42 deeply-sourced fluid and gas samples from the CVZ and the SVZ. He isotopes from the CVZ range from 0.1 to 2.6 R_A (n = 23), following correction for atmospheric contributions. Atmosphere-corrected He isotopes from the SVZ range from 0.7 to 5.0 R_A (n = 19). Taken together, these data reveal a clear southeastward increase in $^3He/^4He$, with the highest values (in the SVZ) plotting below the nominal range of values associated with pure upper mantle He (8 ± 1 R_A; Graham, 2002), approaching the mean He isotope value for arc gases of (5.4 ± 1.9 R_A; Hilton et al., 2002). Notably, the lowest values are found in the CVZ, suggesting more significant crustal contributions (i.e., assimilation) (**Figure 8**) to the He budget. The crustal thickness in the CVZ is up to 70 km, significantly larger than in the SVZ, where it is just ~40 km (Tassara and Echaurren, 2012; Assumpção et al., 2013) (**Figures 1B**, **9**). It thus appears that crustal thickness exerts a primary control on the extent of fluid-crust interaction, as helium and other volatiles rise through the upper plate in the ACM, which is broadly consistent with the findings of several previous studies (e.g., Lages et al., 2021). This suggests a masked mantle influence in the CVZ associated with thicker crust adding ^4He. Carbon isotope compositions ($\delta^{13}CO_2$) vary between −12.0‰ and −1.2‰ in the CVZ and $CO_2/^3He$ values vary over three orders of magnitude (9.0×10^8–1.1×10^{12}). In the SVZ, carbon isotopes ($\delta^{13}CO_2$) vary between −14.0‰ and −8.7‰ and $CO_2/^3He$ values vary by nearly three orders of magnitude (4.7×10^7–3.9×10^{10}). Lower $\delta^{13}CO_2$ and $CO_2/^3He$ values in the SVZ are consistent with calcite precipitation in shallow-level (upper ~20 km) hydrothermal systems (Ray et al., 2009; Barry et al., 2019a). We speculate that the coincidence of modeled calcite precipitation temperature (122°C) and the upper temperature limit for life may be consistent with biological nucleation being important for overcoming kinetic limitations on calcite precipitation. Taken together, the bimodal nature of the He-CO_2 data suggests fundamentally different volatile migration pathways in each volcanic region, indicating complex interplay between mantle degassing, sediment delivery, interaction with continental crust, and volatile sequestration *via* secondary processes. Finally, we emphasize that these competing processes are not unique to the Andes and that these models should be applied to understand the volatile budget in other arc settings around the world.

DATA AVAILABILITY STATEMENT

The datasets presented in this study can be found in online repositories. The names of the repository/repositories and accession number(s) can be found in the article/ **Supplementary Material**. The complete dataset and the R code to reproduce the analysis have been permanently archived on Zenodo at DOI: 10.5281/zenodo.

AUTHOR CONTRIBUTIONS

All authors either helped collect samples or analyzed samples. All authors contributed to writing the manuscript.

FUNDING

This work was principally supported by the NSF-FRES award 2121637 to PB, KL, and JM. Field work was also supported by award G-2016-7206 from the Alfred P. Sloan Foundation and the Deep Carbon Observatory to PB, KL, DG, and JM. Additional support came from The National Fund for Scientific and Technological Development of Chile (FONDECYT) Grant 11191138 (The National Research and Development Agency of Chile, ANID Chile), and COPAS COASTAL ANID FB210021 to GJ. DG was partially supported by funding from the European Research Council (ERC) under the European Union's Horizon 2020 research and innovation program Grant Agreement No. 948972—COEVOLVE—ERC-2020-STG.

ACKNOWLEDGMENTS

We also acknowledge M. Correggia and L. Di Iorio for technical assistance with the water samples carbon data analysis at the University of Naples Federico II.

SUPPLEMENTARY MATERIAL

The Supplementary Material for this article can be found online at: https://www.frontiersin.org/articles/10.3389/feart.2022.897267/full#supplementary-material

REFERENCES

Aguilera, F., Tassi, F., Darrah, T., Moune, S., and Vaselli, O. (2012). Geochemical Model of a Magmatic-Hydrothermal System at the Lastarria Volcano, Northern Chile. *Bull. Volcanol.* 74 (1), 119–134. doi:10.1007/s00445-011-0489-5

Aguilera, F., Cortes, J., González, C., and Layana, S. (2016). *Geología y geoquímica de fluidos del campo geotérmico de Cupo, Región de los Ríos, Chile*. Antofagasta, Chile: Private Report.

Aguilera, F. (2008). *Origen y naturaleza de los fluidos en los sistemas volcánicos, geotermales y termales de baja entalpía de la zona volcánica central (ZVC) entre los 17 43'S y 25 10'S*. Antofagasta, Chile: PhD Thesis: Universidad Católica del Norte.

Agusto, M., Tassi, F., Caselli, A. T., Vaselli, O., Rouwet, D., Capaccioni, B., et al. (2013). Gas Geochemistry of the Magmatic-Hydrothermal Fluid Reservoir in the Copahue–Caviahue Volcanic Complex (Argentina). *J. Volcanol. Geotherm. Res.* 257, 44–56. doi:10.1016/j.jvolgeores.2013.03.003

Aiuppa, A., Fischer, T. P., Plank, T., and Bani, P. (2019). CO2 Flux Emissions from the Earth's Most Actively Degassing Volcanoes, 2005-2015. *Sci. Rep.* 9 (1), 5442–5517. doi:10.1038/s41598-019-41901-y

Andrews, J. N. (1985). The Isotopic Composition of Radiogenic Helium and its Use to Study Groundwater Movement in Confined Aquifers. *Chem. Geol.* 49 (1-3), 339–351.

Arnold, Y. A., Cabassi, J., Tassi, F., Caffe, P. J., and Vaselli, O. (2017). Fluid Geochemistry of a Deep-Seated Geothermal Resource in the Puna Plateau (Jujuy Province, Argentina). *J. Volcanol. Geotherm. Res.* 338, 121–134. doi:10.1016/j.jvolgeores.2017.03.030

Arnold, Y. A., Franco, M. G., Tassi, F., Caffe, P. J., Jofre, C. B., Claros, M., et al. (2020). Geochemical Features of Hydrothermal Systems in Jujuy Province, Argentina: Hints for Geothermal Fluid Exploration. *J. S. Am. Earth Sci.* 101, 102627. doi:10.1016/j.jsames.2020.102627

Assumpção, M., Feng, M., Tassara, A., and Julià, J. (2013). Models of Crustal Thickness for South America from Seismic Refraction, Receiver Functions and Surface Wave Tomography. *Tectonophysics* 609, 82–96. doi:10.1016/j.tecto.2012.11.014

Barry, P. H., Hilton, D. R., Fischer, T. P., de Moor, J. M., Mangasini, F., and Ramirez, C. (2013). Helium and Carbon Isotope Systematics of Cold "Mazuku" CO_2 Vents and Hydrothermal Gases and Fluids from Rungwe Volcanic Province, Southern Tanzania. *Chem. Geol.* 339, 141–156. doi:10.1016/j.chemgeo.2012.07.003

Barry, P. H., Lawson, M., Meurer, W. P., Warr, O., Mabry, J. C., Byrne, D. J., et al. (2016). Noble Gases Solubility Models of Hydrocarbon Charge Mechanism in the Sleipner Vest Gas Field. *Geochimica Cosmochimica Acta* 194, 291–309. doi:10.1016/j.gca.2016.08.021

Barry, P. H., de Moor, J. M., Giovannelli, D., Schrenk, M., Hummer, D. R., Lopez, T., et al. (2019a). Forearc Carbon Sink Reduces Long-Term Volatile Recycling into the Mantle. *Nature* 568 (7753), 487–492. doi:10.1038/s41586-019-1131-5

Barry, P. H., Nakagawa, M., Giovannelli, D., Maarten de Moor, J., Schrenk, M., Seltzer, A. M., et al. (2019b). Helium, Inorganic and Organic Carbon Isotopes of Fluids and Gases across the Costa Rica Convergent Margin. *Sci. Data* 6 (1), 284–288. doi:10.1038/s41597-019-0302-4

Barry, P. H., Negrete-Aranda, R., Spelz, R. M., Seltzer, A. M., Bekaert, D. V., Virrueta, C., et al. (2020). Volatile Sources, Sinks and Pathways: A Helium-Carbon Isotope Study of Baja California Fluids and Gases. *Chem. Geol.* 550, 119722. doi:10.1016/j.chemgeo.2020.119722

Barry, P. H., Bekaert, D. V., Krantz, J. A., Halldórsson, S. A., de Moor, J. M., Fischer, T. P., et al. (2021). Helium-carbon Systematics of Groundwaters in the Lassen Peak Region. *Chem. Geol.* 584, 120535. doi:10.1016/j.chemgeo.2021.120535

Bekaert, D. V., Turner, S. J., Broadley, M. W., Barnes, J. D., Halldórsson, S. A., Labidi, J., et al. (2021). Subduction-driven Volatile Recycling: A Global Mass Balance. *Annu. Rev. Earth Planet. Sci.* 49, 37–70. doi:10.1146/annurev-earth-071620-055024

Benavente, O., Tassi, F., Gutiérrez, F., Vaselli, O., Aguilera, F., and Reich, M. (2013). Origin of Fumarolic Fluids from Tupungatito Volcano (Central Chile): Interplay between Magmatic, Hydrothermal, and Shallow Meteoric Sources. *Bull. Volcanol.* 75 (8), 1–15. doi:10.1007/s00445-013-0746-x

Benavente, O., Tassi, F., Reich, M., Aguilera, F., Capecchiacci, F., Gutiérrez, F., et al. (2016). Chemical and Isotopic Features of Cold and Thermal Fluids Discharged in the Southern Volcanic Zone between 32.5°S and 36°S: Insights into the Physical and Chemical Processes Controlling Fluid Geochemistry in Geothermal Systems of Central Chile. *Chem. Geol.* 420, 97–113. doi:10.1016/j.chemgeo.2015.11.010

Beyerle, U., Aeschbach-Hertig, W., Imboden, D. M., Baur, H., Graf, T., and Kipfer, R. (2000). A Mass Spectrometric System for the Analysis of Noble Gases and Tritium from Water Samples. *Environ. Sci. Technol.* 34 (10), 2042–2050. doi:10.1021/es990840h

Bouilhol, P., Debret, B., Inglis, E. C., Warembourg, M., Grocolas, T., Rigaudier, T., et al. (2022). Decoupling of Inorganic and Organic Carbon during Slab Mantle Devolatilisation. *Nat. Commun.* 13 (1), 308–310. doi:10.1038/s41467-022-27970-0

Capaccioni, B., Aguilera, F., Tassi, F., Darrah, T., Poreda, R. J., and Vaselli, O. (2011). Geochemical and Isotopic Evidences of Magmatic Inputs in the Hydrothermal Reservoir Feeding the Fumarolic Discharges of Tacora Volcano (Northern Chile). *J. Volcanol. Geotherm. Res.* 208 (3-4), 77–85. doi:10.1016/j.jvolgeores.2011.09.015

Chen, Y. W., Wu, J., and Suppe, J. (2019). Southward Propagation of Nazca Subduction Along the Andes. *Nature* 565 (7740), 441–447.

Chiodi, A., Tassi, F., Báez, W., Maffucci, R., Invernizzi, C., Giordano, G., et al. (2015). New geochemical and isotopic insights to evaluate the geothermal resource of the hydrothermal system of Rosario de la Frontera (Salta, northern Argentina). *J. Volcanol. Geotherm. Res.* 295, 16–25. doi:10.1016/j.jvolgeores.2015.03.001

Chiodi, A., Tassi, F., Báez, W., Filipovich, R., Bustos, E., Glok Galli, M., et al. (2019). Preliminary Conceptual Model of the Cerro Blanco Caldera-Hosted Geothermal System (Southern Puna, Argentina): Inferences from Geochemical Investigations. *J. S. Am. Earth Sci.* 94, 102213. doi:10.1016/j.jsames.2019.102213

Clarke, W. B., Jenkins, W. J., and Top, Z. (1976). Determination of Tritium by Mass Spectrometric Measurement of 3He. *Int. J. Appl. Radiat. isotopes* 27 (9), 515–522. doi:10.1016/0020-708x(76)90082-x

Clift, P. D. (2017). A Revised Budget for Cenozoic Sedimentary Carbon Subduction. *Rev. Geophys.* 55 (1), 97–125. doi:10.1002/2016rg000531

Contreras-Reyes, E., Grevemeyer, I., Flueh, E. R., and Reichert, C. (2008). Upper Lithospheric Structure of the Subduction Zone Offshore of Southern Arauco Peninsula, Chile, At~ 38 S. *J. Geophys. Res. Solid Earth* 113 (B07303), 1–19. doi:10.1029/2007JB005569

Contreras-Reyes, E., Flueh, E. R., and Grevemeyer, I. (2010). Tectonic Control on Sediment Accretion and Subduction off South Central Chile: Implications for Coseismic Rupture Processes of the 1960 and 2010 Megathrust Earthquakes. *Tectonics* 29 (TC6018), 1–27. doi:10.1029/2010TC002734

Craig, H. (1953). The Geochemistry of the Stable Carbon Isotopes. *Geochimica cosmochimica acta* 3 (2-3), 53–92. doi:10.1016/0016-7037(53)90001-5

Dawson, P., Chouet, B., and Pitt, A. (2016). Tomographic Image of a Seismically Active Volcano: Mammoth Mountain, California. *J. Geophys. Res. Solid Earth* 121 (1), 114–133. doi:10.1002/2015jb012537

Day, J. M. D., Barry, P. H., Hilton, D. R., Burgess, R., Pearson, D. G., and Taylor, L. A. (2015). The Helium Flux from the Continents and Ubiquity of low-3He/4He Recycled Crust and Lithosphere. *Geochimica Cosmochimica Acta* 153, 116–133. doi:10.1016/j.gca.2015.01.008

De Leeuw, G. A. M., Hilton, D. R., Fischer, T. P., and Walker, J. A. (2007). The He–CO_2 Isotope and Relative Abundance Characteristics of Geothermal Fluids

in el Salvador and Honduras: New Constraints on Volatile Mass Balance of the Central American Volcanic Arc. *Earth Planet. Sci. Lett.* 258 (1-2), 132–146. doi:10.1016/j.epsl.2007.03.028

de Moor, J. M., Aiuppa, A., Avard, G., Wehrmann, H., Dunbar, N., Muller, C., et al. (2016). Turmoil at Turrialba Volcano (Costa Rica): Degassing and Eruptive Processes Inferred from High-Frequency Gas Monitoring. *J. Geophys. Res. Solid Earth* 121 (8), 5761–5775. doi:10.1002/2016jb013150

de Moor, J. M., Fischer, T. P., and Plank, T. (2022). Constraints on the Sulfur Subduction Cycle in Central America from Sulfur Isotope Compositions of Volcanic Gases. *Chem. Geol.* 588, 120627. doi:10.1016/j.chemgeo.2021.120627

De Silva, S. L. (1989). Altiplano-Puna Volcanic Complex of the Central Andes. *Geology* 17 (12), 1102–1106. doi:10.1130/0091-7613(1989)017<1102:apvcot>2.3.co;2

DeMets, C., Gordon, R. G., and Argus, D. F. (2010). Geologically Current Plate Motions. *Geophys. J. Int.* 181 (1), 1–80. doi:10.1111/j.1365-246x.2009.04491.x

Dewey, J. F., and Bird, J. M. (1970). Mountain Belts and the New Global Tectonics. *J. Geophys. Res.* 75 (14), 2625–2647. doi:10.1029/jb075i014p02625

Dunai, T. J., and Baur, H. (1995). Helium, Neon, and Argon Systematics of the European Subcontinental Mantle: Implications for its Geochemical Evolution. *Geochimica Cosmochimica Acta* 59 (13), 2767–2783. doi:10.1016/0016-7037(95)00172-v

Ellis, A. J., and Golding, R. M. (1963). The Solubility of Carbon Dioxide above 100 Degrees C in Water and in Sodium Chloride Solutions. *Am. J. Sci.* 261 (1), 47–60. doi:10.2475/ajs.261.1.47

Filipovich, R., Chiodi, A., Báez, W., Ahumada, M. F., Invernizzi, C., Taviani, S., et al. (2022). Structural Analysis and Fluid Geochemistry as Tools to Assess the Potential of the Tocomar Geothermal System, Central Puna (Argentina). *Geothermics* 98, 102297. doi:10.1016/j.geothermics.2021.102297

Fouke, B. W., Farmer, J. D., Des Marais, D. J., Pratt, L., Sturchio, N. C., Burns, P. C., et al. (2000). Depositional Facies and Aqueous-Solid Geochemistry of Travertine-Depositing Hot Springs (Angel Terrace, Mammoth Hot Springs, Yellowstone National Park, U.S.A.). *J. Sediment. Res.* 70 (3), 565–585. doi:10.1306/2dc40929-0e47-11d7-8643000102c1865d

Fullerton, K. M., Schrenk, M. O., Yücel, M., Manini, E., Basili, M., Rogers, T. J., et al. (2021). Effect of Tectonic Processes on Biosphere-Geosphere Feedbacks across a Convergent Margin. *Nat. Geosci.* 14 (5), 301–306. doi:10.1038/s41561-021-00725-0

Gautheron, C., and Moreira, M. (2002). Helium Signature of the Subcontinental Lithospheric Mantle. *Earth Planet. Sci. Lett.* 199 (1-2), 39–47. doi:10.1016/s0012-821x(02)00563-0

Giggenbach, W. F., and Goguel, R. L. (1989). *Methods for theCollection and Analysis of Geothermal and Volcanic Water and Gas Samples*. Petone, New Zealand: Dept. of Sci. and Ind. Res.

Gilfillan, S. M. V., Lollar, B. S., Holland, G., Blagburn, D., Stevens, S., Schoell, M., et al. (2009). Solubility Trapping in Formation Water as Dominant CO_2 Sink in Natural Gas Fields. *Nature* 458 (7238), 614–618. doi:10.1038/nature07852

Godoy, B., Taussi, M., González-Maurel, O., Renzulli, A., Hernández-Prat, L., le Roux, P., et al. (2019). Linking the Mafic Volcanism with the Magmatic Stages during the Last 1 Ma in the Main Volcanic Arc of the Altiplano-Puna Volcanic Complex (Central Andes). *J. S. Am. Earth Sci.* 95, 102295. doi:10.1016/j.jsames.2019.102295

Graham, D. W. (2002). Noble Gas Isotope Geochemistry of Mid-ocean Ridge and Ocean Island Basalts: Characterization of Mantle Source Reservoirs. *Rev. Mineralogy Geochem.* 47, 247. doi:10.2138/rmg.2002.47.8

Güleç, N., and Hilton, D. R. (2016). Turkish Geothermal Fields as Natural Analogues of CO_2 Storage Sites: Gas Geochemistry and Implications for CO_2 Trapping Mechanisms. *Geothermics* 64, 96–110.

Hamilton, N. E., and Ferry, M. (2018). Ggtern: Ternary Diagrams Using Ggplot2. *J. Stat. Softw. Code Snippets* 87 (3), 1–17. doi:10.18637/jss.v087.c03

Hamza, V. M., Dias, F. J. S. S., Gomes, A. J. L., and Terceros, Z. G. D. (2005). Numerical and Functional Representations of Regional Heat Flow in South America. *Phys. Earth Planet. Interiors* 152 (4), 223–256. doi:10.1016/j.pepi.2005.04.009

Harmon, R. S., Barreiro, B. A., Moorbath, S., Hoefs, J., Francis, P. W., Thorpe, R. S., et al. (1984). Regional O-, Sr-, and Pb-Isotope Relationships in Late Cenozoic Calc-Alkaline Lavas of the Andean Cordillera. *J. Geol. Soc.* 141 (5), 803–822. doi:10.1144/gsjgs.141.5.0803

Hayes, J. M., Strauss, H., and Kaufman, A. J. (1999). The Abundance of 13C in Marine Organic Matter and Isotopic Fractionation in the Global Biogeochemical Cycle of Carbon during the Past 800 Ma. *Chem. Geol.* 161 (1-3), 103–125. doi:10.1016/s0009-2541(99)00083-2

Hilton, D. R., and Porcelli, D. (2003). Noble Gases as Mantle Tracers. *Treatise Geochem.* 2, 568. doi:10.1016/b0-08-043751-6/02007-7

Hilton, D. R., Hammerschmidt, K., Teufel, S., and Friedrichsen, H. (1993). Helium Isotope Characteristics of Andean Geothermal Fluids and Lavas. *Earth Planet. Sci. Lett.* 120 (3-4), 265–282. doi:10.1016/0012-821x(93)90244-4

Hilton, D. R., Fischer, T. P., and Marry, B. (2002). Noble Gases and Volatile Recycling at Subduction Zones. *Rev. Mineralogy Geochem.* 47, 1–73. doi:10.2138/rmg.2002.47.9

Hilton, D. R. (1996). The Helium and Carbon Isotope Systematics of a Continental Geothermal System: Results from Monitoring Studies at Long Valley Caldera (California, U.S.A.). *Chem. Geol.* 127 (4), 269–295. doi:10.1016/0009-2541(95)00134-4

Hoke, L., Hilton, D. R., Lamb, S. H., Hammerschmidt, K., and Friedrichsen, H. (1994). 3He Evidence for a Wide Zone of Active Mantle Melting beneath the Central Andes. *Earth Planet. Sci. Lett.* 128 (3-4), 341–355. doi:10.1016/0012-821x(94)90155-4

Holloway, J. R., and Blank, J. G. (1994). Chapter 6. Application of Experimental Results to C-O-H Species in Natural Melts. *Rev. Mineralogy Geochem.* 30 (1), 187–230. doi:10.1515/9781501509674-012

Howell, J. A., Schwarz, E., Spalletti, L. A., and Veiga, G. D. (2005). The Neuquén Basin: an Overview. *Geol. Soc. Lond. Spec. Publ.* 252 (1), 1–14. doi:10.1144/gsl.sp.2005.252.01.01

Hunt, A. G. (2015). US Geological Survey Noble Gas Laboratory's Standard Operating Procedures for the Measurement of Dissolved Gas in Water Samples *(No. 5-A11)*. Reston, VA: US Geological Survey.

Inostroza, M., Tassi, F., Aguilera, F., Sepúlveda, J. P., Capecchiacci, F., Venturi, S., et al. (2020). Geochemistry of Gas and Water Discharge from the Magmatic-Hydrothermal System of Guallatiri Volcano, Northern Chile. *Bull. Volcanol.* 82 (7), 1–16. doi:10.1007/s00445-020-01396-2

Jacques, G., Hoernle, K., Gill, J., Wehrmann, H., Bindeman, I., and Lara, L. E. (2014). Geochemical Variations in the Central Southern Volcanic Zone, Chile (38–43°S): The Role of Fluids in Generating Arc Magmas. *Chem. Geol.* 371, 27–45. doi:10.1016/j.chemgeo.2014.01.015

James, D. E. (1971). Plate Tectonic Model for the Evolution of the Central Andes. *Geol. Soc. Am. Bull.* 82 (12), 3325–3346. doi:10.1130/0016-7606(1971)82[3325:ptmfte]2.0.co;2

Javoy, M., Pineau, F., and Delorme, H. (1986). Carbon and Nitrogen Isotopes in the Mantle. *Chem. Geol.* 57 (1-2), 41–62. doi:10.1016/0009-2541(86)90093-8

Jordan, T. E., Isacks, B. L., Ramos, V. A., and Allmendinger, R. W. (1983). Mountain Building in the Central Andes. *Episodes* 6 (3), 20–26. doi:10.18814/epiiugs/1983/v6i3/005

Karolytė, R., Johnson, G., Györe, D., Serno, S., Flude, S., Stuart, F. M., et al. (2019). Tracing the Migration of Mantle CO_2 in Gas Fields and Mineral Water Springs in South-East Australia Using Noble Gas and Stable Isotopes. *Geochimica Cosmochimica Acta* 259, 109–128. doi:10.1016/j.gca.2019.06.002

Kay, S. M., and Mpodozis, C. (2002). Magmatism as a Probe to the Neogene Shallowing of the Nazca Plate beneath the Modern Chilean Flat-Slab. *J. S. Am. Earth Sci.* 15 (1), 39–57. doi:10.1016/s0895-9811(02)00005-6

Kimani, C. N., Kasanzu, C. H., Tyne, R. L., Mtili, K. M., Byrne, D. J., Kazimoto, E. O., et al. (2021). He, Ne, Ar and CO_2 Systematics of the Rungwe Volcanic Province, Tanzania: Implications for Fluid Source and Dynamics. *Chem. Geol.* 586, 120584. doi:10.1016/j.chemgeo.2021.120584

Lages, J., Rizzo, A. L., Aiuppa, A., Robidoux, P., Aguilar, R., Apaza, F., et al. (2021). Crustal Controls on Light Noble Gas Isotope Variability along the Andean Volcanic Arc. *Geochem. Persp. Let.* 19, 45–49. doi:10.7185/geochemlet.2134

López-Escobar, L., Parada, M. A., Hickey-Vargas, R., Frey, F. A., Kempton, P. D., and Moreno, H. (1995). Calbuco Volcano and Minor Eruptive Centers Distributed along the Liquiñe-Ofqui Fault Zone, Chile (41–42 S): Contrasting Origin of Andesitic and Basaltic Magma in the Southern Volcanic Zone of the Andes. *Contributions Mineralogy Petrology* 119 (4), 345–361. doi:10.1007/BF00286934

Lopez, T., Aguilera, F., Tassi, F., de Moor, J. M., Bobrowski, N., Aiuppa, A., et al. (2018). New Insights into the Magmatic-Hydrothermal System and Volatile Budget of Lastarria Volcano, Chile: Integrated Results from the 2014 IAVCEI

CCVG 12th Volcanic Gas Workshop. *Geosphere* 14 (3), 983–1007. doi:10.1130/ges01495.1

Mabry, J., Lan, T., Burnard, P., and Marty, B. (2013). High-precision Helium Isotope Measurements in Air. *J. Anal. At. Spectrom.* 28 (12), 1903–1910. doi:10.1039/c3ja50155h

Malowany, K., Stix, J., Van Pelt, A., and Lucic, G. (2015). H_2S Interference on CO_2 Isotopic Measurements Using a Picarro G1101-I Cavity Ring-Down Spectrometer. *Atmos. Meas. Tech.* 8 (10), 4075–4082. doi:10.5194/amt-8-4075-2015

Malowany, K. S., Stix, J., de Moor, J. M., Chu, K., Lacrampe-Couloume, G., and Sherwood Lollar, B. (2017). Carbon Isotope Systematics of Turrialba Volcano, Costa Rica, Using a Portable Cavity Ring-Down Spectrometer. *Geochem. Geophys. Geosyst.* 18 (7), 2769–2784. doi:10.1002/2017gc006856

Mamani, M., Wörner, G., and Sempere, T. (2010). Geochemical Variations in Igneous Rocks of the Central Andean Orocline (13 S to 18 S): Tracing Crustal Thickening and Magma Generation through Time and Space. *GSA Bull.* 122 (1-2), 162–182. doi:10.1130/b26538.1

Marty, B., and Jambon, A. (1987). C/3He in Volatile Fluxes from the Solid Earth: Implications for Carbon Geodynamics. *Earth Planet. Sci. Lett.* 83 (1-4), 16–26. doi:10.1016/0012-821x(87)90047-1

Marty, B., Jambon, A., and Sano, Y. (1989). Helium Isotopes and CO2 in Volcanic Gases of Japan. *Chem. Geol.* 76 (1-2), 25–40. doi:10.1016/0009-2541(89)90125-3

Mason, E., Edmonds, M., and Turchyn, A. V. (2017). Remobilization of Crustal Carbon May Dominate Volcanic Arc Emissions. *Science* 357 (6348), 290–294. doi:10.1126/science.aan5049

Mazor, E., and Wasserburg, G. J. (1965). Helium, Neon, Argon, Krypton and Xenon in Gas Emanations from Yellowstone and Lassen Volcanic National Parks. *Geochimica Cosmochimica Acta* 29 (5), 443–454. doi:10.1016/0016-7037(65)90038-4

McLing, T. L., Smith, R. W., and Johnson, T. M. (2002). *Chemical Characteristics of Thermal Water beneath the.* Geology, Hydrogeology, and Environmental Remediation: Idaho National Engineering And Environmental Laboratory, Eastern Snake River Plain, Idaho, Special Paper 353. Boulder, CO, 205.

Merino, N., Aronson, H. S., Bojanova, D. P., Feyhl-Buska, J., Wong, M. L., Zhang, S., et al. (2019). Living at the Extremes: Extremophiles and the Limits of Life in a Planetary Context. *Front. Microbiol.* 10, 780. doi:10.3389/fmicb.2019.00780

Morrison, P., and Pine, J. (1955). Radiogenic Origin of the Helium Isotopes in Rock. *Ann. N. Y. Acad. Sci.* 62 (3), 71–92. doi:10.1111/j.1749-6632.1955.tb35366.x

Mtili, K. M., Byrne, D. J., Tyne, R. L., Kazimoto, E. O., Kimani, C. N., Kasanzu, C. H., et al. (2021). The Origin of High Helium Concentrations in the Gas Fields of Southwestern Tanzania. *Chem. Geol.* 585, 120542. doi:10.1016/j.chemgeo.2021.120542

Newell, D. L., Jessup, M. J., Hilton, D. R., Shaw, C. A., and Hughes, C. A. (2015). Mantle-Derived Helium in Hot Springs of the Cordillera Blanca, Peru: Implications for Mantle-To-Crust Fluid Transfer in a Flat-Slab Subduction Setting. *Chem. Geol.* 417, 200–209. doi:10.1016/j.chemgeo.2015.10.003

Ohmoto, H., and Rye, R. O., 1979. *Isotopes of Sulfur and Carbon*. New York, NY: Geochemistry of Hydrothermal Ore Deposits pp. 509–567

O'nions, R. K., and Oxburgh, E. R. (1988). Helium, Volatile Fluxes and the Development of Continental Crust. *Earth Planet. Sci. Lett.* 90 (3), 331–347. doi:10.1016/0012-821x(88)90134-3

Ozima, M., and Podosek, F. A. (2002). *Noble Gas Geochemistry*. Cambridge University Press, 160–249.

Ozima, M., and Podosek, F. A. (1983). *Geochemistry of Noble Gases*. Cambridge Univ. Press.

Plank, T., and Manning, C. E. (2019). Subducting Carbon. *Nature* 574 (7778), 343–352. doi:10.1038/s41586-019-1643-z

Plümper, O., King, H. E., Geisler, T., Liu, Y., Pabst, S., Savov, I. P., et al. (2017). Subduction Zone Forearc Serpentinites as Incubators for Deep Microbial Life. *Proc. Natl. Acad. Sci. U. S. A.* 114 (17), 4324–4329. doi:10.1073/pnas.1612147114

Ray, M. C., Hilton, D. R., Muñoz, J., Fischer, T. P., and Shaw, A. M. (2009). The Effects of Volatile Recycling, Degassing and Crustal Contamination on the Helium and Carbon Geochemistry of Hydrothermal Fluids from the Southern Volcanic Zone of Chile. *Chem. Geol.* 266 (1-2), 38–49. doi:10.1016/j.chemgeo.2008.12.026

Robidoux, P., Rizzo, A. L., Aguilera, F., Aiuppa, A., Artale, M., Liuzzo, M., et al. (2020). Petrological and Noble Gas Features of Lascar and Lastarria Volcanoes (Chile): Inferences on Plumbing Systems and Mantle Characteristics. *Lithos* 370-371, 105615. doi:10.1016/j.lithos.2020.105615

Rothstein, D. A., and Manning, C. E. (2003). Geothermal Gradients in Continental Magmatic Arcs; Constraints from the Eastern Peninsular Ranges Batholith, Baja California, Mexico. *Geol. Soc. Am. Special Pap.* 374, 337–354. doi:10.1130/0-8137-2374-4.337

Roulleau, E., Tardani, D., Sano, Y., Takahata, N., Vinet, N., Bravo, F., et al. (2016). New Insight from Noble Gas and Stable Isotopes of Geothermal/Hydrothermal Fluids at Caviahue-Copahue Volcanic Complex: Boiling Steam Separation and Water-Rock Interaction at Shallow Depth. *J. Volcanol. Geotherm. Res.* 328, 70–83. doi:10.1016/j.jvolgeores.2016.10.007

Ryan, W. B., Carbotte, S. M., Coplan, J. O., O'Hara, S., Melkonian, A., Arko, R., et al. (2009). Global Multi-Resolution Topography Synthesis. *Geochem. Geophys. Geosystems* 10 (3), Q03014. doi:10.1029/2008gc002332

Sano, Y., and Marty, B. (1995). Origin of Carbon in Fumarolic Gas from Island Arcs. *Chem. Geol.* 119 (1-4), 265–274. doi:10.1016/0009-2541(94)00097-r

Sano, Y., and Williams, S. N. (1996). Fluxes of Mantle and Subducted Carbon along Convergent Plate Boundaries. *Geophys. Res. Lett.* 23 (20), 2749–2752. doi:10.1029/96gl02260

Scott, E. M., Allen, M. B., Macpherson, C. G., McCaffrey, K. J. W., Davidson, J. P., Saville, C., et al. (2018). Andean Surface Uplift Constrained by Radiogenic Isotopes of Arc Lavas. *Nat. Commun.* 9 (1), 969–978. doi:10.1038/s41467-018-03173-4

Sepúlveda, F., Lahsen, A., and Powell, T. (2007). Gas Geochemistry of the Cordón Caulle Geothermal System, Southern Chile. *geothermics* 36 (5), 389–420. doi:10.1016/j.geothermics.2007.05.001

Shaw, A. M., Hilton, D. R., Fischer, T. P., Walker, J. A., and Alvarado, G. E. (2003). Contrasting He–C Relationships in Nicaragua and Costa Rica: Insights into C Cycling through Subduction Zones. *Earth Planet. Sci. Lett.* 214 (3-4), 499–513. doi:10.1016/s0012-821x(03)00401-1

Spane, F. A., Jr, and Webber, W. D. (1995). Hydrochemistry And Hydrogeologic Conditions within the Hanford Site Upper Basalt Confined Aquifer System *(No. PNL-10817)*. Richland, WA (United States); Pacific Northwest National Lab.PNNL.

Stern, R. J. (2004). Subduction Initiation: Spontaneous and Induced. *Earth Planet. Sci. Lett.* 226 (3-4), 275–292. doi:10.1016/s0012-821x(04)00498-4

Stern, R. J. (2007). When and How Did Plate Tectonics Begin? Theoretical and Empirical Considerations. *Chin. Sci. Bull.* 52 (5), 578–591. doi:10.1007/s11434-007-0073-8

Syracuse, E. M., and Abers, G. A. (2006). Global Compilation of Variations in Slab Depth beneath Arc Volcanoes and Implications. *Geochem. Geophys. Geosystems* 7 (5), Q05017. doi:10.1029/2005gc001045

Takai, K., Nakamura, K., Toki, T., Tsunogai, U., Miyazaki, M., Miyazaki, J., et al. (2008). Cell Proliferation at 122°C and Isotopically Heavy CH_4 Production by a Hyperthermophilic Methanogen Under High-Pressure Cultivation. *Proc. Natl. Acad. Sci. U.S.A.* 105, 10949–10954. doi:10.1073/pnas.0712334105

Tardani, D., Reich, M., Roulleau, E., Takahata, N., Sano, Y., Pérez-Flores, P., et al. (2016). Exploring the Structural Controls on Helium, Nitrogen and Carbon Isotope Signatures in Hydrothermal Fluids along an Intra-arc Fault System. *Geochimica Cosmochimica Acta* 184, 193–211. doi:10.1016/j.gca.2016.04.031

Tardani, D., Roulleau, E., Pinti, D. L., Pérez-Flores, P., Daniele, L., Reich, M., et al. (2021). Structural Control on Shallow Hydrogeochemical Processes at Caviahue-Copahue Volcanic Complex (CCVC), Argentina. *J. Volcanol. Geotherm. Res.* 414, 107228. doi:10.1016/j.jvolgeores.2021.107228

Tassara, A., and Echaurren, A. (2012). Anatomy of the Andean Subduction Zone: Three-Dimensional Density Model Upgraded and Compared against Global-Scale Models. *Geophys. J. Int.* 189 (1), 161–168. doi:10.1111/j.1365-246x.2012.05397.x

Tassi, F., Aguilera, F., Vaselli, O., Medina, E., Tedesco, D., Delgado Huertas, A., et al. (2009). The Magmatic- and Hydrothermal-Dominated Fumarolic System at the Active Crater of Lascar Volcano, Northern Chile. *Bull. Volcanol.* 71 (2), 171–183. doi:10.1007/s00445-008-0216-z

Tassi, F., Aguilera, F., Darrah, T., Vaselli, O., Capaccioni, B., Poreda, R. J., et al. (2010). Fluid Geochemistry of Hydrothermal Systems in the Arica-Parinacota, Tarapacá and Antofagasta Regions (Northern Chile). *J. Volcanol. Geotherm. Res.* 192 (1-2), 1–15. doi:10.1016/j.jvolgeores.2010.02.006

Tassi, F., Aguilera, F., Vaselli, O., Darrah, T., and Medina, E. (2011). Gas Discharges from Four Remote Volcanoes in Northern Chile (Putana, Olca, Irruputuncu and Alitar): a Geochemical Survey. *Ann. Geophys.* 54 (2), 2. doi:10.4401/ag-5173

Tassi, F., Agusto, M., Vaselli, O., and Chiodini, G. (2016). "Geochemistry of the Magmatic-Hydrothermal Fluid Reservoir of Copahue Volcano (Argentina): Insights from the Chemical and Isotopic Features of Fumarolic Discharges," in *Copahue Volcano* (Berlin, Heidelberg: Springer), 119–139. doi:10.1007/978-3-662-48005-2_6

Tassi, F., Agusto, M., Lamberti, C., Caselli, A. T., Pecoraino, G., Caponi, C., et al. (2017). The 2012–2016 Eruptive Cycle at Copahue Volcano (Argentina) versus the Peripheral Gas Manifestations: Hints from the Chemical and Isotopic Features of Fumarolic Fluids. *Bull. Volcanol.* 79 (10), 1–14. doi:10.1007/s00445-017-1151-7

Thorpe, R. S., and Francis, P. W. (1979). Variations in Andean Andesite Compositions and Their Petrogenetic Significance. *Tectonophysics* 57 (1), 53–70. doi:10.1016/0040-1951(79)90101-x

Thorpe, R. S. (1982). "The Andes," in *Andesites: Orogenic Andesites and Related Rocks*, 187–205.

Tormey, D. R., Hickey-Vargas, R., Frey, F. A., and López-Escobar, L. (1991). Recent Lavas from the Andean Volcanic Front (33 to 42°S); Interpretations of Along-Arc Compositional Variations. *Andean magmatism its Tect. setting* 265, 57–78. doi:10.1130/spe265-p57

Tsesarsky, M., Gat, D., and Ronen, Z. (2016). Biological Aspects of Microbial-Induced Calcite Precipitation. *Environ. Geotech.* 5 (2), 69–78.

Turner, S. J., Langmuir, C. H., Dungan, M. A., and Escrig, S. (2017). The Importance of Mantle Wedge Heterogeneity to Subduction Zone Magmatism and the Origin of EM1. *Earth Planet. Sci. Lett.* 472, 216–228. doi:10.1016/j.epsl.2017.04.051

Tyne, R. L., Barry, P. H., Hillegonds, D. J., Hunt, A. G., Kulongoski, J. T., Stephens, M. J., et al. (2019). A Novel Method for the Extraction, Purification, and Characterization of Noble Gases in Produced Fluids. *Geochem. Geophys. Geosyst.* 20 (11), 5588–5597. doi:10.1029/2019gc008552

Varekamp, J. C., Kreulen, R., Poorter, R. P. E., and Bergen, M. J. (1992). Carbon Sources in Arc Volcanism, with Implications for the Carbon Cycle. *Terra nova.* 4 (3), 363–373. doi:10.1111/j.1365-3121.1992.tb00825.x

Varekamp, J. C., deMoor, J. M., Merrill, M. D., Colvin, A. S., Goss, A. R., Vroon, P. Z., et al. (2006). Geochemistry and Isotopic Characteristics of the Caviahue-Copahue Volcanic Complex, Province of Neuquén, Argentina. *Special Papers-Geological Soc. Am.* 407, 317. doi:10.1130/2006.2407(15)

Völker, D., Geersen, J., Contreras-Reyes, E., and Reichert, C. (2013). Sedimentary Fill of the Chile Trench (32–46 S): Volumetric Distribution and Causal Factors. *J. Geol. Soc.* 170 (5), 723–736.

Vogel, J. C., Grootes, P. M., and Mook, W. G. (1970). Isotopic Fractionation between Gaseous and Dissolved Carbon Dioxide. *Z. Phys.* 230 (3), 225–238. doi:10.1007/bf01394688

Wehrmann, H., Hoernle, K., Portnyagin, M., Wiedenbeck, M., and Heydolph, K. (2011). Volcanic CO2 Output at the Central American Subduction Zone Inferred from Melt Inclusions in Olivine Crystals from Mafic Tephras. *Geochem. Geophys. Geosystems* 12 (6), Q06003. doi:10.1029/2010gc003412

Weiss, R. F. (1968). Piggyback Sampler for Dissolved Gas Studies on Sealed Water Samples. *Deep Sea Res. Oceanogr. Abstr.* 15 (6), 695–699. doi:10.1016/0011-7471(68)90082-x

Weiss, R. F. (1971). Solubility of Helium and Neon in Water and Seawater. *J. Chem. Eng. Data* 16 (2), 235–241. doi:10.1021/je60049a019

Wickham, H. (2016). *ggplot2: Elegant Graphics for Data Analysis*. New York: Springer-Verlag. 978-3-319-24277-4.

Wieser, P. E., Turner, S. J., Mather, T. A., Pyle, D. M., Savov, I. P., and Orozco, G. (2019). New Constraints from Central Chile on the Origins of Enriched Continental Compositions in Thick-Crusted Arc Magmas. *Geochimica Cosmochimica Acta* 267, 51–74. doi:10.1016/j.gca.2019.09.008

Conflict of Interest: The authors declare that the research was conducted in the absence of any commercial or financial relationships that could be construed as a potential conflict of interest.

Publisher's Note: All claims expressed in this article are solely those of the authors and do not necessarily represent those of their affiliated organizations, or those of the publisher, the editors and the reviewers. Any product that may be evaluated in this article, or claim that may be made by its manufacturer, is not guaranteed or endorsed by the publisher.

Copyright © 2022 Barry, De Moor, Chiodi, Aguilera, Hudak, Bekaert, Turner, Curtice, Seltzer, Jessen, Osses, Blamey, Amenábar, Selci, Cascone, Bastianoni, Nakagawa, Filipovich, Bustos, Schrenk, Buongiorno, Ramírez, Rogers, Lloyd and Giovannelli. This is an open-access article distributed under the terms of the Creative Commons Attribution License (CC BY). The use, distribution or reproduction in other forums is permitted, provided the original author(s) and the copyright owner(s) are credited and that the original publication in this journal is cited, in accordance with accepted academic practice. No use, distribution or reproduction is permitted which does not comply with these terms.

frontiers | Frontiers in Microbiology

TYPE Original Research
PUBLISHED 11 August 2023
DOI 10.3389/fmicb.2023.1134114

Check for updates

OPEN ACCESS

EDITED BY
Brett J. Baker,
The University of Texas at Austin, United States

REVIEWED BY
Florence Schubotz,
University of Bremen, Germany
Craig Everroad,
National Aeronautics and Space Administration, United States

*CORRESPONDENCE
Donato Giovannelli
✉ donato.giovannelli@unina.it

†These authors share first authorship

‡PRESENT ADDRESS
Alessandra Ferrillo,
Norwegian University of Life Sciences, Aas, Norway

RECEIVED 29 December 2022
ACCEPTED 25 July 2023
PUBLISHED 11 August 2023

CITATION
Barosa B, Ferrillo A, Selci M, Giardina M, Bastianoni A, Correggia M, di Iorio L, Bernardi G, Cascone M, Capuozzo R, Intoccia M, Price R, Vetriani C, Cordone A and Giovannelli D (2023) Mapping the microbial diversity associated with different geochemical regimes in the shallow-water hydrothermal vents of the Aeolian archipelago, Italy. *Front. Microbiol.* 14:1134114. doi: 10.3389/fmicb.2023.1134114

COPYRIGHT
© 2023 Barosa, Ferrillo, Selci, Giardina, Bastianoni, Correggia, di Iorio, Bernardi, Cascone, Capuozzo, Intoccia, Price, Vetriani, Cordone and Giovannelli. This is an open-access article distributed under the terms of the Creative Commons Attribution License (CC BY). The use, distribution or reproduction in other forums is permitted, provided the original author(s) and the copyright owner(s) are credited and that the original publication in this journal is cited, in accordance with accepted academic practice. No use, distribution or reproduction is permitted which does not comply with these terms.

Mapping the microbial diversity associated with different geochemical regimes in the shallow-water hydrothermal vents of the Aeolian archipelago, Italy

Bernardo Barosa[1†], Alessandra Ferrillo[1†‡], Matteo Selci[1], Marco Giardina[1], Alessia Bastianoni[1], Monica Correggia[1], Luciano di Iorio[1], Giulia Bernardi[2], Martina Cascone[1], Rosaria Capuozzo[1], Michele Intoccia[1], Roy Price[3], Costantino Vetriani[4,5], Angelina Cordone[1] and Donato Giovannelli[1,5,6,7,8*]

[1]Department of Biology, University of Naples "Federico II", Naples, Italy, [2]Blue Marine Foundation, London, United Kingdom, [3]School of Marine and Atmospheric Sciences, Stony Brook, NY, United States, [4]Department of Biochemistry and Microbiology, Rutgers University, New Brunswick, NJ, United States, [5]Department of Marine and Coastal Science, Rutgers University, New Brunswick, NJ, United States, [6]Istituto per le Risorse Biologiche e Biotecnologiche Marine, Consiglio Nazionale Delle Ricerche, CNR-IRBIM, Ancona, Italy, [7]Earth-Life Science Institute, Tokyo Institute of Technology, Ookayama, Tokyo, Japan, [8]Marine Chemistry and Geochemistry Department–Woods Hole Oceanographic Institution, Woods Hole, MA, United States

Shallow-water hydrothermal vents are unique marine environments ubiquitous along the coast of volcanically active regions of the planet. In contrast to their deep-sea counterparts, primary production at shallow-water vents relies on both photoautotrophy and chemoautotrophy. Such processes are supported by a range of geochemical regimes driven by different geological settings. The Aeolian archipelago, located in the southern Tyrrhenian sea, is characterized by intense hydrothermal activity and harbors some of the best sampled shallow-water vents of the Mediterranean Sea. Despite this, the correlation between microbial diversity, geochemical regimes and geological settings of the different volcanic islands of the archipelago is largely unknown. Here, we report the microbial diversity associated with six distinct shallow-water hydrothermal vents of the Aeolian Islands using a combination of 16S rRNA amplicon sequencing along with physicochemical and geochemical measurements. Samples were collected from biofilms, fluids and sediments from shallow vents on the islands of Lipari, Panarea, Salina, and Vulcano. Two new shallow vent locations are described here for the first time. Our results show the presence of diverse microbial communities consistent in their composition with the local geochemical regimes. The shallow water vents of the Aeolian Islands harbor highly diverse microbial community and should be included in future conservation efforts.

KEYWORDS

shallow-water vents, Aeolian archipelago, 16S rRNA amplicon sequencing, microbial diversity, marine protected areas, hydrothermal vents

1. Introduction

The vast and diverse metabolic repertoire of microorganisms enables their ubiquitous distribution on our planet, making them key mediators of biogeochemical cycles on a planetary scale (Falkowski et al., 2008). Notwithstanding their ubiquity, their distribution and the environmental factors shaping it, are not fully resolved. However, significant correlations between microbial community composition and environmental geochemistry have been established in diverse environments (Jorgensen et al., 2012; Alsop et al., 2014; Liu et al., 2014; Yamamoto et al., 2019). Geothermal environments are ideal systems to study the complex relationships between community composition and geochemistry due to the wide geochemical gradients present across proximal geographic distances, and relatively constrained microbial communities (Power et al., 2018). Additionally, geothermal ecosystems harbor diverse communities of extremophiles that are an untapped source of potential biotechnological compounds (Sayed et al., 2020). Hence, there is an increasing necessity to characterize in detail the microbial diversity in these ecosystems and to prioritize their conservation.

Marine hydrothermal vents are dynamic systems where water is discharged through the Earth's crust in areas where there is enough heat to drive fluid circulation, e.g., plate boundaries and mid-ocean ridges (Price and Giovannelli, 2017; Brovarone et al., 2020). The interaction between the seawater with the hot, deep-subsurface lithologies, promotes the leaching of inorganic reduced species, such as volatiles and metals (McDermott et al., 2018). Upon arrival at the surface, the mixing of the reduced hydrothermal fluids (enriched in electron donors) with the oxidized sea water (enriched in electron acceptors), creates a thermodynamic disequilibrium that fuels diverse microbial consortia and sustains complex food webs (Dahle et al., 2015; Price et al., 2015; Reed et al., 2015). In contrast with their deep-sea counterparts, shallow-water hydrothermal vents (SWHV) are closer to the surface, thus they are strongly influenced by solar energy. In these shallow systems, the primary production is reliant upon a mixture of phototrophy and chemolithotrophy, making them high-energy environments (Tarasov et al., 2005; Gomez-Saez et al., 2017). Additionally, the shallower depths and the resultant decrease in pressure allow for the presence of a generally abundant free gas phase (Bastianoni et al., 2022). The proximity to landmasses promotes the input of terrigenous organic carbon to the system, while tidal waves and tides make SWHV transient ecosystems subject to strong dynamic forcing (Giovannelli et al., 2013; Yücel et al., 2013; Price and Giovannelli, 2017).

The shallow-water hydrothermal vents of the Aeolian archipelago are some of the most studied marine shallow vents in the world. The archipelago, located north of Sicily, is composed of seven volcanic islands (Stromboli, Vulcano, Panarea, Salina, Lipari, Alicudi, and Filicudi) and several sea-mounts. The archipelago lies between the Tyrrhenian sea back-arc basin and the Calabrian fore-arc. While most of its volcanic activity developed during the Quaternary period, it continues to the present day on some of the islands (Vulcano and Stromboli) in the form of volcanic eruptions and secondary geothermal manifestations (Gamberi et al., 1997). The geomorphism of the region is very dynamic, marked by the presence of rock types belonging mainly to the calc-alkaline, shoshonitic, and potassium associations (De Astis et al., 2000; Peccerillo and Turco, 2004). The islands of Lipari, Salina, and Vulcano, are aligned on an NNW–SSE striking fault, while a NNE–SSW to NE–SW striking fault affects the islands of Stromboli and Panarea (De Astis et al., 2003; Favallim et al., 2005). Most of the described marine geothermal activity is present along the coast of the islands of Vulcano and Panarea, where the majority of microbiological studies on the shallow-water vents have been focused so far. Despite this, additional sites of geothermal activities have been described on the other islands (Cardellini et al., 2003; Inguaggiato et al., 2012, 2013).

Previous studies have mapped the thermodynamic chemical reaction landscape of SWHVs of Vulcano and Panarea islands, showing that a wide range of exergonic chemical reactions are capable of sustaining diverse metabolic strategies (Amend et al., 2003; Rogers and Amend, 2005, 2006; Rogers et al., 2007; Price et al., 2015). Accordingly, through metagenomics analysis, amplicon sequencing, and DGGE analysis, previous studies reported complex and diverse microbial communities inhabiting these ecosystems (Gugliandolo and Italiano, 1999; Simmons and Norris, 2002; Rogers and Amend, 2005, 2006; Rusch et al., 2005; Lentini et al., 2007, 2014; Manini et al., 2008; White et al., 2008; Maugeri et al., 2009, 2010, 2013; Gugliandolo et al., 2012, 2015; Placido et al., 2015; Antranikian et al., 2017; Fagorzi et al., 2019; Gugliandolo and Maugeri, 2019; Sciutteri et al., 2022). These communities were found to be enriched in sulfur-oxidizing chemolithoautotrophic bacteria at higher temperatures and at lower temperatures by heterotrophic and photoautotrophic-based life-styles. Furthermore, thermophilic microorganisms have been isolated from several vents (Hafenbradl et al., 1996; Deckert et al., 1998; Lentini et al., 2007; Gugliandolo et al., 2012). However, only a few studies tried to couple in more detail both the geochemistry of the shallow vents and the microbial communities inhabiting them. In addition, these studies were conducted exclusively on the SWHV of Vulcano and Panarea, with the exception of one study, based on culture-dependent approaches that included communities from Lipari and Stromboli (Gugliandolo and Italiano, 1999). Currently, there is a lack of a more comprehensive survey of the microbial communities associated with the diversity of shallow-water hydrothermal vent ecosystems of the Aeolian archipelago.

To address this, and to understand how geochemically different shallow-water hydrothermal vents shape the microbial community composition, we used a combination of 16S rRNA gene amplicon sequencing and geochemical approaches to survey six shallow-water hydrothermal vents located in four different islands of the Archipelago, including two new locations that have never been characterized in the literature before. Our results show that shallow-water hydrothermal vents of the Aeolian islands are ecosystems that support diverse and complex microbial communities, providing important ecological roles to the surrounding marine environment. For this reason, they should be included in current and future conservation efforts.

2. Materials and methods

2.1. Sampling and site description

The samples were retrieved on the AEO19 expedition to the islands of the Aeolian archipelago: Vulcano, Panarea, Salina, and Lipari in the summer of 2019. Six different locations were sampled:

Vulcano - Levante Bay (LB), Vulcano - Levante Port (PL); Panarea - Bottaro (BO), Panarea - Baia Calcara (BC), Salina - Pollara (PO), and Lipari - Pietra del bagno (PB) (Figure 1), representing different shallow-water geothermal environments. All the samples were retrieved by SCUBA divers, using sterile falcon tubes and syringes. To accomplish a broader characterization of the different sites, different types of samples were collected: sediments, hydrothermal fluids, and biofilms. In the sites Levante Bay, Pollara, Baia Calcara, and Pietra del Bagno, abundant white microbial mats were observed near the venting sites. The shallow vents across the sampled locations were sulfide-rich, with the exception of the Pietra del Bagno site, where the presence of conspicuous orange precipitates suggests the presence of iron-rich hydrothermal fluids. Intense degassing was observed in the Bottaro venting site. All samples were stored either at +4°C or −20°C in accordance to the specific protocols for later processing in the lab. Subsamples used for molecular analysis and organic matter determination were stored frozen at −20°C, while samples for the determination of the major ions were filtered through a 0.22 µm filter and stored at +4°C. Temperature was measured *in situ* using a waterproof thermocouple, while pH, oxidation–reduction potential, conductivity, and dissolved oxygen were measured using a multi-parameter sensor probe (Hanna- multiparameter, model HI98194) on the boat immediately after the dive, with a fluid sample collected with syringes at the seafloor.

2.2. Sedimentary organic matter

The determination of the concentration of pigments (chlorophyll-*a* and phaeopigments) was carried out according to Lorenzen and Downs (1986). Briefly, the samples were supplemented with 90% of acetone and further incubated in the dark, at 4°C, for 12 h. After incubation, in order to remove the sediments, the samples were centrifuged and the concentration of chlorophyll-*a* and phaeopigments was estimated using a spectrofluorometer (at wavelengths of 430 nm and 630 nm), before and after being supplemented with 200 µL of 0.1 N HCl, respectively. Pigment concentrations were normalized to sediment dry weight (Manini et al., 2003).

Total protein concentrations were determined according to Hartree (1972), and further modified for analysis of sediment samples from Fabiano et al. (1995). The total carbohydrate concentrations were determined according to Gerchakov and Hatcher (1972), and expressed as glucose equivalents. Total lipids were extracted from the sediments by a direct elution with chloroform and methyl alcohol (1:1 v/v), and further determined according to Bligh and Dyer (1959). The readings were performed spectrophotometrically. The concentrations of carbohydrates, proteins and lipids were converted to carbon equivalents using the conversion factors, 0.40, 0.49 and 0.75 µg C × µg^{-1}, respectively, and further normalized to sediment dry weight (Fabiano et al., 1995). The biopolymeric carbon (BPC), calculated through the sum of the concentration of carbohydrates,

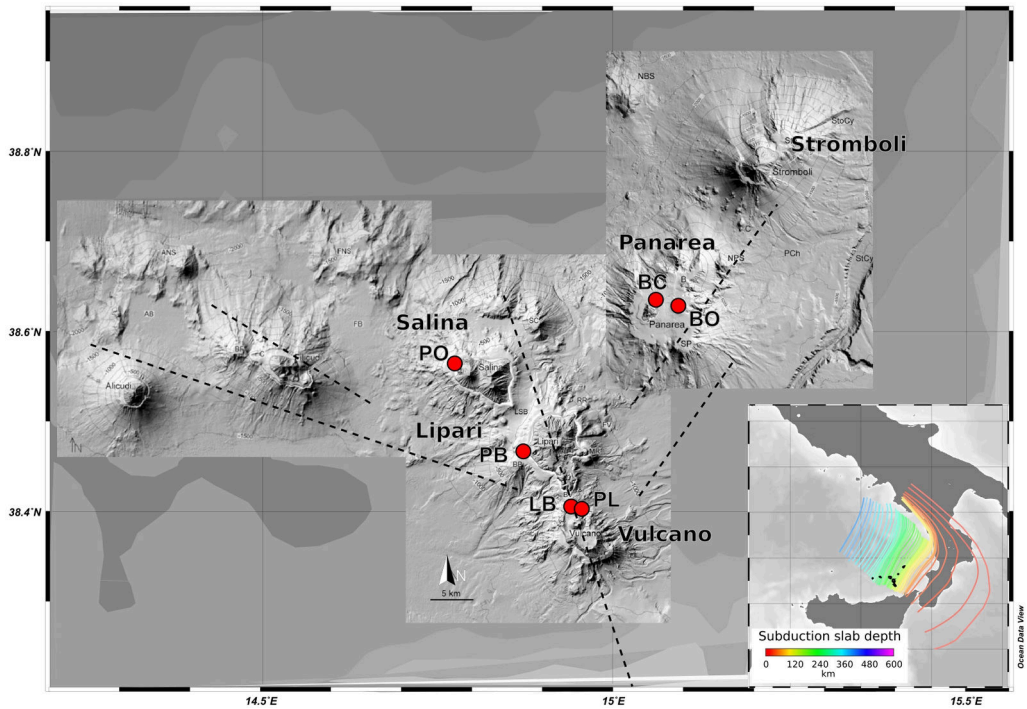

FIGURE 1
Map of the volcanic Aeolian island archipelago, located north of Sicily. Sample sites are shown in red. Major fault systems are illustrated here, as well as the gradient of the different slab depths (100–250 Km).

proteins and lipids, represents the fraction of the total organic carbon potentially available to heterotrophs and benthic consumers in the environment. All measurements are reported as an average of three replicates.

2.3. Geochemical analysis

The concentrations of major cations (sodium-Na^+, potassium-K^+, magnesium-Mg^{2+} and calcium-Ca^+) and anions (chlorine-Cl^-, sulfate-SO_4^{2-} and bromide-Br^-) of the hydrothermal fluids were measured using ion chromatography (ECO, IC Metrohm) equipped with conductivity detectors in two independent measurements. Calibration curves for the ion species of interest were run in the range of 0.1 and 10 ppm with $R \geq 0.999$. In order to reduce the amount of Cl^- and Na^+ entering the system, before the analysis, all samples were filtered (0.22 μm) and diluted to guarantee a conductivity of 600 μS/cm. All dilutions were made using 18.2 MΩ/cm type I water, which was also used as a blank for blank subtractions. Anions were run using a 3.2 mM Na_2CO_3 + 1 mM $NaHCO_3$ mobile phase on a Metrosep A Supp 5 column equipped with a 0.15 M ortho-Phosphoric acid suppressor. The flow of the anionic eluent was 0.7 mL min-1 for 30 min, effective for good resolution of all anions in the standard solution. Cations were run using a 2.5 mM HNO_3 + 0.5 mM $(COOH)_2 \times 2H_2O$ mobile phase on a Metrosep C4 column. The flow of the cationic eluent was 0.9 mL min-1 with a total separation of 35 min, effective for good resolution of all cations in the standard solution. Data acquisition and analysis were carried out through MagIC Net 3.3 software. Additionally, calibration curves were carried out using certified CPA chem external standards for each of the anions and cations analyzed. Detection limits for each of the ions analyzed correspond to 95% confidence levels, and were as follows: Mg^{2+} (0.08 mM), Na^+ (0.3 mM), Ca^{2+} (0.3 mM), K^+ (0.7 mM), SO_4^{2-} (0.03 mM), Br^- (0.02 mM), Cl^- (0.1 mM).

2.4. DNA extraction and amplicon sequencing

DNA extraction was performed using the DNeasy PowerSoil Kit (QIAGEN), following the manufacturer's instructions, with small modifications. The modifications of the protocol included a further elution step to better recover the DNA from the column. For samples where the PowerSoil kit protocol resulted in low quantity of DNA, a modified phenol-chloroform extraction method was employed (Cordone et al., 2005, 2011; Zanfardino et al., 2016), specifically adapted for the conditions found in shallow-water hydrothermal vents, such as the higher presence of clays and anions (Giovannelli et al., 2013, 2016). Briefly, 0.8 g of sediment was suspended in 850 μL of extraction buffer (100 mM Na_2HPO_4 pH 8, 100 mM tris–HCL pH 8, 100 mM EDTA pH 8, 1.5 M NaCl, 1% CTAB) and further supplemented with 100 μL of Lysozyme (100 mg/mL), followed by two incubation periods at 37°C for 30 min, the latter after the addition of 5 μL of Proteinase K (1 mg/mL). Subsequently, 50 μL of 20% SDS was added to the samples and incubated 1 h at 65°C, with regular mixing. The sediments were removed through consecutive centrifugations (2 × 14,000 g) after the addition of a solution of phenol:chloroform:isoamyl alcohol (25:24:1/24:1). The supernatant was collected and supplemented with Na-acetate (0.1 vol) and isopropanol 100%, and incubated at room temperature for 12 h. The precipitated DNA was then washed with 70% ice-cold ethanol, and re-suspended in 50 μL of Tris–HCL. DNA was visualized with agarose gel electrophoresis and quantified spectrophotometrically and spectrofluorimetrically (NanoDrop and Qubit). Obtained DNA was sequenced at the Integrated Microbiome Resource (IMR)[1] using primers targeting the V4-V5 of the 16S rRNA (515FB = GTGYCAGCM GCCGCGGTAA 926R = CCGYCAATTYMTTTRAGTTT515FB), using Illumina MiSeq technology.

2.5. Bioinformatic and statistical analysis

The raw sequence data was processed using the DADA2 package (Callahan et al., 2017). The analysis of the quality profile was carried out after removing primers and adapters. Sequences with an average call quality for each base between 20 and 40, were retained for downstream analysis. DADA2, through estimation of the error profile for each possible transition, identifies amplicon sequencing variants (ASVs). Taxonomy was assigned to the ASVs by matching with the SILVA Database, release 138.1[2] (Quast et al., 2013). Taxonomic assignments, together with the variant abundance table, were used to calculate diversity indices and investigate microbial diversity with the Phyloseq package (McMurdie and Holmes, 2013), as previously reported (Cordone et al., 2022). Briefly, the ASVs count table and the assigned taxonomy were combined into a *phyloseq* object. Mitochondria, Chloroplast, and Eukaryotic sequences were removed. Then, groups related to human pathogens and common DNA extraction contaminants (Sheik et al., 2018) were removed. The remaining reads represented 96.97% of the original reads, with 149,351 reads assigned to 2,145 ASVs preserved for downstream analysis. Diversity analyzes were carried out using the Phyloseq package (McMurdie and Holmes, 2013) with the relative abundance values set to 100%. Top abundance ASVs and genera were further defined as having accumulative abundances above 0.1%. Additionally, the alpha diversity was investigated using Shannon diversity index. The beta diversity was investigated using the UniFrac diversity index (Unweighted and Weighted) as implemented in the vegan package (Oksanen et al., 2018). Subsequently, the resultant similarity matrix was plotted using non-metric multidimensional scaling techniques. The resulting ordination was used to investigate the correlation between the environmental and geochemical variables using environmental fitting (*envfit* and *ordisurf* functions in vegan). All statistical investigations, data processing and plotting were carried out in the R statistical software version 4.1.2 (R Core Team, 2021), using the vegan (Oksanen et al., 2018), ggplot2 (Wickham, 2011), and the packages supra-referred. All the sequences analyzed in this study are available through the European Nucleotide Archive (ENA) under project accession PRJEB54611 under the ENA Umbrella project CoEvolve PRJEB55081. A complete R script containing all the steps to reproduce our analysis is available at https://github.com/giovannellilab/Barosa_et_al_Aeolian_shallow_vent_diversity with

1 https://imr.bio
2 www.arb-silva.de

DOI: https://doi.org/10.5281/zenodo.7480614 together with all the environmental and geochemical data.

3. Results

3.1. Physico-chemical parameters and sedimentary organic matter content

The physico-chemical parameters of the hydrothermal sites sampled in the present study are presented in Table 1. Overall, the physico-chemical parameters measured varied between the sites. The shallow-water vent sediment temperatures at the sampled venting orifice ranged from 28°C in Pollara to 90°C in Baia Calcara. The salinity ranged from 33.0 psu in Levante Bay to 41.5 psu in Pietra del Bagno. Dissolved oxygen (DO) values ranged from 11% in Levante Bay to 57.3% in Pietra del Bagno. Additionally, the oxidation–reduction potential of the different sites was negative for Levante Bay, Bottaro, and Levante Port, while Baia Calcara, Bottaro, and Pietra del Bagno had positive reduction potentials. The pH was slightly acidic for every sample, with the exception of Bottaro, which had circumneutral pH (8).

The sampled sediments showed a wide range of sedimentary organic matter content, with concentrations of biopolymeric organic carbon (BPC) ranging from 99.44 μg C g^{-1} (± 2.22) in Pollara to 3499.0 μg C g^{-1} (± 2740.5) in Bottaro. The higher values of BPC in Bottaro, as well as the high variability between the measured replicates, was hypothesized to be related to the presence of a biofilm ingrained in the coarse sediment. Total protein and carbohydrates ranged from 492.88 μg C g^{-1} (± 39.5) and 39.23 μg C g^{-1} (± 4.64) in Levante Bay to 6547.72 μg C g^{-1} (± 599.9) and 1756.92 μg C g^{-1} (± 279.88) in Bottaro, respectively. Total lipids ranged from 10.17 μgC g^{-1} (± 3.02) in Pollara to 222.48 μg C g-1 (± 65.91) in Levante Port. Protein to carbohydrate ratios ranged from 1.1 in Pietra del Bagno to 15.2 in Baia Calcara. Chlorophyll-*a* concentration values ranged from 0.01 μg g^{-1} (± 0.003) in Levante Bay to 6.9 μg g^{-1} (± 0.126) in Levante Port. The highest chlorophyll-*a* concentrations were measured at the moderate temperature sites, Bottaro and Levante Port, while the lowest values were measured at the high temperature sites, Levante Bay and Baia Calcara (Figure 2).

3.2. Geochemical analysis

The concentration of the major elements in the hydrothermal fluids were measured in the forms of major anions and cations (Figure 3; Table 2). Chloride concentrations ranged from 535.9 (% RDS 0.38) to 701.9 mM (% RDS 0.38), compared to 618.0 mM in seawater. Bottaro, Pollara and Pietra del Bagno have the highest Cl^- values. Sulfate concentrations ranged from 22.71 mM (% RDS 0.69) in Baia Calcara to 27.89 mM (% RDS 0.69) in Pietra del Bagno. Sulfate was depleted in the hydrothermal fluids of all the samples compared to seawater concentrations (32.9 mM). Additionally, Br^- concentrations ranged from 0.74 mM (% RDS 0.59) in Levante Bay to 0.91 mM (% RDS 0.59) in Bottaro, compared to sea water concentrations (0.94 mM). As for the major cations, Mg^{2+} concentrations ranged from 49.04 mM (% RDS 3.8) in Levante Bay to 62.36 mM (% RDS 3.8) in Bottaro, compared to seawater concentrations of 58.3 mM. Bottaro and Pollara were the only sites where fluids were enriched in Mg^{2+}, relative to seawater. The concentrations of K^+, Ca^{2+} and Na^+ ranged from 11.18 mM (% RDS 11.75) in Pollara to 13.23 mM (% RDS 11.75) in Levante Bay, from 8.55 mM (% RDS 10.37) in Pietra del Bagno to 17.87 mM (% RDS 10.37) in Bottaro, and from 445.9 mM (% RDS 7.4) in Levante Port to 551.6 mM (% RDS 7.4) in Bottaro, compared to the seawater concentrations of 11.0 mM, 11.1 mM and 547.0 mM, respectively. Additionally, we combined our data from previous publish data on the geochemistry of the fluids sampled from the shallow water hydrothermal vents of Vulcano, Panarea, and Stromboli (Italiano and Nuccio, 1991; Sedwick and Stüben, 1996; Gugliandolo et al., 2006; Rogers et al., 2007; Sieland, 2009; Tassi et al., 2009; Inguaggiato et al., 2013; Price et al., 2015; Kürzinger, 2019). Fluid data from the present study falls within a mixing trend resembling Type 3 fluids previously described by Price et al., 2015.

3.3. Microbial diversity

The bacterial diversity of the shallow-water hydrothermal vents of the Aeolian archipelago was investigated using the V4-V5 variable region of the 16S rRNA gene. After guaranteeing high-quality data (quality check and data filtering steps), a total of 149,351 reads were obtained, and 2,145 ASVs identified. Regarding the alpha diversity of the different sample types, the biofilm samples had lower alpha diversity measure (3) in comparison with the fluid and sediment samples (4.3 and 4.2, respectively). In terms of variability, the fluid samples showed less sample variability (the difference between the lowest diversity value points to the highest) in relation to the biofilm and sediment samples, which could be related to the differences in the matrix of the different sample types (Figure 4A). For instance, deep

TABLE 1 Location (GPS coordinates), depth, and the physico-chemical parameters measured on the venting fluids at the different sampled locations.

Station	Island	Latitude (°N)	Longitude (°E)	Depth (m)	Temperature (°C)	Salinity (PSU)	DO (%)	ORP (mV)	pH
LB	Vulcano	38.416729	14.959821	0.2	83.9	33.0	11	−295	5.8
PL	Vulcano	38.4161941	14.9611976	6.1	52	37.7	24.4	−202	5.22
BC	Panarea	38.64557	15.076182	15	90	37.5	43	150	5.26
BO	Panarea	38.6388904	15.1104468	6.5	46	40.94	15	−260	5.4
PO	Salina	38.574516	14.799716	10	28	39.0	48	121	5.6
PB	Lipari	38.47514	14.898117	12	45	41.5*	57.3	77	8.08

ORP - Oxido-reduction potential; DO - Dissolved oxygen; *Value of salinity for Pietra del Bagno calculated from Cl– concentrations using the formula: Salinity (ppt) = 0.00180665 × Cl– (mg/L).

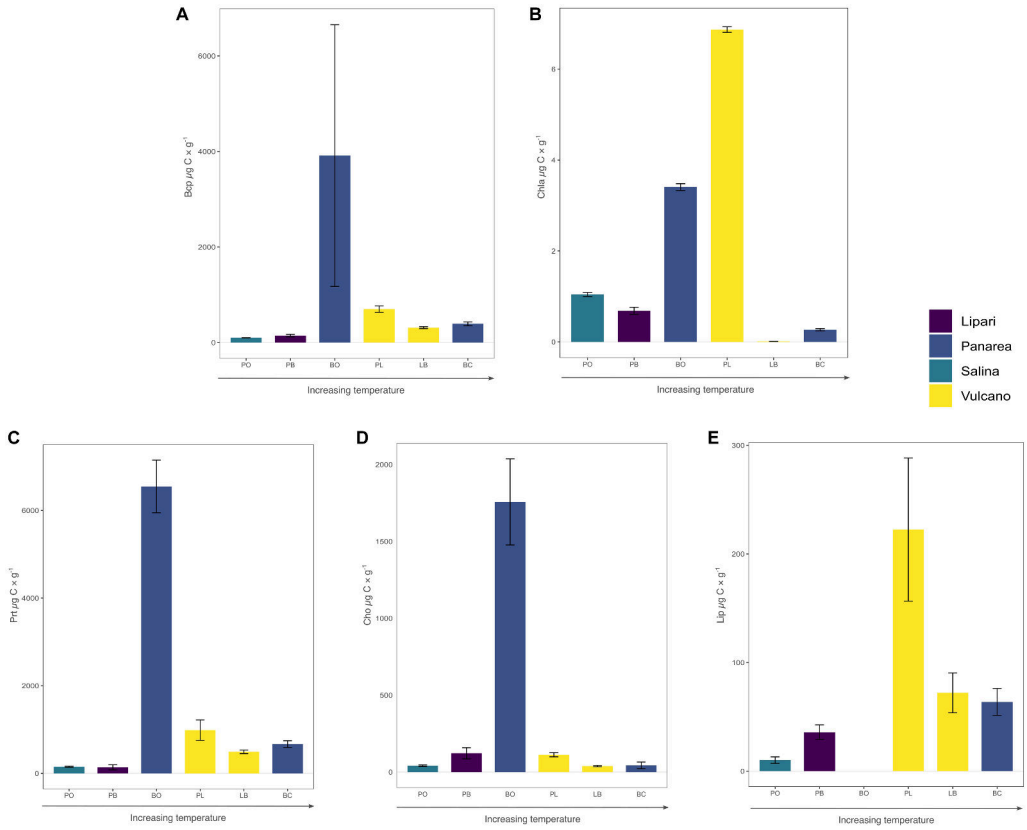

FIGURE 2
Content and quality of the organic matter measured in the sampled sediments. **(A)** Biopolymeric organic carbon (BCP); **(B)** Chlorophyll-a pigments content; **(C)** Proteins; **(D)** Carbohydrates; **(E)** Lipids. All sites are organized by increasing temperatures and are expressed in μg g^{-1} of dry sediment. Error bars represent standard deviation ($n = 3$).

geothermal fluids impose a stronger bottleneck in terms of possible redox couples and ecological niches to the microbial communities, compared to the sediment samples. Additionally, the temperature was found to be a major driver of diversity between samples (Pearson correlation test, $R^2 = 0.41$), where higher temperature sites showed a decrease in alpha diversity (Figure 4B).

The high-temperature sites, Baia Calcara and Levante Bay, characterized by temperatures above 80°C, were dominated by members belonging to Campylobacterota (formerly Epsilonproteobacteria), Proteobacteria, Aquificota, Bacteroidota, Chloroflexi and Acidobacteriota phylum (Figure 5). Among Campylobacterota, the order Campylobacterales was present in high abundances in all the high-temperature sites. Within Campylobacteriales, the genus *Nitratifactor* was only present at higher abundances (44%) in the biofilm sample of Baia Calcara, followed by *Sulfurimonas* (average abundance of 6.08% between the biofilm and sediment samples of Baia Calcara), *Campylobacter* (average abundance of 9% between the fluid and sediment sample of Levante Bay), and *Sulfurovum* genera (6.55% in the fluid sample of Levante Bay). The phylum Proteobacteria was composed entirely by class Gammaproteobacteria in the Baia Calcara site (average abundance of 12% between sediments and biofilm samples), and by Gammaproteobacteria and Alphaproteobacteria in the Levante Bay site (average abundance of 15% in both sample types and 8.5% in the fluid samples, respectively). Within Gammaproteobacteria, the orders Chromatiales and Thiomicrospirales were present in the highest abundances (average abundance of 24.6% at Levante Bay between the fluid and sediment samples, and 13.3% between the sediments and biofilm samples of Baia Calcara and the fluid samples of Levante Bay, respectively), with ASVs classified only to the genus *Candidatus thiobios* and *Thiomicrorhabdus*. The order Nitrococcales was present in lower abundances (average abundance of 6.1% between both sampling sites and all sample types, with the exception of the sediments of Levante Bay), and composed by the genus *Sulfurivirga*. Among Alphaproteobacteria, all ASVs were classified into the order Rhodobacterales in both the fluid and sediment samples of Levante Bay (average abundance of 8.5%), however, it was not possible to resolve them down to the genus level. The phylum Aquificota was composed entirely of members belonging to the order Hydrogenothermales, and the genus *Hydrogenothermus*, and only

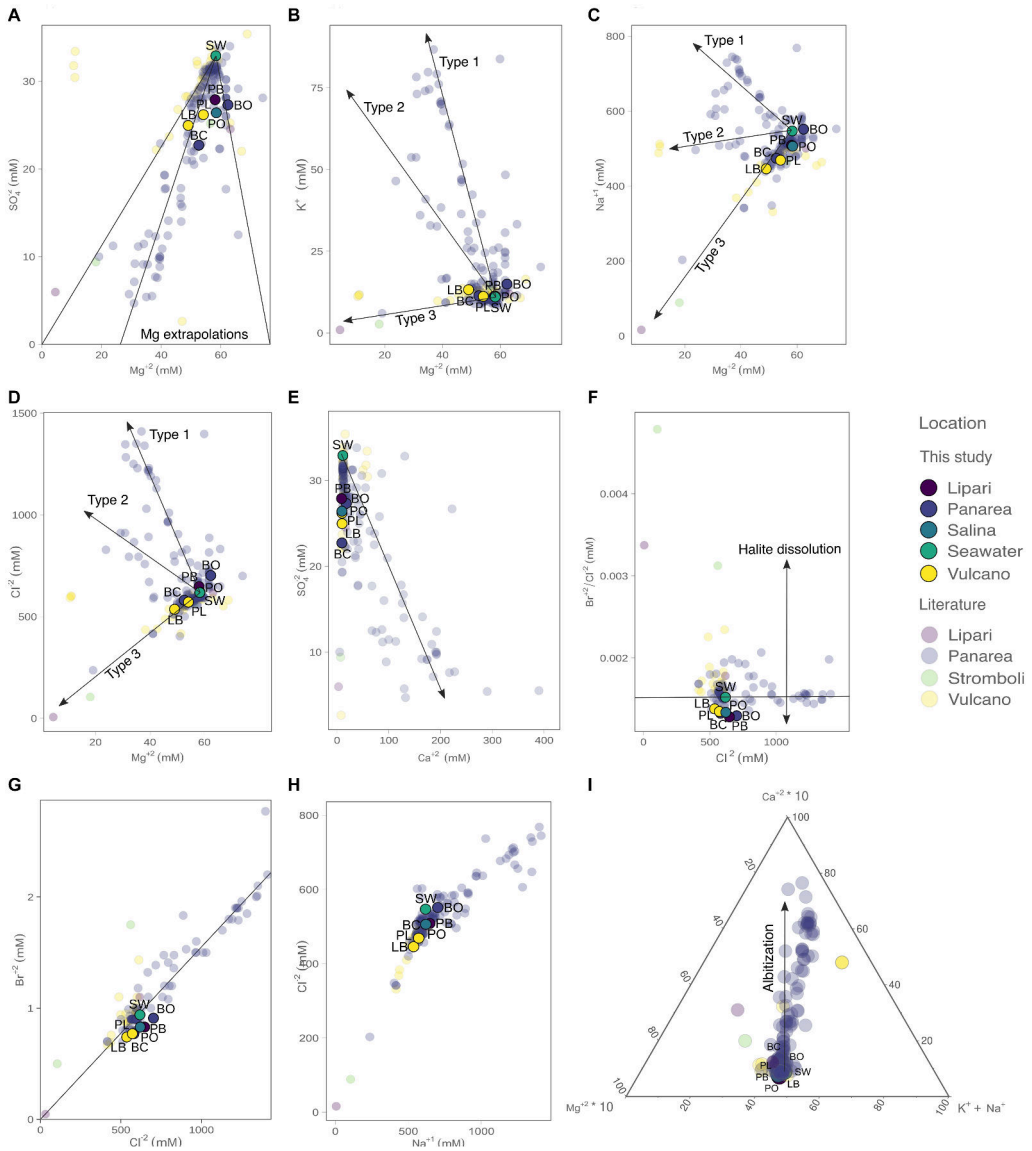

FIGURE 3
Concentrations of the major anions and cations measured in the present study (bold colors), as well as from previous reports from the Literature (opaque colors): **(A)** SO_4^{2-} vs. Mg^{2+}, with the three visible Mg^{2+} end-member extrapolations; **(B)** K^+ vs. Mg^{2+} with the three fluid mixing trends observed; **(C)** Na^+ vs. Mg^{2+}; **(D)** Cl^- vs. Mg^{2+}; **(E)** SO_4^{2-} vs. Ca^{2+} (vector illustrating end-member extrapolation); **(F)** Br^-/Cl^- ratio vs. Cl^-, where it is possible to infer the presence of halite in solution; **(G)** Br^- vs. Cl^- and extrapolations to zero; **(H)** Cl^- vs. Na^+; **(I)** ternary plot with the influence of albitization on the hydrothermal fluids. The literature data was retrieved from Italiano and Nuccio (1991), Sedwick and Stüben (1996), Gugliandolo et al. (2006), Rogers et al. (2007), Sieland (2009), Tassi et al. (2009), Inguaggiato et al. (2013), Price et al. (2015), and Kürzinger (2019).

observed at the sediment samples of Baia Calcara (25.09%). Within Bacteroidota, only the order Flavobacteriales was identified in both the sediment and fluid samples at the Levante Bay site (average abundance of 9.3%), however, no ASVs were classified to the genus level. Acidobacteriota and Chloroflexi, albeit present in lower abundances (5.14% in sediment samples of Baia Calcara and 5.51% in fluid samples of Levante Bay, respectively), had as most abundant, members belonging to the order Thermoanaerobaculares, genus *subgroup* 23, and to the class *Anaerolineae*, respectively (Table 3).

Moderate-temperature sites, such as Bottaro, Pietra del Bagno, and Levante Port, characterized by temperatures ranging from 40°C to 53°C, presented a higher diversity of bacterial phyla. These sites

TABLE 2 Concentrations of the major anions and cations (mM) of the hydrothermal fluids from the Aeolian Shallow-water vents.

Station	Island	Mg^{2+}	Na^{+}	Ca^{2+}	K^{+}	SO_4^{2-}	Br^{-}	Cl^{-}
LB	Vulcano	49.04	445.9	9.65	13.23	24.96	0.74	535.9
PL	Vulcano	54.13	469.1	9.47	11.19	26.19	0.77	571.2
BC	Panarea	52.6	474.1	9.25	11.37	22.71	0.77	580.6
BO	Panarea	62.36	551.6	17.87	14.96	27.31	0.91	701.9
PO	Salina	58.46	506.3	9.41	11.18	26.41	0.83	620.2
PB	Lipari	58.06	508.6	8.55	11.32	27.89	0.83	647.4
Sea Water	–	58.3	547.0	11.1	11.0	32.9	0.94	618.0

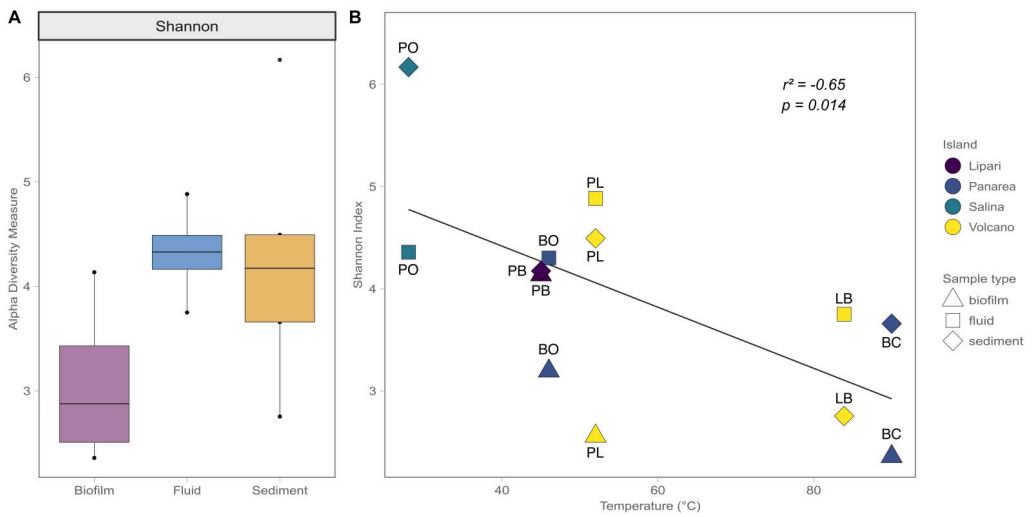

FIGURE 4
Shannon Alpha diversity indexes. **(A)** Alpha diversity measures in relation to the different sample types (Biofilm, Fluid, Sediment). **(B)** Alpha diversity measures in relation to the temperature, with the different Islands sampled, as well the different sample types.

were dominated by members belonging to Campylobacterota, Proteobacteria, Bacteroidota, Calditrichota, Chloroflexi, Cyanobacteria, as well as the Archaeal phylum Crenarchaeota and Altiarchaeota at low abundances. Among Campylobacteriota, the order Campylobacterales was only identified at the sediments and biofilm samples of the Levante Port site, with the highest abundant ASVs belonging to the family *Arcobacteraceae* (37.92% at the sediment samples), without classification to the genus level. Additionally, it was also possible to classify Campylobacterales into the genera *Thiovulum* and *Sulfurimonas* in the biofilm samples (23.40 and 19.40%, respectively), and *Sulfurovum* in the sediment samples (6.51%). Within Proteobacteria, the order Rhodobacterales (21.96% in biofilm sample at Bottaro and 5.70% in biofilm sample of Pietra del Bagno) was the most abundant group, however, it was not possible to classify them down to the genus level. Additionally, the family *Mariprofundaceae* and the assigned genus *Mariprofundus*, was the second most abundant genus within Proteobacteria (15.03%) and only present at the sediment samples of Pietra del Bagno. While in lower abundances, it was possible to identify the family *Thioprofundae*, composed by the genus *Thioprofundum* (7.47% in the sediment samples of Levante Port), and the family *Colwelliaceae*, where all the ASVs were assigned to the genus *Colwellia* (11.54% in biofilm sample of Pietra del Bagno). Moreover, it was also possible to identify the family *Thioglobaceae*, with the ASVs assigned to the clade SUP05 cluster (8.03% in the biofilm samples of Pietra del Bagno). Within the Bacteroidota, the order Flavobactereales constituted most of the ASVs (26.17% in the biofilm sample of Bottaro); however, classification could not be resolved to the genus level. Lower abundance ASVs belonging to Bacteroidota were also assigned to the order Ignobacteriales and the clade LheB3-7 (11.52% in sediment samples of Levante Port). The phyla Aquificota, similarly to the high-temperature sites, was composed entirely of ASVs belonging to the genus *Hydrogenothermus*, and only present at the fluid sample of Bottaro (16.57%). Among Calditrichota, the genus *Caldithrix* represented all the ASVs (17.32% in the sediment sample of Pietra del Bagno and 8.06% in the fluid sample of Bottaro). Additionally, the phototrophic bacterial phyla Cyanobacteria, was composed by the genus *Synechococcus* of the order Synechococcales in only the fluid samples (6.03 and 5.55% in Levante Port and Bottaro, respectively). The Archaeal phyla were detected in low abundances. Archaeal ASVs

10.3389/fmicb.2023.1134114

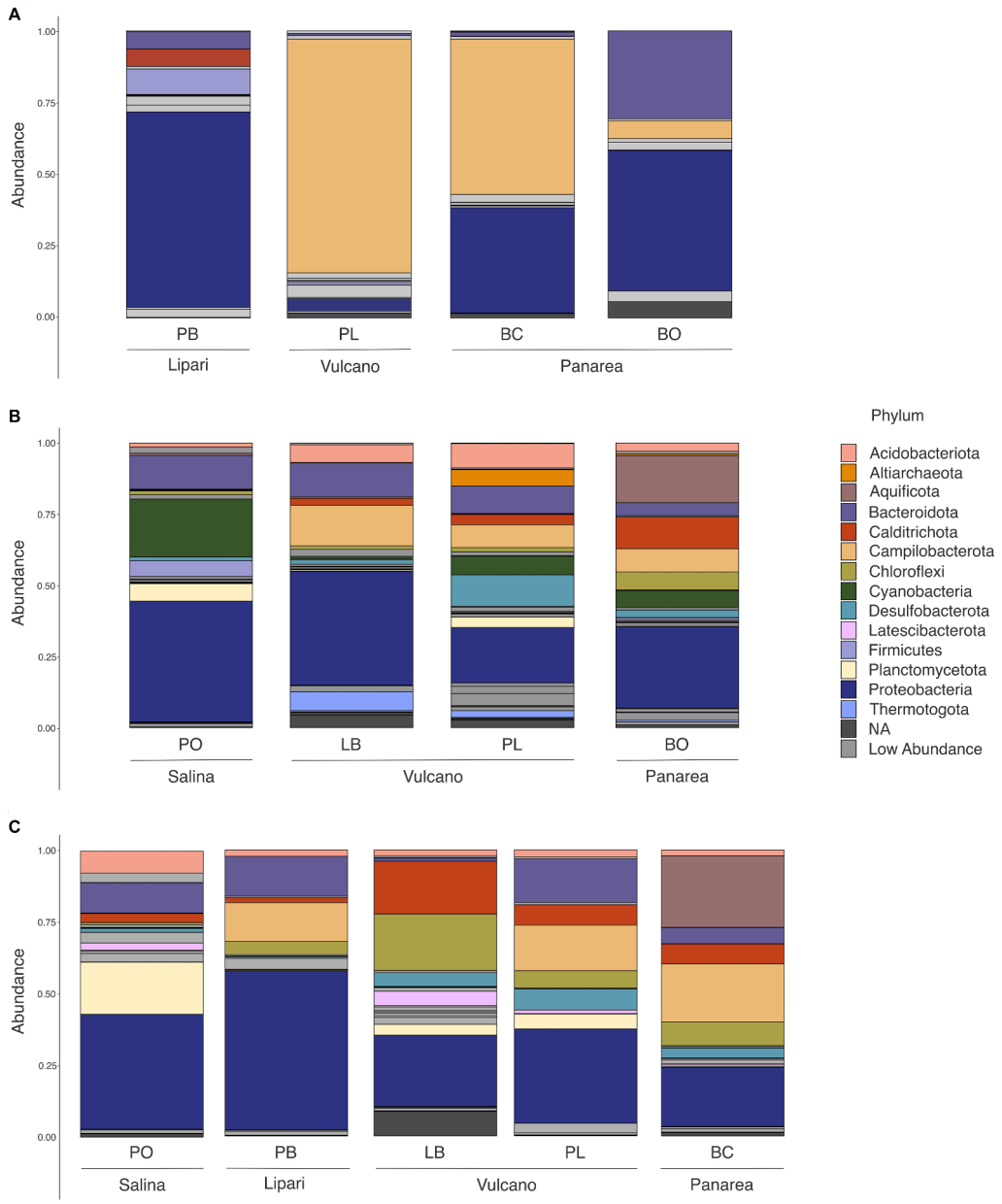

FIGURE 5
Phylum level abundance and distribution of the 16S rRNA diversity in all of the sample sites and sample types at the different islands of the Aeolian Archipelago. For simplicity, only abundances above 5% at each site are illustrated. **(A)** Biofilm samples; **(B)** Fluid samples; **(C)** Sediment samples.

were classified into the genera *Candidatus_Nitrosopumilus* and *Candidatus_Altiarchaeum* (6.06% in the biofilm sample of Pietra del Bagno and 5.76% in the fluid sample of Levante Port, respectively). Interestingly, some lower abundance ASVs could not be classified up to the phylum level (8.59% in the sediment sample of Pietra del Bagno and 5.67% in the biofilm sample of Bottaro, respectively).

The lowest temperature site, Pollara, at the island of Salina, marked by temperatures of 28°C, was dominated by Cyanobacteria, Proteobacteria, Bacteroidota, and Firmicutes. The majority of the ASVs at lower temperatures were assigned to the phylum Cyanobacteria and the species *Synechococcus* sp. CC9902 (20.15% in the fluid sample). The order Alteromonadales with the genus

TABLE 3 Taxonomic affiliation of the most abundant ASVs through SILVA database (to the lowest possible taxonomic resolution) and Ezbiocloud closest relative.

Sample type	SILVA classification	Ez-biocloud classification	Similarity (%)	Acc. no.
Biofilm	*Nitratifractor*	JQ611125_s	97.32	JQ611125
Biofilm	*Thiomicrorhabdus*	*Galenea microaerophila*	99.73	JQ080912
Biofilm	*Sulfurimonas*	JN873929_s	98.39	JN873929
Biofilm	*Sulfurivirga*	*Sulfurivirga caldicuralii*	99.73	jgi.1107633
Biofilm	Bacteria	JF320743_s	95.99	JF320743
Biofilm	*Rhodobacteraceae*	*Actibacterium pelagium*	*100*	NSBU01000007
Biofilm	*Arcobacteraceae*	AY922188_s	100	AY922188
Biofilm	*Flavobacteriaceae*	*Urechidicola croceu*	95.38	KX066850
Biofilm	*Colwellia*	*Colwellia rossensis*	100	U14581
Biofilm	SUP05_cluster	Maorithyas hadalis gill symbiont I	99.2	AB042413
Biofilm	*Nitrincolaceae*	AM402959_s	99.2	AM402959
Biofilm	Candidatus Nitrosopumilus	*Nitrosopumilus cobalaminigenes*	98.67	KX950757
Biofilm	*Sulfitobacter*	EU795102_s	100	EU795102
Biofilm	*Thiovulum*	DQ295692_s	92.25	DQ295692
Sediments	*Hydrogenothermus*	*Hydrogenothermus marinus*	99.2	AJ292525
Sediments	*Thiomicrorhabdus*	*Galenea microaerophila*	99.73	JQ080912
Sediments	*Sulfurivirga*	*Sulfurivirga caldicuralii*	99.73	jgi.1107633
Sediments	*Sulfurimonas*	JN873929_s	98.39	JN873929
Sediments	*Anaerolineae*	JF320743_s	96.52	JF320743
Sediments	Candidatus_Thiobios	AY310506_s	98.13	AY310506
Sediments	*Campylobacter*	JQ287068_s	98.12	JQ287068
Sediments	*Flavobacteriaceae*	*Urechidicola croceus*	95.38	KX066850
Sediments	*Rhodobacteraceae*	*Actibacterium pelagium*	100	NSBU01000007
Sediments	*Anaerolineaceae*	FJ905697_s	94.39	FJ905697
Sediments	*Mariprofundus*	*Mariprofundus aestuarium*	99.73	CP018799
Sediments	*Caldithrix*	*Caldithrix abyssi*	98.94	CM001402
Sediments	Bacteria	JF320743_s	95.99	JF320743
Sediments	*Caldithrix*	DQ925879_s	94.69	DQ925879
Sediments	*Woeseia*	JF344416_s	99.2	JF344416
Sediments	*Rhodothermaceae*	EU925913_s	99.19	EU925913
Sediments	*Rhodobacteraceae*	*Actibacterium pelagium*	100	NSBU01000007
Fluids	*Hydrogenothermus*	*Hydrogenothermus marinus*	99.2	AJ292525
Fluids	*Caldithrix*	*Caldithrix abyssi* DSM 13497(T)	98.94	CM001402
Fluids	*Synechococcus* CC9902	*Synechococcus sp.* CC9902	99.47	CP000097
Fluids	*Rhodobacteraceae*	*Actibacterium pelagium* JN33(T)	100	NSBU01000007
Fluids	Candidatus_Thiobios	AY310506_s	98.13	AY310506
Fluids	*Flavobacteriaceae*	*Urechidicola croceus* LPB0138(T)	95.38	KX066850
Fluids	*Sulfurovum*	HM591450_s	97.32	HM591450
Fluids	*Campylobacter*	JQ287068_s	98.12	JQ287068
Fluids	*Sulfurivirga*	*Sulfurivirga caldicuralii*	99.73	jgi.1107633
Fluids	*Thiomicrorhabdus*	*Galenea microaerophila*	99.73	JQ080912
Fluids	Subgroup_23	EU542513_s	98.39	EU542513
Fluids	Candidatus_Altiarchaeum	*Altarchaeum hamiconexum*	96.55	JAACVF010000098
Fluids	*Pseudoalteromonas*	*Pseudoalteromonas shioyasakiensis*	100	AB720724
Fluids	NS5_marine_group	PAC001209_s	100	PAC001209
Fluids	*Anoxybacillus*	*Anoxybacillus rupiensis*	100	AJ879076

Pseudoalteromonas (7.53% in the fluid sample), and the order Steroidobacterales, with the genus *Woesia* (9.15% in the sediment sample) were the most abundant within Proteobacteria. The phyla Bacteroidetes was composed of the orders Flavobacteriales and Rhodothermales (5.83% in the fluid sample and 5.06% in the sediment sample, respectively).

To understand the role of the environmental parameters and the geochemistry in the structuring of the microbial communities inhabiting the SWHV of the Aeolian islands, we investigated the beta-diversity using both quantitative and qualitative approaches, more specifically, using weighted and unweighted UNIFRAC dissimilarity indexes, respectively, followed by environmental fitting. The unweighted UniFrac nMDS analysis shows a statistically significant separation between the communities of the islands of Lipari and Salina, and Vulcano and Panarea (ADONIS, $p = 0.0016$, $n = 6$). Additionally, the same separation was found between the composition of the communities of the biofilm samples, compared to the other sample types analyzed in the present study (ADONIS, $p = 0.0075$, $n = 6$). Through linear vector fitting versus the nMDS ordination, we observe which are the main parameters that better explain the microbial diversity of our samples (Figure 6). The group of Vulcano and Panarea can be explained by the temperature, and the group of Salina and Lipari, by the major cations and anions, Mg^{2+}, Na^{+}, and Br^{-}. Using the weighted UniFrac, which weights the abundance of the taxa present, we found the same statistically significant separations between the same island groups (ADONIS, $p = 0.0075$, $n = 6$), and between biofilms and the other sample types analyzed in the present study (ADONIS, $p = 0.0475$, $n = 6$). However, we found differences regarding the main parameters explaining the abundance of microbial communities with vector fitting. For instance, here the biofilm samples of Levante Port and Baia Calcara were mainly explained by temperature and longitude. Additionally, the microbial diversity of Bottaro and Levante Port, in contrast with the unweighted version, are also explained by the major anions and cations, with the addition of Cl^{-}.

4. Discussion

Shallow-water hydrothermal vents are marine environments associated with volcanic activity and tectonically active margins. Due to their unique characteristics, such as the presence of light, proximity to landmasses, and dynamic geochemistry, they harbor a highly diverse microbial consortia (Tarasov et al., 2005; Price and Giovannelli, 2017). The Aeolian archipelago is one of the most studied shallow-water hydrothermal systems in the world (Gugliandolo and Italiano, 1999; Simmons and Norris, 2002; Rogers and Amend, 2005; Rusch et al., 2005; Lentini et al., 2007, 2014; Manini et al., 2008; Maugeri et al., 2009, 2010, 2013; Gugliandolo et al., 2015; Gugliandolo and Maugeri, 2019). However, the role of the diverse geochemical environments found in the different islands in controlling the microbial community structure, is still poorly understood, and usually investigated in a handful of sites. To address this, we surveyed 6 different shallow water vents located in four different islands, combining 16S rRNA amplicon sequencing with geochemical and physico-chemical data. To the best of our knowledge, two of the investigated shallow vents (Pietra del Bagno and Pollara) were never reported before in the literature.

4.1. Geochemistry of the Aeolian shallow-water hydrothermal vents

Hydrothermal systems are characterized by the convective circulation of water that percolates into the crust, gets heated, and then is discharged at the sea floor. During this journey, the fluids are chemically and physically transformed by subsurface processes, such as temperature-dependent water-rock reactions, leaching of transition metals and volatiles from the host lithologies, and phase-separation events (Fournier, 2007; German and Seyfried, 2014). These processes, although occurring in a dynamic continuum, are generally separated into three distinct areas: the recharge zone, the reaction zone, and the upflow zone. Due to the inherent characteristics of the locations within the subsurface where they take place, these areas are marked by the occurrence of different processes. The recharge zone is characterized by the fixation of alkali metals, boron, and the fixation of Mg^{2+} associated with the mineralization of smectite and chlorite. Deep in the system (reaction zone), anorthite is transformed to albite (albitization), resulting in the exchange of Na^{+} and Si^{4+} for Ca^{+} into the fluids, as well as metal mobilization. Additionally, the high temperatures and pressures present at depth allow phase separation events, separating the low weight ions (migrate to the vapor phase) from the heavier weight ions (remain in the fluids). Cl^{-}, by remaining in the fluid phase, modifies the salinity content of the hydrothermal fluids. In the upflow zone, further low-temperature water-rock reactions can occur, such as the precipitation of anhydrite and other minerals (Berndt et al., 1988; Tivey, 2007; Alt, 2013; German and Seyfried, 2014). During ascent, the fluids can either be channeled, feeding directly from deep subsurface reservoirs, or diffuse, with significant mixing of end member fluids with seawater prior to discharge. All together these processes entail different ratios of mixing with seawater, contributing to additional alterations to the fluids before they are discharged at the seafloor where they are collected (Price and Giovannelli, 2017). By analyzing the enrichment and depletion of major ions and cations in vent fluids, we can have a deeper understanding of the main processes occurring in the subsurface. These geochemical processes define the geochemical space available for microbial communities to thrive in these ecosystems, and are fundamental in investigating the microbial diversity of shallow-water hydrothermal vents (Price et al., 2015; Price and Giovannelli, 2017).

In the present study, we leverage the information available in the already published literature on the geochemistry of hydrothermal fluids of the shallow vents of Vulcano, Panarea, and Stromboli (Figure 3) combined with new data. Furthermore, we add for the first time geochemical data for the shallow vents of Lipari and Salina (Pietra del Bagno and Pollara, respectively). It is important to note that subsurface processes at shallow-water hydrothermal vents hosted in volcanic arc settings have not been characterized to the same level of detail as Mid-Ocean Ridge hosted deep-sea systems. For this reason, our study relies on previous characterization of Panarea fluids by Price et al. (2015) and conceptually extended to the other shallow vents investigated. By combining published and new geochemical data we identified three mixing trends (Type 1, Type 2, and Type 3) already described for Panarea by Price et al. (2015).

The observed different trends reveal that these hydrothermal fluids evolved differently, and therefore were subjected to different subsurface processes within the Panarea hydrothermal system. Data

10.3389/fmicb.2023.1134114

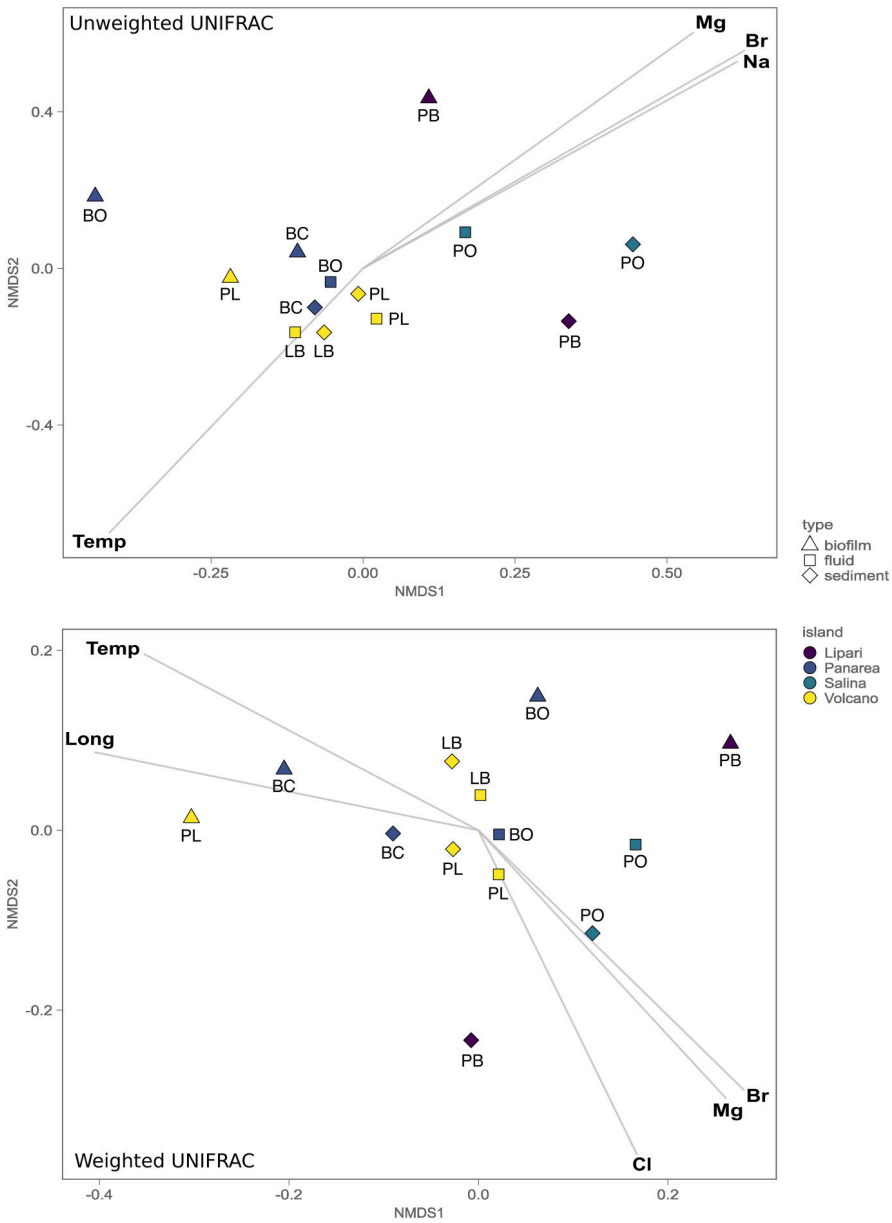

FIGURE 6
Non-metric multidimensional scaling (nMDS, stress 0.075) plot of the 16S gene amplicon microbial diversity based both the weighted and unweighted UniFrac measures, overlaid with environmental vector fitting, illustrating vectors with significant *p* values ($p < 0.01$).

from Vulcano, Lipari, and Salina shallow vents shows that fluids from diverse islands fall within the Type 3 trend (Figure 3). These fluids do not show enrichments of major anions and cations, but instead, show depletions of the major species. The evolution of Type 3 fluids results in acidic fluids, with concentrations of major ions similar to sea-water concentrations, whereas type 1 and type 2 fluids are the result of deep recirculating brine and focused upflow of shallower brines, respectively. This suggests that the difference between these fluid types is directly related to subsurface processes, such as phase-separation deep in the system, the scrubbing of exsoluted gasses that percolate up the crust, as well as the mixing of the diffuse flow fluids with sea-water (Price et al., 2015). Based on our data, it appears that the evolution of

Type 3 fluids might be a common process in the shallow water vents of the Aeolian Archipelago. Additionally, and as evident in Price et al. (2015), most of the fluids, including the ones in the present study, do not extrapolate to zero in both SO_4^{2-} and Mg^{2+}. This can be related to seawater mixing as the fluids approach the surface, due to their diffuse nature. However, in the Bottaro site, the fluids are enriched in Mg^{2+}. It was hypothesized that Mg^{2+} enrichments in Panarea could be related to the leaching of host rocks due to acidification, by means of argillic alteration (Reeves et al., 2011). Since volcanic arc hydrothermal systems are not exposed to the same pressures compared to their deep-sea counterparts (Price and Giovannelli, 2017), the presence of free gas phases may also be contributing to the depletion of Na^+ and Cl^- observed relative to sea water (Figure 3), altering the salinities of the fluids as they percolate through the hydrothermal system. All the fluid samples collected in our study had Br^-/Cl^- ratios lower than seawater, suggesting the presence of dissolved halite in solution. Albitization, which occurs deep in the system and results in the release of Ca^+ in exchange for Na^+ (Alt, 2013), does not seem to be a major process affecting the evolution of our fluid samples, compared to other fluids recovered from Panarea and Vulcano (Figure 3).

While the geochemical composition of the fluids is an important parameter in controlling the diversity of microbial communities, the availability of organic carbon for heterotrophic consumption is fundamental in driving community composition. In hydrothermal systems organic carbon can either be delivered through the subsurface fluids as dissolved organic carbon produced or recycled at depth (Fullerton et al., 2021), or from the water column, either as sinking organic matter particles, lateral advections of surface primary productivity, and terrigenous run offs (Gomez-Saez et al., 2015; Price and Giovannelli, 2017; LaRowe et al., 2020). Additionally, it could be directly produced *in situ* by a diverse community of phototrophic and chemolithotrophic microorganisms (Price and Giovannelli, 2017). The organic carbon delivered to the system is accumulated in the sediments, and analyzing the sedimentary organic matter content can provide an estimate of the organic load on the vent system. In our data the sedimentary organic matter, measured as biopolymeric organic carbon (BPC) was highly variable between the different sites, and did not show linear relationships with temperature, in contrast to what has been observed in a previous study on a shallow-water hydrothermal vent system (Giovannelli et al., 2013; Figure 2A). The lowest amounts of BPC was measured in the site with the lowest temperatures (Pollara, 28°C and Pietra del Bagno, 45°C), and could be related to a to hydrodynamic processes, perturbing the system in these specific locations (Bao et al., 2018), as well as to the fact that these sites are further away from the coast, and thus representing lower amounts of terrigenous inputs to the system. The high concentrations found in Bottaro are instead related to the thick microbial biofilms attached to the sand and gravel. The concentration of chlorophyll-*a* (chl-*a*) pigments was lower at the higher temperatures sites (>80°C; Figure 2B) in line with previous observations (Giovannelli et al., 2013). The presence of Chl-*a* in the sediments can be either related to input of fresh organic carbon from the water column or to the presence of phototrophs in the sediments and biofilms of the vent. The presence of known phototrophs in the sediment and biofilm samples (see below) suggests that the high chlorophyll concentrations found in the same sites are the results of *in situ* production, possibly taking advantage of the nutrients and CO_2 released by the shallow vents. Additionally, the chl-*a* values were higher at the Levante Port and Bottaro sites, which had similar depths (average 6.4 meters), suggesting that beside temperature, the depth of the shallow vent could play a role in controlling the presence and abundance of photosynthetic organisms.

4.2. Microbial diversity

Previous studies conducted at shallow-water hydrothermal vents have demonstrated that a highly diverse microbial consortia inhabit these ecosystems (Hoaki et al., 1995; Sievert et al., 2000; Manini et al., 2008; Maugeri et al., 2009, 2010; Zhang et al., 2012; Price et al., 2013; Kerfahi et al., 2014; Lentini et al., 2014; Dávila-Ramos et al., 2015; Gugliandolo et al., 2015; Gomez-Saez et al., 2017). In the present study, we found that the microbial communities of the Aeolian Islands shallow-water vents are dominated by members belonging to diverse phyla, such as Proteobacteria, Campylobacteriota, Bacteroidota, Cyanobacteria, Chloroflexi, among others present at lower abundances. The major lineages found here have been reported in other shallow-water vents (Maugeri et al., 2010; Zhang et al., 2012; Kerfahi et al., 2014; Lentini et al., 2014; Dávila-Ramos et al., 2015; Gugliandolo et al., 2015; Gomez-Saez et al., 2017; Price and Giovannelli, 2017), illustrating their important ecological role in the functioning of the shallow-water vent ecosystem.

Our data shows that temperature is a major driver explaining the microbial diversity (alpha-diversity, Pearson correlation test, $R^2 = 0.41$, $p < 0.05$). High-temperature sites (>80°C) were characterized by lower diversity in comparison to lower and moderate temperatures sites (28°C to 50°C; Figure 4B). Temperature has been shown to be one of the major factors controlling microbial diversity in a number of diverse geothermal ecosystems, including shallow-water vent environments (Giovannelli et al., 2013; Gugliandolo et al., 2015), deep-sea hydrothermal vents (Dick et al., 2013; Ding et al., 2017), and hot springs (Chan et al., 2017; Fullerton et al., 2021).

High-temperature locations, such as Baia Calcara and Levante Bay sites in the islands of Vulcano and Panarea, respectively, were characterized by temperatures above 80°C. The microbial communities inhabiting these high-temperature shallow vents were dominated by groups related to known chemolithoautotrophic, thermophilic bacteria, harnessing energy through the oxidation of reduced sulfur species and hydrogen. These types of metabolic strategies have been widely reported in shallow-water, deep-sea hydrothermal vents, as well as hot-springs (Tarasov et al., 2005; Yamamoto and Takai, 2011; Inskeep et al., 2013; Price and Giovannelli, 2017). The Baia Calcara and Levante Bay sites had as most abundant, ASVs related to the genera *Nitratifactor*, *Thiomicroarhdbus*, *Hydrogenothermus*, *Candidatus_thiobios,* and the family *Rhodobactereceae*. The biofilm community at the Baia Calcara site was mostly composed of members belonging to *Nitratifactor* and *Thiomicroarhdbus*. *Nitratifactor* has been previously described in shallow and deep-sea hydrothermal systems (Zhang et al., 2012; Zeng et al., 2021). The closest sequence to our ASVs was recovered from a shallow-water hydrothermal system in Kueishan Island, Taiwan (unpublished data). Interestingly, this group was not present in the sediment samples of the same site. Additionally, the genus *Thiomicroarhdbus* was also present in high abundances in the biofilm samples, and in lower abundance also in the sediment sample. It was possible to assign this ASVs to the species *Galenea microaerophila*

(99.73% similarity) (Giovannelli et al., 2012). Initially described from a shallow-water vent from Paleochori Bay, on the island of Milos, *Galenea microaerophila* grows chemolithoautotrophically, through the oxidation of thiosulfate as electron donor, and oxygen (5%) as electron acceptor (Giovannelli et al., 2012). The sediment sample at Baia Calcara was mostly composed by the genus *Hydrogenothermus*, of the phylum Aquificota. This ancestral and deep-branching bacterial phylum is highly prevalent in geothermal environments (Hedlund et al., 2015; Giovannelli et al., 2017), and it is capable of fixing CO_2 into biomass using energy derived from H_2S and H_2 with either elemental sulfur, nitrate or oxygen (at low partial pressures) as electron acceptor. The dominant ASV in our dataset was related to the species *Hydrogenothermus marinus* (99.2% similarity), a hydrogen-oxidizing, chemolithoautotrophic, thermophilic bacterium (Stöhr et al., 2001) originally isolated from sediment samples from Vulcano island.

At the fluid and sediment samples at Levante Bay, the other high temperature site, the family *Rhodobactereceae* and the genus *Candidatus* thiobios were present in highest abundances. The family Rhodobactereceae is widespread in marine environments, and are capable of growing through the utilization of multiple organic, as well as inorganic compounds, contributing to their vast ecological diversity (Pohlner et al., 2019). In our study, it could also be identified in moderate to lower temperature sites. The ASVs classified as *Rhodobactereceae* were further related to the species *Actibacterium pelagium* (100% similarity), which have been isolated from the seawater of the Mediterranean Sea, Pacific and Atlantic Oceans, growing heterotrophically on a variety of organic carbon sources (Guo et al., 2017). Even though members belonging to *Rhodobactereceae* have been previously identified in other hydrothermal systems (Forget et al., 2010; Zhang et al., 2012; Pohlner et al., 2019), to our knowledge, this is the first time this species has been reported in a hydrothermal vent environment. The genus *Candidatus* thiobios is associated with ectosymbiotic bacteria growing on the marie ciliate *Zoothamnium niveum*, commonly found in sulfide-rich habits, including hydrothermal vents (Rinke et al., 2006; Bright et al., 2014). The presence of high abundance of this genus could be related to the presence of the *Zoothamnium niveum* inhabiting this specific site.

Both sites (Baia Calcara and Levante Bay), included lower abundances of sequences assigned to the genus *Sulfurimonas*, *Sulfurivirga*, *Sulforovum*, and *Campylobacter*, all belonging to the Campylobacterota phylum (formerly known as Epsilonproteobacteria). Members of the *Sulfurimonas* genus are widespread in sulfidic environments and are capable of using multiple reduced sulfur species as electron donors, such as thiosulfate, hydrogen sulfide, and elemental sulfur (Han and Perner, 2015). The genus *Sulfurivirga* could be assigned to the species *Sulfurivirga caldiculari* (99.73% similarity), a thiosulfate-oxidizing, thermophilic, chemolithoautotrophic bacterium, described in a shallow-water vent system in Japan (Takai et al., 2006). Similarly, *Sulfurovum* is also associated with thiosulfate oxidation and chemolithoautotrophy (Inagaki et al., 2004). *Campylobacter*, within Campylobacteriota, is ubiquitous in hydrothermal environments, including shallow-water hydrothermal vents (Rinke et al., 2006; Anderson et al., 2011; Giovannelli and Vetriani, 2017; Wang et al., 2017). These genera have been associated with high-temperature high sulfidic locations in other shallow-water, as well as deep-sea hydrothermal systems (Forget et al., 2010; Zhang et al., 2012; Giovannelli et al., 2013; Gugliandolo et al., 2015; Gomez-Saez et al., 2017; Price and Giovannelli, 2017). Members of the Campylobacterota are present in most sites presenting higher temperatures (Levante Bay, Levante Port, Bottaro, Baia Calcara and Pietra del Bagno) and dominate the biofilm communities of Levante Port and Baia Calcara. Hydrothermal vents are often enriched in reduced sulfur species (German and Seyfried, 2014; Price and Giovannelli, 2017). The presence of sulfur-related metabolisms, coupled to inorganic carbon fixation, highlights the importance of these types of metabolic strategies for the function of hydrothermal systems, as well as the importance of these ecosystems to mediate the biogeochemical cycles of sulfur and carbon. Additionally, these high temperature locations had the highest protein/carbohydrate ratios (15.2 in Baia Calcara and 12.6 in Levante Port), suggesting high *in situ* productivity. Since at these locations, recovered ASVs are related to known chemolithoautotrophic groups, indicates that they are major contributors to primary productivity in high temperature shallow water hydrothermal vents. Similarly, Gomez-Saez et al. (2017), reported that chemoautotrophy constitutes an important contribution to fresh organic matter production, accounting for up to 65% of autotrophic carbon fixation in the shallow-water hydrothermal vents of Dominica.

At moderate to low temperatures an increase in phototrophic microbial lineages was observed, also reflected in the quantities of BPC and Chlorophyll-*a*. The prevalent photosynthetic group observed in this study was assigned to the genus *Synechococcus* and to the species *Synechococcus* sp. CC9902 (99.47% similarity), belonging to the phylum Cyanobacteria. The presence of phototrophs in shallow-water hydrothermal systems is well documented, as well as a key feature of these systems (Tarasov et al., 1990, 1999, 2005; Sievert et al., 2000; Zhang et al., 2012; Maugeri et al., 2013; Price et al., 2013; Lentini et al., 2014; Dávila-Ramos et al., 2015; Gugliandolo et al., 2015; Gomez-Saez et al., 2017; Price and Giovannelli, 2017). Here, *Synechococcus* sp. CC9902 was present in lower abundances at moderate temperatures in Bottaro and Levante Port, and high abundances in Pollara, the lowest temperature site. *Synechococcus* sp. CC9902 is widespread in the oceans and is described as having increased plasticity to diverse saline concentrations and light intensities (Ludwig and Bryant, 2012; Kim et al., 2018). Furthermore, the presence of this taxon has already been described in shallow-water hydrothermal vent environments (Maugeri et al., 2013). However, in other shallow-water vents systems, the specific lineages within Cyanobacteria differ. This suggests that in shallow-water hydrothermal vents the photoautotrophic niche space can be occupied by diverse lineages of phototrophic taxa. Notwithstanding, it is important to note that, even though the presence of Cyanobacteria in shallow water hydrothermal vents is well documented, the possibility of mixing with background seawater cannot be discarded. For instance, it has been shown that fluid mixing with seawater could be the result of the convective cells in porous media (Yücel et al., 2013).

The shallow water vent Pietra del Bagno, Lipari, due to the presence of orange precipitates surrounding the venting site, was deemed to be iron-rich. The sediment community was mainly composed by the family *Anaerolineares* of the phylum Chloroflexi, and the genus *Mariprofundus* belonging to Proteobacteria. Members belonging to Chloroflexi are ecologically and physiologically diverse, allowing them to colonize a wide variety of environments (Ward et al., 2018; Vuillemin et al., 2020). Despite being originally associated with anoxygenic phototrophy, they are also known to employ other metabolic strategies (McIlroy et al., 2017). The family *Anaerolineares*

is associated with hydrocarbon oxidation and is known to have important roles in the functioning of anaerobic digestion systems (McIlroy et al., 2017). Nonetheless, they have been reported in deep-sea and shallow-water hydrothermal vents (Rajasabapathy et al., 2018; McGonigle et al., 2020; Wang et al., 2020). The closest relative to our sequences was reported from Fe-rich hydrothermal sediments of two submarine volcanoes of the Tonga volcanic arc (Forget et al., 2010). Interestingly, this bacterial family has also been observed to be present in high abundances in Fe-enriched locations (Hoshino et al., 2016; Ward et al., 2017). Other members of Chloroflexi, such as *Ardenticatena maritima*, grow by dissimilatory iron-reduction (Kawaichi et al., 2013). Thus, it is possible that *Anaerolineares* can couple the oxidation of organic matter to iron-reduction, making them major players in the biomineralization of organic matter in shallow-water vent environments.

The genus *Mariprofundus* of Zetaproteobacteria are well-known iron(II)-oxidizers that couple the iron (II) oxidation to the reduction of oxygen or nitrate (Chiu et al., 2017; McAllister et al., 2019). Members belonging to the phyla Zetaproteobacteria are widespread in hydrothermal Fe-rich environments (Emerson and Moyer, 2002; Emerson et al., 2010; Forget et al., 2010; Gomez-Saez et al., 2017; McAllister et al., 2019). Within *Mariprofundus*, it was possible to assign to the species *Mariprofundus aestuarium* (99.73% similarity), previously isolated from redox-stratified water columns, and capable of growing through the oxidation of iron (II) (Chiu et al., 2017). Additionally, albeit in lower abundances, it was possible to identify the genus *Caldithrix*. More specifically, we could assign our sequences to the species *Caldithrix abyssi* (98.94% similarity). This species is a known chemolithoautotroph, capable of growing anaerobically through the reduction of nitrate, using hydrogen as an electron donor (Miroshnichenko et al., 2003). Our geochemical analysis did not identify nitrate in the fluids at this site (data not shown); however, it was recently found that an environmentally assembled genome (MAG) of this species codes for a homolog of an extracellular respiratory system found in *Geobacter*, associated with iron reduction (Fortney et al., 2018). Given that this terminal electron acceptor was not tested in the original isolate (Miroshnichenko et al., 2003), the coupling of hydrogen oxidation to iron reduction could potentially suggest a metabolic strategy employed by *Caldithrix*. Notably, previous studies conducted at Fe-rich shallow-water vents have reported similar communities to the ones observed at this site (Handley et al., 2010; Meyer-Dombard et al., 2013; Gomez-Saez et al., 2017). Thus, these lineages can be considered to be important in driving the iron cycling in the shallow-water vent ecosystem, making important contributions to the biogeochemical cycles of iron. Interestingly, it was not possible to identify iron oxidizers in the biofilm community in high abundance at the same site. Conversely, the genus *Collwelia* was present in high abundances, followed by the clade SUP05. Members belonging to *Collwelia* are psychrophilic, heterotrophic bacteria, ubiquitous in cold marine environments (Techtmann et al., 2016), including sea ice (Zhang et al., 2008), polar sediments (Wang et al., 2015), and deep-sea trenches (Nogi et al., 2004). Specifically, we identified the species *Colwellia rossensis* (100% similarity), isolated from coastal Antarctic sea ice (Bowman et al., 1998). Colwellia species have been isolated from marine environments, and are characteristically psychrophiles (Bowman et al., 1998). The presence of ASVs related to this species at higher temperatures suggests a bigger temperature gradient to which this group is adapted to. The clade SUP05 is composed of known sulfur-oxidizing bacteria, also described as having a heterotrophic-based metabolism (Spietz et al., 2019; Morris and Spietz, 2022). At this location, the protein to carbohydrate ratios is 1.13. As reported by Pusceddu et al. (2003), since proteins are readily mobilized, as compared to carbohydrates, low ratios suggest the presence of aged organic matter (not freshly produced), and probably indicates external input as a potential source of organic matter to the biofilm communities.

Additionally, in moderate temperatures sites, it was possible to identify in higher abundance the families *Flavobactereceae* and *Arcobactereceae*, in the biofilms of Bottaro and Levante Port, and the genus *IheB3-7* at the sediment sample of Levante Port. The family *Flavobacteriaceae* of the Phylum Bacteroidetes, ubiquitous in marine environments, are known to degrade complex hydrocarbons, with large numbers of glycosyl hydrolases and peptidases encoded in the genomes of this bacterial group (Gavriilidou et al., 2020). Moreover, the family *Arcobactereceae*, also widely distributed in marine environments (Venâncio et al., 2022), has been reported in shallow vent hydrothermal environments (Maugeri et al., 2009; Gugliandolo et al., 2015; Gomez-Saez et al., 2017).

At the lowest temperature site (Pollara), Cyanobacteria was the most abundant group, and with lower abundances, the genera *Pseudoalteromonas*, *Woesia*, NS5 marine group, and *Anoxybacillus*. These microbial groups are associated with heterotrophic metabolisms, and given the protein/carbohydrate ratios at this location of 3.64, as well as Chla-a concentration of 1.0 $\mu g\, g^{-1}$, suggests that these groups rely on the export of organic carbon from the water column into the vent system, coupled with the usage of aged organic matter derived from external input, and *in situ* production from phototrophic organisms. *Pseudoalteromonas*, *Woesia*, and NS5 marine group are widely distributed in marine environments (Holmström and Kjelleberg, 1999; Du et al., 2016; Priest et al., 2022). Additionally, *Anoxybacillus* was also reported in deep-sea hydrothermal vent sediments (Cheng et al., 2021). Here, it was possible to assign *Anoxybacillus* to the species *Anoxybacillus rapiensis* (100% similarity), a thermophilic, anaerobic, heterotrophic bacterium, isolated from diverse hot springs in Bulgaria (Derekova et al., 2007).

While temperature is one of the key variables controlling the microbial diversity in our dataset, other environmental parameters contribute significantly in shaping microbial communities of the different sample types collected (fluids, sediments and biofilms) across the geochemically diverse vents sampled. This has been recently demonstrated in hot springs (Fullerton et al., 2021), where a combination of the geological settings, the aqueous geochemistry and trace element availability provided strong explanatory power of the beta diversity turnover among the sampled springs. In this work unweighted and weighted UniFrac based multivariate analysis (Figure 6) revealed the presence of three statistically significant groups. The first was composed of the biofilm samples, where no significant correlations with the measured parameters were found to significantly explain the diversity. The biofilm composition and architecture are found to be influenced by both deterministic, as well as stochastic effects. For instance, previous studies have shown that biofilm thickness drives the biofilm community and diversity (Suarez et al., 2019), combined with the age of the biofilm and other environmental variables. The second major group, encompassing the samples of fluids and sediments from the islands Vulcano and Panarea, could be explained by the temperature. As discussed above, these

locations were marked by moderate to high temperatures, with ASVs associated with microbial lineages related to the oxidation of hydrogen or reduced sulfur species. In hydrothermal systems fluid ascent is facilitated by the permeability of lithospheric fault systems, allowing a more focused channeling of the fluids to the surface (Pearce et al., 2019). Moreover, hydrothermal systems further away from fault systems are likely to show weak thermal anomalies (Taillefer et al., 2018). Consistent with this, the site with the lowest temperature, Pollara in Salina, is the sampling site further away from known fault systems in the area. Interestingly, we found that temperature and Mg^{2+} follow opposite correlation patterns. Magnesium is depleted in end-member hydrothermal fluids, resulting from water-rock reactions during the circulation of the fluids in the hydrothermal system (Alt, 2013). The presence of higher quantities of Mg^{2+} in low temperature sites, can entail less degree of water-reactions, which could be a function of the weak thermal anomalies found in the island of Salina and Lipari. Consistent with this, these islands present less geothermal activity compared to the other island samples in this study.

In the third group, encompassing the sites from the islands of Salina and Lipari, the microbial diversity was explained by the major anions and cations Mg^{2+}, Br^{-}, and Na^{+}. Despite the geochemical analysis encompassing our samples in combination with the literature available placed our samples within Type 3 fluids, small variations of the major anions and cations show statistically significant correlation with the microbial distribution in both these islands. Diverse subsurface processes could result in similar concentrations of the major anions and cations, but result in a differential enrichment of minor elements, such as trace elements (Rollinson and Pease, 2021). Recent studies have shown that trace elements play key roles in shaping microbial niche occupation, as well as have been used to improve the cultivation of extremophilic organisms from natural hot springs (Meyer-Dombard et al., 2012; Shafiee et al., 2021).

Similarly to the unweighted UniFrac, with the weighted version, which weights the abundance of the taxa present, we found the same statistically significant separation between the communities of Vulcano/Panarea and Salina/Lipari, as well as the biofilm samples and the other samples types. However, conversely to the unweighted UniFrac, we found the temperature to be correlated with the abundance of taxa of Baia Calcara and Levante Port biofilm communities. These were dominated by thermophilic communities belonging to *Nitratifractor* and *Thiomicrorhabdus*. Therefore, both these parameters can act as strong selective pressures, driving not the structuring of the biofilm communities of Baia Calcara and Levante Port, but selecting for thermophilic, chemolithoautotrophic groups. The correlation with longitude could be related with the location of the islands within the Aeolian volcanic arc. It has been previously demonstrated that the magmatic composition of the Aeolian arc exhibits within-islands variations (Peccerillo et al., 2013). These differences could entail differential inputs of magmatic volatiles into the hydrothermal fluids, which in turn could be influencing the microbial communities inhabiting the shallow-water hydrothermal vents. It was also possible to find the major elements correlating with the abundance of the communities of the islands of Lipara and Salina, and with weighted UniFrac, the communities of Vulcano and Salina.

In the Aeolian Archipelago it is possible to find a highly diverse set of marine habitats. These habitats, in turn, harbor an abundant number of species, some of which with endangered status (Álvarez et al., 2019). For this reason, over the years, there have been increasing efforts to enhance the conservation measures on the Aeolian Islands, through the practices of sustainable fishing, tourism, and community education (Álvarez et al., 2019). The presence of high hydrothermal activity should further augment the need for conservation practices in these islands, for different reasons. One is that the microbial communities inhabiting these vents play important ecological roles for the entire shallow marine ecosystem (Tarasov et al., 2005; Price and Giovannelli, 2017), potentially sustaining primary productivity in surrounding ecosystems (Price and Giovannelli, 2017). Given their key roles as primary producers, these microbial communities sustain complex food webs on the surrounding islands. Secondly, extreme environments are often looked upon for the isolation of microorganisms that produce industrially and medically relevant metabolites, such as novel enzymes and antibiotics (Littlechild, 2015; Sayed et al., 2020; Petrillo et al., 2021). For instance, novel enzyme-producing Bacillus have been isolated from the Island of Panarea, whereas novel hydrolases have been identified on environmental DNA libraries from the sediments of the shallow-vents of the island of Vulcano (Lentini et al., 2007; Gugliandolo et al., 2012; Placido et al., 2015). Thirdly, in recent years there have been efforts to apply conservation status to deep-sea hydrothermal vents (Van Dover, 2012; Van Dover et al., 2018). We argue that shallow-water hydrothermal vents play an equally important role in the functioning of marine ecosystems, and should be explicitly acknowledged in marine spatial planning and conservation efforts, not only because of their uniqueness, but because they represent an accessible window for us to appreciate the intricate relationships between the geosphere and biosphere.

5. Conclusion

In conclusion, our study shows that the Aeolian archipelago shallow water hydrothermal vents harbors a highly diverse microbial consortia. In line with previous studies conducted in these unique ecosystems, we found the presence of ASVs related to organisms employing diverse metabolic strategies, ranging from chemolithoautotrophy, heterotrophy and phototrophy. Furthermore, we found those same groups to be correlated strongly with temperature, where we could observe a transition from higher temperatures (mainly ASVs related to chemolithoautotrophic groups) to moderate and lower temperatures (mainly ASVs related to phototrophic and heterotrophic groups). This transition is commonly observed in geothermal environments, and can be considered as a definite characteristic of these systems. Furthermore, through the analysis of BPC, we found that different types of organic matter are available to the resident communities, from terrigenous input exported to the system, as well as *in situ* production by chemolithoautotrophic and phototrophic groups. This supports the literature on how shallow water hydrothermal vents are considered high energy environments. Through beta diversity analysis, we found the presence of three significant groups, composed of the biofilm samples, and the sediment and fluid samples of the islands of Vulcano and Panarea, and Lipari and Salina. The group of Vulcano and Panarea was correlated with temperature, as these locations were marked by moderate to high temperatures, and they were dominated by ASVs related to chemolithoautotrophic groups. As for the group of Lipari and Salina, the distribution of the microbial communities was

correlated with major ions. This suggests that subsurface water rock reactions have an influence on the concentration of the major ions, which in turn, can influence the microbial communities inhabiting these shallow water hydrothermal vents. Additionally, we found that the longitude, together with the temperature, was a significant vector in the weighted UNIFRAC. This correlation could be due to the location of the islands within the Aeolian volcanic arc and the different geothermal activity within each island.

Additionally, our compilation of fluid data from previous studies showed the same trend noted by Price et al. (2015), wherein in these hydrothermal systems, one can find 3 types of fluid evolution, showing differential enrichments and depletions of the major anions and cations, and therefore hinting at different subsurface processes taking place in the different islands. Given that the Aeolian archipelago shallow water hydrothermal vents, and the microbial communities inhabiting them, have important ecological roles for the surrounding marine environment, we think it is important their inclusion into present and future conservation efforts. Finally, shallow-water vents and the volcanic arc lithologies at which they occur are still understudied, compared to the basaltic, mid-ocean ridge lithologies from their deep-sea counter-parts. Our study is the first stage of a deeper characterization of the Aeolian archipelago shallow-water systems, and future studies will shed light on the ecological role of the communities in these systems, as well as on the local biogeochemical cycles.

Data availability statement

The datasets presented in this study can be found in online repositories. The names of the repository/repositories and accession number(s) can be found below: https://www.ebi.ac.uk/ena, PRJEB54611, https://zenodo.org/record/7480614.

Author contributions

BB carried out data analysis, geochemical experiments and wrote the first draft of the manuscript. BB, AF, MS, MG, AB, MCO, and LD produced the geochemical and microbiological data. MS and AF carried out Dada2 and Phyloseq and statistical analysis. AF, AC, MC, GB, RP, MI, CV, and DG planned the expedition and collected the samples. RP, CV, AC, and DG supervised the study. All authors contributed equally to the final version of the manuscript.

Funding

This work is partially funded by the European Research Council (ERC) under the European Union's Horizon 2020 research and innovation program (grant agreement No. 948972) to DG. Partial funding was from the NASA Habitable Worlds program under grant 80NSSC20K0228 to REP.

Acknowledgments

The authors wish to thank the Blue Marine Foundation (https://www.bluemarinefoundation.com/) for support in organizing the sampling expedition and for the use of the zodiac. They also thank the Salina diving center for providing the diving logistics necessary to carry out the sampling and Luca Magni for assistance with the dives and location access.

Conflict of interest

The authors declare that the research was conducted in the absence of any commercial or financial relationships that could be construed as a potential conflict of interest.

Publisher's note

All claims expressed in this article are solely those of the authors and do not necessarily represent those of their affiliated organizations, or those of the publisher, the editors and the reviewers. Any product that may be evaluated in this article, or claim that may be made by its manufacturer, is not guaranteed or endorsed by the publisher.

References

Alsop, E. B., Boyd, E. S., and Raymond, J. (2014). Merging metagenomics and geochemistry reveals environmental controls on biological diversity and evolution. *BMC Ecol.* 14:16. doi: 10.1186/1472-6785-14-16

Alt, J. C. (2013). "Subseafloor processes in Mid-Ocean ridge Hydrothennal systems" in *Geophysical monograph series*. eds. S. E. Humphris, R. A. Zierenberg, L. S. Mullineaux and R. E. Thomson (Washington, DC: American Geophysical Union), 85–114.

Álvarez, H., Perry, A. L., García, S., Blanco, J., and Aguilar, R. (2019). Towards the creation of a marine protected area in the Aeolian Islands. *MarXiv* 2019:b9dqc. doi: 10.31230/osf.io/b9dqc

Amend, J. P., Rogers, K. L., Shock, E. L., Gurrieri, S., and Inguaggiato, S. (2003). Energetics of chemolithoautotrophy in the hydrothermal system of Vulcano Island, southern Italy. *Geobiology* 1, 37–58. doi: 10.1046/j.1472-4669.2003.00006.x

Anderson, I., Sikorski, J., Zeytun, A., Nolan, M., Lapidus, A., Lucas, S., et al. (2011). Complete genome sequence of *Nitratifractor salsuginis* type strain (E9I37-1T). *Stand. Genomic Sci.* 4, 322–330. doi: 10.4056/sigs.1844518

Antranikian, G., Suleiman, M., Schäfers, C., Adams, M. W. W., Bartolucci, S., Blamey, J. M., et al. (2017). Diversity of bacteria and archaea from two shallow marine hydrothermal vents from Vulcano Island. *Extremophiles* 21, 733–742. doi: 10.1007/s00792-017-0938-y

Bao, R., van der Voort, T. S., Zhao, M., Guo, X., Montluçon, D. B., McIntyre, C., et al. (2018). Influence of hydrodynamic processes on the fate of sedimentary organic matter on continental margins. *Glob. Biogeochem. Cycles* 32, 1420–1432. doi: 10.1029/2018GB005921

Bastianoni, A., Cascone, M., De Moor, J. M., Barry, P. H., Price, R., Cordone, A., et al. (2022). *The missing carbon budget puzzle piece: Shallow-water hydrothermal vents contribution to global CO_2 fluxes*.

Berndt, M. E., Seewald, J. S., and Seyfried, W. E. (1988). Hydrothermal alteration processes at Mid Ocean ridges:Constrains from diabase alteration experiments, hot-spring fluids and composition of the oceanic crust. *Can. Mineral.* 26, 787–804.

Bligh, E. G., and Dyer, W. J. (1959). A rapid method of Total lipid extraction and purification. *Can. J. Biochem. Physiol.* 37, 911–917. doi: 10.1139/o59-099

Bowman, J. P., Lewis, T. E., Staley, J. T., and McMeekin, T. A. (1998). *Colwellia demingiae* sp. nov., *Colwellia hornerae* sp. nov., *Colwellia rossensis* sp. nov. and *Colwellia psychrotropica* sp. nov.: psychrophilic Antarctic species with the ability to synthesize

docosahexaenoic acid (22: 63). *Int. J. Syst. Bacteriol.* 48, 1171–1180. doi: 10.1099/00207713-48-4-1171

Bright, M., Espada-Hinojosa, S., Lagkouvardos, I., and Volland, J.-M. (2014). The giant ciliate *Zoothamnium niveum* and its thiotrophic epibiont *Candidatus* Thiobios zoothamnicoli: a model system to study interspecies cooperation. *Front. Microbiol.* 5:145. doi: 10.3389/fmicb.2014.00145

Brovarone, A. V., Butch, C. J., Ciappa, A., Cleaves, H. J., Elmaleh, A., Faccenda, M., et al. (2020). Let there be water: how hydration/dehydration reactions accompany key earth and life processes#. *Am. Mineral.* 105, 1152–1160. doi: 10.2138/am-2020-7380

Callahan, B. J., McMurdie, P. J., and Holmes, S. P. (2017). Exact sequence variants should replace operational taxonomic units in marker-gene data analysis. *ISME J.* 11, 2639–2643. doi: 10.1038/ismej.2017.119

Cardellini, C., Chiodini, G., and Frondini, F. (2003). Application of stochastic simulation to CO_2 flux from soil: mapping and quantification of gas release: simulation of soil CO_2 flux. *J. Geophys. Res. Solid Earth* 108:2165. doi: 10.1029/2002JB002165

Chan, C. S., Chan, K.-G., Ee, R., Hong, K.-W., Urbieta, M. S., Donati, E. R., et al. (2017). Effects of physiochemical factors on prokaryotic biodiversity in Malaysian Circumneutral Hot Springs. *Front. Microbiol.* 8:1252. doi: 10.3389/fmicb.2017.01252

Cheng, J.-H., Wang, Y., Zhang, X.-Y., Sun, M.-L., Zhang, X., Song, X.-Y., et al. (2021). Characterization and diversity analysis of the extracellular proteases of thermophilic *Anoxybacillus caldiproteolyticus* 1A02591 from Deep-Sea hydrothermal vent sediment. *Front. Microbiol.* 12:643508. doi: 10.3389/fmicb.2021.643508

Chiu, B. K., Kato, S., McAllister, S. M., Field, E. K., and Chan, C. S. (2017). Novel pelagic Iron-oxidizing Zetaproteobacteria from the Chesapeake Bay Oxic–anoxic transition zone. *Front. Microbiol.* 8:1280. doi: 10.3389/fmicb.2017.01280

Cordone, A., D'Errico, G., Magliulo, M., Bolinesi, F., Selci, M., Basili, M., et al. (2022). Bacterioplankton diversity and distribution in relation to phytoplankton community structure in the Ross Sea surface waters. *Front. Microbiol.* 13:722900. doi: 10.3389/fmicb.2022.722900

Cordone, A., Lucchini, S., Felice, M., and Ricca, E. (2011). Direct and indirect control of Lrp on LEE pathogenicity genes of *Citrobacter rodentium*. *FEMS Microbiol. Lett.* 325, 64–70. doi: 10.1111/j.1574-6968.2011.02411.x

Cordone, A., Mauriello, E. M. F., Pickard, D. J., Dougan, G., De Felice, M., and Ricca, E. (2005). The lrp gene and its role in type I fimbriation in *Citrobacter rodentium*. *J. Bacteriol.* 187, 7009–7017. doi: 10.1128/JB.187.20.7009-7017.2005

Dahle, H., Økland, I., Thorseth, I. H., Pederesen, R. B., and Steen, I. H. (2015). Energy landscapes shape microbial communities in hydrothermal systems on the Arctic Mid-Ocean ridge. *ISME J.* 9, 1593–1606. doi: 10.1038/ismej.2014.247

Dávila-Ramos, S., Estradas-Romero, A., Prol-Ledesma, R. M., and Juárez-López, K. (2015). Bacterial populations (first record) at two shallow hydrothermal vents of the Mexican Pacific West coast. *Geomicrobiol J.* 32, 657–665. doi: 10.1080/01490451.2014.980526

De Astis, G., Peccerillo, A., Kempton, P. D., La Volpe, L., and Wu, T. W. (2000). Transition from calc-alkaline to potassium-rich magmatism in subduction environments: geochemical and Sr, Nd, Pb isotopic constraints from the island of Vulcano (Aeolian arc). *Contrib. Mineral. Petrol.* 139, 684–703. doi: 10.1007/s004100000172

De Astis, G., Ventura, G., and Vilardo, G. (2003). Geodynamic significance of the Aeolian volcanism (Southern Tyrrhenian Sea, Italy) in light of structural, seismological, and geochemical data: geodynamics of the Aeolian volcanism. *Tectonics* 22:1040. doi: 10.1029/2003TC001506

Deckert, G., Warren, P. V., Gaasterland, T., Young, W. G., Lenox, A. L., Graham, D. E., et al. (1998). The complete genome of the hyperthermophilic bacterium *Aquifex aeolicus*. *Nature* 392, 353–358. doi: 10.1038/32831

Derekova, A., Sjøholm, C., Mandeva, R., and Kambourova, M. (2007). *Anoxybacillus rupiensis* sp. Nov., a novel thermophilic bacterium isolated from Rupi basin (Bulgaria). *Extremophiles* 11, 577–583. doi: 10.1007/s00792-007-0071-4

Dick, G. J., Anantharaman, K., Baker, B. J., Li, M., Reed, D. C., and Sheik, C. S. (2013). The microbiology of deep-sea hydrothermal vent plumes: ecological and biogeographic linkages to seafloor and water column habitats. *Front. Microbiol.* 4:124. doi: 10.3389/fmicb.2013.00124

Ding, J., Zhang, Y., Wang, H., Jian, H., Leng, H., and Xiao, X. (2017). Microbial community structure of deep-sea hydrothermal vents on the ultraslow spreading southwest Indian ridge. *Front. Microbiol.* 8:1012. doi: 10.3389/fmicb.2017.01012

Du, Z.-J., Wang, Z.-J., Zhao, J.-X., and Chen, G.-J. (2016). *Woeseia oceani* gen. Nov., sp. nov., a chemoheterotrophic member of the order Chromatiales, and proposal of Woeseiaceae fam. Nov. *Int. J. Syst. Evol. Microbiol.* 66, 107–112. doi: 10.1099/ijsem.0.000683

Emerson, D., Fleming, E. J., and McBeth, J. M. (2010). Iron-oxidizing Bacteria: an environmental and genomic perspective. *Annu. Rev. Microbiol.* 64, 561–583. doi: 10.1146/annurev.micro.112408.134208

Emerson, D., and Moyer, C. L. (2002). Neutrophilic Fe-oxidizing Bacteria are abundant at the Loihi seamount hydrothermal vents and play a major role in Fe oxide deposition. *Appl. Environ. Microbiol.* 68, 3085–3093. doi: 10.1128/AEM.68.6.3085-3093.2002

Fabiano, M., Danovaro, R., and Fraschetti, S. (1995). A three-year time series of elemental and biochemical composition of organic matter in subtidal sandy sediments of the Ligurian Sea (northwestern Mediterranean). *Cont. Shelf Res.* 15, 1453–1469. doi: 10.1016/0278-4343(94)00088-5

Fagorzi, C., Del Duca, S., Venturi, S., Chiellini, C., Bacci, G., Fani, R., et al. (2019). Bacterial communities from extreme environments: Vulcano Island. *Diversity* 11:140. doi: 10.3390/d11080140

Falkowski, P. G., Fenchel, T., and Delong, E. F. (2008). The microbial engines that drive Earth's biogeochemical cycles. *Science* 320, 1034–1039. doi: 10.1126/science.1153213

Favallim, M., Karátson, D., Mazzuoli, R., Pareschi, M. T., and Ventura, G. (2005). Volcanic geomorphology and tectonics of the Aeolian archipelago (southern Italy) based on integrated DEM data. *Bull. Volcanol.* 68, 157–170. doi: 10.1007/s00445-005-0429-3

Forget, N. L., Murdock, S. A., and Juniper, S. K. (2010). Bacterial diversity in Fe-rich hydrothermal sediments at two South Tonga arc submarine volcanoes: bacterial diversity in Fe oxide samples. *Geobiology* 8, 417–432. doi: 10.1111/j.1472-4669.2010.00247.x

Fortney, N. W., He, S., Converse, B. J., Boyd, E. S., and Roden, E. E. (2018). Investigating the composition and metabolic potential of microbial communities in chocolate pots Hot Springs. *Front. Microbiol.* 9:2075. doi: 10.3389/fmicb.2018.02075

Fournier, R. O. (2007). "Hydrothermal systems and volcano geochemistry" in *Volcano deformation*. ed. D. Dzurisin (Berlin, Heidelberg: Springer Berlin Heidelberg), 323–341.

Fullerton, K. M., Schrenk, M. O., Yücel, M., Manini, E., Basili, M., Rogers, T. J., et al. (2021). Effect of tectonic processes on biosphere–geosphere feedbacks across a convergent margin. *Nat. Geosci.* 14, 301–306. doi: 10.1038/s41561-021-00725-0

Gamberi, F., Marani, M., and Savelli, C. (1997). Tectonic, volcanic and hydrothermal features of a submarine portion of the Aeolian arc (Tyrrhenian Sea). *Mar. Geol.* 140, 167–181. doi: 10.1016/S0025-3227(97)00020-0

Gavriilidou, A., Gutleben, J., Versluis, D., Forgiarini, F., van Passel, M. W. J., Ingham, C. J., et al. (2020). Comparative genomic analysis of Flavobacteriaceae: insights into carbohydrate metabolism, gliding motility and secondary metabolite biosynthesis. *BMC Genomics* 21:569. doi: 10.1186/s12864-020-06971-7

Gerchakov, S. M., and Hatcher, P. G. (1972). Improved technique for analysis of carbohydrates in sediments. 1. *Limnol. Oceanogr.* 17, 938–943. doi: 10.4319/lo.1972.17.6.0938

German, C. R., and Seyfried, W. E. (2014). "Hydrothermal processes" in *Treatise on geochemistry*. ed. K. K. Turekian (Amsterdam, Netherlands: Elsevier), 191–233.

Giovannelli, D., d'Errico, G., Fiorentino, F., Fattorini, D., Regoli, F., Angeletti, L., et al. (2016). Diversity and distribution of prokaryotes within a shallow-water pockmark Field. *Front. Microbiol.* 7:941. doi: 10.3389/fmicb.2016.00941

Giovannelli, D., d'Errico, G., Manini, E., Yakimov, M., and Vetriani, C. (2013). Diversity and phylogenetic analyses of bacteria from a shallow-water hydrothermal vent in Milos island (Greece). *Front. Microbiol.* 4:184. doi: 10.3389/fmicb.2013.00184

Giovannelli, D., Grosche, A., Starovoytov, V., Yakimov, M., Manini, E., and Vetriani, C. (2012). *Galenea microaerophila* gen. Nov., sp. nov., a mesophilic, microaerophilic, chemosynthetic, thiosulfate-oxidizing bacterium isolated from a shallow-water hydrothermal vent. *Int. J. Syst. Evol. Microbiol.* 62, 3060–3066. doi: 10.1099/ijs.0.040808-0

Giovannelli, D., Sievert, S. M., Hügler, M., Markert, S., Becher, D., Schweder, T., et al. (2017). Insight into the evolution of microbial metabolism from the deep-branching bacterium, *Thermovibrio ammonificans*. *Elife* 6:e18990. doi: 10.7554/eLife.18990

Giovannelli, D., and Vetriani, C. (2017). From extreme environments to human pathogens: an evolutionary journey. *Biochemist* 39, 4–9. doi: 10.1042/BIO03906004

Gomez-Saez, G. V., Pop Ristova, P., Sievert, S. M., Elvert, M., Hinrichs, K.-U., and Bühring, S. I. (2017). Relative importance of chemoautotrophy for primary production in a light exposed marine shallow hydrothermal system. *Front. Microbiol.* 8:702. doi: 10.3389/fmicb.2017.00702

Gomez-Saez, G. V., Riedel, T., Niggemann, J., Pichler, T., Dittmar, T., and Bühring, S. I. (2015). Interaction between iron and dissolved organic matter in a marine shallow hydrothermal system off Dominica Island (Lesser Antilles). *Mar. Chem.* 177, 677–686. doi: 10.1016/j.marchem.2015.10.003

Gugliandolo, C., and Italiano, F. (1999). Submarine hydrothermal vents of the Aeolian Islands: relationship between microbial communities and thermal fluids. *Geomicrobiol J.* 16, 105–117. doi: 10.1080/014904599270794

Gugliandolo, C., Italiano, F., and Maugeri, T. L. (2006). *The submarine hydrothermal system of Panarea (southern Italy): Biogeochemical processes at the thermal fluids-sea bottom interface*.

Gugliandolo, C., Lentini, V., Bunk, B., Overmann, J., Italiano, F., and Maugeri, T. L. (2015). Changes in prokaryotic community composition accompanying a pronounced temperature shift of a shallow marine thermal brine pool (Panarea Island, Italy). *Extremophiles* 19, 547–559. doi: 10.1007/s00792-015-0737-2

Gugliandolo, C., Lentini, V., Spanò, A., and Maugeri, T. L. (2012). New bacilli from shallow hydrothermal vents of Panarea Island (Italy) and their biotechnological potential: Bacilli from shallow vents of Panarea Island (Italy). *J. Appl. Microbiol.* 112, 1102–1112. doi: 10.1111/j.1365-2672.2012.05272.x

Gugliandolo, C., and Maugeri, T. L. (2019). Phylogenetic diversity of Archaea in shallow hydrothermal vents of Eolian Islands, Italy. *Diversity* 11:156. doi: 10.3390/d11090156

Guo, L.-L., Wu, Y.-H., Xu, X.-W., Huang, C.-J., Xu, Y.-Y., Cheng, H., et al. (2017). *Actibacterium pelagium* sp. nov., a novel alphaproteobacterium, and emended

description of the genus *Actibacterium*. *Int. J. Syst. Evol. Microbiol.* 67, 5080–5086. doi: 10.1099/ijsem.0.002417

Hafenbradl, D., Keller, M., Dirmeier, R., Rachel, R., Roßnagel, P., Burggraf, S., et al. (1996). *Ferroglobus placidus* gen. Nov., sp. nov., a novel hyperthermophilic archaeum that oxidizes Fe^{2+} at neutral pH under anoxic conditions. *Arch. Microbiol.* 166, 308–314. doi: 10.1007/s002030050388

Han, Y., and Perner, M. (2015). The globally widespread genus Sulfurimonas: versatile energy metabolisms and adaptations to redox clines. *Front. Microbiol.* 6:989. doi: 10.3389/fmicb.2015.00989

Handley, K. M., Boothman, C., Mills, R. A., Pancost, R. D., and Lloyd, J. R. (2010). Functional diversity of bacteria in a ferruginous hydrothermal sediment. *ISME J.* 4, 1193–1205. doi: 10.1038/ismej.2010.38

Hartree, E. F. (1972). Determination of protein: a modification of the Lowry method that gives a linear photometric response. *Anal. Biochem.* 48, 422–427. doi: 10.1016/0003-2697(72)90094-2

Hedlund, B. P., Reysenbach, A.-L., Huang, L., Ong, J. C., Liu, Z., Dodsworth, J. A., et al. (2015). Isolation of diverse members of the Aquificales from geothermal springs in Tengchong, China. *Front. Microbiol.* 6:157. doi: 10.3389/fmicb.2015.00157

Hoaki, T., Nishijima, M., Miyashita, H., and Maruyama, T. (1995). Dense Community of Hyperthermophilic Sulfur-Dependent Heterotrophs in a geothermally heated shallow submarine biotope near Kodakara-Jima Island, Kagoshima, Japan. *Appl. Environ. Microbiol.* 61, 1931–1937. doi: 10.1128/aem.61.5.1931-1937.1995

Holmström, C., and Kjelleberg, S. (1999). Marine *Pseudoalteromonas* species are associated with higher organisms and produce biologically active extracellular agents. *FEMS Microbiol. Ecol.* 30, 285–293. doi: 10.1016/S0168-6496(99)00063-X

Hoshino, T., Kuratomi, T., Morono, Y., Hori, T., Oiwane, H., Kiyokawa, S., et al. (2016). Ecophysiology of Zetaproteobacteria associated with shallow hydrothermal Iron-Oxyhydroxide deposits in Nagahama Bay of Satsuma Iwo-Jima, Japan. *Front. Microbiol.* 6:1554. doi: 10.3389/fmicb.2015.01554

Inagaki, F., Takai, K., Nealson, K. H., and Horikoshi, K. (2004). *Sulfurovum lithotrophicum* gen. Nov., sp. nov., a novel sulfur-oxidizing chemolithoautotroph within the ε-Proteobacteria isolated from Okinawa trough hydrothermal sediments. *Int. J. Syst. Evol. Microbiol.* 54, 1477–1482. doi: 10.1099/ijs.0.03042-0

Inguaggiato, S., Calderone, L., Inguaggiato, C., Mazot, A., Morici, S., and Vita, F. (2012). Long-time variation of soil CO_2 fluxes at the summit crater of Vulcano (Italy). *Bull. Volcanol.* 74, 1859–1863. doi: 10.1007/s00445-012-0637-6

Inguaggiato, S., Jácome Paz, M. P., Mazot, A., Delgado Granados, H., Inguaggiato, C., and Vita, F. (2013). CO_2 output discharged from Stromboli Island (Italy). *Chem. Geol.* 339, 52–60. doi: 10.1016/j.chemgeo.2012.10.008

Inskeep, W. J., Jay, Z. G., Tringe, S. J., Herrgård, M. B., and Rusch, D.YNP Metagenome Project Steering Committee and Working Group Members (2013). The YNP metagenome project: environmental parameters responsible for microbial distribution in the Yellowstone geothermal ecosystem. *Front. Microbiol.* 4:67. doi: 10.3389/fmicb.2013.00067

Italiano, F., and Nuccio, P. M. (1991). Geochemical investigations of submarine volcanic exhalations to the east of Panarea, Aeolian Islands, Italy. *Clin. Lab. Stand. Inst.* 46, 125–141. doi: 10.1016/0377-0273(91)90079-F

Jorgensen, S. L., Hannisdal, B., Lanzen, A., Baumberger, T., Flesland, K., Fonseca, R., et al. (2012). Correlating microbial community profiles with geochemical data in highly stratified sediments from the Arctic Mid-Ocean ridge. *Proc. Natl. Acad. Sci.* 109, E2846–E2855. doi: 10.1073/pnas.1207574109

Kawaichi, S., Ito, N., Kamikawa, R., Sugawara, T., Yoshida, T., and Sako, Y. (2013). *Ardenticatena maritima* gen. Nov., sp. nov., a ferric iron- and nitrate-reducing bacterium of the phylum 'Chloroflexi' isolated from an iron-rich coastal hydrothermal field, and description of *Ardenticatenia classis* nov. *Int. J. Syst. Evol. Microbiol.* 63, 2992–3002. doi: 10.1099/ijs.0.046532-0

Kerfahi, D., Hall-Spencer, J. M., Tripathi, B. M., Milazzo, M., Lee, J., and Adams, J. M. (2014). Shallow water marine sediment bacterial community shifts along a natural CO_2 gradient in the Mediterranean Sea off Vulcano, Italy. *Microb. Ecol.* 67, 819–828. doi: 10.1007/s00248-014-0368-7

Kim, Y., Jeon, J., Kwak, M. S., Kim, G. H., Koh, I., and Rho, M. (2018). Photosynthetic functions of *Synechococcus* in the ocean microbiomes of diverse salinity and seasons. *PLoS One* 13:e0190266. doi: 10.1371/journal.pone.0190266

Kürzinger, V.. (2019). *Determination and differentiation of the hydrothermal precipitates of Panarea, Italy*. Freiberg Online Geoscience, p. 54.

LaRowe, D. E., Arndt, S., Bradley, J. A., Estes, E. R., Hoarfrost, A., Lang, S. Q., et al. (2020). The fate of organic carbon in marine sediments–new insights from recent data and analysis. *Earth-Sci. Rev.* 204:103146. doi: 10.1016/j.earscirev.2020.103146

Lentini, V., Gugliandolo, C., Bunk, B., Overmann, J., and Maugeri, T. L. (2014). Diversity of prokaryotic Community at a Shallow Marine Hydrothermal Site Elucidated by Illumina sequencing technology. *Curr. Microbiol.* 69, 457–466. doi: 10.1007/s00284-014-0609-5

Lentini, V., Gugliandolo, C., and Maugeri, T. L. (2007). Identification of enzyme-producing thermophilic bacilli isolated from marine vents of Aeolian Islands (Italy). *Ann. Microbiol.* 57, 355–361. doi: 10.1007/BF03175073

Littlechild, J. A. (2015). Enzymes from extreme environments and their industrial applications. *Front. Bioeng. Biotechnol.* 3:161. doi: 10.3389/fbioe.2015.00161

Liu, J., Hua, Z.-S., Chen, L.-X., Kuang, J.-L., Li, S.-J., Shu, W.-S., et al. (2014). Correlating microbial diversity patterns with geochemistry in an extreme and heterogeneous environment of mine tailings. *Appl. Environ. Microbiol.* 80, 3677–3686. doi: 10.1128/AEM.00294-14

Lorenzen, C. J., and Downs, J. N. (1986). The specific absorption coefficients of chlorophyllide and pheophorbide in 90% acetone, and comments on the fluorometric determination of chlorophyll and pheopigments1. *Limnol. Oceanogr.* 31, 449–452. doi: 10.4319/lo.1986.31.2.0449

Ludwig, M., and Bryant, D. A. (2012). *Synechococcus* sp. strain PCC 7002 transcriptome: acclimation to temperature, salinity, oxidative stress, and Mixotrophic growth conditions. *Front. Microbiol.* 3:354. doi: 10.3389/fmicb.2012.00354

Manini, E., Fiordelmondo, C., Gambi, C., Pusceddu, A., and Danovaro, R. (2003). Benthic microbial loop functioning in coastal lagoons: a comparative approach. *Oceanol. Acta* 26, 27–38. doi: 10.1016/S0399-1784(02)01227-6

Manini, E., Luna, G. M., Corinaldesi, C., Zeppilli, D., Bortoluzzi, G., Caramanna, G., et al. (2008). Prokaryote diversity and virus abundance in shallow hydrothermal vents of the Mediterranean Sea (Panarea Island) and the Pacific Ocean (North Sulawesi-Indonesia). *Microb. Ecol.* 55, 626–639. doi: 10.1007/s00248-007-9306-2

Maugeri, T. L., Lentini, V., Gugliandolo, C., Cousin, S., and Stackebrandt, E. (2010). Microbial diversity at a hot, Shallow-Sea hydrothermal vent in the southern Tyrrhenian Sea (Italy). *Geomicrobiol J.* 27, 380–390. doi: 10.1080/01490450903451518

Maugeri, T. L., Lentini, V., Gugliandolo, C., Italiano, F., Cousin, S., and Stackebrandt, E. (2009). Bacterial and archaeal populations at two shallow hydrothermal vents off Panarea Island (Eolian Islands, Italy). *Extremophiles* 13, 199–212. doi: 10.1007/s00792-008-0210-6

Maugeri, T. L., Lentini, V., Spanò, A., and Gugliandolo, C. (2013). Abundance and diversity of Picocyanobacteria in shallow hydrothermal vents of Panarea Island (Italy). *Geomicrobiol J.* 30, 93–99. doi: 10.1080/01490451.2011.653088

McAllister, S. M., Moore, R. M., Gartman, A., Luther, G. W., Emerson, D., and Chan, C. S. (2019). The Fe(II)-oxidizing Zetaproteobacteria: historical, ecological and genomic perspectives. *FEMS Microbiol. Ecol.* 95:fiz015. doi: 10.1093/femsec/fiz015

McDermott, J. M., Sylva, S. P., Ono, S., German, C. R., and Seewald, J. S. (2018). Geochemistry of fluids from Earth's deepest ridge-crest hot-springs: Piccard hydrothermal field, mid-Cayman rise. *Geochim. Cosmochim. Acta* 228, 95–118. doi: 10.1016/j.gca.2018.01.021

McGonigle, J. M., Lang, S. Q., and Brazelton, W. J. (2020). Genomic evidence for Formate metabolism by Chloroflexi as the key to unlocking deep carbon in lost City microbial ecosystems. *Appl. Environ. Microbiol.* 86, e02583–e02519. doi: 10.1128/AEM.02583-19

McIlroy, S. J., Kirkegaard, R. H., Dueholm, M. S., Fernando, E., Karst, S. M., Albertsen, M., et al. (2017). Culture-independent analyses reveal novel Anaerolineaceae as abundant primary fermenters in anaerobic digesters treating waste activated sludge. *Front. Microbiol.* 8:1134. doi: 10.3389/fmicb.2017.01134

McMurdie, P. J., and Holmes, S. (2013). Phyloseq: an R package for reproducible interactive analysis and graphics of microbiome census data. *PLoS One* 8:e61217. doi: 10.1371/journal.pone.0061217

Meyer-Dombard, D. R., Amend, J. P., and Osburn, M. R. (2013). Microbial diversity and potential for arsenic and iron biogeochemical cycling at an arsenic rich, shallow-sea hydrothermal vent (Tutum Bay, Papua New Guinea). *Chem. Geol.* 348, 37–47. doi: 10.1016/j.chemgeo.2012.02.024

Meyer-Dombard, D. R., Shock, E. L., and Amend, J. P. (2012). Effects of trace element concentrations on culturing thermophiles. *Extremophiles* 16, 317–331. doi: 10.1007/s00792-012-0432-5

Miroshnichenko, M. L., Kostrikina, N. A., Chernyh, N. A., Pimenov, N. V., Tourova, T. P., Antipov, A. N., et al. (2003). *Caldithrix abyssi* gen. Nov., sp. nov., a nitrate-reducing, thermophilic, anaerobic bacterium isolated from a mid-Atlantic ridge hydrothermal vent, represents a novel bacterial lineage. *Int. J. Syst. Evol. Microbiol.* 53, 323–329. doi: 10.1099/ijs.0.02390-0

Morris, R. M., and Spietz, R. L. (2022). The physiology and biogeochemistry of SUP05. *Annu. Rev. Mar. Sci.* 14, 261–275. doi: 10.1146/annurev-marine-010419-010814

Nogi, Y., Hosoya, S., Kato, C., and Horikoshi, K. (2004). *Colwellia piezophila* sp. nov., a novel piezophilic species from deep-sea sediments of the Japan trench. *Int. J. Syst. Evol. Microbiol.* 54, 1627–1631. doi: 10.1099/ijs.0.03049-0

Oksanen, J., Blanchet, F. G., Friendly, M., Kindt, R., Legendre, P., McGlinn, D., et al. (2018). *Vegan: Community ecology package*. Available at: https://CRAN.R-project.org/package=vegan (Accessed January 23, 2019).

Pearce, R. K., Sánchez de la Muela, A., Moorkamp, M., Hammond, J. O. S., Mitchell, T. M., Cembrano, J., et al. (2019). Interaction between hydrothermal fluids and fault systems in the in the southern Andes revealed by magnetotelluric and seismic data. *Geophysics* 2019:1143. doi: 10.1002/essoar.10501143.1

Peccerillo, A., De Astis, G., Faraone, D., Forni, F., and Frezzotti, M. L. (2013). Compositional variations of magmas in the Aeolian arc: implications for petrogenesis and geodynamics. *Geol. Soc. Lond. Mem.* 37, 491–510. doi: 10.1144/M37.15

Peccerillo, A., and Turco, E. (2004). Petrological and geochemical variations of Plio-quaternary volcanism in the Tyrrhenian Sea area: regional distribution of magma types,

petrogenesis and geodynamic implications. *Per. Mineral* 73, 231–251. doi: 10.1016/S1871-644X(06)80016-1

Petrillo, C., Castaldi, S., Lanzilli, M., Selci, M., Cordone, A., Giovannelli, D., et al. (2021). Genomic and physiological characterization of Bacilli isolated from salt-pans with plant growth promoting features. *Front. Microbiol.* 12:2517. doi: 10.3389/fmicb.2021.715678

Placido, A., Hai, T., Ferrer, M., Chernikova, T. N., Distaso, M., Armstrong, D., et al. (2015). Diversity of hydrolases from hydrothermal vent sediments of the Levante Bay, Vulcano Island (Aeolian archipelago) identified by activity-based metagenomics and biochemical characterization of new esterases and an arabinopyranosidase. *Appl. Microbiol. Biotechnol.* 99, 10031–10046. doi: 10.1007/s00253-015-6873-x

Pohlner, M., Dlugosch, L., Wemheuer, B., Mills, H., Engelen, B., and Reese, B. K. (2019). The majority of active Rhodobacteraceae in marine sediments belong to uncultured genera: a molecular approach to link their distribution to environmental conditions. *Front. Microbiol.* 10:659. doi: 10.3389/fmicb.2019.00659

Power, J. F., Carere, C. R., Lee, C. K., Wakerley, G. L. J., Evans, D. W., Button, M., et al. (2018). Microbial biogeography of 925 geothermal springs in New Zealand. *Nat. Commun.* 9:2876. doi: 10.1038/s41467-018-05020-y

Price, R. E., and Giovannelli, D. (2017). "A review of the geochemistry and microbiology of marine shallow-water hydrothermal vents" in *Reference module in earth systems and environmental sciences* ed. S. A. Elias (Amsterdam, Netherlands: Elsevier).

Price, R. E., LaRowe, D. E., Italiano, F., Savov, I., Pichler, T., and Amend, J. P. (2015). Subsurface hydrothermal processes and the bioenergetics of chemolithoautotrophy at the shallow-sea vents off Panarea Island (Italy). *Chem. Geol.* 407–408, 21–45. doi: 10.1016/j.chemgeo.2015.04.011

Price, R. E., Lesniewski, R., Nitzsche, K. S., Meyerdierks, A., Saltikov, C., Pichler, T., et al. (2013). Archaeal and bacterial diversity in an arsenic-rich shallow-sea hydrothermal system undergoing phase separation. *Front. Microbiol.* 4:158. doi: 10.3389/fmicb.2013.00158

Priest, T., Heins, A., Harder, J., Amann, R., and Fuchs, B. M. (2022). Niche partitioning of the ubiquitous and ecologically relevant NS5 marine group. *ISME J.* 16, 1570–1582. doi: 10.1038/s41396-022-01209-8

Pusceddu, A., Dell'Anno, A., Danovaro, R., Manini, E., Sara, G., and Fabiano, M. (2003). Enzymatically hydrolyzable protein and carbohydrate sedimentary pools as indicators of the trophic state of detritus sink systems: a case study in a Mediterranean coastal lagoon. *Estuaries* 26, 641–650. doi: 10.1007/BF02711976

Quast, C., Pruesse, E., Yilmaz, P., Gerken, J., Schweer, T., Yarza, P., et al. (2013). The SILVA ribosomal RNA gene database project: improved data processing and web-based tools. *Nucleic Acids Res.* 41, D590–D596. doi: 10.1093/nar/gks1219

R Core Team. (2021). *R: A language and environment for statistical computing, 2015*. Vienna, Austria: R Core Team.

Rajasabapathy, R., Mohandass, C., Bettencourt, R., Colaço, A., Goulart, J., and Meena, R. M. (2018). Bacterial diversity at a shallow-water hydrothermal vent (Espalamaca) in Azores Island. *Curr. Sci.* 115:2110. doi: 10.18520/cs/v115/i11/2110-2121

Reed, D. C., Breier, J. A., Jiang, H., Anantharaman, K., Klausmeier, C. A., Toner, B. M., et al. (2015). Predicting the response of the deep-ocean microbiome to geochemical perturbations by hydrothermal vents. *ISME J.* 9, 1857–1869. doi: 10.1038/ismej.2015.4

Reeves, E. P., Seewald, J. S., Saccocia, P., Bach, W., Craddock, P. R., Shanks, W. C., et al. (2011). Geochemistry of hydrothermal fluids from the PACMANUS, northeast Pual and Vienna woods hydrothermal fields, Manus Basin. *Papua New Guinea. Geochim. Cosmochim. Acta* 75, 1088–1123. doi: 10.1016/j.gca.2010.11.008

Rinke, C., Schmitz-Esser, S., Stoecker, K., Nussbaumer, A. D., Molnár, D. A., Vanura, K., et al. (2006). "*Candidatus* Thiobios zoothamnicoli," an Ectosymbiotic bacterium covering the Giant marine ciliate *Zoothamnium niveum*. *Appl. Environ. Microbiol.* 72, 2014–2021. doi: 10.1128/AEM.72.3.2014-2021.2006

Rogers, K. L., and Amend, J. P. (2005). Archaeal diversity and geochemical energy yields in a geothermal well on Vulcano Island, Italy. *Geobiology* 3, 319–332. doi: 10.1111/j.1472-4669.2006.00064.x

Rogers, K. L., and Amend, J. P. (2006). Energetics of potential heterotrophic metabolisms in the marine hydrothermal system of Vulcano Island, Italy. *Geochim. Cosmochim. Acta* 70, 6180–6200. doi: 10.1016/j.gca.2006.08.046

Rogers, K. L., Amend, J. P., and Gurrieri, S. (2007). Temporal changes in fluid chemistry and energy profiles in the Vulcano Island hydrothermal system. *Astrobiology* 7, 905–932. doi: 10.1089/ast.2007.0128

Rollinson, H., and Pease, V. (2021). *Using geochemical data to understand geological processes*. Cambridge, UK: Cambridge University Press.

Rusch, A., Walpersdorf, E., deBeer, D., Gurrieri, S., and Amend, J. P. (2005). Microbial communities near the oxic/anoxic interface in the hydrothermal system of Vulcano Island, Italy. *Chem. Geol.* 224, 169–182. doi: 10.1016/j.chemgeo.2005.07.026

Sayed, A. M., Hassan, M. H. A., Alhadrami, H. A., Hassan, H. M., Goodfellow, M., and Rateb, M. E. (2020). Extreme environments: microbiology leading to specialized metabolites. *J. Appl. Microbiol.* 128, 630–657. doi: 10.1111/jam.14386

Sciutteri, V., Smedile, F., Vizzini, S., Mazzola, A., and Vetriani, C. (2022). Microbial biofilms along a geochemical gradient at the shallow-water hydrothermal system of Vulcano Island, Mediterranean Sea. *Front. Virol.* 13:840205. doi: 10.3389/fmicb.2022.840205

Sedwick, P., and Stüben, D. (1996). Chemistry of shallow submarine warm springs in an arc-volcanic setting: Vulcano Island, Aeolian archipelago, Italy. *Mar. Chem.* 53, 147–161. doi: 10.1016/0304-4203(96)00020-5

Shafiee, R. T., Diver, P. J., Snow, J. T., Zhang, Q., and Rickaby, R. E. M. (2021). Marine ammonia-oxidising archaea and bacteria occupy distinct iron and copper niches. *ISME Commun.* 1:1. doi: 10.1038/s43705-021-00001-7

Sheik, C. S., Reese, B. K., Twing, K. I., Sylvan, J. B., Grim, S. L., Schrenk, M. O., et al. (2018). Identification and removal of contaminant sequences from ribosomal gene databases: lessons from the census of deep life. *Front. Microbiol.* 9:840. doi: 10.3389/fmicb.2018.00840

Sieland, R. (2009). Chemical and isotopic investigations of submarine fluid discharges from Panarea, Aeolian Islands, Italy. *Freiberg Online Geol.*:21:887. doi: 10.23689/fidgeo-887

Sievert, S. M., Kuever, J., and Muyzer, G. (2000). Identification of 16S ribosomal DNA-defined bacterial populations at a shallow submarine hydrothermal vent near Milos Island (Greece). *Appl. Environ. Microbiol.* 66, 3102–3109. doi: 10.1128/AEM.66.7.3102-3109.2000

Simmons, S., and Norris, P. (2002). Acidophiles of saline water at thermal vents of Vulcano, Italy. *Extremophiles* 6, 201–207. doi: 10.1007/s007920100242

Spietz, R. L., Lundeen, R. A., Zhao, X., Nicastro, D., Ingalls, A. E., and Morris, R. M. (2019). Heterotrophic carbon metabolism and energy acquisition in *Candidatus Thioglobus singularis* strain PS1, a member of the SUP05 clade of marine Gammaproteobacteria. *Environ. Microbiol.* 21, 2391–2401. doi: 10.1111/1462-2920.14623

Stöhr, R., Waberski, A., Völker, H., Tindall, B. J., and Thomm, M. (2001). *Hydrogenothermus marinus* gen. Nov., sp. nov., a novel thermophilic hydrogen-oxidizing bacterium, recognition of *Calderobacterium hydrogenophilum* as a member of the genus *Hydrogenobacter* and proposal of the reclassification of *Hydrogenobacter acidophilus* as *Hydrogenobaculum acidophilum* gen. Nov., comb. nov., in the phylum '*Hydrogenobacter*/Aquifex. *Int. J. Syst. Evol. Microbiol.* 51, 1853–1862. doi: 10.1099/00207713-51-5-1853

Suarez, C., Piculell, M., Modin, O., Langenheder, S., Persson, F., and Hermansson, M. (2019). Thickness determines microbial community structure and function in nitrifying biofilms via deterministic assembly. *Sci. Rep.* 9:5110. doi: 10.1038/s41598-019-41542-1

Taillefer, A., Guillou-Frottier, L., Soliva, R., Magri, F., Lopez, S., Courrioux, G., et al. (2018). Topographic and faults control of hydrothermal circulation along dormant faults in an Orogen. *Geochem. Geophys. Geosystems* 19, 4972–4995. doi: 10.1029/2018GC007965

Takai, K., Miyazaki, M., Nunoura, T., Hirayama, H., Oida, H., Furushima, Y., et al. (2006). *Sulfurivirga caldicuralii* gen. Nov., sp. nov., a novel microaerobic, thermophilic, thiosulfate-oxidizing chemolithoautotroph, isolated from a shallow marine hydrothermal system occurring in a coral reef. *Jpn. Int. J. Syst. Evol. Microbiol.* 56, 1921–1929. doi: 10.1099/ijs.0.64297-0

Tarasov, V. G., Gebruk, A. V., Mironov, A. N., and Moskalev, L. I. (2005). Deep-sea and shallow-water hydrothermal vent communities: two different phenomena? *Chem. Geol.* 224, 5–39. doi: 10.1016/j.chemgeo.2005.07.021

Tarasov, V. G., Gebruk, A. V., Shulkin, V. M., Kamenev, G. M., Fadeev, V. I., Kosmynin, V. N., et al. (1999). Effect of shallow-water hydrothermal venting on the biota of Matupi harbour (Rabaul caldera, New Britain Island, Papua New Guinea). *Cont. Shelf Res.* 19, 79–116. doi: 10.1016/S0278-4343(98)00073-9

Tarasov, V. G., Propp, M. V., Propp, L. N., Zhirmunsky, A. V., Namsakakv, B. B., Gorlenko, V. M., et al. (1990). Shallow-water Gasohydrothermal vents of Ushishir volcano and the ecosystem of Kraternaya bight (the Kurile Islands). *Mar. Ecol.* 11, 1–23. doi: 10.1111/j.1439-0485.1990.tb00225.x

Tassi, F., Capaccioni, B., Caramanna, G., Cinti, D., Montegrossi, G., Pizzino, L., et al. (2009). Low-pH waters discharging from submarine vents at Panarea Island (Aeolian Islands, southern Italy) after the 2002 gas blast: origin of hydrothermal fluids and implications for volcanic surveillance. *Appl. Geochem.* 24, 246–254. doi: 10.1016/j.apgeochem.2008.11.015

Techtmann, S. M., Fitzgerald, K. S., Stelling, S. C., Joyner, D. C., Uttukar, S. M., Harris, A. P., et al. (2016). *Colwellia psychrerythraea* strains from distant Deep Sea basins show adaptation to local conditions. *Front. Environ. Sci.* 4:3. doi: 10.3389/fenvs.2016.00033

Tivey, M. K. (2007). Generation of seafloor hydrothermal vent fluids and associated mineral deposits. *Oceanography* 20, 50–65. doi: 10.5670/oceanog.2007.80

Van Dover, C. (2012). Hydrothermal vent ecosystems and conservation. *Oceanography* 25, 313–316. doi: 10.5670/oceanog.2012.36

Van Dover, C. L., Arnaud-Haond, S., Gianni, M., Helmreich, S., Huber, J. A., Jaeckel, A. L., et al. (2018). Scientific rationale and international obligations for protection of active hydrothermal vent ecosystems from deep-sea mining. *Mar. Policy* 90, 20–28. doi: 10.1016/j.marpol.2018.01.020

Venâncio, I., Luís, Â., Domingues, F., Oleastro, M., Pereira, L., and Ferreira, S. (2022). The prevalence of Arcobacteraceae in aquatic environments: a systematic review and Meta-analysis. *Pathogens* 11:244. doi: 10.3390/pathogens11020244

Vuillemin, A., Kerrigan, Z., D'Hondt, S., and Orsi, W. D. (2020). Exploring the abundance, metabolic potential and gene expression of subseafloor Chloroflexi in million-year-old oxic and anoxic abyssal clay. *FEMS Microbiol. Ecol.* 96:fiaa223. doi: 10.1093/femsec/fiaa223

Wang, L., Cheung, M. K., Liu, R., Wong, C. K., Kwan, H. S., and Hwang, J.-S. (2017). Diversity of Total bacterial communities and chemoautotrophic populations in sulfur-rich sediments of shallow-water hydrothermal vents off Kueishan Island, Taiwan. *Microb. Ecol.* 73, 571–582. doi: 10.1007/s00248-016-0898-2

Wang, W., Li, Z., Zeng, L., Dong, C., and Shao, Z. (2020). The oxidation of hydrocarbons by diverse heterotrophic and mixotrophic bacteria that inhabit deep-sea hydrothermal ecosystems. *ISME J.* 14, 1994–2006. doi: 10.1038/s41396-020-0662-y

Wang, F.-Q., Lin, X.-Z., Chen, G.-J., and Du, Z.-J. (2015). *Colwellia arctica* sp. nov., isolated from Arctic marine sediment. *Antonie Van Leeuwenhoek* 107, 723–729. doi: 10.1007/s10482-014-0366-2

Ward, L. M., Hemp, J., Shih, P. M., McGlynn, S. E., and Fischer, W. W. (2018). Evolution of Phototrophy in the Chloroflexi phylum driven by horizontal gene transfer. *Front. Microbiol.* 9:260. doi: 10.3389/fmicb.2018.00260

Ward, L. M., Idei, A., Terajima, S., Kakegawa, T., Fischer, W. W., and McGlynn, S. E. (2017). Microbial diversity and iron oxidation at Okuoku-hachikurou Onsen, a Japanese hot spring analog of Precambrian iron formations. *Geobiology* 15, 817–835. doi: 10.1111/gbi.12266

White, J. R., Escobar-Paramo, P., Mongodin, E. F., Nelson, K. E., and DiRuggiero, J. (2008). Extensive genome rearrangements and multiple horizontal gene transfers in a population of *Pyrococcus* Isolates from Vulcano Island, Italy. *Appl. Environ. Microbiol.* 74, 6447–6451. doi: 10.1128/AEM.01024-08

Wickham, H. (2011). ggplot2. *Wiley Interdiscip. Rev. Comput. Stat.* 3, 180–185. doi: 10.1002/wics.147

Yamamoto, K., Hackley, K. C., Kelly, W. R., Panno, S. V., Sekiguchi, Y., Sanford, R. A., et al. (2019). Diversity and geochemical community assembly processes of the living rare biosphere in a sand-and-gravel aquifer ecosystem in the Midwestern United States. *Sci. Rep.* 9:13484. doi: 10.1038/s41598-019-49996-z

Yamamoto, M., and Takai, K. (2011). Sulfur metabolisms in epsilon- and gamma-Proteobacteria in Deep-Sea hydrothermal fields. *Front. Microbiol.* 2:192. doi: 10.3389/fmicb.2011.00192

Yücel, M., Sievert, S. M., Vetriani, C., Foustoukos, D. I., Giovannelli, D., and Le Bris, N. (2013). Eco-geochemical dynamics of a shallow-water hydrothermal vent system at Milos Island, Aegean Sea (eastern Mediterranean). *Chem. Geol.* 356, 11–20. doi: 10.1016/j.chemgeo.2013.07.020

Zanfardino, A., Migliardi, A., D'Alonzo, D., Lombardi, A., Varcamonti, M., and Cordone, A. (2016). Inactivation of MSMEG_0412 gene drastically affects surface related properties of *Mycobacterium smegmatis*. *BMC Microbiol.* 16:267. doi: 10.1186/s12866-016-0888-z

Zeng, X., Alain, K., and Shao, Z. (2021). Microorganisms from deep-sea hydrothermal vents. *Mar. Life Sci. Technol.* 3, 204–230. doi: 10.1007/s42995-020-00086-4

Zhang, D.-C., Yu, Y., Xin, Y.-H., Liu, H.-C., Zhou, P.-J., and Zhou, Y.-G. (2008). *Colwellia polaris* sp. nov., a psychrotolerant bacterium isolated from Arctic Sea ice. *Int. J. Syst. Evol. Microbiol.* 58, 1931–1934. doi: 10.1099/ijs.0.65596-0

Zhang, Y., Zhao, Z., Chen, C.-T. A., Tang, K., Su, J., and Jiao, N. (2012). Sulfur metabolizing microbes dominate microbial communities in andesite-hosted Shallow-Sea hydrothermal systems. *PLoS One* 7:e44593. doi: 10.1371/journal.pone.0044593

Diversity of Thermophilic Prokaryotes

Oddur Vilhelmsson, M. Audur Sigurbjornsdottir, Gudny Vala Thorsteinsdottir, Martina Cascone, Davide Corso, Luca Tonietti, Flavia Migliaccio, Nunzia Nappi, Annarita Ricciardelli, Matteo Selci, Francesco Montemagno, Bernardo Barosa, Deborah Bastoni, Alessia Bastianoni, Angelina Cordone, and Donato Giovannelli

Abstract The term ”thermophilic prokaryotes” covers an immense taxonomic and functional diversity of bacteria and archaea, spanning the length and breadth of the prokaryotic Tree of Life. Indeed, thermophiles are found within most major prokaryotic lineages and their functional diversity runs the gamut of biochemical and

O. Vilhelmsson (✉)
Natural Resource Sciences, University of Akureyri, Akureyri, Iceland

BioMedical Center, University of Iceland, Reykjavík, Iceland
e-mail: oddurv@unak.is

M. A. Sigurbjornsdottir
Natural Resource Sciences, University of Akureyri, Akureyri, Iceland

G. V. Thorsteinsdottir
Icelandic Institute of Natural History, Akureyri, Iceland

M. Cascone · D. Corso · F. Migliaccio · N. Nappi · A. Ricciardelli · M. Selci · F. Montemagno · B. Barosa · D. Bastoni · A. Bastianoni · A. Cordone
Department of Biology, University of Naples Federico II, Naples, Italy

Department of Science and Technology, Parthenope University of Naples, Naples, Italy

L. Tonietti
Department of Biology, University of Naples Federico II, Naples, Italy

Department of Science and Technology, Parthenope University of Naples, Naples, Italy

National Research Council – Institute of Marine Biological Resources and Biotechnologies - CNR-IRBIM, Ancona, Italy

D. Giovannelli
Department of Biology, University of Naples Federico II, Naples, Italy

Department of Science and Technology, Parthenope University of Naples, Naples, Italy

Department of Marine and Coastal Science, Rutgers University, New Brunswick, NJ, USA

Marine Chemistry and Geochemistry Department, Woods Hole Oceanographic Institution, Woods Hole, MA, USA

Earth-Life Science Institute, Tokyo Institute of Technology, Tokyo, Japan

Department of Science and Technology, University of Naples Parthenope, Naples, Italy

© The Author(s), under exclusive license to Springer Nature Switzerland AG 2023

S. M. Scully, J. Orlygsson (eds.), *Thermophilic Anaerobes*, Emerging Issues and Trends, https://doi.org/10.1007/978-3-031-41720-7_2

physiological adaptations. Thus, examples can be found of thermophilic lithoautotrophs as well as chemoheterotrophs, obligate anaerobes and aerophiles, extreme halophiles, acidophiles and alkaliphiles, and more. Their ecology is likewise diverse, with thermophiles found in a variety of habitats ranging from hydrothermal vents to desert soil to industrial settings and wastewater treatment facilities. It goes without saying that such immense diversity cannot be reviewed comprehensively in a relatively short book chapter. We thus aim to present examples pulled from diverse taxa within the vast menagerie of prokaryotic thermophiles in order to give insights into the metabolic, taxonomic, and ecological diversity of thermophilic prokaryotes rather than attempting an exhaustive review.

Abbreviations

Comammox	Complete ammonia oxidation
MAG	Metagenome-assembled genome

1 Introduction

Thermophilic prokaryotes are found not only at various geothermally heated sites such as hot springs and hydrothermal vents, but also in a variety of other habitats where growth and metabolism at elevated temperatures may confer a selective advantage. Examples include hot desert soils, solar salterns, compost heaps, deep subsurface sites, such as oil reservoirs and deep mine shafts, and various industrial settings. It is therefore not surprising that thermophily has evolved independently within multiple and highly diverse clades and not necessarily limited to deep lineages of microbes. The occurrence of thermophily across multiple lineages can be seen as an evolutionary response to the environment and the ability of microorganisms to adjust and evolve. A recent review counted more than 1200 known thermophilic species of bacteria and archaea (DiGiacomo et al. 2022), making an exhaustive review of their diversity and phylogeny a difficult exercise of dubious applicability. This review is therefore intended to give snapshot examples pulled from the vast menagerie that is thermophile diversity. Notwithstanding the vast diversity of thermophiles, some generalizations can be made about their physiology and metabolism, especially as regards those thermophiles originating from geothermal sites, where the chemical composition of the environment is characteristically mineral rich, resulting in the microbial community to be largely supported by lithotrophic bacteria and archaea. Common metabolism in thermophilic bacteria and archaea is therefore sulfur and iron metabolism, along with gas metabolism such as H_2 and CO oxidation.

In this chapter, we will briefly discuss some of the major thermophilic and hyperthermophilic groups of Bacteria and Archaea, focusing on 14 phyla commonly

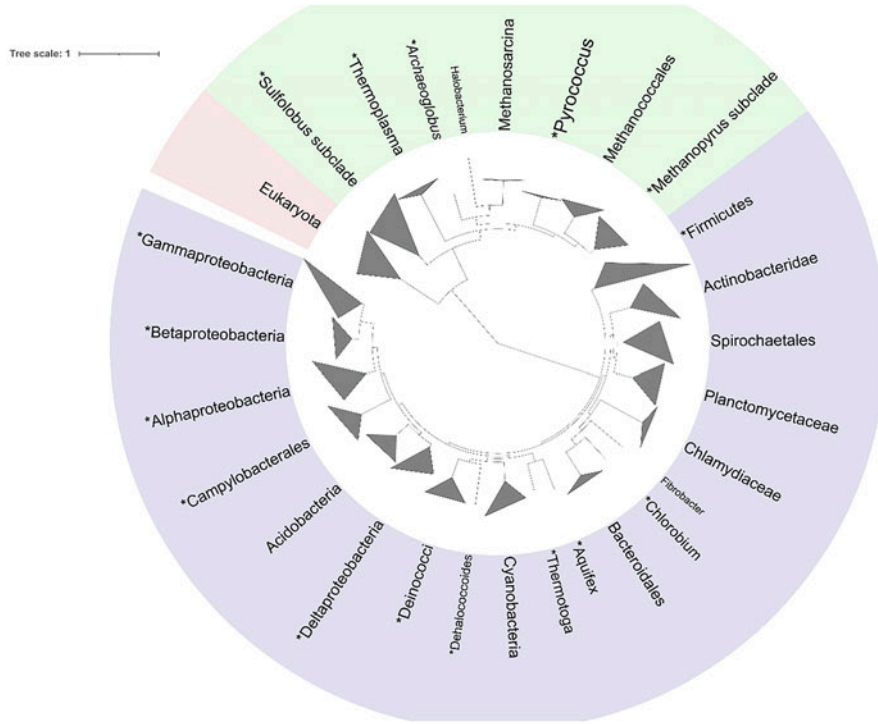

Fig. 1 Tree of life representing the phylogenetic diversity of thermophilic bacteria and archaea. The majority of thermophilic microbes discussed in the chapter belong to the phylogenetic groups shown with asterisk in the Tree of life [based on Ciccarelli et al. (2006) and vizualised with iTOL (Letunic and Bork 2007)]

occurring in diverse natural thermophilic environments. Phylogenetic tree of the different phyla discussed is shown in Fig. 1. We highlight their distribution, physiology, ecology, and potential biotechnological applications where known. Current valid taxonomy and nomenclature as presented on the List of Prokaryotic Names with Standing in Nomenclature (Parte et al. 2020) are followed in this chapter, which includes the major recent changes to the nomenclature of upper-level taxa validly published by Oren and Garrity (2021). To minimize confusion, some of the more commonly used older names are indicated where appropriate.

2 Deinococcota (Previously Deinococcus-Thermus)

The deeply branching Deinococcota (Oren and Garrity 2021) phylum, originally named as Deinococcus-Thermus (Weisburg et al. 1989), due to its resistance to extreme stressors including oxidation, radiation, desiccation, and high temperature, is known as one of the most extremophilic phyla of bacteria (Theodorakopoulos

et al. 2013; Tian and Hua 2010). The first isolated member from this phylum was *Deinococcus radiodurans* strain R1, discovered by Anderson et al. (1956) from X-ray-irradiated canned meat. In 1969, Thomas D. Brock and Hudson Freeze described for the first time *Thermus aquaticus*, and henceforth, organisms belonging to the genus *Thermus* have been considered as the archetypal thermophilic bacteria (Brock and Freeze 1969). Since these discoveries, more than 60 different species have been isolated, all showing an enormous biochemical, physiological, and phenotypic diversity (Garrity et al. 2001b). Their close branching based on 16S rRNA phylogeny suggests that they share a common ancestor, but other than a number of conserved inserts or deletions specific to the groups, there are no distinctive biochemical or molecular signatures exclusive of the phylum (Griffiths and Gupta 2004).

The members of Deinococcota are currently divided into two orders, the *Deinococcales*, composed of the three genera *Deinococcus*, *Deinobacterium*, and *Truepera*, and the order *Thermales*, that comprises five genera: *Thermus*, *Meiothermus*, *Marinithermus*, *Oceanithermus*, and *Vulcanithermus* (Theodorakopoulos et al. 2013). Recently, a new family has been proposed, the *Truperaceae* (Theodorakopoulos et al. 2013). Members belonging to this phylum are generally aerobic chemo-organotrophic bacteria, some of which are dissimilative sulfur oxidizers, using reduced sulfur compounds as electron donors in energy conservation, with O_2 or other organic compounds as electron acceptor (Skirnisdottir et al. 2001), others are dissimilative iron-reducers, coupling for respiration the oxidation of H_2 or organic electron sources with the reduction of ferric iron (Fe^{3+}) as a terminal acceptor (Kieft et al. 1999). Although some members of the Deinococcota stain gram-positively, they are classified as gram-negative bacteria, due to their complex cell envelope that includes an outer membrane-like structure (Thompson and Murray 1981), and a peculiar peptidoglycan, in which ornithine represents the principal diamino acid in the cross-linked chains (Rainey and da Costa 2001). The members of the genus *Deinococcus* exhibit resistance to high ionizing and ultraviolet radiations, and desiccation (Albuquerque et al. 2005; Cox and Battista 2005; Slade and Radman 2011). In contrast, cultured representatives of the *Thermus* genus are either thermophilic or hyperthermophilic, while not having any unusual radiation nor stress resistance capabilities (Brock and Freeze 1969), and have a tolerance temperature range between 45 °C and 80 °C. Most of the organisms belonging to the group have a maximum growth temperature slightly under 80 °C (Brock and Freeze 1969; Chung et al. 2000), and just a few strains, belonging to *T. thermophilus,* can grow at 80 °C or above (Manaia et al. 1995).

This phylum comprises very different species that have been found and isolated from a number of different environments, such as air dust and air samples (Weon et al. 2007; Yoo et al. 2009), desert soils (Rainey et al. 2005), cold environments in Antarctica (Hirsch et al. 2004), hot springs or biofilms, radioactive sites (Siebert and Hirsch 1988), and Phoenix spacecraft surface (Stepanov et al. 2014).

The exploitation of the adaptation strategies of these organisms finds numerous applications in the biotechnological field, for an example the treatment of nuclear energy waste. Indeed, *D. radiodurans* can be directly used for the adsorption of

uranium in radioactive wastewater and for the treatment of mixed radioactive wastes containing ionic mercury (Li et al. 2021). The most noteworthy discovery has been the isolation of the thermostable DNA polymerase (DNA pol) from *Thermus aquaticus* (Taq pol) which revolutionized the history of molecular biology through its use in the polymerase chain reaction (PCR) and paved the way for the development of modern biotechnology (Bessman et al. 1956; Chien et al. 1976).

2.1 Thermales

Bacteria belonging to *Thermales* order are generally rod-shaped, non-motile, gram-negative, aerobic or facultatively anaerobic thermophiles, generally isolated from hydrothermal areas with temperatures of 50–70 °C and neutral to alkaline pH (Rainey and da Costa 2001). The most representative species is *Thermus aquaticus* (Brock and Freeze 1969), which grows at temperatures ranging from 40 to 80 °C, with an optimum at 70 °C, and at a pH of 7.5–7.8.

The genus *Thermus* lists several thermophilic and hyperthermophilic species, mainly isolated from hydrothermal areas, such as Yellowstone National Park and Pacheteaus Calistoga in California (Brock and Freeze 1969), Japan (Oshima and Imahori 1974), Iceland (Pask-Hughes and Williams 1977), continental Portugal, the Island of São Miguel in the Azores (Manaia and da Costa 1991; Santos et al. 1989), and the Australian Artesian Basin (Denman et al. 1991). Isolates of the genus *Thermus* have also been obtained from abyssal geothermal areas in the mid-Atlantic Ridge and in the Guaymas Basin, Gulf of California, at depths of 3500 and 2000 m, respectively (Marteinsson 1999).

The most representative species of this genus is *Thermus aquaticus*, first isolated in 1969 from the Mushroom Spring in the Lower Geyser Basin of Yellowstone National Park by Thomas D. Brock and Hudson Freeze of Indiana University (Brock and Freeze 1969). *T. aquaticus* has been described as a gram-negative, non-sporulating, non-motile, rod-shaped bacterium, able to switch to a long filamentous shape at supraoptimal temperatures or in the stationary phase. Moreover, one of its main reported features is the production of peculiar large spherical bodies in older cultures, probably generated as temporary food and nucleotide storage (Brock and Freeze 1969). Another representative member of this genus is *Thermus thermophilus*, first isolated in 1968 from the thermal water of Mine Hot Spring, in Japan, and originally placed in the genus Flavobacterium (Oshima and Imahori 1971). *T. thermophilus* is used to grow at temperatures ranging from 47 to 85 °C, with an optimum between 65 and 72 °C, and at a pH range of 5.1 and 9.6, with an optimum pH value of around 7.5 (Oshima and Imahori 1974).

3 Nitrospirota (Previously Nitrospirae)

The first member of this phylum, *Nitrospira marina*, a chemolithotrophic nitrite-oxidizing bacterium isolated from water in the Gulf of Maine, was discovered by Watson in 1986. The phylum Nitrospirota, previously known as Nitrospirae, is a diverse group of Gram-negative, curved, vibrioid, or spiral-shaped bacteria (Garrity et al. 2001e). This phylum consists of three genera that have cultured representatives: *Nitrospira*, *Leptospirillum,* and *Thermodesulfovibrio* (Garrity et al. 2001e; Watson et al. 1986; Watson and Waterbury 1971). Phylogenetic surveys based on the 16S rRNA gene show how *Nitrospira* and *Leptospirillum* consistently cluster together, while *Thermodesulfovibrio* forms a separate branch.

The phylum comprises physiologically diverse bacteria, with a big representation of a chemolithoautotrophic, aerobic, nitrite-oxidizing bacteria (NOB) (*Nitrospira*), chemolithoautotrophic, aerobic, ferrous iron (FeIII) oxidizers (*Leptospirillum*), and anaerobic, thermophilic, chemo-organoheterotrophic, or hydrogenotrophic sulfate reducers (SRB) (*Thermodesulfovibrio*) (Daims 2014). Members of this phylum have been found in different natural and man-made ecosystems, like soil (Wang et al. 2019), fresh and groundwater (Ghimire-Kafle et al. 2023; Hovanec et al. 1998; Palomo et al. 2022), wastewater treatment plants (Daims 2014), marine sponge (Off et al. 2010), and geothermal springs with temperatures between 55 °C and 70 °C (Edwards et al. 2013; Lebedeva et al. 2011).

The genus *Nitrospira* represents the most abundant nitrite oxidizer, and it is almost ubiquitously present in oxic habitats, catalyzing an essential step of nitrification for biogeochemical nitrogen cycling. *Leptospirillum* tends to be a thermotolerant acidophilic genus, with optimal temperature growth ranging between 30 and 37 °C, and with only a few moderately thermophilic strains that can grow up to 40 °C (Vardanyan et al. 2023). The *Nitrospira* genus comprises only five formally identified members (Lücker et al. 2010), usually reported as moderately thermophilic, with growth temperature ranges between 28 and 44 °C (Ehrich et al. 1995; Lebedeva et al. 2008). Recently, the most thermophilic NOB known, *Nitrospira calida*, was isolated from Gorjachinsk Hot Spring in the Lake Baikal area (Russia), with a growth temperature optimum of 46–52 °C and an upper temperature for growth of 58 °C (Lebedeva et al. 2011). *Thermodesulfovibrio* is the most thermophilic genus of the phylum, with a temperature range for growth from 40 to 75 °C, and an upper pH limit for growth of 7.7–8.5 for all species, and a lower pH limit from 6.0 to 6.5 (Frank et al. 2016).

This phylum comprises three genera, all with relevant biotechnological use. *Leptospirillum* members are considered the most important microorganisms used in commercial bioleaching, and their iron oxidizing activity has been used in acid mine drainage, while *Thermodesulfovibrio* members are used to degrade organic compounds in anaerobic digesters. Moreover, *Nitrospira* species are used in wastewater treatment plants (WWTPs) to prevent eutrophication (Spasov et al. 2020; Vardanyan et al. 2023).

3.1 Nitrospirales

The genus *Nitrospira* represents a key nitrite oxidizer in nature, and it is almost ubiquitously present in oxic habitats, catalyzing the second and essential step of nitrification for biogeochemical nitrogen cycling. But their metabolism is not limited to nitrite oxidation or comammox, but they are also involved in other functionalities in the nitrogen cycle, either under anoxic or aerobic conditions. Members of this group are generally aerobic chemolithoautotrophic bacteria. They have been found in groundwater, geothermal springs, freshwater, soils, and wastewater treatment plants (WWTPs). But they could also colonize marine sponges, rhizospheres, and leaf surfaces of plants. According to many studies, *Nitrospira* generally have an optimum of growth between 30–35 °C and the optimum pH is in the range 8.0–8.3 (Mehrani et al. 2020), and the only true thermophile found in this genus so far is *Nitrospira calida*, with a growth temperature optimum of 46–52 °C and an upper temperature for growth of 58 °C (Lebedeva et al. 2011).

The genus *Thermodesulfovibrio* is classified as a group of strictly anaerobic, curved rod-shaped, thermophilic bacteria capable of reducing sulfate and other sulfur compounds and even perform oxidation of hydrogen and other organic compounds (Henry et al. 1994). Another ecologically significant physiological capability is the ability to undergo syntrophic degradation of organic compounds in the absence of sulfate. This group shows adaptations to the physico-chemical surroundings found in hot springs, as well as a diverse array of subterranean and terrestrial hot spring ecosystems, where they have been observed to thrive. The growth of *Thermodesulfovibrio* was observed at 40 °C and 70 °C with an optimum at 65 °C with a pH range between 6.8 and 7.0. (Haouari et al. 2008; Henry et al. 1994; Sekiguchi et al. 2008).

4 Chloroflexota (Previously Chloroflexi)

The phylum Chloroflexota (Oren and Garrity 2021), formerly known as Chloroflexi, contains a large number of thermophilic bacteria that differ widely both physiologically and ecologically. They are largely isolated from geothermal habitats, but also from compost heaps and industrial settings. Originally, the Chloroflexota were described as "Green non-sulfur bacteria," suggesting a very specific physiology. However, in recent years, with the increase of isolated strains and with metagenome-assembled genomes (MAGS) reconstructed from environmental samples, the phylum Chloroflexota has expanded to include vast metabolic diversity and abundant numbers in diverse subsurface ecosystems. Studies have been unraveling the true diversity of the phylum, which consists of a wide variety of anaerobic and aerobic bacteria, mesophilic and thermophilic, chemoheterotrophic, chemolithotrophic, or photolithotrophic. Nevertheless, the cell biology of members within the Chloroflexota remains poorly studied.

A commonly occurring physiological trait within the Chloroflexota is their filamentous cell structure with gliding motility (Garrity et al. 2001b) with only a few of them possessing flagella. The cell envelope of Chloroflexota is quite unique and has long been debated if they have a two-layer membrane (diderma) or only one layer (monoderm) since many of them lack the ability to form peptidoglycan (Kube et al. 2005), but it seems that species within the phylum might diverge in this sense as well.

4.1 Anaerolineae

Environmental DNA-based community analyses have revealed that members of the class Anaerolineae frequently occur in geothermal environments in widely disparate geographical locations. Examples include hot methane seeps in Iceland (Þorsteinsdóttir et al. 2020), hot spring microbial mats in Saudi Arabia (Yasir et al. 2020), hot spring water in the Himalayas (Sharma et al. 2020), sediments downstream from a sulfidic hot spring in Sumatra (Okumura et al. 2022), and seafloor hydrothermal vents (McGonigle et al. 2020).

Cultured thermophiles within this class all belong to the order Anaerolineales (Yamada et al. 2006) and are filamentous chemoheterotrophic anaerobes, oxidizing various carbohydrates, and proteinaceous compounds. They are likely to do so synergistically with hydrogenotrophic methanogens, as their growth is enhanced in their presence, indicating that they can use hydrogenotrophs as a hydrogen scavenging system (Yamada and Sekiguchi 2018). The family Anaerolineaceae contains thermophiles in at least four of its genera, *Anaerolinea*, *Bellilinea*, *Thermanaerothrix*, and *Thermomarinilinea*. These include *A. thermophila* isolated from hot spring sulfur-turf (Sekiguchi et al. 2003), *A. thermolimosa* and *B. caldifistulae* from anaerobic thermophilic granular sludge (Yamada et al. 2006, 2007), *Tt. daxenis* isolated from a deep hot aquifer (Gregoire et al. 2011), and the halophilic *Tm. lacunofontana* isolated from a shallow hydrothermal vent (Nunoura et al. 2013).

Most of the members of the Anaerolineae indicated by community analyses have not been cultured and attempts at reconstructing their genomes from metagenomic data are frequently complicated by binning problems (Singleton et al. 2021). Nevertheless, recent MAG-based studies (Ward et al. 2018; Braga et al. 2021; Liu et al. 2022; Rogers et al. 2023) have revealed this class to be considerably more metabolically diverse than previously believed, including sulfur oxidation, nitrogen cycling, and microaerophilic respiration (Rogers et al. 2023).

4.2 *Chloroflexia*

The class Chloroflexia comprises among others the well-known phototrophic mat-forming bacteria that often grow in great abundance in and around hot springs, frequently in association with Cyanobacteria (Pierson and Castenholz 1974; Giovannoni et al. 1987; Jørgensen and Nelson 1988). The chloroflexi proper, forming the family Chloroflexaceae, are gliding filamentous phototrophic thermophiles. Three species have been described, *Chloroflexus aurantiacus*, *C. aggregans*, and *C. islandicus* (Pierson and Castenholz 1974; Hanada et al. 1995; Gaisin et al. 2017). The family Roseoflexaceae contains additional thermophilic mat-formers, *Heliothrix oregonensis* (Pierson et al. 1985) and *Roseiflexus castenholzii* (Hanada et al. 2002). A cellulolytic filamentous thermophile, *Kallotenue papyrolyticum,* is found within the order Kallotenuales (Cole et al. 2013).

4.3 *Ktedonobacteria*

The class Ktedonobacteria harbors aerobic bacteria that stain gram-positive (Cavaletti et al. 2006). In DNA-based environmental studies, they are often encountered in environments such as geothermal fields, volcanic soils, caves, and gas vents (Hernández et al. 2020; Þorsteinsdóttir et al. 2020; Arif et al. 2021). Ktedonobacteria MAGs have been found to be abundant in young volcanic soil where they are thought to use reduced gases, such as H_2 and CO for growth (Hernández et al. 2020). Studies of their functional capabilities have shown diverse degradation abilities, indicating an ecological function comparable to that of actinomycetes and saprotrophic fungi. Genome sequencing has revealed large genome sizes, including megaplasmids, with several unknown functions, while screening has shown broad antimicrobial activities (Zheng et al. 2019). Cultured representatives of thermophiles within the class Ktedonobacteria are thus far limited to two species in one of its seven genera, *Thermosporothrix hazakensis* and *T. narukonensis* (Yabe et al. 2010, 2016).

4.4 *Other Chloroflexota Classes*

The class Ardenticatenia is yet represented only by a single thermophilic species, *Ardenticatena maritima*. This facultatively anaerobic chemoheterotroph reduces iron and nitrate under anaerobic conditions. It was isolated from a hydrothermal field in Japan (Kawaichi et al. 2013).

DNA-based studies on hot methane seeps in Iceland have indicated a dominating presence of uncultured members of the class *Dehalococcoidia* (Þorsteinsdóttir et al. 2020). This class contains obligate organohalide-respiring anaerobic bacteria

(Löffler et al. 2013). MAG-based studies have indicated that uncultured members of the class *Dehalococcoidia* may fix CO_2 via the Wood-Ljungdahl pathway, which has thus far not been observed among the culturable Chloroflexota (Hug et al. 2013).

A recently described class, Tepidiformia, is composed of only a single species, *Tepidiforma bonchosmolovskayae,* which was isolated from a hot spring in Russia. It is an aerobic, chemoheterotrophic thermophile that can grow chemolithoautotrophically with siderite ($FeCO_3$) as the electron donor and oxygen as electron acceptor (Kochetkova et al. 2020).

Thermoflexus hugenholtzii (Dodsworth et al. 2014) is a thermophilic filamentous bacterium within the class Thermoflexia. It is chemoheterotrophic, microaerophilic, and facultatively anaerobic. It is found in terrestrial geothermal systems, occurring prominently in geothermally heated sediments, also found in microbial mats in similar habitats.

5 Pseudomonadota

The phylum Pseudomonadota (Oren and Garrity 2021), previously named Proteobacteria, is an extremely diverse and cosmopolitan phylum. It harbors a number of different types of thermophiles, including anoxygenic phototrophs, heterotrophs, oligotrophs, and diverse chemolithotrophs.

5.1 Acidithiobacillia

Chemolithoautotrophic thermophiles are found within the genera *Acidithiobacillus* and *Thermithiobacillus*. These organisms are obligately aerobic sulfur oxidizers, using reduced inorganic sulfur such as thiosulfate, elemental sulfur, and hydrogen sulfide as electron donors (Boden and Hutt 2019a, b). While most members of these genera are mesophilic, moderate thermophiles are represented by *A. caldus* and *T. tepidarius*. An apparently obligate autotroph, *T. tepidarius* was isolated from a Roman bath and is adapted to a fluctuating environment in terms of oxygen partial pressure (Boden and Hutt 2019a). On the other hand, *A. caldus* is a strictly aerobic mixotroph (Boden and Hutt 2019b).

5.2 Alphaproteobacteria

Although the vast majority of the *Alphaproteobacteria* are considered mesophilic, generally not exhibiting growth at temperatures above 45 °C, this phylogenetically, ecologically, and metabolically highly diverse class nevertheless harbors an astonishing diversity of moderately thermophilic bacteria. Thermophilic members of this

class range from obligate chemoheterotrophs to facultative phototrophs and mixotrophs. They have been isolated from habitats including hot springs, desert soils, and industrial environments.

Unusual cell morphologies, such as prosthecate cells, and complex life cycles are frequently observed among members of the *Caulobacteraceae* family. They are usually chemo-organotrophs and may be quite fastidious, often requiring supplemented peptides, amino acids, and B vitamins. Habitat range is wide, but they are most often found in oligotrophic habitats and are frequently associated with freshwater environments, including submerged surfaces to which they can attach and form a biofilm (Abraham et al. 2014). Some moderately thermophilic species are known within the genus *Phenylobacterium*, including *P. terrae* and *P. lituiforme*, isolated from Pakistani soil and a subsurface aquifer, respectively (Kanso and Patel 2004; Khan et al. 2018). Like other members of the genus, these species are heterotrophic. Atypically for the genus, which classically is described as comprising strict aerobes only, *P. lituiforme* is a facultative anaerobe, reflecting the oxygen-poor environment of the subsurface from where it was isolated.

In the order Parvarculales, the only thus far described species of the genus *Amphiplicatus*, *A. meriothermophilus*, is a prosthecate moderate thermophile and halophile isolated from a Chinese hot spring (Zhen-Li et al. 2014). This species can grow at an optimum temperature between 48 and 50 °C and optimum pH of 7.5.

Within the Rhizobiales, the family Hyphomicrobiaceae, although not particularly large, is morphologically and physiologically highly diverse (Oren and Xu 2014). Prosthecate and budding species are commonly found within the family. Most species are aerobic chemoheterotrophs, although some are facultatively anaerobic denitrifiers, and many are oligocarbophilic. Some are facultative photoheterotrophs, and a few facultative chemolithotrophs have been found within this family (Oren and Xu 2014). Thermophiles are found within the genera *Rhodoplanes* and *Dichotomicrobium*, including *D. thermohalophilum*, *R. azumiensis*, *R. tepidamas*, and *R. tepidicaeni* (DiGiacomo et al. 2022).

Moderately thermophilic species have also been described within the family *Methylobacteriaceae*, which is characterized by pigmented facultatively methylotrophic bacteria that can grow on one-carbon compounds, e.g., formate, formaldehyde, and methanol as sole carbon sources. The thermophiles are within the genus *Microvirga* and were isolated from plant root nodules and desert soil (Reeve et al. 2014; Amin et al. 2016). Other thermophiles within the *Rhizobiales* order include members of the genera *Chelativorans*, *Tepidamorphus*, *Tepdicaulis*, and *Mongoliimonas* (DiGiacomo et al. 2022).

In the Rhodobacterales, thermophily seems rather common in the metabolically diverse family Paracoccaceae (previously Rhodobacteraceae). It contains a variety of slight and moderate thermophiles, including members of the genera: *Albidovulum*, *Jhaorihella*, *Oceanicella*, *Paracoccus*, *Rubellimicrobium*, *Ruegeria*, *Rhodobacter*, *Rhodosalinus*, and *Tranquilimonas* (Xian et al. 2020; DiGiacomo et al. 2022).

The genus *Albidovulum* contains two validly described species, *A. inexpectatum* and *A. xiamenense*, both of which are thermophilic (Albuquerque et al. 2018). While capable of oxidizing thiosulfate to sulfate in the presence of organic substrates,

A. inexpectatum does not grow chemoautotrophically and is therefore characterized as a facultative mixotroph (Albuquerque et al. 2018).

Moderate thermophiles are also found among the sphingomonads, such as *Porphyrobacter tepidarius*, *Altererythrobacter lauratis*, *Sphingomonas astaxanthinifaciens*, and *Thermaurantiacus tibetensis* (Ming et al. 2021; DiGiacomo et al. 2022). Known for the budding mode of reproduction of several of its member species, the genus *Porphyrobacter* currently contains 10 described species (Parte et al. 2020), all of which are strictly aerobic chemo-organoheterotrophs. Members of this genus produce bacteriochlorophyll-*a* esterified with phytol and carotenoids (Hiraishi and Imhoff 2015). They can thus appear purple pigmented, although the presence of carotenoids often renders them orange or red (Tonon et al. 2014). The carotenoids are polar and include carotenoid sulfates and bacteriorubixanthin, as well as nostaxanthin in *P. tepidarius*, and form with bacteriochlorophyll-*a* the core light-harvesting complex and the photosynthetic reaction center. However, they seem to lack the peripheral light-harvesting center, as indeed do other bacteriochlorophyll-containing Alphaproteobacteria (Hiraishi and Imhoff 2015). Also, similarly to many other aerobic photosynthetic bacteria, *Porphyrobacter* species produce bacteriochlorophyll-*a* only in the dark.

The porphyrobacters are primarily associated with freshwater environments, including the neuston (the air-water interface) and some strains are known to degrade biphenyl and dibenzofuran (Hiraishi et al. 2002). The thermophilic species *P. tepidarius*, with an optimum temperature of about 40–48 °C, was isolated from cyanobacterial mats in a brackish hot spring in Japan (Hanada et al. 1997). Another similarly thermophilic (Topt ~45–50 °C) *Porphyrobacter* species, *P. cryptus*, was isolated in 2003 from a Portuguese hot spring (Rainey et al. 2003). Comparing the genomes of *Porphyrobacter* type strains, Xu et al. (2018) concluded that thermophily of *P. cryptus* was at least in part made possible by substitution of glycine and serine to alanine, increasing the frequency of alpha-helices and thus promoting thermostability of proteins.

Although closely related to *Porphyrobacter*, members of the genus *Altererythrobacter* produce carotenoids but no bacteriochlorophyll and do not photosynthesize (Tonon et al. 2014). Two thermophilic *Altererythrobacter* species, *A. palmitatis* and *A. lauratis,* have been described (Yuan et al. 2017) and were both isolated from Tibetan hot springs.

The only species thus far described in the genus *Thermaurantiacus* is the thermophilic species *T. tibetensis*, isolated from a microbial mat in a Tibetan hot spring (Ming et al. 2021). It is moderately thermophilic, with an optimal growth temperature of 45 °C and growth not observed above 55 °C. Carotenoids are present.

5.3 Betaproteobacteria

The order Burkholderiales contains bacteria that are highly diverse in terms of ecology, physiology, and metabolism, ranging from psychrophiles to thermophiles,

and widely distributed in Nature. It contains obligate and facultative chemolithotrophs, nitrogen-fixers, and facultative anaerobes, as well as strict aerobes (Garrity et al. 2015). Accumulation of poly-hydroxybutyrate is a common feature among the Burkholderiales, consistent with organisms adjusted to an oligotrophic environment where storage of carbon in carbonosomes is likely to confer an advantage (Prieto et al. 2014). Among thermophiles in this order are members of the genera *Caldimonas*, *Tepidimonas*, and *Tepidicella*, as well as at least two species of *Schlegelella*, *S. aquatica,* and *S. thermodepolymerans* (Elbanna et al. 2003; Lütke-Eversloh et al. 2004; Chou et al. 2006). Both are moderately thermophilic, the former isolated from a Taiwanese hot spring, while the latter comprises strains isolated from sewage treatment sludges.

5.4 Gammaproteobacteria

The purple sulfur bacteria (PSB) are found within the order Chromatiales, primarily in the families Chromatiaceae and Ectothiorhodospiraceae. While most of the PSBs described so far are mesophilic, a few species in both families are thermophilic, notably *Thermochromatium tepidum* (Imhoff et al. 1998) and the extremely halotolerant *Halorhodospira halochloris* (Imhoff and Trüper 1977). Thermophilic PSBs are found in hot springs and warm soda lakes and salterns. The term "purple bacteria" refers to their reddish-purple color, which in turn is explained by the presence of bacteriochlorophyll and carotenoids. They are thus capable of anoxygenic photosynthesis and typically fix CO_2 via Rubisco and the Calvin-Benson cycle. Electron donors are usually reduced sulfur compounds, often stored in sulfur granules either intracellularly or, in the case of the Ectothiorhodospiraceae, on the cell surface. Non-phototrophic thermophiles are also found within the *Chromatiales*, such as the chemolithoautotrophic sulfur oxidizers *Thiofaba tepidiphila* and *Sulfurivermis fontis*, both isolated from Japanese hot springs (Mori and Suzuki 2008; Kojima et al. 2017).

5.5 Deltaproteobacteria

The class Deltaproteobacteria, recently proposed to be reclassified into the phyla *Desulfobacterota*, *Myxococcota*, and SAR324 (Langwig et al. 2022), is ubiquitous in marine sediments (Wang et al. 2012), soils (Delgado-Baquerizo et al. 2018), subterranean environments (Hug et al. 2016), wetlands (Liu et al. 2014), freshwater, and marine water columns (Swan et al. 2011; Sheik et al. 2015), playing an essential role in global biogeochemical cycling. Despite their importance, our understanding of these bacteria is biased toward cultured organisms. They include gram-negative bacteria, for the major part mesophilic anaerobes, many of which are interesting for their potential biotechnological applications. Notable metabolic features within this

class are the sulfate respiration, using protein complexes sulfate adenylyltransferase (Sat), adenylyl sulfate reductase (Apr), and dissimilatory sulfite reductase (Dsr), most of which have already been characterized (Minz et al. 1999). Members of the class *Deltaproteobacteria* are also known for their ability to reduce elemental metals, such as iron, with species of the families *Geobacteraceae* and *Desulfuromonadaceae* able to use external surfaces as electron acceptors to complete respiration, producing an electrical current (Bond et al. 2002; Holmes et al. 2004). These organisms have a variety of other metabolic abilities, such as inorganic sulfur compounds disproportionation (mainly carried out by members of the orders *Desulfobacterales* and Desulfovibrionales and of one phylogenetically separate species, *Desulfomonile tiedjei* (Deweerd and Suflita 1990; Sorokin et al. 2008)), dissimilatory iron reduction (mainly within Desulfuromonadia) (Lovley and Phillips 1988; Lonergan et al. 1996), nitrogen fixation (Masuda et al. 2017; Tan et al. 2019), mercury methylation (Si et al. 2015), organohalide respiration (Liu and Häggblom 2018), and aliphatic and aromatic hydrocarbon degradation (Bergmann et al. 2011).

Among thermophilic *Deltaproteobacteria*, different strains have been characterized recently and seem to have very similar metabolisms. For instance, an anaerobic thermophilic chemolithoautotroph bacterium called *Desulfurirhabdus thermomarina* has been isolated from a shallow sea hydrothermal vent. It can grow at 50 °C by the disproportionation of sulfite and elemental sulfur (Allioux et al. 2020). Furthermore, among thermophilic *Deltaproteobacteria* there is *Dissulfurimicrobium hydrothermale* Sh68T, which is a motile, anaerobic, chemolithoautotrophic microorganism, isolated from a hydrothermal pond at Uzon caldera, Kamchatka, Russia. Similar to *D. thermomarina*, it is able to produce energy and grow by disproportionation of elemental sulfur, sulfite, and thiosulfate (Yvenou et al. 2021). Another thermophilic deltaproteobacterium able both to disproportionate sulfur compounds and accomplish dissimilatory sulfate reduction at high temperatures corresponds to *Dissulfuribacter thermophilus*, strain S69T (Slobodkin et al. 2013). This microorganism was isolated from a deep-sea hydrothermal vent chimney located on the Eastern Lau Spreading Center and Valu Fa Ridge, Pacific Ocean, at a depth of 1910 m using anoxic medium with elemental sulfur as the only energy source. Its temperature range for growth was 28–70 °C, with an optimum at 61 °C. A metabolically and phylogenetically similar deltaproteobacteria strain was also isolated from a shallow-sea hydrothermal vent where it participates in biogeochemical cycling of sulfur, most probably as a primary producer (Slobodkina et al. 2016).

A different strategy of bacterial predation is found in the members of the order *Myxococcales*, known for their predominantly aerobic, predatory lifestyle with the ability to produce a variety of secondary metabolites (Jurkevitch and Davidov 2007; Berleman and Kirby 2009). During the motile phase of their life, members of this order exhibit complex social behavior, swarm prey organisms, secrete enzymes and proteases to lyse the target cells (Hart and Zahler 1966), and are also able to sporulate. *Myxobacteria* have long been considered mesophiles (Reichenbach 1999). Recently, a thermotolerant strain GT-7, identified as belonging to the genus *Myxococcus* within the Cystobacterineae, was isolated from the soil. Its growth

temperature range is between 42 and 44 °C (Gerth and Müller 2005). It is also known that the occurrence of the myxobacteria in hot spring microbial mats is relatively high and this is probably due to more stable microbial ecosystems existing in the mats, compared to the external environment (Iizuka et al. 2006).

Deltaproteobacteria are one of the most used groups of microorganisms for numerous biotechnological applications. For instance, a subtype of Class II type V CRISPR-Cas effectors from *Deltaproteobacteria* have been reported to produce extensive 5′-overhangs at cleaved DNA targets, which can make it usable for various applications (Selkova et al. 2020). Furthermore, *Deltaproteobacteria* can degrade Polycyclic Aromatic Hydrocarbons, enabling them significant environmental remediation functions in many areas, including groundwater pollution and oil spills (Viggi et al. 2017; Wang et al. 2021). Recent binding analysis of six previously uncharacterized proteins from the magnetotactic deltaproteobacterium *Desulfamplus magnetovallimortis* BW-1, identified two new magnetite-binding proteins which can be used as affinity tags for the immobilization of recombinant fusion proteins to magnetite (Pohl et al. 2021). Members of the *Deltaproteobacteria* class such as *Desulfovibrio magneticus* and *Geobacter sulfurreducens* are defined as "magnetotactic bacteria," because their ability to derive their magnetic orientation from magnetosomes, which are unique organelles containing nanometer-sized crystals of magnetic iron minerals. Nanowires enable bacteria to transfer electrons over micrometer distances to extracellular electron acceptors such as insoluble metal oxides or electrodes (Lovley and Malvankar 2015). Understanding how protein-based nanowires can conduct electrons is intriguing, as proteins are generally considered to be electrical insulators and are widely used in different biotechnological fields. Dissimilatory metal-reducing bacteria have been employed in microbial fuel cells and in bioremediation techniques, and bioengineered nanowires have been proposed for future use in nanobioelectronics (Boesen and Nielsen 2013).

6 Campylobacterota

The phylum Campylobacterota comprises a phylogenetically diverse bacterial group consisting of three classes: *Desulfurellia* (formerly corresponding to the order *Desulfurellales*) and *Campylobacteria* (formerly classified as *Epsilonproteobacteria*) (Waite et al. 2017). Although this phylum is widely known for its pathogenic members such as *Helicobacter pylori* and *Campylobacter jejuni* (Salama 2020; Yeh et al. 2021), a greater number of non-pathogenic mesophilic and thermophilic species have been discovered in diverse natural environments, including deep-sea hydrothermal fields (Shiotani et al. 2020), aquatic redox-stratified systems (Henkel et al. 2022), subterranean estuaries (Huang et al. 2021), terrestrial sulfidic caves (Bizic et al. 2023), terrestrial Mud Volcanoes (Mardanov et al. 2020), and oil fields (Nakagawa and Takaki 2009). These microorganisms are key players in element cycling (Lopez-Fernandez et al. 2018; Di Cesare et al. 2020; Seyler et al. 2021), and in deep-sea hydrothermal vents, they

constitute the dominant members of the microbial community, particularly in sulfide chimney structures where they can represent up to 85% of the total microbial biomass (Nakagawa et al. 2006).

The taxonomically and metabolically diverse members of Campylobacterota are also responsible for chemosynthetic primary productivity of inorganic sources at sub seafloor level (Campbell et al. 2006; McNichol et al. 2018). Although the cultivation of thermophilic Campylobacterota members has increased with the refinement of cultivation conditions, the number of described thermophilic species still only represents 14% of the total number of validly published species within Campylobacterota (Shiotani et al. 2020). Consequently, there is insufficient information on their genomes and intra-specific diversity, leaving the classification of thermophiles unresolved. Within the Campylobacterota, thermophiles are found within the order *Nautiliales* and in the *incertae sedis* genera *Nitratiruptur*, while the majority of the other members in the *Campylobacterales* are represented by mesophiles with some exception showing thermotolerance. All the thermophiles in the phylum have been isolated from deep-sea hydrothermal vents where they are key primary producers sustaining the vent ecosystems (Campbell et al. 2006).

Cultivation, isolation, and characterization of these bacteria have enabled new discoveries about their evolution and diversification (Nakagawa et al. 2007), biogeography (Mino et al. 2017), and their potential of biotechnological applications related to global warming mitigation (Mino et al. 2018; Fukushi et al. 2020). For example, *Nitratiruptor labii* carries out the reduction of N_2O to N_2 (Fukushi et al. 2020), a reaction which could be exploited for nitrogen removal from wastewater. Future studies, including cultivation analysis of N_2O-reducing *Campylobacteria*, transcriptional analysis of nitrous oxide reductase genes, and evaluation of N_2O consumption thermodynamics and kinetics, may provide a broader view of mechanisms allowing to significant N_2O consumption rates.

Vent-derived hydrogen-converting enzymes detected in Campylobacterota have also been widely studied in recent years. Due to the wide range of thermal and chemical conditions featuring vent environments (Miyazaki et al. 2020), thermophilic Campylobacterota hydrogenases genes are of particular interest for the use in hydrogen production as a green energy source and energy generation in biofuel cells (Armstrong et al. 2009; Chenevier et al. 2013).

6.1 Nautiliales

Within the deeply branching group of the *Nautiliales*, sequences have been retrieved exclusively from hydrothermal systems, and cultured representatives of the family are thermophilic, autotrophic, and can reduce elemental sulfur with molecular hydrogen. Deep-sea hydrothermal environments can be regarded as one of the largest reservoirs of diverse environmental Campylobacterota on Earth, whose deeply branching groups correspond to *Nautiliales* and *Nitratiruptor*. The first hydrogen-oxidizing, sulfur-reducing, thermophilic chemolithoautotrophs

Nautiliales successful isolations were from *Alvinella pompejana* symbiont-associated biomass and tube samples (Campbell et al. 2001). *Alvinella pompejana* is a deep-sea hydrothermal vent polychaete, which has an episymbiont community integrated into its dorsal epithelium. Surveys of geochemical conditions within *A. pompejana* tubes revealed high temperature range (∼20–80 °C), anoxia, surprisingly low or trace free hydrogen sulfide (from <0.2 to 46.53 μM), pH values between 5.3 and 6.4, high concentrations of potential electron acceptors such as sulfate, nitrate, and iron, and potentially lethal levels of heavy metals like zinc, nickel, vanadium, copper, lead, cadmium, cobalt, and silver (Di Meo-Savoie et al. 2004; Luther et al. 2001; Cary et al. 1998). The *Nautiliales* isolates from *Alvinella pompejana* were moderately thermophilic sulfur-reducing heterotrophs growing on formate as the energy and carbon source. In addition, two of the isolates were able to grow on sulfur using hydrogen as the electron donor. Optimal growth temperatures of the bacteria ranged from 41 to 45 °C (Campbell et al. 2001). Preliminary analysis of a metagenomic library of the *A. pompejana* symbionts supports the hypothesis that at least a portion of the symbiotic Campylobacterota detoxify sulfide by rendering it biologically unavailable through metal-transport and sulfide-oxidation processes so that *A. pompejana* can thrive in this extreme microhabitat (Barbara J. Campbell et al. 2006). Recently, several previously uncultivated, phylogenetically diverse Campylobacterota groups were isolated from various geologically and geographically distinct deep-sea hydrothermal fields, all showing a diverse range of physiological characteristics and utilization of electron donors, such as hydrogen and sulfur, and electron acceptors, such as sulfur and nitrogen. Additionally, they have been shown to fix inorganic carbon (Voordeckers et al. 2005; Nakagawa et al. 2005a, b) through two autotrophic pathways, the acetyl-coenzyme A pathway and the rTCA cycle.

Therefore, all the Campylobacterota studied so far are chemolithoautotrophs, and it is highly significant from the evolutionary point of view, because chemolithoautotrophy is thought to be the first type of metabolic pathway evolved on Earth (Russell and Hall 1997; Wächtershäuser 1990). Phylogenetic analysis of rTCA genes amplified directly from hydrothermal vent chimney samples, as well as enzymatic expression analyses of the beta subunit of the ATP citrate lyase (aclB), genetic analyses of the cultures of Candidatus *A. sulfidicus,* and the chemolithoautotrophic *Nautilia* sp. strain AmH (Wirsen et al. 2002; Campbell et al. 2003) have demonstrated the potential presence of the rTCA cycle for autotrophic carbon fixation in these environments (Wächtershäuser 1990; Campbell et al. 2003; Ken Takai et al. 2005). Oxygen is not essential for many of the isolated sulfur-reducing or sulfur-oxidizing Campylobacterota, especially for the deeply branching *Nautiliales*, which are obligate anaerobes that use various alternative electron acceptors, such as sulfite, elemental sulfur, and nitrate. Because the metabolic features and environmental adaptation of the studied Campylobacterota, including growth at high temperatures, anaerobic metabolism, and chemoautotrophy, are similar to the members of *Chlorobiaceae* and *Aquificales*, the evolution and significance of the Campylobacterota throughout Earth's history are interesting reasons to pursue in future research.

Nitratiruptor tergarcus is a thermophilic bacterium (growth temperature between 37 and 65 °C) which has been isolated from a deep-sea hydrothermal chimney structure in the Mid-Okinawa Trough (Nakagawa et al. 2005a, b). To this group belongs the recently described species *Nitratiruptor labii*, isolated from the same deep-sea hydrothermal region (Fukushi et al. 2020). Only in the last few years, a new strain EPR55-1 T belonging to the *Nitratiruptoraceae* species was isolated from the East Pacific Rise, being the first thermophilic campylobacterial species which is able to utilize thiosulfate and sulfite as its sole electron acceptor and sulfur source, respectively. This strain possessed lophotrichous flagella, unlike the monotrichous and amphitrichous flagella of *Nitratiruptor labii* and *Nitratiruptor tergarcus*, respectively (Shiotani et al. 2020).

7 Firmicutes

The phylum Firmicutes (today, also known as Bacillota) was originally described by Gibbons and Murray (1978), comprising low G + C Gram-positive bacteria. According to the Taxonomy in NCBI database (Schoch et al. 2020), the phylum consists of nine classes (*Bacilli, Bacillota incertae sedis, Bacillota* sensu stricto *incertae sedis, Clostridia, Culicoidibactera, Desulfuribacilla, Erysipelotrichia, Limnochordia, Negativicutes, Thermolithobacteria,* and *Tissierellia*), however—two of the listed classes have not been validly published according to LPSN (Parte et al. 2020). At least 45 families and 480 genera have been published; consequently, the phylum Firmicutes is highly diverse (Seong et al. 2018). Within the phylum, several thermophilic bacteria are known, such as members of genera *Clostridia, Thermoanaerobacterium, Thermoanaerobacter, Caldanaerobacter,* and *Caldicellulosiruptor*.

7.1 Clostridia

The type genus of the family *Clostridiacea*, *Clostridium*, is a large and diverse group of bacteria, currently containing more than 250 validly published species (Parte et al. 2020). The genus was first described in 1880, and harbors rod-shaped, Gram-positive, spore-forming anaerobic bacteria distributed in diverse habitats, including soil, water, and other ecological niches rich in plant decaying material (Lawson 2016; Wiegel 2015; Figueiredo et al. 2020). The species of genus Clostridium are extremely diverse and their G + C content can vary from 21 to 54%, which is considered to be too extensive for one genus (Lawson 2016). A phylogenetic analysis on *Clostridia* by Collins et al. (1994) leads to the conclusion that more than half of the species assigned to the genus were in fact not closely related to the type species, *C. butyricum*.

Most of the 250 validly described *Clostridium* species are classified as mesophiles, whereas only about 20 are moderately thermophilic, e.g., *C. thermocellum*, *C. thermosuccinogenes*, *C. thermopalmarium,* and *C. stercorarium*. Many of the thermophilic species of *Clostridium* have been extensively studied regarding their ability to degrade complex and lignocellulosic biomass, especially *C. thermocellum* (Akinosho et al. 2014). Some key features of *C. thermocellum* include its complex cellulolytic machinery, high growth rates, and tolerance to high temperatures and ethanol concentrations (Dumitrache et al. 2016; Sudha Rani et al. 1998). In recent years, researchers have been working to engineer *C. thermocellum* to improve its performance and make it a more effective biocatalyst for industrial applications (Sander et al. 2015; Rangel et al. 2020). Several studies have investigated the genetic and biochemical mechanisms underlying the cellulolytic activity of *C. thermocellum*, e.g., Raman et al. (2011) where transcriptomic and proteomic approaches were used to identify key genes and enzymes involved in cellulose degradation.

7.2 Thermoanaerobacterium

Bacteria belonging to the genus *Thermoanaerobacterium* are anaerobic, extreme thermophiles with optimal growth temperature ranging from 55 to 70 °C. In general, their cells have Gram-positive cell wall structure; however, several strains of *Thermoanaerobacterium* appear as Gram-negative during Gram staining. The pH range for growth is also broad, ranging from 3.2 to 8.5 (Onyenwoke and Wiegel 2015). The genus was first described in 1993 when two xylan-degrading bacteria were isolated from Frying Pan Springs in Yellowstone National Park (Lee et al. 1993). Today, the genus consists of eight validly published species: *T. aciditolerans, T. aotearoense, T. butyriciformans, T. polysaccharolyticum, T. saccharolyticum, T. thermosaccharolyticum, T. thermostercoris, T. thermosulfurigenes, T. xylanolyticum*, and *T. zeae* isolated from a variety of extreme environment, such as hot springs, hydrothermal vents, and leachate of waste from canning factories (Parte et al. 2020).

Bacteria of *Thermoanaerobacterium* have been studied extensively for their potential use in industrial biotechnology and are known for their abilities to degrade various sugars present in lignocellulosic biomass. Degradation of lignocellulose, and other substrates, results in a variety of end products, such as ethanol, acetate, lactate, and hydrogen. *Thermoanaerobacterium* species are thus promising candidates for bioethanol production from lignocellulose, although the production of mixed end products limits their use—and the level of ethanol is in general low (Ren et al. 2008; Romano et al. 2010; Sveinsdottir et al. 2009; Wu et al. 2021). For the past two decades or so, various studies have been published on genetical modifications of *Thermoanaerobacterium* species to improve the final ethanol titer and more. *T. saccharolyticum* is one of the most studied bacteria of the *Thermoanaerobacterium* genus and was the first thermophilic bacterium to be

genetically modified to enhance its ethanol production (Desai et al. 2004). Attempts have been made to knock out both acetate and lactate formation, resulting in increased ethanol yields both from glucose and xylose (Shaw et al. 2008). In a recent study, the *T. saccharolyticum pforA* and *ferredoxin* were transferred to strain of *Clostridium thermocellum*, increasing the maximum ethanol titer by 14% (Hon et al. 2018). Similarly, other species of *Thermoanaerobacterium* are known for effective hydrogen production from lignocellulosic biomass, i.e., *T. aotearoense* (Li et al. 2019).

7.3 Thermoanaerobacter and Caldanaerobacter

The genus *Thermoanaerobacter* is composed of obligately anaerobic thermophiles. All species have a Gram-positive cell wall structure, but in some cases the Gram-stain reaction can vary. The optimal growth temperature of *Thermoanaerobacter* ranges from 35 to 78 °C and pH optimum range of 5.8–8.5. *Thermoanaerobacter* are organoheterothropic and use various fermentation pathways, including the Wood-Ljungdahl pathway. Some species of the genus are also able to grow chemolithoheterotrophically and others are facultative chemolithoautotrophs (Onyenwoke and Wiegel 2015). The genus was first described in 1981 when the type species, *T. ethanolicus* was isolated from a hot spring in Yellowstone National Park (Wiegel and Ljungdahl 1981). Today, the genus contains 15 validly published species and 5 subspecies, isolated from extreme environments such as hot springs and oil fields (Parte et al. 2020). Most species can degrade various substrates and sugars and their main end products are ethanol, hydrogen, lactate, and in some cases alanine. *Thermoanaerobacter* species, such as *T. ethanolicus*, *T. brockii,* and *T. thermohydrosulfuricus*, have been extensively studied for their ethanol production (Lacis and Lawford 1988a, b; Lee et al. 2007; Georgieva and Ahring 2007; Lamed and Zeikus 1980a, b) and high yields of ethanol production from sugar observed. The ethanol yields can however vary greatly depending on both species and culture conditions. For example, *Thermoanaerobacter* strain AK5 was shown to produce up to 1.7 mol ethanol from 1 mol glucose in batch culture but when lowering the pH 2 the yields dropped, and end product formation was switched to acetate rather than ethanol (Brynjarsdottir et al. 2012). Recently, the production of branched-chain alcohols from branched-chain amino acids by *Thermoanaerobacter* has gained increased attention and has potential as a source for biofuel production from protein waste in the future (Scully and Orlygsson 2014).

Members of *Thermoanaerobacter* were recently reclassified and moved to the genus *Caldanaerobacter* based on phylogenetic, phenotypic, and metabolic characteristics (Fardeau et al. 2015). Today, *Caldanaerobacter* consists of only two species and four subspecies (Parte et al. Parte et al. 2020). *Caldanaerobacter* bacteria are strictly anaerobic heterotrophs and ferment glucose to L-alanine in nearly equal molar amounts (Fardeau et al. 2015). In a recent study on the genomes of three species of *C. subterraneus*, a variety of hydrolases were found, concluding bacteria

of the genus *Caldanaerobacter* to harbor enzymes with great biotechnological potential (Sant'Anna et al. 2015). Novel thermostable lipases originating from *Calanaerobacter* have furthermore been cloned and expressed in *E. coli*. The two lipases identified showed high thermoactivity and stability (90 °C, pH11) and were also found resistant to various organic solvents, which makes these enzymes greatly interesting for multiple biotechnological processes (Royter et al. 2009).

7.4 Caldicellulosiruptor

Members of the genus *Caldicellulosiruptor* are Gram-negative, strictly anaerobic and have optimal growth temperatures ranging from 65 to 75 °C. They have a broad substrate spectrum and degrade mono-, di- and polysaccharides, e.g., cellulose, cellobiose, xylan, and xylose (Rainey 2015). The type species, *C. saccharolyticus*, was described by Rainey et al. (1994), and today, the genus contains ten validly published species: *C. saccharolyticus, C. acetigenus, C. bescii, C. changaiensis, C. diazotrophicus, C. hydrothermalis, C. kristjanssonii, C. kronotskyensis, C. lactoaceticus,* and *C. owensensis* (Parte et al. 2020). All species of *Caldicellulosiruptor* have been isolated from geothermal environments such as hot springs and lake sediments (Rainey et al. 1994; Yang et al. 2010). Unlike the previously mentioned *Thermoanaerobacter* and *Thermoanaerobacterium*, *Caldicellulosiruptor* species do not produce ethanol at high titer. They are, however, excellent candidates for hydrogen production, and some have been extensively studied for their H_2 production from sugar and hydrolysates from lignocellulosic biomass (Kádár et al. 2004; Vrije et al. 2007; Zeidan and van Niel 2010). High ethanol yields have however been observed by one species, *C. bescii*, by genetical modification of the wild type (Chung et al. 2015). The genomes of all validly published *Caldicellulosiruptor* type species have been whole sequenced, revealing enzymes that can be useful for pharmaceutical production, as well as in textile and paper processing (Blumer-Schuette 2020). Furthermore, *Caldicellulosiruptor* species are now being investigated for the formation of metal nanoparticles (Bing et al. 2018) and heavy metal reduction (Bai et al. 2018).

8 Thermotogae

The Thermotogae phylum is composed of generally thermophilic, anaerobic gram-negative eubacteria characterized by the presence of an outer sheath-like envelope, referred to as "toga," the absence of an outer membrane and a rod-like shape (Frock et al. 2010; Bhandari and Gupta 2014a; Counts et al. 2017), able to thrive at different temperature ranges, from mesophilic to thermophilic and extremely thermophilic organisms. This phylum includes four orders *Kosmotogales*, *Mesoaciditogales*, *Petrotogales,* and *Thermotogales*. At present, the *Thermotogales* order includes

two families, *Fervidobacteriaceae* and *Thermotogaceae* (Bhandari and Gupta 2014a; Schoch et al. 2020).

For the most part, members of the class have been isolated from submarine geothermal features (Jannasch et al. 1988; Boniface et al. 2006; Conners et al. 2006), either shallow or deep (Wery et al. 2001; Alain et al. 2002; Postec et al. 2005, 2010; Nunoura et al. 2007; L'Haridon et al. 2019), oil reservoirs (Ravot et al. 1995; Fardeau et al. 1997; Takahata et al. 2001), continental solfataric (Windberger et al. 1989), and/or acidic springs (Itoh et al. 2016). The majority of the members of this class are able to grow on a myriad of carbon sources, including hexoses, pentoses, disaccharides, glucans, xylans, glucomannan, galactomannan, pectin, chitin, and amorphous cellulose (Conners et al. 2006; Vanfossen et al. 2008; Latif et al. 2015).

All members of the *Thermotogae* class are characterized by the presence of a toga-like outer membrane and are generally rod-shaped cells, although some members can also have cocci-shaped ones (Bhandari and Gupta 2014b; Reysenbach 2015). While most of them are obligate anaerobes, some exhibit oxygen tolerance and can survive under concentrations below 15% (DiPippo et al. 2009). The most distinctive feature of all members of this class is the toga-like outer membrane, which has been reported to have a rather unusual composition regarding other bacteria, leading to their classification as atypical Gram-negative bacteria rather than the prototypical diderm Gram-negative bacteria. Other unusual features of the membranes of the Thermotogae are the presence of long-chain C30, C32, and C34 dicarboxylic acids in lipids from *Kosmotoga*, *Thermotoga*, *Fervidobacterium,* and *Thermosipho*, which are considered an adaptation to grow in high-temperature environments. This consideration is further supported by their absence in the lipids of *Mesotoga prima* (Bhandari and Gupta 2014b).

The members of this phylum are all chemo-organotrophs capable of coupling the degradation of various types of carbon substrates, from simple forms of sugars to more complex organic matter, and to the oxidation of different forms of sulfur. The metabolic pathways involved in sugar degradation are the Entner–Doudoroff and the Embden–Meyerhof–Parnas pathways along with the non-oxidative portion of the pentose-phosphate pathway. The presence of genes that coded for different sugar metabolisms was also observed by (Zhaxybayeva et al. 2009) after functionally annotating large fractions of genomes besides the one studied previously from *T. maritima* (Nelson et al. 1999). One of the main products of glucose fermentation, H_2, inhibits growth for most of the species. However, this effect can be overcome in the presence of sulfur, thiosulfate, or cysteine, depending on the species, and the production of H_2S is thought of as a kind of a detoxification reaction. (Bhandari and Gupta 2014a; Huber and Hannig 2006).

The potentially high yields of H_2 as a metabolic product, as well as the capability to use a myriad of carbon substrates, and its thermophilic and hyperthermophilic nature has sparked great interest for technological applications. Thermotolerant enzymes present in these bacteria can be industrially used to increase reaction velocities and solubility of substrates and they can easily be overproduced in *E. coli* through recombinant vectors (Bhandari and Gupta 2014a). Their capability

to use different types of carbon substrates has also been used in large-scale industrial production of sugars, artificial sweeteners, and syrups. Enzymes from *Thermotogae* species have also been applied in the pretreatment of pulp and for the braking of fluids in oil wells. A more detailed description of all the other applications of enzymes isolated from this class can be found in (Bhandari and Gupta 2014a). The high yield of H_2 reported from the degradation of various carbon sources, as well as the fact that both *Thermotoga maritima* and *Thermotoga neapolitana* reach the Thauer limit (i.e., completely efficient fermentation of sugar into the production of H_2) these species represent prime candidates for the production of clean, renewable energy (Auria et al. 2016; Eriksen et al. 2011; Frock et al. 2010; Van Ooteghem et al. 2002, 2004).

8.1 Thermotogales

Thermotogales are widespread cosmopolitan bacteria, able to grow at high temperatures (optimal growth temperature around 80 °C and maximum temperature of 90 °C) making them, together with members of the phylum Aquificota (formerly known as Aquificae), the bacteria with the highest growth temperature known now. Its thermophilic nature explains its predominance in volcanically or geothermally heated environments, and its organotrophic nature reflects its capability of degrading complex organic substrates (Huber and Hannig 2006). They also exhibit a broad range of tolerance to salinity conditions, with some species restricted to growth under low salinity ranges while others can thrive at higher salt concentrations. The capability to use a wide variety of carbon sources also explains its biotechnological application to produce clean energy and the degradation of organic pollutants (Blumer-Schuette et al. 2008; Bhandari and Gupta 2014a; Latif et al. 2015). The first isolated organisms from the phylum all belong to the *Thermotogales* order, either to the *Fervidobacteriacea* class *(Fervidobacterium nodosum*, Patel et al. 1985) or the *Thermotogaceae* class (*Termotoga maritima*, Huber et al. 1986). Generally speaking, members of this class are heterotrophic thermophiles capable of using both simple and complex forms of carbon to transform them into H_2, CO_2, and acetate.

The Fervidobacteriaceae family includes two genera, *Fervidobacterium* and *Thermosipho*, both of them composed of thermophilic bacteria, able to grow at temperatures between 65 and 80 °C, neutral pH and low salinity (<1% salt concentration). All members of this family are strictly anaerobic and able to reduce sulfur to sulfide and have been found in hot springs, terrestrial geothermal aquifers, shallow and deep-sea hydrothermal vents, and deep oil reservoirs (Farrell et al. 2021). Their growth is inhibited by the presence of H_2 and they can utilize different types of carbon substrates with various degrees of complexity, from glucose and sucrose to starch, and lactose (Huber et al. 1990; Patel et al. 1985; Kanoksilapatham et al. 2016). The G + C content in the DNA of members of this family ranges between 29.5 and 45.8 mol%. The type genus for this family is *Fervidobacterium*, with its type

species being *F. nodosum*, isolated in 1985 by Patel et al. from a hot spring in New Zealand. The other species that compose the *Fervidobacterium* genus are *Fervidobacterium changbaicum*, *Fervidobacterium gondwanense, Fervidobacterium islandicum, Fervidobacterium pennivorans, Fervidobacterium riparium,* and *Fervidobacterium thailandense*.

On the other hand, the *Thermosipho* genus is made up of eight species *Thermosipho africanus, Thermosipho melanesiensis, Thermosipho japonicus, Thermosipho geolei, Thermosipho atlanticus, Thermosipho affectus, Thermosipho globiformans,* and *Thermosipho activus* (Nesbø et al. 2022). The type species for this genus is *T. africanus*, which was isolated by Huber et al. (1989) from a marine hydrothermal area in Obock, Djibouti (Africa). *T. africanus* differs from other members of the *Thermotogales* order in their GC content (29.5–31.5 mol%), the presence of a divergent RNA polymerase, and lower growth temperatures (from 35 to 77 °C). All species of the *Thermosipho genus* share over 91% of their 16S rRNA with each other and are closely related with genus *Fervidobacterium* (Bhandari and Gupta 2014a). Species have been isolated from shallow and deep-sea hydrothermal vents and deep subsurface oil reservoirs, and all have shown growth inhibition in the presence of H_2.

Thermotogaceae members are thermophilic and hyperthermophilic bacteria, with optimal growth temperatures between 60 and 80 °C and that require anaerobic conditions to grow. They are fermentative and hydrogen-producing rod-shaped bacteria that can use a wide variety of carbon sources (Zhaxybayeva et al. 2019). This family is divided into two, *Thermotoga* and *Pseudothermotoga*, with the type genus being *Thermotoga*, as defined by (Huber et al. 1986). All species from both families are known to occur in geothermally heated sediments, shallow-depth marine hydrothermal vents, hot springs, solfataric springs, oil reservoirs, and bioreactors (Bhandari and Gupta 2014a; Huber and Hannig 2006; Jannasch et al. 1988; Zhaxybayeva et al. 2019). Species from the *Thermotogaceae* family have a G + C content between 38.7 and 51.3 mol, and within the *Thermotoga* genus, the species can be differentiated based on the presence of the lipid 15, 16-dimethyl-30-glyceryloxytriacontanoic acid (Bhandari and Gupta 2014a).

The *Thermotoga* genus is composed of four validly named species, *T. maritima, T. neapolitana, T. naphthophila,* and *T. petrophila,* with *T. maritima* being the type species for the genus, while the *Pseudothermotoga* genus consists of *Pseudothermotoga thermarum, Pseudothermotoga elfii, Pseudothermotoga hypogea, Pseudothermotoga Profunda,* and *Pseudothermotoga caldifontis,* with *P. thermarum* being the type species (Farrell et al. 2021). Members of the *Pseudothermotoga* genus are able to use thiosulfate as an electron acceptor and different carbon substrates, like xylose, glucose, sucrose, and starch, while for the type species, *P. thermarum*, elemental sulfur can inhibit growth, as well as the presence of H_2 (Windberger et al. 1989).

8.2 Kosmotogales

The *Kosmotogales* order was proposed by Bhandari and Gupta (2014b) to include all bacteria that were either rod or cocci-shaped and had a thermophilic or mesophilic nature, with the genus *Kosmotoga* as its nomenclature type. Within the *Kosmotogales*, the *Kosmotogaceae* family includes two genera *Kosmotoga* and *Mesotoga* and is characterized by a G + C content between 36.4 and 48.3 mol% (Nesbø et al. 2019). All the members of this order are known to be present in hydrothermal vents, marine sediments, crustal fluids, deep aquifers, oil reservoirs, environments contaminated with hydrocarbons, and other anthropic environments. The genus *Kosmotoga* is composed of three species, *K. olearia, K. arenicorallina,* and *K. shengliensis*, all of them thermophiles, with an optimum growth temperature between 60 and 65 °C (DiPippo et al. 2009; Feng et al. 2010; Nunoura et al. 2010). The name *Kosmotoga* was proposed by DiPippo et al. (2009) to indicate the fact that its members are present in different environments, from oil fields to marine sediments and hot springs. Among the substances that inhibit its growth are sulfite, acetate, lactate, and propionate (DiPippo et al. 2009). The fact that Kosmotoga species can grow at temperatures from 20 °C to 79 °C has been considered as evidence of high phenotypic flexibility in expressing genes associated with energy and carbohydrate metabolic activity at high temperatures, and up-regulation of amino acid production at lower temperatures (Pollo et al. 2017). However, not all species from this family share the same tolerance to anaerobiosis and capability to use alternative electron acceptors. For instance, *K. arenicorallina* is an obligate anaerobe and chemo-organotroph that grows in a very narrow temperature range, between 50 and 65 °C, and unable to reduce thiosulfate (Nunoura et al. 2010). The *Mesotoga* genus includes mesophilic obligate heterotrophs that grow optimally between 37 and 45 °C and is composed of two species *M. prima* (type species, described by Nesbø et al. 2012) and *M. infera*.

8.3 Mesoaciditogales

This order was proposed by Itoh et al. (2016) to accommodate the deeply branched, more acidic, low salinity, anaerobic, chemo-organotrophic bacteria that belonged to the Thermotogae. Accordingly, *Mesoaciditogales* are divided into two families, *Athalassotoga* and *Mesoacidotoga*, which include one species each (Itoh et al. 2016; Reysenbach et al. 2013). The only member of the *Athalassotoga* family, *Athalassotoga saccharophila*, has short rod cells that prefer mildly acidic (pH 4.5–7.5) and thermophilic (between 30 and 60 °C) conditions for growth as well as low salinity (< 1.0% NaCl), and anaerobic conditions. They can use different types of complex carbon substrates and can reduce Fe (III), thiosulfate, and L-cystine as electron acceptors. The G + C content is 41 mol% (Itoh et al. 2016). The family *Mesoaciditoga*, composed only of *Mesoaciditoga lauensis* (Reysenbach et al. 2013),

is characterized by moderately thermophilic (45 to 65 °C) acidophilic (pH between 5.5 and 5.7) bacteria with cells shaped like short rods or cocci and a G + C content of 45 mol%. They grow under anaerobic conditions and are chemo-organotrophs capable of fermenting a broad range of carbohydrates, proteinaceous substrates, and yeast, reducing elemental sulfur to H_2S. Members of this family, similarly to other Thermotogae, have been isolated from deep-sea hydrothermal sediments (*M. lauensis*) or acidic hot spring waters (*A. saccharophila*).

8.4 Petrotogales

Petrotogales are all thermophilic (growth temperature between 45 and 70 °C) bacteria known to occur in oil reservoirs or deep-sea hydrothermal vents or chimneys. This order has only one family, *Petrotogaceae* that is composed of six genera: *Defluviitoga, Geotoga, Marinitoga, Oceanotoga, Petrotoga,* and *Tepiditoga. Petrotoga* is the type genus of the *Petrotogaceae* family, with *Geotoga petraea* as the type species. All members of the Petrogales order are also anaerobic, able to use elemental sulfur as an electron acceptor, have rod-shaped cells, and can degrade different types of carbon substrates.

Geotoga petraea was isolated and described by Davey et al. (1993) from oil field brines, along with *G. subterranea*, also isolated and characterized first by Davey et al. (1993) from brines in oil fields in Texas and Oklahoma. As all other *Thermotogae*, both are obligate anaerobes, and capable of fermentation and of reducing elemental sulfur to H_2S. They also share some morphological features like rod-shaped cells and a sheath-like outer structure. However, unlike other members of the *Thermotogales* class, they grow optimally at temperatures between 45 and 50 °C (Bhandari and Gupta 2014a; Davey et al. 1993) and are considered as halophilic since they grow optimally at salt concentrations between 3 to 4% and can tolerate salt concentrations of up to 10%.

Other relevant members of this order are the six species of the genus *Marinitoga* (*M. camini, M. piezophila, M. hydrogenotolerans, M. okinawensis, M. litoralis,* and *M. lauensis*). These species are capable of growth at low pH (4.5–5) and high salinity (from 2 to 4%) conditions as well as temperatures between 55 and 65 °C. This is thought to reflect the environmental conditions of their habitats (Alain et al. 2002; Bhandari and Gupta 2014a; L'Haridon et al. 2019; Nunoura et al. 2007; Postec et al. 2005, 2010; Wery et al. 2001). One peculiarity is the fact that *M. hydrogenotolerans* and *M. okinawensis*, unlike most members of the *Marinotoga* genus, and the *Petrotogaceae* family, are able to grow under 100% H_2 in the absence of sulfur (Nunoura et al. 2007).

The *Petrotoga* genus includes seven moderately thermophilic and halophilic species: *P. halophila, P. japonica, P. mexicana, P. miotherma. P. mobilis, P. olearia,* and *P. sibirica*, all isolated from oil brines, oil reservoirs, or oil wells. These bacteria are able to grow at temperatures that range from 35 to 65 °C (optimal temperature between 55 and 60 °C), at a pH range between 5.5 and 9.0, and variable

salinity conditions (between 0.5 and 10% NaCl) with an optimum from 2.0 to 4.0% (Bhandari and Gupta 2014b; Davey et al. 1993; Lien et al. 1998; Miranda-Tello et al. 2004, 2007; Purwasena et al. 2014). The other three genera, *Defluviitoga, Oceanotoga,* and *Tepiditoga*, are all composed of just one species each: *D. tunisiensis, O. teriensis,* and *T. spiralis*, all of them exhibiting more of a moderate thermophilic nature, with an optimum growth temperature around 50 °C (Ben Hania et al. 2012; Jayasinghearachchi and Lal 2011; Mori et al. 2020).

9 Thermodesulfobacteria

Thermodesulfobacterias are thermophilic chemolithoautotrophs and heterotrophs that can use oxidized sulfur and iron compounds as terminal electron acceptors (Vick et al. 2010). The phylum contains one class *Thermodesulfobacteria*, one order *Thermodesulfobacteriales*, and one family *Thermodesulfobacteriaceae* with four valid genera: *Thermodesulfobacterium, Thermodesulfatator, Caldimicrobium, Thermosulfurimonas,* and the candidate genus *Geothermobacterium* (Mori 2014). Although there is one family in this phylum, it is one of the deeply branching lineages within the domain Bacteria, with a sequence divergence of the 16S rRNA gene is 11.6 b% (Mori 2014).

Members of this group inhabit different thermal environments. They were isolated from terrestrial hot spring in Yellowstone (U.S.A.) (Kashefi et al. 2002; Zeikus et al. 1983), in Kamchatka (Russia) (Miroshnichenko et al. 2009), in Iceland (Sonne-Hansen and Ahring 1999), from stratal waters of oil deposits (Hatchikian et al. 2001), from deep-sea hydrothermal vents at Guaymas Basin (Jeanthon et al. 2002), Central Indian Ridge (Moussard et al. 2004), mid-Atlantic Ridge (Alain et al. 2010), and Eastern Lau Spreading Center (Slobodkin et al. 2012). In addition, Thermodesulfobacterium species were retrieved from oil field waters from oil production platforms in the Norwegian sector of the North Sea (Christensen et al. 1992).

In general, they have cells morphologically rod-shaped and motile with single or some polar flagella (with some exceptions (Hatchikian et al. 2001; Sonne-Hansen and Ahring 1999)). Their Gram reaction is negative and spore formation is not reported. They are thermophilic, neutrophilic, and strictly anaerobic, with some exceptions. For example, species members of the genus *Thermodesulfobacterium* are chemolithoautotrophs growing using sulfur compounds or Fe(III) as an energy source, and CO_2 as a carbon source. Moreover, organic compounds can be used for growth by some species of the genera *Thermodesulfobacterium* and *Thermodesulfatator* (Mori 2014).

10 Aquificota

The phylum Aquificota (formerly referred to as Aquificae) is widespread in hydrothermal environments, both marine and terrestrial (Gupta 2014). Aquificota is composed of both thermophilic and hyperthermophilic bacteria, with the species *Aquifex aeolicus* holding the record of the highest temperature for the Bacterial domain, being able to grow at above 90 °C (Clarke 2014; Dworkin et al. 2006). The vast majority of members belonging to Aquificota are chemolithoautotrophs, being able to derive energy from inorganic compounds, such as different oxidation states of sulfur, hydrogen, ferrous iron, nitrate, and oxygen, coupled to inorganic carbon fixation using the reductive citrate cycle (rTCA) (Gupta, 2014b). Their versatility in the usage of electron donors and acceptors, as well as their abundance in geothermal environments, makes them key players in the biogeochemical cycles in these ecosystems. Notably, they have been used as a model to infer the evolution of metabolism for different reasons: they inhabit what could be referenced as relic ecosystems, which resemble the conditions present in the early Earth, as well as the fact that they root deeply in the phylogenetic tree of Life (Braakman et al. 2014; Giovannelli et al. 2017). This means that these organisms carry both ancestral and acquired genes. For instance, Braakman et al. (2014), using a novel approach nominated phylometabolics, which merges phylogenetic inference with metabolic reconstructions, was able to show three classes of innovations in metabolic evolution studying the genomic architecture of *Aquifex aeolicus*. The phylum Aquificota is composed of only one class, nominated *Aquificae*, and two orders, the *Aquificales*, and *Desulfurobacterales*. The order *Aquificales* encompasses aerobic and microaerophilic bacteria, while *Desulfurobacteriales*, only strictly anaerobic bacteria. This implies that they are able to colonize different niches in geothermal environments given the disponibility of oxygen in the ecosystem. Within *Aquificales*, two families have been described, *Hydrogenothermaceae* and *Aquificaceae*, while within *Desulfurobacteriales*, only the family *Desulfurobacteriaceae* has been described.

10.1 Aquificae

Aquificae > Aquificales > Hydrogenothermaceae.

The family *Hydrogenothermaceae*, within the phylum Aquificota, is composed by the genera *Hydrogenothermus*, *Persephonella*, *Sulfurihydrogenibium*, and *Venenivibrio*. All of the members belonging to this family are known thermophiles, with optimum growth temperatures ranging from 60 to 73 °C, using a diverse set of electron donors, such as elemental sulfur, thiosulfate, ferrous iron, and hydrogen, coupled to the reduction of oxygen and nitrate. One of the key characteristics of this family is the usage of oxygen as an electron acceptor.

The genus *Hydrogenothermus*, represented by the type strain *Hydrogenothermus marinus* VM1t, was firstly isolated from a marine shallow-water hydrothermal vent in the island of Vulcano, Italy (Stöhr et al. 2001). This organism grows chemolithoautotrophically, through the oxidation of hydrogen, coupled to the reduction of oxygen, and with an optimum temperature of 65 °C. Characterized by being a gram-negative bacterium, *H. marinus* has an optimum growth between pH5 and 7. *Hydrogenothermus marinus* have been reported from diverse geothermal environments, such as the deep-sea hydrothermal vents along the Eastern Lau Spreading Center (Ferrera et al. 2014), the hot springs of Tengchong, China (Briggs et al. 2014), as well as the mariana back-arc venting fluids (Trembath-Reichert et al. 2019). Previous studies have shown that this organism is able to grow on high abundances of perchlorates, naturally found in arid regions such as the Atacama Desert, Chile, with maintained growth patterns up to 200 mM perchlorate. Since high concentrations of perchlorates are also found on Mars, *H. marinus* was suggested to be considered as a model organism for future space experiments (Beblo-Vranesevic et al. 2017b). Given their ecological role in geothermal systems, the capabilities of coupling hydrogen oxidation to oxygen reduction means that this group occupies the aerobic niche in hydrothermal systems, coupling the reduction of hydrothermal fluids with the oxidized sea water, taking the advantage of the thermodynamic equilibrium formed.

The genus *Persephonella*, represented by the type strain *Persephonella marina*, was initially isolated in deep-sea hydrothermal vents in the Pacific Ocean (Gotz 2002). It is characterized by being a strictly chemolithoautotrophic, microaerophilic, hydrogen-oxidizing bacteria, with an optimum growth temperature of 73 °C and pH6. Other species belonging to *Persephonella* genus include *Persephonella guaymasensis*, isolated from the deep-sea hydrothermal vents of the Guaymas Basin (Gotz 2002), *Persephonella hydrogeniphila* (Nakagawa et al. 2003), isolated from the deep-sea hydrothermal vents of the Suyiyo Seamount in the Izu-Bonin Arc, Japan, and *Persephonella atlantica*, isolated from deep-sea hydrothermal chimney collected from the Lucky Strike hydrothermal vent field on the Mid-Atlantic Ridge (François et al. 2021). For this reason, they are thought to be major colonizers of the deep-sea hydrothermal vent ecosystem (Mino et al. 2013). Members of this genus are known to use hydrogen and thiosulfate as electron donors, coupled with the reduction of oxygen and nitrate, and have similar optimum growth temperatures (~70 °C). However, only *Persephonella atlantica* is not able to utilize elemental sulfur as an electron donor. Due to their thermophilic way of life, members belonging to *Persephonella* have been used for carbon sequestration technologies, for instance, by the utilization of their high temperature adapted carbonic anhydrase used in an amine-based absorption process (Kanth et al. 2014).

The genus *Sulfurihydrogenibium*, represented by the type strain *Sulfurihydrogenibium subterraneum*, was initially isolated from a hot subsurface aquifer in a Japanese gold mine. Having an optimum growth temperature of 60–65 °C, this species grows chemolithoautotrophically, using hydrogen, sulfur, and thiosulfate as electron donors, coupled to oxygen reduction (Takai et al. 2003). Other species belonging to this genus include *Sulfurihydrogenibium azorense*, isolated

from terrestrial hot spring in the Azores, Portugal (Aguiar et al. 2004), *Sulfurihydrogenibium kristjanssonii*, isolated from terrestrial Icelandic hot spring (Flores et al. 2008), and *Sulfurihydrogenibium rodmanii* isolated from terrestrial hot springs in the Geyser Valley and the Uzon Caldera, Kamchatka, Russia (O'Neill et al. 2008). These species have been demonstrated to use a diverse set of electron donors, encompassing hydrogen, ferrous iron, sulfide, sulfate, thiosulfate, sulfur, coupled to oxygen as electron acceptor. Their optimum temperature ranges from 55 °C to 70 °C, and they are morphologically characterized by being gram-negative with motile rods.

The genus *Venenivibrio* is the least characterized genus from the *Hydrogenothermaceae*, with only one described species. The type strain, *Venenivibrio stagnispumantis*, is a thermophilic, hydrogen-oxidizing bacterium, isolated from a hot spring in Waiotapu, New Zealand (Hetzer et al. 2008). This species is able to grow using hydrogen as an electron donor, and oxygen as an electron acceptor, with an optimum temperature for growth at 70 °C, with elemental sulfur and thiosulfate shown to be essential for growth. Additionally, *V. stagnispumantis* is gram-negative, rod-shaped, and motile bacteria, growing with an optimum pH of 5.4.

The family Aquificaceae, together with *Hydrogenothermaceae*, make up the order *Aquificales.* This family encompasses the most thermophilic members belonging to the Aquificota, with optimum growth temperatures ranging from 65 to 90 °C, and spanning five different genera: *Hydrogenivirga*, *Hydrogenobacter*, *Hydrogenobaculum*, *Thermocrinis*, and *Aquifex*. As a whole, members belonging to the *Aquificaceae* are obligate chemolithoautotrophs, using hydrogen as the most preferred electron donor, and oxygen as electron acceptor. However, some species are also able to use sulfur species as electron donors, and nitrate as electron acceptor.

The genus *Hydrogenivirga* is composed of chemolithoautotrophic and thermophilic bacteria. Represented by the type species, *Hydrogenivirga caldilitoris*, a bacterium isolated from a coastal hot spring in Ibusuki, Kagoshima Prefecture, Japan. This species is able to grow at an optimum temperature of 75 °C and optimum pH of 6.5–7, using sulfur and hydrogen as electron donors, and nitrate and oxygen (microaerophilic) as electron acceptors Nakagawa et al. 2004a, b). The other species belonging to this genus is Hydrogenivirga okinawensis, a chemolithoautotrophic, thermophilic bacteria, isolated from a deep-sea hydrothermal field at the Yonaguni Knoll IV, Southern Okinawa Trough (Nunoura et al. 2008a, b). Compared to the other species of this genus, *H. okinawensis* can use thiosulfate as an electron donor, instead of hydrogen, and is able to grow at an optimum temperature of 70–75 °C and at an optimum pH of 6.9–7.5.

The genus *Hydrogenobacter,* represented by the type species *Hydrogenobacter thermophilus*, was initially isolated from hot springs located in Izu and Kyushu, Japan, and was regarded as the first obligate chemolithoautotroph described among the aerobic, hydrogen-oxidizing bacteria (Kawasumi et al. 1984). This thermophilic species grows through the oxidation of hydrogen, coupled to the reduction of oxygen, and has an optimum growth temperature between 70 and 75 °C, at neutral pH. Interestingly, it was on *H. thermophilus* that it was discovered a novel pathway

of the reductive TCA cycle, where the cleavage of citrate was carried out by citryl-CoA synthetase (CCS), instead of the known enzyme ATP citrate lyase (ACL) (Aoshima et al. 2004). Other species of this genus include *Hydrogenobacter halophilus,* isolated from a seaside saline hot spring in Izu Peninsula, Japan. This species grows at an optimum temperature of 70 °C (Nishihara et al. 1990), and compared to the other species of the genus, *H. halophilus* can utilize elemental sulfur and thiosulfate as alternative electron donors to hydrogen. Furthermore, the species *Hydrogenobacter hydrogenophilum* (formerly classified as *Calderobacterium hydrogenophilum*) was isolated from the hydrothermal vents of the Kamchatka region (Ludvík and Benada 1994) and is able to grow at an optimum temperature of 74 °C, using hydrogen as an electron donor, and oxygen as an electron acceptor.

The genus *Hydrogenobaculum* was created to accommodate the species *Hydrogenobaculum acidophilum,* which was previously classified as *Hydrogenobacter acidophilus,* belonging to the genus *Hydrogenobacter.* This species was isolated from a solfataric field in Tsumagoi, Japan (Shima and Suzuki 1993), and it is the only thermoacidophile belonging to the Aquificota, with an optimum pH between 3 and 4, and an optimum growth temperature of 65 °C (Stöhr et al. 2001). This species can utilize hydrogen and reduced sulfur species as electron donors, with oxygen as electron acceptor.

The genus *Thermocrinis*, represented by the type species *Thermocrinis ruber*, is a thermophilic bacterium isolated from the Octopus spring in the Yellowstone National Park (H. Huber 2002). This species can grow at 89 °C in neutral to alkaline pH, using hydrogen, thiosulfate, and elemental sulfur as electron donors, and with oxygen as an electron acceptor. *T. ruber* was shown to be able to grow both chemolithoautotrophically, as well as heterotrophically. Additionally, a previous study reported the ability of *Thermocrinis ruber* to utilize arsenite as a sole electron donor, producing arsenate (Härtig et al. 2014). Other species belonging to this genus include *Thermocrinis minervae*, isolated from a Costa Rican terrestrial hot spring, a chemolithoautotrophic bacteria, growing at an optimum temperature of 75 ° C, and 5.9–6.5 pH (Caldwell et al. 2010). Similar to *T. ruber*, this species is able to utilize elemental sulfur, thiosulfate, and hydrogen as electron donors, and oxygen as electron acceptor. Moreover, the species *Thermocrinis jamiesonii* was isolated from the water column of Great Boiling Spring, Nevada, USA (Dodsworth et al. 2015). It can grow chemolithoautotrophically, using hydrogen and thiosulfate as electron donors and oxygen as an electron acceptor, having an optimum growth temperature of 80 °C, and an optimum pH of 7.25. However, the most thermophilic species within the genus *Thermocrinis* is *Thermocrinis albus,* which grows at an optimum temperature of 89 °C, and similar to the other species of this genus, is able use hydrogen, thiosulfate, and sulfur as electron donors, and oxygen as electron acceptor (Eder and Huber 2002).

The genus *Aquifex,* represented by the type species *Aquifex pyrophilus*, was initially isolated from hot marine sediments, retrieved from the Kolbeinsey Ridge, Iceland (R. Huber et al. 1992). This species is characterized by being a strictly chemolithoautotroph, growing at an optimum growth temperature of 85 °C and optimum pH of 6.8. It can use hydrogen, thiosulfate, and elemental sulfur as electron

donors, and oxygen (microaerophilic) and nitrate as electron acceptors. The other species belonging to *Aquifex,* and the most studied member within the Aquificota is *Aquifex aeolicus*. As one of the most thermophilic bacteria known (growing at 95 ° C), *A. aeolicus* has sparked the interest of the scientific community. Similar to other members of the genus *Aquifex,* this species can utilize hydrogen as an electron donor, and oxygen (microaerophilic) as electron acceptor (Deckert et al. 1998), but contrary to *A. pyrophilus,* it has not been observed to perform nitrate respiration. Given its observed resistance to higher temperatures, it has been screened for temperature-resistant enzymes which could provide essential biotechnological applications (Guiral et al. 2012).

The family *Desulfurobacteriaceae,* the only described family within the order *Desulfurobacteriales,* is widely distributed in marine geothermal environments (Gupta 2014). It is composed of four genera: *Balnearium, Desulfurobacterium, Phorcysia, and Thermovibrio*. Conversely to the other families of Aquificota, *Desulfurobacteriaceae* is composed entirely of obligate anaerobic, chemolithoautotrophic, thermophilic bacteria (60–75 °C) (Giovannelli et al. 2017). Their inability to use oxygen as a terminal electron acceptor is reflected by the diversity of inorganic electron acceptors used to derive energy for growth, such as sulfur, polysulfide, thiosulfate, sulfite, and nitrate, coupled to hydrogen oxidation. Furthermore, similar to all the Aquificota, members belonging to this family are able to fix inorganic carbon using the reverse citrate cycle. However, they represent the only lineage within Aquificota to retain a complete reductive acetyl-coA pathway, including the oxygen-sensitive enzyme carbon monooxidase (*CodH*) (Giovannelli et al. 2017).

The genus *Desulfurobacterium* is ubiquitous in deep-sea hydrothermal vent environments. Represented by the type species *Desulfurobacterium thermolithotrophum*, it was initially isolated from a deep-sea hydrothermal chimney sample, retrieved from the mid-Atlantic ridge (L'Haridon et al. 1998). Other known species belonging to this genus include *Desulfurobacterium atlanticum,* isolated from East Pacific rise deep-sea hydrothermal vents, *Desulfurobacterium pacificum*, isolated from the mid-ocean ridge, *Desulfurobacterium crinifex*, isolated from the Juan de Fuca Ridge, and *Desulfurobacterium indicum*, isolated from a high temperature, deep-sea hydrothermal vent (Cao et al. 2017; L'Haridon et al. 2006; Alain et al. 2003). Members of this genus can oxidize hydrogen, coupled to a variety of electron acceptors, such as elemental sulfur, thiosulfate, sulfite, and nitrate. Additionally, this genus comprises only thermophilic bacteria, with optimum growth temperatures ranging from 60 °C to 75 °C, and pH 6.

The genus *Thermovibrio* is composed of three known species: *Themovibrio guaymasensis*, isolated from a deep-sea hydrothermal vent chimney at Guaymas Basin, *Thermovibrio ammonificans,* isolated from the East Pacific Rise hydrothermal field, and *Thermovibrio ruber*, isolated from a hydrothermal system off the beach of Lihir Island, Papua New Guinea (H. Huber 2002; Vetriani et al. 2004; L'Haridon et al. 2006). Of all the known species within *Thermovibrio, T. ruber*, the type species, remains the only microorganism that is not obtained from a deep-sea hydrothermal system. It is characterized by being a strictly anaerobic,

chemolithoautotrophic, thermophilic bacteria (75 ° C), growing through the oxidation of hydrogen, coupled to the reduction of sulfur or nitrate. Interestingly, compared to the genus *Desulfurobacterium* of the *Desulfurobacteriaceae,* members belonging to *Thermovibrio* possess less flexibility regarding electron acceptors, mainly using sulfur and nitrate to produce H_2S and ammonium, respectively. For this reason, they have been considered key players in the nitrogen cycle on hydrothermal systems (Giovannelli et al. 2017). Additionally, all members of this genus possess similar optimum growth temperatures (75 °C to 80 °C), and optimum pH between 5.5 and 6.0.

The genus *Phorcysia* has only one described species, the type species *Phorcysia thermohydrogeniphila*, isolated from the tube of *Alvinella pompejana* tubeworms, collected from the wall of a sulfide structure on the East Pacific Rise deep-sea hydrothermal vents (Perez et al. 2012). Characterized by being an anaerobic, chemolithoautotrophic bacteria, *P. thermohydrogeniphila* can grow using hydrogen as the sole electron donor, and nitrate and sulfur as electron acceptors, producing ammonium and hydrogen sulfide, respectively.

The genus *Balnearium* is represented by only one identified species, *Balnearium lithotrophicum,* a strictly anaerobic, hydrogen-oxidizing, and chemolithoautotrophic bacteria. This species is a known thermophile, having an optimum growth temperature ranging from 70 to 75 °C, and the lowest optimum pH within the *Desulfurobacteriaceae,* 5.4 (K. Takai 2003). Contrarily to the other genus of this family, *Balnearium lithotrophicum* can grow using hydrogen as a sole electron acceptor, and elemental sulfur as the sole electron acceptor, therefore presenting the lowest metabolic plasticity of the family.

11 Deferribacterota

The phylum Deferribacterota, described in 2001, consists of a family formerly known as *Deferribacteres* (Huber and Stetter 2001) and is widespread in marine environments, deep hydrothermal vents, contaminated soils and oil reservoirs, and the gut mucus of rodents. Ten Gram-negative, anaerobic (rarely microaerophilic), and rod- or vibrio-shaped genera are grouped in the phylum, e.g., *Calditerrivibrio, Deferribacter, Denitrovibrio, Flexistipes, Geovibrio, Deferrivibrio, Limisalsivibrio, Petrothermobacter, Selenivibrio*, and *Mucispirillum*. Of these, only five are thermophilic, able to live and survive above 41 °C, e.g., *Calditerrivibrio, Deferribacters, Flexistipes, Deferrivibrio,* and *Petrothermobacter*. Members belonging to Deferribacterota employ different metabolic strategies, such as chemo-organotrophy and chemolithotrophy. In general, they are capable of deriving energy from the anaerobic respiration of various organic substrates and the use of nitrate, iron (II), manganese (IV), sulfur-reduced compounds, and cobalt (III) as terminal electron acceptors. However, they can also be able to grow heterotrophically by fermentation (Huber and Stetter 2001). The dissimilatory metal reduction is a metabolic pathway that some members of the Deferribacterota phylum can use to thrive on iron and

manganese oxides as electron acceptors. The thermophilic genera of this phylum are commonly found in sulfur-rich and deep-sea hydrothermal systems, making them key players in the biogeochemical cycles in these environments (Slobodkin et al. 2019), while the other genera can be found in contaminated soils and oil reservoirs (Hidalgo et al. 2021), with the exception for *Mucispirillum* sp. that showed a unique lifestyle connected to gut mucus of rodents (Robertson et al. 2005). The presence of some genera in deep-sea systems is also supported by their halophilic and halotolerant capabilities.

11.1 Deferribacteres

The genus *Calditerrivibrio* is an important nitrate reducer in nature and was discovered in hot spring waters in Yumata, Nagano, Japan ($T = 60$ °C) (Iino et al. 2008). The only known species is *Calditerrivibrio nitroreducens,* an anaerobic, thermophilic bacterium with an optimum growth temperature between 30 °C and 65 °C, and a pH optimum between 7.0 and 7.5 (Iino et al. 2008). From a metabolic point of view, *C. nitroreducens* can be defined as a chemo-organotrophic, non-fermentative organism. It is involved in the nitrogen biogeochemical cycle due to its ability to use nitrate as the only electron acceptor during growth, having ammonium as the final product. Other types of electron acceptors are not used in their metabolic activities. *C. nitroreducens* use different organic carbon species as electron donors (Iino et al. 2008).

The genus *Deferribacters*, composed of four different species, is of fundamental importance in the biogeochemical cycling of iron and other metal oxides as part of their respiratory metabolism. Only four species belong to this genus: *D. abyssi, D. autotrophicus, D. desulfuricans*, and *D. thermophilus*. All four species are thermophiles able to grow between 40 °C and 70 °C with an optimum temperature of 60 °C. *D. abyssi, D. autotrophicus,* and *D. desulfuricans* have been isolated from deep-sea hydrothermal environments between the Mid-Atlantic Ridge, and the deep-sea hydrothermal vents on the Izo-Bonin Arc in Japan (Miroshnichenko et al. 2003; Takai et al. 2003). Furthermore, *D. autotrophicus* was isolated from the deepest known ocean hydrothermal field at a depth of 4100 m (Slobodkina et al. 2009). *D. thermophilus* was discovered in the North Sea's Beatrice oil field, UK. Metabolically, *D. abyssi* is a chemolithoautotrophic bacteria capable of using molecular hydrogen and inorganic carbon compounds as electron donors, and reduced sulfur, iron (III), and nitrate species as electron acceptors (Miroshnichenko et al. 2003). The same is for *D. autotrophicus* but it adds manganese (IV) to the plethora of electron acceptors. All four species can use hydrogen or organic substances as energy sources and carbon sources, and elemental sulfur and nitrate as electron acceptors (Greene et al. 1997). Additionally, *D. desulfuricans* has been shown to be able to use arsenate as an electron acceptor, making it a major player in the arsenic biogeochemical cycle (Takai et al. 2003).

The genus *Flexistipes*, along with the only known species *F. sinusarabici*, has been isolated from the hot brines of the Atlantis II Deep at the bottom of the Red Sea, one of the most extreme environments on our planet, e.g., temperature of 64 °C and salinity values of 26% NaCl, high concentration of heavy metals, and no free oxygen (Hartmann 1985; Brewer and Spencer 1969). *F. sinusarabici* is a thermophile organism that can grow in a range of temperatures between 30 °Cand 53 °C with an optimum temperature between 45 °C and 50 °C. It is a chemo-organotroph capable of metabolizing complex organic compounds under anaerobic growth using molecular nitrogen, carbon dioxide, molecular hydrogen, and methane. It has been found that *F. sinusarabici* can produce sulfur hydrides in the presence of elemental sulfur (Fiala et al. 1990).

The genus *Deferrivibrio* is a key actor in the biogeochemical cycling of elements in hot and haline mineral water deposits. *D. essentukiensis* is the only known species of this genus, isolated for the first time in the Yessentukskoye mineral water deposit in Russia (Zavarzina et al. 2022). It is a moderate thermophile capable of growing at a temperature between 30 °C and 54 °C and a pH between 6.2 and 7.9. In addition, it is an anaerobic halotolerant organism able to thrive in haline environments with a concentration of NaCl between 0 and 18 g/L. *D. essentukiensis* is a chemo-organotroph that uses carbonic organic compounds as electron donors and ferrihydrite as the sole electron acceptor (Zavarzina et al. 2022).

The single species known as *Petrothermobacter organivorans* makes up the entire genus *Petrothermobacter*. *P. organivorans* has been isolated for the first time in a deep subsurface oil field in Japan. It is an anaerobic, chemoheterotrophic organism capable of oxidizing carbon compounds while reducing iron (III), manganese (IV), nitrate, and sulfate as electron acceptors. It has an optimum of growth at 55 °C and the optimum pH is in the range of 6.0–8.0 (Tamazawa et al. 2017). *P. organivorans* has a relatively broad substrate range and can utilize pyruvate, fumarate, succinate, malate, yeast extract, and peptone for fermentative growth. Due to its metabolic capabilities, it can be considered as an essential organism for the biogeochemical cycling of various metals, such as iron and manganese (Tamazawa et al. 2017).

12 Chlorobi

The phylum Chlorobi has long been regarded as a monophyletic group of strictly anaerobic and anoxygenic, sulfur-oxidizing, photolithoautotroph microorganisms, generally referred to as the Green Sulfur Bacteria (GSB) (Frigaard and Dahl 2009; Fröstl and Overmann 2000; Gregersen et al. 2011; Imhoff 2003; van Niel 1932; Overmann and Tuschak 1997; Trüper Hans and Pfennig 1992). Photosynthesis is carried out due to bacteriochlorophylls and photosynthetic pigments—similar to plant, algal, and cyanobacterial chlorophyll—hosted in the chlorosomes. Sulfide and hydrogen sulfide are used as electron donors to fix CO_2 via reverse TCA cycle (Bello et al. 2022; Trüper Hans and Pfennig 1992).

Chlorobi traditionally included a single monotypic class *Chlorobia*, in turn consisting of one order (*Chlorobiales*) and family (*Chlorobiaceae*) (Gibson et al. 1984; Imhoff 2003), which is further divided into several genera (e.g., *Chlorobium*, *Ancalochloris*, *Chloroherpeton*, *Pelodicyton*, and *Prostheocochloris*) (Fröstl and Overmann 2000; Garrity et al. 2001a, b, c, d, e, f). The only metabolic exception was believed to concern the species *Chlorobium ferroxidans* and *Chlorobium phaeoferrooxidans*, which use ferrous iron rather than sulfur as electron donor in a metabolic pathway termed photoferrotrophy (Beatty et al. 2005; Frigaard and Bryant 2004; Frigaard and Dahl 2009; Garcia et al. 2021; Ghosh and Dam 2009; Hegler et al. 2008; Heising et al. 1999; Hiras et al. 2016; Imhoff 2003). However, later studies demonstrated that the cultured representative GSB are rather part of a wider and more diverse taxonomic group (Hiras et al. 2016). Firstly, a second class termed *Ignavibacteria* was included in the phylum when the anaerobic chemo-organoheterotrophic thermophilic species *Ignavibacterium album* (Iino et al. 2010) and *Melioribacter roseus* (Podosokorskaya et al. 2013) were discovered. Then, metagenomic approaches widened the class *Chlorobi* by revealing uncultured aerobic photoheterotrophic genome species, namely *Thermochlorobacter aerophylum*, and *Chlorobium* sp. GBChlB, and Chlorobi-445 (Liu et al. 2012; Roy et al. 2019); these latter have been proposed as part of the novel family *Chloroherpetonaceae* (Bello et al. 2022). Lastly, the aerobic chemo-organoheterotrophic OPB56 clade, whose clones are reported to be ubiquitous in thermal environments, was proposed to have the same common ancestor as Chlorobi and Ignavibacterium classes based on both concatenated ribosomal protein tree and concatenated single copy genes tree (Hiras et al. 2016; Soo et al. 2014).

12.1 Chlorobia

Besides GSB, the order Chlorobiales encompasses various thermophilic microorganisms whose optimal growth temperature range is 45 °C – 55 °C, and 4.5 and 6 for pH. The species *Chlorobium tepidum* was in fact isolated from an anoxygenic mat in a volcanic area in New Zealand and consists of anaerobic, phototrophic—either autotrophic or heterotrophic—microorganisms (Wahlund et al. 1991). Likewise, *Thermochlorobacter aerophilum* was isolated from microbial mats of alkaline siliceous hot spring at the Yellowstone National Park, but it is an aerobic phototrophic species, unable to oxidize sulfur compounds and to fix both N_2 and CO_2 (Liu et al. 2012). Conversely, the GSB1 species, which has been molecularly correlated to the *Chlorobium* and *Prosthecochloris*, was isolated from water collected at the plume of a 2 km-deep black smoker on the East Pacific rise. GSB1 retrieval is surprising as its growth requires anaerobiosis, sulfide or hydrogen sulfide, CO_2, and light, which in such an environment can only derive from geothermal activity (Beatty et al. 2005).

12.2 Ignavibacteria

The order *Ignavibacteriales* only harbors two thermophilic species, namely *Ignavibacterium album* and *Melioribacter roseus*, isolated from a sulfide-rich hot spring in Japan and water springing from a 2775 m-deep artesian borehole in Western Siberia, respectively. Both isolates have been cultured, thus demonstrating to be able to grow both aero- and anaerobically via chemo-organotrophic metabolism, with their optimal growth temperature spanning between 35 °C and 60 °C (Iino et al. 2010; Podosokorskaya et al. 2013).

Notably, *Melioribacter roseus* has 2 L-asparaginases, whose activity can be widely exploited by various biotechnological fields: these enzymes can both promote apoptosis in cancer cells and catalyze L-asparagine hydrolysis (thus preventing the formation of acrylamide, a human carcinogen). One of the two *M. roseus* enzymes exhibits the highest rate of activity at 70 °C, and thermophilic enzymes have been demonstrated to exhibit higher enzymatic activity, despite increased KM. Adaptation to high temperatures is given by the low abundance of thermolabile residues and the high frequency of thermostable residues (Dumina et al. 2021).

13 Thaumarchaeota

Thaumarchaeota is Gram-negative, short-rod, microbial group, including members of 0.3–0.6 μm in diameter and 0.6–1.0 μm long (Jung et al. 2018). Most of them possess a wider range of cell envelope structures than bacteria, and they differ from bacteria in the absence of peptidoglycan in the cell walls. Thaumarchaeota range among the most abundant archaea on Earth, and in particular in soil systems where they constitute about 5% of all prokaryotic biomass (Schleper and Nicol 2010). Initially classified as "mesophilic Crenarchaeota," comparative genomics has recently revealed that they form a separate and deep-branching phylum within the Archaea (Zhang and He 2012). Everything starts back in 1992, when Jed Fuhrman's team and Ed DeLong reported the discovery of a novel clade of archaeal 16S rRNA sequences from ocean surface waters, which formed a mesophilic sister group to the hyperthermophilic Crenarchaeota (DeLong 1992; Fuhrman et al. 1992). When it became apparent that this novel group contained autotrophic ammonia-oxidizing archaea, these organisms were consequently also referred to as mesophilic Crenarchaeota. When Brochier-Armanet and colleagues analyzed a concatenated data set of 53 ribosomal proteins common to Archaea and Eukarya, they observed that *C. symbiosum* branched off before the separation of Crenarchaeota and Euryarchaeota. Based on this phylogenetic analysis, on gene presence/absence data, and on the diversity and wide distribution of autotrophic ammonia-oxidizing archaea, they proposed that these organisms belong to the phylum Thaumarchaeota (Brochier-Armanet et al. 2008). This novel phylum includes all known archaeal

ammonia oxidizers and additionally several clusters of environmental sequences representing microorganisms with unknown energy metabolism (Pester et al. 2011).

Aerobic ammonia oxidation, the first and rate-limiting step in nitrification, is the only biological process converting reduced to oxidized inorganic nitrogen species on Earth (Gruber and Galloway 2008). The Thaumarchaeota are the first example of nitrification in the Archaea kingdom, a metabolism previously thought to be restricted to a few proteobacterial lineages (Könneke et al. 2005). Most of the ammonia-oxidizing archaea that have been identified to date have not been fully characterized because it is extremely difficult to obtain pure cultures of these organisms. Autotrophic CO_2 fixation on low NH_3 concentrations is the primary anabolic process in thaumarchaeal ammonia oxidizers; however, a potential for mixotrophic growth has also been reported (Hatzenpichler 2012; Stahl and de la Torre 2012). They have an extremely high affinity for substrate (Martens-Habbena and Stahl 2011), which means that they are frequently the dominant ammonia-oxidizing organisms in natural environments with low NH_3 concentrations. These environments include oligotrophic open ocean waters and nutrient-poor soils (Verhamme et al. 2011). They also seem to be adapted to growth at low pH, low dissolved oxygen concentrations, and high temperatures (Hatzenpichler 2012) and are the primary ammonia oxidizers in acidic forest soils (Lehtovirta-Morley et al. 2011), coastal waters (Urakawa et al. 2010), in the Atlantic and Pacific Oceans (Aylward and Santoro 2020), marine sediments (Dang et al. 2013), wastewater treatment bioreactors (Badar et al. 2022), in a coffee compost (Papale et al. 2021) and geothermal habitats (Beam et al. 2014; Hedlund et al. 2013; Nishizawa et al. 2016).

The presence of Thaumarchaeota, both in mesophilic and in thermophilic environments (De la Torre et al. 2008), confirms the wide spectrum of phenotypes belonging to this phylum. Different studies show that ammonia-oxidizing archaea are widely distributed in terrestrial geothermal systems (De la Torre et al. 2008) featured by diverse environmental variables. For example, ammonia-oxidizing archaea growth has been demonstrated up to 74 °C (de la Torre et al. 2008) and in situ activity measurements and quantitative studies of these microbial populations have revealed high activity and abundance up to ~81 °C (Cole et al. 2013; Dodsworth et al. 2011). In addition, studies about the distribution and relative abundance of the isoprenoid glycerol dialkyl glycerol tetraether (iGDGT) crenarchaeol, a potential biomarker for ammonia-oxidizing archaea, suggest this microbe's higher abundance compared to other archaea at 45–50 °C (Zhang et al. 2006). We also know that hyperthermophiles constitute the first diverging lineages of the currently described archaeal phyla (Crenarchaeota, Euryarchaeota, Korarchaeota) indicating that the last common ancestor of Archaea might have been a hyperthermophile (Forterre 2002; Woese 1987; Woese et al. 1990). Mesophily in some thaumarchaeal lineages is a derived character that helped their adaptation to colder habitats. The analysis of environmental sequences from Thaumarchaeota indicates that adaptation to mesophilia may have happened through horizontal gene transfer from bacteria or from mesophilic archaea (López-García et al. 2015). Because secondary adaptations to mesophily are also observed in

Euryarchaeota, this would be consistent with the hypothesis of multiple independent adaptations to mesophily in the Archaea from thermophilic or hyperthermophilic ancestors.

There are clear biotechnological applications related to the Thaumarchaeota group, mainly related to its thermostable enzyme properties (Saghatelyan et al. 2021). It is known, for example, that the type IB DNA topoisomerases are very important targets for antitumoral drugs in humans (Pommier 2009). Recent studies suggest that the archaeal type IB topoisomerases are much more similar to the eukaryotic enzymes than the Vaccinia virus type IB topoisomerase, which has been widely used as model system to understand human enzyme (Dahmane et al. 2016). These characteristics indicate that the Cs-TopIB or others thaumarchaeal TopIB might be promising new models for phylogenetic and structural studies of the type IB DNA topoisomerases.

14 Archaeoglobi

Archaeoglobi is a class of archaea that includes two orders, namely the *Archaeoglobales* and the *Desulfurococcales*. Members of the *Archaeoglobales* reduce sulfate, thiosulfate, iron, and nitrate, while they are facultative autotrophs or heterotrophs that reduce sulfate and thiosulfate to hydrogen sulfide. Archaeoglobi are strict anaerobes and hyperthermophiles that thrive in high-temperature environments, typically between 60 °C and 95 °C, and pH 5.5–7.5. They occur singly and in pairs and are gram-negative. Thermophilic archaeoglobi are generally small, spherical, or rod-shaped, and lack motility structures such as flagella. They typically have a cell wall made of pseudomurein, a type of peptidoglycan-like polymer that is unique to the Archaea domain.

Archaeoglobi are found in various locations around the world, such as Iceland, Italy, Japan, New Zealand, Russia, and the United States, and in a wide range of extreme habitats, such as deep-sea hydrothermal vents, hot springs, and oil reservoirs.

There are two orders of marine generalist archaea that are both considered Archaeoglobi: the *Archaeoglobales* in the Euryarchaeota and the *Desulfurococcales* in the Crenarchaeota.

The family *Archaeoglobaceae* is composed of *Archaeoglobi, Geoglobus*, and *Ferroglobus*. Archaeoglobi includes five species with validly published names: *A. fulgidus*, *A. profundus*, *A. veneficus*, *A. infectus*, and *A. sulfaticallidus*. Archaeoglobi can use a wide range of electron donors and acceptors, including sulfate, sulfite, thiosulfate, iron, nitrate, and various organic compounds. Members of the *Archaeoglobales* order, including Archaeoglobi, are able to grow by reduction of sulfite and thiosulfate. *A. sulfaticallidus* is the only species capable of lithoautotrophic growth with sulfate as a terminal electron acceptor.

The cell envelope of Archaeoglobi consists of an S-layer composed of subunits in hexagonal array containing a periodate-Schiff-positive polypeptide. Cells contain phytanyl ether lipids.

A complete oxidative TCA cycle has been shown to function in the cells of Archaeoglobi members such as *A. fulgidus*, *A. profundus*, *F. placidus*, *Geoglobus ahangari*, and *Geoglobus acetivorans*. The recently discovered species of Archaeoglobus, named *A. lithotrophicus*, has been found to be capable of lithoautotrophic growth using hydrogen gas and carbon dioxide as electron donor and acceptor, respectively.

One of the defining characteristics of thermophilic archaeoglobi is their ability to use molecular hydrogen (H_2) as an electron donor and sulfate (SO_4^{2-}) as an electron acceptor for energy production. This process, known as sulfate reduction, produces hydrogen sulfide (H_2S) as a byproduct. The ability of thermophilic archaeoglobi to carry out sulfate reduction is believed to be a key factor in their success in extreme environments, as sulfate is often abundant in such environments. Thermophilic archaeoglobi are also capable of carrying out a number of other metabolic processes, including the oxidation of organic compounds and the reduction of elemental sulfur. Some species are even capable of using carbon monoxide (CO) or methanol as electron donors.

There is growing interest in the biotechnological applications of Archaeoglobi due to their unique metabolic capabilities, which make them potentially useful for a range of industrial processes. Archaeoglobi are known, for example, for their ability to degrade a variety of hydrocarbons, including alkanes and aromatic compounds, under anaerobic conditions. This makes them a potential tool for bioremediation of contaminated environments, such as oil spills or petroleum-contaminated soils. Archaeoglobi can use hydrogen and carbon dioxide to produce methane, making them useful for the production of biogas as a renewable energy source. This archaeal group is also able to produce a range of enzymes that have potential biocatalytic applications. For example, some archaeal enzymes are known to be highly stable and active under extreme conditions of temperature, pH, and salinity, and this is why they are widely used in the production of chiral compounds for pharmaceuticals and agrochemicals, and in various industrial processes that require high stability and activity under extreme conditions. Some species of Archaeoglobi are capable of oxidizing sulfide minerals, making them useful for bioleaching of metal ores. Overall, there is significant potential for biotechnological applications of Archaeoglobi, and research in this area is ongoing.

15 Euryarcheota

The Euryarcheota phyla belongs to the Archaea domain and is composed of organisms that show very diverse physiological traits. These characteristics are known since the greatest number of cultured and diverse archaeal lineages belong to the Euryarchaeota phyla, in particular from the thermophilic classes *Archaeoglobi*,

Methanopyri, and *Thermococci* (Baker et al. 2020). Generally speaking, the Euryarchaeota can occur as rods, cocci, irregular cocci, triangular, square, lancet, spiral, or disk-shaped cells. Its nature with regard to Gram staining can be either positive or negative, based on the presence or absence of pseudomurein in cell walls (Garrity et al. 2001a, b, c, d, e, f). This phylum includes hyperthermophilic, halophilic, and methanogenic organisms. This diversity also poses a sharp contrast among organisms classified as Euryarcheota, since methanogens are the most strict type of anaerobes described, while halophiles are for the most part primarily aerobes (Pesaro and Widmer 2002; Baker et al. 2020). Euryarchaeota thermophiles belong to the *Thermoplasmatales* order, which includes three genera: *Thermoplasma, Picrophilus,* and *Ferroplasma,* with the *Thermoplasma* having the peculiarity of not having cell walls (Garrity et al. 2001a, b, c, d, e, f). There are three key genera of hyperthermophiles, two of them (*Thermococcus* and *Pyrococcus*) make up a distinct taxonomic order, the *Thermococcales* while the other one (*Methanopyrus*) is a methanogen that despite its similarity with the other methanogens has the peculiarity of being able to thrive at high temperatures. The growth temperatures reported for these thermophiles range from 55 °C (*Thermoplasma*) to as high as 110 °C (*Methanopyrus*). Other hyperthermophiles belonging to the *Thermoplasmatales* include *Archaeoglobus* and *Ferroglobus.* Thermophilic and hyperthermophilic Euryarcheaota metabolisms are varied, spanning from methanogenesis like in *Methanopyrus* to chemoheterotrophy, where proteins such as starch or maltose are used as electron donors and Fe, sulfate or S^0 act as a terminal electron acceptor in *Thermococcus, Pyrococcus, Thermoplasma*, and *Picrophilus* (Leigh and Whitman 2013a, b).

15.1 Thermoplasmatales

The key genera of this class are *Thermoplasma, Picrophilus,* and *Ferroplasma.* All members of this class are facultative aerobes capable of heterotrophic growth, under acidic conditions; however, only *Thermoplasma* and *Picrophilus* can thrive under thermophilic conditions. *Thermoplasma* lacks cell walls and grows optimally at temperatures near 55 °C (Garrity et al. 2001a, b, c, d, e, f; Leigh and Whitman 2013a, b). *Thermoplasma* species are facultative aerobes, chemo-organotrophic organisms, able to perform sulfur respiration through the degradation of organic compounds. These archaea are also acidophiles (optimum pH2.0) and are able to cope with the high temperatures and low pH due to the production of lipoglycan inside its cytoplasmic membranes. Members of the *Thermoplasma* have been found in self-heating coal refuse piles, terrestrial solfataras, and acid hot springs, with *T. acidophilum* being the first species described by Darland et al. (1970). Other members of this genus are *T. volcanium* (Segerer et al. 1988) and *T. thiooxidans* (Li et al. 1994).

Picrophilus is the other thermophilic member of the *Thermoplasmatales.* This genus differs from *Thermoplasmata* in the fact that it has a cell membrane.

Picrophilus species have an optimum growth temperature between 47 and 60 °C and is able to grow at pH values below 0, making it an hyperacidophile. It has also been shown that its growth is inhibited by high salt concentrations, which supports the hypothesis of a distribution restricted to terrestrial geothermal settings (Garrity et al. 2001a, b, c, d, e, f). This genus is composed of two species, both of them isolated from solfataric springs in Japan by Schleper et al. (1996) and capable of forming a highly acid-impermeable membrane at pH values below 4.

15.2 Thermococcales

The Thermococcales order includes all the hyperthermophilic genera belonging to the Euryarchaeota. They are heterotrophic archaea able to grow optimally at temperatures between 75 and 100 °C using sulfur respiration. They are commonly found in deep and shallow marine hydrothermal vents, although they have also been isolated from terrestrial hot springs (Garrity et al. 2001a, b, c, d, e, f). The genera included in this order are as follows: *Thermococcus* and *Pyrococcus*. *Thermococcus* are obligate chemo-organotrophic anaerobes that can grow metabolizing proteins and other complex C sources due to the reduction of elemental sulfur (Zillig et al. 1983a, b). The optimum growth temperature for these archaea is between 75 and 88 °C (Zillig et al. 1983a, b; Garrity et al. 2001a, b, c, d, e, f), in the presence of salt (between 2 and 4%). There are at least 15 species formally recognized as members of this genus, most of them isolated from terrestrial hot springs, coastal and marine solfataras, and deep-sea hydrothermal vents (Garrity et al. 2001a, b, c, d, e, f). The other member of the *Thermococcales* order is *Pyrococcus*. Members of this genus have a higher optimum growth temperature, between 70 and 106 °C, with this being the major difference among the two genera. From a metabolic point of view, they are also very similar, since both genera are heterotrophs that couple degradation of complex carbon substrates to the reduction of elemental sulfur to form H_2S. Species belonging to the *Pyrococcus* genus have been isolated from geothermally heated marine sediments such as *P. furiosus* (Fiala and Stetter 1986), deep-sea hydrothermal vents such as *P. abyssi, P. glycovorans, P. chitonophagus, P. horikoshii, P. kukulkanii, P. woesei*, and *P. yayanosii* (Zillig et al. 1987; Erauso et al. 1993; González et al. 1998; Barbier et al. 1999; Lepage et al. 2004; Birrien et al. 2011).

15.3 Methanopyrus

Methanopyrus organisms are hyperthermophilic archaea able to grow optimally at temperatures of 98 °C (Garrity et al. 2001a, b, c, d, e, f). Members of this genus have the peculiarity that they share phenotypic properties with both methanogens and hyperthermophiles. They can grow autotrophically through chemolithoautotrophy, coupling the reduction of CO_2 to CH_4, to the oxidation of H_2. The membrane lipids

found in the cell membranes of these archaea are an unsaturated form of diphytanoyl tetraethers and are thought to be able to stabilize the cytoplasmic membrane at high temperatures.

16 Crenarchaeota

The phylum Crenarchaeota (Garrity et al., 2001) were identified as a physiologically homogeneous group characterized by thermophilic taxa like *Sulfolobus* spp. (Brock et al. 1972; Woese 1987; Woese et al. 1990; Pesaro and Widmer 2002) but also by hyperthermophiles like *Pyrolobus* spp. (Blöchl et al. 1997). Most Crenarchaeota species were first isolated from submarine and terrestrial environments such as deep-sea hydrothermal vents, terrestrial hot springs, and hot acidic mudpots (Zillig et al. 1983a, b; Nakagawa et al. 2004a, b; Leigh and Whitman 2013a, b). The only class within the Crenarchaeota is named *Thermoprotei* which is divided in further orders among which the *Acidilobales, Desulfurococcales, Fervidicoccales, Sulfolobales,* and *Thermoproteales* (Offre et al. 2013). Energy-generating metabolism known for Crenarchaeota includes autotrophic pathways during which carbon is assimilated from oxidized inorganic compounds, i.e., carbon dioxide or bicarbonate, and reduced to form simple organic molecules (Berg et al. 2010). Some lineages of Crenarchaeota include facultative autotrophic organisms as well as obligate heterotrophs which utilize proteins and sugars as main carbon source (Kletzin 2007). The Crenarchaeota include some of the first cultivated lineages of archaea belonging to the *Sulfolobus* genus that were isolated for the first time from the hot acid springs in Yellowstone National Park by Thomas Brock (Brock et al. 1972) and then become one of the main models of thermophile archaea investigations (Zhang et al. 2018).

16.1 Thermoprotei

Sulfolobus species present an aerobic and microaerophilic way of life, able to thrive at temperatures around 75–80 °C and pH 2–3 (Brock et al. 1972). Most species are chemo-organoheterotrophs, e.g., *S. solfataricus* which uses a wide range of carbon substrates (i.e., sugars, tryptone, peptides, and amino acids) (Hanner et al. 1990; Wolf et al. 2016) while others like *S. acidocaldarius* are considered facultative autotrophic, involved in the respiration of sulfur and the utilization of CO_2 or HCO_3—as source of carbon (Brock et al. 1972; Schönheit and Schäfer 1995; Leigh and Whitman 2013a, b). Among the eight *Sulfolobus* species known in literature, only three (*S. islandicus, S. solfataricus, and S. acidocaldarius*) are well described as model organisms for comparative genomics and genetics, host–virus interactions, investigation of catabolic enzymes, and industrial applications (Held and Whitaker 2009; Reno et al. 2009; Chavan and Deshpande 2013; Bräsen et al. 2014). Indeed, the genus *Sulfolobus* has a key role in several biotechnological

applications since it is a source of unique enzymes, biomaterials, and unique catabolic pathways (i.e., the Entner–Doudoroff (ED) pathway and the Weimberg and Dahms pathway) involved in the degradation of pentoses and hexoses for the exploitation of novel products (Siebers and Schönheit 2005; Nunn et al. 2010; Kouril et al. 2013; Besse et al. 2015; Quehenberger et al. 2017).

17 Conclusions

This chapter was intended to give an overview of thermophilic bacteria, found within the prokaryotic Tree of Life. At this present date, more than 1200 species of thermophilic bacteria have been discovered and are found in at least 15 phyla. Thermophilic prokaryotes are found in a wide range of extreme environments, including hot springs, geothermal vents, deep-sea hydrothermal vents, and desert soil. In general, thermophilic bacteria have diverse metabolic activity and are capable of utilizing a wide range of substrates. Their diversity and adaptation to extreme environments make them a promising source of biotechnological applications, including production of enzymes and biofuels as was addressed in the present chapter.

References

Abraham W-R, Rohde M, Bennasar A (2014) The family Caulobacteraceae. In: Rosenberg E, DeLong EF, Lory S et al (eds) The prokaryotes: alphaproteobacteria and betaproteobacteria. Springer, Berlin, pp 179–205

Aguiar P, Beveridge TJ, Reysenbach A-L (2004) *Sulfurihydrogenibium azorense*, sp. nov., a thermophilic hydrogen-oxidizing microaerophile from terrestrial hot springs in the Azores. Int J Syst Evol Microbiol 54:33–39. https://doi.org/10.1099/ijs.0.02790-0

Akinosho H, Yee K, Close D et al (2014) The emergence of *Clostridium thermocellum* as a high utility candidate for consolidated bioprocessing applications. Front Chem 2(Aug):66. https://doi.org/10.3389/fchem.2014.00066

Alain K, Marteinsson VT, Miroshnichenko ML et al (2002) *Marinitoga piezophila* sp. nov., a rod-shaped, thermo-piezophilic bacterium isolated under high hydrostatic pressure from a deep-sea hydrothermal vent. Int J Syst Evol Microbiol 52:1331–1339. https://doi.org/10.1099/00207713-52-4-1331

Alain K, Rolland S, Crassous P et al (2003) *Desulfurobacterium crinifex* sp. nov., a novel thermophilic, pinkish-streamer forming, chemolithoautotrophic bacterium isolated from a Juan de Fuca Ridge hydrothermal vent and amendment of the genus *Desulfurobacterium*. Extremophiles 7:361–370. https://doi.org/10.1007/s00792-003-0329-4

Alain K, Postec A, Grinsard E et al (2010) *Thermodesulfatator atlanticus* sp. nov., a thermophilic, chemolithoautotrophic, sulfate-reducing bacterium isolated from a mid-Atlantic ridge hydrothermal vent. Int J Syst Evol Microbiol 60:33–38. https://doi.org/10.1099/ijs.0.009449-0

Albuquerque L, Simões C, Nobre MF et al (2005) *Truepera radiovictrix* gen. nov., sp. nov., a new radiation resistant species and the proposal of Trueperaceae fam. nov. FEMS Microbiol Lett 247:161–169. https://doi.org/10.1016/j.femsle.2005.05.002

Albuquerque L, Froufe H, Egas C et al (2018) Albidovulum. In: Boone DR, Castenholz RW, Garrity GM (eds) Bergey's manual of systematics of archaea and bacteria. Springer, New York, pp 1–8

Allioux M, Yvenou S, Slobodkina G et al (2020) Genomic characterization and environmental distribution of a thermophilic anaerobe *Dissulfurirhabdus thermomarina* SH388(T) involved in disproportionation of sulfur compounds in shallow sea hydrothermal vents. Microorganisms 8: 1132. https://doi.org/10.3390/microorganisms8081132

Amin A, Ahmed I, Habib N et al (2016) *Microvirga pakistanensis* sp nov., a novel bacterium isolated from desert soil of Cholistan, Pakistan. Arch Microbiol 198:933–939. https://doi.org/10.1007/s00203-016-1251-3

Anderson A, Nordan H, Cain R et al (1956) Studies on a radioresistant *Micrococcus*. I. Isolation, morphology, cultural characteristics and resistance to gamma radiation. Food Technol 10:575–578

Aoshima M, Ishii M, Igarashi Y (2004) A novel enzyme, citryl-CoA synthetase, catalysing the first step of the citrate cleavage reaction in *Hydrogenobacter thermophilus* TK-6: Citryl-CoA synthetase in *H. thermophilus*. Mol Microbiol 52:751–761. https://doi.org/10.1111/j.1365-2958.2004.04009.x

Arif S, Willenberg C, Dreyer A et al (2021) Sasso Pisano geothermal field environment harbours diverse *Ktedonobacteria* representatives and illustrates habitat-specific adaptations. Microorganisms 9(7):1402. https://doi.org/10.3390/microorganisms9071402

Armstrong FA, Belsey NA, Cracknell JA et al (2009) Dynamic electrochemical investigations of hydrogen oxidation and production by enzymes and implications for future technology. Chem Soc Rev 38:36–51. https://doi.org/10.1039/b801144n

Auria R, Boileau C, Davidson S et al (2016) Hydrogen production by the hyperthermophilic bacterium *Thermotoga maritima* part II: modeling and experimental approaches for hydrogen production. Biotechnol Biofuels 19(9):268. https://doi.org/10.1186/s13068-016-0681-0

Aylward FO, Santoro AE (2020) Heterotrophic Thaumarchaea with small genomes are widespread in the dark ocean. MSystems 5:10–128. https://doi.org/10.1128/msystems.00415-20

Badar A, Mukhtar S, Mehnaz S, Malik KA (2022) Microbial diversity analysis of Hudiara Drain wastewater using cultureindependent and culture-dependent approaches. Environ Sustain 5:65–76. https://doi.org/10.1007/s42398-022-00215-y

Bai YN, Lu YZ, Shen N et al (2018) Investigation of Cr (VI) reduction potential and mechanism by *Caldicellulosiruptor saccharolyticus* under glucose fermentation condition. J Hazard Mater 344:585–592. https://doi.org/10.1016/j.jhazmat.2017.10.059

Baker BJ, De Anda V, Seitz KW et al (2020) Diversity, ecology and evolution of archaea. Nat Microbiol 5:887–900. https://doi.org/10.1038/s41564-020-0715-z

Barbier G, Godfroy A, Meunier JR, et al (1999) *Pyrococcus glycovorans* sp. nov., a hyperthermophilic archaeon isolated from the East Pacific rise. Int J Syst Bacteriol 49(4):1829–1837. https://doi.org/10.1099/00207713-49-4-1829

Beam JP, Jay ZJ, Kozubal MA, Inskeep WP (2014) Niche specialization of novel Thaumarchaeota to oxic and hypoxic acidic geothermal springs of Yellowstone National Park. ISME J 8:938–951. https://doi.org/10.1038/ismej.2013.193

Beatty J, Overmann J, Lince MT et al (2005) An obligately photosynthetic bacterial anaerobe from a deep-sea hydrothermal vent. Proc Natl Acad Sci U S A 102:9306–9310. https://doi.org/10.1073/pnas.0503674102

Beblo-Vranesevic K, Huber H, Rettberg P (2017b) High tolerance of *Hydrogenothermus marinus* to sodium perchlorate. Front Microbiol 8:1369. https://doi.org/10.3389/fmicb.2017.01369

Bello S, Howard-Azzeh M, Schellhorn HE et al (2022) Phylogenomic analyses and molecular signatures elucidating the evolutionary relationships amongst the *Chlorobia* and *Ignavibacteria* species: robust demarcation of two family-level clades within the order *Chlorobiales* and proposal for the family *Chloroherpetonaceae* fam. nov. Microorganisms 10(7):1312. https://doi.org/10.3390/microorganisms10071312

Ben Hania W, Godbane R, Postec A, et al (2012) *Defluviitoga tunisiensis* gen. nov., sp. nov., a thermophilic bacterium isolated from a mesothermic and anaerobic whey digester. Int J Syst Evol Microbiol 62:1377–1382. https://doi.org/10.1099/ijs.0.033720-0

Berg IA, Kockelkorn D, Ramos-Vera WH et al (2010) Autotrophic carbon fixation in archaea. Nat Rev Microbiol 8:447–460. https://doi.org/10.1038/nrmicro2365

Bergmann F, Selesi D, Weinmaier T et al (2011) Genomic insights into the metabolic potential of the polycyclic aromatic hydrocarbon degrading sulfate-reducing deltaproteobacterium N47. Environ Microbiol 13:1125–1137. https://doi.org/10.1111/j.1462-2920.2010.02391.x

Berleman JE, Kirby JR (2009) Deciphering the hunting strategy of a bacterial wolfpack. FEMS Microbiol Rev 33:942–957. https://doi.org/10.1111/j.1574-6976.2009.00185.x

Besse A, Peduzzi J, Rebuffat S, Carre-Mlouka A (2015) Antimicrobial peptides and proteins in the face of extremes: lessons from archaeocins. Biochimie 118:344–355. https://doi.org/10.1016/j.biochi.2015.06.004

Bessman MJ, Kornberg A, Lehman IR et al (1956) Enzymic synthesis of deoxyribonucleic acid. Biochim Biophys Acta 21(1):197–198. https://doi.org/10.1016/0006-3002(56)90127-5

Bhandari V, Gupta RS (2014a) Molecular signatures for the phylum (class) Thermotogae and a proposal for its division into three orders (*Thermotogales, Kosmotogales* ord. nov. and *Petrotogales* ord. nov.) containing four families (*Thermotogaceae, Fervidobacteriaceae* fam. nov., *Kosmotogaceae* fam. nov. and *Petrotogaceae* fam. nov.) and a new genus *Pseudothermotoga* gen. nov. with five new combinations. Antonie Van Leeuwenhoek 105:143–168. https://doi.org/10.1007/s10482-013-0062-7

Bhandari V, Gupta RS (2014b) The phylum Thermotogae. In: Rosenberg E, DeLong EF, Lory S, Stackebrandt E, Thompson F (eds) The prokaryotes. Springer, Heidelberg, pp 989–1015. https://doi.org/10.1007/978-3-642-38954-2_118

Bing W, Sun H, Wang F et al (2018) Hydrogen-producing hyperthermophilic bacteria synthesized size-controllable fine gold nanoparticles with excellence for eradicating biofilm and antibacterial applications. J Mater Chem B 6(28):4602–4609. https://doi.org/10.1039/c8tb00549d

Birrien J-L, Zeng X, Jebbar M, et al (2011) *Pyrococcus yayanosii* sp. nov., an obligate piezophilic hyperthermophilic archaeon isolated from a deep-sea hydrothermal vent. Int J Syst Evol Microbiol 61:2827–2881. https://doi.org/10.1099/ijs.0.024653-0

Bizic M, Brad T, Ionescu D et al (2023) Cave *Thiovulum* (Candidatus *Thiovulum stygium*) differs metabolically and genomically from marine species. ISME J 17:340–353. https://doi.org/10.1038/s41396-022-01350-4

Blöchl E, Rachel R, Burggraf S et al (1997). *Pyrolobus fumarii*, gen. and sp. nov., represents a novel group of archaea, extending the upper temperature limit for life to 113 C Extremophiles 1:14–21

Blumer-Schuette SE (2020) Insights into thermophilic plant biomass hydrolysis from *Caldicellulosiruptor* systems biology. Microorganisms 8(3):385. https://doi.org/10.3390/microorganisms8030385

Blumer-Schuette SE, Kataeva I, Westpheling J et al (2008) Extremely thermophilic microorganisms for biomass conversion: status and prospects. Curr Opin Biotechnol 19:210–217. https://doi.org/10.1016/j.copbio.2008.04.007

Boden R, Hutt LP (2019a) Thermithiobacillus. In: Boone DR, Castenholz RW, Garrity GM (eds) Bergey's manual of systematics of archaea and bacteria. Springer, New York, pp 1–11

Boden R, Hutt LP (2019b) Bergey's manual of systematics of archaea and bacteria. In: Boone DR, Castenholz RW, Garrity GM (eds) Acidithiobacillus. Springer, New York, pp 1–19

Boesen T, Nielsen LP (2013) Molecular dissection of bacterial nanowires. MBio 4:e00270–e00213. https://doi.org/10.1128/mBio.00270-13

Bond DR, Holmes DE, Tender LM et al (2002) Electrode-reducing microorganisms that harvest energy from marine sediments. Science 295:483–485. https://doi.org/10.1126/science.1066771

Boniface A, Bouhss A, Mengin-Lecreulx D et al (2006) The MurE synthetase from *Thermotoga maritima* is endowed with an unusual D-lysine adding activity. J Biol Chem 281:15680–15686. https://doi.org/10.1074/jbc.M506311200

Braga LPP, Pereira RV, Martins LF et al (2021) Genome-resolved metagenome and metatranscriptome analyses of thermophilic composting reveal key bacterial players and their metabolic interactions. BMC Genomics 22:1–19. https://doi.org/10.1186/s12864-021-07957-9

Bräsen C, Esser D, Rauch B et al (2014) Carbohydrate metabolism in archaea: current insights into unusual enzymes and pathways and their regulation. Microbiol Mol Biol Rev 78:89–175. https://doi.org/10.1128/MMBR.00041-13

Brewer PG, Spencer DW (1969) A note on the chemical composition of the Red Sea brines. In: Hot brines and recent heavy metal deposits in the Red Sea: a geochemical and geophysical account, pp 174–179. https://doi.org/10.1007/978-3-662-28603-6_19

Briggs BR, Brodie EL, Tom LM et al (2014) Seasonal patterns in microbial communities inhabiting the hot springs of Tengchong, Yunnan Province, China: PhyloChip and physicochemical analyses. Environ Microbiol 16:1579–1591. https://doi.org/10.1111/1462-2920.12311

Brochier-Armanet C, Boussau B, Gribaldo S, Forterre P (2008) Mesophilic Crenarchaeota: proposal for a third archaeal phylum, the Thaumarchaeota. Nat Rev Microbiol 6:245–252. https://doi.org/10.1038/nrmicro1852

Brock T, Freeze H (1969) *Thermus aquaticus* gen. n and sp. n., a non-sporulating extreme thermophile. J Bacteriol 98:289–297.

Brock, TD, Brock, KM, Belly, RT et al (1972) *Sulfolobus*: a new genus of sulfur-oxidizing bacteria living at low pH and high temperature. Arch Mikrobiol 84:54–68. doi: https://doi.org/10.1007/BF00408082

Brynjarsdottir H, Wawiernia B, Orlygsson J (2012) Ethanol production from sugars and complex biomass by *Thermoanaerobacter* AK5: the effect of electron-scavenging systems on end-product formation. Energy Fuel 26(7):4568–4574. https://doi.org/10.1021/ef300754q

Caldwell SL, Liu Y, Ferrera I, et al (2010) *Thermocrinis minervae* sp. nov., a hydrogen- and sulfur-oxidizing, thermophilic member of the Aquificales from a Costa Rican terrestrial hot spring. Int J Syst Evol Microbiol 60:338–343. https://doi.org/10.1099/ijs.0.010496-0

Campbell BJ, Jeanthon C, Kostka JE et al (2001) Growth and phylogenetic properties of novel bacteria belonging to the epsilon subdivision of the proteobacteria enriched from *Alvinella pompejana* and deep-sea hydrothermal vents. Appl Environ Microbiol 67(10):4566–4572. https://doi.org/10.1128/AEM.67.10.4566-4572.2001

Campbell BJ, Stein JL, Cary JS (2003) Evidence of chemolithoautotrophy in the bacterial community associated with *Alvinella pompejana*, a hydrothermal vent polychaete. Appl Environ Microbiol 69(9):5070–5078. https://doi.org/10.1128/AEM.69.9.5070-5078.2003

Campbell BJ, Engel AS, Porter ML et al (2006) The versatile ε-proteobacteria: key players in sulphidic habitats. Nat Rev Microbiol 4(6):458–468. https://doi.org/10.1038/nrmicro1414

Cao J, Birien T, Gayet N et al (2017) *Desulfurobacterium indicum* sp. nov., a thermophilic sulfur-reducing bacterium from the Indian Ocean. Int J Syst Evol Microbiol 67:1665–1668. https://doi.org/10.1099/ijsem.0.001837

Cary SC, Shank T, Stein J (1998) Worms bask in extreme temperatures. Nature 391:545–546. https://doi.org/10.1038/35286

Cavaletti L, Monciardini P, Bamonte R et al (2006) New lineage of filamentous, spore-forming, gram-positive bacteria from soil. Appl Environ Microbiol 72:4360–4369. https://doi.org/10.1128/AEM.00132-06

Chavan SB, Deshpande MV (2013) Chitinolytic enzymes: an appraisal as a product of commercial potential. Biotechnol Prog 29:833–846. https://doi.org/10.1002/btpr.1732

Chenevier P, Mugherli L, Darbe S et al (2013) Hydrogenase enzymes: application in biofuel cells and inspiration for the design of noble-metal free catalysts for H-2 oxidation. C R Chim 16:491–505. https://doi.org/10.1016/j.crci.2012.11.006

Chien A, Edgar DB, Trela JM (1976) Deoxyribonucleic acid polymerase from the extreme thermophile *Thermus aquaticus*. J Bacteriol 127:1550–1557. https://doi.org/10.1128/jb.127.3.1550-1557.1976

Chou Y-J, Sheu S-Y, Sheu D-S et al (2006) *Schlegelella aquatica* sp. nov., a novel thermophilic bacterium isolated from a hot spring. Int J Syst Evol Microbiol 56:2793–2797. doi: https://doi.org/10.1099/ijs.0.64446-0

Christensen B, Torsvik T, Lien T (1992) Immunomagnetically captured thermophilic sulfate-reducing bacteria from North Sea oil field waters. Appl Environ Microbiol 58:1244–1248. https://doi.org/10.1128/aem.58.4.1244-1248.1992

Chung AP, Rainey FA, Valente M, et al (2000) *Thermus igniterrae* sp. nov. and *Thermus antranikianii* sp. nov., two new species from Iceland. Int J Syst Evol Microbiol 50:209–217. https://doi.org/10.1099/00207713-50-1-209

Chung D, Cha M, Snyder EN et al (2015) Cellulosic ethanol production via consolidated bioprocessing at 75°C by engineered *Caldicellulosiruptor bescii*. Biotechnol Biofuels 8(1): 163. https://doi.org/10.1186/s13068-015-0346-4

Ciccarelli FD, Doerks T, von Mering C et al (2006) Toward automatic reconstruction of a highly resolved tree of life. Science 311(5765):1283–1287. https://doi.org/10.1126/science.1123061

Clarke A (2014) The thermal limits to life on earth. Int J Astrobiol 13:141–154. https://doi.org/10.1017/S1473550413000438

Cole JK, Gieler BA, Heisler DL et al (2013) *Kallotenue papyrolyticum* gen. nov., sp. nov., a cellulolytic and filamentous thermophile that represents a novel lineage (Kallotenuales ord. nov., Kallotenuaceae fam. nov.) within the class Chloroflexia. Int J Syst Evol Microbiol 63: 4675–4682. https://doi.org/10.1099/ijs.0.053348-0

Collins MD, Lawson PA, Willems A et al (1994) The phylogeny of the genus *Clostridium* - proposal of 5 new genera and 11 new species combinations. Int J Syst Bacteriol 44:812–826. https://doi.org/10.1099/00207713-44-4-812

Conners SB, Mongodin EF, Johnson MR et al (2006) Microbial biochemistry, physiology, and biotechnology of hyperthermophilic *Thermotoga* species. FEMS Microbiol Rev 30:872–905. https://doi.org/10.1111/j.1574-6976.2006.00039.x

Counts JA, Zeldes BM, Lee LL et al (2017) Physiological, metabolic and biotechnological features of extremely thermophilic microorganisms. Wiley Interdiscip Rev Syst Biol Med 9:e1377. https://doi.org/10.1002/wsbm.1377

Cox MM, Battista JR (2005) *Deinococcus radiodurans* — the consummate survivor. Nat Rev Microbiol 3:882–892. https://doi.org/10.1038/nrmicro1264

Dahmane N, Gadelle D, Delmas S et al (2016) topIb, a phylogenetic hallmark gene of *Thaumarchaeota encodes* a functional eukaryote-like topoisomerase IB. Nucl Acids Res 44: 2795–2805. https://doi.org/10.1093/nar/gkw097

Dang H, Zhou H, Yang J et al (2013) Thaumarchaeotal signature gene distribution in sediments of the northern South China Sea: an indicator of the metabolic intersection of the marine carbon, nitrogen, and phosphorus cycles? Appl Environ Microbiol 79:2137–2147. https://doi.org/10.1128/AEM.03204-12

Daims H (2014) The family Nitrospiraceae. In: Rosenberg E, DeLong EF, Lory S, Stackebrandt E, Thompson F (eds) The prokaryotes. Springer, Berlin. https://doi.org/10.1007/978-3-642-38954-2_126

Darland G, Brock TD, Samsonoff W et al (1970) A thermophilic, acidophilic *mycoplasma* isolated from a coal refuse pile. Science 170:1416–1418. https://doi.org/10.1126/science.170.3965.1416

Davey ME, Wood WA, Key R et al (1993) Isolation of three species of *Geotoga* and *Petrotoga*: two new genera, representing a new lineage in the bacterial line of descent distantly related to the "Thermotogales". Syst Appl Microbiol 16:191–200. https://doi.org/10.1016/S0723-2020(11)80467-4

Deckert G, Warren PV, Gaasterland T et al (1998) The complete genome of the hyperthermophilic bacterium *Aquifex aeolicus*. Nature 392:353–358. https://doi.org/10.1038/32831

De la Torre JR, Walker CB, Ingalls AE, Könneke M, Stahl DA (2008) Cultivation of a thermophilic ammonia oxidizing archaeon synthesizing crenarchaeol. Env Microbiol 10:810–818. https://doi.org/10.1111/j.1462-2920.2007.01506.x

DeLong EF (1992) Archaea in coastal marine environments. Proc Nat Acad Sci 89:5685–5689. https://doi.org/10.1073/pnas.89.12.5685

Delgado-Baquerizo M, Oliverio AM, Brewer TE et al (2018) A global atlas of the dominant bacteria found in soil. Science 359:320–325. https://doi.org/10.1126/science.aap9516

Denman S, Hampson K, Patel BKC (1991) Isolation of strains of *Thermus aquaticus* from the Australian Artesian Basin and a simple and rapid procedure for the preparation of their plasmids. FEMS Microbiol Lett 82:73–78. https://doi.org/10.1111/j.1574-6968.1991.tb04842.x

Desai SG, Guerinot ML, Lynd LR (2004) Cloning of L-lactate dehydrogenase and elimination of lactic acid production via gene knockout in *Thermoanaerobacterium saccharolyticum* JW/SL-YS485. Appl Microbiol Biotechnol 65(5):600–605. https://doi.org/10.1007/s00253-004-1575-9

Deweerd KA, Suflita JM (1990) Anaerobic aryl reductive dehalogenation of Halobenzoates by cell extracts of "*Desulfomonile tiedjei*". Appl Environ Microbiol 56:2999–3005. https://doi.org/10.1128/aem.56.10.2999-3005.1990

Di Cesare A, Pjevac P, Eckert E et al (2020) The role of metal contamination in shaping microbial communities in heavily polluted marine sediments. Environ Pollut 265:114823. https://doi.org/10.1016/j.envpol.2020.114823

DiGiacomo J, McKay C, Davila A (2022) ThermoBase: a database of the phylogeny and physiology of thermophilic and hyperthermophilic organisms. PLoS One 17:e0268253. https://doi.org/10.1371/journal.pone.0268253

DiPippo JL, Nesbø CL, Dahle H et al (2009). *Kosmotoga olearia* gen. nov., sp. nov., a thermophilic, anaerobic heterotroph isolated from an oil production fluid. Int J Syst Evol Microbiol, 59: 2991–3000. https://doi.org/10.1099/ijs.0.008045-0

Dodsworth JA, Hungate BA, Hedlund BP (2011) Ammonia oxidation, denitrification and dissimilatory nitrate reduction to ammonium in two US Great Basin hot springs with abundant ammonia-oxidizing archaea. Env Microbiol 13:2371–2386. https://doi.org/10.1111/j.1462-2920.2011.02508.x

Dodsworth JA, Gevorkian J, Despujos F et al (2014) *Thermoflexus hugenholtzii* gen. nov., sp. nov., a thermophilic, microaerophilic, filamentous bacterium representing a novel class in the Chloroflexi, Thermoflexia classis nov., and description of Thermoflexaceae fam. nov. and Thermoflexales ord. nov. Int J Syst Evol Microbiol 64:2119–2127. https://doi.org/10.1099/ijs.0.055855-0

Dodsworth JA, Ong JC, Williams AJ et al (2015) *Thermocrinis jamiesonii* sp. nov., a thiosulfate-oxidizing, autotropic thermophile isolated from a geothermal spring. Int J Syst Evol Microbiol 65:4769–4775. https://doi.org/10.1099/ijsem.0.000647

Dumina M, Zhgun A, Pokrovskaya M et al (2021) Highly active thermophilic L-asparaginase from *Melioribacter roseus* represents a novel large Group of Type II bacterial L-asparaginases from Chlorobi-Ignavibacteriae-Bacteroidetes clade. Int J Mol Sci 22:13632. https://doi.org/10.3390/ijms222413632

Dumitrache A, Akinosho H, Rodriguez M et al (2016) Consolidated bioprocessing of populus using *Clostridium (Ruminiclostridium) thermocellum*: a case study on the impact of lignin composition and structure. Biotechnol Biofuels 9(31). https://doi.org/10.1186/s13068-016-0445-x

Dworkin M, Falkow S, Rosenberg E et al (eds) (2006) The prokaryotes. Springer, New York

Eder W, Huber R (2002) New isolates and physiological properties of the Aquificales and description of *Thermocrinis albus* sp. nov. Extremophiles 6:309–318. https://doi.org/10.1007/s00792-001-0259-y

Edwards TA, Calica NA, Huang DA et al (2013) Cultivation and characterization of thermophilic *Nitrospira* species from geothermal springs in the US Great Basin, China, and Armenia. FEMS Microbiol Ecol 85(2):283–292. https://doi.org/10.1111/1574-6941.12117

Ehrich S, Behrens D, Lebedeva E et al (1995) A new obligately chemolithoautotrophic, nitrite-oxidizing bacterium, *Nitrospira moscoviensis* sp. nov. and its phylogenetic relationship. Arch Microbiol 164:16–23

Elbanna K, Lütke-Eversloh T, Van Trappen S et al (2003) *Schlegelella thermodepolymerans* gen. nov., sp. nov., a novel thermophilic bacterium that degrades poly(3-hydroxybutyrate-co-3-

mercaptopropionate). Int J Syst Evol Microbiol 53:1165–1168. https://doi.org/10.1099/ijs.0.02562-0

Erauso G, Reysenbach A-L, Godfroy A et al (1993) *Pyrococcus abyssi* sp. nov., a new hyperthermophilic archaeon isolated from a deep-sea hydrothermal vent. Arch Microbiol 160:338–349. https://doi.org/10.1007/BF00252219

Eriksen NT, Riis ML, Holm NK et al (2011) H_2 synthesis from pentoses and biomass in *Thermotoga* spp. Biotechnol Lett 33(2):293–300. https://doi.org/10.1007/s10529-010-0439-x

Fardeau ML, Ollivier B, Patel BK et al (1997) *Thermotoga hypogea* sp. nov., a xylanolytic, thermophilic bacterium from an oil-producing well. Int J Syst Bacteriol 47:1013–1019. https://doi.org/10.1099/00207713-47-4-1013

Fardeau ML, Ollivier B, Jl C (2015) *Caldanaerobacter*. In: Trujillo ME, Dedysh S, DeVos P et al (eds) Bergey's manual of systematics of archaea and bacteria. Springer, New York. https://doi.org/10.1002/9781118960608.gbm00745

Farrell AA, Nesbø CL, Zhaxybayeva O et al (2021) Fervidobacteriaceae. In: Trujillo ME, Dedysh S, DeVos P, Hedlund B, Kämpfer P, Rainey FA, Whitman WB (eds) Bergey's manual of systematics of archaea and bacteria. Springer, New York. https://doi.org/10.1002/9781118960608.fbm00360

Feng Y, Cheng L, Zhang X et al (2010) *Thermococcoides shengliensis* gen. nov., sp. nov., a new member of the order Thermotogales isolated from oil-production fluid. Int J Syst Evol Microbiol 60:932–937. https://doi.org/10.1099/ijs.0.013912-0

Ferrera I, Banta AB, Reysenbach A-L (2014) Spatial patterns of Aquificales in deep-sea vents along the eastern Lau spreading Center (SW Pacific). Syst Appl Microbiol 37:442–448. https://doi.org/10.1016/j.syapm.2014.04.002

Fiala G, Stetter KO (1986) *Pyrococcus furiosus* sp. nov. represents a novel genus of marine heterotrophic archaebacteria growing optimally at 100°C. Arch Microbiol 145:56–61. https://doi.org/10.1007/BF00413027

Fiala G, Woese CR, Langworthy TA, Stetter KO (1990) *Flexistipes sinusarabici*, a novel genus and species of eubacteria occurring in the Atlantis II Deep brines of the Red Sea. Arch Microbiol 154:120–126. https://doi.org/10.1007/BF00423320

Figueiredo GGO, Lopes VR, Romano T et al (2020) In beneficial microbes in Agro-ecology. Academic, Cambridge, pp 477–491. isbn:978-0-12-823414-3

Flores GE, Liu Y, Ferrera I et al (2008) *Sulfurihydrogenibium kristjanssonii* sp. nov., a hydrogen- and sulfur-oxidizing thermophile isolated from a terrestrial Icelandic hot spring. Int J Syst Evol Microbiol 58:1153–1158. https://doi.org/10.1099/ijs.0.65570-0

François DX, Godfroy A, Mathien C et al (2021) *Persephonella atlantica* sp. nov.: how to adapt to physico-chemical gradients in high temperature hydrothermal habitats. Syst Appl Microbiol 44:126176. https://doi.org/10.1016/j.syapm.2020.126176

Forterre P (2002) The origin of DNA genomes and DNA replication proteins. Curr Op Microbiol 5:525–532. https://doi.org/10.1016/S1369-5274(02)00360-0

Frank YA, Kadnikov VV, Lukina AP et al (2016) Characterization and genome analysis of the first facultatively alkaliphilic *Thermodesulfovibrio* isolated from the deep terrestrial subsurface. Front Microbiol 7:2000. https://doi.org/10.3389/fmicb.2016.02000

Frigaard N-U, Bryant DA (2004) Seeing Green bacteria in a new light: genomics-enabled studies of the photosynthetic apparatus in Green Sulfur bacteria and filamentous anoxygenic phototrophic bacteria. Arch Microbiol 182:265–276. https://doi.org/10.1007/s00203-004-0718-9

Frigaard N-U, Dahl C (2009) Sulfur metabolism in phototrophic Sulfur bacteria. Adv Microb Physiol 54:103–200. https://doi.org/10.1016/S0065-2911(08)00002-7

Frock AD, Notey JS, Kelly RM (2010) The genus *Thermotoga*: recent developments. Environ Technol 31:1169–1181. https://doi.org/10.1080/09593330.2010.484076

Fröstl JM, Overmann J (2000) Phylogenetic affiliation of the bacteria that constitute phototrophic consortia. Arch Microbiol 174:50–58. https://doi.org/10.1007/s002030000172

Fuhrman JA, McCallum K, Davis AA (1992) Novel major archaebacterial group from marine plankton. Nature 356:148–149. https://doi.org/10.1038/356148a0

Fukushi M, Mino S, Tanaka H et al (2020) Biogeochemical Implications of N_2O-reducing thermophilic campylobacteria in deep-sea vent fields, and the description of *Nitratiruptor labii* sp. nov. iScience 23:101462. https://doi.org/10.1016/j.isci.2020.101462

Gaisin VA, Kalashnikov AM, Grouzdev DS et al (2017) *Chloroflexus islandicus* sp. nov., a thermophilic filamentous anoxygenic phototrophic bacterium from a geyser. Int J Syst Evol Microbiol 67:1381–1386. https://doi.org/10.1099/ijsem.0.001820

Garcia SL, Mehshad M, Buck M et al (2021) Freshwater *Chlorobia* exhibit metabolic specialization among cosmopolitan and endemic populations. mSystems 6(3):e01196–e01120. https://doi.org/10.1128/mSystems.01196-20

Garrity GM, Holt JG, Castenholz RW et al (2001a) Phylum BVI. Chloroflexi phy. nov. In: Boone DR, Castenholz RW, Garrity GM (eds) BT - Bergey's manual of systematic bacteriology, Volume one: the archaea and the deeply branching and phototrophic bacteria. Springer, New York, pp 427–446

Garrity GM, Holt JG, Reysenbach A-L et al (2001b) Phylum Al Crenarchaeota phy. nov. In: Boone DR, Castenholz RW, Garrity GM (eds) Bergey's manual of systematic bacteriology, Volume one: the archaea and the deeply branching and phototrophic bacteria. Springer, New York, pp 169–210. https://doi.org/10.1007/978-0-387-21609-6_16

Garrity GM, Holt JG, Battista JR et al (2001c) Phylum BIV. Deinococcus-Thermus. In: Boone DR, Castenholz RW, Garrity GM (eds) Bergey's manual of systematic bacteriology. Springer, New York, pp 395–420

Garrity GM, Holt JG, Overmann J et al (2001d) Phylum BXI. Chlorobi phy. nov. In: Boone DR, Castenholz RW, Garrity GM (eds) Bergey's manual of systematic bacteriology. Springer, New York, pp 601–623. https://doi.org/10.1007/978-0-387-21609-6_28

Garrity GM, Holt JG, Whitman WB et al (2001e) Phylum all. Euryarchaeota phy. nov. In: Boone DR, Castenholz RW, Garrity GM (eds) Bergey's manual of systematic bacteriology, Volume one: the archaea and the deeply branching and phototrophic bacteria. Springer, New York, pp 211–355

Garrity GM, Holt JG, Spieck E et al (2001f) Phylum BVIII Nitrospirae phy. nov. in. In: Boone DR, Castenholz RW, Garrity GM (eds) Bergey's manual of systematic bacteriology. Springer, New York, NY, pp 451–464

Garrity GM, Bell JA, Lilburn T (2015) Burkholderiales ord. nov. In: Boone DR, Castenholz RW, Garrity GM (eds) Bergey's manual of systematics of archaea and bacteria. Springer, New York, p 1

Georgieva T, Ahring BK (2007) Evaluation of continuous ethanol fermentation of dilute-acid corn Stover hydrolysate using thermophilic anaerobic bacterium *Thermoanaerobacter* BG1L1. Appl Microbiol Biotechnol 77:61–68. https://doi.org/10.1007/s00253-007-1149-8

Gerth K, Müller R (2005) Moderately thermophilic myxobacteria: novel potential for the production of natural products isolation and characterization. Environ Microbiol 7:874–880. https://doi.org/10.1111/j.1462-2920.2005.00761.x

Ghimire-Kafle S, Weaver ME Jr, Bollmann A (2023) Ecophysiological and genomic characterization of the freshwater complete ammonia oxidizer *Nitrospira* sp. strain BO4. Appl Environ Microbiol 89(2):e01965–e01922. https://doi.org/10.1128/aem.01965-22

Ghosh W, Dam B (2009) Biochemistry and molecular biology of lithotrophic Sulfur oxidation by taxonomically and ecologically diverse bacteria and archaea. FEMS Microbiol Rev 33(6): 999–1043. https://doi.org/10.1111/j.1574-6976.2009.00187.x

Gibbons NE, Murray RGE (1978) Proposals concerning the higher taxa of bacteria. Int J Syst Bacteriol 28:1–6

Gibson J, Pfennig N, Waterbury JB (1984) *Chloroherpeton thalassium* gen. nov. et spec. nov., a non-filamentous, flexing and gliding Green Sulfur bacterium. Arch Microbiol 138:96–101, https://doi.org/10.1007/BF00413007

Giovannoni SJ, Revsbech NP, Ward DM et al (1987) Obligately phototrophic *Chloroflexus*: primary production in anaerobic hot spring microbial mats. Arch Microbiol 147:80–87. https://doi.org/10.1007/BF00492909

Giovannelli D, Sievert SM, Hügler M et al (2017) Insight into the evolution of microbial metabolism from the deep-branching bacterium, *Thermovibrio ammonificans*. Elife 6:e18990. https://doi.org/10.7554/eLife.18990

González JM, Masuchi Y, Robb FT et al (1998) *Pyrococcus horikoshii* sp. nov., a hyperthermophilic archaeon isolated from a hydrothermal vent at the Okinawa trough. Extremophiles 2:123–130. https://doi.org/10.1007/s007920050051

Gotz D (2002) *Persephonella marina* gen. nov., sp. nov. and *Persephonella guaymasensis* sp. nov., two novel, thermophilic, hydrogen-oxidizing microaerophiles from deep-sea hydrothermal vents. Int J Syst Evol Microbiol 52:1349–1359. https://doi.org/10.1099/ijs.0.02126-0

Greene AC, Patel BK, Sheehy AJ (1997) *Deferribacter thermophilus* gen. nov., sp. nov., a novel thermophilic manganese-and iron-reducing bacterium isolated from a petroleum reservoir. Int J Syst Evol Microbiol 47:505–509. https://doi.org/10.1099/00207713-47-2-505

Gregersen L, Bryant DA, Frigaard NU (2011) Mechanisms and evolution of oxidative sulfur metabolism in green sulfur bacteria. Front Microbiol 2:116. https://www.frontiersin.org/articles/10.3389/fmicb.2011.00116

Gregoire P, Fardeau M-L, Joseph M et al (2011) Isolation and characterization of *Thermanaerothrix daxensis* gen. nov., sp. nov., a thermophilic anaerobic bacterium pertaining to the phylum "Chloroflexi", isolated from a deep hot aquifer in the Aquitaine Basin. Syst Appl Microbiol 34:494–497. https://doi.org/10.1016/j.syapm.2011.02.004

Griffiths E, Gupta RS (2004) Distinctive protein signatures provide molecular markers and evidence for the monophyletic nature of the Deinococcus-Thermus phylum. J Bacteriol 186:3097–3107. https://doi.org/10.1128/JB.186.10.3097-3107.2004

Gruber N, Galloway JN (2008) An Earth-system perspective of the global nitrogen cycle. Nature 451:293–296. https://doi.org/10.1038/nature06592

Guiral M, Prunetti L, Aussignargues C et al (2012) The Hyperthermophilic bacterium *Aquifex aeolicus*. Adv Microb Physiol:125–194

Gupta RS (2014) The phylum aquificae. In: Rosenberg E, DeLong EF, Lory S et al (eds) The prokaryotes. Springer, Berlin, pp 417–445

Hanada S, Hiraishi A, Shimada K et al (1995) *Chloroflexus aggregans* sp. nov., a filamentous phototrophic bacterium which forms dense cell aggregates by active gliding movement. Int J Syst Bacteriol 45:676–681. https://doi.org/10.1099/00207713-45-4-676

Hanada S, Kawase Y, Hirashi A et al (1997) *Porphyrobacter tepidarius* sp. nov., a moderately thermophilic aerobic photosynthetic bacterium isolated from a hot spring. Int J Syst Bacteriol 47:408–413. https://doi.org/10.1099/00207713-47-2-408

Hanada S, Takaichi S, Matsuura K et al (2002) *Roseiflexus castenholzii* gen. nov., sp. nov., a thermophilic, filamentous, photosynthetic bacterium that lacks chlorosomes. Int J Syst Evol Microbiol 52:187–193. https://doi.org/10.1099/00207713-52-1-187

Hanner M, Redl B, Stöffler G (1990) Isolation and characterization of an intracellular aminopeptidase from the extreme thermophilic archaebacterium *Sulfolobus solfataricus*. Biochim Biophys Acta 1033:148–153. https://doi.org/10.1016/0304-4165(90)90005-H

Haouari O, Fardeau ML, Cayol JL et al (2008) *Thermodesulfovibrio hydrogeniphilus* sp. nov., a new thermophilic sulphate-reducing bacterium isolated from a Tunisian hot spring. Syst Appl Microbiol 31(1):38–42. Doi:https://doi.org/10.1016/j.syapm.2007.12.002

Hart BA, Zahler SA (1966) Lytic enzyme produced by *Myxococcus xanthus*. J Bacteriol 92:1632–1637. https://doi.org/10.1128/jb.92.6.1632-1637.1966

Härtig C, Lohmayer R, Kolb S et al (2014) Chemolithotrophic growth of the aerobic hyperthermophilic bacterium *Thermocrinis ruber* OC 14/7/2 on monothioarsenate and arsenite. FEMS Microbiol Ecol 90:747–760. https://doi.org/10.1111/1574-6941.12431

Hatchikian EC, Ollivier B, Garcia JL (2001) Family I. Thermodesulfobacteriaceae fam. nov. In: Boone DR, Castenholz RW, Garrity GM (eds) Bergey's manual of systematic bacteriology, Volume one: The archaea and the deeply branching of phototrophic bacteria, 2nd edn. Springer, New York, pp 390–394

Hatzenpichler R (2012) Diversity, physiology, and niche differentiation of ammonia-oxidizing archaea. Appl Environ Microbiol 78:7501–7510. https://doi.org/10.1128/AEM.01960-12

Hartmann M (1985) Atlantis-II Deep geothermal brine system. Chemical processes between hydrothermal brines and Red Sea deep water. Mar Geol 64:157–177. https://doi.org/10.1016/0025-3227(85)90166-5

Hedlund BP, Dodsworth JA, Cole JK, Panosyan HH (2013) An integrated study reveals diverse methanogens, Thaumarchaeota, and yet-uncultivated archaeal lineages in Armenian hot springs. Antonie Van Leeuwenhoek 104:71–82. https://doi.org/10.1007/s10482-013-9927-z

Hegler F, Posth NR, Jiang J et al (2008) Physiology of phototrophic iron(II)-oxidizing bacteria: implications for modern and ancient environments. FEMS Microbiol Ecol 66:250–260. https://doi.org/10.1111/j.1574-6941.2008.00592.x

Heising S, Richter L, Ludwig W, Schink B (1999) *Chlorobium ferrooxidans* sp. nov., a phototrophic Green Sulfur bacterium that oxidizes ferrous iron in coculture with a '*Geospirillum'* sp. strain. Arch Microbiol 172:116–124, https://doi.org/10.1007/s002030050748

Held NL, Whitaker RJ (2009) Viral biogeography revealed by signatures in *Sulfolobus islandicus* genomes. Environ Microbiol 11:457–466. https://doi.org/10.1111/j.1462-2920.2008.01784.x

Henkel JV, Schulz-Vogt HN, Dellwig O et al (2022) Biological manganese-dependent sulfide oxidation impacts elemental gradients in redox-stratified systems: indications from the Black Sea water column. ISME J 16:1523–1533. https://doi.org/10.1038/s41396-022-01200-3

Henry EA, Devereux R, Maki JS et al (1994) Characterization of a new thermophilic sulfate-reducing bacterium: *Thermodesulfovibrio yellowstonii*, gen. nov. and sp. nov.: its phylogenetic relationship to *Thermodesulfobacterium commune* and their origins deep within the bacterial domain. Arch Microbiol 161:62–69. https://doi.org/10.1007/s002030050022

Hernández M, Vera-Gargallo B, Calabi-Floody M et al (2020) Reconstructing genomes of carbon monoxide oxidisers in volcanic deposits including members of the class Ktedonobacteria. Microorganisms 8(12):1880. https://doi.org/10.3390/microorganisms8121880

Hetzer A, McDonald IR, Morgan HW (2008) *Venenivibrio stagnispumantis* gen. nov., sp. nov., a thermophilic hydrogen-oxidizing bacterium isolated from champagne Pool, Waiotapu, New Zealand. Int J Syst Evol Microbiol 58:398–403. https://doi.org/10.1099/ijs.0.64842-0

Hidalgo KJ, Sierra-Garcia IN, Zafra G, de Oliveira VM (2021) Genome-resolved meta-analysis of the microbiome in oil reservoirs worldwide. Microorganisms 9:1812. https://doi.org/10.3390/microorganisms9091812

Hiraishi A, Imhoff JF (2015) Porphyrobacter. In: Boone DR, Castenholz RW, Garrity GM (eds) Bergey's manual of systematics of archaea and bacteria. Springer, New York, pp 1–6

Hiraishi A, Yonemitsu Y, Matsushita M et al (2002) Characterization of *Porphyrobacter sanguineus* sp. nov., an aerobic bacteriochlorophyll-containing bacterium capable of degrading biphenyl and dibenzofuran. Arch Microbiol 178:45–52. https://doi.org/10.1007/s00203-002-0423-5

Hiras J, Wu YW, Eichorst SA et al (2016) Refining the phylum chlorobi by resolving the phylogeny and metabolic potential of the representative of a deeply branching, uncultivated lineage. ISME J 10:833–845. https://doi.org/10.1038/ismej.2015.158

Hirsch P, Gallikowski CA, Siebert J et al (2004) *Deinococcus frigens* sp. nov., *Deinococcus saxicola* sp. nov., and *Deinococcus marmoris* sp. nov., low temperature and draught-tolerating, UV-resistant bacteria from continental Antarctica. Syst Appl Microbiol 27:636–645. https://doi.org/10.1078/0723202042370008

Holmes DE, Nicoll JS, Bond DR, Lovley DR (2004) Potential role of a novel psychrotolerant member of the family Geobacteraceae, *Geopsychrobacter electrodiphilus* gen. nov., sp. nov., in electricity production by a marine sediment fuel cell. Appl Environ Microbiol 70:6023–6030. https://doi.org/10.1128/AEM.70.10.6023-6030.2004

Hon S, Holwerda EK, Worthen RS et al (2018) Expressing the *Thermoanaerobacterium saccharolyticum* pforA in engineered *clostridium thermocellum* improves ethanol production. Biotechnol Biofuels 11:242. https://doi.org/10.1186/s13068-018-1245-2

Hovanec TA, Taylor LT, Blakis A et al (1998) *Nitrospira*-like bacteria associated with nitrite oxidation in freshwater aquaria. Appl Environ Microbiol 64(1):258–264. https://doi.org/10.1128/AEM.64.1.258-264.1998

Huang L, Bae H-S, Young C et al (2021) Campylobacterota dominate the microbial communities in a tropical karst subterranean estuary, with implications for cycling and export of nitrogen to coastal waters. Environ Microbiol 23:6749–6763. https://doi.org/10.1111/1462-2920.15746

Huber H (2002) *Thermovibrio ruber* gen. nov., sp. nov., an extremely thermophilic, chemolithoautotrophic, nitrate-reducing bacterium that forms a deep branch within the phylum Aquificae. Int J Syst Evol Microbiol 52:1859–1865. https://doi.org/10.1099/ijs.0.02235-0

Huber H, Stetter KO (2001) Class I. Deferribacteres class. nov. Bergey's manual of systematic bacteriology 1:465

Huber R, Hannig M (2006) Thermotogales. In: Dworkin M, Falkow S, Rosenberg E et al (eds) The prokaryotes. Springer, New York. https://doi.org/10.1007/0-387-30747-8_38

Huber R, Langworthy TA, König H et al (1986) *Thermotoga maritima* sp. nov. represents a new genus of unique extremely thermophilic eubacteria growing up to 90°C. Arch Microbiol 144:324–333. https://doi.org/10.1007/BF00409880

Huber R, Woese CR, Langworthy TA, Fricke H, Stetter KO (1989) *Thermosipho africanus* gen. nov., represents a new genus of thermophilic eubacteria within the "Thermotogales". Syst Appl Microbiol 12:32–37. https://doi.org/10.1016/S0723-2020(89)80037-2

Huber R, Woese CR, Langworthy TA et al (1990) *Fervidobacterium islandicum* sp. nov., a new extremely thermophilic eubacterium belonging to the "Thermotogales". Arch Microbiol 154:105–111. https://doi.org/10.1007/BF00423318

Huber R, Wilharm T, Huber D et al (1992) *Aquifex pyrophilus* gen. nov. sp. nov., represents a novel group of marine Hyperthermophilic hydrogen-oxidizing bacteria. Syst Appl Microbiol 15:340–351. https://doi.org/10.1016/S0723-2020(11)80206-7

Hug LA, Castelle CJ, Wrighton KC et al (2013) Community genomic analyses constrain the distribution of metabolic traits across the Chloroflexi phylum and indicate roles in sediment carbon cycling. Microbiome 1:22. https://doi.org/10.1186/2049-2618-1-22

Hug LA, Baker BJ, Anantharaman K et al (2016) A new view of the tree of life. Nat Microbiol 1:1–6

Iino T, Nakagawa T, Mori K et al (2008) *Calditerrivibrio nitroreducens* gen. nov., sp. nov., a thermophilic, nitrate-reducing bacterium isolated from a terrestrial hot spring in Japan. Int J Syst Evol Microbiol 58:1675–1679. doi: https://doi.org/10.1099/ijs.0.65714-0.18599715

Iino T, Mori K, Uchino Y et al (2010) *Ignavibacterium album* gen. nov., sp. nov., a moderately thermophilic anaerobic bacterium isolated from microbial Mats at a terrestrial hot spring and proposal of Ignavibacteria classis Nov., for a novel lineage at the periphery of Green Sulfur bacteria. Int J Syst Evol Microbiol 60:1376–1382, https://doi.org/10.1099/ijs.0.012484-0

Iizuka T, Tokura M, Jojima Y et al (2006) Enrichment and phylogenetic analysis of moderately thermophilic myxobacteria from hot springs in Japan. Microbes Environ 21:189–199

Imhoff JF (2003) Phylogenetic taxonomy of the family Chlorobiaceae on the basis of 16S RRNA and Fmo (Fenna-Matthews-Olson protein) gene sequences. Int J Syst Evol Microbiol 53:941–951. https://doi.org/10.1099/ijs.0.02403-0

Imhoff JF, Trüper HG (1977) *Ectothiorhodospira halochloris* sp. nov., a new extremely halophilic phototrophic bacterium containing bacteriochlorophyll b. Arch Microbiol 114:115–121. https://doi.org/10.1007/BF00410772

Imhoff JF, Süling J, Petri R (1998) Phylogenetic relationships among the *Chromatiaceae,* their taxonomic reclassification and description of the new genera *Allochromatium, Halochromatium, Isochromatium, Marichromatium, Thiococcus, Thiohalocapsa* and *Thermochromatium*. Int J Syst Bacteriol 48(Pt 4):1129–1143. https://doi.org/10.1099/00207713-48-4-1129

Itoh T, Onishi M, Kato S et al (2016) *Athalassotoga saccharophila* gen. nov., sp. nov., isolated from an acidic terrestrial hot spring, and proposal of Mesoaciditogales Ord. Nov. and

Mesoaciditogaceae fam. nov. in the phylum Thermotogae. Int J Syst Evol Microbiol 66:1045–1051. https://doi.org/10.1099/ijsem.0.000833

Jannasch HW, Wirsen CO, Molyneaux SJ et al (1988) Extremely thermophilic fermentative archaebacteria of the genus *Desulfurococcus* from deep-sea hydrothermal vents. Appl Environ Microbiol 54:1203–1209. https://doi.org/10.1128/aem.54.5.1203-1209.1988

Jayasinghearachchi HS, Lal B (2011) *Oceanotoga teriensis* gen. nov., sp. nov., a thermophilic bacterium isolated from offshore oil-producing wells. Int J Syst Evol Microbiol 61:554–560. https://doi.org/10.1099/ijs.0.018036-0

Jeanthon C, L'Haridon S, Cueff V et al (2002) *Thermodesulfobacterium hydrogeniphilum* sp. nov., a thermophilic, chemolithoautotrophic, sulfate-reducing bacterium isolated from a deep-sea hydrothermal vent at Guaymas Basin, and emendation of the genus *Thermodesulfobacterium*. Int J Syst Evol Microbiol 52:765–772. https://doi.org/10.1099/00207713-52-3-765

Jørgensen BB, Nelson DC (1988) Bacterial zonation, photosynthesis, and spectral light distribution in hot spring microbial mats of Iceland. Microb Ecol 16(2):133–147. https://doi.org/10.1007/BF02018909

Jung MY, Islam MA, Gwak JH, Kim JG, Rhee SK (2018) *Nitrosarchaeum koreense* gen. nov., sp. nov., an aerobic and mesophilic, ammonia-oxidizing archaeon member of the phylum Thaumarchaeota isolated from agricultural soil. Int J Syst Evol Microbiol 68:3084–3095. https://doi.org/10.1099/ijsem.0.002926

Jurkevitch E, Davidov Y (2007) Phylogenetic diversity and evolution of predatory prokaryotes. In: Jurkevitch E (ed) BT - predatory prokaryotes: biology, ecology and evolution. Springer, Berlin, pp 11–56

Kádár Z, de Vrijek T, van Noorden GE et al (2004) Yields from glucose, xylose, and paper sludge hydrolysate during hydrogen production by the extreme thermophile *Caldicellulosiruptor saccharolyticus*. Appl Biochem Biotechnol 113–116:497–508

Kanoksilapatham W, Pasomsup P, Keawram P, et al (2016) *Fervidobacterium thailandense* sp. nov., an extremely thermophilic bacterium isolated from a hot spring. Int J Syst Evol Microbiol 66:5023–5027. https://doi.org/10.1099/ijsem.0.001463

Kanso S, Patel BKC (2004) *Phenylobacterium lituiforme* sp. nov., a moderately thermophilic bacterium from a subsurface aquifer, and emended description of the genus *Phenylobacterium*. Int J Syst Evol Microbiol 54:2141–2146. https://doi.org/10.1099/ijs.0.63138-0

Kanth BK, Jun S-Y, Kumari S, Pack SP (2014) Highly thermostable carbonic anhydrase from *Persephonella marina* EX-H1: its expression and characterization for CO_2-sequestration applications. Process Biochem 49:2114–2121. https://doi.org/10.1016/j.procbio.2014.10.011

Kashefi K, Holmes DE, Reysenbach A-L et al (2002) Use of Fe(III) as an electron acceptor to recover previously uncultured hyperthermophiles: isolation and characterization of *Geothermobacterium ferrireducens* gen. nov., sp. nov. Appl Environ Microbiol 68:1735–1742. https://doi.org/10.1128/AEM.68.4.1735-1742.2002

Kawaichi S, Ito N, Kamikawa R et al (2013) *Ardenticatena maritima* gen. nov., sp. nov., a ferric iron- and nitrate-reducing bacterium of the phylum "Chloroflexi" isolated from an iron-rich coastal hydrothermal field, and description of Ardenticatenia classis nov. Int J Syst Evol Microbiol 63:2992–3002. https://doi.org/10.1099/ijs.0.046532-0

Kawasumi T, Igarashi Y, Kodama T et al (1984) *Hydrogenobacter thermophilus* gen. nov. , sp. nov. , an extremely thermophilic, aerobic, hydrogen-oxidizing bacterium. Int J Syst Bacteriol 34:5–10. doi: https://doi.org/10.1099/00207713-34-1-5

Khan IU, Habib N, Xiao M et al (2018) *Phenylobacterium terrae* sp. nov., isolated from a soil sample of Khyber-Pakhtun-Khwa, Pakistan. Antonie Van Leeuwenhoek 111:1767–1775. https://doi.org/10.1007/s10482-018-1064-2

Kieft TL, Fredrickson JK, Onstott TC et al (1999) Dissimilatory reduction of Fe(III) and other electron acceptors by a *Thermus* isolate. Appl Environ Microbiol 65:1214–1221. https://doi.org/10.1128/AEM.65.3.1214-1221.1999

Kletzin A (2007) General characteristics and important model organisms. In: Cavicchioli R (ed) Archaea. Wiley, pp 14–92. https://doi.org/10.1128/9781555815516.ch2

Kochetkova TV, Zayulina KS, Zhigarkov VS et al (2020) *Tepidiforma bonchosmolovskayae* gen. nov., sp. nov., a moderately thermophilic Chloroflexi bacterium from a Chukotka hot spring (Arctic, Russia), representing a novel class, Tepidiformia, which includes the previously uncultivated lineage OLB14. Int J Syst Evol Microbiol 70:1192–1202. https://doi.org/10.1099/ijsem.0.003902

Kojima H, Watanabe M, Fukui M (2017) *Sulfurivermis fontis* gen. nov., sp. nov., a sulfur-oxidizing autotroph, and proposal of Thioprofundaceae fam. nov. Int J Syst Evol Microbiol 67:3458–3461. https://doi.org/10.1099/ijsem.0.002137

Könneke M, Bernhard AE, de La Torre JR, Walker CB, Waterbury JB, Stahl DA (2005) Isolation of an autotrophic ammoniaoxidizing marine archaeon. Nature 437:543–546. https://doi.org/10.1038/nature03911

Kouril T, Wieloch P, Reimann J et al (2013) Unraveling the function of the two Entner–Doudoroff branches in the thermoacidophilic crenarchaeon *Sulfolobus solfataricus* P2. FEBS J 280:1126–1138. https://doi.org/10.1111/febs.12106

Kube M, Beck A, Zinder SH et al (2005) Genome sequence of the chlorinated compound–respiring bacterium *Dehalococcoides* species strain CBDB1. Nat Biotechnol 23:1269–1273. https://doi.org/10.1038/nbt1131

L'Haridon S, Cilia V, Messner P et al (1998) *Desulfurobacterium thermolithotrophum* gen. nov., sp. nov., a novel autotrophic, Sulphur-reducing bacterium isolated from a deep-sea hydrothermal vent. Int J Syst Bacteriol 48:701–711. https://doi.org/10.1099/00207713-48-3-701

L'Haridon S, Reysenbach A-L, Tindall BJ et al (2006) *Desulfurobacterium atlanticum* sp. nov., *Desulfurobacterium pacificum* sp. nov. and *Thermovibrio guaymasensis* sp. nov., three thermophilic members of the Desulfurobacteriaceae fam. nov., a deep branching lineage within the bacteria. Int J Syst Evol Microbiol 56:2843–2852. https://doi.org/10.1099/ijs.0.63994-0

L'Haridon S, Gouhier L, John ES et al (2019) *Marinitoga lauensis* sp. nov., a novel deep-sea hydrothermal vent thermophilic anaerobic heterotroph with a prophage. Syst Appl Microbiol 42:343–347. https://doi.org/10.1016/j.syapm.2019.02.006

Lacis LS, Lawford HG (1988a) Effect of growth rate on ethanol production by *Thermoanaerobacter ethanolicus* in glucose-or xylose-limited continuous culture. Biotechnol Lett 10(8). https://doi.org/10.1007/BF01027138

Lacis LS, Lawford HG (1988b) Ethanol production from xylose by *Thermoanaerobacter ethanolicus* in batch and continuous culture. Arch Microbiol 150:48–55. https://doi.org/10.1007/BF00409717

Lamed R, Zeikus JG (1980a) Glucose fermentation pathway of *Thermoanaerobium brockii*. J Bacteriol 141(3):1251–1257. https://doi.org/10.1128/JB.141.3.1251-1257.1980

Lamed R, Zeikus JG (1980b) Ethanol production by thermophilic bacteria: relationship between fermentation product yields of and catabolic enzyme activities in *Clostridium thermocellum* and *Thermoanaerobium brockii*. J Bacteriol 144(2):569–578. https://doi.org/10.1128/JB.144.2.569-578.1980

Meo-Savoie D, Carol A, George W et al (2004) Physicochemical characterization of the microhabitat of the epibionts associated with *Alvinella pompejana*, a hydrothermal vent annelid 1 1Associate editor: P O'Day'. Geochim Cosmochim Acta 68(9):2055–2066. https://doi.org/10.1016/j.gca.2003.10.039

Langwig MV, De Anda V, Dombrowski N et al (2022) Large-scale protein level comparison of deltaproteobacteria reveals cohesive metabolic groups. ISME J 16:307–320. https://doi.org/10.1038/s41396-021-01057-y

Latif H, Sahin M, Tarasova J et al (2015) Adaptive evolution of *Thermotoga maritima* reveals plasticity of the ABC transporter network. Appl Environ Microbiol 81:5477–5485. https://doi.org/10.1128/AEM.01365-15

Lawson PA (2016) The taxonomy of the genus clostridium: current status and future perspectives. Microbiol China 43(05):1070–1074

Lebedeva EV, Alawi M, Maixner F et al (2008) Physiological and phylogenetic characterization of a novel lithoautotrophic nitrite-oxidizing bacterium, 'Candidatus *Nitrospira bockiana*'. Int J Syst Evol Microbiol 58(1):242–250. https://doi.org/10.1099/ijs.0.65379-0

Lebedeva EV, Off S, Zumbrägel S et al (2011) Isolation and characterization of a moderately thermophilic nitrite-oxidizing bacterium from a geothermal spring. FEMS Microbiol Ecol 75(2): 195–204. https://doi.org/10.1111/j.1574-6941.2010.01006.x

Lehtovirta-Morley LE, Stoecker K, Vilcinskas A, Prosser JI, Nicol GW (2011) Cultivation of an obligate acidophilic ammonia oxidizer from a nitrifying acid soil. Proc Nat Acad Sci 108: 15892–15897. https://doi.org/10.1073/pnas.1107196108

Lee YJ, Dashti M, Prange A et al (2007) *Thermoanaerobacter sulfurigignens* sp. nov., an anaerobic thermophilic bacterium that reduces 1 M thiosulfate to elemental sulfur and tolerates 90 mM sulfite. Int J Syst Evol Microbiol 57(7):1429–1434. doi: https://doi.org/10.1099/ijs.0.64748-0

Lee YE, Jain MK, Lee CY et al (1993) Taxonomic distinction of saccharolytic thermophilic anaerobes - description of *Thermoanaerobacterium xylanolyticum* gen-nov, sp-nov, and *Thermoanaerobacterium saccharolyticum* gen-nov, sp-nov - reclassification of *Thermoanaerobium brockii, Clostridium thermosulfurogenes*, and *Clostridium thermohydrosulfuricum* E100–69 as *Thermoanaerobacter brockii* comb-nov, *Thermoanaerobacterium thermosulfurigenes* comb-nov, and *Thermoanaerobacter thermohydrosulfuricus* comb-nov, respectively - and transfer of *Clostridium thermohydrosulfuricum* 39E to *Thermoanaerobacter ethanolicus*. Int J Syst Bacteriol 43:41–51. https://doi.org/10.1099/00207713-43-1-41

Leigh JA, Whitman WB (2013a) Archaeal genetics. In: Brenner's encyclopedia of genetics. Elsevier, pp 188–191. https://doi.org/10.1016/B978-0-12-374984-0.00093-0

Leigh JA, Whitman WB (2013b) Archaeal genetics. In: Hughes K, Maloy S (eds) Brenner's encyclopedia of genetics. Elsevier, pp 188–191

Lepage E, Marguet E, Geslin C et al (2004) Molecular diversity of new *Thermococcales* isolates from a single area of hydrothermal Deep-Sea vents as revealed by randomly amplified polymorphic DNA fingerprinting and 16S rRNA gene sequence analysis. Appl Environ Microbiol 70:1277–1286. https://doi.org/10.1128/AEM.70.3.1277-1286.2004

Letunic I, Bork P (2007) Interactive tree of life (iTOL): an online tool for phylogenetic tree display and annotation. Bioinformatics 23(1):127–128. https://doi.org/10.1093/bioinformatics/btl529

Lien T, Madsen M, Rainey FA et al (1998) *Petrotoga mobilis* sp. nov., from a North Sea oil-production well. Int J Syst Evol Microbiol 48:1007–1013. https://doi.org/10.1099/00207713-48-3-1007

Li S, Zhu Q, Luo J et al (2021) Application progress of *Deinococcus radiodurans* in biological treatment of radioactive uranium-containing wastewater. Indian J Microbiol 61:417–426. https://doi.org/10.1007/s12088-021-00969-9

Li Y, Hu J, Qu C et al (2019) Engineered *Thermoanaerobacterium aotearoense* with nfnAB knockout for improved hydrogen production from lignocellulose hydrolysates. Biotechnol Biofuels 12:214. https://doi.org/10.1186/s13068-019-1559-8

Liu Z, Klatt CG, Ludwig M et al (2012) 'Candidatus *Thermochlorobacter Aerophilum*:' an aerobic Chlorophotoheterotrophic member of the phylum Chlorobi defined by metagenomics and Metatranscriptomics. ISME J 6:1869–1882. https://doi.org/10.1038/ismej.2012.24

Liu J, Häggblom MM (2018) Genome-guided identification of organohalide-respiring deltaproteobacteria from the marine environment. MBio 9:e02471–e02418. https://doi.org/10.1128/mBio.02471-18

Li Y, Liu G, Zhong H (1994) A new species of *Thermoplasma*. Wei Sheng Wu Xue Bao 34:255–260

Liu Y, Zhang J, Zhao L, Zhang X, Xie S (2014) Spatial distribution of bacterial communities in high-altitude freshwater wetland sediment. Limnology 15:249–256. https://doi.org/10.1007/s10201-014-0429-0

Liu R, Wei X, Song W et al (2022) Novel Chloroflexi genomes from the deepest ocean reveal metabolic strategies for the adaptation to deep-sea habitats. Microbiome 10(1):1–17. https://doi.org/10.1186/s40168-022-01263-6

Löffler F, Yan J, Ritalahti K et al (2013) *Dehalococcoides mccartyi* gen. nov., sp. nov., obligately organohalide-respiring anaerobic bacteria relevant to halogen cycling and bioremediation, belong to a novel bacterial class, Dehalococcoidia classis nov., order Dehalococcoidales Ord. Nov. and family. Int J Syst Evol Microbiol 63:625–635. https://doi.org/10.1099/ijs.0.034926-0

Lonergan DJ, Jenter HL, Coates JD et al (1996) Phylogenetic analysis of dissimilatory Fe(III)-reducing bacteria. J Bacteriol 178:2402–2408. https://doi.org/10.1128/jb.178.8.2402-2408.1996

López-García P, Zivanovic Y, Deschamps P, Moreira D (2015) Bacterial gene import and mesophilic adaptation in archaea. Nature Rev Microbiol 13:447–456. https://doi.org/10.1038/nrmicro3485

Lopez-Fernandez M, Broman E, Turner S et al (2018) Investigation of viable taxa in the deep terrestrial biosphere suggests high rates of nutrient recycling. FEMS Microbiol Ecol 94:fiy121. https://doi.org/10.1093/femsec/fiy121

Lovley DR, Malvankar NS (2015) Seeing is believing: novel imaging techniques help clarify microbial nanowire structure and function. Environ Microbiol 17:2209–2215. https://doi.org/10.1111/1462-2920.12708

Lovley DR, Phillips EJ (1988) Novel mode of microbial energy metabolism: organic carbon oxidation coupled to dissimilatory reduction of iron or manganese. Appl Environ Microbiol 54:1472–1480. https://doi.org/10.1128/aem.54.6.1472-1480.1988

Lücker S, Wagner M, Maixner F et al (2010) *Nitrospira* metagenome illuminates the physiology and evolution of globally important nitrite-oxidizing bacteria. Proc Natl Acad Sci U S A 107(30):13479–13484. doi: https://doi.org/10.1073/pnas.1003860107

Ludvík J, Benada O, Mikuh'k K (1994) Ultrastructure of an extreme thermophilic hydrogen-oxidizing bacterium *Calderobacterium hydrogenophilum*. Arch Microbiol 162:267–271

Luther GW, Rozan TF, Taillefert M et al (2001) Chemical speciation drives hydrothermal vent ecology. Nature 410:813–816. https://doi.org/10.1038/35071069

Lütke-Eversloh T, Elbanna K, Cnockaert MC et al (2004) *Caenibacterium thermophilum* is a later synonym of *Schlegelella thermodepolymerans*. Int J Syst Evol Microbiol 54:1933–1935. doi: https://doi.org/10.1099/ijs.0.63204-0

Manaia CM, da Costa MS (1991) Characterization of halotolerant *Thermus* isolates from shallow marine hot springs on S. Miguel, Azores. Microbiology 137:2643–2648. https://doi.org/10.1099/00221287-137-11-2643

Manaia CM, Hoste B, Carmen Gutierrez M et al (1995) Halotolerant *Thermus* strains from marine and terrestrial hot springs belong to *Thermus thermophilus* (ex Oshima and Imahori, 1974) nom. Rev. emend. Syst Appl Microbiol 17:526–532. https://doi.org/10.1016/S0723-2020(11)80072-X

Mardanov AV, Kadnikov VV, Beletsky AV et al (2020) Sulfur and methane-oxidizing microbial community in a terrestrial mud volcano revealed by metagenomics. Microorganisms 8(9):1333. https://doi.org/10.3390/microorganisms8091333

Marteinsson VT (1999) Isolation and characterization of *Thermus thermophilus* Gy1211 from a deep-sea hydrothermal vent. Extremophiles 3:247–251. https://doi.org/10.1007/s007920050123

Martens-Habbena W, Stahl DA (2011) Nitrogen metabolism and kinetics of ammonia-oxidizing archaea. Meth Enzymol 496:465–487. https://doi.org/10.1016/B978-0-12-386489-5.00019-1

Masuda Y, Itoh H, Shiratori Y et al (2017) Predominant but previously-overlooked prokaryotic drivers of reductive nitrogen transformation in Paddy soils, revealed by Metatranscriptomics. Microbes Environ 32:180–183. https://doi.org/10.1264/jsme2.ME16179

McGonigle JM, Lang SQ, Brazelton WJ (2020) Genomic evidence for formate metabolism by Chloroflexi as the key to unlocking deep carbon in lost City microbial ecosystems. Appl Environ Microbiol 86:e02583–e02519. https://doi.org/10.1128/AEM.02583-19

McNichol J, Stryhanyuk H, Sylva SP et al (2018) Primary productivity below the seafloor at deep-sea hot springs. Proc Natl Acad Sci U S A 115:6756–6761. https://doi.org/10.1073/pnas.1804351115

Mehrani MJ, Sobotka D, Kowal P et al (2020) The occurrence and role of *Nitrospira* in nitrogen removal systems. Bioresour Technol 303:122936. https://doi.org/10.1016/j.biortech.2020.122936

Ming Y-Z, Liu L, Lv A-P et al (2021) *Thermaurantiacus tibetensis* gen. nov., sp. nov., a novel moderately thermophilic bacterium isolated from hot spring microbial mat in Tibet. Antonie Van Leeuwenhoek 114:445–455. https://doi.org/10.1007/s10482-021-01530-w

Mino S, Makita H, Toki T et al (2013) Biogeography of *Persephonella* in deep-sea hydrothermal vents of the Western Pacific. Front Microbiol 4:107. https://doi.org/10.3389/fmicb.2013.00107

Mino S, Nakagawa S, Makita H et al (2017) Endemicity of the cosmopolitan mesophilic chemolithoautotroph Sulfurimonas at deep-sea hydrothermal vents. ISME J 11:909–919. https://doi.org/10.1038/ismej.2016.178

Mino S, Yoneyama N, Nakagawa S et al (2018) Enrichment and genomic characterization of a N_2O-reducing Chemolithoautotroph from a Deep-Sea hydrothermal vent. Front Bioeng Biotechnol 6:184. https://doi.org/10.3389/fbioe.2018.00184

Minz D, Flax JL, Green SJ et al (1999) Diversity of sulfate-reducing bacteria in oxic and anoxic regions of a microbial mat characterized by comparative analysis of dissimilatory sulfite reductase genes. Appl Environ Microbiol 65:4666–4671. https://doi.org/10.1128/AEM.65.10.4666-4671.1999

Miranda-Tello E, Fardeau M-L, Joulian C et al (2007) *Petrotoga halophila* sp. nov., a thermophilic, moderately halophilic, fermentative bacterium isolated from an offshore oil well in Congo. Int J Syst Evol Microbiol 57:40–44. https://doi.org/10.1099/ijs.0.64516-0

Miroshnichenko ML, Slobodkin AI, Kostrikina NA et al (2003) *Deferribacter abyssi* sp. nov., an anaerobic thermophile from deep-sea hydrothermal vents of the Mid-Atlantic Ridge. Int J Syst Evol Microbiol 53:1637–1641. https://doi.org/10.1099/ijs.0.02673-0

Miranda-Tello E, Fardeau M-L, Thomas P et al (2004) *Petrotoga mexicana* sp. nov., a novel thermophilic, anaerobic and xylanolytic bacterium isolated from an oil-producing well in the Gulf of Mexico. Int J Syst Evol Microbiol 54:169–174. https://doi.org/10.1099/ijs.0.02702-0

Miroshnichenko ML, Lebedinsky AV, Chernyh NA et al (2009) *Caldimicrobium rimae* gen. nov., sp. nov., an extremely thermophilic, facultatively lithoautotrophic, anaerobic bacterium from the Uzon caldera, Kamchatka. Int J Syst Evol Microbiol 59:1040–1044. https://doi.org/10.1099/ijs.0.006072-0

Miyazaki J, Ikuta T, Watsuji T et al (2020) Dual energy metabolism of the Campylobacterota endosymbiont in the chemosynthetic snail Alviniconcha Marisindica. ISME J 14(5):1273–1289. https://doi.org/10.1038/s41396-020-0605-7

Mori K, Sakurai K, Hosoyama A et al (2020) Vestiges of adaptation to the mesophilic environment in the genome of *Tepiditoga spiralis* gen. nov., sp. nov. Microbes Environ 35:ME20046. https://doi.org/10.1264/jsme2.ME20046

Mori K, Suzuki K (2008) *Thiofaba tepidiphila* gen. nov., sp. nov., a novel obligately chemolithoautotrophic, sulfur-oxidizing bacterium of the Gammaproteobacteria isolated from a hot spring. Int J Syst Evol Microbiol 58:1885–1891. https://doi.org/10.1099/ijs.0.65754-0

Mori K (2014) The family Thermodesulfobacteriaceae. In: Rosenberg E, DeLong EF, Lory S et al (eds) The prokaryotes: firmicutes and Tenericutes. Springer, Berlin, pp 381–388

Moussard H, L'Haridon S, Tindall BJ et al (2004) *Thermodesulfatator indicus* gen. nov., sp. nov., a novel thermophilic chemolithoautotrophic sulfate-reducing bacterium isolated from the central Indian ridge. Int J Syst Evol Microbiol 54:227–233. https://doi.org/10.1099/ijs.0.02669-0

Nakagawa S, Takai K, Horikoshi K et al (2004b) *Aeropyrum camini* sp. nov., a strictly aerobic, hyperthermophilic archaeon from a deep-sea hydrothermal vent chimney. Int J Syst Evol Microbiol 54, 329–335. doi: https://doi.org/10.1099/ijs.0.02826-0

Nakagawa S, Inagaki F, Takai K et al (2005a) '*Thioreductor micantisoli* gen. nov., sp. nov., a novel mesophilic, Sulfur-reducing Chemolithoautotroph within the ε-proteobacteria isolated from

hydrothermal sediments in the mid-Okinawa trough'. Int J Syst Evol Microbiol 55(2):599–605. https://doi.org/10.1099/ijs.0.63351-0

Nakagawa S, Nakamura S, Inagaki F et al (2004a) *Hydrogenivirga caldilitoris* gen. nov., sp. nov., a novel extremely thermophilic, hydrogen- and sulfur-oxidizing bacterium from a coastal hydrothermal field. Int J Syst Evol Microbiol 54:2079–2084. https://doi.org/10.1099/ijs.0.03031-0

Nakagawa S, Takai K, Horikoshi K et al (2003) *Persephonella hydrogeniphila* sp. nov., a novel thermophilic, hydrogen-oxidizing bacterium from a deep-sea hydrothermal vent chimney. Int J Syst Evol Microbiol 53:863–869. https://doi.org/10.1099/ijs.0.02505-0

Nakagawa S, Takai K, Inagaki F et al (2005b) *Nitratiruptor tergarcus* gen. nov., sp. nov. and *Nitratifractor salsuginis* gen. nov., sp. nov., nitrate-reducing chemolithoautotrophs of the epsilon-proteobacteria isolated from a deep-sea hydrothermal system in the mid-Okinawa trough. Int J Syst Evol Microbiol 55:925–933. https://doi.org/10.1099/ijs.0.63480-0

Nakagawa S, Takaki Y, Shimamura S et al (2007) Deep-sea vent epsilon-proteobacterial genomes provide insights into emergence of pathogens. Proc Natl Acad Sci U S A 104:12146–12150. https://doi.org/10.1073/pnas.0700687104

Nakagawa S, Takaki Y (2009) Nonpathogenic epsilonproteobacteria. In: Cullen KE (ed) Encyclopedia of life sciences. Wiley. https://doi.org/10.1002/047001590X

Nakagawa T, Takai K, Suzuki Y et al (2006) Geomicrobiological exploration and characterization of a novel deep-sea hydrothermal system at the TOTO caldera in the Mariana volcanic arc. Environ Microbiol 8:37–49. https://doi.org/10.1111/j.1462-2920.2005.00884.x

Nelson KE, Clayton RA, Gill SR et al (1999) Evidence for lateral gene transfer between archaea and bacteria from genome sequence of *Thermotoga maritima*. Nature 399(6734):323–329. https://doi.org/10.1038/20601

Nesbø C, Farrell AA, Zhaxybayeva O et al (2022) Thermosipho. In: Trujillo ME, Dedysh S, DeVos P, Hedlund B, Kämpfer P, Rainey FA, Whitman WB (eds) Bergey's manual of systematics of archaea and bacteria. Wiley. https://doi.org/10.1002/9781118960608.gbm01272.pub2

Nesbø CL, Bradnan DM, Adebusuyi A et al (2012*) Mesotoga prima* gen. nov., sp. nov., the first described mesophilic species of the Thermotogales. Extremophiles 16:387–393. https://doi.org/10.1007/s00792-012-0437-0

Nesbø CL, Farrell AA, Zhaxybayeva O et al (2019) Thermotoga. In: Trujillo ME, Dedysh S, DeVos P, Hedlund B, Kämpfer P, Rainey FA, Whitman WB (eds) Bergey's manual of systematics of archaea and bacteria. Wiley, pp 1–13. https://doi.org/10.1002/9781118960608.gbm01273.pub2

Nishihara H, Igarashi Y, Kodama T (1990) A new isolate of *Hydrogenobacter*, an obligately chemolithoautotrophic, thermophilic, halophilic and aerobic hydrogen-oxidizing bacterium from seaside saline hot spring. Arch Microbiol 153:294–298. https://doi.org/10.1007/BF00249085

Nishizawa M, Sakai S, Konno U et al (2016) Nitrogen and oxygen isotope effects of ammonia oxidation by thermophilic Thaumarchaeota from a geothermal water stream. Appl Environ Microbiol 82:4492–4504. https://doi.org/10.1128/AEM.00250-16

Nunn CE, Johnsen U, Schönheit P et al (2010) Metabolism of pentose sugars in the hyperthermophilic archaea *Sulfolobus solfataricus* and *Sulfolobus acidocaldarius*. J Biol Chem 285:33701–33709. https://doi.org/10.1074/jbc.M110.146332

Nunoura T, Hirai M, Imachi H et al (2010) *Kosmotoga arenicorallina* sp. nov. a thermophilic and obligately anaerobic heterotroph isolated from a shallow hydrothermal system occurring within a coral reef, southern part of the Yaeyama archipelago, Japan, reclassification of *Thermococcoides shengliensis* as *Kosmotoga shengliensis* comb. nov., and emended description of the genus Kosmotoga. Arch Microbiol 192:811–819. https://doi.org/10.1007/s00203-010-0611-7

Nunoura T, Hirai M, Miyazaki M et al (2013) Isolation and characterization of a thermophilic, obligately anaerobic and heterotrophic marine Chloroflexi bacterium from a Chloroflexi-dominated microbial community associated with a Japanese shallow hydrothermal system,

and proposal for Thermomarinili. Microbes Environ 28:228–235. https://doi.org/10.1264/jsme2.me12193

Nunoura T, Miyazaki M, Suzuki Y et al (2008a) *Hydrogenivirga okinawensis* sp. nov., a thermophilic sulfur-oxidizing chemolithoautotroph isolated from a deep-sea hydrothermal field, southern Okinawa trough. Int J Syst Evol Microbiol 58:676–681. https://doi.org/10.1099/ijs.0.64615-0

Nunoura T, Oida H, Miyazaki M et al (2007) *Marinitoga okinawensis* sp. nov., a novel thermophilic and anaerobic heterotroph isolated from a deep-sea hydrothermal field, southern Okinawa trough. Int J Syst Evol Microbiol 57:467–471. https://doi.org/10.1099/ijs.0.64640-0

Nunoura T, Oida H, Miyazaki M et al (2008b) *Thermosulfidibacter takaii* gen. nov., sp. nov., a thermophilic, hydrogen-oxidizing, sulfur-reducing chemolithoautotroph isolated from a deep-sea hydrothermal field in the southern Okinawa trough. Int J Syst Evol Microbiol 58:659–665. https://doi.org/10.1099/ijs.0.65349-0

Off S, Alawi M, Spieck E (2010) Enrichment and physiological characterization of a novel *Nitrospira*-like bacterium obtained from a marine sponge. Appl Environ Microbiol 76(14):4640–4646. https://doi.org/10.1128/AEM.00320-10

Offre P, Spang A, Schleper C (2013) Archaea in biogeochemical cycles. Annu Rev Microbiol 67:437–457. https://doi.org/10.1146/annurev-micro-092412-155614

Okumura T, Takashima C, Yanagawa K et al (2022) Stromatolite formation by Anaerolineae-dominated microbial communities in hot spring travertine in North Sumatra, Indonesia. Sediment Geol 440:106263. https://doi.org/10.1016/j.sedgeo.2022.106263

Onyenwoke RU, Wiegel J (2015) *Thermoanaerobacterium*. In: Trujillo ME, Dedysh S, DeVos P, Hedlund B, Kämpfer P, Rainey FA, Whitman WB (eds) Bergey's manual of systematics of archaea and bacteria. Wiley. https://doi.org/10.1002/9781118960608.gbm00755

Oren A, Garrity GM (2021) Valid publication of the names of forty-two phyla of prokaryotes. Int J Syst Evol Microbiol 71:005056. https://doi.org/10.1099/ijsem.0.005056

Oren A, Xu X-W (2014) The family Hyphomicrobiaceae. In: Rosenberg E, DeLong EF, Lory S et al (eds) The prokaryotes: Alphaproteobacteria and betaproteobacteria. Springer, Berlin, pp 247–281

Oshima T, Imahori K (1971) Isolation of an extreme thermophile and thermostability of its transfer ribonucleic acid and ribosomes. J Gen Appl Microbiol 17:513–517. https://doi.org/10.2323/jgam.17.513

Oshima T, Imahori K (1974) Description of *Thermus thermophilus* (Yoshida and Oshima) comb. nov., a nonsporulating thermophilic bacterium from a Japanese thermal spa. Int J Syst Bacteriol 24:102–112. https://doi.org/10.1099/00207713-24-1-102

Overmann J, Tuschak C (1997) Phylogeny and molecular fingerprinting of Green Sulfur bacteria. Arch Microbiol 167:302–309. https://doi.org/10.1007/s002030050448

O'Neill AH, Liu Y, Ferrera I et al (2008) *Sulfurihydrogenibium rodmanii* sp. nov., a sulfur-oxidizing chemolithoautotroph from the Uzon caldera, Kamchatka peninsula, Russia, and emended description of the genus *Sulfurihydrogenibium*. Int J Syst Evol Microbiol 58:1147–1152. https://doi.org/10.1099/ijs.0.65431-0

Palomo A, Dechesne A, Pedersen AG et al (2022) Genomic profiling of *Nitrospira* species reveals ecological success of comammox *Nitrospira*. Microbiome 10(1):204. https://doi.org/10.1186/s40168-022-01411-y

Papale M, Romano I, Finore I et al (2021) Prokaryotic diversity of the composting thermophilic phase: the case of ground coffee compost. Microorganisms 9:218. https://doi.org/10.3390/microorganisms9020218

Parte AC, Sardà Carbasse J, Meier-Kolthoff JP et al (2020) List of prokaryotic names with standing in nomenclature (LPSN) moves to the DSMZ. Int J Syst Evol Microbiol 70:5607–5612. https://doi.org/10.1099/ijsem.0.004332

Pask-Hughes RA, Williams RAD (1977) Yellow-pigmented strains of *Thermus* spp. from Icelandic hot springs. Microbiology 102:375–383. https://doi.org/10.1099/00221287-102-2-375

Patel BKC, Morgan HW, Daniel RM (1985) *Fervidobacterium nodosum* gen. nov. and spec. nov., a new chemoorganotrophic, caldoactive, anaerobic bacterium. Arch Microbiol 141:63–69. https://doi.org/10.1007/BF00446741

Perez-Rodríguez I, Grosche A, Massenburg L et al (2012) *Phorcysia thermohydrogeniphila* gen. nov., sp. nov., a thermophilic, chemolithoautotrophic, nitrate-ammonifying bacterium from a deep-sea hydrothermal vent. Int J Syst Evol Microbiol 62:2388–2394. https://doi.org/10.1099/ijs.0.035642-0

Pesaro M, Widmer F (2002) Identification of novel Crenarchaeota and Euryarchaeota clusters associated with different depth layers of a forest soil. FEMS Microbiol Ecol 42:89–98. https://doi.org/10.1111/j.1574-6941.2002.tb00998.x

Pester M, Schleper C, Wagner M (2011) The Thaumarchaeota: an emerging view of their phylogeny and ecophysiology. Curr Op Microbiol 14:300–306. https://doi.org/10.1016/j.mib.2011.04.007

Pierson BK, Castenholz RW (1974) A phototrophic gliding filamentous bacterium of hot springs, *Chloroflexus aurantiacus*, gen. and sp. nov. Arch Microbiol 100:5–24. https://doi.org/10.1007/BF00446302

Pierson BK, Giovannoni SJ, Stahl DA et al (1985) *Heliothrix oregonensis*, gen. nov., sp. nov., a phototrophic filamentous gliding bacterium containing bacteriochlorophyll a. Arch Microbiol 142:164–167. https://doi.org/10.1007/BF00447061

Podosokorskaya O, Kadnikov VV, Gavrilov SN et al (2013) Characterization of Melioribacter roseus gen. nov., sp. nov., a novel facultatively anaerobic thermophilic cellulolytic bacterium from the class Ignavibacteria, and a proposal of a novel bacterial phylum Ignavibacteriae. Environ Microbiol 15:1759–1771. https://doi.org/10.1111/1462-2920.12067

Pohl A, Young SAE, Schmitz TC et al (2021) Magnetite-binding proteins from the magnetotactic bacterium *Desulfamplus magnetovallimortis* BW-1. Nanoscale 13:20396–20400. https://doi.org/10.1039/d1nr04870h

Pollo SMJ, Adebusuyi AA, Straub TJ et al (2017) Genomic insights into temperature-dependent transcriptional responses of *Kosmotoga olearia*, a deep-biosphere bacterium that can grow from 20 to 79 °C. Extremophiles 21:963–979. https://doi.org/10.1007/s00792-017-0956-9

Pommier Y (2009) DNA topoisomerase I inhibitors: chemistry, biology, and interfacial inhibition. Chem Rev 109:2894–2902. https://doi.org/10.1021/cr900097c

Postec A, Le Breton C, Fardeau M-L et al (2005) *Marinitoga hydrogenitolerans* sp. nov., a novel member of the order Thermotogales isolated from a black smoker chimney on the mid-Atlantic ridge. Int J Syst Evol Microbiol 55:1217–1221. https://doi.org/10.1099/ijs.0.63550-0

Postec A, Ciobanu M, Birrien J-L et al (2010) *Marinitoga litoralis* sp. nov., a thermophilic, heterotrophic bacterium isolated from a coastal thermal spring on Ile Saint-Paul, southern Indian Ocean. Int J Syst Evol Microbiol 60:1778–1782. https://doi.org/10.1099/ijs.0.017574-0

Prieto MA, Escapa IF, Martínez VV et al (2014) A holistic view of polyhydroxyalkanoate metabolism in pseudomonas putida. Environ Microbiol 18(2):341–357. https://doi.org/10.1111/1462-2920.12760

Purwasena IA, Sugai Y, Sasaki K (2014) *Petrotoga japonica* sp. nov., a thermophilic, fermentative bacterium isolated from Yabase oilfield in Japan. Arch Microbiol 196:313–321. https://doi.org/10.1007/s00203-014-0972-4

Quehenberger J, Shen L, Albers SV et al (2017) Sulfolobus – a potential Key organism in future biotechnology. Front Microbiol 8. https://www.frontiersin.org/articles/10.3389/fmicb.2017.02474. Accessed 7 Apr 2023

Rainey FA, da Costa MS (2001) Order II. Thermales Ord. Nov. In: Garrity GM, Boone DR, Castenholz RW (eds) Bergey's manual of systematic bacteriology, Volume one: the archaea and the deeply branching and phototrophic bacteria, 2nd edn. Springer, New York, p 403

Rainey FA, Ray K, Ferreira M et al (2005) Extensive diversity of ionizing-radiation-resistant bacteria recovered from Sonoran Desert soil and description of nine new species of the genus *Deinococcus* obtained from a single soil sample. Appl Environ Microbiol 71:5225–5235. https://doi.org/10.1128/AEM.71.9.5225-5235.2005

Rainey FA, Silva J, Nobre MF et al (2003) *Porphyrobacter cryptus* sp. nov., a novel slightly thermophilic, aerobic, bacteriochlorophyll a-containing species. Int J Syst Evol Microbiol 53: 35–41. https://doi.org/10.1099/ijs.0.02308-0

Rainey FA (2015) Caldicellulosiruptor. In: Trujillo ME, Dedysh S, Devos P, Hedlund B, Kämpfer P, Rainey FA, Whitman WB (eds) Bergey's manual of systematics of archaea and bacteria. Wiley. https://doi.org/10.1002/9781118960608.gbm00754

Rainey FA, Donnison AM, Janssen PH et al (1994) Description of *Caldicellulosiruptor saccharolyticus* gen. nov., sp. nov: an obligately anaerobic, extremely thermophilic, cellulolytic bacterium. FEMS Microbiol Lett 120:263–266. https://doi.org/10.1016/0378-1097(94)90481-2

Rangel AE, Croft T, González Barrios AF et al (2020) Transcriptomic analysis of a *Clostridium thermocellum* strain engineered to utilize xylose: responses to xylose versus cellobiose feeding. Sci Rep 10(1):14517. https://doi.org/10.1038/s41598-020-71428-6

Raman B, McKeown CK, Rodriguez M et al (2011) Transcriptomic analysis of *Clostridium thermocellum* ATCC 27405 cellulose fermentation. BMC Microbiol 11:134. https://doi.org/10.1186/1471-2180-11-134

Ravot G, Magot M, Fardeau ML et al (1995) *Thermotoga elfii* sp. nov., a novel thermophilic bacterium from an African oil-producing well. Int J Syst Bacteriol 45:308–314. https://doi.org/10.1099/00207713-45-2-308

Reeve W, Ardley J, Tian R et al (2014) Genome sequence of the Listia angolensis microsymbiont *Microvirga lotononidis* strain WSM3557(T). Stand Genomic Sci 9:540–550. 10.4056/sigs.4548266 WE - science citation index expanded (SCI-EXPANDED)

Reichenbach H (1999) The ecology of the myxobacteria. Environ Microbiol 1:15–21. https://doi.org/10.1046/j.1462-2920.1999.00016.x

Ren N, Cao G, Wang A et al (2008) Dark fermentation of xylose and glucose mix using isolated *Thermoanaerobacterium thermosaccharolyticum* W16. Int J Hydro Energy 33(21):6124–6132. https://doi.org/10.1016/j.ijhydene.2008.07.107

Reno ML, Held NL, Fields CJ et al (2009) Biogeography of the *Sulfolobus islandicus* pan-genome. Proc Natl Acad Sci U S A 106:8605–8610. https://doi.org/10.1073/pnas.0808945106

Reysenbach A-L, Liu Y, Lindgren AR et al (2013) *Mesoaciditoga lauensis* gen. nov., sp. nov., a moderately thermoacidophilic member of the order Thermotogales from a deep-sea hydrothermal vent. Int J Syst Evol Microbiol 63:4724–4729. https://doi.org/10.1099/ijs.0.050518-0

Reysenbach AL (2015) Thermotogae class. nov. In: Trujillo ME, Dedysh S, Devos P et al (eds) Bergey's manual of systematics of archaea and bacteria. Wiley. https://doi.org/10.1002/9781118960608.cbm00051

Robertson BR, O'Rourke JL, Neilan BA et al (2005) *Mucispirillum schaedleri* gen. nov., sp. nov., a spiral-shaped bacterium colonizing the mucus layer of the gastrointestinal tract of laboratory rodents. Int J Syst Evol Microbiol 55:1199–1204. https://doi.org/10.1099/ijs.0.63472-0

Rogers TJ, Buongiorno J, Jessen GL et al (2023) Chemolithoautotroph distributions across the subsurface of a convergent margin. ISME J 17:140–150. https://doi.org/10.1038/s41396-022-01331-7

Romano I, Dipasquale L, Orlando P et al (2010) *Thermoanaerobacterium thermostercus* sp., nov, a new anaerobic thermophilic hydrogen-producing bacterium from buffalo-dung. Extremophiles 14(2):233–240. Doi:https://doi.org/10.1007/s00792-010-0303-x

Roy C, BAkshi U, Rameez MJ et al (2019) Phylogenomics of an uncultivated, aerobic and thermophilic, photoheterotrophic member of chlorobia sheds light into the evolution of the phylum chlorobi. Comput Biol Chem 80:206–216. https://doi.org/10.1016/j.compbiolchem.2019.04.001

Royter M, Schmidt M, Elend C et al (2009) Thermostable lipases from the extreme thermophilic anaerobic bacteria *Thermoanaerobacter thermohydrosulfuricus* SOL1 and *Caldanaerobacter subterraneus* subsp. tengcongensis. Extremophiles 13:769–783. https://doi.org/10.1007/s00792-009-0265-z

Russell MJ, Hall AJ (1997) The emergence of life from iron Monosulphide bubbles at a submarine hydrothermal redox and PH front. J Geol Soc 154(3):377–402. https://doi.org/10.1144/gsjgs.154.3.0377

Saghatelyan A, Margaryan A, Panosyan H, Birkeland NK (2021) Microbial diversity of terrestrial geothermal springs in Armenia and Nagorno-Karabakh: a review. Microorganisms 9:1473. https://doi.org/10.3390/microorganisms9071473

Salama NR (2020) Cell morphology as a virulence determinant: lessons from helicobacter pylori. Curr Opin Microbiol 54:11–17. https://doi.org/10.1016/j.mib.2019.12.002

Sander K, Wilson C, Rodriguez M et al (2015) *Clostridium thermocellum* DSM1313 transcriptional responses to redox perturbation. Biotechnol Biofuels 8(1). doi:https://doi.org/10.1186/s13068-015-0394-9

Sant'Anna FH, Lebedinsky AV, Sokolova TG et al (2015) Analysis of three genomes within the thermophilic bacterial species *Caldanaerobacter subterraneus* with a focus on carbon monoxide dehydrogenase evolution and hydrolase diversity. BMC Genomics 16:757. https://doi.org/10.1186/s12864-015-1955-9

Santos MA, Williams RAD, Da Costa MS (1989) Numerical taxonomy of *Thermus* isolates from hot springs in Portugal. Syst Appl Microbiol 12:310–315. https://doi.org/10.1016/S0723-2020(89)80079-7

Schleper C, Nicol GW (2010) Ammonia-oxidising archaea - physiology, ecology and evolution. Adv Microb Physiol 57:1–41. https://doi.org/10.1016/B978-0-12-381045-8.00001-1

Schleper C, Puehler G, Klenk H-P et al (1996) *Picrophilus oshimae* and *Picrophilus torridus* fam. nov., gen. nov., sp. nov., two species of Hyperacidophilic, thermophilic, heterotrophic, aerobic archaea. Int J Syst Evol Microbiol 46:814–816. https://doi.org/10.1099/00207713-46-3-814

Schoch CL, Ciufo S, Domrachev M et al (2020) NCBI Taxonomy: a comprehensive update on curation, resources and tools, Database, Volume 2020, 2020, baaa062, https://doi.org/10.1093/database/baaa062

Schönheit P, Schäfer T (1995) Metabolism of hyperthermophiles. World J Microbiol Biotechnol 11:26–57. https://doi.org/10.1007/BF00339135

Scully SM, Orlygsson J (2014) Branched-chain alcohol formation from branched-chain amino acids by *Thermoanaerobacter brockii* and *Thermoanaerobacter yonseiensis*. Anaerobe 30:82–84. https://doi.org/10.1016/j.anaerobe.2014.09.003

Segerer A, Langworthy TA, Stetter KO (1988) *Thermoplasma acidophilum* and *Thermoplasma volcanium* sp. nov. from solfatara Fields. Syst Appl Microbiol 10:161–171. https://doi.org/10.1016/S0723-2020(88)80031-6

Sekiguchi Y, Yamada T, Hanada S et al (2003) *Anaerolinea thermophila* gen. nov., sp. nov. and *Caldilinea aerophila* gen. nov., sp. nov., novel filamentous thermophiles that represent a previously uncultured lineage of the domain bacteria at the subphylum level. Int J Syst Evol Microbiol 53:1843–1851. https://doi.org/10.1099/ijs.0.02699-0

Sekiguchi Y, Muramatsu M, Imachi H et al (2008) *Thermodesulfovibrio aggregans* sp. nov. and *Thermodesulfovibrio thiophilus* sp. nov., anaerobic, thermophilic, sulfate-reducing bacteria isolated from thermophilic methanogenic sludge, and emended description of the genus *Thermodesulfovibrio*. Int J Syst Evol Microbiol 58(11):2541–2548. doi: https://doi.org/10.1099/ijs.0.2008/000893-0

Selkova P, Vasileva A, Pobegalov G et al (2020) Position of deltaproteobacteria Cas12e nuclease cleavage sites depends on spacer length of guide RNA. RNA Biol 17:1472–1479. https://doi.org/10.1080/15476286.2020.1777378

Seong CN, Kang JW, Lee JH et al (2018) Taxonomic hierarchy of the phylum firmicutes and novel firmicutes species originated from various environments in Korea. J Microbiol 56(1):1–10. https://doi.org/10.1007/s12275-018-7318-x

Seyler LM, Trembath-Reichert E, Tully BJ et al (2021) Time-series transcriptomics from cold, oxic subseafloor crustal fluids reveals a motile, mixotrophic microbial community. ISME J 15:1192–1206. https://doi.org/10.1038/s41396-020-00843-4

Sharma N, Kumar J, Abedin MM et al (2020) Metagenomics revealing molecular profiling of community structure and metabolic pathways in natural hot springs of the Sikkim Himalaya. BMC Microbiol 20:246. https://doi.org/10.1186/s12866-020-01923-3

Shaw AJ, Podkaminer KK, Desai SG et al (2008) Metabolic engineering of a thermophilic bacterium to produce ethanol at high yield. Proc Natl Acad Sci U S A 105:13769–13774

Sheik CS, Anantharaman K, Breier JA et al (2015) Spatially resolved sampling reveals dynamic microbial communities in rising hydrothermal plumes across a back-arc basin. ISME J 9:1434–1445. https://doi.org/10.1038/ismej.2014.228

Shima S, Suzuki K-I (1993) *Hydrogenobacter acidophilus* sp. nov., a Thermoacidophilic, aerobic, hydrogen-oxidizing bacterium requiring elemental Sulfur for growth. Int J Syst Bacteriol 43:703–708. https://doi.org/10.1099/00207713-43-4-703

Shiotani T, Mino S, Sato W et al (2020) *Nitrosophilus alvini* gen. nov., sp. nov., a hydrogen-oxidizing chemolithoautotroph isolated from a deep-sea hydrothermal vent in the East Pacific rise, inferred by a genome-based taxonomy of the phylum "Campylobacterota". PLoS One 15:e0241366. https://doi.org/10.1371/journal.pone.0241366

Siebers B, Schönheit P (2005) Unusual pathways and enzymes of central carbohydrate metabolism in archaea. Curr Opin Microbiol 8:695–705. https://doi.org/10.1016/j.mib.2005.10.014

Siebert J, Hirsch P (1988) Characterization of 15 selected coccal bacteria isolated from antarctic rock and soil samples from the McMurdo-dry valleys (South-Victoria land). Polar Biol 9:37–44. https://doi.org/10.1007/BF00441762

Singleton CM, Petriglieri F, Kristensen JM et al (2021) Connecting structure to function with the recovery of over 1000 high-quality metagenome-assembled genomes from activated sludge using long-read sequencing. Nat Commun 12:2009. https://doi.org/10.1038/s41467-021-22203-2

Si Y, Zou Y, Liu X et al (2015) Mercury methylation coupled to iron reduction by dissimilatory iron-reducing bacteria. Chemosphere 122:206–212. https://doi.org/10.1016/j.chemosphere.2014.11.054

Skirnisdottir S, Hreggvidsson GO, Holst O et al (2001) Isolation and characterization of a mixotrophic sulfur-oxidizing *Thermus scotoductus*. Extremophiles 5:45–51. https://doi.org/10.1007/s007920000172

Slade D, Radman M (2011) Oxidative stress resistance in *Deinococcus radiodurans*. Microbiol Mol Biol Rev 75:133–191. https://doi.org/10.1128/MMBR.00015-10

Slobodkina GB, Kolganova TV, Chernyh NA, Querellou J, Bonch-Osmolovskaya EA, Slobodkin AI (2009) *Deferribacter autotrophicus* sp. nov., an iron (III)-reducing bacterium from a deep-sea hydrothermal vent. Int J Syst Evol Microbiol 59:1508–1512. https://doi.org/10.1099/ijs.0.006767-0

Slobodkina GB, Kolganova T V, Kopitsyn DS et al (2016) *Dissulfurirhabdus thermomarina* gen. nov., sp. nov., a thermophilic, autotrophic, sulfite-reducing and disproportionating deltaproteobacterium isolated from a shallow-sea hydrothermal vent. Int J Syst Evol Microbiol 66:2515–2519. https://doi.org/10.1099/ijsem.0.001083

Slobodkin AI, Reysenbach A-L, Slobodkina GB et al (2012) *Thermosulfurimonas dismutans* gen. nov., sp. nov., an extremely thermophilic sulfur-disproportionating bacterium from a deep-sea hydrothermal vent. Int J Syst Evol Microbiol 62:2565–2571. https://doi.org/10.1099/ijs.0.034397-0

Slobodkin AI, Reysenbach A-L, Slobodkina GB et al (2013) *Dissulfuribacter thermophilus* gen. nov., sp. nov., a thermophilic, autotrophic, sulfur-disproportionating, deeply branching deltaproteobacterium from a deep-sea hydrothermal vent. Int J Syst Evol Microbiol 63:1967–1971. https://doi.org/10.1099/ijs.0.046938-0

Slobodkin A, Slobodkina G, Allioux M et al (2019) Genomic insights into the carbon and energy metabolism of a thermophilic deep-sea bacterium *Deferribacter autotrophicus* revealed new metabolic traits in the phylum Deferribacteres. Genes 10:849. https://doi.org/10.3390/genes10110849

Sonne-Hansen J, Ahring BK (1999) *Thermodesulfobacterium hveragerdense* sp. nov., and *Thermodesulfovibrio islandicus* sp. nov., two thermophilic sulfate reducing bacteria isolated from a Icelandic hot spring. Syst Appl Microbiol 22:559–564. https://doi.org/10.1016/S0723-2020(99)80009-5

Soo RM, Skennerton CT, Sekiguchi Y et al (2014) An expanded genomic representation of the phylum cyanobacteria. Genome Biol Evol 6(5):1031–1045. https://doi.org/10.1093/gbe/evu073

Sorokin DY, Tourova TP, Mussmann M et al (2008) *Dethiobacter alkaliphilus* gen. nov. sp. nov., and *Desulfurivibrio alkaliphilus* gen. nov. sp. nov.: two novel representatives of reductive sulfur cycle from soda lakes. Extremophiles 12:431–439. https://doi.org/10.1007/s00792-008-0148-8

Spasov E, Tsuji JM, Hug LA et al (2020) High functional diversity among *Nitrospira* populations that dominate rotating biological contactor microbial communities in a municipal wastewater treatment plant. ISME J 14(7):1857–1872. https://doi.org/10.1038/s41396-020-0650-2

Stahl DA, De La Torre JR (2012) Physiology and diversity of ammonia-oxidizing archaea. Annu Rev Microbiol 66:83–101. https://doi.org/10.1146/annurev-micro-092611-150128

Stepanov VG, Vaishampayan P, Venkateswaran K et al (2014) Draft genome sequence of *Deinococcus phoenicis*, a novel strain isolated during the Phoenix Lander spacecraft assembly. Genome Announc 2:e00301–e00314. https://doi.org/10.1128/genomeA.00301-14

Stöhr R, Waberski A, Völker H, Tindall BJ, Thomm M (2001) *Hydrogenothermus marinus* gen. nov., sp. nov., a novel thermophilic hydrogen-oxidizing bacterium, recognition of *Calderobacterium hydrogenophilum* as a member of the genus *Hydrogenobacter* and proposal of the reclassification of *Hydrogenobacter acidophilus* as *Hydrogenobaculum acidophilum* gen. nov., comb. nov., in the phylum'Hydrogenobacter/Aquifex'. Int J Syst Evol Microbiol 51: 1853–1862. https://doi.org/10.1099/00207713-51-5-1853

Sudha Rani K, Swamy MV, Seenayya G (1998) Production of ethanol from various pure and natural cellulosic biomass by *clostridium thermocellum* strains SS21 and SS22. Process Biochem 33(4):435–440. https://doi.org/10.1016/S0032-9592(97)00095-2

Sveinsdottir M, Beck SR, Orlygsson J (2009) Ethanol production from monosugars and lignocellulosic biomass by thermophilic bacteria isolated from Icelandic hot springs. Icel Agric Sci 22: 45–58

Swan BK, Martinez-Garcia M, Preston CM et al (2011) Potential for chemolithoautotrophy among ubiquitous bacteria lineages in the dark ocean. Science 333:1296–1300. https://doi.org/10.1126/science.1203690

Takahata Y, Nishijima M, Hoaki T et al (2001) *Thermotoga petrophila* sp. nov. and *Thermotoga naphthophila* sp. nov., two hyperthermophilic bacteria from the Kubiki oil reservoir in Niigata, Japan. Int J Syst Evol Microbiol 51:1901–1909. https://doi.org/10.1099/00207713-51-5-1901

Takai K, Campbell BJ, Cary SC et al (2005) Enzymatic and genetic characterization of carbon and energy metabolisms by Deep-Sea hydrothermal chemolithoautotrophic isolates of Epsilonproteobacteria. Appl Environ Microbiol 71(11):7310–7320. https://doi.org/10.1128/AEM.71.11.7310-7320.2005

Takai K, Kobayashi H, Nealson KH et al (2003) Sulfurihydrogenibium subterraneum gen. nov., sp. nov., from a subsurface hot aquifer. Int J Syst Evol Microbiol 53:823–827. https://doi.org/10.1099/ijs.0.02506-0

Takai K (2003) *Balnearium lithotrophicum* gen. nov., sp. nov., a novel thermophilic, strictly anaerobic, hydrogen-oxidizing chemolithoautotroph isolated from a black smoker chimney in the Suiyo seamount hydrothermal system. Int J Syst Evol Microbiol 53:1947–1954. https://doi.org/10.1099/ijs.0.02773-0

Tamazawa S, Mayumi D, Mochimaru H et al (2017) *Petrothermobacter organivorans* gen. nov., sp. nov., a thermophilic, strictly anaerobic bacterium of the phylum Deferribacteres isolated from a deep subsurface oil reservoir. Int J Syst Evol Microbiol 67:3982–3986. https://doi.org/10.1099/ijsem.0.002234

Tan S, Liu J, Fang Y et al (2019) Insights into ecological role of a new deltaproteobacterial order Candidatus Acidulodesulfobacterales by metagenomics and metatranscriptomics. ISME J 13: 2044–2057. https://doi.org/10.1038/s41396-019-0415-y

Theodorakopoulos N, Bachar D, Christen R et al (2013) Exploration of Deinococcus-Thermus molecular diversity by novel group-specific PCR primers. Microbiology 2:862–872. https://doi.org/10.1002/mbo3.119

Thompson BG, Murray RG (1981) Isolation and characterization of the plasma membrane and the outer membrane of *Deinococcus radiodurans* strain sark. Can J Microbiol 27:729–734. https://doi.org/10.1139/m81-111

Þorsteinsdóttir GV, Blischke A, Sigurbjörnsdóttir A et al (2020) Gas seepage pockmark microbiomes suggest the presence of sedimentary coal seams in the Oxarfjordur graben of NE-Iceland. Can J Microbiol 66:25–38. https://doi.org/10.1139/cjm-2019-0081

Tian B, Hua Y (2010) Carotenoid biosynthesis in extremophilic Deinococcus–Thermus bacteria. Trends Microbiol 8:512–520. https://doi.org/10.1016/j.tim.2010.07.007

Tonon LAC, Moreira APB, Thompson F (2014) The family Erythrobacteraceae. In: Rosenberg E, DeLong EF, Lory S et al (eds) The prokaryotes: alphaproteobacteria and betaproteobacteria. Springer, Berlin, pp 213–235

Trembath-Reichert E, Butterfield DA, Huber JA (2019) Active subseafloor microbial communities from Mariana back-arc venting fluids share metabolic strategies across different thermal niches and taxa. ISME J 13:2264–2279. https://doi.org/10.1038/s41396-019-0431-y

Trüper Hans G, Pfennig N (1992) The family Chlorobiaceae. In: Balows A et al (eds) The Prokaryotes. Springer, New York, pp 3583–3592. https://doi.org/10.1007/978-1-4757-2191-1_33

Urakawa H, Martens-Habbena W, Stahl DA (2010) High abundance of ammonia-oxidizing Archaea in coastal waters, determined using a modified DNA extraction method. Appl Env Microbiol 76:2129–2135. https://doi.org/10.1128/AEM.02692-09

Vanfossen AL, Lewis DL, Nichols JD et al (2008) Polysaccharide degradation and synthesis by extremely thermophilic anaerobes. Ann NY Acad Sci 1125:322–337. https://doi.org/10.1196/annals.1419.017

van Niel CB (1932) On the morphology and physiology of the purple and Green Sulphur bacteria. Arch Mikrobiol 3(1):1–112. https://doi.org/10.1007/BF00454965

Van Ooteghem SA, Beer SK, Yue PC (2002) Hydrogen production by the thermophilic bacterium *Thermotoga neapolitana*. Appl Biochem Biotechnol 98:177–189. https://doi.org/10.1385/ABAB:98-100:1-9:177

Van Ooteghem SA, Jones A, Van Der Lelie D et al (2004) H2 production and carbon utilization by *Thermotoga neapolitana* under anaerobic and microaerobic growth conditions. Biotechnol Lett 26(15):1223–1232. https://doi.org/10.1023/B:BILE.0000036602.75427.88

Vardanyan A, Khachatryan A, Castro L et al (2023) Bioleaching of sulfide minerals by *Leptospirillum ferriphilum* CC from polymetallic mine (Armenia). Fortschr Mineral 13(2): 243. https://doi.org/10.3390/min13020243

Verhamme DT, Prosser JI, Nicol GW (2011) Ammonia concentration determines differential growth of ammonia-oxidising archaea and bacteria in soil microcosms. ISME J 5:1067–1071. https://doi.org/10.1038/ismej.2010.191

Vetriani C, Speck MD, Ellor SV et al (2004) *Thermovibrio ammonificans* sp. nov., a thermophilic, chemolithotrophic, nitrate-ammonifying bacterium from deep-sea hydrothermal vents. Int J Syst Evol Microbiol 54:175–181. https://doi.org/10.1099/ijs.0.02781-0

Vick TJ, Dodsworth JA, Costa KC et al (2010) Microbiology and geochemistry of little Hot Creek, a hot spring environment in the Long Valley caldera. Geobiology 8:140–154. https://doi.org/10.1111/j.1472-4669.2009.00228.x

Viggi CC, Matturro B, Frascadore E et al (2017) Bridging spatially segregated redox zones with a microbial electrochemical snorkel triggers biogeochemical cycles in oil-contaminated river Tyne (UK) sediments. Water Res 127:11–21. https://doi.org/10.1016/j.watres.2017.10.002

Voordeckers, J, Starovoytov V, Vetriani C (2005) *Caminibacter mediatlanticus* sp. nov., a thermophilic, chemolithoautotrophic, nitrate-ammonifying bacterium isolated from a Deep-Sea hydrothermal vent on the mid-Atlantic ridge'. Int J Syst Evol Microbiol 55 (2): 773–779. https://doi.org/10.1099/ijs.0.63430-0

Vrije GJ, Mars AE, Budde MAW et al (2007) Glycolytic pathway and hydrogen yield studies of the extreme thermophile *Caldicellulosiruptor saccharolyticus*. Appl Microbiol Biotechnol 74: 1358–1367. https://doi.org/10.1007/s00253-006-0783-x

Wächtershäuser G (1990) The case for the chemoautotrophic origin of life in an iron-Sulfur world. Orig Life Evol Biosph 20(2):173–176. https://doi.org/10.1007/BF01808279

Wahlund T, Woese CR, Castenholz RW et al (1991) A thermophilic green sulfur bacterium from New Zealand hot springs, *Chlorobium tepidum* sp. nov. Arch Microbiol 156:81–90. https://doi.org/10.1007/BF00290978

Waite DW, Vanwonterghem I, Rinke C et al (2017) Comparative genomic analysis of the class Epsilonproteobacteria and proposed reclassification to Epsilonbacteraeota (phyl. nov.). Frontiers Microbiol 8:682. https://doi.org/10.3389/fmicb.2017.00682

Wang Z, Cao Y, Zhu-Barker X et al (2019) Comammox *Nitrospira* clade B contributes to nitrification in soil. Soil Biol Biochem 135:392–395. https://doi.org/10.1016/j.soilbio.2019.06.004

Wang M, Sha C, Wu J et al (2021) Bacterial community response to petroleum contamination in brackish tidal marsh sediments in the Yangtze River estuary, China. J Environ Sci (China) 99: 160–167. https://doi.org/10.1016/j.jes.2020.06.015

Ward LM, McGlynn SE, Fischer WW (2018) Draft genome sequences of two basal members of the Anaerolineae class of Chloroflexi from a sulfidic hot spring. Genome Announc 6(25):e00570–e00518. https://doi.org/10.1128/genomeA.00570-18

Watson SW, Waterbury JB (1971) Characteristics of two marine nitrite oxidizing bacteria, *Nitrospina gracilis* nov. gen. nov. sp. and *Nitrococcus mobilis* nov. gen. nov. sp. Arch Mikrobiol 77:203–230. https://doi.org/10.1007/BF00454947

Watson SW, Bock E, Valois FW et al (1986) *Nitrospira marina* gen. nov. sp. nov.: a chemolithotrophic nitrite-oxidizing bacterium. Arch Microbiol 144:1–7. doi: https://doi.org/10.1007/BF00454947

Weisburg WG, Giovannoni SJ, Woese CR (1989) The Deinococcus-Thermus phylum and the effect of rRNA composition on phylogenetic tree construction. Syst Appl Microbiol 11:128–134. https://doi.org/10.1016/s0723-2020(89)80051-7

Weon H-Y, Kim B-Y, Schumann P et al (2007) *Deinococcus cellulosilyticus* sp. nov., isolated from air. Int J Syst Evol Microbiol 57(8):1685–1688. https://doi.org/10.1099/ijs.0.64951-0

Wery N, Lesongeur F, Pignet P et al (2001) *Marinitoga camini* gen. nov., sp. nov., a rod-shaped bacterium belonging to the order Thermotogales, isolated from a deep-sea hydrothermal vent. Int J Syst Evol Microbiol 51:495–504. https://doi.org/10.1099/00207713-51-2-495

Wiegel J, Ljungdahl LG (1981) *Thermoanaerobacter ethanolicus* gen. nov., spec. nov., a new, extreme thermophilic, anaerobic bacterium. Arch Microbiol 128:343–348. https://doi.org/10.1007/BF00405910

Wiegel J (2015) Clostridiaceae. In: Trujillo ME, Dedysh S, DeVos P, Hedlund B, Kämpfer P, Rainey FA, Whitman WB (eds) Bergey's manual of systematics of archaea and bacteria. Wiley. https://doi.org/10.1002/9781118960608.fbm00129

Windberger E, Huber R, Trincone A et al (1989) *Thermotoga thermarum* sp. nov. and *Thermotoga neapolitana* occurring in African continental solfataric springs. Arch Microbiol 151:506–512. https://doi.org/10.1007/BF00454866

Wirsen CO, Sievert SM, Cavanaugh CM et al (2002) Characterization of an autotrophic Sulfide-oxidizing marine arcobacter Sp. that produces filamentous Sulfur. Appl Environ Microbiol 68(1):316–325. https://doi.org/10.1128/AEM.68.1.316-325.2002

Woese CR, Kandler O, Wheelis ML (1990) Towards a natural system of organisms: proposal for the domains archaea, bacteria, and Eucarya. Proc Natl Acad Sci U S A 87:4576–4579. https://doi.org/10.1073/pnas.87.12.4576

Woese CR (1987) Bacterial evolution. Microbiol Rev 51:221–271. https://doi.org/10.1128/mr.51.2.221-271.1987

Wolf J, Stark H, Fafenrot K, Albersmeier A, Pham TK, Müller KB et al (2016) A systems biology approach reveals major metabolic changes in the thermoacidophilic archaeon *Sulfolobus*

solfataricus in response to the carbon source L-fucose versus D-glucose. Mol Microbiol 102: 882–908. https://doi.org/10.1111/mmi.13498

Wu M, Jiang Y, Liu Y et al (2021) Microbial application of thermophilic *Thermoanaerobacterium* species in lignocellulosic biorefinery. Appl Microbiol Biotechnol 105:5739–5749. https://doi.org/10.1007/s00253-021-11450-4

Xian W-D, Liu Z-T, Li M-M et al (2020) Rhodobacter flagellatus sp. nov., a thermophilic bacterium isolated from a hot spring. Int J Syst Evol Microbiol 70:1541–1546. https://doi.org/10.1099/ijsem.0.003929

Xu L, Wu Y-H, Zhou P et al (2018) Investigation of the thermophilic mechanism in the genus Porphyrobacter by comparative genomic analysis. BMC Genomics 19:385. https://doi.org/10.1186/s12864-018-4789-4

Yabe S, Aiba Y, Sakai Y et al (2010) *Thermosporothrix hazakensis* gen. nov., sp. nov., isolated from compost, description of *Thermosporotrichaceae* fam. nov. within the class Ktedonobacteria Cavaletti et al. 2007 and emended description of the class Ktedonobacteria. Int J Syst Evol Microbiol 60:1794–1801. https://doi.org/10.1099/ijs.0.018069-0

Yabe S, Sakai Y, Yokota A (2016) *Thermosporothrix narukonensis* sp. nov., belonging to the class Ktedonobacteria, isolated from fallen leaves on geothermal soil, and emended description of the genus Thermosporothrix. Int J Syst Evol Microbiol 66:2152–2157. https://doi.org/10.1099/ijsem.0.001004

Yamada T, Imachi H, Ohashi A et al (2007) *Bellilinea caldifistulae* gen. nov., sp. nov. and *Longilinea arvoryzae* gen. nov., sp. nov., strictly anaerobic, filamentous bacteria of the phylum Chloroflexi isolated from methanogenic propionate-degrading consortia. Int J Syst Evol Microbiol 57:2299–2306. https://doi.org/10.1099/ijs.0.65098-0

Yamada T, Sekiguchi Y, Hanada S et al (2006) *Anaerolinea thermolimosa* sp. nov., *Levilinea saccharolytica* gen. nov., sp. nov. and *Leptolinea tardivitalis* gen. nov., sp. nov., novel filamentous anaerobes, and description of the new classes Anaerolineae classis nov. and Caldilineae classis nov in the phylum Chloroflexi. Int J Syst Evol Microbiol 56:1331–1340. https://doi.org/10.1099/ijs.0.64169-0

Yamada T, Sekiguchi Y (2018) Anaerolineaceae. In: Trujillo ME, Dedysh S, DeVos P, Hedlund B, Kämpfer P, Rainey FA, Whitman WB (eds) Bergey's manual of systematics of archaea and bacteria. Wiley, pp 1–5

Yang S, Kataeva I, Wiegel J et al (2010) Classification of *Anaerocellum thermophilum* strain DSM 6725 as *Caldicellulosiruptor bescii* sp. nov. Int J Syst Evol Microbiol 60:2011–2015. https://doi.org/10.1099/ijs.0.017731-0

Yasir M, Qureshi AK, Srinivasan S et al (2020) Domination of filamentous anoxygenic phototrophic bacteria and prediction of metabolic pathways in microbial mats from the Hot Springs of Al Aridhah. Folia Biol (Praha) 66:24–35

Yeh H-Y, Awad A, Rothrock MJ (2021) Detection of C*ampylobacter jejuni* diversity by clustered regularly interspaced short palindromic repeats (CRISPR) from an animal farm. Vet Med Sci 7: 2381–2388. https://doi.org/10.1002/vms3.622

Yoo S-H, Weon H-Y, Kim S-J et al (2009) *Deinococcus aerolatus* sp. nov. and *Deinococcus aerophilus* sp. nov., isolated from air samples. Int J Syst Evol Microbiol 60:1191–1195. https://doi.org/10.1099/ijs.0.016030-0

Yuan C-G, Chen X, Jiang Z et al (2017) *Altererythrobacter lauratis* sp. nov. and *Altererythrobacter palmitatis* sp. nov., isolated from a Tibetan hot spring. Antonie Van Leeuwenhoek 110:1077–1086. https://doi.org/10.1007/s10482-017-0882-y

Yvenou S, Allioux M, Slobodkin A et al (2021) Genetic potential of *Dissulfurimicrobium hydrothermale*, an obligate sulfur-disproportionating thermophilic microorganism. Microorganisms 10. https://doi.org/10.3390/microorganisms10010060

Zavarzina DG, Prokofeva MI, Pikhtereva VA et al (2022) *Deferrivibrio essentukiensis* sp. nov., gen. nov., a Representative of Deferrivibrionaceae fam. nov., Isolated from the subsurface aquifer of caucasian mineral drinking waters. Microbiology 91:143–159. https://doi.org/10.1134/S0026261722020114

Zeidan AA, van Niel EWJ (2010) A quantitative analysis of hydrogen production efficiency of the extreme thermophile *Caldicellulosiruptor owensensis* OLT. Int J Hydro Energy 35:1128–1137. https://doi.org/10.1016/j.ijhydene.2009.11.082

Zeikus JG, Dawson MA, Thompson TE et al (1983) Microbial ecology of volcanic Sulphidogenesis: isolation and characterization of *Thermodesulfobacterium commune* gen. nov. and sp. nov. Microbiology 129:1159–1169. https://doi.org/10.1099/00221287-129-4-1159

Zhang L, He J (2012) A novel archaeal phylum: Thaumarchaeota-a review. Wei Sheng wu xue Bao Acta Microbiol Sin 52:411–421. PMID: 22799205

Zhang CL, Pearson A, Li YL, Mills G, Wiegel J (2006) Thermophilic temperature optimum for crenarchaeol synthesis and its implication for archaeal evolution. Appl Environ Microbiol 72: 4419–4422. https://doi.org/10.1128/AEM.00191-06

Zhang C, Phillips APR, Wipfler RL et al (2018) The essential genome of the crenarchaeal model *Sulfolobus islandicus*. Nat Commun 9:4908. https://doi.org/10.1038/s41467-018-07379-4

Zhaxybayeva O, Nesbø CL, Farrell AA et al (2019) Thermotogaceae. In: Trujillo ME, Dedysh S, Devos P, Hedlund B, Kämpfer P, Rainey FA et al (eds) Bergey's manual of systematics of archaea and bacteria. Wiley. https://doi.org/10.1002/9781118960608.fbm00253.pub2

Zhaxybayeva O, Swithers KS, Lapierre P et al (2009) On the chimeric nature, thermophilic origin, and phylogenetic placement of the Thermotogales. Proc Natl Acad Sci U S A 106(14): 5865–5870. https://doi.org/10.1073/pnas.0901260106

Zheng Y, Saitou A, Wang C-M et al (2019) Genome features and secondary metabolites biosynthetic potential of the class Ktedonobacteria. Front Microbiol 10:893. https://doi.org/10.3389/fmicb.2019.00893

Zhen-Li Z, Xin-Qi Z, Nan W et al (2014) *Amphiplicatus metriothermophilus* gen. nov., sp. nov., a thermotolerant alphaproteobacterium isolated from a hot spring. Int J Syst Evol Microbiol 64: 2805–2811. https://doi.org/10.1099/ijs.0.062471-0

Zillig W, Gierl A, Schreiber G et al (1983a) The archaebacterium *Thermofilum pendens* represents, a novel genus of the thermophilic, anaerobic Sulfur respiring Thermoproteales. Syst Appl Microbiol 4:79–87. https://doi.org/10.1016/S0723-2020(83)80035-6

Zillig W, Holz I, Janekovic D et al (1983b) The archaebacterium *Thermococcus celer* represents, a novel genus within the thermophilic branch of the archaebacteria. Syst Appl Microbiol 4:88–94. https://doi.org/10.1016/S0723-2020(83)80036-8

Zillig W, Holz I, Klenk H-P et al (1987) *Pyrococcus woesei*, sp. nov., an ultra-thermophilic marine archaebacterium, representing a novel order, *Thermococcales*. Syst Appl Microbiol 9:62–70. https://doi.org/10.1016/S0723-2020(87)80057-7

PLOS ONE

RESEARCH ARTICLE

Complex organic matter degradation by secondary consumers in chemolithoautotrophy-based subsurface geothermal ecosystems

Raegan Paul[1], Timothy J. Rogers[1], Kate M. Fullerton[1], Matteo Selci[2], Martina Cascone[2], Murray H. Stokes[1], Andrew D. Steen[1], J. Maarten de Moor[3,4], Agostina Chiodi[5], Andri Stefánsson[6], Sæmundur A. Halldórsson[6], Carlos J. Ramirez[7], Gerdhard L. Jessen[8,9], Peter H. Barry[10], Angelina Cordone[2], Donato Giovannelli[2,10,11,12,13]*, Karen G. Lloyd[1]*

1 Microbiology Department, University of Tennessee, Knoxville, TN, United States of America, **2** Department of Biology, University of Naples "Federico II", Naples, Italy, **3** Observatorio Volcanológico y Sismológico de Costa Rica (OVSICORI) Universidad Nacional, Heredia, Costa Rica, **4** Department of Earth and Planetary Sciences, University of New Mexico, Albuquerque, NM, United States of America, **5** Instituto de Bio y Geociencias del NOA (IBIGEO, UNSa-CONICET), Salta, Argentina, **6** NordVulk, Institute of Earth Sciences, University of Iceland, Reykjavík, Iceland, **7** Servicio Geologico Ambiental, Heredia, Costa Rica, **8** Instituto de Ciencias Marinas y Limnológicas, Universidad Austral de Chile, Valdivia, Chile, **9** Center for Oceanographic Research COPAS COASTAL, Universidad de Concepción, Concepción, Chile, **10** Marine Chemistry & Geochemistry Department, Woods Hole Oceanographic Institution, Woods Hole, MA, United States of America, **11** National Research Council–Institute of Marine Biological Resources and Biotechnologies—CNR-IRBIM, Ancona, Italy, **12** Department of Marine and Coastal Science, Rutgers University, New Brunswick, NJ, United States of America, **13** Earth-Life Science Institute, Tokyo Institute of Technology, Tokyo, Japan

* klloyd@utk.edu (KGL); donato.giovannelli@unina.it (DG)

Check for updates

OPEN ACCESS

Citation: Paul R, Rogers TJ, Fullerton KM, Selci M, Cascone M, Stokes MH, et al. (2023) Complex organic matter degradation by secondary consumers in chemolithoautotrophy-based subsurface geothermal ecosystems. PLoS ONE 18(8): e0281277. https://doi.org/10.1371/journal.pone.0281277

Editor: Yanbin Yin, University of Nebraska-Lincoln, UNITED STATES

Received: January 18, 2023

Accepted: July 30, 2023

Published: August 18, 2023

Copyright: © 2023 Paul et al. This is an open access article distributed under the terms of the Creative Commons Attribution License, which permits unrestricted use, distribution, and reproduction in any medium, provided the original author and source are credited.

Data Availability Statement: Data is available in the NCBI SRA with project ID PRJNA627197 and project ID PRJNA914269. Iceland assemblies metagenomic workflow is available on Kbase at https://narrative.kbase.us/narrative/107494. Scripts used in R studio are available on github at rpaul5/terrestrial-geothermal-systems.

Funding: This work was supported by funding from the Deep Carbon Observatory at the Alfred P. Sloan Foundation (G-2016-7206), the Census of

Abstract

Microbial communities in terrestrial geothermal systems often contain chemolithoautotrophs with well-characterized distributions and metabolic capabilities. However, the extent to which organic matter produced by these chemolithoautotrophs supports heterotrophs remains largely unknown. Here we compared the abundance and activity of peptidases and carbohydrate active enzymes (CAZymes) that are predicted to be extracellular identified in metagenomic assemblies from 63 springs in the Central American and the Andean convergent margin (Argentinian backarc of the Central Volcanic Zone), as well as the plume-influenced spreading center in Iceland. All assemblies contain two orders of magnitude more peptidases than CAZymes, suggesting that the microorganisms more often use proteins for their carbon and/or nitrogen acquisition instead of complex sugars. The CAZy families in highest abundance are GH23 and CBM50, and the most abundant peptidase families are M23 and C26, all four of which degrade peptidoglycan found in bacterial cells. This implies that the heterotrophic community relies on autochthonous dead cell biomass, rather than allochthonous plant matter, for organic material. Enzymes involved in the degradation of cyanobacterial- and algal-derived compounds are in lower abundance at every site, with volcanic sites having more enzymes degrading cyanobacterial compounds and non-volcanic sites having more enzymes degrading algal compounds. Activity assays showed that many

Deep Life, NSF-EAR 2121670 to K.G.L., D.G., M. dM., and P.H.B., NSF-OCE-2151015 to K.G.L. and P.H.B., NSF-DEB 2132774 and Simons Foundation 404586 to K.G.L., FONDECYT Grant 11191138 (ANID Chile) to G.L.J. The funders had no role in study design, data collection and analysis, decision to publish, or preparation of the manuscript.

Competing interests: The authors have declared that no competing interests exist.

of these enzyme classes are active in these samples. High temperature sites (> 80˚C) had similar extracellular carbon-degrading enzymes regardless of their province, suggesting a less well-developed population of secondary consumers at these sites, possibly connected with the limited extent of the subsurface biosphere in these high temperature sites. We conclude that in < 80˚C springs, chemolithoautotrophic production supports heterotrophs capable of degrading a wide range of organic compounds that do not vary by geological province, even though the taxonomic and respiratory repertoire of chemolithoautotrophs and heterotrophs differ greatly across these regions.

Introduction

Terrestrial geothermal systems emit volatiles from the Earth's interior (i.e., mantle and crust) to the atmosphere. Often, meteoric water permeates into the subsurface hydrothermal system, where it is heated and rises to the surface, bringing with it volatiles from the deep subsurface [1]. The differential enrichment of these volatiles into geothermal fluids creates environmental niches that can be saturated with deeply-derived inorganic carbon and other compounds [2–4]. In convergent margins such as those of the Central American and the Andean Central Volcanic Zone, inorganic carbon is derived from the mantle, overlying crust and/or down-going slab [5]. In divergent spreading centers and/or areas with mantle plume-influenced volcanism, such as Iceland, geothermal systems are often dominated by deep mantle gases (e.g., Harðardóttir et al. 2018 [6]). These geological systems create a large diversity of surface-emitting springs that range in temperature, pH, inorganic carbon content, and availability of redox active compounds that together make the driving force of microbial community composition [4, 7, 8]. Sampling fluid emissions from natural surface springs provides access to these deeply-sourced microbial communities and the volatiles that support them [8–11].

The important role that chemolithoautotrophs play in these geothermal ecosystems is well-established (e.g., [4, 12–14]). The heterotrophic communities within these systems are less often studied, even though heterotrophs have been shown to be dominant within heavily-sedimented subsurface ecosystems (e.g., [15]). These heavily-sedimented systems do not have a constant supply of redox active volatiles and are therefore dependent on allocthonously-derived organic matter, and likely differ greatly from geothermal ecosystems. Recent work has focused on understanding the heterotrophic community within terrestrial geothermal systems [16, 17] and many industrially useful carbohydrate- and peptide-degrading enzymes have been isolated from these microbial communities [18, 19]. Specifically, carbohydrate active enzymes and peptidases have been found in hot spring fluids [17, 20, 21]. However, a survey of the full complement of all the carboyhdrate active enzymes and peptidases have not been made from metagenomes from hot springs, to our knowledge. The taxonomy and respiratory pathways of primary producers and heterotrophs are known to vary along geological gradients according to changes in deep volatile delivery [4, 7, 8]. However, it is not known whether organic carbon degradation pathways vary along with them. Different types of chemolithoautotrophs may promote different compositions of carbon-degrading enzymes in the ecosystems they support. Thus, it is important to investigate the heterotrophic community because it actively participates in the geochemical cycle of terrestrial geothermal environments by consuming organic carbon and releasing inorganic carbon.

Hot springs typically contain little photosynthetically-derived organic matter, potentially leading heterotrophs to depend primarily on the byproducts of the chemolithoautotrophic

community [22]. To access these organic byproducts, heterotrophs use extracellular enzymes to break down larger organic molecules into smaller molecules that can permeate their cell membrane more readily [23] ultimately recycling carbon through this autotroph-heterotroph mutualism. The composition of carbon-degrading enzymes may therefore show whether chemolithoautotrophy or photosynthesis is more important for heterotrophic communities. Here, we focus on two broad classes of extracellular enzymes: peptidases which break down proteins and carbohydrate-active enzymes (CAZymes) which break down polysaccharides and related macromolecules.

We compare springs across the Central American and the Andean (Argentinian backarc of the Central Volcanic Zone) convergent margins as well as the plume-influenced Iceland plate boundary. These regions are defined by their position across the convergent margin or continental intra-plate setting toward an oceanic plate boundary. The Costa Rican subduction zone is driven by the Cocos-Nazca plate subducting under the Caribbean plate. Northern Costa Rica is characterized by having higher volcanic activity than the other areas [24]. The Panama slab window is a result of a tear within the Nazca plate where arc volcanism ceases [25]. The formation of the slab window is also responsible for the cease in volcanism within the Cordillera Talamanca region [26], and a change in the rock chemistry in the area that shows hot spot-like compositions [27]. The Andean convergent margin is driven by the Nazca plate subducting under the South American plate [28], whereas Iceland is associated with spreading along the Mid-Atlantic Ridge under the influence of a mantle plume (e.g., [2, 29, 30]). Environmental factors also vary significantly between the sites due to large variations in latitude, elevation, and rainfall. This wide range of geological and environmental settings provides an opportunity to study geochemically diverse springs. Sites from Argentina and Iceland were placed into their own categories because they have different tectonic processes than those of Central America. The sites are then color coded based on these different geological processes that distinguish them (Fig 1).

Enzyme assays and bioinformatics analyses on metagenomes were used to analyze the microbial community interactions within diverse geothermal systems. To study the heterotrophic activity within geothermal systems, assemblies from the Costa Rican convergent margin, the Argentina backarc of the Andean convergent margin and the subaerial section of the Mid-Atlantic ridge (Iceland) were annotated using dbcan2 database and the run_dbcan package to find CAZymes and DRAM to annotate the MEROPS families [32, 33]. MEROPS classifies proteolytic enzymes using hierarchical classification by homologous sequences [34]. The CAZyme database splits carbohydrate-active enzymes into classes of glycoside hydrolases (GH), glycosyl transferases (GT), polysaccharide lyases (PL), carbohydrate esterases (CE), auxiliary activities (AA), and carbohydrate binding molecules (CBM), defined by sequence similarity [35]. Enzyme commission numbers are based on the reactions catalyzed instead of sequence homology [36]. Using these different tools allows for a broad analysis of the potential organic matter degrading functions of proteins based on their sequence homology. Hierarchical clustering and principal coordinate analysis were used to find correlations between the sites and the enzyme families found within them. By combining the maximum potential enzymatic activity, measured by low molecular mass fluorogenic substrate proxies, with the metagenomic annotations, we can see a larger scope of the potential heterotrophic activity within these sites.

Materials and methods

Sampling

DNA extraction and sequencing for all samples has been previously described [3, 4] Sample collection was performed following the protocols previously described [3, 4, 7] and using the

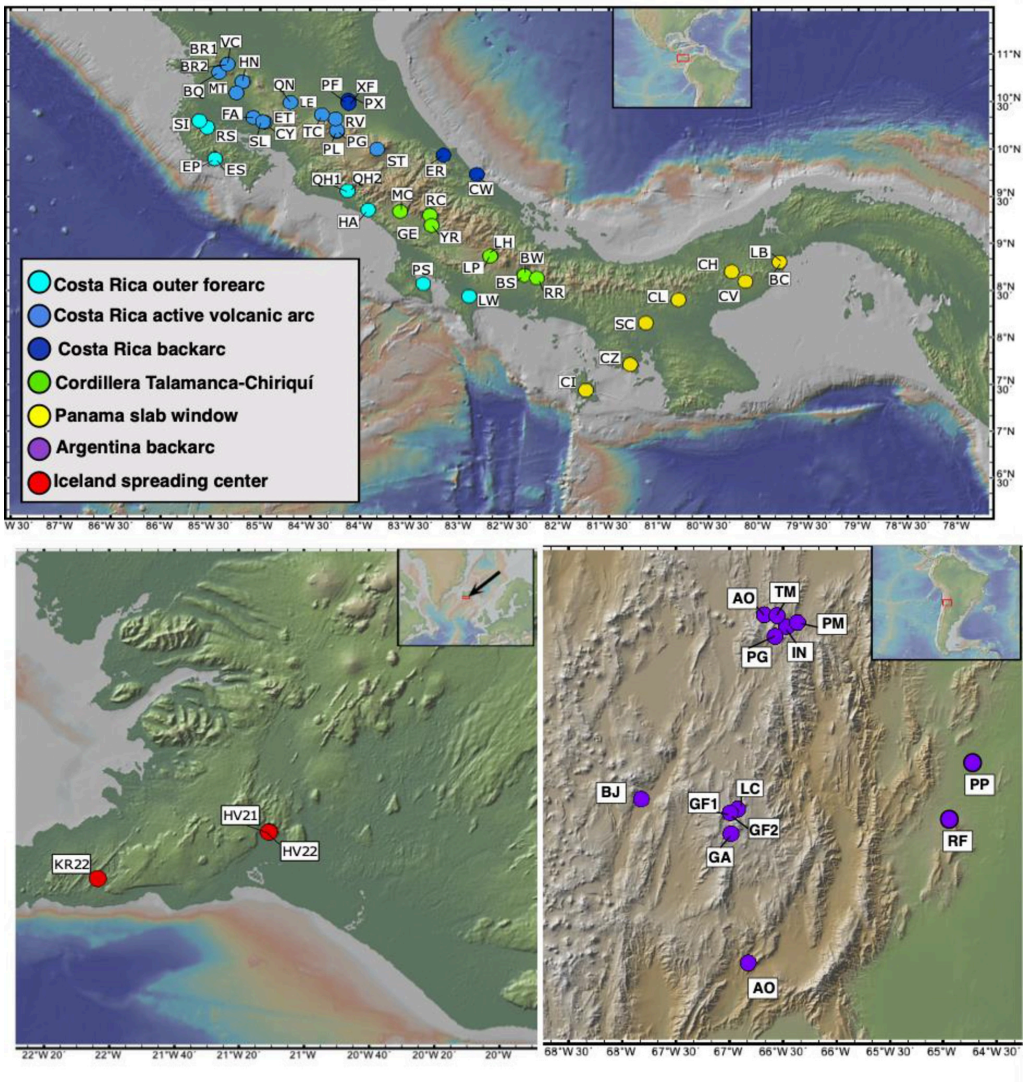

Fig 1. Maps of site locations. A. Costa Rica and Panama sites are color coded to match the different geological provinces. **B.** Iceland sites are all active volcanic hot spot and spreading center. **C.** Argentina sites are all backarc. Figure made with GeoMapApp (www.geomapapp.org) / CC BY / CC BY [31].

https://doi.org/10.1371/journal.pone.0281277.g001

rationale described by Giovannelli et al. 2022 [11]. Sites are color coded based on province (Fig 1) [31]. GPS coordinates, site names, temperature and pH measurements are shown in Table 1. Coauthors located at the University of Salta, Observatorio Volcanológico y Sismológico de Costa Rica (OVSICORI) Universidad Nacional, and NordVulk, Institute of Earth Sciences, University of Iceland, regularly visit these sites and required local verbal permission

Table 1. Site name and abbreviation supplemented with province, latitude, longitude, temperature, and pH. NM means not measured.

ABBREV.	SAMPLE NAME	SITE NAME	REGION	LAT	LONG	PROVINCE	TEMP ˚C	PH
AO19	AO190224	Antuco	Argentina	-24.182136	-66.674029	Argentina backarc	27.8	6.3
AR17	AR170220	Arenal Horse Farm	Costa Rica	10.4864	-84.6872	Costa Rica active volcanic arc	NM	NM
BC18	BC180410	Los Bajos the Corera	Panama	8.806037	-79.790968	Panama slab window	31.8	7.5
BJ19	BJ190227	Botijuela	Argentina	-25.743034	-67.823245	Argentina backarc	40	6.4
BQ17	BQ170218	Borinquen	Costa Rica	10.810883	-85.413707	Costa Rica active volcanic arc	88.9	2.1
BR117	BR170218_1	Blue River Spring 1	Costa Rica	10.89837	-85.32839	Costa Rica active volcanic arc	59	6.2
BR217	BR170218_2	Blue River Spring 2	Costa Rica	10.89837	-85.32853	Costa Rica active volcanic arc	53.8	5.9
BS18	BS180407	Bajo Mendez Spring	Costa Rica	8.66645	-82.3491	Cordillera Talamanca-Chiriquí	40.9	9.1
BW18	BW180407	Bajo Mendez Well	Costa Rica	8.66581	-82.34867	Cordillera Talamanca-Chiriquí	43.2	9.1
CH18	CH180410	Chiguiri Abajo	Panama	8.70508	-80.26919	Panama slab window	31.1	7
CI18	CI180408	Coiba Island	Panama	7.44104	-81.73277	Panama slab window	48.3	9
CL18	CL180409	Calobre	Panama	8.40448	-80.80375	Panama slab window	50.9	7.5
CV18	CV180410	Casa Valmor	Panama	8.5992	-80.13162	Panama slab window	34.9	7.5
CW18	CW180415	Cauhita Well	Costa Rica	9.735746	-82.825737	Costa Rica backarc	35	7.2
CY17	CY170214	Rio Cayuco	Costa Rica	10.287497	-84.955524	Costa Rica active volcanic arc	72	6.3
CZ18	CZ180409	Salitral Carrizal	Panama	7.71407	-81.28832	Panama slab window	26.3	10
EP17	EP170215	Espabel	Costa Rica	9.901885	-85.454327	Costa Rica outer forearc	26.4	9.9
ES17	ER180415	Rio Blanco Er Resbala	Costa Rica	9.938223	-83.161331	Costa Rica backarc	35	9.5
ER18	ES170215_1	Estrada	Costa Rica	9.899005	-85.453514	Costa Rica outer forearc	27.9	9.7
ET17	ET170220_1	Eco Thermales	Costa Rica	10.484006	-84.675853	Costa Rica active volcanic arc	40	6.1
FA17	FA170219_1	Finca Ande	Costa Rica	10.336843	-85.069499	Costa Rica active volcanic arc	55.2	5.9
GA19	GA190226	Galán Aguas Calientes	Argentina	-25.825416	-66.922496	Argentina backarc	67	6.7
GE18	GE180403	Gevi	Costa Rica	9.19483333	-83.280806	Cordillera Talamanca-Chiriquí	35.8	7.8
GF119	GF190226_1	Galán Fumaroles 1	Argentina	-25.858188	-66.992695	Argentina backarc	80	7.8
GF219	GF190226_2	Galán Fumaroles 2	Argentina	-25.858243	-66.992818	Argentina backarc	80	3.2
HA18	HA180403	Hattillo	Costa Rica	9.36022	-83.91664	Cordillera Talamanca-Chiriquí	33	8.9
HV121	HV1210602	Hveragerdi 1	Iceland	64.008117	-21.17949	Iceland spreading center	93.5	2.7
HV221	HV2210602	Hveragerdi 2	Iceland	64.007062	-21.180739	Iceland spreading center	25.7	1.8
IN19	IN190223	Incachule	Argentina	-24.282129	-66.466761	Argentina backarc	46.9	6.5
KR21	KR2210530	Krysuvik upper pool	Iceland	63.895451	-22.057004	Iceland spreading center	93	2
LB18	LB180410	Los Bajos	Panama	8.80736	-79.79061	Panama slab window	34.8	NM
LC19	LC190226	Galán La Colcha	Argentina	-26.032911	-66.986094	Argentina backarc	84	6.9
LE18	LE180416	Las Estrella	Costa Rica	10.427103	-84.368543	Cordillera Talamanca-Chiriquí	34.7	NM
LH18	LH180406	Los Pozos Thermales	Panama	8.87095	-82.6899	Cordillera Talamanca-Chiriquí	55.4	6.7
LP18	LP180406	Los Pozos Thermales	Panama	8.86966	-82.69282	Cordillera Talamanca-Chiriquí	39.1	6.5
LW18	LW180405	Laurel	Costa Rica	8.44119	-82.90487	Costa Rica outer forearc	31.5	7.1
MC18	MC180404	Montecarlo—Bernardino	Costa Rica	9.34391	-83.59565	Cordillera Talamanca-Chiriquí	31.8	9.6
MT17	MT170219	Termales Salitral	Costa Rica	10.595774	-85.238451	Costa Rica active volcanic arc	59.1	6.3
PB17	PB170224	Poas Volcano background soil	Costa Rica	10.196777	-84.229892	Costa Rica active volcanic arc	NM	NM
PF17	PF170222	Pompilo's finca	Costa Rica	10.518466	-84.11518	Costa Rica backarc	28.7	5.8
PG19	PG190225	Pastos Grandes	Argentina	-24.364589	-66.571132	Argentina backarc	44.9	8.7
PG17	PG172224	Poas Volcano Laguna	Costa Rica	10.188962	-84.227388	Costa Rica active volcanic arc	19.2	NM
PL17	PL170224	Poas Volcano Lake	Costa Rica	10.196777	-84.229892	Costa Rica active volcanic arc	37.6	0.8
PM19	PM190223	Pompeya	Argentina	-24.246688	-66.362722	Argentina backarc	50.3	6.5
PP19	PP190301	El Galpón Pio Perez	Argentina	-24.40986	-64.59146	Argentina backarc	54.3	8.5
PS18	PS180405	Playa Sandalo	Costa Rica	8.57554	-83.36416	Costa Rica outer forearc	33	8.2
PX18	PX180416	Praxair well 24	Costa Rica	10.488755	-84.113598	Costa Rica backarc	28.7	NM

(*Continued*)

Table 1. (Continued)

ABBREV.	SAMPLE NAME	SITE NAME	REGION	LAT	LONG	PROVINCE	TEMP ˚C	PH
QH117	QH170213_1	Quepos Hot springs	Costa Rica	9.56171	-84.123251	Costa Rica outer forearc	48.7	8.5
QH217	QH170213_2	Quepos Hot springs	Costa Rica	9.561575	-84.123468	Costa Rica outer forearc	36.7	8.7
QN17	QN170220	Quebrada naranja	Costa Rica	10.495573	-84.696714	Costa Rica active volcanic arc	22.9	5.6
RC18	RC180404	Ujarassa	Costa Rica	9.30283	-83.29782	Cordillera Talamanca-Chiriquí	60	7.7
RF19	RF190301	Rosario de la Frontera	Argentina	-25.40986	-64.59134	Argentina backarc	82	8.2
RR18	RR180407	"Rockslide"	Costa Rica	8.63591	-82.22369	Cordillera Talamanca-Chiriquí	41.3	NM
RS17	RS170216	Ranchero etl Salitral	Costa Rica	10.232331	-85.531602	Costa Rica outer forearc	29.4	9.9
RV17	RV170221	Recreo Verde	Costa Rica	10.321576	-84.243686	Costa Rica active volcanic arc	42.7	6.2
SC18	SC180411	El Salao Campollano	Panama	8.15755	-81.13097	Panama slab window	29.9	7
SI17	SI170217	El Sitio	Costa Rica	10.301239	-85.610549	Costa Rica outer forearc	35.9	9.8
SL17	SL170214	Santa Lucia	Costa Rica	10.290599	-84.972435	Costa Rica active volcanic arc	57	6.1
TC17	TC170221	El Tucano bubbling site	Costa Rica	10.366486	-84.381208	Costa Rica active volcanic arc	60	6.2
TM19	TM190224	Tocomar	Argentina	-24.18778	-66.55451	Argentina backarc	69.2	7.1
VV19	VV190228	Villa Vil	Argentina	-27.112858	-66.822241	Argentina backarc	38.2	9.1
XF18	XF180416	Praxair well 19	Costa Rica	10.485523	-84.113229	Costa Rica backarc	28.9	7
YR18	YR180404	Yheri	Costa Rica	9.19492	-83.28059	Cordillera Talamanca-Chiriquí	26	8.9

https://doi.org/10.1371/journal.pone.0281277.t001

from landowners for each one of them. The samples we report here have been published previously [3, 4, 7, 37]. From each site, temperature and pH were measured directly in the fluids using a portable YSI Plus 6-Series Sonde Multimeter (YSI Incorporated, Yellow springs, OH) and 0.5 to 1.5 liters of hydrothermal fluids venting from the subsurface were collected. Care was taken when collecting fluids to do this as close to the perceived fluid source as possible. Fluids were immediately filtered through Sterivex 0.22 μm filter cartridges (MilliporeSigma) and quick-frozen onsite in a liquid nitrogen-cooled dry shipper. When fluid sampling was complete and to avoid resuspension, ~10 mL of surface sediments constantly overwashed by the venting source were placed into a sterile plastic vial and frozen onsite along with the filters. Sample names ending in (F) are from filtered fluids and those ending in (S) are from surface sediments.

Bioinformatic processing

For the Iceland metagenomes, raw reads were trimmed with Trimmomatic (v 0.39) [38] and assembled using the MetaWRAP (v 1.3.2) pipeline [39]. The quality of the Iceland assemblies was determined using Quast (v4.4) [40] on Kbase [41]). All other assemblies were generated by trimming raw reads with Trimmomatic (v 0.38). Reads were assembled *de novo* with metaSPAdes with a minimum contig length of 1.5 kb [7]. Reads from LC19F, LC19S, RF19S, and TM19S were assembled using MEGAHIT (v 1.2.9) [42]. The assemblies were annotated using prokka (v 1.14.5) [43] and dbcan2 [32]. For peptidase annotations the assemblies were uploaded to KBase [41] and annotated with DRAM (v.0.1.0) [33]. Secreted proteins were identified using SignalP (v 2.0) [44]. The clean reads were mapped back to the assemblies for read coverage using bowtie2 (v 2.3.5.1) and samtools (v1.15.1) [45, 46]. Hierarchical clustering based on spearman correlation, was performed using hclust from the base R package (R version 4.2.1). Total microbial community analysis of these sites is the focus of previous work, therefore, taxonomic identification was only performed for contigs for the high temperature sites HV121S, HV221S, and KR21S using gottcha2 on Kbase (S1 Fig in S1 File) [4, 7, 47–49].

CAZy family abundances were annotated using dbcan2. Annotations were selected if they were annotated with at least two tools: HMMER and DIAMOND. The annotated gene IDs

were then combined with the prokka gene ID and contigs to gain the abundance of each contig. Read coverage was calculated as previously described [7] Then the read coverage of each annotation normalized to the total assembly size was used to generate a heatmap with hierarchical clustering of the CAZyme families and site locations. All annotations that are presented also were annotated for having a signal peptide sequence by SignalP [44]. Protein annotations that are not present within 75% of the assemblies were removed for better visualization.

Enzyme commission numbers were assigned with dbcan2 database and combined with the SignalP annotations to estimate secretion. Enzyme commission groupings are only shown for class 3 hydrolases where the enzyme commission number was present in at least 75% of the assemblies. MEROPS peptidase annotations were completed using DRAM on Kbase and annotated using SignalP. The gene IDs were then matched to contigs of the assemblies to get the normalized read coverage.

Enzymatic assays

Enzymatic assays were performed following the methods of Bell (2013) [50] with slight modifications. Briefly, sediments were weighed out at 2.75 grams wet weight. The sediments were then combined with 91 mL of 0.5 M Tris-HCl buffer with a matching pH to the original site locations. The sediment slurries were blended for one minute to homogenize them. Then 800 μL of each slurry was pipetted into deep well plates in duplicate. 200 μL of substrates with a concentration of 200 μM were then added to each well. The substrates used were 4-Methylumbelliferyl α-D-glucopyranoside (AG), 4-Methylumbelliferyl β-D-glucopyranoside (BG), 4-Methylumbelliferyl β-D-cellobiosidase (CB), 4-Methylumbelliferyl N-acetyl-β-d-glucosaminidase (NAG), L-Leucine-7-amido-4-methylcoumarin (LEU), 4-Methylumbelliferyl phosphate (PHOS), 4-Methylumbelliferyl sulfate potassium salt (SULF), 4-Methylumbelliferyl-β-D-xylopyranoside (XYL). Each deep well plate was incubated for 3 hours at 30–70˚C, and time points were taken at 0 hours, 1.5 hours, and 3 hours. To take each time point, 200 μL was pipetted from the deep well plate to a black flat bottom 96 well plate. The fluorescence was measured at 455 nm after excitation at 355 nm using a Tecan Infinite M200 Pro Fluorimeter. Differences in enzyme activities among provinces were tested using a Kruskal-Wallis test, implemented in R, due to the strong non-normal distribution of activities in the data set.

Results

Sites

Three different geographical areas were analyzed: the Central American and Andean convergent margins, and Iceland (mantle plume-influenced spreading center). Large variations in fluid sources (i.e. mantle, slab, crust, or surficial) are expected due to the contrasting geologic and environmental settings of the studied areas. We include data from 22 sites in Costa Rica that are influenced by the convergent margin, with analyses of the geochemistry, respirations, and taxonomic identities of the 22 sites published previously [3, 4, 7, 51]. We include 47 additional sites spanning Costa Rica and Panama that are also influenced by the convergent margin, 13 sites from the Andean convergent margin and 3 sites from Iceland. Sites were grouped by geographic-tectonic setting: Costa Rica outer forearc, Costa Rica active volcanic arc, Costa Rica backarc, Cordillera Talamanca, Panama, Argentina backarc, and Iceland (Fig 1, Table 1). These groupings allow us to explore large variations in fluid sources and physicochemical characteristics which are ultimately related to their tectonic setting. For example, in Costa Rica the distance to the trench (outer forearc to active arc to backarc) correlates with large variations in temperature, pH, and mantle-derived components that affect chemical compositions of the fluids and the microbial communities [3, 4]. In total 13 sites have the lowest temperatures

(19.2–29.9˚C) and eight sites have the highest temperatures (80–93.5˚C) (Table 1). Seven sites have the lowest pH (0.85–3.21), while 11 sites have the highest pH (9.0–10.0).

Enzyme activities

Most of the hydrolysis rates measured were indistinguishable from zero (Fig 2). This could mean either that few of the enzymes were being expressed at the time of sampling or that we were unable to properly recreate the geochemical conditions present *in situ*. Of the enzymes tested, carbon-acquiring enzymes (AG, BG, CB, XYL) were more active than enzymes associated with phosphorus and sulfur acquisition (PHOS and SULF) (S3 Table in S1 File). LEU hydrolysis was orders of magnitude lower than the other enzymes assayed, in contrast to soils where LEU often has high hydrolysis rates [52]. NAG hydrolysis was positive at more sites

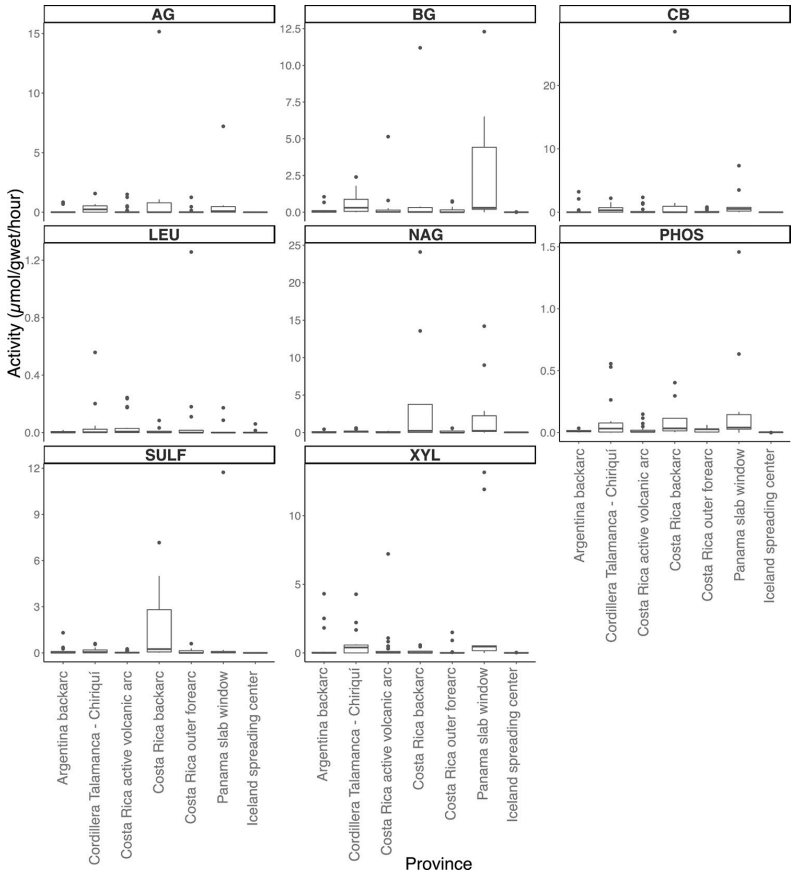

Fig 2. Enzyme activity box plot. Activities for each site were grouped together based on province. Activity measurements were only performed on sediment samples. Each activity is presented in μmol/g_{wet}/h. Enzyme substrates were separated into different panels. Enzymes abbreviations are alpha-glucosidase (AG), beta-glucosidase (BG), cellobiohydrolase (CB), leucine aminopeptidase (LEU), N-acetyl-β-D-glucosaminidase (NAG), phosphatase (PHOS), sulfatase (SULF), and xylosidase (XYL).

https://doi.org/10.1371/journal.pone.0281277.g002

than the other substrates. PHOS hydrolysis had only one site with zero activity, CL18S. From the Kruskal-Wallis statistical analysis, no significant differences ($p>0.05$) were observed for any enzyme activities between provinces.

Metagenomic assemblies

Of the three metagenomic assemblies from Iceland, HV221S has 4,344 contigs, KR21S has 3,214, and HV121S has 912 (S1 Table in S1 File). The total length of these assemblies is 5,645,364 bp for HV121S, 7,802,221 bp for HV221S, and 12,561,178 bp for KR22. The total contig numbers for the Costa Rica, Panama and Argentina assemblies range from 488 to 164,798 (S2 Table in S1 File). The total sizes of the Costa Rica, Panama and Argentina assemblies range from 8,678,655 to 509,373,734 (S2 Table in S1 File). Genus level taxonomy classification was done using gottcha2 on Kbase (S1 Fig in S1 File) [41, 47]. At the genus level, HV121S has 70% of reads annotated as *Sulfolobus*, 15% as *Acidianus*, and the 8% as *Thermoproteus*.The remaining reads are distributed across *Methylorubrum*, *Pseudomonas*, and *Stenotrophomonas*. HV21S had 38% of reads annotated as *Sulfolobus*, 21% as *Thermoproteus*, 10% as *Cutibacterium*, and the rest are distributed across other genera. KR21S has 45% of reads identified as *Acidianus*, 8% as *Sulfolobus*, and 5% as *Thermoproteus*, with the remaining taxonomy distributed across other genera.

Peptidases

In total, there are 144 MEROPS family annotations predicted to be secreted (Fig 3), M (Metallo) with 59, S (Serine) with 32, C (Cysteine) with 29, A (Aspartic) with 9, N (Asparagine) with 5, T (Threonine) with 4, U (Unknown) with 4, G (Glutamic) with 1, and P (Mixed) with 1 (Fig 3). Of these 144 families, 88 are present in every assembly. The total read abundance of annotations for MEROPS is 283,488,080, which is much greater than those of CAZy at 1,729,668, and EC3 at 633,511, which are discussed below. Important MEROPS families are listed in Table 2.

The highest read abundance normalized to total assembly size is 5,316,108.99 for M23 in site GF1f. The most abundant MEROPS normalized read abundances are S09 (prolyl oligopeptidase), M23 (beta-lytic metallopeptidase), C26 (gamma-glutamyl hydrolase), S33 (prolyl aminopeptidase), M38 (isoaspartyl dipeptidase), C44 (amidophosphoribosyl transferase precursor), S49 (signal peptide peptidase A), M20 (glutamate carboxypeptidase), M50 (site 2 peptidase), and S16 (Lon-A peptidase). The sites with the least amount of MEROPS annotations are GF219F, HV121S, GF219S, and GF119F.

Within the spearman correlation hierarchical clustering of sites based on the MEROPS families, the highest temperature sites (GF219S, GF119F, GF219F, HV221S, HV121S, and KR21S) cluster together. Some sites' sediment and fluid assemblies cluster together: SC18F, LW18F, EP17F, RS17F, and BR117F. One cluster consists of only fluid samples CZ18F, RV17F, LH18F, BS18F, CI18F, BW18F, LE18F, RR18F, XF18F, CV18F, and LP18F. For the hierarchical clustering of MEROPS families based on their distribution across sites, one cluster contains MEROPS families S53, A37, U56, A22, G01, that are highly present in only the very hot sites. It has been shown that these peptidase families are associated with acidophilic or thermophilic archaea [60].

CAZymes

CAZy families predicted to be secreted are present in all sites at orders of magnitude lower read abundance than peptidases. Of the six CAZy classes, the most abundant are the glycosyl hydrolases (GH). CAZy families that are abundant in all sites are GH23 (peptidoglycan lyase),

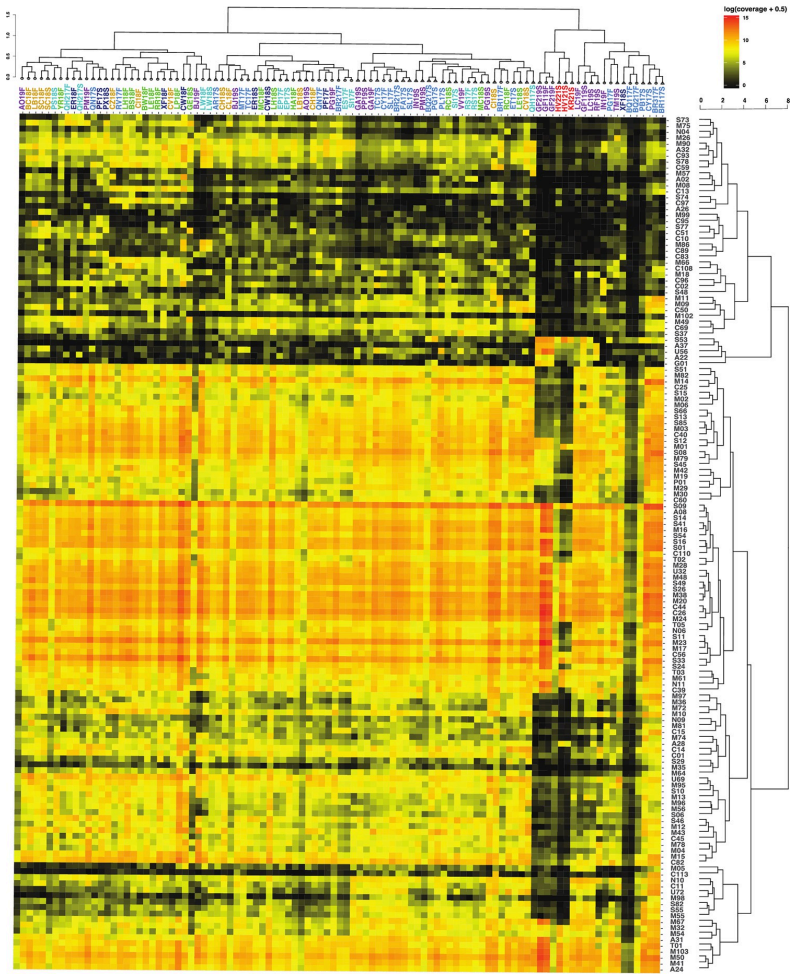

Fig 3. Heatmap with hierarchical correlation of read abundances of MEROPS families (y axis) per site (x axis) based on spearman rank correlation. Abundance shown in log of normalized contig abundance with 0.5 added to avoid zeros for visualization. Untransformed abundances were used for the spearman correlation. Sites are colored by the geological provinces shown in Fig 1.

https://doi.org/10.1371/journal.pone.0281277.g003

CBM50 (binds peptidoglycan and chitin), GH102 (peptidoglycan lytic transglycosylase), and GH103 (peptidoglycan lytic transglycosylase). All five CAZy classes are present in 76 of the assemblies with 89 annotations from glycoside hydrolases (GH), 31 from carbohydrate binding modules (CBM), 17 from polysaccharide lyases (PL), 10 from carbohydrate esterases (CE), 7 from glycosyltransferases (GT), and 2 from auxiliary activities (AA). There are a total of 156 CAZy families present. The assemblies with the least number of CAZyme annotations are HV121S, KR21S, GF119F, GF219F, GF219S and BQ217F. Sites BQ117F, BQ217F, GF119F, GF219F, GF219S, HV121S, KR21S, LC19s, and RF19S, had less than 75% of the total CAZyme annotations presented, all of which had temperatures over 80˚C.

Table 2. CAZy and MEROPS families listed based on the substrate group preference. The groups associated with cell degradation are chitin and peptidoglycan. Photosynthate degradation groups are xylan and cellulose [53–59].

GROUP	CAZY FAMILY	MEROPS FAMILY
CHITIN	GH5, GH7, GH8, GH18, GH19, GH20, GH46, CBM5	
PEPTIDOGLYCAN	GH22, GH23, GH24, GH25, GH102, GH103, GH108, CBM50, CE4	S11, M23, S13, S66, M15, M74, M14, C51
STARCH/ GLYCOGEN	GH3, GH13, GH14, GH15, GH27, GH31, GH38, GH57, GH72, GH77, GH89, GH119, GH126, AA13, GT35, CBM20	
TREHALOSE	GH37, GH65	
XYLAN	GH3, GH5, GH7, GH8, GH10, GH11, GH43, GH67	
CELLULOSE	GH1, GH3, GH5, GH8, GH9, GH10, GH16, GH43, GH51, GH74, GH116	

https://doi.org/10.1371/journal.pone.0281277.t002

Within the spearman correlation of the site clustering, we see a grouping of sites that are from the Argentina backarc and have a higher temperature range (Fig 4). These sites cluster together due to the low abundance of enzyme annotations within their assemblies. Some sites' sediment and fluid samples cluster together such as, LB18, SC18, BJ19, QN17, AO19, RS17, QH217, ER18, and LC19.

Enzyme commission

Enzymes from EC3 are hydrolases, so many of them overlap with those in the CAZyme and MEROPS groups, but the EC categories are more finely divided than CAZyme groups, so they describe hydrolase functionality more precisely. As with CAZymes, EC3 annotations (0–49,251.04) have orders of magnitude lower read abundance than the MEROPs peptidases (0–5,316,108.99) (Fig 5). There are a total of 117 EC hydrolase annotations. The EC hydrolases are subdivided into 3.1 (ester hydrolases), 3.2 (glycosylases), 3.3 (ether hydrolases), 3.4 (peptidases), 3.5 (other non-peptide carbon and nitrogen hydrolases), 3.6 (acid anhydride hydrolases), 3.7 (other carbon-carbon bond hydrolases), 3.8 (halide hydrolases), 3.9 (other phosphorus nitrogen bond hydrolases), 3.10 (sulfur nitrogen bond hydrolases), 3.11 (other carbon phosphorus bond hydrolases), 3.12 (sulfur-sulfur bond hydrolases), 3.13 (carbon sulfur bond hydrolases). The spearman site correlation shows a clustering of sites with very few hydrolases present (Fig 5). The sites that have less than 75% of the protein annotations shown are IN19F, LC19F, HV221S, RF19S, BQ117F, GF119S, BQ217F, KR21S, HV121S, LC19S, GF219S, GF219F, and GF119F. All these sites except for IN19 fall within the highest temperature range (80–93.5˚C). The most abundant EC annotation is 3.4.21.107 (peptidase Do). Other ECs in high abundance are N-acetylmuramoyl-L-alanine amidase (3.5.1.28), subtilisin (3.4.21.62), C-terminal processing peptidase (3.4.21.102), prolyl oligopeptidase (3.4.21.26), oryzin (3.4.21.63), triacylglycerol lipase (3.1.1.3), and beta-lactamase (3.5.2.6). The most common category among these high abundance enzymes is EC group 3.4, which are peptidases.

The EC numbers that are present in all assemblies are alkaline phosphatase (3.1.3.1), (3.2.1.1), beta-glucosidase (3.2.1.21), alpha-L-fucosidase (3.2.1.51), dipeptidyl-peptidase IV (3.4.14.5), peptidyl-dipeptidase A (3.4.15.1), peptidyl-dipeptidase Dcp (3.4.15.5), peptidase Do (3.4.21.107), subtilisin (3.4.21.62), oryzin (3.4.21.63), and endothelin-converting enzyme 1 (3.4.24.71). Three of the EC numbers that are present in all assemblies are also some of the most abundant (3.4.21.107, 3.4.21.62, and 3.4.21.63). Of the eleven EC numbers present in all assemblies, seven are within the family of peptidases. As with the MEROPS and CAZymes annotations, some of the fluid and sediments from the same site group together: AO19, LB18, SC18, PF17, CI18, QN17, QH217, and ER18.

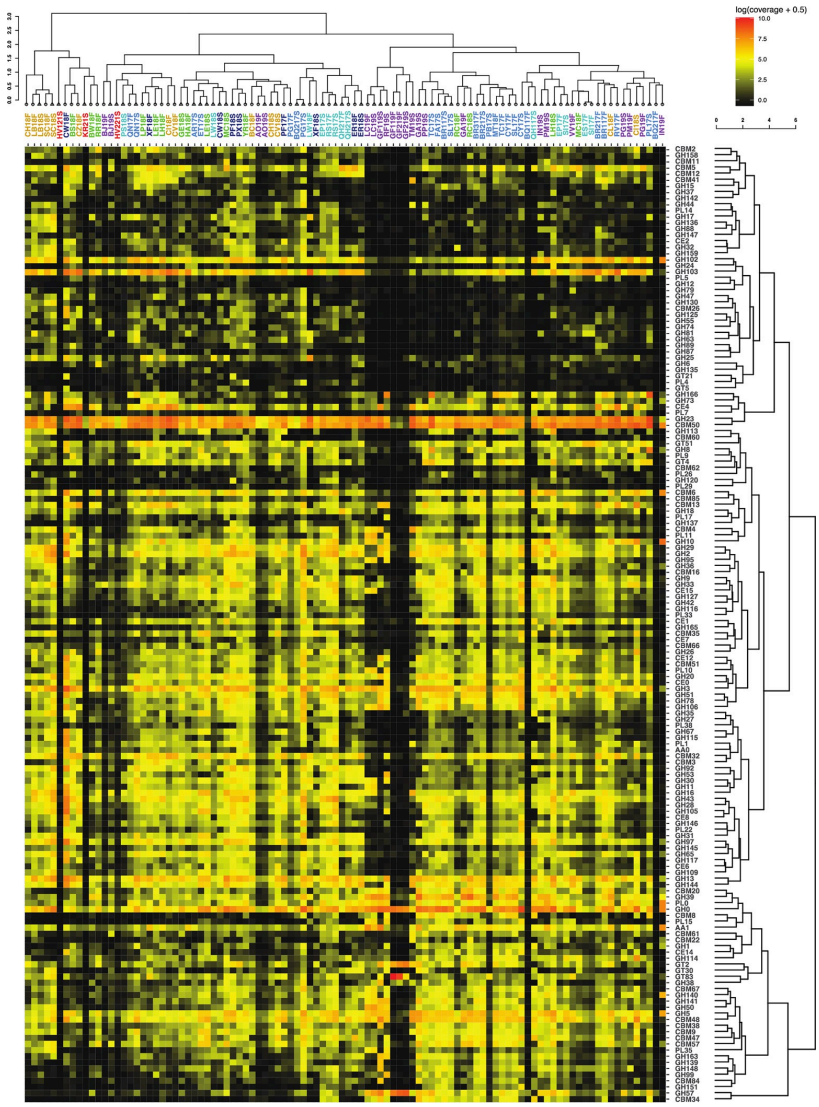

Fig 4. Heatmap with hierarchical correlation of read abundance of CAZy families (y axis) per site (x axis) based on spearman rank correlation. Visualization details are the same as Fig 3.

https://doi.org/10.1371/journal.pone.0281277.g004

CAZy degradation groupings

We summed the abundance of CAZy families that are either part of chitin/peptidoglycan degradation (bacterial necromass) or xylan degradation (plant products) (Tables 2 and 3). In total cell-degrading enzymes are in higher read abundance (521,794.37) than photosynthate-degrading enzymes (227,434.98) (Table 3). The assemblies with the highest percentage of cell-

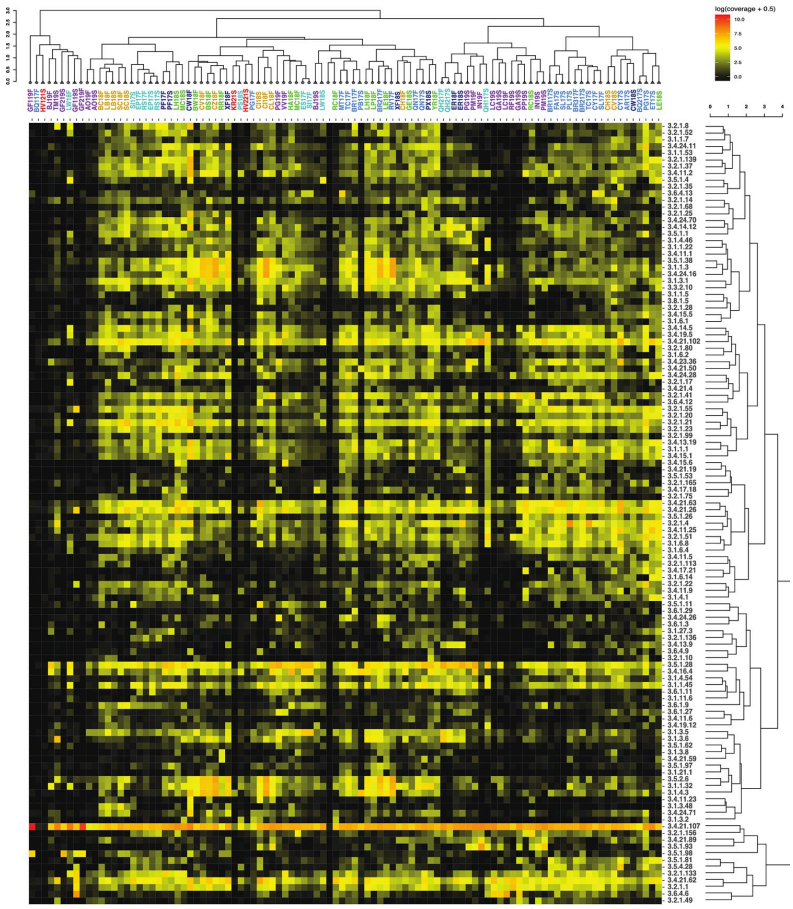

Fig 5. Heatmap with hierarchical correlation of read abundance of hydrolases (EC 3, y axis) per site, based on spearman rank correlation. Visualization details are the same as Fig 3.

https://doi.org/10.1371/journal.pone.0281277.g005

degrading enzymes are BJ18F, SI17F, KR21S, ES17F, RV17F, and CI18F. Only 20 assemblies have fewer than 50% of the cell-degrading enzyme annotations. The abundance of these enzymes for each site, with sediment and fluid components, is shown in a stacked bar plot to visualize the differing quantity across sediments and fluids (Fig 6). Overall, cell-degrading enzymes are more abundant than photosynthate-degrading enzymes. Photosynthate-degrading enzymes are more abundant in sediments than in fluids, whereas the cell-degrading enzymes are more abundant in fluids than in sediments (Table 3). CAZy family GH103 is more abundant in fluids than in sediments (Fig 6). CAZy families GH18 and GH3 are more abundant in sediments than fluids.

Table 3. Sums of enzymes associated with cell and photosynthate degradation. Cell enzymes are in the chitin and peptidoglycan groups of Table 3. The photosynthate enzymes are in the groups xylan and cellulose of Table 3. The total of these two groups are summed for each site.

Site	Cell	Plant	Province	Type	Temp °C	pH	% cell degradation
RS17S	2303.35	7311.38	Costa Rica outer forearc	Sediment	29.4	9.96	0.24
PG17S	2717.43	7824.97	Active volcanic arc	Sediment	19.2		0.26
BQ217S	275.26	702.8	Active volcanic arc	Sediment	88.9	2.11	0.28
FA17S	1356.01	3157.92	Active volcanic arc	Sediment	55.2	5.93	0.3
RS17F	1793.86	3927.14	Costa Rica outer forearc	Fluid	29.4	9.96	0.31
LE18S	1779.26	3744.37	Cordillera Talamanca	Sediment	34.7		0.32
BR117S	1790.83	3507.56	Active volcanic arc	Sediment	53.8	5.87	0.34
SL17S	1608.47	2395.79	Active volcanic arc	Sediment	57	6.12	0.4
SC18S	4231.4	5974.49	Panama slab window	Sediment	29.9	6.5	0.41
IN19S	1951.11	2651.99	Argentina backarc	Sediment	46.9	6.52	0.42
CY17S	2782.04	3678.12	Active volcanic arc	Sediment	72	6.31	0.43
BR317F	2259.54	2880.35	Active volcanic arc	Fluid	59	6.16	0.44
PP19S	2768.98	3466.71	Argentina backarc	Sediment	54.3	8.47	0.44
YR18F	3699.46	4556.12	Cordillera Talamanca	Fluid	26	8.9	0.45
RC18S	3124.49	3563.44	Cordillera Talamanca	Sediment	60	7.7	0.47
GA19S	3880.17	4421.99	Argentina backarc	Sediment	67	6.7	0.47
CW18F	16280.11	18463.25	Active volcanic backarc	Fluid	35	7.19	0.47
IN19F	4897.84	5482.85	Argentina backarc	Fluid	46.9	6.52	0.47
GF219S	8.21	8.62	Argentina backarc	Sediment	80	3.21	0.49
CW18S	1102.96	1140.82	Active volcanic backarc	Sediment	35	7.19	0.49
ET17S	3686.85	3635.11	Active volcanic arc	Sediment	40	6.06	0.5
BR217S	3714.33	3629.83	Active volcanic arc	Sediment	53.8	5.87	0.51
LH18S	8995.25	8393.51	Cordillera Talamanca	Sediment	55.4	6.7	0.52
SL17F	2882.97	2547.03	Active volcanic arc	Fluid	57	6.12	0.53
PM19S	4557.13	3980.86	Argentina backarc	Sediment	50.3	6.53	0.53
CV18S	2364.68	1971.3	Panama slab window	Sediment	34.9	7.46	0.55
RF19S	2319.97	1777.15	Argentina backarc	Sediment	82	8.23	0.57
GE18S	2650.99	1939.12	Cordillera Talamanca	Sediment	35.8	7.8	0.58
LC19S	4152.17	3007.55	Argentina backarc	Sediment	84	6.94	0.58
PF17S	5696.03	4077.12	Active volcanic backarc	Sediment	28.7	5.81	0.58
SI17S	3655.49	2607.84	Costa Rica outer forearc	Sediment	35.9	9.83	0.58
MC18S	7088.09	5020.36	Cordillera Talamanca	Sediment	31.8	9.6	0.59
HV121S	5.04	3.52	Spreading center hot spot	Sediment	93.5	2.72	0.59
EP17S	4095.65	2760.82	Costa Rica outer forearc	Sediment	26.4	9.99	0.6
AR17S	1015.94	613.94	Active volcanic arc	Sediment			0.62
PF17F	5945.38	3326.85	Active volcanic backarc	Fluid	28.7	5.81	0.64
GA19F	3232.45	1772.08	Argentina backarc	Fluid	67	6.7	0.65
LB18S	1799.92	907.5	Panama slab window	Sediment	34.8	5.951	0.66
RR18F	2427.99	1216.93	Cordillera Talamanca	Fluid	41.3	7.2756	0.67
BR117F	5777.06	2784.88	Active volcanic arc	Fluid	59	6.16	0.67
PX18S	7241.69	3328.99	Active volcanic backarc	Sediment	42.9225	6.3077	0.69
XF18S	1378.69	617.31	Active volcanic backarc	Sediment	28.9	7	0.69
CH18S	1497.87	644.82	Panama slab window	Sediment	31.1	7	0.7
QN17S	8016.9	3343.38	Active volcanic arc	Sediment	22.9	5.6	0.71
VV19F	4672.04	1821.79	Argentina backarc	Fluid	38.2	9.09	0.72
SC18F	6730.07	2555.04	Panama slab window	Fluid	29.9	6.5	0.72

(*Continued*)

Table 3. (Continued)

Site	Cell	Plant	Province	Type	Temp °C	pH	% cell degradation
BC18F	3840.09	1452.1	Panama slab window	Fluid	31.8	7.5	0.73
CI18S	10418.56	3918.02	Panama slab window	Sediment	48.3	9	0.73
BS18F	9438.61	3449.51	Cordillera Talamanca	Fluid	40.9	9.05	0.73
TC17S	11507.98	4132.12	Active volcanic arc	Sediment	60	6.24	0.74
ER18F	4408.88	1580.28	Active volcanic backarc	Fluid	35	9.51	0.74
TC17F	6889.35	2454.24	Active volcanic arc	Fluid	60	6.24	0.74
BQ117F	4.55	1.61	Active volcanic arc	Fluid	88.9	2.11	0.74
LB18F	6797.71	2293.94	Panama slab window	Fluid	34.8	5.951	0.75
QH217S	5764.17	1913.66	Costa Rica outer forearc	Sediment	36.7	8.69	0.75
CL18F	10123.52	3243.36	Panama slab window	Fluid	50.9	7.5	0.76
MT17F	7584.31	2352.33	Active volcanic arc	Fluid	59.1	6.32	0.76
CY17F	5257.73	1501	Active volcanic arc	Fluid	72	6.31	0.78
TM19S	10956.68	3105.54	Argentina backarc	Sediment	69.2	7.13	0.78
QH117S	5565.26	1527.88	Costa Rica outer forearc	Sediment	36.7	8.69	0.78
GF119S	7954.31	2174.13	Argentina backarc	Sediment	80	7.75	0.79
LH18F	11274.13	3025.97	Cordillera Talamanca	Fluid	55.4	6.7	0.79
EP17F	3224.4	850.89	Costa Rica outer forearc	Fluid	26.4	9.99	0.79
AO19S	315.56	82.69	Argentina backarc	Sediment	27.8	6.25	0.79
LC19F	7355.95	1836.67	Argentina backarc	Fluid	84	6.94	0.8
PG19S	5290.06	1307.15	Argentina backarc	Sediment	43.9	8.74	0.8
PS18S	1165.03	286.77	Costa Rica outer forearc	Sediment	33	8.2	0.8
PL17S	20079.51	4798.48	Active volcanic arc	Sediment	37.6	0.85	0.81
LE18F	5406.9	1289.32	Cordillera Talamanca	Fluid	34.7		0.81
BJ19S	2057.82	474.15	Argentina backarc	Sediment	40	6.44	0.81
LP18F	8018.62	1783.25	Cordillera Talamanca	Fluid	39.1	6.5	0.82
GF219F	25.72	5.37	Argentina backarc	Fluid	80	3.21	0.83
ER18S	7225.99	1464.14	Active volcanic backarc	Sediment	35	9.51	0.83
QH217F	4871.79	978.15	Costa Rica outer forearc	Fluid	48.7	8.53	0.83
HV221S	142.26	28.35	Spreading center hot spot	Sediment	25.7	1.82	0.83
MC18F	7154.79	1377.19	Cordillera Talamanca	Fluid	31.8	9.6	0.84
XF18F	11532.69	2192.06	Active volcanic backarc	Fluid	28.9	7	0.84
PG17F	917.39	169.35	Active volcanic arc	Fluid	19.2		0.84
LW18S	2907.58	491.44	Costa Rica outer forearc	Sediment	31.5	7.1	0.86
HA18F	5644.82	936.25	Cordillera Talamanca	Fluid	33	8.9	0.86
BR217F	12377.42	1729.54	Active volcanic arc	Fluid	59	6.16	0.88
PM19F	10782.76	1501.85	Argentina backarc	Fluid	50.3	6.53	0.88
AO19F	399.1	54.82	Argentina backarc	Fluid	27.8	6.25	0.88
GF119F	12.49	1.69	Argentina backarc	Fluid	80	7.75	0.88
BW18F	3514.44	451.47	Cordillera Talamanca	Fluid	43.2	9.05	0.89
BQ217F	3.79	0.44	Active volcanic arc	Fluid	88.9	2.11	0.9
LW18F	14067.82	1595.78	Costa Rica outer forearc	Fluid	31.5	7.1	0.9
QN17F	6016.9	676.83	Active volcanic arc	Fluid	22.9	5.6	0.9
CH18F	4852.63	515.69	Panama slab window	Fluid	31.1	7	0.9
CV18F	9161.27	951.7	Panama slab window	Fluid	34.9	7.46	0.91
CZ18F	16531	1610.23	Panama slab window	Fluid	26.3	10	0.91
RC18S	5817.55	391.52	Cordillera Talamanca	Fluid	60	7.7	0.94
PG19F	8315.79	515.92	Argentina backarc	Fluid	43.9	8.74	0.94

(*Continued*)

Table 3. (Continued)

Site	Cell	Plant	Province	Type	Temp °C	pH	% cell degradation
PB17S	2689.73	112.99	Active volcanic arc	Sediment			0.96
CI18F	16955.03	682.48	Panama slab window	Fluid	48.3	9	0.96
RV17F	15451.3	576.05	Active volcanic arc	Fluid	42.7	6.19	0.96
ES17F	7007.89	259.52	Costa Rica outer forearc	Fluid	27.9	9.75	0.96
KR21S	61.39	1.58	Spreading center hot spot	Sediment	93	2.04	0.97
SI17F	7079.4	161.59	Costa Rica outer forearc	Fluid	35.9	9.83	0.98
BJ19F	3362.49	20.58	Argentina backarc	Fluid	40	6.44	0.99
Total	**521794.37**	**227434.98**					

https://doi.org/10.1371/journal.pone.0281277.t003

Multivariate analysis

We performed multivariate analysis on the datasets using a principal component analysis (PCA) to perform an unconstrained coordination analysis. For cell-degrading enzymes, sites do not cluster based on province (Fig 7A). Instead, we see that high temperature sites (HV121, HV221, KR21, GF119, GF219, BQ1, and BQ2) cluster together while all other sites are indistinguishable based on cell-degrading enzyme abundance. Photosynthate-degrading enzyme abundances, however, do cluster by provinces, with the Costa Rica active volcanic arc and Argentina active volcanic backarc tending to group together. Sites with volcanic activity correlate with CAZyme families GH1, GH5, GH9, GH51, and GH116, which are specifically related to cellulose degradation [58]. Here, high temperature sites continue to cluster together, but do not correlate with any specific enzymes. The nonvolcanic sites correlate with CAZy families GH16, GH43, GH74, GH11, and GH67. Families GH11, GH43, and GH67 are known to be directly related to xylan degradation [59].

To further support the idea that province separation is driven by photosynthate-degrading carbohydrate-active enzymes, rather than all peptidases, a PCA analysis was done on all the MEROPS, CAZy, and EC family annotations, as well as the annotations that correspond to the enzymes that were the target of the activity assays (S2-S5 Figs in S1 File). These PCA analyses show that there are no distinct clusters based on province. However, we see province clustering for a PCA plot of only cell-degrading and photosynthate-degrading CAZy enzymes (S6 Fig in S1 File).

Discussion

All 63 sites produced a high diversity of enzymes predicted to be capable of breaking down organic matter outside the cell. This suggests that hot spring communities can break down a wide variety of organic compounds ranging from proteins and carbohydrates to structural molecules, as has been previously suggested [17, 61–63]. Below we will describe how the distribution of organic carbon degrading enzymes across these sites suggest these communities are primarily supported by microbial biomass, rather than plant detritus, consistent with a chemolithoauotrophically-based ecosystem. But these heterotrophic enzymes are less directly influenced by geological features than the taxonomic compositions or respiratory capabilities of these communities [64–67].

Nature of the heterotrophic enzymes across all seeps and hot springs

We propose that the heterotrophic community in these terrestrial seeps and hot springs primarily use the organic matter of dead bacterial necromass produced *in situ* rather than allochthonous surface-derived material from plant matter. The heterotrophic community may

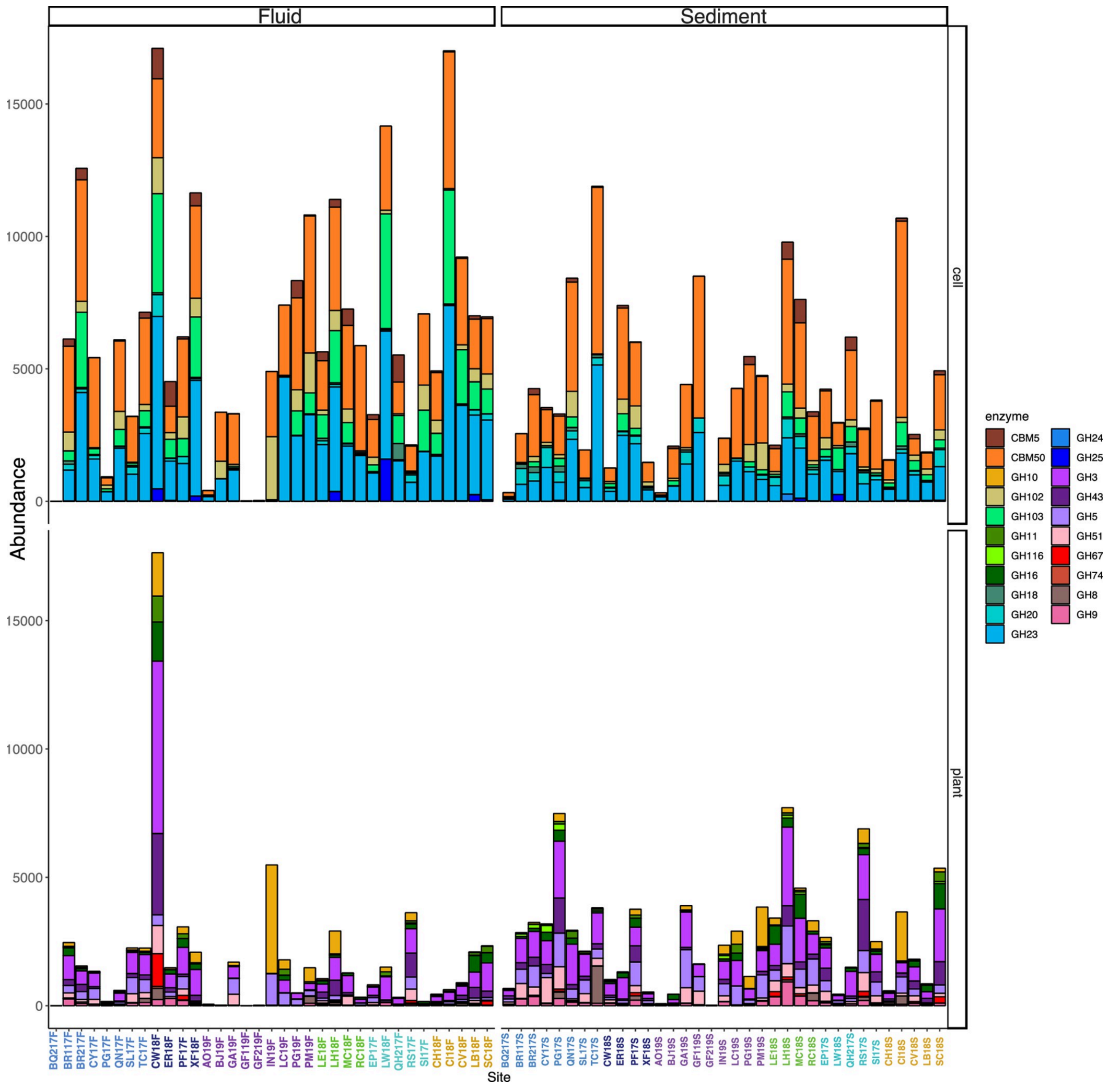

Fig 6. Read abundance of cell-degrading and photosynthate-degrading enzymes in metagenomic assemblies from sediments and fluids, with sites separated by geological province. Sites are colored by the geological provinces shown in Fig 1.

https://doi.org/10.1371/journal.pone.0281277.g006

include autotrophs that are also capable of metabolizing organic compounds. To consume complex organic matter, heterotrophs rely on extracellular enzymes such as CAZymes and peptidases to degrade the larger organic molecules so they can bring them into the cell [64]. CAZymes are important for geochemical cycling because they facilitate the breakdown of complex carbon substrates [65]. Another subset of enzymes involved in the biogeochemical cycling of heterotrophs are peptidases, which cleave peptide bonds between amino acids [60, 66]. Protein degradation has

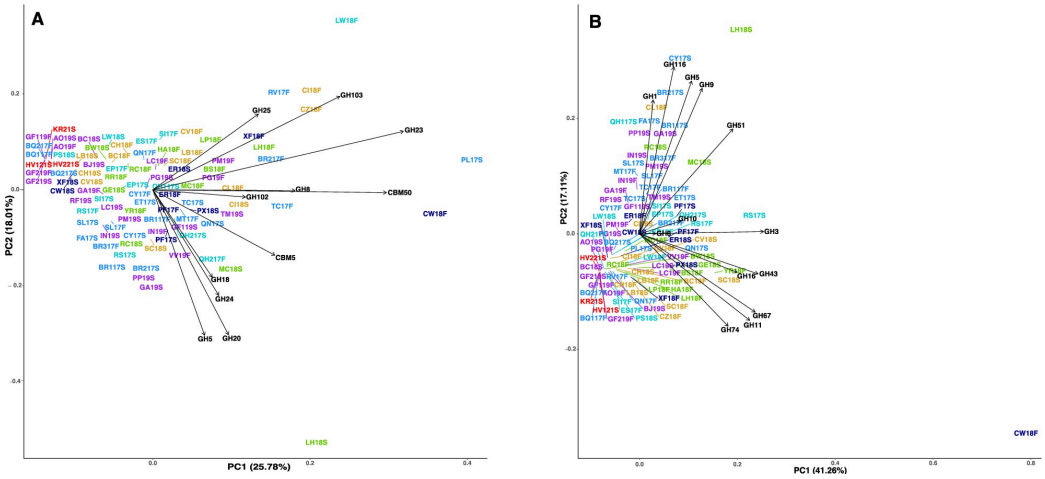

Fig 7. PCA plot CAZy family abundance. A. PCA plot of the abundance of CAZy families involved in the degradation of chitin and peptidoglycan, inferred to be cell-degrading. **B.** PCA plot of the abundance of CAZy families involved in the degradation of xylan and cellulose, inferred to be photosynthate-degrading. Sites are colored by the geological provinces shown in Fig 1.

https://doi.org/10.1371/journal.pone.0281277.g007

been shown to be important for heterotrophs within the subsurface [67, 68]. Heterotrophs within these springs may rely on protein from dead cells (necromass) for carbon and nitrogen acquisition, as they do in marine sediments [67, 69]. EC annotations are based on the reactions catalyzed which allows for analysis of different reactions within the assemblies, and much of the important heterotrophic enzymes fall under EC3, hydrolases [36]. The enzyme annotation methods do not distinguish between prokaryotic and eukaryotic sources [34, 36, 65]. Thus, the set of enzymes present in an environment can indicate the chemical nature, and therefore the source, of organic matter being consumed by heterotrophs [70].

An ecosystem supported by bacterial and archaeal cell necromass should contain more enzymes involved in peptidoglycan and chitin degradation such as chitinases, N-acetylglucosaminidase, and lysozymes [53–56]. Enzymes that are involved in the degradation of plant material, which in the case of subsurface springs would indicate allocthonous material from the surface, are often cellulases, xylanases, and glucosidases [57–59]. These enzymes have been characterized into CAZy families (Table 2). In our metagenomic assemblies, enzymes associated with cell necromass degradation are the most numerous overall, i.e., twice the amount of photosynthate-degrading enzyme families (Table 3). Enzymes for cell necromass consumption include those that break down peptidoglycan, a key component in bacterial cell walls. CAZyme families associated with peptidoglycan degradation are GH103, GH102, GH73, GH25, GH24, GH23, and CBM50 (Table 2) [56]. These families are found in most of the assemblies (Fig 4). The CAZyme families with the highest abundance are GH23 (peptidoglycan lyase) and CBM50 (LysM domain). These two CAZyme families are integral to the degradation of peptidoglycan.

Another facet of the heterotrophic community utilizing necromass for essential nutrients is the acquisition of starch, glycogen, and trehalose [71]. These compounds may also be derived from photosynthate materials. The CAZy families that are present within all assemblies are from the families GH13, GH15, GH31, GH57, GH122, and GH133 (Fig 4), which are involved in starch degradation [72]. This suggests that the possibility of using starches is a common heterotrophic metabolism across these sites.

The peptidase annotations also support the idea that the heterotrophic community relies on necromass for carbon and energy acquisition. Peptidase families such as S11, M23, S13, S66, M15, M74, M14, and C51 are used for peptidoglycan degradation (Fig 3). These families' biological functions are associated with lysis or degradation of bacterial cell walls [53]. Of the eight listed cell wall degrading/lysing peptidases, all except M74 and C51 are present in every assembly. Peptidase family M74 is present in all but four of the assemblies, GF119F, GF119S, GF219F, and GF219S. Peptidase family C51 is present in all but eight of the assemblies, BQ117F, GF119F, GF119S, GF219F, GF219S, HV121S, KR21S, and RF19S. All the samples lacking M74 and C51 fall within the temperature range (80–93.5˚C) in magmatic steam-heated springs. This may suggest that M74, which is a murein endopeptidase and C51, a D-alanyl-glycyl peptidase, are not adapted to high temperatures.

CAZyme families associated with plant degradation have lower total abundance in comparison to cell degradation even though there are more possibilities for plant degrading families to be found (Table 3). Of the 45 assemblies that have more than 30% plant degrading enzymes out of all the enzymes related to cell and plant degradation (Table 2), 34 are sediment samples (Table 3). Therefore, sediment assemblies contain more annotations for photosynthate-degrading enzymes than fluid samples. This may be caused by additions of photosynthetically-derived material to the sediments deposited at the surface.

The dominance of cellular biomass as the main organic matter source for the heterotrophic community is consistent with chemolithoautotrophic biomass forming the major primary production. This agrees with the findings from Barry et al., 2019a, who used helium and carbon isotopes from the same sites to show that the dissolved inorganic carbon was almost entirely derived from deep (i.e., mantle and subduction-related) sources [3]. Since hot spring enzymes related to cell necromass are more abundant in our metagenomes, we propose that hot springs microbes primarily subsist using necromass derived from chemoautotrophs rather than surficially-derived organic carbon ultimately derived from plants.

Independent confirmation of enzyme activity with substrate proxy analyses

Extracellular enzyme assays were used as a proxy for the activity of heterotrophic organisms within the seeps and hot spring derived sediment samples. Enzymes that are commonly-assayed in soils are often associated with cellulose and lignin degradation along with enzymes that hydrolyze proteins [70]. Degradation of plant litter is often demonstrated using assays for AG, BG, CB, and XYL, as they degrade cellulose and xylan. LEU assays represent carbon and nitrogen acquisition from proteins alongside NAG which is a proxy of the degradation of peptidoglycan and chitin [73]. Extracellular enzyme assays can reveal different organic carbon and nitrogen sources for microbial communities, allowing for inferences about biogeochemical cycling within the system. Enzymes involved in carbon and nitrogen acquisition have been used to demonstrate the limitations of nutrients within various systems [70, 73, 74]. The results for these assays predicted that these organisms are not highly active (S4 Table in S1 File). However, the fact that activity could be observed at all suggests that at least some of the enzymes we identified in our metagenomic annotations were active in natural samples and the lack of extracellular enzymatic activity may be the result of not recreating the ideal geochemical parameters for the hydrolysis within the lab setting [75].

Highest temperature magmatic steam-heated springs have low diversity of heterotrophic enzymes

Lower diversity microbial communities tend to be found at very high temperature springs [55]. Accordingly, our high temperature and low pH sites (GF219S, GF119F, GF219F,

HV121S, and KR21S) have fewer annotations for both CAZymes and peptidases than more mesophilic springs. This is likely due to the small number of organisms present within these sites (S1 Fig in S1 File). Although these sites are driven by heat and volatiles originating from the subsurface, they are not representative of deep subsurface communities. The depth of the subsurface biosphere at these sites is shallow (<50m) due to the high heat flow in the area and near boiling temperature that limit the possible distribution of microorganisms at depth [11]. The shallow subsurface nature and lower residence time of the communities in these sites combined with the lack of phylogenetic diversity is the likely cause of the lower functional diversity of the heterotrophic community.

The extracellular enzymatic assays demonstrate that many high temperature sites may not be expressing the enzymes found within their metagenomes (S4 Table in S1 File). The sites with the highest extracellular activities are within the temperature range of 32.5–50˚C. Extracellular enzymes require energy to produce, so organisms that are already spending energy surviving in very high temperature and low pH sites may not have excess capacity for extracellular enzyme production [67, 76, 77]. Therefore, because the hyperthermic sites are energy-limited they are not expressing as many extracellular enzymes as the more mesothermic springs.

Heterotrophic metabolism is not influenced by geological processes

Chemolithoautotrophic metabolisms and the redox couples that provide power for them vary depending on geological province across the Central America convergent margin [4, 7]. We hypothesized that the heterotrophic community's enzymatic functions would also vary across the provinces, since their taxonomic identities and respiratory properties do [4, 7]. However, most of the extracellular enzymes in our metagenomic assemblies do not correlate with geological provinces. Based on hierarchical clustering of spearman correlations, all sites except for the very high temperature magmatic steam-heated sites are difficult to distinguish based on abundance of predicted extracellular enzymes for peptide and carbohydrate degradation. Even though the populations of chemolithoautotrophs vary by geological setting, the biomass they produce may be similar enough that it can be broken down by similar sets of enzymes (Fig 7A), even though the heterotrophic taxa that make these enzymes also vary by geological setting [4, 7].

One group of extracellular enzymes, however, does differentiate by geological province. The PCA analysis of the photosynthate-degrading enzymes shows slight clustering of the Costa Rica active volcanic arc and backarc and the Argentina backarc (Fig 7B). These sites have the same amount of photosynthate-degrading and cell-degrading enzymes as the other provinces, but the composition of the photosynthate-degrading enzymes more closely reflects cellulose degradation with enzymes such as GH5, GH9, GH116, and GH1. Springs and seeps that lack direct magmatic influence, such as the Costa Rica outer forearc, the Cordillera Talamanca, and Panama cluster separately from the volcanic sites, with more xylan-degrading enzymes. When all CAZy families for xylan, chitin, and peptidoglycan degradation are combined, clustering based on province still occurs, suggesting a strong association of volcanic sites with cellulose-degradation and non-volcanic sites with xylan-degradation (S6 Fig in S1 File).

Since these photosynthate-degrading enzymes are more abundant in surficial sediments than in the freshly-expressed fluids, they are likely degrading surface-derived organic matter rather than chemolithoautotrophic production in the subsurface. The surface-derived substrates that are cleaved by photosynthate-degrading enzymes, however, are unlikely to come from plants, since our sites in the Costa Rica volcanic arc are in a dense jungle and our sites

from the Argentina backarc that group with them are from the high altiplano desert, which is extremely dry with little vegetation. If the photosynthate-degrading enzymes were mostly driven by introduction of surrounding plants, then the Costa Rica volcanic zone should have more similar enzymes to the other Costa Rica and Panama sites, since they are close together and have similarly dense vegetation. A more likely potential source of xylan for these springs is thermophilic algae [78, 79]. Volcanic springs are often associated with higher temperatures, average 55.4˚C, while the non-volcanic springs are less thermophilic with an average temperature of 37.1˚C. The lower temperatures of the non-volcanic springs are closer to the optimal temperatures of growth for diverse algae, some of which are also well adapted to sulfidic and acidic sites [80]. Therefore, the non-volcanic sites may allow for algae to grow and act as a source of xylan for the heterotrophic organisms. Cellulose, which is more common in volcanic sites, is often found in cyanobacteria [81], which have a higher temperature tolerance than eukaryotic algae [82]. However, we cannot rule out the alternate possibility that these enzymes are responding to delivery of different types of subsurface-derived organic matter in the volcanic vs. non-volcanic systems.

Conclusions

Here we present extracellular carbohydrate- and peptide-degrading enzyme potential from the metagenomes of 63 seeps and hot springs across the Central American and the Andean convergent margin (Argentinian backarc of the Central Volcanic Zone), and Iceland (mantle plume-influenced spreading center). Throughout the seven tectonic-geographic sample groups examined, we see that the heterotrophic community primarily relies on the degradation of proteins rather than carbohydrates. This is supported by the MEROPS annotations that are found in high abundance across all assemblies. The highest CAZyme and peptidase annotations are for families associated with peptidoglycan degradation. This supports the hypothesis that most of the metabolic function for heterotrophs is derived from the degradation of dead microbial cells, consistent with the major source of organic matter in this system being subsurface chemolithoautotrophic production. Very high temperature (>75˚C), low pH sites (< 4), that are heated by volcanic inputs, differ from the rest of the sites based on their CAZymes and peptidases. Except for a few thermophilic peptidases, they had fewer extracellular carbon-degrading enzymes, suggesting that the secondary trophic level is less well-developed at these sites, possibly because they must put more energy into survival in these extreme conditions. Except for these high temperature sites, most extracellular CAZyme, hydrolase, and peptidase families did not differ by geological province. This suggests that, even though the taxonomic identities and respirations of the chemolithoautotrophs and heterotrophs vary by geological province [4, 7], their organic matter degrading capabilities do not. The exceptions are the photosynthate-degrading enzymes which comprised a minor component of the carbon-degrading enzymes. Volcanic sites had more cyanobacteria-degrading enzymes while non-volcanic arc sites had more algae-degrading enzymes, likely due to the difference in temperature preference of those two types of phototrophs. This study revealed that the secondary community within terrestrial geothermal systems actively participates in the carbon budget within these sites by consuming chemolithoautotrophically-derived dead cell material, with enzymatic capabilities that are independent of geological province.

Supporting information

S1 Checklist. Inclusivity in global research.
(DOCX)

S1 File. All supplemental tables and figures referred to in the text.
(DOCX)

Acknowledgments

The authors wish to thank Emilce Bustos, Ruben Filipovich, Joy Buongiorno, Matthew O. Schrenk, Patrick Beaudry, Bernard Marty, Diana Roman, Forrest Horton, Alan Seltzer, Maja Rasmussen, and Eemu Ranta.

Author Contributions

Conceptualization: Raegan Paul, Donato Giovannelli, Karen G. Lloyd.

Data curation: Raegan Paul, Timothy J. Rogers, Kate M. Fullerton, Martina Cascone.

Formal analysis: Raegan Paul.

Funding acquisition: J. Maarten de Moor, Andri Stefánsson, Sæmundur A. Halldórsson, Carlos J. Ramirez, Gerdhard L. Jessen, Peter H. Barry, Donato Giovannelli, Karen G. Lloyd.

Investigation: Raegan Paul, Matteo Selci, Murray H. Stokes, Agostina Chiodi, Angelina Cordone.

Methodology: Raegan Paul, Timothy J. Rogers, Kate M. Fullerton, Martina Cascone, Donato Giovannelli, Karen G. Lloyd.

Project administration: Donato Giovannelli, Karen G. Lloyd.

Resources: Timothy J. Rogers, Kate M. Fullerton, Martina Cascone, Andrew D. Steen, J. Maarten de Moor, Andri Stefánsson, Sæmundur A. Halldórsson, Carlos J. Ramirez, Gerdhard L. Jessen, Peter H. Barry, Donato Giovannelli, Karen G. Lloyd.

Software: Timothy J. Rogers, Kate M. Fullerton, Andrew D. Steen, J. Maarten de Moor, Andri Stefánsson, Sæmundur A. Halldórsson, Carlos J. Ramirez, Gerdhard L. Jessen, Peter H. Barry.

Supervision: Andrew D. Steen, J. Maarten de Moor, Andri Stefánsson, Sæmundur A. Halldórsson, Carlos J. Ramirez, Gerdhard L. Jessen, Peter H. Barry.

Visualization: Raegan Paul.

Writing – original draft: Raegan Paul.

Writing – review & editing: Raegan Paul, Timothy J. Rogers, Kate M. Fullerton, Matteo Selci, Martina Cascone, Murray H. Stokes, Andrew D. Steen, J. Maarten de Moor, Agostina Chiodi, Andri Stefánsson, Sæmundur A. Halldórsson, Carlos J. Ramirez, Gerdhard L. Jessen, Peter H. Barry, Angelina Cordone, Donato Giovannelli, Karen G. Lloyd.

References

1. Muffler LJP. Tectonic and hydrologic control of the nature and distribution of geothermal resources. 1975.
2. Stefánsson A, Hilton DR, Sveinbjörnsdóttir ÁE, Torssander P, Heinemeier J, Barnes JD, et al. Isotope systematics of Icelandic thermal fluids. Journal of Volcanology and Geothermal Research. 2017; 337: 146–164. https://doi.org/10.1016/J.JVOLGEORES.2017.02.006
3. Barry PH, de Moor JM, Giovannelli D, Schrenk M, Hummer DR, Lopez T, et al. Forearc carbon sink reduces long-term volatile recycling into the mantle. Nature 2019 568:7753. 2019; 568: 487–492. https://doi.org/10.1038/s41586-019-1131-5 PMID: 31019327

4. Fullerton KM, Schrenk MO, Yücel M, Manini E, Basili M, Rogers TJ, et al. Effect of tectonic processes on biosphere–geosphere feedbacks across a convergent margin. Nat Geosci. 2021; 14: 301–306. https://doi.org/10.1038/s41561-021-00725-0

5. Bekaert D, Turner SJ, Broadley MW, Labidi J, Bekaert D v, Turner SJ, et al. Subduction-Driven Volatile Recycling: A Global Mass Balance Metallic components of the lunar regolith View project Looking for indigenous noble gases on the Moon View project Subduction-Driven Volatile Recycling: A Global Mass Balance. The Annual Review of Earth and Planetary Sciences is online at earth.annualreviews.org. 2021; 49: 37–70. https://doi.org/10.1146/annurev-earth-071620-055024

6. Harðardóttir S, Halldórsson SA, Hilton DR. Spatial distribution of helium isotopes in Icelandic geothermal fluids and volcanic materials with implications for location, upwelling and evolution of the Icelandic mantle plume. Chem Geol. 2018; 480: 12–27. https://doi.org/10.1016/J.CHEMGEO.2017.05.012

7. Rogers TJ, Buongiorno J, Jessen GL, Schrenk MO, Fordyce JA, de Moor JM, et al. Chemolithoautotroph distributions across the subsurface of a convergent margin. The ISME Journal 2022. 2022; 1–11. https://doi.org/10.1038/s41396-022-01331-7 PMID: 36257972

8. Reysenbach AL, St John E, Meneghin J, Flores GE, Podar M, Dombrowski N, et al. Complex subsurface hydrothermal fluid mixing at a submarine arc volcano supports distinct and highly diverse microbial communities. Proc Natl Acad Sci U S A. 2020; 117: 32627–32638. https://doi.org/10.1073/pnas.2019021117 PMID: 33277434

9. Arnórsson S, Bjarnason JÖ, Giroud N, Gunnarsson I, Stefánsson A. Sampling and analysis of geothermal fluids. Geofluids. 2006; 6: 203–216. https://doi.org/10.1111/J.1468-8123.2006.00147.X

10. Summit M, Baross JA. A novel microbial habitat in the mid-ocean ridge subseafloor. Proceedings of the National Academy of Sciences. 2001; 98: 2158–2163. https://doi.org/10.1073/pnas.051516098 PMID: 11226209

11. Giovannelli D, Barry PH, de Moor JM, Jessen GL, Schrenk MO, Lloyd KG. Sampling across large-scale geological gradients to study geosphere-biosphere interactions. Front Microbiol. 2022; 13. https://doi.org/10.3389/fmicb.2022.998133 PMID: 36386678

12. Urschel MR, Kubo MD, Hoehler TM, Peters JW, Boyd ES. Carbon source preference in chemosynthetic hot spring communities. Appl Environ Microbiol. 2015; 81: 3834–3847. https://doi.org/10.1128/AEM.00511-15 PMID: 25819970

13. Schuler CG, Havig JR, Hamilton TL. Hot spring microbial community composition, morphology, and carbon fixation: Implications for interpreting the ancient rock record. Front Earth Sci (Lausanne). 2017; 5: 97. https://doi.org/10.3389/FEART.2017.00097/BIBTEX

14. Power JF, Carere CR, Lee CK, Wakerley GLJ, Evans DW, Button M, et al. Microbial biogeography of 925 geothermal springs in New Zealand. Nature Communications 2018 9:1. 2018; 9: 1–12. https://doi.org/10.1038/s41467-017-02088-w

15. Biddle JF, Lipp JS, Lever MA, Lloyd KG, Sørensen KB, Anderson R, et al. Heterotrophic Archaea dominate sedimentary subsurface ecosystems off Peru. Proc Natl Acad Sci U S A. 2006; 103: 3846–3851. https://doi.org/10.1073/pnas.0600035103 PMID: 16505362

16. Kaushal G, Kumar J, Sangwan RS, Singh SP. Metagenomic analysis of geothermal water reservoir sites exploring carbohydrate-related thermozymes. Int J Biol Macromol. 2018; 119: 882–895. https://doi.org/10.1016/j.ijbiomac.2018.07.196 PMID: 30081126

17. Jun Liew K, Hung Liang C, Ting Lau Y, Suriaty Yaakop A, Chan K-G, Shahar S, et al. Thermophiles and carbohydrate-active enzymes (CAZymes) in biofilm microbial consortia that decompose lignocellulosic plant litters at high temperatures. Scientific Reports |. 2022; 12. https://doi.org/10.1038/s41598-022-06943-9 PMID: 35181739

18. Sahoo K, Sahoo RK, Gaur M, Subudhi E. Cellulolytic thermophilic microorganisms in white biotechnology: a review. Folia Microbiol (Praha). 2020; 65: 25–43. https://doi.org/10.1007/s12223-019-00710-6 PMID: 31102141

19. Strazzulli A, Cobucci-Ponzano B, Iacono R, Giglio R, Maurelli L, Curci N, et al. Discovery of hyperstable carbohydrate-active enzymes through metagenomics of extreme environments. FEBS Journal. 2020; 287: 1116–1137. https://doi.org/10.1111/febs.15080 PMID: 31595646

20. Vishnivetskaya TA, Hamilton-Brehm SD, Podar M, Mosher JJ, Palumbo A V., Phelps TJ, et al. Community Analysis of Plant Biomass-Degrading Microorganisms from Obsidian Pool, Yellowstone National Park. Microb Ecol. 2015; 69: 333–345. https://doi.org/10.1007/s00248-014-0500-8 PMID: 25319238

21. Cai R, Zhang J, Liu R, Sun C. Metagenomic Insights into the Metabolic and Ecological Functions of Abundant Deep-Sea Hydrothermal Vent DPANN Archaea. Appl Environ Microbiol. 2021; 87: 1–11. https://doi.org/10.1128/AEM.03009-20 PMID: 33608296

22. Simkus DN, Slater GF, Lollar BS, Wilkie K, Kieft TL, Magnabosco C, et al. Variations in microbial carbon sources and cycling in the deep continental subsurface. Geochim Cosmochim Acta. 2016; 173: 264–283. https://doi.org/10.1016/j.gca.2015.10.003

23. Arnosti C, Bell C, Moorhead DL, Sinsabaugh RL, Steen AD, Stromberger M, et al. Extracellular enzymes in terrestrial, freshwater, and marine environments: Perspectives on system variability and common research needs. Biogeochemistry. 2014. pp. 5–21. https://doi.org/10.1007/s10533-013-9906-5

24. Montero W, Lewis JC, Araya MC. The Guanacaste Volcanic Arc Sliver of Northwestern Costa Rica. Scientific Reports 2017 7:1. 2017; 7: 1–9. https://doi.org/10.1038/s41598-017-01593-8 PMID: 28496117

25. Zimmer MM, Fischer TP, Hilton DR, Alvarado GE, Sharp ZD, Walker JA. Nitrogen systematics and gas fluxes of subduction zones: Insights from Costa Rica arc volatiles. Geochemistry, Geophysics, Geosystems. 2004;5. https://doi.org/10.1029/2003GC000651

26. Abratis M, Wörner G. Ridge collision, slab-window formation, and the flux of Pacific asthenosphere into the Caribbean realm. Geology. 2001; 127. Available: www.geosociety.org/pubs/

27. Bekaert D v., Gazel E, Turner S, Behn MD, de Moor JM, Zahirovic S, et al. High 3He/4He in central Panama reveals a distal connection to the Galapagos plume. Proc Natl Acad Sci U S A. 2021; 118: e2110997118. https://doi.org/10.1073/PNAS.2110997118/SUPPL_FILE/PNAS.2110997118.SD03.XLSX

28. Peacock SM, van Keken PE, Holloway SD, Hacker BR, Abers GA, Fergason RL. Thermal structure of the Costa Rica–Nicaragua subduction zone. Physics of the Earth and Planetary Interiors. 2005; 149: 187–200. https://doi.org/10.1016/J.PEPI.2004.08.030

29. White RS, Bown JW, Smallwood JR. The temperature of the Iceland plume and origin of outward- propagating V-shaped ridges. Journal—Geological Society (London). 1995; 152: 1039–1045. https://doi.org/10.1144/GSL.JGS.1995.152.01.26

30. Barry PH, Hilton DR, Füri E, Halldórsson SA, Grönvold K. Carbon isotope and abundance systematics of Icelandic geothermal gases, fluids and subglacial basalts with implications for mantle plume-related CO2 fluxes. Geochim Cosmochim Acta. 2014; 134: 74–99. https://doi.org/10.1016/J.GCA.2014.02.038

31. Ryan WBF, Carbotte SM, Coplan JO, O'Hara S, Melkonian A, Arko R, et al. Global Multi-Resolution Topography synthesis. Geochemistry, Geophysics, Geosystems. 2009;10. https://doi.org/10.1029/2008GC002332

32. Zhang H, Yohe T, Huang L, Entwistle S, Wu P, Yang Z, et al. dbCAN2: a meta server for automated carbohydrate-active enzyme annotation. Nucleic Acids Res. 2018; 46: W95–W101. https://doi.org/10.1093/nar/gky418 PMID: 29771380

33. Shaffer M, Borton MA, McGivern BB, Zayed AA, la Rosa SL, Solden LM, et al. DRAM for distilling microbial metabolism to automate the curation of microbiome function. Nucleic Acids Res. 2020; 48: 8883–8900. https://doi.org/10.1093/nar/gkaa621 PMID: 32766782

34. Rawlings ND, Barrett AJ, Bateman A. MEROPS: the peptidase database. Nucleic Acids Res. 2010; 38: D227. https://doi.org/10.1093/nar/gkp971 PMID: 19892822

35. Lombard V, Golaconda Ramulu H, Drula E, Coutinho PM, Henrissat B. The carbohydrate-active enzymes database (CAZy) in 2013. Nucleic Acids Res. 2014; 42: D490–D495. https://doi.org/10.1093/nar/gkt1178 PMID: 24270786

36. Hu QN, Zhu H, Li X, Zhang M, Deng Z, Yang X, et al. Assignment of EC Numbers to Enzymatic Reactions with Reaction Difference Fingerprints. PLoS One. 2012; 7. https://doi.org/10.1371/journal.pone.0052901 PMID: 23285222

37. Barry PH, De Moor JM, Chiodi A, Aguilera F, Hudak MR, Bekaert D V., et al. The Helium and Carbon Isotope Characteristics of the Andean Convergent Margin. Front Earth Sci (Lausanne). 2022; 10: 985. https://doi.org/10.3389/FEART.2022.897267/BIBTEX

38. Bolger AM, Lohse M, Usadel B. Trimmomatic: a flexible trimmer for Illumina sequence data. Bioinformatics. 2014; 30: 2114–2120. https://doi.org/10.1093/bioinformatics/btu170 PMID: 24695404

39. Uritskiy G v., Diruggiero J, Taylor J. MetaWRAP—A flexible pipeline for genome-resolved metagenomic data analysis. Microbiome. 2018; 6: 1–13. https://doi.org/10.1186/S40168-018-0541-1/FIGURES/7

40. Gurevich A, Saveliev V, Vyahhi N, Tesler G. QUAST: quality assessment tool for genome assemblies. Bioinformatics. 2013; 29: 1072–1075. https://doi.org/10.1093/bioinformatics/btt086 PMID: 23422339

41. Arkin AP, Cottingham RW, Henry CS, Harris NL, Stevens RL, Maslov S, et al. KBase: The United States Department of Energy Systems Biology Knowledgebase. Nature Biotechnology 2018 36:7. 2018; 36: 566–569. https://doi.org/10.1038/nbt.4163 PMID: 29979655

42. Li D, Liu C-M, Luo R, Sadakane K, Lam T-W. MEGAHIT: an ultra-fast single-node solution for large and complex metagenomics assembly via succinct de Bruijn graph. Bioinformatics. 2015; 31: 1674–1676. https://doi.org/10.1093/bioinformatics/btv033 PMID: 25609793

43. Seemann T. Prokka: rapid prokaryotic genome annotation. Bioinformatics. 2014; 30: 2068–2069. https://doi.org/10.1093/bioinformatics/btu153 PMID: 24642063

44. Armenteros JJA, Salvatore M, Emanuelsson O, Winther O, von Heijne G, Elofsson A, et al. Detecting sequence signals in targeting peptides using deep learning. Life Sci Alliance. 2019;2. https://doi.org/10.26508/LSA.201900429 PMID: 31570514

45. Langmead B, Salzberg SL. Fast gapped-read alignment with Bowtie 2. Nat Methods. 2012; 9: 357. https://doi.org/10.1038/nmeth.1923 PMID: 22388286

46. Danecek P, Bonfield JK, Liddle J, Marshall J, Ohan V, Pollard MO, et al. Twelve years of SAMtools and BCFtools. Gigascience. 2021; 10: 1–4. https://doi.org/10.1093/gigascience/giab008 PMID: 33590861

47. Freitas TAK, Li PE, Scholz MB, Chain PSG. Accurate read-based metagenome characterization using a hierarchical suite of unique signatures. Nucleic Acids Res. 2015;43. https://doi.org/10.1093/nar/gkv180 PMID: 25765641

48. Basili M, Rogers TJ, Fullerton K, Nakagawa M, Yucel M, de Moor JM, et al. Regional patterns in microbial communities of deeply-sourced spring fluids across the Central America subduction zone. In Prep.

49. Cascone M, Bastianoni A, Selci M, Correggia M, Di Lorio L, Cordone A, et al. Deeply-sourced springs of the Argentina backarc as windows into the subsurface. In Prep. 2022.

50. Bell CW, Fricks BE, Rocca JD, Steinweg JM, McMahon SK, Wallenstein MD. High-throughput Fluorometric Measurement of Potential Soil Extracellular Enzyme Activities. JoVE (Journal of Visualized Experiments). 2013; e50961. https://doi.org/10.3791/50961 PMID: 24299913

51. Barry PH, Nakagawa M, Giovannelli D, Maarten de Moor J, Schrenk M, Seltzer AM, et al. Helium, inorganic and organic carbon isotopes of fluids and gases across the Costa Rica convergent margin. Scientific Data 2019 6:1. 2019; 6: 1–8. https://doi.org/10.1038/s41597-019-0302-4 PMID: 31767867

52. Sipes K, Paul R, Fine A, Li P, Liang R, Boike J, et al. Permafrost Active Layer Microbes From Ny Ålesund, Svalbard (79˚N) Show Autotrophic and Heterotrophic Metabolisms With Diverse Carbon-Degrading Enzymes. Front Microbiol. 2022; 12. https://doi.org/10.3389/fmicb.2021.757812 PMID: 35185810

53. Vermassen A, Leroy S, Talon R, Provot C, Popowska M, Desvaux M. Cell wall hydrolases in bacteria: Insight on the diversity of cell wall amidases, glycosidases and peptidases toward peptidoglycan. Frontiers in Microbiology. Frontiers Media S.A.; 2019. https://doi.org/10.3389/fmicb.2019.00331 PMID: 30873139

54. Zhou Z, Tran PQ, Kieft K, Anantharaman K. Genome diversification in globally distributed novel marine Proteobacteria is linked to environmental adaptation. ISME Journal. 2020; 14: 2060–2077. https://doi.org/10.1038/s41396-020-0669-4 PMID: 32393808

55. Donhauser J, Qi W, Bergk-Pinto B, Frey B. High temperatures enhance the microbial genetic potential to recycle C and N from necromass in high-mountain soils. Glob Chang Biol. 2021; 27: 1365–1386. https://doi.org/10.1111/gcb.15492 PMID: 33336444

56. Ren C, Zhang X, Zhang S, Wang J, Xu M, Guo Y, et al. Altered microbial CAZyme families indicated dead biomass decomposition following afforestation. Soil Biol Biochem. 2021;160. https://doi.org/10.1016/j.soilbio.2021.108362

57. Dodd D, Mackie RI, Cann IKO. Xylan degradation, a metabolic property shared by rumen and human colonic Bacteroidetes. Molecular Microbiology. 2011. pp. 292–304. https://doi.org/10.1111/j.1365-2958.2010.07473.x PMID: 21219452

58. Escuder-Rodríguez JJ, Decastro ME, Cerdán ME, Rodríguez-Belmonte E, Becerra M, González-Siso MI. Cellulases from thermophiles found by metagenomics. Microorganisms. MDPI AG; 2018. https://doi.org/10.3390/microorganisms6030066 PMID: 29996513

59. Knapik K, Becerra M, González-Siso MI. Microbial diversity analysis and screening for novel xylanase enzymes from the sediment of the Lobios Hot Spring in Spain. Sci Rep. 2019; 9. https://doi.org/10.1038/s41598-019-47637-z PMID: 31371784

60. Nguyen TTH, Myrold DD, Mueller RS. Distributions of extracellular peptidases across prokaryotic genomes reflect phylogeny and habitat. Front Microbiol. 2019; 10. https://doi.org/10.3389/fmicb.2019.00413 PMID: 30891022

61. Cheng JH, Wang Y, Zhang XY, Sun ML, Zhang X, Song XY, et al. Characterization and Diversity Analysis of the Extracellular Proteases of Thermophilic Anoxybacillus caldiproteolyticus 1A02591 From Deep-Sea Hydrothermal Vent Sediment. Front Microbiol. 2021; 12. https://doi.org/10.3389/fmicb.2021.643508 PMID: 33796092

62. Choure K, Parsai S, Kotoky R, Srivastava A, Tilwari A, Rai PK, et al. Comparative Metagenomic Analysis of Two Alkaline Hot Springs of Madhya Pradesh, India and Deciphering the Extremophiles for Industrial Enzymes. Front Genet. 2021;12. https://doi.org/10.3389/fgene.2021.643423 PMID: 33763123

63. DeCastro ME, Doane MP, Dinsdale EA, Rodríguez-Belmonte E, González-Siso MI. Exploring the taxonomical and functional profile of As Burgas hot spring focusing on thermostable β-galactosidases. Sci Rep. 2021; 11. https://doi.org/10.1038/s41598-020-80489-6 PMID: 33420292

64. Benz R, Bauer K. Permeation of hydrophilic molecules through the outer membrane of gram-negativ bacteria. Eur J Biochem. 1988; 176: 1–19. https://doi.org/10.1111/J.1432-1033.1988.TB14245.X PMID: 2901351

65. Garron ML, Henrissat B. The continuing expansion of CAZymes and their families. Curr Opin Chem Biol. 2019; 53: 82–87. https://doi.org/10.1016/j.cbpa.2019.08.004 PMID: 31550558

66. Van Der Velden VHJ, Hulsmann AR. Peptidases: structure, function and modulation of peptide-mediated effects in the human lung. Clinical and Experimental Allergy. 1999; 29: 445. https://doi.org/10.1046/j.1365-2222.1999.00462.x PMID: 10202358

67. Steen AD, Kevorkian RT, Bird JT, Dombrowski N, Baker BJ, Hagen SM, et al. Kinetics and identities of extracellular peptidases in subsurface sediments of the White Oak River Estuary, North Carolina. Appl Environ Microbiol. 2019; 85: 102–121. https://doi.org/10.1128/AEM.00102-19 PMID: 31324636

68. Lloyd KG, May MK, Kevorkian RT, Steen AD. Meta-analysis of quantification methods shows that archaea and bacteria have similar abundances in the subseafloor. Appl Environ Microbiol. 2013; 79: 7790–7799. https://doi.org/10.1128/AEM.02090-13 PMID: 24096423

69. Bradley JA, Amend JP, LaRowe DE. Necromass as a Limited Source of Energy for Microorganisms in Marine Sediments. J Geophys Res Biogeosci. 2018; 123: 577–590. https://doi.org/10.1002/2017JG004186

70. Sinsabaugh RL, Lauber CL, Weintraub MN, Ahmed B, Allison SD, Crenshaw C, et al. Stoichiometry of soil enzyme activity at global scale. Ecol Lett. 2008; 11: 1252–1264. https://doi.org/10.1111/j.1461-0248.2008.01245.x PMID: 18823393

71. Žifčáková L, Větrovský T, Lombard V, Henrissat B, Howe A, Baldrian P. Feed in summer, rest in winter: microbial carbon utilization in forest topsoil. Microbiome. 2017; 5: 122. https://doi.org/10.1186/s40168-017-0340-0 PMID: 28923122

72. Møller MS, Svensson B. Structural biology of starch-degrading enzymes and their regulation. Current Opinion in Structural Biology. Elsevier Ltd; 2016. pp. 33–42. https://doi.org/10.1016/j.sbi.2016.07.006 PMID: 27450115

73. Luo L, Meng H, Gu JD. Microbial extracellular enzymes in biogeochemical cycling of ecosystems. J Environ Manage. 2017; 197: 539–549. https://doi.org/10.1016/j.jenvman.2017.04.023 PMID: 28419976

74. Schimel JP, Weintraub MN. The implications of exoenzyme activity on microbial carbon and nitrogen limitation in soil: a theoretical model. Soil Biol Biochem. 2003; 35: 549–563. https://doi.org/10.1016/S0038-0717(03)00015-4

75. German DP, Weintraub MN, Grandy AS, Lauber CL, Rinkes ZL, Allison SD. Optimization of hydrolytic and oxidative enzyme methods for ecosystem studies. Soil Biol Biochem. 2011; 43: 1387–1397. https://doi.org/10.1016/J.SOILBIO.2011.03.017

76. Breyer E, Zhao Z, Herndl GJ, Baltar F. Global contribution of pelagic fungi to protein degradation in the ocean. Microbiome. 2022; 10. https://doi.org/10.1186/s40168-022-01329-5 PMID: 36050758

77. Baker-Austin C, Dopson M. Life in acid: pH homeostasis in acidophiles. Trends in Microbiology. 2007. pp. 165–171. https://doi.org/10.1016/j.tim.2007.02.005 PMID: 17331729

78. Hirooka S, Miyagishima S ya. Cultivation of acidophilic algae galdieria sulphuraria and pseudochlorella sp. YKT1 in media derived from acidic hot springs. Front Microbiol. 2016; 7: 2022. https://doi.org/10.3389/fmicb.2016.02022 PMID: 28066348

79. Hsieh YSY, Harris PJ. Xylans of Red and Green Algae: What Is Known about Their Structures and How They Are Synthesised? Polymers (Basel). 2019; 11. https://doi.org/10.3390/polym11020354 PMID: 30960338

80. Singh SP, Singh P. Effect of temperature and light on the growth of algae species: A review. Renewable and Sustainable Energy Reviews. 2015; 50: 431–444. https://doi.org/10.1016/J.RSER.2015.05.024

81. Nobles DR, Romanovicz DK, Brown J. Cellulose in cyanobacteria. Origin of vascular plant cellulose synthase? Plant Physiol. 2001; 127: 529–542. https://doi.org/10.1104/PP.010557 PMID: 11598227

82. Lürling M, Eshetu F, Faassen EJ, Kosten S, Huszar VLM. Comparison of cyanobacterial and green algal growth rates at different temperatures. Freshw Biol. 2013; 58: 552–559. https://doi.org/10.1111/J.1365-2427.2012.02866.X

Check for updates

Essays in Biochemistry (2023) **67** 653–670
https://doi.org/10.1042/EBC20230012

PORTLAND PRESS

Review Article

Oxidoreductases and metal cofactors in the functioning of the earth

Bruno Hay Mele[1], Maria Monticelli[1,2], Serena Leone[3], Deborah Bastoni[1], Bernardo Barosa[1], Martina Cascone[1], Flavia Migliaccio[1], Francesco Montemagno[1], Annarita Ricciardelli[1], Luca Tonietti[1,4], Alessandra Rotundi[4], Angelina Cordone[1] and Donato Giovannelli[1,4,5,6,7,8]

[1]Department of Biology, University of Naples Federico II, Naples, Italy; [2]National Research Council - Institute of Biomolecular Chemistry - CNR-ICB, Pozzuoli, Italy; [3]Dipartimento di Biologia ed Evoluzione degli Organismi Marini, Stazione Zoologica Anton. Dohrn, Napoli, Italy; [4]Department of Science and Technology, University of Naples Parthenope, Naples, Italy; [5]National Research Council - Institute of Marine Biological Resources and Biotechnologies - CNR-IRBIM, Ancona, Italy; [6]Department of Marine and Coastal Science, Rutgers University, New Brunswick, NJ, U.S.A.; [7]Marine Chemistry and Geochemistry Department - Woods Hole Oceanographic Institution, MA, U.S.A.; [8]Earth-Life Science Institute, Tokyo Institute of Technology, Tokyo, Japan

Correspondence: Donato Giovannelli (donato.giovannelli@unina.it) or Bruno Hay Mele (bruno.haymele@unina.it)

OPEN ACCESS

Life sustains itself using energy generated by thermodynamic disequilibria, commonly existing as redox disequilibria. Metals are significant players in controlling redox reactions, as they are essential components of the engine that life uses to tap into the thermodynamic disequilibria necessary for metabolism. The number of proteins that evolved to catalyze redox reactions is extraordinary, as is the diversification level of metal cofactors and catalytic domain structures involved. Notwithstanding the importance of the topic, the relationship between metals and the redox reactions they are involved in has been poorly explored. This work reviews the structure and function of different prokaryotic organometallic–protein complexes, highlighting their pivotal role in controlling biogeochemistry. We focus on a specific subset of metal-containing oxidoreductases (EC1 or EC7.1), which are directly involved in biogeochemical cycles, i.e., at least one substrate or product is a small inorganic molecule that is or can be exchanged with the environment. Based on these inclusion criteria, we select and report 59 metalloenzymes, describing the organometallic structure of their active sites, the redox reactions in which they are involved, and their biogeochemical roles.

Introduction

Life is fundamentally electric [1]. The thermodynamic disequilibria present in the environment as geochemical gradients are exploited by life to drive its metabolic reactions. The two energy sources used by life, chemical for chemotrophs and light for phototrophs, are always linked or converted to redox disequilibria. Thus life's need for thermodynamic disequilibrium is ultimately a requirement for redox chemistry imbalance. Thermodynamically favorable redox reactions (e.g., glucose oxidation coupled to oxygen respiration) are chopped by life into sub reactions decoupling the flow of electrons and protons through the electron transport chain and the cell membrane to create a chemiosmotic gradient (Figure 1). This separation effectively converts a scalar (directionless) redox chemical reaction into a vectorial (gradient-forming) process, producing chemical and mechanical work. In a sense, life has solved the need for energy to drive biochemical reactions anticipating Alessandro Volta's battery by nearly four billion years [2].

Biology has evolved proteins that act stepwise to control redox reactions, transferring electrons across redox states between the opening donor and the ultimate acceptor. These proteins, called oxidoreductases (classified under the Enzyme Commission classes 1 and 7.1), are overwhelmingly metal-containing. To precisely and efficiently transfer electrons to and from a wide range of molecules, they finely tune their

Received: 14 May 2023
Revised: 03 July 2023
Accepted: 10 July 2023

Version of Record published:
11 August 2023

© 2023 The Author(s). This is an open access article published by Portland Press Limited on behalf of the Biochemical Society and distributed under the Creative Commons Attribution License 4.0 (CC BY).

Downloaded from http://portlandpress.com/essaysbiochem/article-pdf/67/4/653/948905/ebc-2023-0012c.pdf by Universita degli Studi di Napoli Federico II user on 07 January 2025

Essays in Biochemistry (2023) 67 653–670
https://doi.org/10.1042/EBC20230012

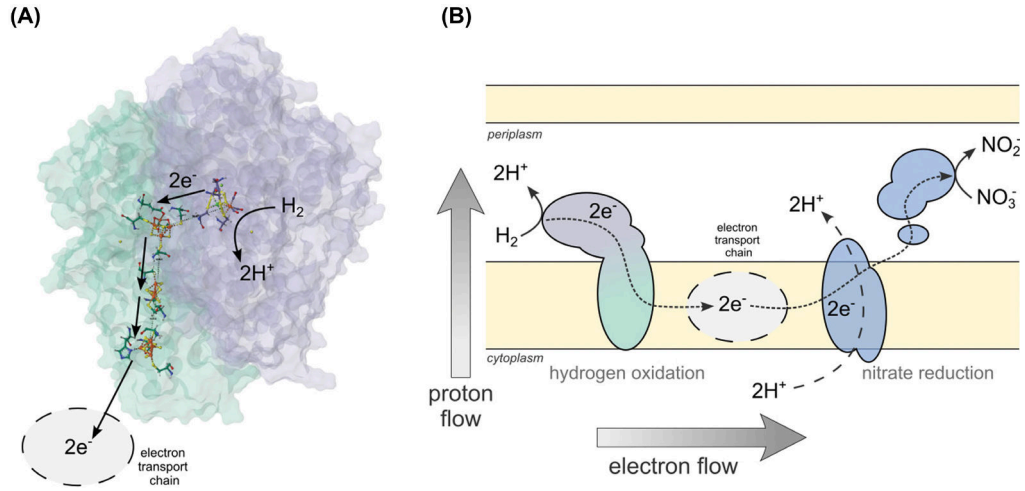

Figure 1. Oxidoreductase proteins and electron stranspor chain used by life to capture redox disequilibrium.
(**A**) The heterodimeric structure of the periplasmic [NiFe]-hydrogenase from *Desulfovibrio vulgaris* (hyd, 5XLF) showing the [NiFe] catalytic center and the iron-sulfur clusters responsible for the electron transport. (**B**) Cellular model of the coupling between the periplasmic membrane-bound [NiFe]-hydrogenase Hyd and the periplasmic molybdopterin-containing nitrate reductase Nap in *Thermovibrio ammonificans* showing the decoupling between electrons and protons across the membrane (adapted from [83]).

conjugated metals' midpoint electric potential by controlling the coordination sphere, geometry, and accessibility of the active site [3]. Elements incorporated in the oxidoreductases' catalytic centers include transition metals such as Fe, Mo, W, Zn, Cu, V, Mn, Ni, Mg, Co and Se and non-metals like S, coordinated either directly or through organometallic structures in the active center [4] (Figure 2). Despite the critical role of metalloproteins in biology, our understanding of the diversity of elements and structures they use is still limited. For example, recent work has demonstrated that lanthanides, a group of elements previously believed to be inert for life, are used by an enzyme catalyzing a key step in the aerobic respiration of methane [5].

The functioning of our planet: a focus on biogeochemistry

Redox couples are recycled on a planetary scale by coupled geological and biological processes happening at diverse spatial and temporal scales. Within biology, redox cycling of key macromolecule-building elements (e.g., carbon, hydrogen, nitrogen, oxygen, and sulfur, also known as CHNOS elements) is primarily carried out by microorganisms inhabiting diverse ecosystems [6]. We did not consider phosphorus, an essential building block in biochemistry, since its biogeochemical cycle is governed by Lewis acid–base chemistry rather than redox chemistry [7].

Most key reactions that control biogeochemistry are carried out by a small set of microbial-encoded proteins containing a redox-sensitive transition metal as core catalytic center [8]. Life can exploit thermodynamic disequilibria present in natural systems using these enzymes whenever the kinetics of the abiotic reactions is slow enough or the activation energy required is big enough for life to outcompete it [9].

Here we discuss the diversity of metal-containing catalytic structures in essential biogeochemical redox proteins and their importance in our planet's functioning. While all enzymes participating in a given metabolic pathway are essential, and all are critical in biogeochemistry regardless of the metabolism itself, this review focused on a small subset of enzymes selected following these criteria:

1. They are exclusively oxidoreductases (EC1 or EC7.1), given the dependence of life on redox chemistry.
2. They are metal-containing proteins (metalloproteins). Metals often occur in multiple subunits participating in the redox reaction and passing electrons within the enzyme complex. Here, we have considered only oxidoreductases in which the metal directly participates in the primary redox reactions.

© 2023 The Author(s). This is an open access article published by Portland Press Limited on behalf of the Biochemical Society and distributed under the Creative Commons Attribution License 4.0 (CC BY).

Downloaded from http://portlandpress.com/essaysbiochem/article-pdf/67/4/653/948905/ebc-2023-0012c.pdf by Universita degli Studi di Napoli Federico II user on 07 January 2025

Essays in Biochemistry (2023) **67** 653–670
https://doi.org/10.1042/EBC20230012

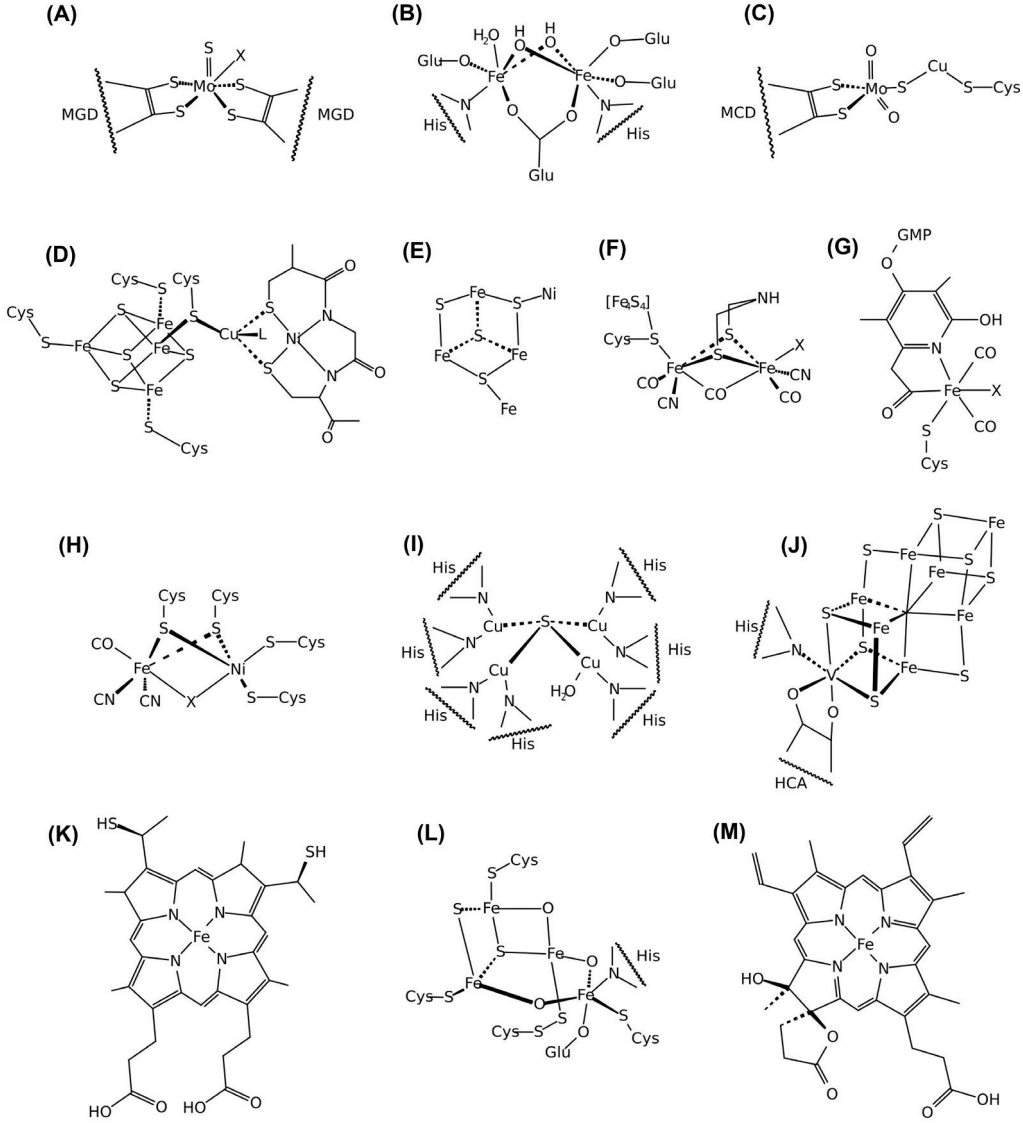

Figure 2. Chemical structures of biogeochemically relevant metal-containing cofactors from prokaryotic oxidoreductases.

(**A**) the Mo-containing catalytic site of Formate dehydrogenase (*fdhF*, 1FDO; shown in Figure 3D); (**B**) the FeO cluster of the soluble methane monooxygenase hydroxylase (*mmoX*,1MHY); (**C**) the Mo-Cu-containing cluster in the active site of CO dehydrogenase (*coxL*, 1ZXI); (**D**) the Ni-Fe-Cu center (cluster A) and (**E**) the Fe-[NiFe3S4] cofactor (cluster C) of the anaerobic carbon monoxide dehydrogenase (*codh*, 1MJG); (**F**) the catalytic centers of the [FeFe]-hydrogenase (*hydA*, 6N59; shown in Figure 3A), [Fe]-hydrogenase (**G**) (*hmd*, 6HAV; shown in Figure 3C) and [NiFe]-hydrogenase (**H**) (*hydB*, 5XLF; shown in Figure 3B); (**I**) the [Cu_4S] cluster of the nitrous oxide reductase (*nosZ*, 1FWX); (**J**) the FeVco cofactor of the V-containing nitrogenase (*vnfD*, 5N6Y; shown in Figure 3G); (**K**) the Heme C contained in several oxidoreductases (*hzsA, hdh, nrfA, nirS, hao, tsdA* [5C2V, 6HIF, 2J7A, 6TSI, 1FGJ, 4V2K]); (**L**) the hybrid cluster from the the Hybrid Cluster Protein from Desulfovibrio vulgaris (*hcp*, 1E1D); (**M**) the Cis-heme hydroxychlorin gamma-spirolactone (*cydA* and *appC*, 6RKO and 7OY2).

© 2023 The Author(s). This is an open access article published by Portland Press Limited on behalf of the Biochemical Society and distributed under the Creative Commons Attribution License 4.0 (CC BY).

Downloaded from http://portlandpress.com/essaysbiochem/article-pdf/67/4/653/948905/ebc-2023-0012c.pdf by Universita degli Studi di Napoli Federico II user on 07 January 2025

PORTLAND PRESS

Essays in Biochemistry (2023) **67** 653–670
https://doi.org/10.1042/EBC20230012

3. They are biogeochemically relevant, i.e., they catalyze a reaction where the substrate/product is a small inorganic molecule that is (or can be) directly exchanged with the environment. Enzymes interacting with molecules like CO_2, CO, H_2, NO_3^-, NH_4^+, SO_4^{2-}, H_2S, and many other compounds fall in this category. Methane (CH_4), considered an organic molecule, is included in this work's list of valid biogeochemical compounds.

These criteria exclude all the enzymes that, while fundamental for the functioning of metabolism, interact with metabolic intermediates and all the key enzymes that do not deal with redox reactions-for example, the key enzyme for the Calvin–Benson–Bassam cycle, Rubisco (EC 4.1.1.39), and many essential genes involved in carbon fixation. In addition, metal-containing oxidoreductase complexes without a metal in the active site are excluded. An example in this category is the flavocytochrome c sulfide dehydrogenase (EC 1.8.5.4), responsible for the reversible conversion of sulfide to elemental sulfur in several sulfide oxidizers and anoxygenic phototrophs. While the heterodimer contains two heme cofactors (making it an iron-containing metalloprotein) and interacts with both H_2S and elemental sulfur, the active site of the catalytic subunit does not contain any metal. It uses instead two flavin-adenine dinucleotide (FAD) cofactors [10]. Under these criteria, the number of biogeochemically-relevant metal-containing oxidoreductases involved in key steps of the CHNOS cycles is reduced to 59 (Table 1 and Supplementary Figure S1). These effectively control the biogeochemistry at the interface between the geosphere and biosphere and are more likely to be influenced by the environmental availability of their metal cofactor [11].

Carbon cycle

At the most fundamental level, life is carbon-based. Hence, life plays a vital role in mediating the biogeochemical cycles of carbon on earth's surface [12,13]. Inorganic carbon is a building block for assembling complex C molecules [12] through autotrophy-based metabolic strategies. At the same time, CH_4 can be oxidized to yield energy for cellular growth and maintenance, ultimately releasing CO_2 [14,15]. While oxidoreductases are involved in the pathways responsible for the uptake and release of inorganic carbon compounds, few are metal-containing oxidoreductases. The KEGG database lists 66 enzymatic classes involved in carbon fixation pathways, of which 21 are classified as oxidoreductases. However, only three (5% of all enzymatic classes involved in carbon fixation pathways) fall within our definition (Table 1). Other carbon-related metabolisms important at the biogeochemical level are methanogenesis, aerobic and anaerobic methane oxidation, and carbon monoxide utilization. KEGG lists 33 enzymatic classes involved in these pathways; 15 are oxidoreductases, and only three fall within our definition (9%; Table 1).

Consulting KEGG, we observed that the active centers of oxidoreductases in the seven carbon fixation pathways usually consist of organic cofactors such as ferredoxin, FAD, and NAD (see supplementary online materials). A few exceptions exist. *Escherichia coli* formate dehydrogenase (*fdhF* [1FDO], Figures 2A and 3D) and *Methanothermobacter wolfeii* formylmethanofuran dehydrogenase (*fwdA* [5T5I], Figure 3E and Supplementary Figure S2) are homologous enzymes involved in CO_2 fixation. Their active site enzymes contain a molybdenum ion bound to two molybdopterin guanine dinucleotide (PDB accession MGD) and a selenocysteine or a tungsten ion bound to two MGD and a cysteine, respectively.

The carbon monoxide dehydrogenase (*coxL* [1ZXI], Figure 2C) is also a metal-containing oxidoreductase of biogeochemical interest. It uses either a Cu-S-Mo cluster for the aerobic variant or a Cu-Ni or Ni-only cofactor for the anaerobic variant of the enzyme (*codh* [1MGJ], Figure 2D) [16,17]. The Cu-S-Mo cluster associated with the aerobic CODH interacts with a single molybdopterin cytosine dinucleotide (MCN) rather than two (as in the FDH). The two oxygens of the cluster replace the dithiolate group of the second MCN in defining the metal geometry (here constrained to be distorted pyramidal) [18]. For anaerobic CODH, Ni is integrated within a Fe-[$NiFe_3S_4$] cluster rather than being bridged to a cubane [Fe_4S_4] [19].

Within the methane cycle, two additional enzymes match our definition of biogeochemically relevant metal oxidoreductase: the membrane-bound particulate Methane monooxygenase (pMMO, *pmoB1/B2* [3RGB]), which uses Cu as a catalytic cofactor, and the cytoplasmic, copper starvation-induced soluble Methane monooxygenase (sMMO, *mmoX* [1MHY], Figure 2B), which in turn uses Fe-Fe. Albeit both catalyze methane oxidation, they are entirely different from a structural standpoint.

Despite the low number of biogeochemical metal-containing oxidoreductases present, the carbon cycle is very diverse in its metal requirement, with Fe, Mo, W, Cu, and Ni involved in key steps of the cycle (Figure 4A).

Nitrogen cycle

Nitrogen is abundant in earth's atmosphere in the form of dinitrogen (N_2) gas and it is present in significant quantities also in the mantle. This element is vital in building nucleic acids, proteins, and enzymes. At the enzymatic level, nitrogen can be transformed between different compounds with different redox states, e.g., NH_4^+, NO, NO_2, N_2O,

© 2023 The Author(s). This is an open access article published by Portland Press Limited on behalf of the Biochemical Society and distributed under the Creative Commons Attribution License 4.0 (CC BY).

Downloaded from http://portlandpress.com/essaysbiochem/article-pdf/67/4/653/948905/ebc-2023-0012c.pdf by Universita degli Studi di Napoli Federico II user on 07 January 2025

Table 1 List of biogeochemically relevant metals containing oxidoreductases controlling the major CHNOS cycles

Cycle	Pathway	Step	Uniprot	Protein name	Gene	EC	KO	PFAM	Metal in the active center	Organometallic structure [PDB ligand accession]	PDB	Representative organism
Carbon	Aerobic methane oxidation	Oxygenation of methane to methanol	G1UBD1	Particulate methane monooxygenase α subunit	*pmoB1, pmoB2*	1.14.18.3	K10944	PF04744	Cu	Cu (II)-Cu (II) [CUA]	3RGB	*Methylococcus capsulatus*
			P27354	(soluble) Methane monooxygenase component A β chain	*mmoX*	1.14.13.25	K16157	PF02332	Fe	2 Fe (III) [FE]	1MHY	*Methylosinus trichosporium*
	Carbon fixation	CO_2 reduction to formate	P07658	Formate dehydrogenase H	*fdhF*	1.17.98.4	K22015	PF04879	Mo	Mo (VI) [MO] molybdenum-bis (molybdopterin guanine dinucleotide) [MGD]	1FDO	*Escherichia coli*
		CO_2 reduction to formylmethanofuran	O74030	Tungsten formylmethanofuran dehydrogenase subunit fwdA	*fwdA*	1.2.7.12	K00200	PF00384	W	W (VI) [W], molybdenum-bis (molybdopterin guanine dinucleotide) [MGD]	5T5I	*Methanothermobacter wolfeii*
		Oxidation of CO to CO_2	P19920	(aerobic) Carbon monoxide dehydrogenase medium chain	*coxL*	1.2.5.3	K03520	PF02738, PF20256	CuMo	Cu (I) -S- Mo (VI) (= O) OH Cluster [CUM]	1ZXI	*Oligotropha carboxidovorans*
		Reduction of CO_2 to CO	P27988	(anaerobic) Carbon monoxide dehydrogenase/acetyl-CoA synthase subunit alpha	*codh*	1.2.7.4	K00192	PF03063	CuNi/Ni	Fe(4)-Ni(1)-S (4) Cluster [XCC] + Cu Ion [CU1]	1MJG	*Moorella thermoacetica*
Hydrogen	Hydrogen oxidation	F420 reduction	D9PYF9	(NiFe) F420-reducing hydrogenase, subunit α	*frhA*	1.12.98.1	K00440	PF00374	NiFe	Formyl [bis(hydrocyanato -1kappaC)] Fe-Ni [NFU]	4OMF	*Methanthermobacter marburgensis str. Marburg*
		H_2-respiration	Q58194	5,10-methenyl tetrahydromethanopterin hydrogenase	*hmd*	1.12.98.2	K13942	PF03201	Fe	Fe (II) [FE2] coordinated by 5'-O-[(S)-hydroxy {[2-hydroxy-3,5-dimethyl-6-(2-oxoethyl)pyridin-4-yl]oxy} phosphoryl] guanosine [I2C]	3F47	*Methancaldococcus jannaschii*

Continued over

© 2023 The Author(s). This is an open access article published by Portland Press Limited on behalf of the Biochemical Society and distributed under the Creative Commons Attribution License 4.0 (CC BY).

Downloaded from http://portlandpress.com/essaysbiochem/article-pdf/67/4/653/948905/ebc-2023-0012c.pdf by Universita degli Studi di Napoli Federico II user on 07 January 2025

Essays in Biochemistry (2023) **67** 653–670
https://doi.org/10.1042/EBC20230012

PORTLAND PRESS

Table 1 List of biogeochemically relevant metals containing oxidoreductases controlling the major CHNOS cycles (Continued)

Cycle	Pathway	Step	Uniprot	Protein name	Gene	EC	KO	PFAM	Metal in the active center	Organometallic structure [PDB ligand accession]	PDB	Representative organism
			P21852	Periplasmic [NiFe] hydrogenase large subunit	*hydB*	1.12.2.1	K00437	PF00374	NiFe / NiFeSe	Ni-Fe oxidized active center [NFV] or NiFeSe	5XLF	*Desulfovibrio vulgaris*
	Hydrogen production	H_2-production	P29166	(FeFe) Iron hydrogenase 1	*hydA*	1.12.7.2	K00533	PF02906	Fe	dicarbonyl [bis(cyanide-kappaC)]-mu-(imin dimethanethiol-atato-1kappaS: 2kappaS)-mu -(oxomethylidene) diiron (II) [402]	6N59	*Clostridium pasteurianum*
		H_2-production/Mrp Antiporter	Q8U0Z6	(NiFe) Membrane-bound hydrogenase subunit α	*mbhL*	1.12.7.2	K18016	PF1434	NiFe	Formyl [bis(hydrocyanato-1kappaC)]Fe-Ni [NFU]	6CFW	*Pyrococcus furiosus*
Nitrogen	Anammox	From ammonia to hydrazine	Q1Q0T3	Hydrazine synthase subunit γ	*hzsA*	1.7.2.7	K20932	PF18582	Fe	HEME C [HEC]	5C2V	*Candidatus Kuenenia stuttgartiensis*
		From hydrazine to nitrogen	Q1PW30	Hydrazine de-hydrogenase	*hdh*	1.7.2.8	K20935	PF13447	Fe	HEME C [HEC]	6HIF	*Candidatus Kuenenia stuttgartiensis*
	Assimilatory nitrate reduction	From nitrate to nitrite	P73448	Nitrate reductase	*narB*	1.7.7.2	K00367	PF00355	Mo	Mo (VI [MO] + 2 molybdenum-bis (molyb-dopterin guanine dinucleotide) [MGD]	AF-P73448-F1	*Synechocystis* sp. PCC 6803
		From ammonia to nitrite	P9WJ03	Ferredoxin-nitrite reductase	*nirA*	1.7.7.1	K00366	PF01077, PF03460	Fe	Siroheme [SRM]	1ZJ8	*Mycobacterium tuberculosis H37Rv*
	Dissimilatory nitrite reduction	From ammonia to nitrite	Q72EF3	Cytochrome *c* nitrite reductase subunit NrfA	*nrfA*	1.7.2.2	K03385	PF02335	Fe	HEME C [HEC]	2J7A	*Desulfovibrio vulgaris str. Hildenborough*
	Denitrification	From nitrate to nitrite	P09152	Respiratory nitrate reductase 1 α chain	*narG*	1.7.5.1	K00370	PF00384, PF01568	Mo	Mo (VI) [MO] + 2 PO4-(2-amino-4-oxo-3,4,5,6,-tetrahydro-pteridic-6-YL)-2-hydroxy-3,4-dimercapto-butenyl ester guamylate [MD1]	1Y4Z	*Escherichia coli*

Continued over

© 2023 The Author(s). This is an open access article published by Portland Press Limited on behalf of the Biochemical Society and distributed under the Creative Commons Attribution License 4.0 (CC BY).

Downloaded from http://portlandpress.com/essaysbiochem/article-pdf/67/4/653/948905/ebc-2023-0012c.pdf by Universita degli Studi di Napoli Federico II user on 07 January 2025

Essays in Biochemistry (2023) **67** 653–670
https://doi.org/10.1042/EBC20230012

Table 1 List of biogeochemically relevant metals containing oxidoreductases controlling the major CHNOS cycles (Continued)

Cycle	Pathway	Step	Uniprot	Protein name	Gene	EC	KO	PFAM	Metal in the active center	Organometallic structure [PDB ligand accession]	PDB	Representative organism
			P81186	Periplasmic nitrate reductase	*napA*	1.9.6.1	K02567	PF04879, PF00384, PF01568	Mo	Mo (VI) [MO] + 2 molybdenum-bis (molyb-dopterin guanine dinucleotide) [MGD]	2JIM	*Desulfovibrio desulfuricans*
		From Nitric oxide to nitrite	E8PLV7	Copper-containing nitrite reductase	*nirK*	1.7.2.1	K00368	PF00394, PF00732	Cu	Cu (II) [CU]	6HBE	*Thermus scotoductus*
			P24474	Nitrite reductase	*nirS*	1.7.2.1	K15864	PF02239, PF13442	Fe	HEME C [HEC]	6TSI	*Pseudomonas aeruginsa*
		From nitrite to nitrate	P49050	Nitrate reductase [NADPH]	*nasA*	1.7.7.2	K00372	PF04879, PF00384, PF01568	Mo	(Molybdopterin -S,S)-dioxo-thio-Mo (IV) [MTV]	2BIH	*Ogataea angusta*
		From nitrogen to nitrous oxide	Q51705	Nitrous-oxide reductase	*nosZ*	1.7.2.4	K00376	PF00116, PF18764, PF18793	Cu	Cu4S [CUZ]	1FWX	*Paracoccus denitrificans*
		From nitrous oxide to nitric oxide	B3Y963	Nitric oxide reductase	*norB*	1.7.2.5	K04561	PF00115	Fe	Protoporph-yrin IX containing Fe [HEM]	3AYF	*Geobacillus stearother-mophilus*
	Nitrification	From ammonia to hydroxylamine	Q04508	(Cupredoxin) Ammonia monooxyge-nase beta subunit	*amoB1; amoB2*	1.14.99.39	K10944	PF02461	Cu	Cu (II) [CU]	AF-Q04508-F1	*Nitrosomonas europaea*
			P31101	Hydroxylamine reductase	*hcp*	1.7.99.1	K05601	PF03063	Fe	Iron/Sulfur/ Oxygen Hybrid Cluster [FSO]	1E1D	*Desulfovibrio vulgaris*
		From ammonia to nitrite	P08201	Nitrite reductase (NADH) large subunit	*nirB*	1.7.1.15	K00363	PF04324, PF01077, PF03460, PF07992, PF18267	Fe	–	AF-P08201-F1	*Escherichia coli (strain K12)*
		From hydroxilamine to nitrite	Q50925	Hydroxylamine oxidoreduc-tase	*hao*	1.7.2.6	K10535	PF13447	Fe	HEME C [HEC]	1FGJ	*Nitrosomonas europaea*
		From nitrite to nitrate	Q1PZD8	Nitrite oxidore-ductase subunit A	*nrxA*	1.7.99.-	K00370	PF09459	Mo	Mo (VI) [MO] + 2 PO4-(2-amino-4 -oxo-3,4,5,6,-tetrahydro-pteridic-6 -YL)-2-hydroxy-3, 4-dimercapto-butenyl ester guamylate [MD1]	7B04	*Candidatus Kuenenia stuttgartiensis*

Continued over

© 2023 The Author(s). This is an open access article published by Portland Press Limited on behalf of the Biochemical Society and distributed under the Creative Commons Attribution License 4.0 (CC BY).

Downloaded from http://portlandpress.com/essaysbiochem/article-pdf/67/4/653/948905/ebc-2023-0012c.pdf by Universita degli Studi di Napoli Federico II user on 07 January 2025

Essays in Biochemistry (2023) **67** 653–670
https://doi.org/10.1042/EBC20230012

PORTLAND PRESS

Table 1 List of biogeochemically relevant metals containing oxidoreductases controlling the major CHNOS cycles (Continued)

Cycle	Pathway	Step	Uniprot	Protein name	Gene	EC	KO	PFAM	Metal in the active center	Organometallic structure [PDB ligand accession]	PDB	Representative organism
	Nitrogen fixation	From nitrogen to ammonia	-[a]	Nitrogenase iron–iron protein	*anfD*	1.18.6.1	K00531	PF00148	Fe	FeFeco[a]	8OIE[a]	*Azotobacter Vinelandi*
			P07328	Nitrogenase molybdenum–iron protein alpha chain	*nifD*	1.18.6.1	K02586	PF00148	Mo	FeMoco [ICS]	3U7Q	*Azotobacter Vinelandi*
			P16855	Nitrogenase vanadium–iron protein α chain	*vnfD*	1.18.6.1	K22896	PF00148	V	FeVco [8P8]	5N6Y	*Azotobacter Vinelandi*
Oxygen	Oxygen radicals detoxification	Hydrogen peroxide detoxification	Q3JNW6	Catalase-peroxidase	*katG*	1.11.1.21	K03782	PF00141	Fe	Protoporph-yrin IX Containing FE [HEM]	5SW4	*Burkholderia pseudomallei*
		Oxygen detoxification	P0ABE5	Superoxide oxidase CybB	*cybB*	1.10.3.17	K12262	PF01292	Fe	Protoporph-yrin IX Containing FE [HEM]	5OC0	*Escherichia coli*
		Superoxide detoxification	P80734	Superoxide dismutase [Ni]	*sodN*	1.15.1.1	K00518	PF09055	Ni	Ni (II) [NI]	1Q0G	*Streptomyces seoulensis*
			P00446	Superoxide dismutase [Cu-Zn]	*sodC*	1.15.1.1	K04565	PF00080	Cu	Cu (II) [CU]	1BZO	*Photobacterium leiognathi*
			Q9RUV2	Superoxide dismutase [Mn]	*sodA*	1.15.1.1	K04564	PF02777, PF00082	Fe / Mn	Fe (III) [FE] / Mn (II) [MN]	1Y67, 3KKY	*Deincoccus radiodurans*
			P82385	Superoxide reductase	*sorA*	1.15.1.2	K05919	PF06397, PF01880	Fe	Fe (III) [FE]	1DQI	*Desulfovibrio desulfuricans*
	Oxygen respiration	Oxidative phosphoryla-tion	D9IA44	*Cbb3*-type cytochrome *c* oxidase (subunit II)	*ccoN*	7.1.1.9	K00404	PF00115	Cu	Cu (II) [CU] + Protopor-phyrin IX [HEM]	5DJQ	*Stutzerimonas stutzeri*
			P34956	Cytochrome ba quinol oxidase subunit 1	*qoxB*	7.1.1.5	K02827	PF00115	Cu	Cu (II) [CU] + Heme-A [HEA]	6KOB	*Bacillus subtilis*
			P0ABJ9	Cytochrome bd-I ubiquinol oxidase subunit 1	*cydA*	7.1.1.7	K00425	PF01654	Fe	Cis-heme D hydroxychlorin gamma-spirolactone [HDD]	6RKO	*Escherichia coli*
			P24244	Putative cytochrome bd-II ubiquinol oxidase subunit AppX	*appC*	7.1.1.7	K00425	PF01654	Fe	Cis-heme D hydroxychlorin gamma-spirolactone [HDD]	7OY2	*Escherichia coli*
			P0ABJ6	Cytochrome bo(3) ubiquinol oxidase subunit 4	*cyoB*	7.1.1.3	K02298	PF00115	Cu	Cu (II) [CU] + HEME-O [HEO]	7N9Z	*Escherichia coli*

Continued over

© 2023 The Author(s). This is an open access article published by Portland Press Limited on behalf of the Biochemical Society and distributed under the Creative Commons Attribution License 4.0 (CC BY).

Downloaded from http://portlandpress.com/essaysbiochem/article-pdf/67/4/653/948905/ebc-2023-0012c.pdf by Universita degli Studi di Napoli Federico II user on 07 January 2025

Essays in Biochemistry (2023) 67 653–670
https://doi.org/10.1042/EBC20230012

Table 1 List of biogeochemically relevant metals containing oxidoreductases controlling the major CHNOS cycles (Continued)

Cycle	Pathway	Step	Uniprot	Protein name	Gene	EC	KO	PFAM	Metal in the active center	Organometallic structure [PDB ligand accession]	PDB	Representative organism
			P98005	Cytochrome-*c* oxidase polypeptide I + III	*ctaD*	7.1.1.9	K02274	PF00115	Cu	Cu (II) [CU] + Heme-AS [HAS]	2YEV	*Thermus thermophilus*
	Oxygenic photosynthesis	Water oxidation to oxygen	P0A444	Photosystem II protein D1 1	*psbA1*	1.10.3.9	K02703	PF00124	Mn	Oxygen evolving system [OEC]	3KZI	*Thermosynechococcus elongatus*
Sulfur	Aerobic sulfur disproportionation	From S-sulfanylglutathione to glutathione + sulfite	A5VWI3	Sulfur dioxygenases	*sdoA*	1.13.11.18	–	PF00753	Fe	Fe (III) [FE]	4YSK	*Pseudomonas putida*
		Catalyzes the simultaneous oxidation and reduction of elemental sulfur in the presence of oxygen	P29082	Sulfur oxygenase/reductase	*sor*	1.13.11.55	K16952	PF07682	Fe	Fe (III) [FE]	2CB2	*Acidianus ambivalens*
	Assimilatory sulfate reduction	Reduction of sulfite to sulfide	A0A920E3E6	Assimilatory sulfite reductase (ferredoxin)	*sir*	1.8.7.1	K00392	PF03460, PF01077	Fe	SIROHEME [SRM]	–	*Synechococcus* sp. PCC7942
			P17846	Sulfite reductase [NADPH] hemoprotein beta-component	*cysL*	1.8.1.2	K00381	PF01077, PF03460	Fe	SIROHEME [SRM]	1AOP	*Escherichia coli*
	DMSO reduction	Catalyzes the conversion of DMSO to dimethyl sulfide	Q57366	Dimethyl sulfoxide/trimethylamine N-oxide reductase	*dmsA*	1.8.5.3	K07306	PF04879, PF01568, PF00384	Mo	Mo (VI [MO] + 2 molybdenum-bis (molybdopterin guanine dinucleotide) [MGD]	1EU1	*Rhodobacter sphaeroides*
		DMSO reduction	Q8GPG4	Dimethylsulfide dehydrogenase subunit α	*ddhA*	1.8.2.4	K16964	PF00384, PF01568	Mo	Mo (VI [MO] + 2 molybdenum-bis (molybdopterin guanine dinucleotide) [MGD]	AF-Q8GPG4-F1	*Rhodovulum sulfidophilum*
	Sulfate reduction	Catalyzes the reduction of sulfite to sulfide	Q59109	Sulfite reductase, dissimilatory-type subunit α	*dsrA*	1.8.99.5	K11180	PF03460, PF01077	Fe	Siroheme [SRM]	3MM5	*Archeoglobus fulgidus*

Continued over

© 2023 The Author(s). This is an open access article published by Portland Press Limited on behalf of the Biochemical Society and distributed under the Creative Commons Attribution License 4.0 (CC BY).

Downloaded from http://portlandpress.com/essaysbiochem/article-pdf/67/4/653/948905/ebc-2023-0012c.pdf by Universita degli Studi di Napoli Federico II user on 07 January 2025

Essays in Biochemistry (2023) **67** 653–670
https://doi.org/10.1042/EBC20230012

PORTLAND PRESS

Table 1 List of biogeochemically relevant metals containing oxidoreductases controlling the major CHNOS cycles (Continued)

Cycle	Pathway	Step	Uniprot	Protein name	Gene	EC	KO	PFAM	Metal in the active center	Organometallic structure [PDB ligand accession]	PDB	Representative organism
	Sulfite oxidation	Sulfite oxidation to sulfate	D3RNN8	Sulfite dehydrogenase subunit A	*soeA*	1.8.5.6	K21307	PF04879, PF00384, PF01568	Mo	Mo (VI [MO] + 2 molybdenum-bis (molybdopterin guanine dinucleotide) [MGD]	AF-D3RNN8-F1	*Allochromatium vinosum*
	Sulfur disproportionation	From sulfite to sulfate	Q9LA16	Sulfite: cytochrome c oxidoreductase subunit A	*sorA*	1.8.2.1	K05301	PF00174, PF03404	Mo	(molybdopterin- S,S)-oxo -Mo [MSS]	2BPB	*Starkeya novella*
	Sulfur reduction	Catalyzes the cytoplasmic production of hydrogen sulfide in the presence of elemental sulfur	–	Sulfhydrogenase	*shyB*	1.12.98.4	K17995, K17996	PF17179, PF00175, PF10418	Fe	–	–	*Pyrococcus furiosus*
		Sulfur reduction	Q8NKK1	Sulfur reductase molybdopterin subunit	*sreA*	1.97.1.3 / 1.12.98.4	K17219	PF04879, PF01568, PF00384	Mo	Mo (VI) [MO] + 2 molybdenum-bis (molybdopterin guanine dinucleotide) [MGD]	AF-Q8NKK1-F1	*Acidianus ambivalens*
	Thiosulfate oxidation	From thiosulfate to sulfate	O07819	Sulfur-oxidation complex	*soxCD*	1.8.2.6	K17225	PF00174, PF03404	MoCo	Mo (IV) oxide [2MO] + Co (II) [CO]	2XTS	*Paracoccus pantotrophus*
		From thiosulfate to tetrathionate	D3RVD4	Thiosulfate dehydrogenase	*tsdA*	1.8.2.2	K19713	PF13442	Fe	HEME C [HEC]	4V2K	*Allochromatium vinosum*
	Thiosulfate reduction	From thiosulfate to hydrogen sulfide	Q72LA6	Polysulfide reductase chain A	*phsA/psrA*	1.8.5.5	K08352	PF04879, PF00384, PF01568	Mo	Mo (VI) [MO] + 2 molybdenum-bis (molybdopterin guanine dinucleotide) [MGD]	2VPX	*Thermus thermophilus*
	Sulfite reduction	Reduces sulfite to sulfide	Q58280	Coenzyme F420-dependent sulfite reductase	*fsr*	1.8.98.3	K21816	PF00037, PF04432, PF04422, PF01077, PF03460	Fe	SIROHEME [SRM]	7NP8	*Methanocaldococcus jannaschii*

PDB and UniProt accessions are reported for each gene, together with Ligand ID; AlphafoldDB codes are reported when a crystallographic structure is unavailable. For enzymes known to be cambialistic (i.e., accept alternative metals in the active site) in experimental setups, the alternative metals are reported separated by a "/". An extended version of the table reporting all the other cofactors present in the catalytic subunit of the enzyme is available as supplementary online material and published on a permanent archive with doi: 10.5281/zenodo.7934782. *a* - the structure, organometallic structure and Uniprot accession number for the Fe nitrogenase is on hold at the time of writing and awaiting release.

© 2023 The Author(s). This is an open access article published by Portland Press Limited on behalf of the Biochemical Society and distributed under the Creative Commons Attribution License 4.0 (CC BY).

Downloaded from http://portlandpress.com/essaysbiochem/article-pdf/67/4/653/948905/ebc-2023-0012c.pdf by Universita degli Studi di Napoli Federico II user on 07 January 2025

Essays in Biochemistry (2023) 67 653–670
https://doi.org/10.1042/EBC20230012

Essays in Biochemistry (2023) **67** 653–670
https://doi.org/10.1042/EBC20230012

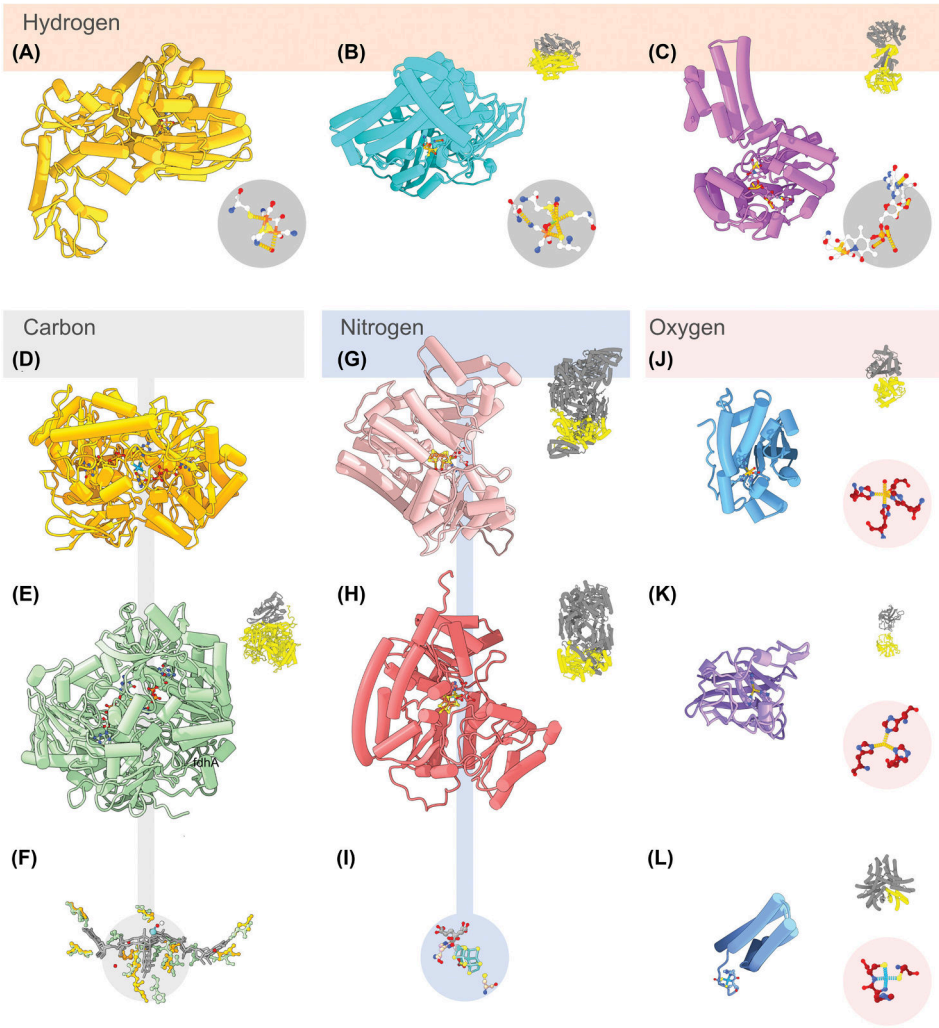

Figure 3. Structures of metal-containing subunits associated with prokaryotic metalloproteins relevant for biogeochemical cycles.

The structures reported are relative to the hydrogen, carbon, nitrogen, and oxygen cycle and have been selected because they have isoforms containing different metals in their catalytic site or show some degree of cofactor cambialism. For each pdb, the coordinated metal/organometallic complex is displayed within a circle, together with a miniature of the assembly highlighting in yellow the catalytic subunit. Hydrogen cycle-related structures: (**A**) FeFe-hydrogenase small subunit (*hydA*) from *Clostridium pasteurianum* (6N59); (**B**) NiFe-hydrogenase large subunit (*hydB*) from *C. pasteurianum* (5XLF; *hydA-hydB* heterodimeric assembly [AB]); (**C**) activated Fe-hydrogenase (*hmd*) from *Methanococcus aeolicus Nankai-3* (6HAV). **Carbon cycle-related structures:** (**D**) formate dehydrogenase H α-chain (*fdhF*) from *Escherichia coli* (1FDO); (**E**) Tungsten formylmethanofuran dehydrogenase chain α (*fwdA*) from *Methanothermobacter wolfeii* (5t5i, dodecameric assembly 2x[ABCDFG]); (**F**) the Mo/W-bis(molybdopterin guanine dinucleotide) cofactor common to both enzymes. Nitrogen cycle-related structures: (**G**) V containing nitrogenase α-chain (*vnfD*) from *Azotobacter vinelandii* (5N6Y; hexameric assembly 2x[ABC]); (**H**) Mo containing nitrogenase α-chain (*nifD*) from *A. vinelandii* (53U7Q; tetrameric assembly 2x[AC]); (**I**) the FeMoco/FeVco cofactor. Oxygen cycle-related structures: (**J**) Superoxide dismutase (*sodA*) from *Deinococcus radiodurans* (1Y67, 3KKY; homodimeric assembly); (**K**) Superoxide dismutase (*sodC*) from *Photobacterium leiognathi* (1BZ0; homodimeric assembly); (**L**) Ni-containing superoxide dismutase (*sodN*) from *Streptomyces selenosis* (1Q0G; hexameric assembly).

© 2023 The Author(s). This is an open access article published by Portland Press Limited on behalf of the Biochemical Society and distributed under the Creative Commons Attribution License 4.0 (CC BY).

Downloaded from http://portlandpress.com/essaysbiochem/article-pdf/67/4/653/948905/ebc-2023-0012c.pdf by Universita degli Studi di Napoli Federico II user on 07 January 2025

Essays in Biochemistry (2023) 67 653–670
https://doi.org/10.1042/EBC20230012

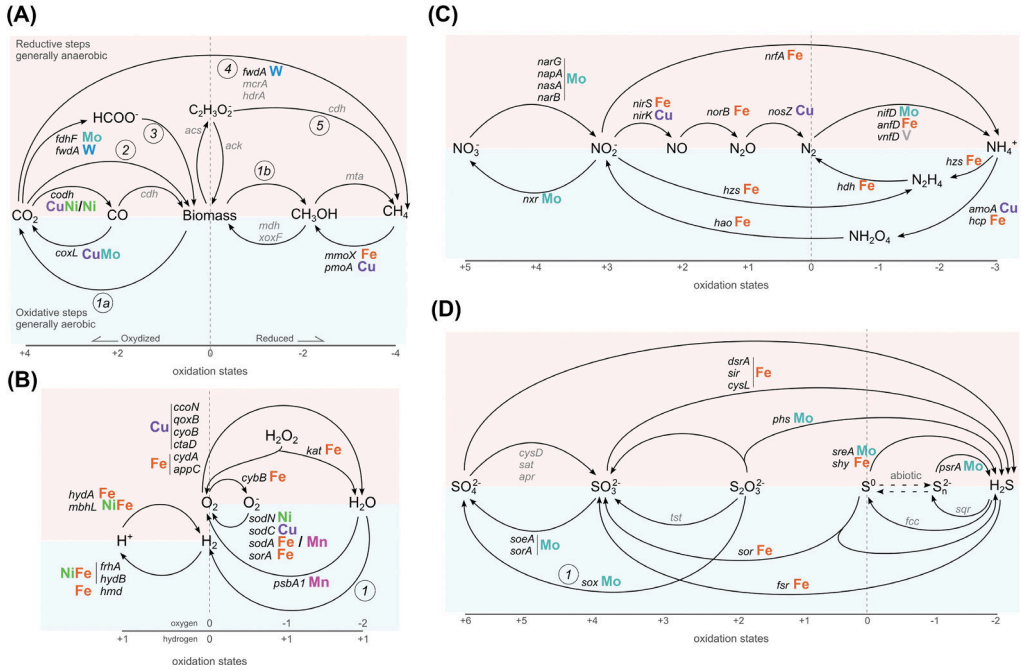

Figure 4. Biogeochemical cycles of the major CHNOS elements.

The reductive side of each cycle is reported on the upper side of each cycle and highlighted in light red, while the oxidative side is on the bottom and highlighted in light blue. Molecules in each element are ordered left to right based on the oxidation state starting with the most oxidized form. Key enzymes for each step of each cycle are reported: in black the names of enzymes that do not meet our criteria of biogeochemically relevant metal containing oxidoreductases, while in light gray other enzymes. Enzyme names are based on the KEGG names and reported in Supplementary Table S1. The catalytic metal is reported for each biogeochemical oxidoreductase colored according to Jmol color scheme. The numbers in a circle represent complex pathways/processes. (**A**) Carbon cycle: 1a and 1b, heterotrophy and fermentation: no enzyme meets our criteria in these pathways; 2, carbon fixation; 3, formate assimilation; 4, methanogenesis pathway: the reported enzyme catalyze key steps in this multi-enzyme pathway; 5, acetoclastic methanogenesis. (**B**) Hydrogen and oxygen cycle: 1, abiotic and biotic hydrogen formation; note that the oxidation scale for oxygen and hydrogen are distinct, and hydrogen is reported with the same oxidation state on both sides. (**C**) Nitrogen cycle. (**D**) Sulfur cycle: 1, sulfur/thiosulfate oxidation is accomplished by a complex group of enzymes (*sox*) of which *soxCD* meets our criteria (Table 1).

NO_3^-, NO_2^-, hydroxylamine, and amino acids, moving from +5 in NO_3^- to -3 in ammonia [20] (Figure 4C). The 22 different EC numbers present in the energetic nitrogen cycle on KEGG are oxidoreductases, and 16 (73%) of them are metalloenzymes relevant in our context. The most frequent metal is Fe, followed by Mo, Cu, and V (Table 1).

Nitrification is governed by Fe, except for the Cu-containing cofactor known as cupredoxin [21–23]. The most utilized metal cofactor for denitrification involves Mo, followed by Fe and Cu, with different geometry inside the enzymatic cofactors. The dissimilatory nitrite reduction and the assimilatory nitrate/nitrite reduction are controlled by Fe, except for the nitrate reductases, in which the catalytic metal is Mo [24]. The anaerobic oxidation of ammonia is carried out by Fe-containing enzymes (Figure 4C). The nitrogen fixation pathway is carried out by the Nitrogenase enzyme (Figures 2F and 3G,H), which exists in three different isoforms partnering with a unique cofactor: FeMoco (*nifD* [3U7Q], Figure 3H), FeVco (*vnfD* [5N6Y], Figures 2I and 3G,I and Supplementary Figure S3), or FeFeco [25]. Fe is the leading metal in every step of the nitrogen cycle associated with the more reduced nitrogen molecules. In contrast, Mo and Cu are associated with the most oxidized forms of nitrogen or enzymes directly involving molecular oxygen (e.g., Ammonia monooxygenase) (Figure 4C).

© 2023 The Author(s). This is an open access article published by Portland Press Limited on behalf of the Biochemical Society and distributed under the Creative Commons Attribution License 4.0 (CC BY).

Downloaded from http://portlandpress.com/essaysbiochem/article-pdf/67/4/653/948905/ebc-2023-0012c.pdf by Universita degli Studi di Napoli Federico II user on 07 January 2025

Essays in Biochemistry (2023) **67** 653–670
https://doi.org/10.1042/EBC20230012

PORTLAND PRESS

Sulfur cycle

Sulfur is the 10th most abundant element on Earth. Despite only a small fraction of it being bound to biomass, it is essential in all organisms. Life plays key roles in the global sulfur cycle through its assimilation into methionine and cysteine, enzyme cofactors (i.e., iron-sulfur clusters), and through its use as electron donor/acceptor in dissimilatory energy-yielding reactions (mainly restricted to prokaryotes) [26]. The sulfur cycle involves reactions between eight valence states, from the most reduced H_2S (−2) to the most oxidized SO_4^{2-} (+6, Figure 4D). Among the 19 enzymes involved in the cycle, 14 are oxidoreductases, and 11 of these fall within our definition (79% of all sulfur cycle enzymatic classes), relying on the presence of either Mo or Fe for their catalytic activity and having a direct biogeochemical impact through their function (Table 1).

The aerobic sulfur disproportionation, assimilatory sulfate reduction, and sulfate reduction pathways are catalyzed by Fe-containing enzymes (Table 1 and Figure 4D). DMSO reduction, sulfite oxidation, sulfur disproportionation, and thiosulfate reduction pathways are catalyzed by Mo-containing enzymes. Interestingly, both dimethyl sulfide:cytochrome c2 reductase (DMSO reduction) and sulfite dehydrogenase (sulfite oxidation) contain a molybdenum-bis (molybdopterin guanine dinucleotide) geometry. Additionally, some pathways of the sulfur cycle involve steps catalyzed by enzymes containing both Fe and Mo. For instance, sulfhydrogenase (Fe-containing, part of a NiFe hydrogenase multienzyme complex) and sulfur reductase (Mo-containing) can catalyze sulfur reduction [27]. The same pattern is observed in the thiosulfate oxidation pathway, with sulfane dehydrogenase (Mo-containing) and Thiosulfate dehydrogenase (Fe-containing). This difference could be due to the different substrates these enzymes interact with, as sulfhydrogenase interacts with hydrogen and sulfur reductase with oxygen, suggesting that the redox potential of these substrates could provide selective pressures for specific metal utilization.

Oxygen cycle

The great availability of oxygen in earth's extant atmosphere results from the emergence of oxygenic photosynthesis, which, coupled with a complex series of geological feedbacks, was responsible for the Great Oxidation Event (GOE, 2.5–2.3 billion years ago) [28,29]. Photosystem II (PS-II) is the main protein complex involved in oxygenic photosynthesis. The oxygen-evolving complex (OEC) represents the PS-II catalytic site where the manganese-dependent photo-oxidation of water occurs, with subsequent release of oxygen (Figure 4B) [30,31]. The presence of Mn ions in the OEC catalytic center is supposedly a consequence of its abundance in the Archean oceans and its hypothetical former use as a phototrophic electron donor [32–34]. Furthermore, enhanced oxygen availability prompted the evolution of both O_2-respiratory and -detoxifying mechanisms [35].

Oxygen high electronegativity makes it a suitable terminal acceptor in oxidative phosphorylation, the hallmark of aerobic respiration, where oxygen reduction to water is carried out by cytochrome oxidases (classified as translocases, EC 7.1) (Figure 4B) [36–38]. These enzymes generally require Cu as a metal cofactor, directly located in the catalytic center and coordinated by a heme group. Cytochrome *bd* ubiquinol oxidases make an exception, as their only metal cofactor is Fe, complexed in a heme group (*cydA, appC* [6RKO, 7OY2] Figure 2L; Table 1) [31,38–42]. In *E. coli*, Cu-containing cytochrome *bo* is maximally synthesized under high oxygen availability. Conversely, iron-containing cytochromes *bd* predominate in microaerophilic conditions [43], showing a very low K_m for oxygen and a less efficient proton motive force [44,45]. This evidence suggests that the nature of the metal cofactor is crucial in determining cytochromes' performance and their affinity for oxygen.

On the other hand, aerobic respiration induces the formation of reactive species of oxygen (ROS) (Figure 4B), which are responsible for cell damage [46]. Superoxide radical anions can be detoxified by three superoxide dismutase (SOD) families, which differ in the catalytic metal (*e.g.*, Fe/Mn, Cu, and Ni) (*sodA, sodC, sodN* [1Y67/3KKY, 1BZ0, 1Q0G] Figure 3J,K,L; Table 1) [47–49]. Among them, the Fe/Mn family is highly flexible in cofactor utilization, representing a clear example of a cambialistic enzyme (*sodA/B* [1y67/3kky], Supplementary Figure S2) [48,50]. Hydrogen peroxide produced by SODs is rapidly detoxified by the catalase-peroxidase, whose metal cofactor is Fe in a heme conformation (Figure 4B) [51].

Hydrogen cycle

Hydrogen is a key reduced compound in the redox balance of the planet. It is produced by several abiotic processes, including water photolysis/radiolysis, hydrothermal reactions, magmatic degassing, and hydration of iron-rich ultramafic rocks [52]. Hydrogen is also produced and consumed by microorganisms and used as an electron donor—it is one of the main energetic currencies exchanged within microbial communities [53]. Microorganisms can interact with molecular hydrogen through a group of diverse enzymes called hydrogenases, which catalyze the conversion of molecular hydrogen to protons and electrons and H_2 regeneration through the reverse reaction [54,55] (Figure 4B).

© 2023 The Author(s). This is an open access article published by Portland Press Limited on behalf of the Biochemical Society and distributed under the Creative Commons Attribution License 4.0 (CC BY).

Downloaded from http://portlandpress.com/essaysbiochem/article-pdf/67/4/653/948905/ebc-2023-0012c.pdf by Universita degli Studi di Napoli Federico II user on 07 January 2025

PORTLAND PRESS

Essays in Biochemistry (2023) **67** 653–670
https://doi.org/10.1042/EBC20230012

Their specialized metallic centers coordinate dihydrogen, polarizing the molecule to induce its heterolytic splitting into a proton and a hydride ion.

There are three main groups of hydrogenases, NiFe containing hydrogenases (*hydA* [6N59] Figures 2E and 3A), FeFe hydrogenases (*hydB* [5XLF] Figures 2G and 3B), and Fe-only hydrogenases (*hmD* [6HAV] Figure 3C). [NiFe]-hydrogenases are found in many Bacteria and Archaea, [FeFe]-hydrogenases in Bacteria and some eukaryotes, and [Fe]-hydrogenases only in Archaea [53]. Of the 30+ classes of hydrogenases known, we report here an example of H_2-consuming and H_2-producing hydrogenases from the main [NiFe], [FeFe], and [Fe] hydrogenases (Table 1 and Figure 4). [NiFe]-hydrogenases are mainly involved in H_2 oxidation but have many other functions such as H_2 evolution, sensing, CO respiration, electron bifurcation, and cofactors reduction [53,56,57]. In selenium-rich conditions, some Bacteria, like *Desulfovibrio vulgaris*, downregulate the production of [NiFe]-hydrogenases in favor of protein variants with selenocysteine as one of Ni ligands, displaying lower inhibition by molecular hydrogen and lower O_2 sensitivity [58–60]. [FeFe]-hydrogenases also serve diverse physiological functions such as H_2 uptake, sensing, evolution, electron bifurcation, and CO_2 fixation [61]. [Fe]-hydrogenases, the least characterized type of hydrogenases, have only been detected in methanogenic Archaea where they are expressed when Ni is limiting [62,63].

Cofactor cambialism at the core of biogeochemistry

Diverse factors constrain the choice of metals at the core of metabolisms: the environmental availability of the element of interest, its suitability for the specific redox reaction to be catalyzed, and the ability to control its binding to the target enzyme. Theoretically, metal-binding affinities of natural proteins are defined by the ligand field stabilization energy of metal ions and follow the Irving–Williams (IW) series ($Mn^{2+} < Fe^{2+} < Co^{2+} < Ni^{2+} < Cu^{2+} > Zn^{2+}$) [64]. In practice, cells tend to maintain the availability of metal ions inverse to the IW series [65] so that binding is more regulated by ion availability in the immediate environment of the metalloprotein (or the metallochaperone), with very high spatial granularity-cells are not ideal solutions. Moreover, ions' concentration can change to the point that different metals can be acquired when folding in different places [66]. The environmental concentration is modulated by metal transport and the metal bioavailability in the outer environment—computational studies have shown that if one removes metallochaperones, metal specificity becomes strongly correlated with metal abundance in the environment. The situation is further complicated because cations have overlapping characteristics that impede absolute specificity. For some metals, similarity in binding affinity and preference over coordination environments is associated with different redox chemistry (e.g., $Mn^{2+}/Mg^{2+}/Fe^{2+}$ and Mo/W). In this context, excluding the wrong metals from proteins may be more challenging than acquiring the right ones [67], and having a metallochaperone or an additional metal center (as in binuclear Mg^{2+}, [68] could reduce mismetallation.

At the environmental level, the (bio)availability of metals might control to a first order its utilization by biology [11]. However, the metal used also depends on the enzyme's evolutionary trajectory. The idea that ancient, promiscuous oxidoreductases were constrained to use bioavailable metals to catalyze redox reactions and that a contingency shaped evolution of more 'focused' metalloenzymes differing in metal utilization is supported by comparison of proteomes across life domains [69]. It is worth remembering that many of the transition metals detailed in this review were readily available in ancient times due to the low oxygen/high sulfur environment, except for Cu, Mo, and Zn (that are sparingly soluble in those conditions) and that the Paleozoic oxidation event (GOE) reverted this trend [70]. At the same time, it is essential to consider that selection 'locked in' some crucial enzymes (*e.g.*, Fe-S proteins, [71] relying on once-plentiful metal species (after the GOE, iron is primarily available in the low-solubility ferric form).

Currently, biogeochemical cycles are dominated by Fe as a key catalytic metal (Figure 4 and Supplementary Figure S4). However, its ability to interact with oxidized substrates is often limited to low-concentration conditions requiring high affinity (like in the Fe-containing cytochromes used under microaerophilic conditions). As a result, cells rely on Cu and Mo to attain the higher redox potential needed to interact with powerful oxidants-such as oxygen in full aerobic conditions, nitrate, and other oxidized nitrogen species. Determining the *in vivo* utilization of metal ions by biomolecules is challenging since complicated metal centers can remain poorly defined even after structure determination due to, *e.g.*, experimental procedure-related substitutions.

Conclusion

Life sustains itself through redox reactions that capitalize on environmental thermodynamic disequilibria. A reasonable hypothesis is that life became proficient in redox reactions as it evolved. In prebiotic Earth, metal ions alone were sufficient redox agents. As the concentration of organic molecules in the environment increased, organometallic complexes formed. The existence of these complexes, in turn, created the context for metallopeptides evolutions that eventually developed into metalloproteins [72]. Extant life is capable of catalyzing a large number of redox reactions,

© 2023 The Author(s). This is an open access article published by Portland Press Limited on behalf of the Biochemical Society and distributed under the Creative Commons Attribution License 4.0 (CC BY).

Downloaded from http://portlandpress.com/essaysbiochem/article-pdf/67/4/653/948905/ebc-2023-0012c.pdf by Universita degli Studi di Napoli Federico II user on 07 January 2025

despite this a quantitative understanding of the diversity and distribution of thermodynamic plausible (i.e., energy yielding) reactions are lacking, and a number of theoretically possible reactions have yet to be identified in nature [73].

The requirement of life for metals as cofactors in key biogeochemical reactions attests to the vital role that metals play in the functioning of Earth and the intricate relationship between the biosphere and the geosphere. Complex stellar processes, protoplanetary disk accretion, and planetary differentiation [74], changing redox conditions during planetary evolution [75,76], plate tectonics, supercontinent assembly [77], and changes in dominant volcanism [78], all contributed to the complex interactions between metal bioavailability and the evolution of biogeochemistry. Nevertheless, our understanding of the role of metals in controlling microbial metabolism and biogeochemistry is still in its infancy. Critical questions about selective pressures imposed by redox potentials of substrates and reaction products in selecting specific metals and the effect of metal environmental availability remain open. In addition, we still need a complete catalog of the elements life uses in protein structure; the diversity of organometallic structures has been poorly examined in environmental—and mostly unculturable [79]—microbes, making it problematic to investigate protein structures and cofactors using traditional approaches. Increasing our knowledge of organometallic cofactors from uncultured microbial groups can revolutionize our understanding of how redox chemistry mediates the interaction between life and our planet, offering promising possibilities in the green chemistry industry and opening our transition to a more sustainable economy [80–82].

Summary

- There is a universal need for redox chemistry by life to use thermodynamic disequilibrium.
- Biogeochemical cycles, and therefore the functioning of our planet, are controlled by a small number of biogeochemically relevant redox proteins, most of which use metal cofactors. The metal used is generally tuned together with the protein structure to the midpoint potential of the reaction catalyzed, although alternatives are possible.
- Metal choice is dictated on the first order by availability and active transport and refined by protein structure. Besides, evolution contributed to 'frozen accidents' that irreversibly paired some metals to specific cycles.
- The correlation between the diversity of metal cofactors and the biogeochemical redox reactions in which they are involved is still unclarified.
- Despite their importance for our planet's functioning, we have limited information regarding the organometallic structure found in oxidoreductases of uncultured lineages of microorganisms.

Competing Interests

The authors declare that there are no competing interests associated with the manuscript.

Funding

This work was supported by funding from the European Research Council (ERC) under the European Union's Horizon 2020 research and innovation program [grant number 948972-COEVOLVE-ERC-2020-STG (to D.G.).] L.T. and A.R. were partially funded by the PhD program PON 'Ricerca e Innovazione' 2014–2020, DM n.1061 (10/08/2021) and n. 1233 (30/07/2020) by the Ministero dell'Università e della Ricerca (MUR); the ASI-INAF agreements (I/024/12/0 and 2020-4-HH.0), by the Italian Space Agency (ASI).

Abbreviations

GOE, Great Oxidation Event; MCN, molybdopterin cytosine dinucleotide; OEC, oxygen-evolving complex; ROS, reactive species of oxygen; SOD, superoxide dismutase.

References

1 Trefil, J., Morowitz, H.J. and Smith, E. (2009) The origin of life: a case is made for the descent of electrons. *Am. Sci.* **97**, 206–213

© 2023 The Author(s). This is an open access article published by Portland Press Limited on behalf of the Biochemical Society and distributed under the Creative Commons Attribution License 4.0 (CC BY).

Downloaded from http://portlandpress.com/essaysbiochem/article-pdf/67/4/653/948905/ebc-2023-0012c.pdf by Universita degli Studi di Napoli Federico II user on 07 January 2025

2 Jelen, B.I., Giovannelli, D. and Falkowski, P.G. (2016) The role of microbial electron transfer in the coevolution of the biosphere and geosphere. *Annu. Rev. Microbiol.* **70**, 45–62, https://doi.org/10.1146/annurev-micro-102215-095521
3 Moore, E.K., Jelen, B.I., Giovannelli, D., Raanan, H. and Falkowski, P.G. (2017) Metal availability and the expanding network of microbial metabolisms in the Archaean eon. *Nat. Geosci.* **10**, 629–636, https://doi.org/10.1038/ngeo3006
4 Kim, J.D., Senn, S., Harel, A., Jelen, B.I. and Falkowski, P.G. (2013) Discovering the electronic circuit diagram of life: structural relationships among transition metal binding sites in oxidoreductases. *Philos. Trans. R. Soc. Lond. B Biol. Sci.* **368**, 20120257, https://doi.org/10.1098/rstb.2012.0257
5 Nakagawa, T., Mitsui, R., Tani, A., Sasa, K., Tashiro, S., Iwama, T. et al. (2012) A catalytic role of XoxF1 as La3+-dependent methanol dehydrogenase in methylobacterium extorquens strain AM1. *PLOS ONE, Public Library of Science* **7**, e50480, https://doi.org/10.1371/journal.pone.0050480
6 Falkowski, P.G., Fenchel, T. and Delong, E.F. (2008) The microbial engines that drive earth's biogeochemical cycles. *Science* **320**, 1034–1039, https://doi.org/10.1126/science.1153213
7 Filippelli, G.M. (2008) The global phosphorus cycle: past, present, and future. *Elements* **4**, 89–95, https://doi.org/10.2113/GSELEMENTS.4.2.89
8 Harel, A., Bromberg, Y., Falkowski, P.G. and Bhattacharya, D. (2014) Evolutionary history of redox metal-binding domains across the tree of life. *Proc. Natl. Acad. Sci.* **111**, 7042–7047, https://doi.org/10.1073/pnas.1403676111
9 Shock, E.L. and Boyd, E.S. (2015) Principles of geobiochemistry. *Elements* **11**, 395–401, https://doi.org/10.2113/gselements.11.6.395
10 Chen, Z., Koh, M., Van Driessche, G., Van Beeumen, J.J., Bartsch, R.G., Meyer, T.E. et al. (1994) The structure of flavocytochrome c sulfide dehydrogenase from a purple phototrophic bacterium. *Science, American Assoc. Advancement Sci.* **266**, 430–432, https://doi.org/10.1126/science.7939681
11 Giovannelli, D. (2022) Geosphere and Biosphere coevolution: the role of trace metals availability in the evolution of biogeochemistry. *EarthArXiv*, https://doi.org/10.31223/X5QH1G
12 Hügler, M. and Sievert, S.M. (2011) Beyond the calvin cycle: autotrophic carbon fixation in the ocean. *Annu. Rev. Mar. Sci.* **3**, 261–289, https://doi.org/10.1146/annurev-marine-120709-142712
13 Rousk, J. and Bengtson, P. (2014) Microbial regulation of global biogeochemical cycles. *Front. Microbiol.* **5**, 103, https://doi.org/10.3389/fmicb.2014.00103
14 Daniels, L., Fuchs, G., Thauer, R.K. and Zeikus, J.G. (1977) Carbon monoxide oxidation by methanogenic bacteria. *J. Bacteriol.* **132**, 118–126, https://doi.org/10.1128/jb.132.1.118-126.1977
15 Hakemian, A.S. and Rosenzweig, A.C. (2007) The biochemistry of methane oxidation. *Annu. Rev. Biochem.* **76**, 223–241, https://doi.org/10.1146/annurev.biochem.76.061505.175355
16 Gnida, M., Ferner, R., Gremer, L., Meyer, O. and Meyer-Klaucke, W. (2003) A novel binuclear [CuSMo] cluster at the active site of carbon monoxide dehydrogenase: characterization by X-ray absorption spectroscopy. *Biochemistry* **42**, 222–230, https://doi.org/10.1021/bi026514n
17 Jeoung, J.-H. and Dobbek, H. (2007) Ni, Fe-containing carbon monoxide dehydrogenases. In *Handbook of Metalloproteins* (Messerschmidt, A., Huber, R., Poulas, T., Wieghardt, K., Cygler, M. and Bode, W., eds), John Wiley & Sons, Ltd, Chichester, p met213, https://doi.org/10.1002/0470028637.met213
18 Resch, M., Dobbek, H. and Meyer, O. (2005) Structural and functional reconstruction in situ of the [CuSMoO2] active site of carbon monoxide dehydrogenase from the carbon monoxide oxidizing eubacterium Oligotropha carboxidovorans. *JBIC J. Biol. Inorg. Chem.* **10**, 518–528, https://doi.org/10.1007/s00775-005-0006-4
19 Doukov, T.I., Iverson, T.M., Seravalli, J., Ragsdale, S.W. and Drennan, C.L. (2002) A Ni-Fe-Cu center in a bifunctional carbon monoxide dehydrogenase/acetyl-CoA synthase. *Science* **298**, 567–572, https://doi.org/10.1126/science.1075843
20 Fowler, D., Coyle, M., Skiba, U., Sutton, M.A., Cape, J.N., Reis, S. et al. (2013) The global nitrogen cycle in the twenty-first century. *Philos. Trans. R Soc. Lond. B Biol. Sci.* **368**, 20130164, https://doi.org/10.1098/rstb.2013.0164
21 Lancaster, K.M., Caranto, J.D., Majer, S.H. and Smith, M.A. (2018) Alternative bioenergy: updates to and challenges in nitrification metalloenzymology. *Joule* **2**, 421–441, https://doi.org/10.1016/j.joule.2018.01.018
22 Zhang, L., Wüst, A., Prasser, B., Müller, C. and Einsle, O. (2019) Functional assembly of nitrous oxide reductase provides insights into copper site maturation. *Proc. Natl. Acad. Sci.* **116**, 12822–12827, https://doi.org/10.1073/pnas.1903819116
23 Lawton, T.J., Ham, J., Sun, T. and Rosenzweig, A.C. (2014) Structural conservation of the B subunit in the ammonia monooxygenase/particulate methane monooxygenase superfamily. *Proteins Struct. Funct. Bioinforma.* **82**, 2263–2267, https://doi.org/10.1002/prot.24535
24 Kaneko, T., Sato, S., Kotani, H., Tanaka, A., Asamizu, E., Nakamura, Y. et al. (1996) Sequence analysis of the genome of the unicellular cyanobacterium *Synechocystis* sp. strain PCC6803. II. Sequence determination of the entire genome and assignment of potential protein-coding regions. *DNA Res. Int. J. Rapid Publ. Rep. Genes Genomes* **3**, 109–136, https://doi.org/10.1093/dnares/3.3.109
25 Rees, J.A., Bjornsson, R., Kowalska, J.K., Lima, F.A., Schlesier, J., Sippel, D. et al. (2017) Comparative electronic structures of nitrogenase FeMoco and FeVco. *Dalton Trans.* **46**, 2445–2455, https://doi.org/10.1039/C7DT00128B
26 Dahl, C. (2020) Chapter 3 A biochemical view on the biological sulfur cycle. In *Environmental technologies to treat sulfur pollution: principles and engineering* (Lens, P.N.L., ed.), pp. 55–96, IWA Publishing, London, https://doi.org/10.2166/9781789060966˙0055
27 Guiral, M., Tron, P., Aubert, C., Gloter, A., Iobbi-Nivol, C. and Giudici-Orticoni, M.-T. (2005) A membrane-bound multienzyme, hydrogen-oxidizing, and sulfur-reducing complex from the hyperthermophilic bacterium aquifex aeolicus. *J. Biol. Chem.* **280**, 42004–42015, https://doi.org/10.1074/jbc.M508034200
28 Schirrmeister, B.E., Gugger, M. and Donoghue, P.C.J. (2015) Cyanobacteria and the great oxidation event: evidence from genes and fossils. *Palaeontology* **58**, 769–785, https://doi.org/10.1111/pala.12178
29 Castresana, J., Lübben, M., Saraste, M. and Higgins, D.G. (1994) Evolution of cytochrome oxidase, an enzyme older than atmospheric oxygen. *EMBO J.* **13**, 2516–2525, https://doi.org/10.1002/j.1460-2075.1994.tb06541.x

© 2023 The Author(s). This is an open access article published by Portland Press Limited on behalf of the Biochemical Society and distributed under the Creative Commons Attribution License 4.0 (CC BY).

Downloaded from http://portlandpress.com/essaysbiochem/article-pdf/67/4/653/948905/ebc-2023-0012c.pdf by Universita degli Studi di Napoli Federico II user on 07 January 2025

30 Paul, S., Neese, F. and Pantazis, D.A. (2017) Structural models of the biological oxygen-evolving complex: achievements, insights, and challenges for biomimicry. *Green Chem., Royal Soc. Chem.* **19**, 2309–2325, https://doi.org/10.1039/C7GC00425G
31 Wikström, M., Krab, K. and Sharma, V. (2018) Oxygen activation and energy conservation by cytochrome c oxidase. *Chem. Rev., Am. Chem. Soc.* **118**, 2469–2490, https://doi.org/10.1021/acs.chemrev.7b00664
32 Fischer, W.W., Hemp, J. and Johnson, J.E. (2015) Manganese and the evolution of photosynthesis. *Orig. Life Evol. Biospheres* **45**, 351–357, https://doi.org/10.1007/s11084-015-9442-5
33 Fischer, W.W., Hemp, J. and Valentine, J.S. (2016) How did life survive earth's great oxygenation? *Curr. Opin. Chem. Biol.* **31**, 166–178, https://doi.org/10.1016/j.cbpa.2016.03.013
34 Johnson, J.E., Webb, S.M., Thomas, K., Ono, S., Kirschvink, J.L. and Fischer, W.W. (2013) Manganese-oxidizing photosynthesis before the rise of cyanobacteria. *Proc. Natl. Acad. Sci.* **110**, 11238–11243, https://doi.org/10.1073/pnas.1305530110
35 Falkowski, P.G. (2006) Evolution. Tracing oxygen's imprint on earth's metabolic evolution. *Science* **311**, 1724–1725, https://doi.org/10.1126/science.1125937
36 Deshpande, O.A. and Mohiuddin, S.S. (2023) Biochemistry, Oxidative Phosphorylation. *StatPearls*, StatPearls Publishing, Treasure Island (FL)
37 Brzezinski, P. and Gennis, R.B. (2008) Cytochrome c oxidase: exciting progress and remaining mysteries. *J. Bioenerg. Biomembr.* **40**, 521–531, https://doi.org/10.1007/s10863-008-9181-7
38 Borisov, V.B., Siletsky, S.A., Paiardini, A., Hoogewijs, D., Forte, E., Giuffrè, A. et al. (2021) Bacterial oxidases of the cytochrome bd family: redox enzymes of unique structure, function, and utility as drug targets. *Antioxid. Redox Signal.* **34**, 1280–1318, https://doi.org/10.1089/ars.2020.8039
39 Yi, S.M., Taguchi, A.T., Samoilova, R.I., O'Malley, P.J., Gennis, R.B. and Dikanov, S.A. (2015) Plasticity in the high affinity menaquinone binding site of the cytochrome aa3-600 menaquinol oxidase from Bacillus subtilis. *Biochemistry, Am. Chem. Soc.* **54**, 5030–5044, https://doi.org/10.1021/acs.biochem.5b00528
40 Sousa, F.L., Alves, R.J., Ribeiro, M.A., Pereira-Leal, J.B., Teixeira, M. and Pereira, M.M. (2012) The superfamily of heme-copper oxygen reductases: Types and evolutionary considerations. *Biochim. Biophys. Acta BBA - Bioenerg.* **1817**, 629–637, https://doi.org/10.1016/j.bbabio.2011.09.020
41 Pitcher, R.S. and Watmough, N.J. (2004) The bacterial cytochrome cbb3 oxidases. *Biochim. Biophys. Acta BBA - Bioenerg.* **1655**, 388–399, https://doi.org/10.1016/j.bbabio.2003.09.017
42 Bhagi-Damodaran, A., Michael, M.A., Zhu, Q., Reed, J., Sandoval, B.A., Mirts, E.N. et al. (2017) Why copper is preferred over iron for oxygen activation and reduction in haem-copper oxidases. *Nat. Chem., Nature Publishing Group* **9**, 257–263, https://doi.org/10.1038/nchem.2643
43 Fu, H.A., Iuchi, S. and Lin, E.C. (1991) The requirement of ArcA and Fnr for peak expression of the cyd operon in *Escherichia coli* under microaerobic conditions. *Mol. Gen. Genet. MGG* **226**, 209–213, https://doi.org/10.1007/BF00273605
44 D'mello, R., Hill, S. and Poole, R.K. (1996) The cytochrome bd quinol oxidase in *Escherichia coli* has an extremely high oxygen affinity and two oxygen-binding haems: implications for regulation of activity *in vivo* by oxygen inhibition. *Microbiology, Microbiol. Soc.* **142**, 755–763, https://doi.org/10.1099/00221287-142-4-755
45 Jasaitis, A., Borisov, V.B., Belevich, N.P., Morgan, J.E., Konstantinov, A.A. and Verkhovsky, M.I. (2000) Electrogenic reactions of cytochrome bd. *Biochemistry, Am. Chem. Soc.* **39**, 13800–13809, https://doi.org/10.1021/bi001165n
46 Schieber, M. and Chandel, N.S. (2014) ROS function in redox signaling and oxidative stress. *Curr. Biol. CB* **24**, R453–R462, https://doi.org/10.1016/j.cub.2014.03.034
47 Pelmenschikov, V. and Siegbahn, P.E.M. (2005) Copper−Zinc superoxide dismutase: theoretical insights into the catalytic mechanism. *Inorg. Chem., Am. Chem. Soc.* **44**, 3311–3320, https://doi.org/10.1021/ic050018g
48 Valenti, R., Jabłońska, J. and Tawfik, D.S. (2022) Characterization of ancestral Fe/Mn superoxide dismutases indicates their cambialistic origin. *Protein Sci. Publ. Protein Soc.* **31**, e4423, https://doi.org/10.1002/pro.4423
49 Barondeau, D.P., Kassmann, C.J., Bruns, C.K., Tainer, J.A. and Getzoff, E.D. (2004) Nickel superoxide dismutase structure and mechanism. *Biochemistry, Am. Chem. Soc.* **43**, 8038–8047, https://doi.org/10.1021/bi0496081
50 Frye, K.A., Sendra, K.M., Waldron, K.J. and Kehl-Fie, T.E. (2022) Old dogs, new tricks: New insights into the iron/manganese superoxide dismutase family. *J. Inorg. Biochem.* **230**, 111748, https://doi.org/10.1016/j.jinorgbio.2022.111748
51 Carpena, X., Wiseman, B., Deemagarn, T., Singh, R., Switala, J., Ivancich, A. et al. (2005) A molecular switch and electronic circuit modulate catalase activity in catalase-peroxidases. *EMBO Rep.* **6**, 1156–1162, https://doi.org/10.1038/sj.embor.7400550
52 Vitale Brovarone, A., Sverjensky, D.A., Piccoli, F., Ressico, F., Giovannelli, D. and Daniel, I. (2020) Subduction hides high-pressure sources of energy that may feed the deep subsurface biosphere. *Nat. Commun.* **11**, 3880, https://doi.org/10.1038/s41467-020-17342-x
53 Vignais, P.M. and Billoud, B. (2007) Occurrence, classification, and biological function of hydrogenases: an overview. *Chem. Rev., ACS Publications* **107**, 4206–4272, https://doi.org/10.1021/cr050196r
54 Lubitz, W., Ogata, H., Rüdiger, O. and Reijerse, E. (2014) Hydrogenases. *Chem. Rev.* **114**, 4081–4148, https://doi.org/10.1021/cr4005814
55 Schilter, D., Camara, J.M., Huynh, M.T., Hammes-Schiffer, S. and Rauchfuss, T.B. (2016) Hydrogenase enzymes and their synthetic models: the role of metal hydrides. *Chem. Rev.* **116**, 8693–8749, https://doi.org/10.1021/acs.chemrev.6b00180
56 Schuchmann, K., Chowdhury, N.P. and Müller, V. (2018) Complex multimeric [FeFe] hydrogenases: biochemistry, physiology and new opportunities for the hydrogen economy. *Front. Microbiol.* **9**, 2911, https://doi.org/10.3389/fmicb.2018.02911
57 Feng, X., Schut, G.J., Haja, D.K., Adams, M.W.W. and Li, H. (2022) Structure and electron transfer pathways of an electron-bifurcating NiFe-hydrogenase. *Sci. Adv., Am. Assoc. Advancement Sci.* **8**, eabm7546, https://doi.org/10.1126/sciadv.abm7546
58 Wombwell, C., Caputo, C.A. and Reisner, E. (2015) [NiFeSe]-hydrogenase chemistry. *Acc. Chem. Res., Am. Chem. Soc.* **48**, 2858–2865, https://doi.org/10.1021/acs.accounts.5b00326
59 Khangulov, S.V., Gladyshev, V.N., Dismukes, G.C. and Stadtman, T.C. (1998) Selenium-containing formate dehydrogenase H from Escherichia coli: a molybdopterin enzyme that catalyzes formate oxidation without oxygen transfer. *Biochemistry* **37**, 3518–3528, https://doi.org/10.1021/bi972177k

Downloaded from http://portlandpress.com/essaysbiochem/article-pdf/67/4/653/948905/ebc-2023-0012c.pdf by Universita degli Studi di Napoli Federico II user on 07 January 2025

© 2023 The Author(s). This is an open access article published by Portland Press Limited on behalf of the Biochemical Society and distributed under the Creative Commons Attribution License 4.0 (CC BY).

Essays in Biochemistry (2023) **67** 653–670
https://doi.org/10.1042/EBC20230012

60 Shaw, F.L., Mulholland, F., Le Gall, G., Porcelli, I., Hart, D.J., Pearson, B.M. et al. (2012) Selenium-Dependent Biogenesis of Formate Dehydrogenase in Campylobacter jejuni Is Controlled by the fdhTU Accessory Genes. *J. Bacteriol.* **194**, 3814–3823, https://doi.org/10.1128/JB.06586-11
61 Morra, S. (2022) Fantastic [FeFe]-Hydrogenases and Where to Find Them. *Front. Microbiol.* **13**, 853626, https://doi.org/10.3389/fmicb.2022.853626
62 Wang, C., Lai, Z., Huang, G. and Pan, H.-J. (2022) Current State of [Fe]-hydrogenase and its biomimetic models. *Chem. - Eur. J., John Wiley & Sons, Ltd* **28**, e202201499, https://doi.org/10.1002/chem.202201499
63 Afting, C., Kremmer, E., Brucker, C., Hochheimer, A. and Thauer, R.K. (2000) Regulation of the synthesis of H2-forming methylenetetrahydromethanopterin dehydrogenase (Hmd) and of HmdII and HmdIII in Methanothermobacter marburgensis. *Arch. Microbiol.* **174**, 225–232, https://doi.org/10.1007/s002030000197
64 Irving, H. and Williams, R.J.P. (1948) Order of Stability of Metal Complexes. *Nature* **162**, 746–747
65 Osman, D., Martini, M.A., Foster, A.W., Chen, J., Scott, A.J.P., Morton, R.J. et al. (2019) Bacterial sensors define intracellular free energies for correct enzyme metalation. *Nat. Chem. Biol.* **15**, 241–249, https://doi.org/10.1038/s41589-018-0211-4
66 Tottey, S., Waldron, K.J., Firbank, S.J., Reale, B., Bessant, C., Sato, K. et al. (2008) Protein-folding location can regulate manganese-binding versus copper- or zinc-binding. *Nature* **455**, 1138–1142, https://doi.org/10.1038/nature07340
67 Waldron, K.J., Rutherford, J.C., Ford, D. and Robinson, N.J. (2009) Metalloproteins and metal sensing. *Nature, Nature Publishing Group* **460**, 823–830, https://doi.org/10.1038/nature08300
68 Dudev, T. and Lim, C. (2008) Metal binding affinity and selectivity in metalloproteins: insights from computational studies. *Annu. Rev. Biophys.* **37**, 97–116, https://doi.org/10.1146/annurev.biophys.37.032807.125811
69 Dupont, C.L., Yang, S., Palenik, B. and Bourne, P.E. (2006) Modern proteomes contain putative imprints of ancient shifts in trace metal geochemistry. *Proc. Natl. Acad. Sci.* **103**, 17822–17827, https://doi.org/10.1073/pnas.0605798103
70 Zerkle, A.L., House, C.H. and Brantley, S.L. (2005) Biogeochemical signatures through time as inferred from whole microbial genomes. *Am. J. Sci.* **305**, 467–502, https://doi.org/10.2475/ajs.305.6-8.467
71 Wade, J., Byrne, D.J., Ballentine, C.J. and Drakesmith, H. (2021) Temporal variation of planetary iron as a driver of evolution. *Proc. Natl. Acad. Sci.* **118**, e2109865118, https://doi.org/10.1073/pnas.2109865118
72 Aithal, A., Dagar, S. and Rajamani, S. (2023) Metals in prebiotic catalysis: a possible evolutionary pathway for the emergence of metalloproteins. *ACS Omega, American Chemical Society* **8**, 5197–5208, https://doi.org/10.1021/acsomega.2c07635
73 Amend, J.P., Aronson, H.S., Macalady, J. and LaRowe, D.E. (2020) Another chemolithotrophic metabolism missing in nature: sulfur comproportionation. *Environ. Microbiol.* **22**, 1971–1976, https://doi.org/10.1111/1462-2920.14982
74 Covone, G. and Giovannelli, D. (2022) Stellar metallicity is a key parameter for the search of life in the universe. *arXiv*, https://doi.org/10.48550/arXiv.2207.03748
75 Ostrander, C.M., Johnson, A.C. and Anbar, A.D. (2021) Earth's first redox revolution. *Annu. Rev. Earth Planet. Sci.* **49**, 337–366, https://doi.org/10.1146/annurev-earth-072020-055249
76 Reinhard, C.T. and Planavsky, N.J. (2020) Biogeochemical controls on the redox evolution of earth's oceans and atmosphere. *Elements* **16**, 191–196, https://doi.org/10.2138/gselements.16.3.191
77 Hazen, R.M., Liu, X.-M., Downs, R.T., Golden, J., Pires, A.J. and Grew, E.S. (2014) Mineral evolution: episodic metallogenesis, the supercontinent cycle, and the coevolving geosphere and biosphere. In *Building Exploration Capability for the 21st Century* (Kelley, K.D., Golden, H.C. et al., eds), Society of Economic Geologists, https://doi.org/10.5382/SP.18.01
78 Edmonds, M., Mather, T.A. and Liu, E.J. (2018) A distinct metal fingerprint in arc volcanic emissions. *Nat. Geosci.* **11**, 790–794, https://doi.org/10.1038/s41561-018-0214-5
79 Steen, A.D., Crits-Christoph, A., Carini, P., DeAngelis, K.M., Fierer, N., Lloyd, K.G. et al. (2019) High proportions of bacteria and archaea across most biomes remain uncultured. *ISME J* **13**, 3126–3130, https://doi.org/10.1038/s41396-019-0484-y
80 Crabtree, R.H. (2011) An organometallic future in green and energy chemistry? *Organometallics* **30**, 17–19, https://doi.org/10.1021/om1009439
81 Ganesh, K.N., Zhang, D., Miller, S.J., Rossen, K., Chirik, P.J., Kozlowski, M.C. et al. (2021) Green chemistry: a framework for a sustainable future. *Org. Process Res. Dev.* **25**, 1455–1459, https://doi.org/10.1021/acs.oprd.1c00216
82 Large, B., Baranska, N.G., Booth, R.L., Wilson, K.S. and Duhme-Klair, A.-K. (2021) Artificial metalloenzymes: The powerful alliance between protein scaffolds and organometallic catalysts. *Curr. Opin. Green Sustain. Chem.* **28**, 100420, https://doi.org/10.1016/j.cogsc.2020.100420
83 Giovannelli, D., Sievert, S.M., Hügler, M., Markert, S., Becher, D., Schweder, T. et al. (2017) Insight into the evolution of microbial metabolism from the deep-branching bacterium, Thermovibrio ammonificans. *eLife* **6**, e18990, https://doi.org/10.7554/eLife.18990
84 Bowman, S.E.J. and Bren, K.L. (2008) The chemistry and biochemistry of hemec: functional bases for covalent attachment. *Nat. Prod. Rep* **25**, 1118–1130, https://doi.org/10.1039/b717196j

Downloaded from http://portlandpress.com/essaysbiochem/article-pdf/67/4/653/948905/ebc-2023-0012c.pdf by Universita degli Studi di Napoli Federico II user on 07 January 2025

© 2023 The Author(s). This is an open access article published by Portland Press Limited on behalf of the Biochemical Society and distributed under the Creative Commons Attribution License 4.0 (CC BY).

Italian Journal of Animal Science

ISSN: (Print) (Online) Journal homepage: www.tandfonline.com/journals/tjas20

Ruminal microbiota, carbohydrate-active enzymes and milk bioactive compounds in Italian Mediterranean dairy buffaloes fed total mixed ration with or without green forage

Angela Salzano, Anella Saggese, Elisa Martino, Gianluca Neglia, Martina Cascone, Matteo Selci, Loredana Baccigalupi, Nunzia D'Onofrio, Donato Giovannelli, Giovanna Bifulco, Ezio Ricca, Maria Luisa Balestrieri, Michael D'Occhio & Giuseppe Campanile

To cite this article: Angela Salzano, Anella Saggese, Elisa Martino, Gianluca Neglia, Martina Cascone, Matteo Selci, Loredana Baccigalupi, Nunzia D'Onofrio, Donato Giovannelli, Giovanna Bifulco, Ezio Ricca, Maria Luisa Balestrieri, Michael D'Occhio & Giuseppe Campanile (2024) Ruminal microbiota, carbohydrate-active enzymes and milk bioactive compounds in Italian Mediterranean dairy buffaloes fed total mixed ration with or without green forage, Italian Journal of Animal Science, 23:1, 1681-1694, DOI: 10.1080/1828051X.2024.2417711

To link to this article: https://doi.org/10.1080/1828051X.2024.2417711

© 2024 The Author(s). Published by Informa UK Limited, trading as Taylor & Francis Group.

View supplementary material

Published online: 04 Nov 2024.

Submit your article to this journal

Article views: 215

View related articles

View Crossmark data

Full Terms & Conditions of access and use can be found at
https://www.tandfonline.com/action/journalInformation?journalCode=tjas20

ITALIAN JOURNAL OF ANIMAL SCIENCE
2024, VOL. 23, NO. 1, 1681–1694
https://doi.org/10.1080/1828051X.2024.2417711

Taylor & Francis
Taylor & Francis Group

RUMINANTS NUTRITION AND FEEDING

OPEN ACCESS Check for updates

Ruminal microbiota, carbohydrate-active enzymes and milk bioactive compounds in Italian Mediterranean dairy buffaloes fed total mixed ration with or without green forage

Angela Salzano[a*], Anella Saggese[b*], Elisa Martino[c], Gianluca Neglia[a], Martina Cascone[b], Matteo Selci[b], Loredana Baccigalupi[d], Nunzia D'Onofrio[c], Donato Giovannelli[b], Giovanna Bifulco[a], Ezio Ricca[b], Maria Luisa Balestrieri[c], Michael D'Occhio[e] and Giuseppe Campanile[a]

[a]Dipartimento di Medicina Veterinaria e Produzioni Animali, University of Naples, "Federico II", Napoli, Italy; [b]Dipartimento di Biologia, University of Naples "Federico II", Napoli, Italy; [c]Dipartimento di Medicina di Precisione, University of Campania "Luigi Vanvitelli", Napoli, Italy; [d]Dipartimento di Medicina Molecolare e Biotecnologie Mediche, University of Naples "Federico II", Napoli, Italy; [e]School of Life and Environmental Sciences, Faculty of Science, The University of Sydney, Sydney, Australia

ABSTRACT

The aim of the present study was to determine the effect of including green forage in the diet of Italian Mediterranean dairy buffaloes on the ruminal microbiota, CAZymes profile, functional biomolecules and total antioxidant activity in bulk milk. Sixteen buffaloes were randomly assigned according to lactation number and daily milk production to two homogeneous groups, and for 60 days received each: Group 1, a standard total mixed ration (TMR) or group 2, TMR + ryegrass green forage (30% of diet). The diets of the two groups were iso-nitrogenous and iso-energetic and differed only in the proportion of green forage. Buffaloes that received TMR + green feed had a higher ($p < .01$) representation of bacteria belonging to the orders *Veillonellales*, *Selenomonadales* and *Bradymonadales* compared with buffaloes that received TMR. The former buffaloes also had a greater ($p < .01$) abundance of CAZymes of the GT class (GHT4, GT14, GT20, GT26, GT39) and AA class (AA1, AA3, AA6). The milk of buffaloes that received TMR + green feed had a higher ($p < .01$) antioxidant capacity and greater ($p < .01$) amounts of the functional biomolecules L-carnitine, propionyl-L-carnitine, acetyl-L-carnitine and δ-valerobetaine. The findings have provided evidence for metabolic and biosynthetic pathways that link green forage with rumen bacteria, CAZymes and the synthesis of amino acids and functional biomolecule in buffaloes.

HIGHLIGHTS

- Green feed diet in dairy buffaloes favours ruminal microbiota that produces CAZymes.
- CAZymes support the synthesis of amino acids and functional biomolecules in milk.
- Functional milk from animals fed natural diets will be more appreciated by consumers.

ARTICLE HISTORY
Received 16 May 2024
Revised 1 October 2024
Accepted 11 October 2024

KEYWORDS
Green forage; rumen microbiome; CAZymes; biomolecules; dairy buffalo

Introduction

Buffaloes are a major global livestock of economic and social importance in both developing and developed economies (Deb et al. 2016). They are productive on a relatively low-quality diet and have milk of high nutritional value (Arrichiello et al. 2022). The latter is due partly to the unique rumen microbiota of buffaloes which is distinctively different to the microbiota of other ruminants with relatively high fibre degradation and reduced methane production (Hamid et al. 2017; Iqbal et al. 2018; Malik et al. 2021; Sun et al. 2021). Based on the global importance of buffaloes as a source of milk, it is important to gain a deeper understanding of the relationships between diet, ruminal function and milk quality in buffaloes.

Consumers prefer food products sourced from animals fed natural diets (El-Zaiat and Abdalla 2019; Sallam et al. 2019). Cattle and buffaloes fed green forage produce milk with greater antioxidant and anti-inflammatory activity (Salzano et al. 2021, 2022).

CONTACT Giovanna Bifulco giovanna.bifulco@unina.it
*Both authors contributed equally to this work.

Supplemental data for this article can be accessed online at https://doi.org/10.1080/1828051X.2024.2417711.

© 2024 The Author(s). Published by Informa UK Limited, trading as Taylor & Francis Group.
This is an Open Access article distributed under the terms of the Creative Commons Attribution License (http://creativecommons.org/licenses/by/4.0/), which permits unrestricted use, distribution, and reproduction in any medium, provided the original work is properly cited. The terms on which this article has been published allow the posting of the Accepted Manuscript in a repository by the author(s) or with their consent.

The inclusion of green forage in the diet of buffaloes is associated with distinctive changes in the ruminal metabolome (Neglia, Cotticelli, et al. 2023) and transcriptome (Salzano et al. 2023) and this may be probably due to the higher amount of simple sugars that are able to improve rumen efficiency and nutrient utilisation (Mordenti et al. 2021). It can be, hence, assumed that the changes in the ruminal metabolome and transcriptome in buffaloes fed green forage enhances the health-promoting properties of buffalo milk.

The ruminal microbiota produces carbohydrate-active enzymes (CAZymes) which include lignocellulolytic enzymes that fundamentally determine the degradation and debranching of plant polysaccharides (Hobson and Stewart 1997; Cantarel et al. 2009). The breakdown of complex carbohydrates by CAZymes produces several metabolites, including volatile fatty acids (VFAs) and hydrogen (Li et al. 2022). CAZymes are grouped into families depending on their specific enzymatic activity (Cantarel et al. 2009). The major CAZymes families are glycoside hydrolases (GHs, hydrolyse and/or rearrange glycosidic bonds), glycosyl transferases (GTs, form glycosidic bonds), polysaccharide lyases (PLs, non-hydrolytic cleavage of glycosidic bonds), carbohydrate esterases (CEs, hydrolyse carbohydrate esters) and auxiliary activities (AAs, redox enzymes that act in conjunction with CAZymes). Diet influences the CAZymes profile in cattle and buffaloes (Patel et al. 2014; Wang et al. 2019; Pantoja-Feliciano et al. 2023). The present study sought to describe relationships between the ruminal microbiota, ruminal CAZymes and milk quality, in buffaloes that received green feed. The relationships were compared to buffaloes that received a standard total mixed ration (TMR). The new information could be used to develop diets incorporating green feed which favour rumen microbiota that produce CAZymes profiles that enhance milk quality in buffaloes. The hypothesis tested was that green feed induces changes in the ruminal microbiota composition and CAZymes profile resulting in enhanced synthesis of amino acids and precursors of functional health-promoting biomolecules in milk of buffaloes.

Materials and methods

For this trial, standard veterinary practices were followed and institutional approval was obtained from the Ethical Animal Care and Use Committee of the University of Napoli "Federico II" (Protocol Number 0025532/2022).

Animals, dietary treatment and ruminal tissue collection

The study was carried out over a period of 60 days using Italian Mediterranean dairy buffaloes ($n = 16$; 8.5 ± 2.0 years old) at a commercial farm in southern Italy. The animals were acclimatised in pens with concrete floors and were machine milked twice daily. They were randomly assigned on parity and daily milk production to two homogeneous groups and received either a standard TMR (5.6 ± 0.6 parity; 6.0 ± 0.6 kg/day milk) or TMR + green forage (5.3 ± 0.6 parity; 6.4 ± 0.5 kg/day milk) (Table 1). The green feed consisted of ryegrass (about 30% of the diet on dry matter) at the re-blossoming stage that was cut twice daily to avoid fermentation, and immediately put into the mixer wagon and fed without storage. The ratio of forage to concentrate was 56:44 for buffaloes that received TMR and 69:31 for buffaloes that received TMR + green forage. The two diets were iso-nitrogenous and iso-energetic and differed only in the proportion of green forage (Table 1). The animals were fed in the morning and evening. Refusals were recorded and then removed. Energy values (milk forage units = 1700 kcal) were calculated using equations provided by the INRA (2007).

Average feed intake for each pen was determined daily from unconsumed feed before the next feeding. The amount and composition of refusals were used to

Table 1. Feed and chemical composition of the buffalo diets fed without total mixed ration (TMR group) or with (TMR + green feed) approximately 30% green ryegrass.

	TMR % feed	TMR + green feed % feed
Ryegrass	0.0	50.3
Corn silage	68.5	35.6
Alfalfa hay	12.5	5.2
Soybean meal, 48%	1.8	0.0
Concentrate	11.8	5.1
Wheat straw	3.1	2.3
Hydrogenated fats	0.9	0.7
Calcium carbonate	0.4	0.4
Salt 1:3	0.6	0.4
Vitamins	0.4	0.0
Total	100	100
	Composition, % of dry matter	
Dry matter	16.0	16.1
CP	14.5	14.4
Fat	4.8	5.0
NDF	38.0	38.5
ADF	24.0	23.4
NSC	34.6	33.1
Starch	21.0	15.5
Ash	8.1	9.0
Calcium	0.9	1.0
Phosphorus	0.4	0.4
MFU	0.93	0.91

CP: crude protein; NDF: neutral detergent fibre; ADF: acid detergent fibre; NSC: non-structural carbohydrates; MFU: milk forage units.

calculate DMI and diet composition. Individual feed intake and differences (Δ) between nutritive intake and relative requirements were estimated as previously reported (Campanile et al. 1998):

$$\text{Dry matter (DM) intake} = 91\ \text{g} \times \text{MW} + 0.27\ \text{kg} \times \text{kg ECM}$$

$$\Delta\text{CP} = \text{g CP intake} - (80\ \text{g CP} \times 100\ \text{kg live weight} + 2.7\ \text{g CP} \times \text{g milk protein yield})$$

$$\Delta\text{MFU} = \text{MFU intake} - [(1.4 + 0.6 \times 100\ \text{kg live weight}) \times 1.1 + 0.44\ \text{MFU} \times \text{kg ECM}]$$

At day 60, samples of bulk milk were obtained for each group, the milk production was recorded and the animals were slaughtered and processed under commercial conditions. The rumen of each animal was made available and samples were collected from different locations within the rumen and pooled. Rumen fluid samples (50 mL) for each animal were collected in a falcon tube, immediately frozen in dry ice, and then stored at −80 °C until analyses.

Bulk milk analysis

Samples were analysed in triplicate using IR spectroscopy (Milkoscan 139, Foss Electric, Hillerød, Denmark) that was calibrated with a buffalo standard. Energy corrected milk (ECM = 740 kcal) was calculated using the formula for buffalo cows (Campanile et al. 1998): ([{fat ($g \cdot kg^{-1}$) - 40 + protein ($g \cdot kg^{-1}$) - 31} × 0.01155] + 1) × milk yield. The content of γ-butyrobetaine, glycine betaine, δ-valerobetaine, L-carnitine, acetyl-L-carnitine and propionyl-L-carnitine was determined in duplicate pooled soluble milk extract samples as previously described (Servillo, D'Onofrio, Giovane, et al. 2018). Briefly, samples of milk were centrifuged at 3000 × *g* for 15 min at 4 °C to recover fat globules. The latter were filtered through a 5 μm Millipore filter (Burlington, MA) to remove high MW components and any precipitate that may have been transferred when recovering fat globules. This was followed by filtration through an Amicon Ultra 0.5 mL centrifugal filter with a 3 kDa molecular weight cut-off to yield low MW components, including short-chain acylcarnitines (between 161.2 and 245.3 molecular weight), glycine betaine (153.6 molecular weight), γ-butyrobetaine (146.1 molecular weight) and δ-valerobetaine (159.23 molecular weight). The antioxidant and antineoplastic activity in Amicon Ultra-filtrates are not due to low MW peptides as activity is retained during treatment at 100 °C to produce ricotta cheese (Salzano et al. 2019). Analysis involved HPLC-ESI-MS/MS with an Agilent LC-MSD SL quadrupole ion trap and a 1100 series liquid chromatograph (Supelco Discovery C8 column, 250 × 3.0 mm, particle size 5 μm) under isocratic conditions, 0.1% formic acid in water, at flow rate of 100 μL/min. Quantification of each compound involved comparison of the peak area of its most intense MS2 fragment with the respective calibration curve built with solutions of standards products (L-carnitine, acetyl-L-carnitine propionyl-L-carnitine, glycine betaine and γ-butyrobetaine) from Sigma-Aldrich (Milan, Italy) (Servillo, D'Onofrio, Neglia, et al. 2018). δ-Valerobetaine was prepared as previously described (Servillo, D'Onofrio, Neglia, et al. 2018). Standard solutions were prepared by serial dilution of standard stock solutions (2 mg/L) with water containing 0.1% formic acid. Linearity was assessed by correlation coefficients (r^2) >0.99 for all compounds. Precision and accuracy for all compounds in milk ranged from 95% to 105%.

Ferric reducing antioxidant power and total antioxidant assay

Milk ferric reducing antioxidant power (FRAP; Assay Kit (MBS169262) and total antioxidant capacity (TAC; Assay Kit (#K274-100) were determined in pooled milk samples according to the manufacturer. Milk samples (four replicates) were diluted 1:10 (v/v) with H_2O and a 1 μL aliquot was used for each assay. Samples were incubated at room temperature for 90 min protected from light, before measuring the absorbance at 570 nm, or monitoring the increase in absorbance at 594 nm for 1 h at 37 °C for TAC and FRAP assay, respectively. The positive control comprised ascorbic acid (1 μg/mL). FRAP value was expressed as Fe^{2+} iron equivalents (μM; range = 10–250 × μg/mL of ascorbic acid) and TAC was expressed as Trolox equivalent capacity (range = 10–250 × nmol μg/mL of ascorbic acid).

DNA extraction

Bacterial genomic DNA was extracted using the QIAMP DNA Stool mini kit (QIAGEN, Hilden, Germany) according to the manufacturer and included negative extraction controls (Saggese et al. 2016; Saggese, Giglio, et al. 2022). The amount and the quality of the extracted DNA were evaluated using Nanodrop ND-2000 (Nanodrop, Wilmington, DE) and a high-sensitivity Qubit™ fluorometer (Saggese, De Luca, et al. 2022).

Sequencing, bioinformatics and statistical analyses of 16S rRNA gene sequences

Partial 16S rRNA gene sequences were obtained using primers specific for the V4–V5 region (515FB = GTGYCAGCMGCCGCGGTAA and 926R = CCG YCAATTYMTTTRAGTTT 515FB) (Parada et al. 2016) and were sequenced at the Integrated Microbiome Resource (IMR, https://imr.bio) using an Illumina MiSeq machine (San Diego, CA). All sequences were imported in R, and analysed with the DADA2 package (Callahan et al. 2016). Following the package guidelines, quality plots were performed to check the sequences' quality. Post-QC reads were trimmed using the filterAndTrim command [truncLen = c(260,190), maxN = 0, maxEE = c(2,2), truncQ = 2, rm.phix = TRUE, trimLeft = c(20,21)]. After this step, a parametric error model, based on the convergence between the estimation of error rate and the inference of the sample composition, was performed. Paired-end reads were merged and exact amplicon sequence variants (ASVs) were inferred using the dada algorithm. Chimeric sequences were removed and prokaryotic taxonomy was assigned using the naive Bayesian classifier method against the Silva Database (r138). ASVs abundance table obtained from DADA2 was further processed in R using *Phyloseq*, *Vegan* and *Microbiome* packages (Lahti and Shetty 2017; Oksanen et al. 2020). Sequences are available in the NCBI Sequence Read Archive (SRA) database under the BioProject number PRJNA993601. BioSample accession number for each sequence is included in Supplementary Table S1.

After the Phyloseq object creation, low abundance ASVs (less than three reads across the dataset), mitochondria, chloroplast and potential contaminants (Sheik et al. 2018) were removed. The remaining ASVs represented ∼99% of the original reads, with 1,139,005 reads classified as 8222 individual ASVs used for downstream statistical investigations (Maia et al. 2020). ASVs counts were normalised to the median library size across the dataset. Diversity analyses were carried out using the Phyloseq package (McMurdie and Holmes 2013) with relative abundance set to 100% after the removal of sequences described above. Top abundance ASVs and Genera were defined as having a cumulative relative abundance above 0.1% in our dataset. The alpha diversity was investigated using the Simpson diversity index among the two sampled areas. The beta diversity was investigated using the Jaccard diversity index as implemented in the vegan package (Oksanen et al. 2012). Both the abundance weighted and unweighted versions of the index were used.

Sequencing, bioinformatics and statistical analyses of metadata

Microbiomes were investigated through metagenomic analysis using the Giovannelli Lab metagenomics narrative created on Kbase (Arkin et al. 2018). Metagenomic data are available in the NCBI SRA with project ID PRJNA993601. BioSample accessions for each metagenome are included in Supplementary Table S1. This pipeline is designed to analyse raw metagenomic sequences obtained from various microbiomes and includes three main approaches: a read-based approach, an assembly-based approach and a genome-resolved approach. The read-based approach first involves quality control of the raw sequences using FastQC (v0.11.9) to evaluate sequence quality, followed by a trimming step with Trimmomatic (v0.36) to remove primers and poorly sequenced extremities. The trimmed sequences are then subjected to taxonomic classification using Kaiju (v1.7.3). The read-based functional profiling was obtained through the software mi-faser (functional annotation of sequencing reads; Zhu et al. 2018) which combines faser (an optimised algorithm for mapping reads) with the reference database of protein functions and annotates each microbiome as a set of molecular functions. The assembly-based approach involves the use of three different assembly software programs for each sample: metaSPAdes (v3.15.3), MEGAHIT-high and low sensitivity (v1.2.9) and IDBA-UD (v1.1.3). The resulting assemblies are evaluated using QUAST (v1.1.2) to select the best assembly based on contiguity and completeness. The functional annotation of the contigs obtained from the assembly is carried out using the Database of Rapid Annotation using Subsystems Technology (RAST).

The genome-resolved approach involves binning the contigs obtained from the assembly step using three different binning software programs: MaxBin2 (v2.2.4), MetaBAT2 (v1.7) and CONCOCT (v1.1). The resulting bins are refined using consensus assignments with the software DAS-tool (v1.1.2) to ensure bins with at least 50% completeness. Quality control of the bins is performed using CheckM (v1.0.18), which uses a built-in library of high-quality conserved marker genes to estimate the completeness and contamination of the metagenomic bins. The taxonomic classification of the high-quality bins is carried out using the Genome Taxonomy Database Toolkit (GTDB-Tk) database (Chaumeil et al. 2019), which provides objective taxonomic assignments for bacterial and archaeal genomes, placing the bins within a phylogenetic tree with high-quality reference genomes.

CAZyme annotation of metadata

All samples were further functionally characterised by analysis of the CAZyme database (www.cazy.org), which allows the identification of CAZymes. CAZymes, including those encoded by GHs, glycosyltransferases (GTs), CEs, PLs and AAs genes in the rumen metagenome, were identified and annotated using the HMMER 3.0 package (http://hmmer.org/) with the dbCAN CAZyme database (www.cazy.org; Yin et al. 2012). The CAZyme results of the gene were searched against the sequences in the NR database using the BLASTP algorithm with an *E*-value cut-off of 1×10^{-5}.

Statistical analyses

Statistical analyses were performed using SPSS (23.0) for Windows 10 (SPSS Inc., Chicago, IL). The buffalo was used as the experimental unit. One-way ANOVA was used to compare data for dry matter intake (DMI), milk yield and quality, total antioxidant activity (TAC), FRAP and functional molecules of milk. A statistically significant difference was accepted at $p < .05$.

Results

Animal productions

As shown in Table 1, total DMI was similar between TMR and TMR + green feed buffaloes (16.0 ± 0.2 and 16.1 ± 0.2 kg/day respectively for TMR and TMR + green feed buffaloes, $p = .89$). Average milk yield and ECM throughout the experimental period did not differ significantly between the two groups (12.3 ± 0.1 vs. 12.5 ± 0.2 kg respectively for TMR and TMR + green feed group, $p = .87$). No differences were found on milk quality traits between the two groups (data not shown).

Milk biomolecules and antioxidant capacity

Results for functional biomolecules in milk and total antioxidant power are shown in Table 2. Buffaloes that received green feed had higher ($p < .01$) concentrations of L-carnitine, propionyl-L-carnitine, acetyl-L-carnitine and δ-valerobetaine compared with buffaloes that received the TMR. Concentrations of glycine, betaine and γ-butyrobetaine did not differ between groups. The antioxidant capacity of milk was higher ($p < .01$) in buffaloes that received green feed, both when determined by TAC and FRAP assays.

Table 2. Functional biomolecules and antioxidant power in milk for buffaloes that received a total mixed ratio (TMR group) and buffaloes that received TMR + fresh ryegrass (approximately 30% of the diet; TMR + green feed group).

	TMR, mg/L	TMR + green feed, mg/L
L-Carnitine	30.4 ± 0.7 A	41.0 ± 0.6 B
Acetyl-L-carnitine	38.6 ± 0.5 A	48.4 ± 0.6 B
Propionyl-L-carnitine	15.7 ± 1.0 A	22.1 ± 0.5 B
γ-Butyrobetaine	4.4 ± 0.3	3.8 ± 0.2
δ-Valerobetaine	19.1 ± 0.6 A	23.4 ± 0.6 B
Glycine betaine	7.3 ± 0.1	7.4 ± 0.3
TAC	220.3 ± 5.5 A	249.5 ± 7.7 B
FRAP	194.3 ± 4.2 A	225.8 ± 4.8 B

FRAP: ferric reducing antioxidant power assay; TAC: total antioxidant capacity.
Results are mg/L, mean ± SEM. (A, B) $p < .01$.

Taxonomic analysis of the rumen microbial composition

A total of 1,139,005 sequences with an average sequence length of 370 bp were found and 8221 ASVs were identified. Of these, 6192 ASVs were common to the two groups. There were 734 unique for buffaloes that received TMR and 1295 were unique for buffaloes that received TMR + green feed. The taxonomic analysis assigned the bacterial community to 14 bacterial phyla (Supplementary Table S2 Figure S1). *Firmicutes* (now renamed *Bacillota*) and *Bacteroidota* were the most abundant phyla in both groups (over 92% of the total bacteria). Other bacterial phyla that accounted for more than 1% of the sample were *Proteobacteria* and *Planctomycetota* (Supplementary Table S2). At the order level, *Bacteroidales*, *Christensenellales*, *Oscillospirales* and *Lachnospirales* were most abundant in both groups (Supplementary Table S3 and Figure S2). At the genus level, *Christensenellaceae_R-7_group*, *Rikenellaceae_RC9_gut_group*, *NK4A214_group*, *Prevotella* and *Butyrivibrio* were the most common in buffaloes that received TMR and *Lachnospiraceae_XPB1014_group* replaced *Butyrivibrio* in buffaloes that received TMR + green feed (Supplementary Table S4 and Figure S3).

Rumen microbial diversity

The overall microbial composition of the rumen did not differ markedly between the two groups (Supplementary Figures S1–S3). No differences were observed at the phylum level (Supplementary Figure S1 and Table S2) and there were relatively minor differences at the order and genus level (Supplementary Figures S2 and S3, Tables S3 and S4). At the order level, *Peptostreptococcales–Tissierellales* were more abundant in buffaloes that received TMR and *Veillonellales–Selenomonadales* and *Bradymonadales*

were more abundant in buffaloes that received TMR + green feed (Supplementary Table S3). Relatively few statistically significant differences were observed at the genus level and these were mostly due to poorly represented genera: *Prevotellaceae_YAB2003_group* (*Bacteroidota* phylum) and *Colidextribacter* (*Bacillota* phylum) were more abundant in buffaloes that received TMR whilst *Selenomonas*, *Prevotellaceae-UCG-007*, *Quinella*, *Oscillospira* and *Tyzzerella* (all *Bacillota* phylum) were more abundant in buffaloes that received TMR + green feed (Supplementary Table S4).

The microbial diversity of the two groups was further characterised by analysing alpha and beta diversity. Alpha diversity was analysed using the richness and Simpson indices, the former taking into account all sequences obtained and the latter focusing only on the most abundant ones. A higher number of species and greater species diversity were observed in the buffaloes that received TMR + green feed (Figure 1(A)). However, when the analysis focused only on the most abundant sequences, the results were reversed, and a higher number of species were found in buffaloes that received TMR (Figure 1(B)). Taken together, these results could be interpreted to suggest (1) buffaloes that received TMR + green feed had a greater biodiversity of rumen microbial composition than buffaloes that received TMR and (2) the greater number of species found in buffaloes that received TMR + green feed was due to rare species. This was supported by analysis of beta diversity by the nMDS-Jacard index. The unweighted analysis showed that the samples of buffaloes that received TMR + green feed (green symbols in Figure 2(A)) were scattered in a larger area than samples of buffaloes that received TMR (yellow symbols in Figure 2(A)). This indicated a greater species diversity in buffaloes that received TMR + green feed. The weighted nMDS analysis, where the most abundant ASV are given more weight, showed that the samples of the two groups were similarly distributed, indicating that the clusters observed in the unweighted analysis were mostly due to rare species (Figure 2(B)).

Metagenomic analysis of the rumen microbiota

Total DNA from rumen samples was also used for shotgun metagenome sequencing at the IMR (https://imr.bio). Microbial community metagenomes were generated using the Illumina Nextera Flex Kit for MiSeq + NextSeq and we used a 2× depth (∼8 M PE reads). Metagenomic data were used to assess the presence of archaea and viral DNA. Significantly fewer archaeal and viral sequences were found compared to bacterial sequences. Members of the phylum *Euryarchaeota* accounted for 2.5 ± 1.3% (TMR) and 2.4 ± 1.0% (TMR + green feed) of the total rumen microbiota. At the genus level, the abundance of *Methanobrevibacter* did not differ between the two groups (TMR 1.80%; TMR + green feed 1.74%). The total amount of viral DNA in rumen samples was very low and similar between the two groups (TMR 0.26%; TMR + green feed 0.22%).

Enzymes of the transferases (EC2) and hydrolases (EC3) classes were more abundant in both groups and did not differ (Figure 3). Analysis of functional alpha diversity showed the highest Simpson's diversity index for buffaloes that received TMR + green feed (Figure 4). This was supported by an nMDS analysis based on weighted Jaccard similarity, which showed that samples for buffaloes that received TMR + green feed (green symbols in Figure 5) were scattered in a larger area than samples for buffaloes that received TMR (yellow symbols in Figure 5).

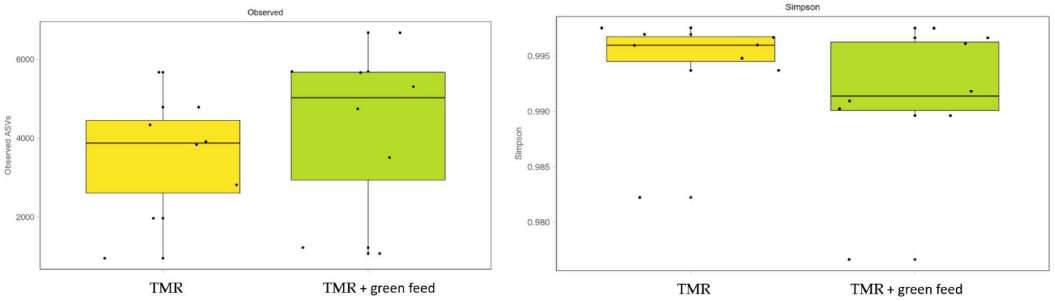

Figure 1. Alpha diversity between the two diet groups. (A) Observed number of ASVs (simply the number of ASVs present in the sample) and (B) Simpson diversity index (taking into account the number of taxa as well as the abundance, thus downplaying the role of rare species). Based on this, the total mixed ration (TMR) + green diet has a larger number of rare species compared to the TMR diet.

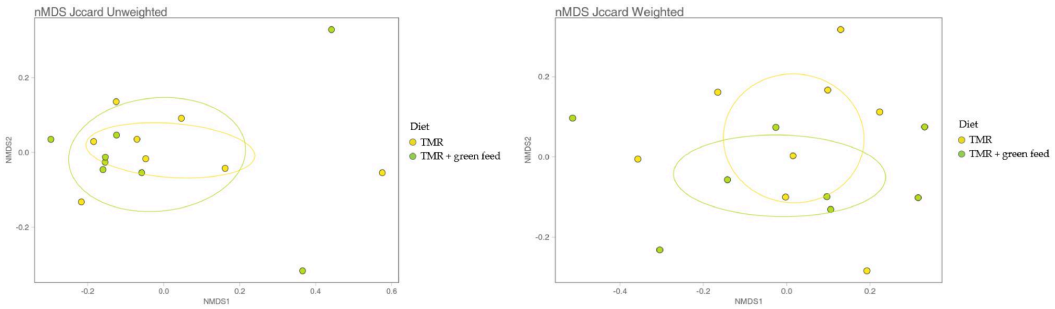

Figure 2. Ordination (nMDS) based on weighted (top) and unweighted (bottom) Jaccard similarity coloured according to the diet group. Ellipses correspond to the 95% confidence interval of the barycentre for the group.

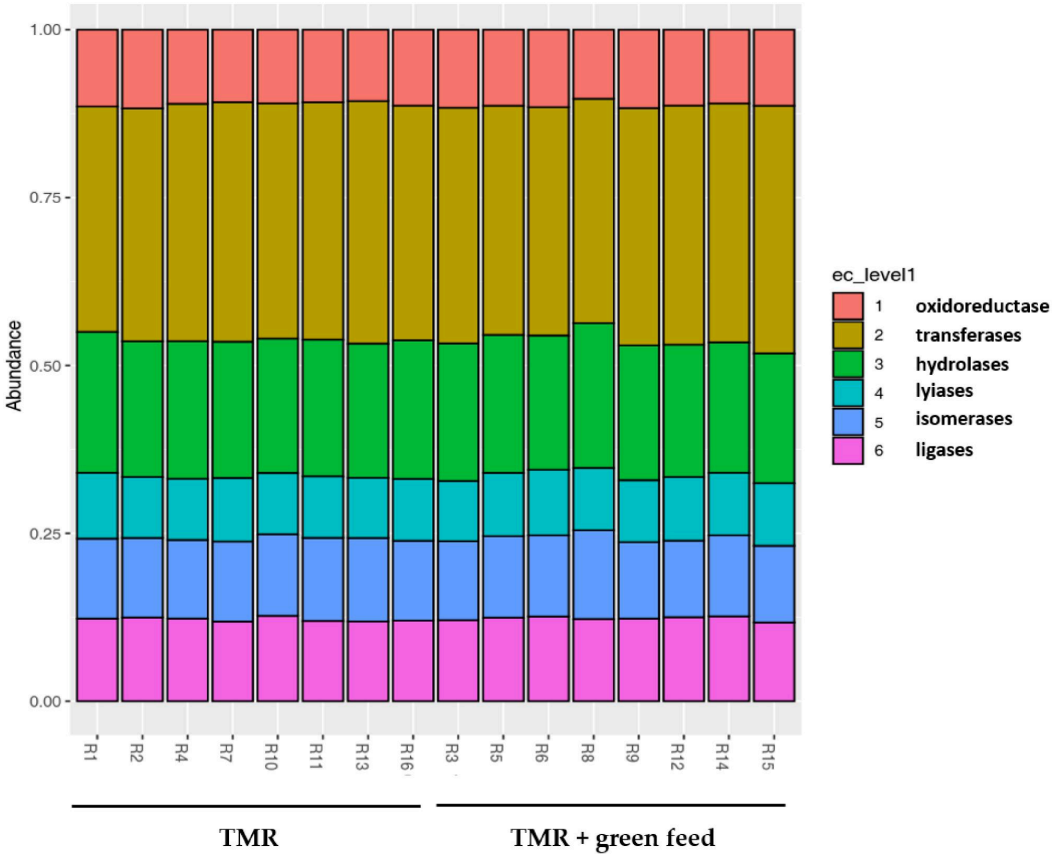

Figure 3. Enzyme code (EC) class distributions in the buffalo group fed with standard total mixed ratio (TMR) or with TMR + ryegrass green forage.

Metagenomic analysis of carbohydrate-active enzymes

Members of all six classes of CAZymes (GHs, GTs, CBMs, CEs, PLs and AAs) were identified, with classes GH and GT being the most abundant in both groups (Supplementary Table S5, summarised in Table 3). Buffaloes that received TMR + green feed had a lower average number of CAZymes of the classes GHs, CBMs and CEs, and an increased number of the classes GTs and AAs (Table 3). Analysis of the most abundant GH

Table 3. Distribution of CAZymes in the rumen of buffaloes that received a total mixed ration (TMR group) and buffaloes that received TMR + fresh ryegrass (approximately 30% of the diet; TMR + green feed group).

	TMR		TMR + green feed	
	Average number/animal	%	Average number/animal	%
GH: glycoside hydrolases	328.37	84.39	251.42	82.47
GT: glycosyl transferases	33.25	8.54	32.00	10.50
CBM: carbohydrate binding modules	1.37	0.35	0.71	0.23
CE: carbohydrate esterases	20.87	5.36	14.25	4.69
PL: polysaccharide lyases	3.25	0.84	2.71	0.89
AA: auxiliary activities	2.00	0.51	3.71	1.22
Total CAZymes	389.11		304.80	

and GT families showed that enzymes belonging to 73 GH and 26 GT families were present, with seven GH and seven GT families present only in buffaloes that received TMR and six GH and 1 GT families present only in buffaloes that received TMR + green feed (Supplementary Table S5, summarised in Table 4). The most abundant GH families (GH2, GH13 and GH30) were all more abundant in buffaloes that received TMR (Figure 6(A)). Families with GH10, GH35, GH54, GH67, GH95, GH104, GH105, GH115 and GH133 more abundant in buffaloes that received TMR + green feed (Figure 6(B)). Analysis of the GT family showed that GT4, GT14, GT20, GT26 and GT39 were more abundant in buffaloes that received TMR + green feed and GT5, GT10, GT30, GT83 and GT112 were more abundant in buffaloes that received TMR (Figure 7). The GT families that were more abundant in the Green group are also produced by some of the genera detected as more abundant in the Green group (Table 5). Some of the remaining GH and GT families were present in the rumen of the two 3p experimental groups to different extents.

Discussion

The present study tested the hypothesis that green feed induces changes in the ruminal microbiota and CAZymes which results in enhanced milk quality in buffaloes. In support of the hypothesis, the inclusion of green feed in the diet of buffaloes favoured subpopulations of bacteria that produced a distinct subset of CAZymes. Also, whole milk of buffaloes that received TMR + green feed had higher amounts of L-carnitine, propionyl-L-carnitine, acetyl-L-carnitine and δ-valerobetaine (Salzano et al. 2021; Neglia, Cotticelli, et al. 2023). These functional biomolecules have health-promoting properties and *in vitro* suppress human cancer cell lines (D'Onofrio, Cacciola, et al. 2020; D'Onofrio, Mele, et al. 2020; Cacciola et al. 2022).

Buffaloes that received TMR + green feed had a higher representation of bacteria belonging to the orders *Veillonellales*, *Selenomonadales* and *Bradymonadales*. *Veillonellaceae* ferment lactate to acetate and propionate which is related to fatty acid metabolism (Zeng et al. 2019). At the genus level, *Quinella*, *Selenomonas*, *Prevotellaceae-UCG-007*, *Oscillospira* and *Tyzzerella* were more abundant in buffaloes that received TMR + green feed. Members of the genus *Prevotella*, and other genera of the family *Prevotellaceae*, are dominant rumen bacteria and show changes in response to changing diets (Paradiso et al. 2021; Rabee et al. 2022; Yi et al. 2022). In weaned calves, *Succiniclastum*, *Selenomonas 1* and the *Prevotellaceae YAB2003* group were positively correlated with total short chain fatty acids and propionic, valeric, acetic and butyric acids, and acetate and butyrate concentrations in the rumen (Hartinger et al. 2022). In the present study, the proportion of highly fermentable carbohydrates/sugars was higher in buffaloes that received TMR + green feed consistent with a greater prevalence of *Prevotella*. Buffaloes that received the TMR diet had a greater abundance of bacteria in the orders *Peptostreptococcales* and *Tissierellales*. *Peptostreptococcales* ferment butyrate, which is used by cells of the rumen wall as an energetic substrate with the formation of β-hydroxybutyrate (Palakawong Na Ayudthaya et al. 2018; Gharechahi et al. 2021). A diet high in concentrates increased acetate and butyrate in the rumen (Sinha et al. 2017) and ruminal fluid *in vitro* in buffaloes (Neglia, Calabrò, et al. 2023).

The capacity of the rumen to convert feed into fermentable sugars is dependent on polysaccharide hydrolysing enzymes, CAZymes, that are produced by rumen microbes. In the present study, differences in rumen bacteria subpopulations between buffaloes that received TMR and TMR + green feed were associated with different ruminal profiles of CAZymes. The total CAZymes were higher in buffaloes that received TMR compared to the TMR + green feed group. In TMR buffaloes, a greater abundance of *Prevotellaceae* was associated with a higher percentage of CAZymes GH, CBM, CE and PL (Wang et al. 2019). Buffaloes that

Table 4. Glycoside hydrolases (GH) and Glycosyl transferases (GT) families present only in one group.

TMR		TMR + green feed	
GH	Activities in the family	GH	Activities in the family
GH4	Maltose-6-phosphate glucosidase (EC 3.2.1.122); α-glucosidase (EC 3.2.1.20); α-galactosidase (EC 3.2.1.22); 6-phospho-β-glucosidase (EC 3.2.1.86); α-glucuronidase (EC 3.2.1.139); α-galacturonase (EC 3.2.1.67); palatinase (EC 3.2.1.-)	GH11	Endo-β-1,4-xylanase (EC 3.2.1.8); exo-1,4-β-xylosidase (EC 3.2.1.-)
GH50	β-Agarase (EC 3.2.1.81)	GH63	Processing α-glucosidase (EC 3.2.1.106); α-1,3-glucosidase (EC 3.2.1.84); α-glucosidase (EC 3.2.1.20); mannosylglycerate α-mannosidase/ mannosylglycerate hydrolase (EC 3.2.1.170); glucosylglycerate hydrolase (EC 3.2.1.208)
GH76	α-1,6-Mannanase (EC 3.2.1.101); α-glucosidase (EC 3.2.1.20)	GH65	α,α-Trehalase (EC 3.2.1.28); maltose phosphorylase (EC 2.4.1.8); trehalose phosphorylase (EC 2.4.1.64); kojibiose phosphorylase (EC 2.4.1.230); trehalose-6-phosphate phosphorylase (EC 2.4.1.216); nigerose phosphorylase (EC 2.4.1.279); 3-O-α-glucopyranosyl-L-rhamnose phosphorylase (EC 2.4.1.282); 1,2-α-glucosylglycerol phosphorylase (EC 2.4.1.332); α-glucosyl-1,2-β-galactosyl-L-hydroxylysine α-glucosidase (EC 3.2.1.107); 1,3-α-oligoglucan phosphorylase (EC 2.4.1.334); α-1,2-glucosidase (EC 3.2.1.-); α-glucan phosphorylase (EC 2.4.1.-); kojibiose glucohydrolase (α-1,2-glucosidase) (configuration inverting) (EC 3.2.1.216); branched-dextran exo-1,2-α-glucosidase (EC 3.2.1.115)
GH141	α-L-Fucosidase (EC 3.2.1.51); xylanase (EC 3.2.1.8)	GH85	Endo-β-N-acetylglucosaminidase (EC 3.2.1.96)
GH144	Endo-β-1,2-glucanase (EC 3.2.1.71); β-1,2-glucooligosaccharide sophorohydrolase (EC 3.2.1.214)	GH89	α-N-Acetylglucosaminidase (EC 3.2.1.50)
GH158	Endo-β-1,3-glucanase (EC 3.2.1.39)	GH112	Lacto-N-biose phosphorylase or galacto-N-biose phosphorylase (EC 2.4.1.211); D-Galactosyl-β-1,4-L-rhamnose phosphorylase (EC 2.4.1.247)
GH 159	β-D-Galactofuranosidase (EC 3.2.1.146); α-L-arabinofuranosidase (EC 3.2.1.55)		
GT	Activities in the family	GT	Activities in the family
GT11	GDP-L-Fuc: galactoside α-1,2-L-fucosyltransferase (EC 2.4.1.69); GDP-L-Fuc: β-LacNac α-1,3-L-fucosyltransferase (EC 2.4.1.-)	GT56	TDP-Fuc4NAc: lipid II Fuc4NAc transferase (EC 2.4.1.-)
GT66	Dolichyl-diphosphooligosaccharide – protein glycotransferase (EC 2.4.99.18); undecaprenyl-diphosphooligosaccharide – protein glycotransferase (EC 2.4.99.19)		
GT84	Cyclic β-1,2-glucan synthase (EC 2.4.1.-)		
GT102	dTDP-β-L-Rhap: O-antigen-polysaccharide α-1,3-L-rhamnosyltransferase (EC 2.4.1.289)		
GT108	GDP-α-D-Manp: β-1,2-D-mannosyltransferase (EC 2.4.1.374)		
GT111	UDP-Galf: β-1,3-galactofuranosyltransferase (EC 2.4.1.-)		
GT113	Glucosyltransferase (2.4.1.-); hexosyltransferase (2.4.1.-)		

received TMR + green feed had a higher percentage of CAZymes GT and AA. The GH CAZymes, together with CE and PL have a complex process of lignocellulose breakdown and can degrade complex sugars (Lombard et al. 2014) whilst CBMs can enhance the catalytic efficiency of enzymes by specifically binding polysaccharides and improving enzyme concentration (Jones et al. 2018).

In both cattle and buffaloes, a change from green to dry roughage was associated with an increase in GH CAZymes (Bohra et al. 2019). In the present study, buffaloes that received TMR had a greater amount of GH CAZymes compared to the TMR + green feed group.

Buffaloes that received TMR + green feed had a greater abundance of CAZymes of the GT class (GHT4, GT14, GT20, GT26, GT39) and AA class (AA1, AA3, AA6). The AA CAZymes class is most abundant in wood degrading fungi and have lignocellulose degradation and antioxidant activity (Sützl et al. 2018). The

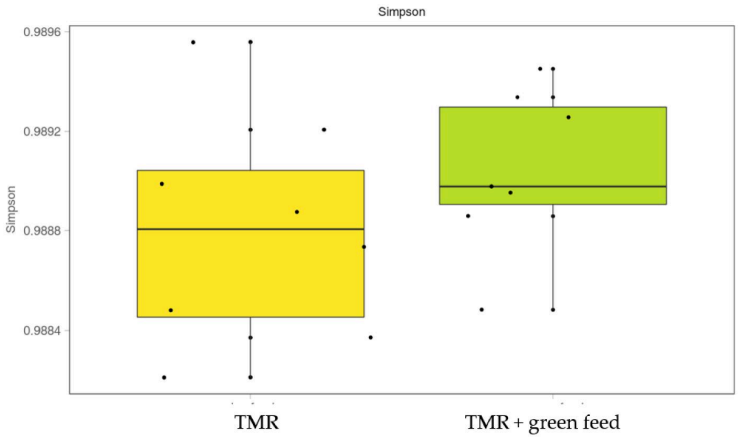

Figure 4. Functional alpha diversity (Simpson) based on the shotgun metagenome functional read assignment for the two diet groups.

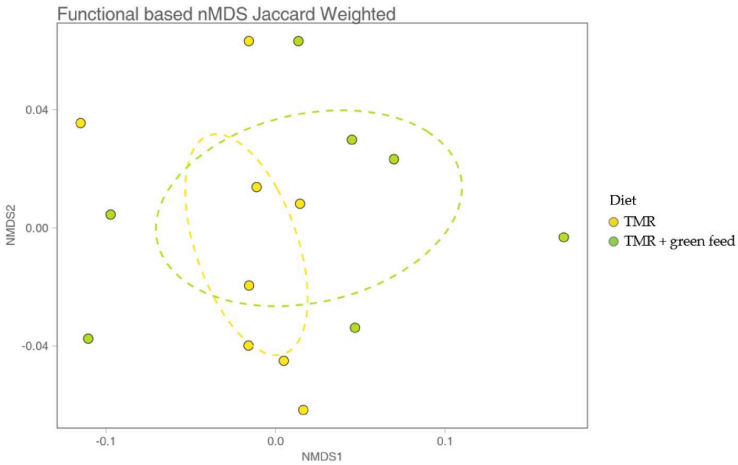

Figure 5. Functional based nMDS based on weighted Jaccard similarity among the shotgun metagenome functional read assignment for the two diet groups.

latter finding could explain the higher antioxidant activity in whole milk of buffaloes that received TMR + green feed in the present study. A higher expression of genes linked to oxidative stress and cellular responses in buffalo ruminal cells *in vitro* correlated with a greater abundance of bacteria that produce GT4 and G26 (*Selenomonas*, *Prevotella*, *Oscillospiraceae*); GT14 and GT20 (*Prevotella*); GT30 (*Selenomonas*, uncultured *Prevotella*); GT39 (*Oscillospiraceae*). The GT CAZymes are involved in the biosynthesis of glycosidic bonds from phospho-activated sugar donors (Coutinho and Henrissat 1999; Benson et al. 2004; Yip and Withers 2006). The specificity of GT CAZymes residues in their ability to selectively modify the correct hydroxyl group on an acceptor containing many equally reactive hydroxyls (e.g. complex oligosaccharides) (Varki 2017). As many bacteria synthesise polysaccharides that mimic human glycosylation, bacterial GT CAZymes can be used for the synthesis of glycoproteins with eukaryotic glycosylation patterns (Varki 2017).

Diet clearly determines the profile of CAZymes in ruminants. The CAZymes profile in buffaloes that received TMR + green feed in the present study could partly explain the ruminal wall cellular transcriptome of buffaloes that received green feed (Salzano et al. 2023). The latter would influence the metabolome of ruminal fluid (Neglia, Cotticelli, et al. 2023) which, in

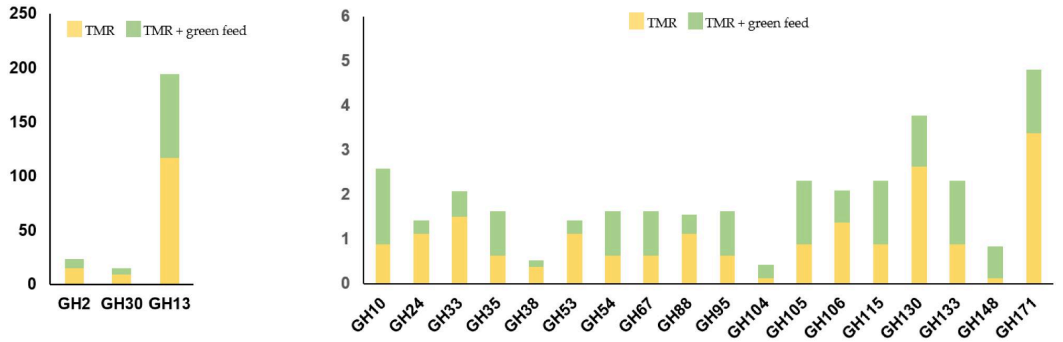

Figure 6. The most abundant Glycoside hydrolases (GH) families in the buffalo group fed with standard total mixed ration (TMR) or with TMR + ryegrass green forage (A). GH families whose abundances show a clear difference between the two experimental groups (B).

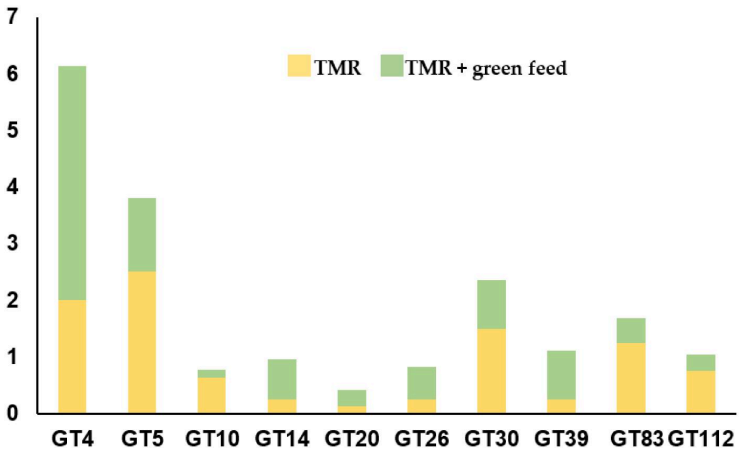

Figure 7. Abundance of the Glycosyl transferases (GT) families in the buffalo group fed with standard total mixed ration (TMR) or with TMR + ryegrass green forage.

Table 5. Genera detected in total mixed ration (TMR) + green feed group rumen samples that encoded the more abundant Gglycosyl transferases (GT) in TMR + green feed group.

GT	Genus
GT4	*Selenomonas, Prevotella, Oscillospiraceae*
GT14	*Prevotella*
GT20	*Prevotella*
GT26	*Selenomonas, Prevotella, Oscillospiraceae*
GT30	*Selenomonas, uncultured Prevotella*
GT39	*Oscillospiraceae*
GT56	–

turn, would influence systemic and milk metabolites in buffaloes fed green forage (Salzano et al. 2021, 2022). This pathway of CAZymes influencing cellular processes would be considered analogous to sugar nucleotide-dependent glycosyltransferases (UGT enzymes) and glycosylation pathways in human cells (Audet-Delage et al. 2022). Nε-trimethyllysine (TML) is the main precursor (Servillo et al. 2014) of the functional biomolecules observed in buffaloes provided with green forage (Salzano et al. 2021, 2022). This precursor is derived by lysine methylation (Lee et al. 2004) which most likely occurs in ruminal wall cells. Leafy vegetables, such as ryegrass, contain relatively high amounts of TML, which participates in carnitine biosynthesis (Servillo et al. 2014). Moreover, they are also known to produce favourable nutrient profiles in cattle in terms of gross composition, macroelements and trace elements (Callahan et al. 2016; Gulati et al. 2018). The higher amount of TML in the rumen of animals fed green forage may hence explain the production of milk with higher nutritional profile.

Overall, the findings in the present study, combined with our previous reports noted above, show that buffaloes fed green forage have higher expression of genes involved in amino acid metabolism. The present findings provide strong support for the proposed metabolic

and biosynthetic pathways that link green forage with rumen bacteria, CAZymes and the synthesis of amino acids and biomolecule in buffaloes. This information can inform the development of diets incorporating green forage that achieve good animal health and well-being whilst producing high amounts of functional biomolecules in milk, for both buffaloes and cattle.

Conclusions

Our analyses indicate that whilst the overall microbial composition of the rumen is not drastically affected by the experimental diet, it increases the microbial biodiversity with an increased abundance of low represented bacterial genera. The inclusion of green feed in the diet of dairy buffaloes favours ruminal microbiota that produce CAZymes that support the synthesis of functional biomolecules. The latter enhances the health-promoting properties of whole milk. The findings provide incentive to further refine feeding strategies that meet consumer preference for food products sourced from animals fed natural diets. The approach adopted in the present study for buffaloes should also be applicable to dairy cattle.

Ethical approval

All experimental procedures were approved by the Ethical Animal Care and Use Committee of the University of Naples "Federico II" (Protocol No. 25532-2022). The authors confirm that the ethical policies of the journal, as noted on the journal's author guidelines page, have been adhered to and the appropriate ethical review committee approval has been received. The authors confirm that they have followed EU standards for the protection of animals used for scientific purposes.

Disclosure statement

No potential conflict of interest was reported by the author(s).

Funding

This research was supported by Project "CAPSULE: Ottimizzazione delle teCniche di Allevamento e dei Processi produttivi del Settore lattiero-caseario bUfalino e del vino per la produzione di aLimEnti funzionali", PON I&C 2014–2020, Project No. F/200016/01-03/X45. CUP: B61B20000170005. PSR REGIONE CAMPANIA 2014–2020 measure 16.1.2. Project "STRABUF: Strategie per il miglioramento della redditività dell'allevamento bufalino (Strategies for improving the profitability of buffalo breeding)". CUP: B68H19005200009. This study was carried out within the Agritech National Research Center and received funding from the European Union Next-Generation EU (PIANO NAZIONALE DI RIPRESA E RESILIENZA (PNRR) – MISSIONE 4 COMPONENTE 2, INVESTIMENTO 1.4 – D.D. 1032 17/06/2022, CN00000022).

ORCID

Anella Saggese http://orcid.org/0000-0002-0968-8644
Elisa Martino http://orcid.org/0000-0003-4070-2894
Gianluca Neglia http://orcid.org/0000-0002-0989-6072
Martina Cascone http://orcid.org/0000-0001-6674-3585
Matteo Selci http://orcid.org/0009-0007-1919-6284
Loredana Baccigalupi http://orcid.org/0000-0003-3070-161X
Nunzia D'Onofrio http://orcid.org/0000-0002-5300-9530
Donato Giovannelli http://orcid.org/0000-0001-7182-8233
Giovanna Bifulco http://orcid.org/0009-0000-4413-7656
Ezio Ricca http://orcid.org/0000-0002-7355-0332
Maria Luisa Balestrieri http://orcid.org/0000-0001-6001-1789
Michael D'Occhio http://orcid.org/0000-0001-8952-3091

Data availability statement

The data sets used and/or analysed during the current study are available from the corresponding author on reasonable request.

References

Arkin AP, Cottingham RW, Henry CS, Harris NL, Stevens RL, Maslov S, Dehal P, Ware D, Perez F, Canon S, et al. 2018. KBase: the United States Department of Energy Systems Biology Knowledgebase. Nat Biotechnol. 36(7):566–569. doi: 10.1038/nbt.4163.

Arrichiello A, Auriemma G, Sarubbi F. 2022. Comparison of nutritional value of different ruminant milks in human nutrition. Int J Funct Nutr. 3(4):5. doi: 10.3892/ijfn.2022.28.

Audet-Delage Y, Rouleau M, Villeneuve L, Guillemette C. 2022. The glycosyltransferase pathway: an integrated analysis of the cell metabolome. Metabolites. 12(10):1006. doi: 10.3390/metabo12101006.

Benson DA, Karsch-Mizrachi I, Lipman DJ, Ostell J, Wheeler DL. 2004. GenBank: update. Nucleic Acids Res. 32(Database issue):D23–D26. doi: 10.1093/nar/gkh045.

Bohra V, Dafale NA, Purohit HJ. 2019. Understanding the alteration in rumen microbiome and CAZymes profile with diet and host through comparative metagenomic approach. Arch Microbiol. 201(10):1385–1397. doi: 10.1007/s00203-019-01706-z.

Cacciola NA, Salzano A, D'Onofrio N, Venneri T, Cicco P, Vinale F, Petillo O, Martano M, Maiolino P, Neglia G, et al. 2022. Buffalo milk whey activates necroptosis and apoptosis in a xenograft model of colorectal cancer. Int J Mol Sci. 23(15):8464. doi: 10.3390/ijms23158464.

Callahan BJ, McMurdie PJ, Rosen MJ, Han AW, Johnson AJA, Holmes SP. 2016. DADA2: high-resolution sample inference from Illumina amplicon data. Nat Methods. 13(7):581–583. doi: 10.1038/nmeth.3869.

Campanile G, De Filippo C, Di Palo R, Taccone W, Zicarelli L. 1998. Influence of dietary protein on urea levels in blood and milk of buffalo cows. Livest Prod Sci. 55(2):135–143. doi: 10.1016/S0301-6226(98)00123-7.

Cantarel BL, Coutinho PM, Rancurel C, Bernard T, Lombard V, Henrissat B. 2009. The carbohydrate-active enzymes database (CAZy): an expert resource for glycogenomics. Nucleic Acids Res. 37(Database issue):D233–D238. doi: 10.1093/nar/gkn663.

Chaumeil PA, Mussig AJ, Hugenholtz P, Parks DH. 2019. GTDB-Tk: a toolkit to classify genomes with the Genome Taxonomy Database. Bioinformatics. 36(6):1925–1927. doi: 10.1093/bioinformatics/btz848.

Coutinho PM, Henrissat B. 1999. Carbohydrate-active enzymes: an integrated database approach. In: Gilbert HJ, Davies G, Henrissat H, Svensson B, editors. Recent advances in carbohydrate bioengineering. Cambridge: The Royal Society of Chemistry; p. 3–12.

D'Onofrio N, Cacciola NA, Martino E, Borrelli F, Fiorino F, Lombardi A, Neglia G, Balestrieri ML, Campanile G. 2020. ROS-mediated apoptotic cell death of human colon cancer LoVo cells by milk δ-valerobetaine. Sci Rep. 10(1):8978. doi: 10.1038/s41598-020-65865-6.

D'Onofrio N, Mele L, Martino E, Salzano A, Restucci B, Cautela D, Tatullo M, Balestrieri ML, Campanile G. 2020. Synergistic effect of dietary betaines on SIRT1-mediated apoptosis in human oral squamous cell carcinoma Cal 27. Cancers. 12(9):2468. doi: 10.3390/cancers12092468.

Deb GK, Nahar TN, Duran PG, Presicce GA. 2016. Safe and sustainable traditional production: the water buffalo in Asia. Front Environ Sci. 4:38. doi: 10.3389/fenvs.2016.00038.

El-Zaiat HM, Abdalla AL. 2019. Potentials of patchouli (*Pogostemon cablin*) essential oil on ruminal methanogenesis, feed degradability, and enzyme activities in vitro. Environ Sci Pollut Res Int. 26(29):30220–30228. doi: 10.1007/s11356-019-06198-4.

Gharechahi J, Vahidi MF, Bahram M, Han J-L, Ding X-Z, Salekdeh GH. 2021. Metagenomic analysis reveals a dynamic microbiome with diversified adaptive functions to utilize high lignocellulosic forages in the cattle rumen. ISME J. 15(4):1108–1120. doi: 10.1038/s41396-020-00837-2.

Gulati A, Galvin N, Lewis E, Hennessy D, O'Donovan M, McManus JJ, Fenelon MA, Guinee TP. 2018. Outdoor grazing of dairy cows on pasture versus indoor feeding on total mixed ration: Effects on gross composition and mineral content of milk during lactation. Journal of Dairy Science. 101(3):2710–2723. doi: 10.3168/jds.2017-13338.

Hamid M, Siddiky M, Rahman M, Hossain K. 2017. Scopes and opportunities of buffalo farming in Bangladesh: a review. SAARC J Agric. 14(2):63–77. doi: 10.3329/sja.v14i2.31246.

Hartinger T, Pacífico C, Poier G, Terler G, Klevenhusen F, Zebeli Q. 2022. Shift of dietary carbohydrate source from milk to various solid feeds reshapes the rumen and fecal microbiome in calves. Sci Rep. 12(1):12383. doi: 10.1038/s41598-022-16052-2.

Hobson PN, Stewart CS. 1997. The rumen microbial ecosystem. 2nd ed. New York: Blackie Academic & Professional.

INRA. 2007. Alimentation des bovins, ovins et caprins – besoins des animaux – valeurs des aliments – tables INRA 2007. Versailles, France: Editions Quae; p. 307.

Iqbal MW, Zhang Q, Yang Y, Li L, Zou C, Huang C, Lin B. 2018. Comparative study of rumen fermentation and microbial community differences between water buffalo and Jersey cows under similar feeding conditions. J Appl Anim Res. 46(1):740–748. doi: 10.1080/09712119.2017.1394859.

Jones DR, Thomas D, Alger N, Ghavidel A, Inglis GD, Abbott DW. 2018. SACCHARIS: an automated pipeline to streamline discovery of carbohydrate active enzyme activities within polyspecific families and de novo sequence datasets. Biotechnol Biofuels. 11(1):27. doi: 10.1186/s13068-018-1027-x.

Lahti L, Shetty S. 2017. Tools for microbiome analysis in R Version. http://microbiome.github.com/microbiome.

Lee J, Cheng D, Bedford MT. 2004. Techniques in protein methylation. Methods Mol Biol. 284:195–208. doi: 10.1385/1-59259-816-1:195.

Li LP, Peng KL, Xue MY, Zhu SL, Liu JX, Sun HZ. 2022. An age effect of rumen microbiome in dairy buffaloes revealed by metagenomics. Microorganisms. 10(8):1491. doi: 10.3390/microorganisms10081491.

Lombard V, Golaconda Ramulu H, Drula E, Coutinho PM, Henrissat B. 2014. The carbohydrate-active enzymes database (CAZy) in 2013. Nucleic Acids Res. 42(Database issue):D490–D495. doi: 10.1093/nar/gkt1178.

Maia AR, Reyes-Ramírez R, Pizarro-Guajardo M, Saggese A, Castro-Córdova P, Isticato R, Ricca E, Paredes-Sabja D, Baccigalupi L. 2020. Induction of a specific humoral immune response by nasal delivery of $Bcla_2$ctd of *Clostridioides difficile*. Int J Mol Sci. 21(4):1277. doi: 10.3390/ijms21041277.

Malik PK, Trivedi S, Mohapatra A, Kolte AP, Sejian V, Bhatta R, Rahman H. 2021. Comparison of enteric methane yield and diversity of ruminal methanogens in cattle and buffaloes fed on the same diet. PLOS One. 16(8):e0256048. doi: 10.1371/journal.pone.0256048.

McMurdie PJ, Holmes S. 2013. phyloseq: an R package for reproducible interactive analysis and graphics of microbiome census data. PLOS One. 8(4):e61217. doi: 10.1371/journal.pone.0061217.

Mordenti AL, Giaretta E, Campidonico L, Parazza P, Formigoni A. 2021. A review regarding the use of molasses in animal nutrition. Animals 11:115. doi: 10.3390/ani11010115.

Neglia G, Calabrò S, Cotticelli A, Salzano A, Matera R, Vastolo A, D'Onofrio N, Giorgino A, Martino E, Balestrieri ML, et al. 2023. Use of former food products in dairy buffalo nutrition: in vitro and in vivo evaluation. J Anim Physiol Anim Nutr. 107(6):1347–1355. doi: 10.1111/jpn.13830.

Neglia G, Cotticelli A, Vassetti A, Matera R, Staropoli A, Vinale F, Salzano A, Campanile G. 2023. Buffalo milk and rumen fluid metabolome are significantly affected by green feed. Sci Rep. 13(1):1381. doi: 10.1038/s41598-022-25491-w.

Oksanen J, Blanchet FG, Friendly M, Kindt R, Legendre P, McGlinn D, Minchin PR, O'Hara RB, Simpson GL, Solymos P, et al. 2020. vegan: community ecology package. https://CRAN.R-project.org/package=vegan.

Oksanen J, Blanchet FG, Kindt R, Legendre P, Minchin PR, O'Hara RB, Simpson GL, Solymos P, Henry M, Stevens H, et al. 2012. vegan: community ecology package. R package version 20-7. http://CRAN.R-project.org/package=vegan.

Palakawong Na Ayudthaya S, van de Weijer AHP, van Gelder AH, Stams AJM, de Vos WM, Plugge CM. 2018. Organic acid production from potato starch waste fermentation by rumen microbial communities from Dutch and Thai dairy cows. Biotechnol Biofuels. 11(1):13. doi: 10.1186/s13068-018-1012-4.

Pantoja-Feliciano IG, Karl JP, Perisin M, Doherty LA, McClung HL, Armstrong NJ, Renberg R, Racicot K, Branck T, Arcidiacono S, et al. 2023. In vitro gut microbiome response to carbohydrate supplementation is acutely affected by a sudden change in diet. BMC Microbiol. 23(1):32. doi: 10.1186/s12866-023-02776-2.

Parada AE, Needham DM, Fuhrman JA. 2016. Every base matters: assessing small subunit rRNA primers for marine microbiomes with mock communities, time series and global field samples. Environ Microbiol. 18(5):1403–1414. doi: 10.1111/1462-2920.13023.

Paradiso R, Borriello G, Bolletti Censi S, Salzano A, Cimmino R, Galiero G, Fusco G, De Carlo E, Campanile G. 2021. Different non-structural carbohydrates/crude proteins (NCS/CP) ratios in diet shape the gastrointestinal microbiota of water buffalo. Vet Sci. 8(6):96. doi: 10.3390/vetsci8060096.

Patel DD, Patel AK, Parmar NR, Shah TM, Patel JB, Pandya PR, Joshi CG. 2014. Microbial and carbohydrate active enzyme profile of buffalo rumen metagenome and their alteration in response to variation in the diet. Gene. 545(1):88–94. doi: 10.1016/j.gene.2014.05.003.

Rabee AE, Younan BR, Kewan KZ, Sabra EA, Lamara M. 2022. Modulation of rumen bacterial community and feed utilization in camel and sheep using combined supplementation of live yeast and microalgae. Sci Rep. 12(1):12990. doi: 10.1038/s41598-022-16988-5.

Saggese A, De Luca Y, Baccigalupi L, Ricca E. 2022. An antimicrobial peptide specifically active against *Listeria monocytogenes* is secreted by *Bacillus pumilus* SF214. BMC Microbiol. 22(1):3. doi: 10.1186/s12866-021-02422-9.

Saggese A, Giglio R, D'Anzi N, Baccigalupi L, Ricca E. 2022. Comparative genomics and physiological characterization of two aerobic spore formers isolated from human ileal samples. Int J Mol Sci. 23(23):14946. doi: 10.3390/ijms232314946.

Saggese A, Isticato R, Cangiano G, Ricca E, Baccigalupi L. 2016. CotG-like modular proteins are common among spore-forming *Bacilli*. J Bacteriol. 198(10):1513–1520. doi: 10.1128/JB.00023-16.

Sallam S, Attia MFA, El-Din ANMN, El-Zarkouny SZ, Saber AM, El-Zaiat HM, Zeitoun MM. 2019. Involvement of quebracho tannins in diet alters productive and reproductive efficiency of postpartum buffalo cows. Anim Nutr. 5(1):80–86. doi: 10.1016/j.aninu.2018.08.003.

Salzano A, Di Meo MC, D'Onofrio N, Bifulco G, Cotticelli A, Licitra F, Iraci Fuintino A, Cascone G, Balestrieri ML, Varricchio E, et al. 2022. Breed and feeding system impact the bioactive anti-inflammatory properties of bovine milk. Int J Mol Sci. 23(19):11088. doi: 10.3390/ijms231911088.

Salzano A, Fioriniello S, D'Onofrio N, Balestrieri ML, Aiese Cigliano R, Neglia G, Della Ragione F, Campanile G. 2023. Transcriptomic profiles of the ruminal wall in Italian Mediterranean dairy buffaloes fed green forage. BMC Genomics. 24(1):133. doi: 10.1186/s12864-023-09215-6.

Salzano A, Licitra F, D'Onofrio N, Balestrieri ML, Limone A, Campanile G, D'Occhio MJ, Neglia G. 2019. Space allocation in intensive Mediterranean buffalo production influences the profile of functional biomolecules in milk and dairy products. J Dairy Sci. 102(9):7717–7722. doi: 10.3168/jds.2019-16656.

Salzano A, Neglia G, D'Onofrio N, Balestrieri ML, Limone A, Cotticelli A, Marrone R, Anastasio A, D'Occhio MJ, Campanile G. 2021. Green feed increases antioxidant and antineoplastic activity of buffalo milk: a globally significant livestock. Food Chem. 344:128669. doi: 10.1016/j.foodchem.2020.128669.

Servillo L, D'Onofrio N, Giovane A, Casale R, Cautela D, Castaldo D, Iannaccone F, Neglia G, Campanile G, Balestrieri ML. 2018. Ruminant meat and milk contain δ-valerobetaine, another precursor of trimethylamine N-oxide (TMAO) like γ-butyrobetaine. Food Chem. 260:193–199. doi: 10.1016/j.foodchem.2018.03.114.

Servillo L, D'Onofrio N, Neglia G, Casale R, Cautela D, Marrelli M, Limone A, Campanile G, Balestrieri ML. 2018. Carnitine precursors and short-chain acylcarnitines in water buffalo milk. J Agric Food Chem. 66(30):8142–8149. doi: 10.1021/acs.jafc.8b02963.

Servillo L, Giovane A, Cautela D, Castaldo D, Balestrieri ML, Pastore A. 2014. Where does Nε-trimethyllysine for the carnitine biosynthesis in mammals come from? PLOS One. 9(1):e84589. doi: 10.1371/journal.pone.0084589.t001.

Sheik CS, Reese BK, Twing KI, Sylvan JB, Grim SL, Schrenk MO, Sogin ML, Colwell FS. 2018. Identification and removal of contaminant sequences from ribosomal gene databases: lessons from the census of deep life. Front Microbiol. 9:840. doi: 10.3389/fmicb.2018.00840.

Sinha SK, Chaturvedi VB, Singh P, Chaudhary LC, Ghosh M, Shivani S. 2017. Effect of high and low roughage total mixed ration diets on rumen metabolites and enzymatic profiles in crossbred cattle and buffaloes. Vet World. 10(6):616–622. doi: 10.14202/vetworld.2017.616-622.

Sun H-Z, Peng K-L, Xue M-Y, Liu J-X. 2021. Metagenomics analysis revealed the distinctive ruminal microbiome and resistive profiles in dairy buffaloes. Anim Microb. 3(1):44. doi: 10.1186/s42523-021-00103-6.

Sützl L, Laurent CVFP, Abrera AT, Schütz G, Ludwig R, Haltrich D. 2018. Multiplicity of enzymatic functions in the CAZy AA3 family. Appl Microbiol Biotechnol. 102(6):2477–2492. doi: 10.1007/s00253-018-8784-0.

Varki A. 2017. Biological roles of glycans. Glycobiology. 27(1):3–49. doi: 10.1093/glycob/cww086.

Wang L, Zhang G, Xu H, Xin H, Zhang Y. 2019. Metagenomic analyses of microbial and carbohydrate-active enzymes in the rumen of holstein cows fed different forage-to-concentrate ratios. Front. Microbiol. 10:649. doi: 10.3389/fmicb.2019.00649.

Yi S, Dai D, Wu H, Chai S, Liu S, Meng Q, Zhou Z. 2022. Dietary concentrate-to-forage ratio affects rumen bacterial community composition and metabolome of yaks. Front Nutr. 9:927206. doi: 10.3389/fnut.2022.927206.

Yin Y, Mao X, Yang JC, Chen X, Mao F, Xu Y. 2012. dbCAN: a web resource for automated carbohydrate-active enzyme annotation. Nucleic Acids Res. 40(Web Server issue):W445–W451. doi: 10.1093/nar/gks479.

Yip VL, Withers SG. 2006. Breakdown of oligosaccharides by the process of elimination. Curr Opin Chem Biol. 10(2):147–155. doi: 10.1016/j.cbpa.2006.02.005.

Zeng H, Guo C, Sun D, Seddik HE, Mao S. 2019. The ruminal microbiome and metabolome alterations associated with diet-induced milk fat depression in dairy cows. Metabolites. 9(7):154. doi: 10.3390/metabo9070154.

Zhu C, Miller M, Marpaka S, Vaysberg P, Rühlemann MC, Wu G, Heinsen F-A, Tempel M, Zhao L, Lieb W, et al. 2018. Functional sequencing read annotation for high precision microbiome analysis. Nucleic Acids Res. 46(4):e23. doi: 10.1093/nar/gkx1209.

Earth Planet. Sci. Lett. 651 (2025) 119169

Contents lists available at ScienceDirect

Earth and Planetary Science Letters

journal homepage: www.elsevier.com/locate/epsl

Carbon, nitrogen, and noble gas isotopes reveal deep volatile signatures in thermal springs in the Central Volcanic Zone (CVZ) of the Andes

PH Barry [a,*], JM de Moor [b,c], MW Broadley [a,d], AM Seltzer [a], DV Bekaert [a,e], K Patil [a,f], CGE Bartels [a], ED Young [g], BE Longworth [a], B Barosa [a,h], A Bastianoni [h], D Bastoni [h], M Cascone [h], SJ Turner [i], RL Tyne [a,d], M Anderson [a], K Li [a], J Curtice [a], N Kumar [a], GL Jessen [j,k], JM Blamey [l], CJ Ramírez [m], A Chiodi [n], F Aguilera [o,p], S Layana [o], C González [o], M Aguilera [p,q], GPJ Masías Alvarez [r], B Marty [e], KG Lloyd [s], D Giovannelli [a,h,t,u,v,*]

[a] Woods Hole Oceanographic Institution, Woods Hole, MA, USA
[b] Observatorio Vulcanológico y Sismológico de Costa Rica (OVSICORI), Universidad Nacional, San Jose, Costa Rica
[c] University of New Mexico, Albuquerque, NM, USA
[d] Department of Earth and Environmental Science, University of Manchester, Manchester, UK
[e] Université de Lorraine, CNRS, CRPG, 54000 Nancy, France
[f] Brown University, Providence RI, USA
[g] University of California Los Angeles, Los Angeles CA, USA
[h] Department of Biology, University of Naples "Federico II", Naples, Italy
[i] University of Houston, Houston, TX, USA
[j] Instituto de Ciencias Marinas y Limnológicas, Universidad Austral de Chile, Valdivia, Chile
[k] Centro de Investigación Oceanográfica COPAS Coastal, Universidad de Concepción, Concepción, Chile
[l] Fundación Biociencia, Universidad de Santiago de Chile, Santiago, Chile
[m] Servicio Geológico Ambiental (SeGeoAm), Heredia, Costa Rica
[n] Instituto de Bio y Geociencias del NOA (IBIGEO, UNSa-CONICET), Salta, Argentina
[o] Millennium Institute on Volcanic Risk Research - Ckelar Volcanoes, Antofagasta, Chile
[p] Departamento de Ciencias Geológicas, Universidad Católica del Norte, Antofagasta, Chile
[q] Programa de Doctorado en Ciencias mención Geologia, Universidad Católica del Norte, Antofagasta, Chile
[r] Instituto Geológico Minero y Metalúrgico (INGEMMET), Arequipa, Perú
[s] University of Southern California, Los Angeles CA, USA
[t] Earth-Life Science Institute, Tokyo Institute of Technology, Tokyo, Japan
[u] National Research Council, Institute of Marine Biological Resources and Biotechnologies—CNR-IRBIM, Ancona, Italy
[v] Department of Marine and Coastal Science, Rutgers University, New Brunswick, NJ, USA

ARTICLE INFO

Editor: Dr R. Hickey-Vargas

Keywords:
Subduction zones
Noble gases
Nitrogen
Carbon
Radiocarbon
Volatiles

ABSTRACT

In subduction zones, thermal springs release deeply-sourced volatiles from Earth's mantle, crust, and/or subducted slab-derived material. The origin and apparent ages of these volatiles are important for understanding the deep volatile cycle, which in turn affects the distribution of microbial life in the subsurface. Here, we report carbon (^{13}C, ^{14}C), noble gas (He, Ne, Ar, Kr and Xe), and clumped nitrogen isotope data in gas and water samples from thermal springs within the Central Volcanic Zone (CVZ) of the Andean Convergent Margin (ACM). He isotopes show that CVZ gases are predominantly sourced from the crust (~77 %), with smaller mantle contributions (~23 %), consistent with previous studies from the CVZ. Thermal spring samples with non-atmospheric He-Ne characteristics have low ^{14}C activities, and are deeply derived (i.e., from the mantle and crust) and old (>22,000 years). To gain additional constraints on volatile sources, a gas sample from Pirquitas Argentina was analyzed using a new high-precision technique to reveal significant geogenic anomalies in argon ($^{40}Ar/^{36}Ar$ = 492), fissiogenic xenon (88 % crustal), and helium (84 % crustal) isotopes. Clumped N_2 isotopologue results also indicate that the N_2-rich Pirquitas sample is dominated by crustal and magmatic N_2, which was unambiguously released at high temperatures (indicated by Δ_{30} of ~0‰). When taken together, all carbon, noble gas and

* Corresponding authors.
E-mail address: pbarry@whoi.edu (P. Barry).

https://doi.org/10.1016/j.epsl.2024.119169
Received 5 September 2024; Received in revised form 13 November 2024; Accepted 7 December 2024
Available online 21 December 2024
0012-821X/© 2024 The Authors. Published by Elsevier B.V. This is an open access article under the CC BY license (http://creativecommons.org/licenses/by/4.0/).

clumped N_2 isotope data from CVZ thermal springs point toward a predominantly crustal source of volatile elements, which is consistent with the thick crust beneath the arc. We conclude that thermal springs with noble gas isotopic evidence for minimal air contributions are old, suggesting that any microbial communities entrained in them are also supported by deeply-derived and old organic carbon.

1. Introduction

In subduction zone settings, deeply-sourced volatile elements (e.g., carbon, noble gases, nitrogen) are primarily derived from Earth's mantle, crust, and/or subducted slab-derived material (e.g., Hilton et al., 1993; 2002; Barry et al., 2019). Mafic lavas and high temperature fumarolic gases are typically considered the best archives of deep volatile sources. However, eruptive materials are not always accessible and volcanic summits are often difficult (or impossible) to reach. Warm and hot "thermal springs" are generally easier to access, and He-C isotopes from such samples often reveal vital information about deeply-sourced volatiles as well as processes occurring deep within Earth's crust (e.g., Ray et al., 2009; Barry et al., 2022). For example, helium isotopes ($^3He/^4He$) and $^4He/^{20}Ne$ values have been used to show the extent of mixing with air components, and $CO_2/^3He$ and $\delta^{13}C$ have been extensively utilized to estimate mantle vs slab contributions to volcanic and thermal manifestations (Sano and Marty, 1995). Furthermore, interpreting noble gases alongside ^{14}C data can provide information about the duration of time that subsurface fluids have been isolated from surface reservoirs (e.g., radiocarbon-dead samples imply apparent ages >40,000 (Stuiver and Polach, 1977; Mook and Van Der Plicht, 1999)). Measurement of low ^{14}C activity provides confidence that samples are deeply-derived and have not extensively mixed with surface-equilibrated fluids. Using such a multipronged isotope approach allows for the deconvolution of deep and shallow source signals, which is critical for robust interpretations of volatile sources from thermal springs in subduction zone settings.

Understanding volatile sources is also important for geomicrobiology, as Earth's crust is home to a sizable microbial ecosystem (Kallmeyer et al., 2012; Magnabosco et al., 2018), sustained by deeply-sourced volatiles (Fullerton et al., 2021). In turn, the subsurface microbial biosphere plays a crucial role in regulating global biogeochemical cycles by influencing the subsurface redox state and can be used to determine the distribution of minerals, gases, and organic matter within the crust (D'Hondt et al., 2019). Despite their significance in surface geological processes and the cycling of volatiles throughout deep time, we know far less about subsurface microbial ecosystems than those at the surface. This knowledge gap primarily stems from the challenges of accessing deep subsurface environments. Typically, direct access to the subsurface microbiome is achieved through scientific drilling programs, which have provided unprecedented opportunities to explore subsurface fluids and their accompanying ecosystems. However, deep drilling projects are costly and infrequent (Orcutt and Edwards, 2014). An alternative, and potentially fruitful approach to studying the deep subsurface biosphere is through thermal features (i.e., springs) that are thought to be deeply-sourced (Summit and Baross 2001). Therefore, a

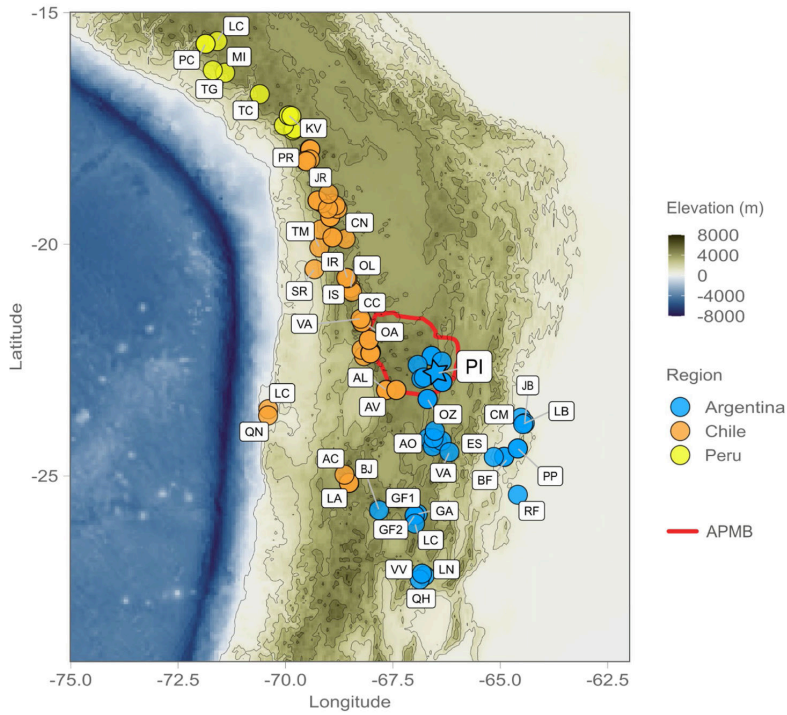

Fig. 1. Map showing sample localities throughout the CVZ. The two letter sample ID corresponds to the sample IDs in the tables. Topography is shown as elevation in meters above mean sea level (MAMSL). The location of the Altiplano Puna Magma Body (APMB) is shown as a red outline (Perkins et al., 2016). As in all figures, the star symbol is used to denote gas phase sample PI230308 from Piquiras, as this sample was targeted for high precision Ar, Kr, Xe and clumped N_2 measurements.

deeper look at the noble gas, carbon and nitrogen isotopic systems is crucial for determining whether such thermal springs can be used to passively sample subsurface microbial communities, massively expanding our ability to sample such ecosystems beyond the small number of locations accessible by drilling.

Here, we present new $\delta^{13}C$, ^{14}C, noble gas (He, Ne, Ar, Kr, Xe), $\delta^{15}N$ and clumped N_2 isotope data from natural springs in the Central Volcanic Zone (CVZ) of the Andean Convergent Margin (ACM) (Fig. 1; Tables 1–5). These data are used to determine 1) the time since fluids were exposed to surface reservoirs, and 2) the origin (mantle and crustal) of non-surface derived volatiles. In this way, we can investigate the interplay between subsurface and surface processes, providing insights into large scale geological processes such as the deep volatile recycling budget. Furthermore, these data will provide important context for future subsurface biological studies that aim to assess microbial community structure and function of microbial populations.

2. Geological setting

The ACM consists of more than 200 Quaternary volcanoes and twelve large caldera/ignimbrite systems formed by the subduction of the Nazca Plate beneath South America (e.g., Stern, 2004). Volcanism is distributed across four distinct segments: the Northern Volcanic Zone (12°N-5°S), Central Volcanic Zone (5–33°S), Southern Volcanic Zone (33–49°S), and Austral Volcanic Zone (49–56°S) (Stern, 2004). The young (32 Ma) Nazca plate subducts beneath the CVZ at a shallow angle (27°) with a convergence rate of 74 km/Ma, and carries a thinner sediment layer compared to the Southern margin (Syracuse and Abers, 2006; Clift, 2017; Lages et al., 2021).

The CVZ is home to 62 (potentially) active volcanoes (de Silva and Francis, 1991; Aguilera et al., 2022), and is built on the thickest crust (60–70 km) of any volcanic arc on Earth (McGlashan et al., 2008; Profeta et al., 2015). Volcanic materials consist mostly of andesites and dacites. Hydrothermal activity occurs throughout the CVZ, observed in geothermal fields and thermal springs. Beginning at 38 Ma, the region from 14 to 20°S experienced a flat slab subduction event, leading to a cessation of magmatism at the prior arc front location and an eastward migration of volcanism (Ramos and Folguera, 2008). The region of flat subduction (and cessation of volcanism) then progressed southward towards 20–24°S from 18 to 12 Ma, which may have led to hydration or alteration of the lower crustal region (Newell et al., 2015).

Around 11 Ma, large ignimbrite complexes were formed over the Altiplano-Puna Volcanic Complex (APVC) within the CVZ, many of which retain a well-mixed crustal-mantle signature, indicating large amounts of mixing deep within the crust (Kay et al., 2009; de Silva et al., 2006; Salisbury, 2011; de Silva and Kay, 2018). Notably, the Altiplano-Puna Magma Body (APMB) is located approximately 10–20 km beneath the APVC (Fig. 1). High resolution tomography shows that this magma body has a diameter of ~200 km and a total volume of ~500,000 km^3 (e.g., Ward et al., 2014) making it the largest known active magma body on Earth (Perkins et al., 2016). However, the CVZ crust over the APMB remains thickened (Perkins et al., 2016). The complex interplay between the thick crust and the APMB likely impacts the geochemical signatures of emitted volatiles, however this remains poorly understood.

3. Results and discussion

He and C isotopes are often considered to be the ‘gold standard’ of tracers for deep volcanically derived source features, because geogenic He and C isotopic signals are often very clearly identifiable. However, detecting meaningful geothermal signals from isotopes of the heavier noble gases (Ne, Ar, Kr and Xe) and N isotopes is more challenging for two reasons. First, there is a large discrepancy between these two groups of elements (i.e., He/C vs Ne/Ar/Kr/Xe/N) in terms of mass balance considerations in gas and water systems. Namely, the amount of He and C emanating from deep reservoirs far outweighs surface (i.e., atmospheric) inputs of He and C in volcanically active geothermal systems. In contrast, Ne, Ar, Kr, Xe and N are found in trace amounts in the mantle and crust, relative to their atmospheric abundances (e.g., Butler et al., 1963). Second, mantle and crustal isotope endmembers for Ne, Kr, Xe, and N closely resemble the atmospheric composition, unlike He and C, therefore making it difficult to resolve deep geothermal anomalies from atmospheric signals. As a result, heavy noble gases have seldom been reported or exploited in volcanic settings, whereas He-C systematics have been used extensively (e.g., Hilton et al., 1993; Ray et al., 2009; Barry et al., 2013; 2019; 2022; Bekaert et al., 2021).

Below we discuss new He-C results alongside radiocarbon activity data, which clearly show that these tracers are robust indicators of old (i.e., >22,000 year) and deep (mantle and crustal) sources. We also present Ne, Ar and Xe data from a subset of samples, along with high precision Xe and clumped N_2 data for a single sample. All noble gas and stable isotope results are detailed in Tables 2–5. The single “case-study” sample (i.e., Pirquitas; PI230308) has a large Ar isotope anomaly ($^{40}Ar/^{36}Ar > 463$), which is significantly higher than air, suggesting that Pirquitas retains a deep signature despite overwhelming atmospheric heavy noble gas contents in the system. Using a recently developed high precision technique, enabled by dynamic mass spectrometry (e.g., Seltzer and Bekaert, 2022), we show that high-precision Xe isotopes can be used to resolve small, yet significant, deep geogenic signals that provide important information about the extent of mantle and crust feeding Pirquitas. Furthermore, the Pirquitas sample was analyzed for clumped N_2 isotopes, which confirms that atmosphere-derived N_2 is completely overprinted by N_2 of a high-temperature origin, as is evidenced by high N_2/Ar and non-atmospheric Δ_{30} values (see Section 3.6). This finding is intriguing because it unambiguously indicates crust-mantle interaction occurring at high temperatures in the subsurface.

3.1. Data integrity

In Fig. 2 we plot $^3He/^4He$ vs $^4He/^{20}Ne$ for all gas and water samples, along with “air”. Mixing lines are also shown to indicate mixing between “air” (or air saturated water) and deep mantle and crustal endmembers. We show that the vast majority of samples have $^4He/^{20}Ne$ values >2, strongly suggesting a deep (crust + mantle) He source. Data are consistent with those previously published from the CVZ (e.g., Lages et al., 2021; Barry et al., 2022 and references within). Due to the deep source of He, it has long been asserted that C is also deeply derived, as it is the major volatile (along with water) in volcanic gases and the likely carrier of noble gases and other trace volatile elements in volcanically influenced thermal spring samples. For CVZ gas and water samples, this assertion is broadly consistent with $CO_2/^3He$ and ^{13}C isotopes, which also suggest deep (i.e., mantle or crustal derived C sources). For example, in Fig. 3 the majority of samples plot inside a three component mixing envelope defined by mantle and slab derived (sediment and limestone) endmembers (Sano and Marty, 1995). For reference, “air” has a $\delta^{13}C$ of ~−8‰ vs. PDVB and a $CO_2/^3He$ of $\sim 6 \times 10^7$, which plots distinctly below the envelope defined by mantle and slab mixing.

3.2. Bimodal ^{14}C signals: deep and “dead” vs. shallow and “active”

We also report radiocarbon (^{14}C) activities of dissolved inorganic carbon (DIC) with fraction modern ($F^{14}C$) between 0 (i.e., below the detection limit) and 0.84, corresponding to apparent groundwater residence times of between >41,100 and 1380 years in water samples from the CVZ. These data are presented along with noble gases and $\delta^{13}C$ of DIC and gaseous $\delta^{13}C$ of CO_2 from thermal springs in the CVZ. We show a striking relationship between radiocarbon activities (F Modern DIC), $^3He/^4He$ (Fig. 4a) and $^4He/^{20}Ne$ (Fig. 4b). Every sample with non-atmospheric He-Ne signature (i.e., $^3He/^4He > 1.8\ R_A$ and $^4He/^{20}Ne > 2$) is also essentially radiocarbon dead (i.e., $F^{14}C < 0.07$). This implies that

Table 1
Meta data for all localities sampled, including latitude, longitude, elevation, temperature and pH of the thermal springs. Temperatures are given in Celsius and elevations are in meters above sea level. Measurements were made in the field.

Region	Name	Site ID	Lat	Long	Elev	T (°C)	pH
Chile	La Chimba	LC220316	−23.5629	−70.40019	13	40.3	7.34
Chile	Quebrada Negra	QN220317	−23.69785	−70.40637	94	26.4	7.11
Chile	El Chitór	CH220319	−22.41729	−68.1726	3754	21.7	5.77
Chile	Rio Salado	RS220319	−22.27811	−68.22771	3084	22.24	6.01
Chile	Alitar fumaroles	AL220320	−23.14591	−67.65525	4747	82.5	NA
Chile	Alitar fumaroles	AL230302	−23.14588	67.65518	4740	85.1	NA
Chile	Alitar verde	AV220320	−23.14915	−67.65849	4705	68.2	5.95
Chile	Laguna Negra	LN220321	−23.14677	−67.41922	4227	52.3	6.58
Chile	El Tatio_Bubbling pool	ET220322	−22.33071	−68.01182	4278	86.8	6.31
Chile	El Tatio_River	ET220322R	−22.34071	−68.02614	4237	NA	NA
Chile	Geyser Blanco	GB220322	−22.35696	−68.02258	4287	83.1	6.58
Chile	Cabana	CA220323	−22.06502	−68.05921	4061	25	7.36
Chile	Olca Volcano_Fum1	OL220324	−20.9412	−68.48334	5312	147.1	NA
Chile	Vega Churchilla	CC220324	−21.02515	−68.45084	4266	20.3	7.85
Chile	Carcote	CR220324	−22.06499	−68.05932	4125	42.2	7.92
Chile	Ojo de Ascotán vertiente 11	OA220325	−21.6879	−68.21487	3736	27.5	6.96
Chile	Vertiente 10 Ascotán	VA220325	−21.60952	−68.25012	3795	22.2	7.15
Chile	Termales Mamiña	TM220326	−20.07042	−69.21176	2804	53.9	8.84
Chile	Termales Cancosa	CN220327	−19.88536	−68.6013	3906	37.2	6.23
Chile	Termales Lirima	LR220327	−19.85184	−68.90653	3999	68.7	6.28
Chile	Irruputuncu fumaroles	IR220328	−20.73451	−68.55741	4977	408	1.24
Chile	Irruputuncu acid spring	IS220328	−20.72589	−68.58618	4042	38.41	2.38
Chile	Santa Rosita	SR220328	−20.54046	−69.32597	1322	34.8	8.26
Chile	Termales Chusmiza	CZ220329	−19.68348	−69.17722	3423	41.7	8.2
Chile	Puchuldiza outflow	PZ220330	−19.40849	−68.95853	4205	74	7.17
Chile	Puchuldiza outflow_pool2	PZ220330	−19.40849	−68.95853	4205	NA	NA
Chile	Puchuldiza fumarole	PD220330	−19.41281	−68.95793	4222	85.9	7.1
Chile	Puchuldiza boiling pool	PD220330	−19.41281	−68.95793	4222	85.1	8.02
Chile	Parajaya	PJ220330	−19.12084	−68.90981	4242	29.6	6.74
Chile	Termales Enquelga	EQ220330	−19.23506	−68.79199	3901	30.1	6.02
Chile	Isluga volcano	IV220331	−19.16223	−68.83487	5163	97	1.29
Chile	Termal Tana	TT220331	−19.11342	−69.13836	4067	66.6	6.31
Chile	Laguna Amarilla	LA220331	−19.05879	−69.25277	3728	35.5	6.77
Chile	Laguna Roja	LR220331	−19.85176	−68.90614	4079	24.3	5.5
Chile	Laguna Verde	LV220331	−19.05701	−69.2534	3731	49.1	5.6
Chile	Laguna Parinacota	LP220401	−19.23299	−69.0104	4157	24.9	7.45
Chile	Baño Polio Quieres (?) Salar Surire	PQ220401	−18.91319	−68.99922	4283	63.4	5.75
Chile	Colpitas	CP220402	−17.95005	−69.43621	4151	16	3.81
Chile	Colpitas East	CE220402	−17.95554	−69.42357	4141	53.5	6.19
Chile	Las Cuevas	CU220402	−18.16997	−69.43094	4473	33.7	6.44
Chile	Putre	PR220403	−18.19791	−69.53851	3785	35.8	6.33
Chile	Termales Jurasi	JR220403	−18.2102	−69.51053	4050	65.4	6.9
Chile	Lastarria volcano_Fum1	LA220409	−25.15544	−68.51953	5124	230	1.22
Chile	Lastarria volcano_Fum2	LA220409	−25.1527	−68.52339	4966	310	1.12
Chile	Salar Aguas Calientes	AC220410	−24.97643	−68.62558	3675	24.4	6.85
Peru	La Calera	LCL221109	−15.61489	−71.58689	3620	68.2	6.3
Peru	Pinchollo_boiling pool	PC221110	−15.67377	−71.86186	4363	85	6.05
Peru	Pinchollo_fumarole	PC221110C	−15.67377	−71.86186	4363	86.6	6.25
Peru	Ticsani	TC221112(1)C	−16.75915	−70.60103	5315	80.8	4.3
Peru	Misti	MI221116C	−16.2976	−71.40578	5585	255	1.58
Peru	Llavemoco	LL221118C	−17.54163	−69.82695	4862	86	5.84
Peru	Casiri	CA221118	−17.50861	−69.80222	4616	47.8	6.36
Peru	Putina	PT221119	−17.43421	−70.03834	3314	50.3	7.51
Peru	Kovire	KV221120	−17.21906	−69.92208	4381	86.4	7.65
Peru	Kovire	KV221120C	−17.21906	−69.92208	4381	86.4	7.3
Peru	Calachaca	CL221120	−17.23272	−69.8628	4298	45.6	6.59
Peru	El Tigre/Yura	TG221122	−16.24527	−71.69355	2519	32.6	6.13
Argentina	Banos Fleming	BF230316	−24.59134	−64.91012	595	29.15	7.66
Argentina	Botijuela	BJ190227	−25.74303	−67.82325	3524	40	6.44
Argentina	Caimancito	CM230315	−23.74437	−64.51974	385	56.6	8.26
Argentina	Coranzuli	CZ230307	−22.97502	−66.3491	4148	33.53	7.48
Argentina	El Sauce	ES230304	−24.59445	−65.15059	838	35.18	6.8
Argentina	Galán Aguas Calientes	GA190226	−25.82542	−66.9225	4482	67	6.7
Argentina	Galán Fumaroles	GF190226_1	−25.85819	−66.9927	4644	80	7.75
Argentina	Galán Fumaroles	GF190226_2	−25.85824	−66.99282	4651	80	3.21
Argentina	Incachule	IN190223	−24.28213	−66.46676	4470	46.9	6.52
Argentina	Well YPF JB5	JB230315	−23.86217	−64.43037	560	71.5	7.2
Argentina	Laguna La Brea	LB230315	−23.88503	−64.46661	635	59.4	6.32
Argentina	Galán La Colcha	LC190226	−26.03291	−66.98609	4728	84	6.94
Argentina	Lagunilla del Farallon	LF230308	−22.41294	−66.59731	3890	53.7	6.51
Argentina	Los Nacimientos	LN230313	−27.15565	−66.75972	2097	38.52	6.55
Argentina	Laguna de Vilama	LV230309	−22.60727	−66.92273	4489	30.2	5.96
Argentina	Orosmayo	OY230308	−22.53242	−66.36244	3996	25.39	8.04

(*continued on next page*)

Table 1 (*continued*)

Region	Name	Site ID	Lat	Long	Elev	T (°C)	pH
Argentina	Olaruz	OZ230305	−23.34416	−66.69222	3939	14.4	6.2
Argentina	Pastos Grandes	PG290225	−24.36459	−66.57113	4305	44.9	8.74
Argentina	Pirquitas	PI230308	−22.73454	−66.46609	4105	23.35	6.34
Argentina	Pompeya	PM190223	−24.24669	−66.36272	3889	50.3	6.53
Argentina	El Galpón	PP190301	−24.40986	−64.59146	493	54.3	8.47
Argentina	Pairique	PQ230306	−22.9028	−66.8383	4292	43.35	7.16
Argentina	Quebrada de Hualfil	QH230313	−27.24069	−66.87535	1847	37.18	8.94
Argentina	Rosario de Coyaguima	RC1230306	−22.87706	−66.77885	4328	55.6	6.61
Argentina	Rosario de la Frontera	RF190301	−25.40986	−64.59134	425	82	8.23
Argentina	Tocomar	TM190224	−24.18778	−66.55451	4333	69.2	7.13
Argentina	Termas de Tuzgle	TZ230310	−24.02815	−66.52361	4213	55.6	6.27
Argentina	Vega Acida	VA230311	−24.48921	−66.18411	3918	15.58	3.95
Argentina	Villa Vil	VV190228	−27.11286	−66.82224	2143	38.2	9.09

any sample with non-atmospheric He-Ne characteristics is derived from a deep carbon pool that has not equilibrated with air for at least ~22,000 years. However, apparent ages in hydrothermal fluids are fundamentally uncertain and it is important to point out that low radiocarbon activities may reflect the addition of dead magmatic C and may not truly reflect time elapsed since exposure to the atmosphere. This is because radiocarbon activities are not solely representative of the atmospheric value, but instead a complex function of the mass ratio of atmospheric C and alkalinity-related carbonate. For this reason, apparent ages should be considered maximum estimates, because if the carbon pool is in fact dominated by deep, dead mantle carbon, waters could be younger than they appear. Nonetheless, these findings indicate that volatiles in these thermal spring samples are unequivocally old and deeply derived. Notably, the bimodal distribution between radiocarbon-active and old water samples is more readily apparent when plotted vs. He-Ne systematics than it is versus other (first order) indicators of depth, such as temperature (Fig. 4c) and pH (Fig. 4d). This indicates that He isotope and $^{4}He/^{20}Ne$ signatures are more faithful proxies for sample age and source/depth than temperature and pH, which can be more easily influenced by shallower factors, such as flow rates or local lithology.

In order to contextualize the importance of these findings, we note that in previous He-C studies in volcanic regions (e.g., Barry et al., 2019) the origin of carbon was essential to the broader interpretation of how volatiles move through subduction zone systems. For instance, isotopically light $\delta^{13}C$ of DIC could either be interpreted as being surface-derived (i.e., decay of organic material in the vicinity of the springs) or resulting from isotopic fractionation at depth. This has important implications for reconstructing the history of volatile cycling between surface reservoirs (i.e., atmosphere, ocean, crust) and for identifying potentially important carbon sinks in Earth's crust. There are also important ramifications for microbiological interpretations, as Earth's crust is home to a sizeable microbial ecosystem (Kallmeyer et al., 2012; Magnabosco et al., 2018) much of which may be sustained by deeply-derived volatile elements such as H, C and S (Fullerton et al., 2021) used by microorganisms as energy sources (Hay Mele et al., 2023). Determining the source (deep vs shallow, magmatic vs crustal, old vs young/surface derived) of the volatiles feeding the microorganisms in the deep subsurface is thus critically important, because the deep microbial biosphere plays a potentially important role in regulating global biogeochemical cycles (Giovannelli, 2023) by influencing the redox state of the crust and determining the redistribution of minerals, gases, and organic matter transformations (D'Hondt et al., 2019). These results support the idea that thermal springs with noble gas isotopic evidence for minimal air contributions can be considered windows into the subsurface (Giovannelli et al., 2022), and are indeed deeply-derived. As a result, microbiological communities that are flushed to the surface at thermal springs can be sampled to investigate the interactions of the community with geothermal waters that are replete with ancient carbon derived from deep within the crust and/or mantle. Noble gas systematics are thus an attractive way to determine which natural springs can be used as passive sampling ports for subsurface ecosystems, without requiring deep drilling of boreholes to access them (Giovannelli et al., 2022).

These new radiocarbon activity findings thus confirm that carbon in samples with deeply-derived (i.e., non-atmospheric) He-Ne, is deeply sourced, confirming biological interpretations of deep signals based off of He isotopes (Fullerton et al., 2021; Rogers et al., 2023; Basili et al. 2024). Traditionally, high-temperature fluids were considered most representative of the deep subsurface. Our findings open the possibility of also considering lower-temperature fluids to study deep volatiles, greatly expanding the locations that can be sampled.

3.3. Volatile sources

3.3.1. Helium

Helium isotope results ($^{3}He/^{4}He$ of sample = R) are reported relative to air (R_A), corrected for the occurrence of atmospheric He (to R_C/R_A) and blank contributions, which are consistently less than 5 %. The $^{4}He/^{20}Ne$ value (Tables 2 and 3) is used to apply an atmospheric correction to all samples, assuming ^{20}Ne is derived from air ($^{4}He/^{20}Ne$ = 0.32) or fresh air saturated water ($^{4}He/^{20}Ne$ = 0.26 at 15 °C; Hilton, 1996; Ozima and Podosek, 2002). Uncorrected helium isotopes range from 0.4 to 5.6 R_A in gas samples and 0.1 to 3.5 R_A in water samples. When the $^{3}He/^{4}He$ is corrected (using methods of Hilton, 1996), the highest $^{3}He/^{4}He$ values found are 5.8 R_A in gas samples and 4.4 R_A in water samples, which is consistent with previous findings (e.g., Lages et al., 2021; Barry et al., 2022). Barry et al. (2022) showed that $^{3}He/^{4}He$ values in thermal springs range from 0.1 R_A to 2.6 R_A, and are slightly lower (more radiogenic) than recent reports of He isotopes from waters and gases within the region (which range from 0.1 R_A to 5.5 R_A; e.g., Lages et al., 2021). These findings suggest overprinting by crustal signatures throughout the CVZ (Fig. 2), which is broadly consistent with the thick crust found throughout the CVZ. Notably, however, high temperature CVZ volcanic gas samples have $^{3}He/^{4}He$ values (Barry et al., 2022; de Moor et al., In Review) approaching the arc endmember value of ~5.4 ± 1.9 R_A (Hilton et al., 2002).

Helium can be derived from the mantle, crust, and/or atmosphere, and the relative contributions of these different sources will ultimately control the $^{3}He/^{4}He$ of a given sample. The average air corrected He isotopes value reported here is 1.9 R_A. Using the methods of Barry et al. (2013) we calculate that the CVZ is characterized by 23 % mantle He and 77 % crustal He on average, which is nearly identical to previous findings from the area (Barry et al., 2022), despite the samples being collected at different locations. The extent of mixing between crustal and mantle components is considered to be controlled by the thickness of the crust (e.g., Barry et al., 2022). We note that in the CVZ, where the crust is ~70 km thick on average, the mean $^{3}He/^{4}He$ is lower (R_C/R_A = 1.9 R_A) than in other parts of the ACM as well as in other subduction zones globally (Hilton et al., 2002). As hydrothermal fluids migrate through thicker sections of crust in the overriding plate, they incorporate radiogenic ^{4}He due to interaction with the U- and Th-rich country

Table 2
Noble gas isotope and carbon isotope data for gas phase samples. Uncertainties are less than 5 % for all isotopes, concentrations, and elemental ratio reported. Noble gas data were acquired by static mass spectrometer in the Barry Lab at WHOI. Carbon (13C) measurements were done at OVSICORI.

Region	Site ID	$^{3}He/^{4}He$ R/RA	$^{4}He/^{20}Ne$	$^{3}He/^{4}He$ RC/RA	$CO_2/^{3}He$	$^{20}Ne/^{22}Ne$	$^{21}Ne/^{22}Ne$	$^{40}Ar/^{36}Ar$	^{4}He (cm3STP/cm3)	^{20}Ne (cm3STP/cm3)	^{36}Ar (cm3STP/cm3)	CO_2	He	$\delta^{13}C$ CO_2 vs PDB
Chile	CH220319	1.03	0.33	1.89	8.77E+10				4.38E-06	1.34E-05		94.7 %	0.00076 %	−6.6
Chile	RS220319	0.99	0.29	1.13	1.57E+10				4.33E-06	1.47E-05		93.8 %	0.00434 %	−5.5
Chile	AL220320	3.16	11,498.43	3.16	2.14E+10				2.92E-06	2.54E-10		0.4 %	0.00000 %	−10.6
Chile	AV220320	3.28	65.56	3.29	6.04E+10				7.99E-07	1.22E-08		99.4 %	0.00036 %	−8.7
Chile	LN220321	1.83	45.10	1.84	2.82E+09				2.86E-04	6.33E-06		72.1 %	0.01005 %	−12.2
Chile	OL220324	1.71	12.63	1.72	3.00E+10				2.33E-06	1.84E-07		0.7 %	0.00001 %	−4.8
Chile	OA220325	0.99	1.45	0.98	7.33E+09				8.31E-06	5.71E-06		17.5 %	0.00174 %	−9.3
Chile	CN220327	1.03	0.29	0.68	6.65E+11				4.07E-06	1.38E-05		99.8 %	0.00011 %	−6.9
Chile	LR220327	1.05	0.29	0.53	9.31E+8				4.25E-06	1.48E-05		48.4 %	0.03563 %	−3.6
Chile	IR220328	5.59	7.56	5.79	2.99E+10				6.72E-07	8.89E-08		3.1 %	0.00001 %	−5.4
Chile	PZ220330	1.91	12.97	1.93	2.05E+10				1.13E-05	8.69E-07		95.3 %	0.00175 %	−4.9
Chile	PD220330	1.66	1653.06	1.66					6.16E-07	3.73E-10				
Chile	IV220331	4.46	35.75	4.49	6.01E+10				1.36E-06	3.79E-08		2.5 %	0.00001 %	−6.2
Chile	LA220331	2.29	101.52	2.29					5.24E-05	5.16E-07				
Chile	LV220331	2.20	29.93	2.21	1.93E+10				1.23E-05	4.10E-07		96.3 %	0.00163 %	
Chile	CE220402	1.71	41.93	1.72					6.14E-08	1.46E-09		99.9 %		−7.0
Chile	CU220402	1.22	25.35	1.22					8.08E-05	3.19E-06				
Chile	LA220409	5.35	4172.62	5.35	7.46E+9				3.46E-06	8.30E-10		4.1 %	0.00007 %	−3.3
Peru	LCL221109	1.53	786.30	1.53	5.75E+09	9.65	0.03	311.63	1.18E-05	1.50E-08	9.79E-08	96.8 %	0.00792 %	−8.5
Peru	PC221110	1.35	567.18	1.35	2.29E+09	9.88	0.03	325.50	4.48E-04	7.89E-07	3.92E-06	0.9 %	0.00020 %	−6.3
Peru	PC221110C	1.36	234.85	1.36	1.37E+10	10.03	0.03	316.14	7.42E-06	3.16E-08	7.03E-08	10.5 %	0.00041 %	
Peru	TC221112(1)C	3.31	2.03	3.75	1.96E+10	10.27	0.03	292.51	1.05E-05	5.17E-06	8.20E-06	7.9 %	0.00009 %	−6.8
Peru	MI221116C	5.23	12.67	5.32	1.39E+10	10.47	0.03	292.15	3.87E-05	3.05E-06	1.73E-06	2.2 %	0.00002 %	−4.9
Peru	LL221118C	3.77	170.32	3.77	1.47E+10	9.86	0.03	302.55	1.09E-04	6.42E-07	1.69E-06	1.2 %	0.00002 %	−6.4
Peru	CA221118	3.64	2.11			9.98	0.03	291.84	4.76E-09	2.25E-09	1.43E-09	99.8 %		−7.4
Peru	KV221120	2.66	1.13			10.12	0.03	291.99	5.67E-06	5.00E-06	1.38E-05			
Peru	TG221122	0.66	35.67	0.65	5.20E+10	9.90	0.03	334.75	2.43E-07	6.82E-09	1.98E-08	89.5 %	0.00188 %	−6.9
Argentina	BF230316	0.80	0.41	0.13		9.65	0.0289	298.0	6.68E-07	1.62E-06	3.37E-06			
Argentina	CZ230307	1.89	138.47	1.90		9.82	0.0291	308.2	7.94E-04	5.73E-06	3.51E-05			−16.0
Argentina	ES230304	0.32	11,323.93	0.32	1.73E+07	9.89	0.0348	351.6	1.03E-03	9.13E-08	2.54E-06	11.2 %	1.44207 %	−12.2
Argentina	JB230315	0.45	55.17	0.45		9.79	0.0286	301.5	6.88E-05	1.25E-06	5.66E-06			
Argentina	LB230315	0.34	2886.76	0.34		9.69	0.0281	348.0	1.42E-03	4.93E-07	1.23E-05			
Argentina	LF230308	1.05	492.39	1.05	6.43E+08	9.88	0.0285	305.3	4.92E-05	1.00E-07	9.85E-07	31.8 %	0.03372 %	−8.6
Argentina	LN230313													
Argentina	LV230307	2.71	243.75	2.71		9.70	0.0286	305.5	1.82E-05	7.46E-08	9.31E-07			
Argentina	LV230309											86.2 %	0.04314 %	−11.1
Argentina	OY230308													
Argentina	OZ230305	1.03	66.82	1.03		10.01	0.0290	301.6	3.54E-05	5.29E-07	2.40E-06			
Argentina	PG230225													
Argentina	PI230308	1.32	2560.73	1.32	2.73E+08	9.38	0.0283	492.5	1.37E-05	5.34E-09	5.41E-08	18.5 %	0.03690 %	−11.9
Argentina	PQ230306	1.58	37.27	1.59	1.81E+07	9.68	0.0290	306.2	3.18E-04	8.54E-06	3.25E-05	0.8 %	0.01982 %	−13.4
Argentina	QH230313													
Argentina	RC1230306	2.77	17.31	2.80		10.01	0.0293	292.0	8.44E-08	4.87E-09	3.83E-08	99.1 %		−10.7
Argentina	TZ230310	5.19	30.46	5.23	2.76E+10	10.03	0.0302	295.5	1.55E-06	5.10E-08	4.59E-07	99.1 %	0.00050 %	−6.8
Argentina	VA230311													

Table 3
Noble gas isotope and carbon isotope data for water phase samples. Uncertainties are less than 5 % for all isotopes, concentrations, and elemental ratio reported. Noble gas data were acquired by static mass spectrometer in the Barry Lab at WHOI. Carbon (13C) measurements were done at OVSICORI. Radiocarbon (14C) measurements were made at NOSAMS at WHOI.

Region	Site ID	$^3He/^4He$	$^4He/^{20}Ne$	$^3He/^4He$	$CO_2/^3He$	$^{20}Ne/^{22}Ne$	$^{21}Ne/^{22}Ne$	$^{40}Ar/^{36}Ar$	^4He	^{20}Ne	^{36}Ar	DIC	$\delta^{13}C$ DIC	^{14}C DIC	^{14}C DIC	^{14}C DIC	^{14}C DIC
		R/R_A		R_C/R_A					$cm^3STP/g\ H_2O$	$cm^3STP/g\ H_2O$	$cm^3STP/g\ H_2O$	mol/l	vs PDB	F Modern	Fm Err	Age	Age Err
Chile	LC220316	1.06	0.27	2.10	3.49E+11				5.39E-08	2.00E-07		0.0012	−7.88	0.5325	0.0065	5060	100
Chile	QN220317	1.79	0.28	9.81	6.72E+11				2.82E-08	1.01E-07		0.0021	−8.63	0.8424	0.0092	1380	90
Chile	LN220321	1.57	12.49	1.58	#######				7.18E-07	5.75E-08		0.0013	−5.05	0.0330	0.0067	27,400	1600
Chile	GB220322	1.55	0.83	1.81	1.98E+12				1.93E-08	2.32E-08		0.0037	−3.53	0.0011	0.0059	> 39,800	43,500
Chile	CA220323	1.25	0.31	2.30	4.18E+11				3.46E-08	1.10E-07		0.0011	−1.5	0.1795	0.0059	13,800	270
Chile	CC220324	1.18	0.22	0.02	3.21E+11				2.64E-08	1.23E-07		0.0006		0.3661	0.0093	8070	200
Chile	CR220324	1.20	0.45	1.47	3.34E+11				3.05E-08	6.81E-08		0.0008		0.3658	0.0072	8080	160
Chile	OA220325	1.10	0.63	1.18	#######				9.38E-08	1.50E-07		0.0017		0.0623	0.0059	22,300	760
Chile	VA220325	1.04	1.19	1.05	2.15E+11				1.09E-07	9.14E-08		0.0015	0.49	0.0631	0.0059	22,200	750
Chile	TM220326	0.08	23.34	0.06	#######				2.63E-06	1.13E-07		0.0003	−10.88				
Chile	IS220328	2.01	0.41	3.70					3.07E-08	7.55E-08		0.0000		0.0005	0.0061	> 40,400	#######
Chile	PZ220330	1.74	6.03	1.77	6.32E+11				3.07E-08	5.08E-09		0.0021	−0.92	−0.0120	0.0060	> 41,100	
Chile	PJ220330	2.26	0.43	4.35	1.66E+11				6.60E-08	1.53E-07		0.0015	−5.46	0.0615	0.0060	22,400	780
Chile	EQ220330	2.84	3.21	3.01	1.68E+11				2.95E-07	9.20E-08		0.0087	−1.45	0.0049	0.0059	> 36,400	9800
Chile	TT220331	3.51	1.63	4.00	5.76E+11				4.61E-08	2.83E-08		0.0058					
Chile	LA220331											0.0048	3.93	−0.0064	0.0060	> 41,200	
Chile	LP220401	1.44	0.25		1.53E+11				4.03E-08	1.62E-07		0.0005	−5.21	0.6381	0.0160	3610	200
Chile	CP220402	1.91	1.42	2.12	2.16E+12				3.69E-07	2.59E-07		0.0941					
Chile	CE220402	2.55	1.19	2.98	6.18E+13				1.83E-09	1.53E-09		0.0179	0.58				
Chile	JR220403	0.92	17.93	0.92	1.48E+10				1.12E-06	6.25E-08		0.0009	−4.78	0.0104	0.0061	36,700	4700
Argentina	BF230316	0.88	0.31		2.86E+11	9.75	0.027	296.7	9.01E-08	2.89E-07	1.19E-06	0.0014	−8.26				
Argentina	CM230315	0.54	29.69		9.82E+09	7.44	0.0289	299.0	3.02E-06	1.02E-07	8.22E-07	0.0010	−8.55				
Argentina	CZ230307	1.90	54.70		1.15E+10	9.92	0.0333	296.0	2.45E-06	4.49E-08	3.96E-07	0.0033	−6.69				
Argentina	LF230308	1.14	21.96		1.16E+12			292.6	1.82E-07	8.27E-09	2.55E-08	0.0149	−6.49				
Argentina	LN230313	0.58	1049.79		1.20E+10			304.1	3.03E-05	2.88E-08	1.97E-07	0.0131	0.16	0.0166	0.0032	32,900	1500
Argentina	OY230308	0.74	19.39		3.84E+10	9.91	0.0286	297.0	1.51E-06	7.79E-08	6.48E-07	0.0026	−9.67				
Argentina	OZ230305	1.06	23.94		3.89E+11	9.71	0.0307	299.0	4.36E-07	1.82E-08	1.68E-07	0.0112	−6.19				
Argentina	PG230225	1.34	107.70	1.34					2.70E-06								
Argentina	PI230308	1.30	1.26		1.88E+13			291.3	3.07E-08	2.44E-08	2.52E-08	0.0464	−3.41				
Argentina	PQ230306											0.0055	−10.95	0.0424	0.0033	25,400	620
Argentina	QH230313	1.06	98.59		1.22E+09	8.04	0.0281	299.9	9.41E-06	9.54E-08	5.42E-07	0.0008	−8.9				
Argentina	RC1230306											0.0152	−4.15	0.0014	0.0038	> 42,200	22,000
Argentina	TZ230310											0.0102	−2.87	0.0296	0.0032	28,300	870
Argentina	VA230311	2.79	2.36		2.42E+12	9.67	0.0286	296.2	3.09E-07	1.31E-07	8.81E-07	0.1293	0.83				

Table 4
High precision dynamic mass spectrometry (DMS) data for the Pirquitas sample. Individual uncertainties are provided for each isotope ratio. DMS data were obtained in the Seltzer Lab at WHOI.

	$^{40}Ar/^{36}Ar$	error	$\delta^{38}Ar/^{36}Ar$	error	$\delta^{86}Kr/^{84}Kr$	error	$\delta^{86}Kr/^{82}Kr$	error	$\delta^{136}Xe/^{130}Xe$	error	$\delta^{134}Xe/^{130}Xe$	error	$\delta^{132}Xe/^{130}Xe$	error	$\delta^{131}Xe/^{130}Xe$	error	$\delta^{129}Xe/^{130}Xe$	error	$\delta^{128}Xe/^{130}Xe$	error
Pirquitas; PI230308	463.27	0.03	2.7	0.1	0.714	0.028	0.773	0.033	2.801	0.139	1.983	0.13	0.425	0.109	0.051	0.127	0.718	0.109	0.314	0.234

Table 5
Nitrogen isotope and clumped nitrogen isotope data for the Pirquitas sample. Individual uncertainties are provided for each isotope ratio. Data were measured in the Young Lab at UCLA.

	$\delta^{15}N$	±1s	$\Delta_{30}N$	±1s
Pirquitas; PI230308	+6.13	0.01	+0.79	0.30

Nitrogen isotopes in permil deviations from atmosphere

rock (e.g., Hilton et al., 1993; Inostroza et al., 2020). We note that the residence time of these fluids in the crust is also likely much longer compared with high temperature volcanic gas emissions (e.g., summit fumaroles), as thermal springs require specific structural conditions (i.e., deep fault structures) and circuitous paths to reach the surface, whereas volcanic conduits likely allow a faster and more direct pathway for fluids to the surface. For these reasons, high temperature magmatic gases and olivine-hosted fluid inclusions from the CVZ indicate much higher mantle He percentages (de Moor et al., In Review). For example, our highest temperature gas sample (408 °C; 5.8 R_A), from Irruputuncu volcano, contains 72 % mantle He, and gas samples from Lascar volcano (Tassi et al., 2011) have $^3He/^4He$ values as high as 7.3 R_A, indicating 90 % mantle helium.

3.3.2. Carbon

Carbon in thermal spring samples can be derived from the mantle, the overlying crust, or from subducted carbon-rich sediments, which release volatiles that migrate to surface springs across the arc (e.g., Sano and Marty, 1995). $CO_2/^3He$ and $\delta^{13}C$ data have been extensively used to differentiate between various carbon sources; however, it is often challenging to distinguish between carbon additions from subduction versus those derived from the overlying crust.

Previous studies in the ACM have noted the role of subducted sediment-derived fluids in melting the Sub-Andean mantle (e.g., Stern, 2007) and supplying volatiles to hydrothermal fluid samples (Ray et al., 2009). Previous work from our group (i.e., Barry et al., 2022) indicated that He and C are likely released across the entire convergent margin (outer forearc, forearc, arc, backarc) and that adopting such a narrow view of where these volatiles are released is likely an oversimplification. It is therefore important to sample across the entire arc system, so that carbon output estimates can be more accurately compared with input estimates.

To quantify the extent of slab-derived CO_2 to thermal springs, we adopt the approach of Sano and Marty (1995), which uses observed He-CO_2 characteristics to deconvolute mantle- versus subduction-derived (i.e., organic sediments and inorganic limestones) components. This approach implicitly assumes that all $CO_2/^3He$ and $\delta^{13}C$ variations are the result of mixing between subduction and mantle derived components and that there is no crustal input from the overriding slab. We note that these assumptions may not be valid, and we explore alternative scenarios below. However, if these assumptions are in fact valid, He–CO_2 characteristics (relative abundances and $\delta^{13}C$ systematics) can be used to resolve CO_2 contributions from three distinct sources: limestone (L) from subducted sediment and mineralized within slab basement, sedimentary (organic) carbon (S) from subducted sediment, and the mantle wedge (M). Each endmember source component is assumed to have a distinctive $CO_2/^3He$ ($M = 2 \times 10^9$; $L = 1 \times 10^{13}$; $S = 1 \times 10^{13}$) and $\delta^{13}C$ ($M = -5‰$; $L = 0‰$; $S = -30‰$) signature. Notably, a recent study suggests that subducting sediments may be higher (~−22.5‰; Xu et al., 2021), which would change the relative contributions slightly. In Fig. 3, we plot the $CO_2/^3He$ values as a function of $\delta^{13}C$ for all samples, together with binary mixing trajectories. In order to quantify the relative proportions of CO_2 derived from each respective endmember component, mass fractions of three major sources of carbon are calculated following the methods of (Sano and Marty, 1995).

Using this approach, we calculate that the average CO_2 provenance in the CVZ to be L:S:M = 75:17:8, which is broadly similar to what Barry

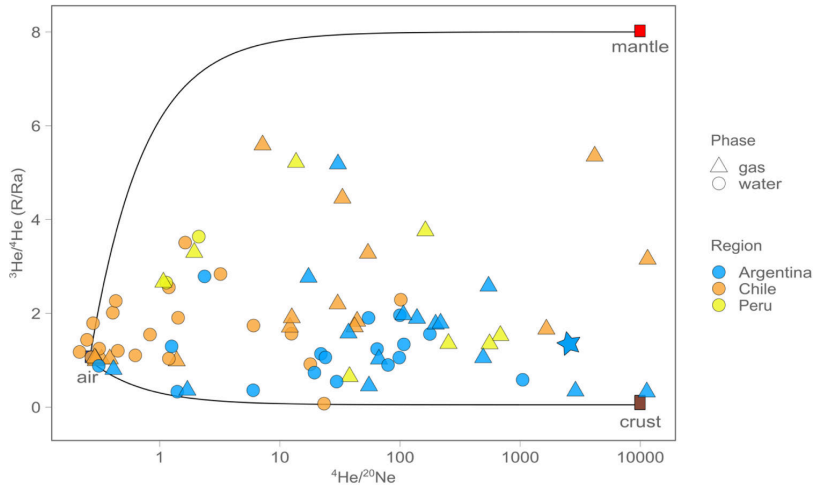

Fig. 2. Helium isotopes (^{3}He/^{4}He) vs. ^{4}He/^{20}Ne for gas (triangles) and water (circles) phase samples. Nearly all samples can be explained by three-component mixing between air, mantle (red square) and crust (brown square). As in all figures, the star symbol is used to denote gas phase sample PI230308 from Piquiras.

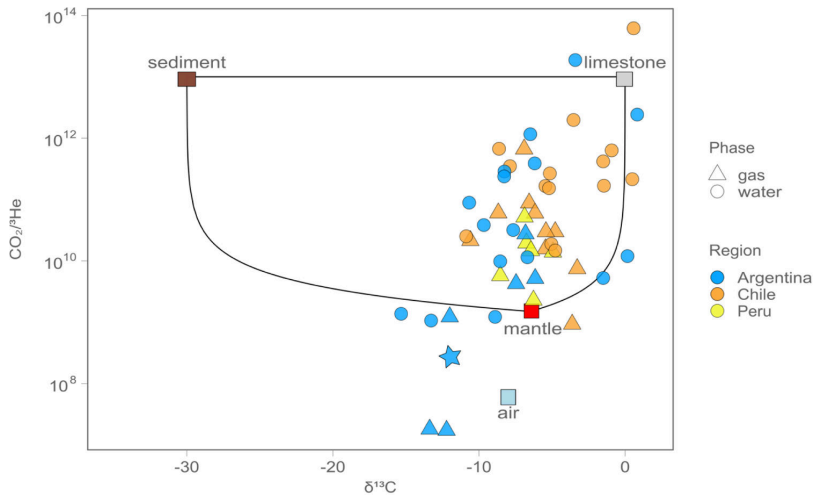

Fig. 3. $CO_2/^3$He vs. δ^{13}C (‰) vs. PDVB of CO_2 for all gas (triangles) and DIC for water (circles) samples respectively from this study. The uncertainties on the $CO_2/^3$He vs. δ^{13}C of CO_2 data are lower than given by the size of the symbols. Subduction-related source end-member compositions for mantle (M), limestone (L), and sediment (S) are plotted for reference, along with binary mixing lines between these three endmember, after Sano and Marty (1995). For reference, air is also plotted. Notably, calcite deposition or dissolution processes could result in the values that plot below the mixing envelope. As in all figures, the star symbol is used to denote gas phase sample PI230308 from Piquiras.

et al. (2022) found (L:S:M = 70:22:8) using an entirely separate set of samples from the CVZ. These calculations equate to an average L/S of 4.9 (this work) versus an average L/S 3.2 in Barry et al. (2022) and an average ($L + S$)/M of 11.9 for the CVZ, which is identical to what Barry et al. (2022) found. This approach implies that slab-derived contributions dominate the CO_2 budget. See Barry et al. (2022) for a more detailed discussion about this approach and its limitations.

The above approach assumes all He-C characteristics are controlled by subduction and mantle inputs and that there is no significant input of assimilated crustal CO_2. While this assumption is likely valid for high temperature volcanic arc samples (e.g., fumaroles) marked by high ^{3}He/^{4}He, here we report thermal spring data from across the entire arc system (i.e., forearc, arc, backarc), with a wide range in ^{3}He/^{4}He. An alternative explanation is that crustal assimilation may be modifying $CO_2/^3$He and δ^{13}C. This hypothesis is compelling in the CVZ, due to the exceedingly thick crust and evidence of carbonate assimilation in some CVZ melts (Matthews et al., 1996). However, δ^{13}C values that are lower than typical mantle and carbonate values (Fig. 3) suggests either incorporation of isotopically light organic carbon in the crust, perhaps from sediments (Sano and Marty, 1995; DeCelles et al., 2011; Quade et al., 2015; Giambiagi et al., 2022), or a negative carbon isotope excursion due to carbonate precipitation (Fig. 3) at depth (Ray et al., 2009; Barry et al., 2019; 2022). Notably, the crustal assimilation hypothesis is supported by He isotope data (Barry et al., 2022), which are highly variable and lower on average versus typical arcs (Hilton et al., 2002), suggesting significant radiogenic overprinting due to interaction

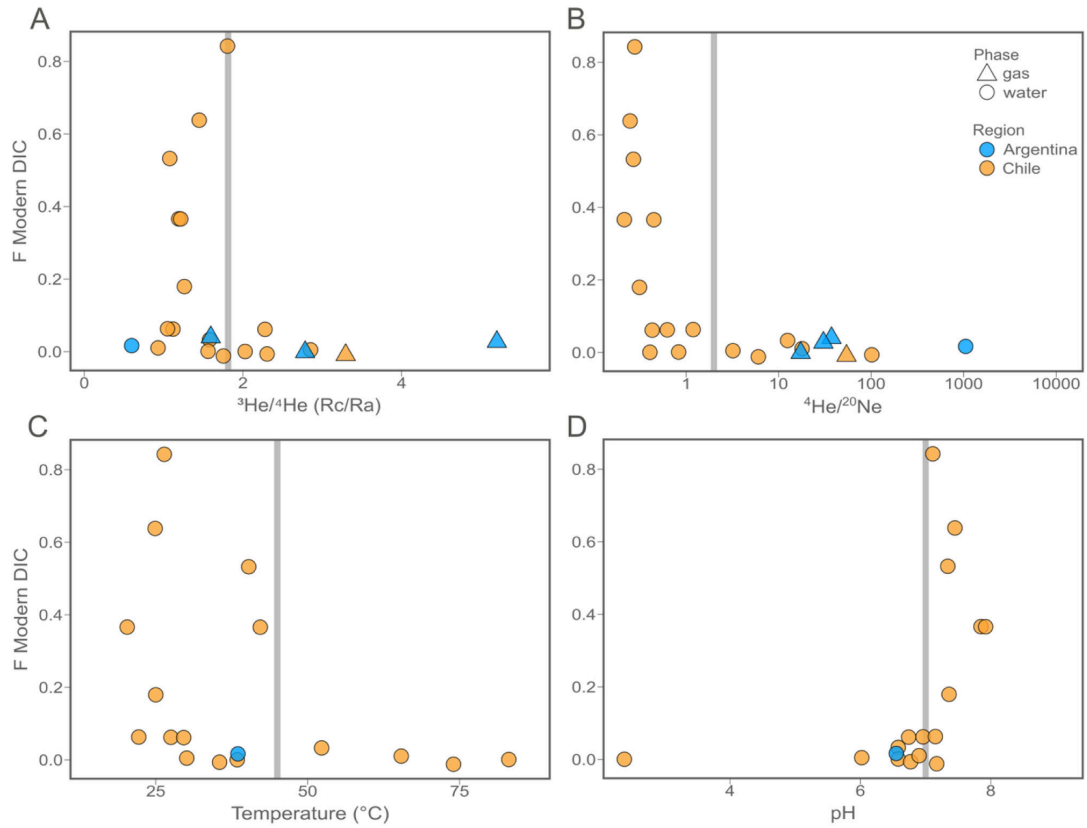

Fig. 4. a-d. Radiocarbon (^{14}C) activities (expressed as fraction modern dissolved inorganic carbon (F^{14}C DIC) vs ^{3}He/^{4}He (Fig. 4a), ^{4}He/^{20}Ne (Fig. 4b), Temperature (Fig. 4c) and pH (Fig. 4d). The gray vertical lines illustrate the bimodal nature of the data. Notably, a handful (n = 4) gas samples are plotted on Figs. 4a and 4b, where there are water phase ^{14}C data, but no corresponding water phase He-Ne data, in which case we plot the gas phase ^{3}He/^{4}He and ^{4}He/^{20}Ne from that particular site against F modern DIC.

with the crust. In Section 3.3.1 we suggested that He isotope variations are primarily controlled by the thickness of the crust, with approximately 77 % of helium derived from the crust on average in thermal springs from this study. We surmise that similar processes could affect the carbon systematics, as $CO_2/^3$He is higher (1.6×10^{12}) than the mantle on average in the CVZ (1-sigma standard deviation = 8.3×10^{12}). Additionally, δ^{13}C is −7.9‰ (1-sigma standard deviation = 3.5‰) is lighter than the mantle on average in the CVZ. Notably, if only arc samples are considered (de Moor et al., In Review), the average $CO_2/^3$He is significantly lower and δ^{13}C is isotopically higher than mantle, meaning these lower temperature thermal spring samples heavily skew the average δ^{13}C to lighter values.

Carbon removal due to calcite precipitation or gas dissolution is yet another process that can affect $CO_2/^3$He and δ^{13}C. However, there is not strong evidence for carbon loss in Chile samples and most data fall within the mixing envelope in Fig. 3. Peru thermal spring data span a much wider range, with $CO_2/^3$He spanning ~7 orders of magnitude. Argentina has two data points clearly below the mantle line, and interestingly these have the lowest δ^{13}C values observed, suggesting that calcite precipitation may be occurring in this region (e.g., Ray et al., 2009; Barry et al., 2022). Similarly, gas loss due to dissolution in water can also result in a decrease in $CO_2/^3$He in both gas and water phase samples (Gilfillan et al., 2009; Güleç and Hilton, 2016). Notably, the trends that are predicted are similar to those anticipated from calcite precipitation (e.g., Güleç and Hilton, 2016). In short, as gases ascend towards the surface, they likely come into contact with gas-undersaturated aquifers. When this occurs, the gas phase preferentially loses the more soluble gas species (i.e., C) relative to the less soluble gas species (i.e., He), resulting in lower $CO_2/^3$He in the gas phase which ultimately manifests at the surface (Barry et al., 2022).

3.4. Neon and argon isotopes

Neon and argon isotopes are not routinely reported in thermal spring samples, as they are commonly air-dominated. In CVZ thermal spring samples, most Ne isotope data (Tables 2 and 3) indeed cluster around air values, which is consistent with our understanding of the overall mass balance of volatiles in volcanic hydrothermal systems, whereby small amounts of atmospheric Ne circulating in the hydrothermal system can easily overwhelm the deep (crustal and mantle) signals. For this reason, Ne isotopes are of somewhat limited utility for interpreting source features in thermal spring samples. Argon isotopes in isolation cannot distinguish between crustal and mantle sources, as both are marked by elevated ^{40}Ar/^{36}Ar values relative to air. Instead, Ar isotope data are best interpreted alongside other tracers (e.g., He, C, Xe, N_2 isotopes). In CVZ thermal spring samples, Ar isotopes vary from 296 to 492 (for reference, air ^{40}Ar/^{36}Ar = 298.6) and point toward mixing between a crustal endmember, marked by radiogenic ^{3}He/^{4}He and non-atmospheric ^{40}Ar/^{36}Ar and a second endmember with variable ^{3}He/^{4}He (i.e., between air and mantle) and broadly air-like ^{40}Ar/^{36}Ar

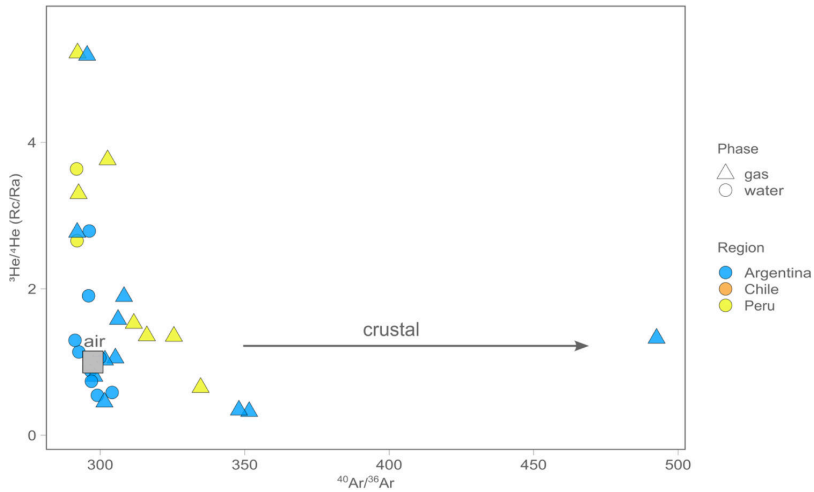

Fig. 5. He isotopes vs Ar isotopes. Ar isotopes vary from 296 to 492 (for reference, air $^{40}Ar/^{36}Ar = 298.6$) and point towards mixing between a crustal endmember, marked by radiogenic $^3He/^4He$ and non-atmospheric $^{40}Ar/^{36}Ar$ and a second endmember with variable $^3He/^4He$ (i.e., between air and mantle) and broadly air-like $^{40}Ar/^{36}Ar$. Uncertainties on He isotopes are better than 5 %, and uncertainties on Ar isotopes are better than 6 %.

(Fig. 5). Again, mass balance considerations can explain this trend, whereby mantle He isotope anomalies are observed in several samples, even when Ar isotopes are swamped by atmospheric contributions, suggesting decoupling between He and Ar.

3.5. High precision Ar, Kr and Xe

High precision Ar, Kr, and Xe results are reported in Table 4. Data were obtained using dynamic mass spectrometry (DMS), which yields significantly higher analytical precision relative to traditional static (SMS) noble gas techniques (methods described in Seltzer and Bekaert, 2022). High precision DMS $^{40}Ar/^{36}Ar$ values for the Pirquitas sample

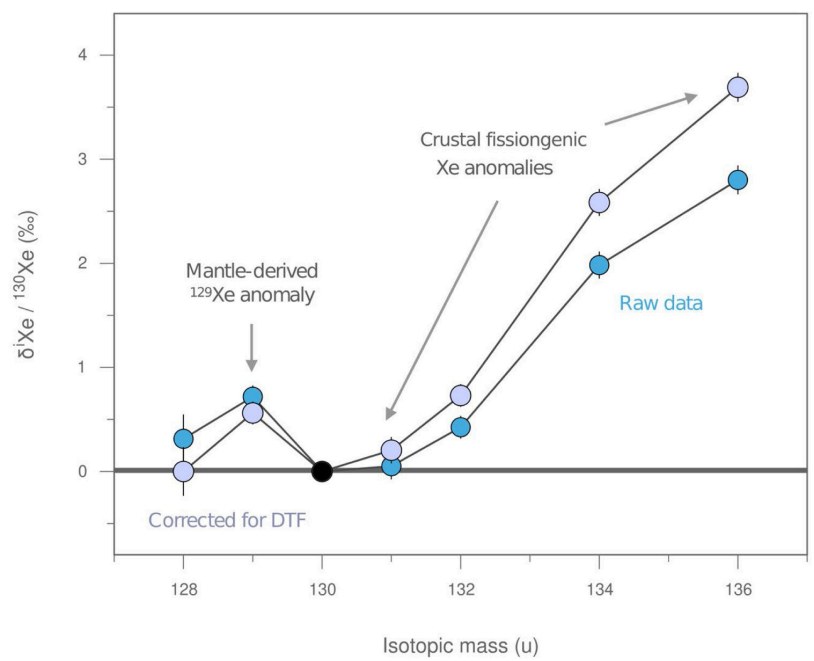

Fig. 6. Xenon spectra for the Pirquitas sample. Assuming a pure mantle $^{129}Xe^*/^{136}Xe^* \sim 1$, then the observed $^{136}Xe/^{129}Xe$ of 3.9 suggests that only 12 % of the $^{136}Xe^*$ is coming from the mantle, with the reminder (88 %) deriving from the crust. This agrees remarkably well with He isotope constraints, which independently implies a 84 % mantle contribution to the Pirquitas sample.

($^{40}Ar/^{36}Ar = 463.27 \pm 0.03$) are in broad agreement with SMS results from the Barry Lab ($^{40}Ar/^{36}Ar = 492 \pm 30$), with both values being in marked excess of the atmospheric ratio ($^{40}Ar/^{36}Ar = 296.8$; Lee et al. 2006). While most $^{40}Ar/^{36}Ar$ values measured in subduction zones worldwide exhibit only slight - if any - excesses relative to the atmospheric value (Bekaert et al., 2023), the elevated $^{40}Ar/^{36}Ar$ observed in the Pirquitas sample (Fig. 5) reflects the contribution of radiogenic ^{40}Ar ($^{40}Ar^*$) from radioactive decay of ^{40}K via electron capture in the continental crust and/or mantle.

One way to distinguish between crustal and mantle-derived noble gas inputs is to use Xe isotope systematics (Fig. 6). This is because the mantle exhibits a marked excess of ^{129}Xe ($^{129}Xe^*$) relative to primordial Xe isotopes (e.g., ^{130}Xe) when normalized to the atmospheric composition, due to the radiogenic decay of ^{129}I ($T_{1/2} = 15.7$ Myr) within the first ~100 Myr of our planet's evolution. Here, we observe that the high precision Xe isotope composition of Pirquitas indeed exhibits a significant $^{129}Xe^*$, which is however accompanied by additional excesses in the light (^{128}Xe) and heavy ($^{131-136}Xe$) isotopes. The latter reflects the contribution of fissiogenic Xe production via spontaneous fission of now extinct ^{244}Pu ($T_{1/2} = 80$ Myr) and/or still extant ^{238}U ($T_{1/2} = 4.468$ Gyr) (Porcelli and Ballentine 2002). While the mantle still preserves some minor remnants of fissiogenic Xe from ^{244}Pu (Kunz et al., 1998; Bekaert et al., 2024), crustal environments are characterized by pure ^{238}U-derived Xe excesses. Thus, both the mantle and crust may contribute heavy, fissiogenic Xe isotopes to the Pirquitas gas sample. Regarding the ^{128}Xe excess, there are two potential explanations, neither of which involve nuclear reactions. The first one is the occurrence of a deep, primordial component that is mass dependently enriched in the light Xe isotopes relative to the present-day atmosphere (as would for instance be expected if the Earth had preserved a chondritic Xe isotope component, inherited from its planetary building blocks; e.g., Caffee et al., 1999; Holland and Ballentine, 2006; Broadley et al., 2020). The second possibility is physical fractionation of the noble gas signals within hydrothermal systems, via diffusive transport fractionation (DTF; Bekaert et al., 2023). In both cases, propagating the correction for the occurrence of this mass dependent light Xe isotope enrichment toward heavier isotopes would tend to exacerbate the heavy Xe isotope excesses observed from the raw data.

Here, we rely on both (i) the recent finding that the upper mantle is largely devoid of primordial heavy noble gases (Bekaert et al., 2024), and (ii) the fact that non-radiogenic Kr and Xe isotope systematics for the Pirquitas sample are consistent with the global diffusive transport fractionation (DTF) line (Fig. 7), to correct for physical fractionation of Xe isotopes in the Pirquitas gas using Kr isotope systematics (Fig. 7; Bekaert et al. 2023). We find that the heavy fissiogenic Xe isotope excesses are much greater than expected based on the $^{129}Xe^*$ (typical $^{129}Xe^*/^{136}Xe^* \sim 1$ for most mantle sources worldwide; Bekaert et al. 2024; Marty et al., in review), indicating significant contribution from crustal (^{238}U-derived) Xe. Assuming a pure mantle $^{129}Xe^*/^{136}Xe^* \sim 1$ (Bekaert et al., 2019, 2024; Marty et al., in review), then the observed $^{136}Xe/^{129}Xe$ of 3.9 suggests that only 12 % of the $^{136}Xe^*$ is coming from the mantle, with the remainder (88 %) deriving from the crust. This agrees remarkably well with He isotope constraints, which independently implies a 84 % crustal contribution to the Pirquitas sample. To our knowledge this is the first time that both He and Xe isotopes have yielded such close agreement in a subduction related sample. This result also appears consistent with the large amount of $^{40}Ar^*$, with both signatures arguably arising from the occurrence of an anomalously thick

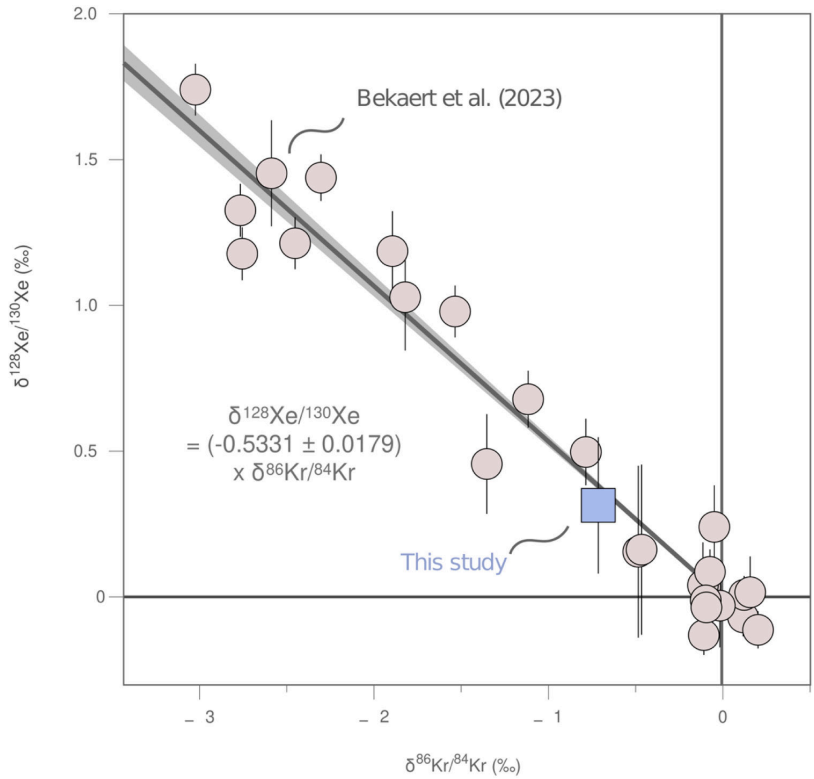

Fig. 7. Xe isotopes vs Kr isotopes from various hydrothermal spring samples. All data are from Bekaert et al., 2023, apart from the Pirquitas sample (this study), which plots along the global diffusive transport fractionation (DTF) line. As such, a correction can be applied to all Xe isotope data to account for DTF.

continental crust in this part of the CVZ. Xenon isotopes were not measured in other samples, due to low $^{40}Ar/^{36}Ar$, implying that Xe isotopes will essentially be indistinguishable from air (Bekaert et al., 2023).

3.6. Clumped N_2

We also measured clumped N_2 isotopes ($^{15}N^{15}N$) (Young et al., 2016; Yeung et al., 2017; Labidi et al., 2020; 2021) in the Pirquitas sample (Table 5). Specifically, we use $^{15}N^{15}N$ to estimate the extent of sample contamination by atmospheric nitrogen, the most abundant gas in air. We use the Δ_{30} notation, whereby the $^{15}N^{15}N$ concentration is reported relative to a random distribution of ^{14}N and ^{15}N atoms among N_2 molecules, as expected for equilibrium at high temperature. The Δ_{30} tracer is defined as $\Delta_{30}={}^{30}R/({}^{15}R)^2 - 1$ (‰), where $^{30}R= {}^{15}N^{15}N/ {}^{14}N^{14}N$ and $^{15}R={}^{15}N/{}^{14}N$. N_2 formed by geological processes at high temperatures (i.e., ~800 °C; Yeung et al., 2017), results in equilibrium among N_2 isotopologues reflected by Δ_{30} values from 0.5 to 0.1‰, respectively (Yeung et al., 2017). This applies for all deeply-derived (i.e., magmatic and crustal) N_2, (Labidi et al., 2020). In contrast, air has a diagnostic disequilibrium $^{15}N^{15}N$ enrichment, resulting in an atmospheric Δ_{30} value of 19.1 ± 0.3‰ (2σ) (Yeung et al., 2017), although high temperatures (>800 °C) may also reorder atmospheric N_2 towards high temperature equilibrium (Yeung et al., 2017).

We find a Δ_{30} of 0.79 ± 0.30‰ and a $\delta^{15}N$ of +6.13 ± 0.01‰ for the Pirquitas sample. In Fig. 8, we plot the Pirquitas sample together with eight fumaroles and seven bubbling springs from a previous study (Labidi et al., 2021) of arc gases from Central America. In light of the high N_2/Ar (=1445) of this sample (>17 times greater than the atmospheric N_2/Ar ratio), it is clear that geologically-sourced N_2 must dominate the N_2 content in this system. The finding of Δ_{30} ~ 0‰ confirms that any atmospheric N_2 content is negligible relative to the large geogenic component (Fig. 8). The fact that He and Xe isotopes both indicate that the Pirquitas sample is composed of >84 % crustal and <16 % mantle gas suggests that the positive $^{15}N^{15}N$ in Pirquitas also likely reflects a predominantly crustal signal. We surmise that this low Δ_{30} nitrogen component, marked by a crustal-like $\delta^{15}N$ value, reflects formation of N_2 at high temperature in the crust, while preserving the original $\delta^{15}N$. This would imply that the thick crust beneath the CVZ is effectively being baked and co-releasing N_2 and noble gases (He through Xe) to the surface. We surmise that He and Xe are coupled and effectively released from the crust due to interaction with the Altiplano-Puna Magma Body (APMB) (Fig. 1), beneath the Pirquitas region. Alternatively, the N_2 signature could be a direct result of sufficiently heated subducted N in sediments, resulting in low Δ_{30}, but decoupled from noble gases and C systematics. The first scenario is more plausible, as it does not require decoupling between different volatile elements. However, differentiating between old overlying crust-derived and subduction (N_2-rich) related fluids is difficult. Notably, the APMB (the largest magma body on Earth) is located directly below the CVZ and provides a potential mechanism for the high temperature release of crustal volatiles (i.e., He, Ar, Xe and N_2) towards the surface. Notably, ignimbrites in the CVZ are sourced by crustal derived magmas (i.e., APMB), whereby intruding magmas resulted in crustal melting and assimilation. This led to the development of crustal-scale intrusive complexes and eventually the APVC (de Silva et al., 2006) in the CVZ. Our combined noble gas and clumped N_2 results indicate these crustally-influenced magmas are the source of the volatiles in the thermal springs throughout the region as well.

4. Summary

When taken together, carbon, noble gases and clumped N_2 isotopes data from thermal springs in the CVZ point towards a dominantly crustal source of volatile elements. The salient take-home points are:

- He-C isotope data are remarkably consistent with previous studies from the CVZ and suggest volatiles released by thermal springs in the CVZ are dominantly sourced from the crust (~77 %), with smaller (~23 %) mantle contributions.
- He-C isotopes are still the "gold-standard" for tracing source features in thermal springs, due to mass balance constraints.
- Thermal spring samples with non-atmospheric He-Ne characteristics have low radiocarbon activities, indicating that dissolved carbon (available for use by microbes) is deeply (i.e., mantle and crustal) derived and old (>22,000 years).

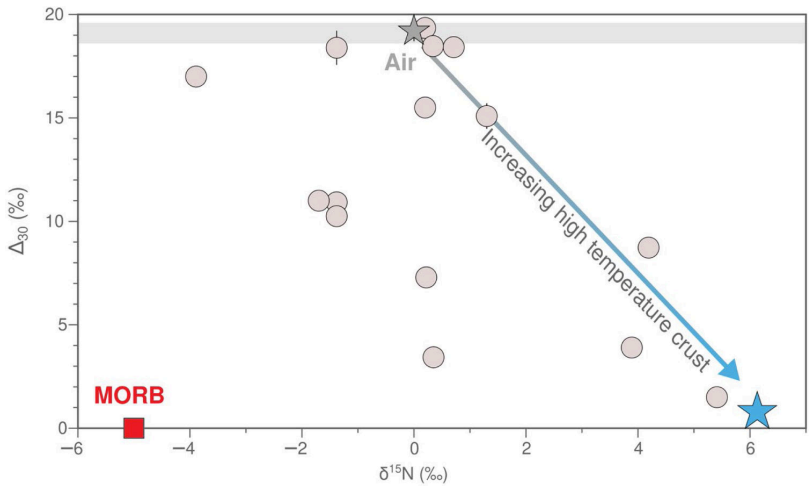

Fig. 8. The nitrogen isotopic composition of volcanic discharges in central America (gray circles) as reported by Labidi et al., 2021 together with the Pirquitas sample (this study; blue star). Variable Δ30 values indicated that Central America arc samples have variable amounts of atmospheric nitrogen. The Pirquitas sample (this study), has the lowest Δ30 value of all arc samples, implying the lowest air-derived N_2 contributions of any known arc sample. Similarly to the findings of Labidi et al., 2021, the high-temperature components (Δ30 approaching zero) have positive $\delta^{15}N$ values. The fact that He, C and Xe strongly suggest that this sample is >80 % crustal and <20 % mantle, suggests that we are observing high temperature crustal nitrogen.

- Argon isotope anomalies are most apparent in the Pirquitas gas sample from the Argentinian backarc.
- High precision Xe isotopes in the Pirquitas gas sample suggest a similar amount of crustal and mantle Xe as suggested independently by He isotopes. This points to a coupled release of all crustal noble gases, likely requiring bulk degassing of the crust via melting rather than low-temperature diffusive loss.
- Clumped N_2 results suggest that the Pirquitas gas sample has essentially no air-derived N_2 and suggests that crustal N_2 (and not just magmatic N_2) can be released at high temperatures (i.e., those marked by Δ_{30} of ~0‰).
- Future microbiological studies that aim to characterize the deep biosphere should target samples with 1) low (<0.1) ^{14}C activities, 2) non-atmospheric He isotopes (>1.8 R_A or <0.5 R_A), 3) elevated (>2) $^4He/^{20}Ne$, and 4) temperatures > 45 °C.

CRediT authorship contribution statement

PH Barry: Conceptualization, Funding acquisition, Investigation, Writing – original draft. **JM de Moor:** Writing – review & editing, Writing – original draft, Methodology, Formal analysis, Conceptualization. **MW Broadley:** Writing – review & editing, Writing – original draft, Formal analysis, Data curation. **AM Seltzer:** Writing – review & editing, Writing – original draft, Visualization, Methodology, Formal analysis, Data curation. **DV Bekaert:** Writing – review & editing, Writing – original draft, Visualization, Formal analysis, Data curation, Conceptualization. **K Patil:** Writing – review & editing, Formal analysis, Data curation. **CGE Bartels:** Writing – review & editing, Formal analysis, Data curation. **ED Young:** Writing – review & editing, Formal analysis, Data curation. **BE Longworth:** Writing – review & editing, Formal analysis. **B Barosa:** Writing – review & editing, Formal analysis. **A Bastianoni:** Formal analysis. **D Bastoni:** Formal analysis. **M Cascone:** Formal analysis. **SJ Turner:** Writing – review & editing, Writing – original draft, Formal analysis, Conceptualization. **RL Tyne:** Writing – review & editing, Writing – original draft, Formal analysis, Data curation. **M Anderson:** Writing – review & editing. **K Li:** Writing – review & editing. **J Curtice:** Formal analysis, Data curation. **N Kumar:** Writing – review & editing, Formal analysis. **GL Jessen:** Writing – review & editing, Writing – original draft, Funding acquisition. **JM Blamey:** Writing – review & editing, Conceptualization. **CJ Ramírez:** Writing – review & editing, Investigation, Conceptualization. **A Chiodi:** Writing – review & editing, Writing – original draft, Formal analysis, Data curation. **F Aguilera:** Writing – review & editing, Writing – original draft. **S Layana:** Writing – review & editing, Conceptualization. **C González:** Writing – review & editing. **M Aguilera:** Writing – review & editing, Conceptualization. **GPJ Masías Alvarez:** Investigation, Writing – review & editing. **B Marty:** Writing – review & editing, Conceptualization. **KG Lloyd:** Writing – review & editing, Writing – original draft, Supervision, Methodology, Investigation, Funding acquisition, Formal analysis, Data curation, Conceptualization. **D Giovannelli:** Writing – review & editing, Writing – original draft, Visualization, Supervision, Methodology, Investigation, Funding acquisition, Formal analysis, Data curation, Conceptualization.

Declaration of competing interest

Lead author Barry declares that none of the authors have any financial or personal relationships with other people or organizations that could inappropriately influence or bias this work.

Acknowledgments

This work was supported by NSF award 2121637 to PHB, JMdM, and KGL. We also acknowledge NSF awards 2152551 to PHB and KGL and 2151120 to PHB, AMS and DVB. DG has received funding from the European Research Council (ERC) under the European Union's Horizon 2020 research and innovation programme (grant agreement No 948972) acronym CoEvolve. GLJ acknowledges COPAS COASTAL ANID FB210021. MWB acknowledges support from NERC grant NE/X01732X/1. RLT acknowledged support from the Weston Howland Junior and Dame Kathleen Ollerenshaw Fellowships. FA, SL, CG and MA acknowledge the FONDECYT project (1211220) as well as the Millennium Scientific Initiative (ICN_038) and the Millennium Institute on Volcanic Risk Research - Ckelar Volcanes. Additionally, SL acknowledges a FONDECYT postdoctoral project (3240283). We acknowledge WHOI's NOSAMS facility, where ^{14}C measurements were made and Susan Lang and Roberta Hansman for consulting on these data. We thank the field participants in the 2022 Chile, 2023 Argentina and 2023 Peru field campaigns. We would also like to thank Lauren Tafla, Sarah Marcum and Jiarui Liu for their help in running clumped nitrogen isotopes at UCLA.

Supplementary materials

Supplementary material associated with this article can be found, in the online version, at doi:10.1016/j.epsl.2024.119169.

Data availability

Data will be made available on request.

References

Aguilera, F., Apaza, F., Del Carpio, J., Grosse, P., Jiménez, N., Ureta, G., Inostroza, M., Báez, W., Layana, S., Gonzalez, C., Rivera, M., 2022. Advances in scientific understanding of the Central Volcanic Zone of the Andes: a review of contributing factors. Bull. Volcanol. 84 (3), 22.

Barry, P.H., Hilton, D.R., Fischer, T.P., De Moor, J.M., Mangasini, F., Ramirez, C., 2013. Helium and carbon isotope systematics of cold "mazuku" CO2 vents and hydrothermal gases and fluids from Rungwe Volcanic Province, southern Tanzania. Chem. Geol. 339, 141–156.

Barry, P.H., De Moor, J.M., Giovannelli, D., Schrenk, M., Hummer, D.R., Lopez, T., Pratt, C.A., Segura, Y.A., Battaglia, A., Beaudry, P., Bini, G., 2019. Forearc carbon sink reduces long-term volatile recycling into the mantle. Nature 568 (7753), 487–492.

Barry, P.H., De Moor, J.M., Chiodi, A., Aguilera, F., Hudak, M.R., Bekaert, D.V., Turner, S.J., Curtice, J., Seltzer, A.M., Jessen, G.L., Osses, E., 2022. The helium and carbon isotope characteristics of the Andean Convergent Margin. Frontiers in Earth Science 10, 897267.

Basili, M., Rogers, T.J., Nakagawa, M., Yücel, M., de Moor, J.M., Barry, P.H., Schrenk, M. O., Jessen, G.L., Zahirovic, S., Bekaert, D. and Ramirez, C.J., 2024. Subsurface microbial community structure shifts along the geological features of the Central American Volcanic Arc.

Bekaert, D.V., Turner, S.J., Broadley, M.W., Barnes, J.D., Halldórsson, S.A., Labidi, J., Wade, J., Walowski, K.J., Barry, P.H., 2021. Subduction-driven volatile recycling: a global mass balance. Annu. Rev. Earth Planet. Sci. 49 (1), 37–70.

Bekaert, D.V., Barry, P.H., Broadley, M.W., Byrne, D.J., Marty, B., Ramírez, C.J., de Moor, J.M., Rodriguez, A., Hudak, M.R., Subhas, A.V., Halldórsson, S.A., 2023. Ultrahigh-precision noble gas isotope analyses reveal pervasive subsurface fractionation in hydrothermal systems. Sci. Adv. 9 (15), eadg2566.

Bekaert, D.V., Caracausi, A., Marty, B., Byrne, D.J., Broadley, M.W., Caro, G., Barry, P.H., Seltzer, A.M., 2024. The low primordial heavy noble gas and 244Pu-derived Xe contents of Earth's convecting mantle. Earth Planet. Sci. Lett. 642, 118886.

Broadley, M.W., Barry, P.H., Bekaert, D.V., Byrne, D.J., Caracausi, A., Ballentine, C.J., Marty, B., 2020. Identification of chondritic krypton and xenon in Yellowstone gases and the timing of terrestrial volatile accretion. Proceed. National Acad. Sci. 117 (25), 13997–14004.

Butler, W.A., Jeffery, P.M., Reynolds, J.H., Wasserburg, G.J., 1963. Isotopic variations in terrestrial xenon. J. Geophys. Res. 68 (10), 3283–3291.

Caffee, M.W., Hudson, G.B., Velsko, C., Huss, G.R., Alexander Jr, E.C., Chivas, A.R., 1999. Primordial noble gases from Earth's mantle: identification of a primitive volatile component. Science 285 (5436), 2115–2118.

Clift, P.D., 2017. A revised budget for Cenozoic sedimentary carbon subduction. Reviews of Geophysics 55 (1), 97–125.

DeCelles, P.G., Carrapa, B., Horton, B.K., Gehrels, G.E., 2011. Cenozoic foreland basin system in the central Andes of northwestern Argentina: implications for Andean geodynamics and modes of deformation. Tectonics 30 (6).

D'Hondt, S., Pockalny, R., Fulfer, V.M., Spivack, A.J., 2019. Subseafloor life and its biogeochemical impacts. Nat. Commun. 10 (1), 3519.

de Moor, J.M., Barry, P.H., Rodríguez, J., Aguilera, F., Aguilera, M., Gonzalez, C., Layana, S., Chiodi, A., Apaza, F., Masias, P., Kern, C., Barnes, J., Cullen, J., Bastoni, D., Bastianoni, A., Cascone, M., Jimenez, C., Salas-Navarro, J., Ramírez, C. J., Jessen, G., Giovannelli, D., Lloyd, K., 2024. Origins and Fluxes of Gas Emissions from the Central Volcanic Zone of the Andes. EPSL. In Review.

de Silva, S.L., Francis, P., 1991. Volcanoes of the Central Andes, 21. Springer-Verlag, Berlin, 6.
de Silva, S., Zandt, G., Trumbull, R., Viramonte, J.G., Salas, G., Jiménez, N., 2006. Large ignimbrite eruptions and volcano-tectonic depressions in the Central Andes: a thermomechanical perspective. In: Geological Society, London, Special Publications, 269, pp. 47–63.
de Silva, S.L., Kay, S.M., 2018. Turning up the heat: high-flux magmatism in the Central Andes. Elements: An Int. Magazine of Mineral., Geochem., Petrol. 14 (4), 245–250.
Fullerton, K.M., Schrenk, M.O., Yücel, M., Manini, E., Basili, M., Rogers, T.J., Fattorini, D., Di Carlo, M., d'Errico, G., Regoli, F., Nakagawa, M., 2021. Effect of tectonic processes on biosphere–geosphere feedbacks across a convergent margin. Nat. Geosci. 14 (5), 301–306.
Giambiagi, L., Tassara, A., Echaurren, A., Julve, J., Quiroga, R., Barrionuevo, M., Liu, S., Echeverría, I., Mardónez, D., Suriano, J., Mescua, J., 2022. Crustal anatomy and evolution of a subduction-related orogenic system: insights from the Southern Central Andes (22-35 S). Earth-Sci. Rev. 232, 104138.
Gilfillan, S.M., Lollar, B.S., Holland, G., Blagburn, D., Stevens, S., Schoell, M., Cassidy, M., Ding, Z., Zhou, Z., Lacrampe-Couloume, G., Ballentine, C.J., 2009. Solubility trapping in formation water as dominant CO2 sink in natural gas fields. Nature 458 (7238), 614–618.
Giovannelli, D., Barry, P.H., de Moor, J.M., Jessen, G.L., Schrenk, M.O., Lloyd, K.G., 2022. Sampling across large-scale geological gradients to study geosphere–biosphere interactions. Front. Microbiol. 13, 998133.
Giovannelli, D., 2023. Trace metal availability and the evolution of biogeochemistry. Nature Reviews Earth & Environment 4 (9), 597–598.
Güleç, N., Hilton, D.R., 2016. Turkish geothermal fields as natural analogues of CO2 storage sites: gas geochemistry and implications for CO2 trapping mechanisms. Geothermics 64, 96–110.
Hay Mele, B., Monticelli, M., Leone, S., Bastoni, D., Barosa, B., Cascone, M., Migliaccio, F., Montemagno, F., Ricciardelli, A., Tonietti, L., Rotundi, A., 2023. Oxidoreductases and metal cofactors in the functioning of the earth. Essays Biochem. 67 (4), 653–670.
Hilton, D.R., Hammerschmidt, K., Teufel, S., Friedrichsen, H., 1993. Helium isotope characteristics of Andean geothermal fluids and lavas. Earth Planet. Sci. Lett. 120 (3–4), 265–282.
Hilton, D.R., Fischer, T.P., Marty, B., 2002. Noble gases and volatile recycling at subduction zones. Rev. Mineral. Geochem. 47 (1), 319–370.
Hilton, D.R., 1996. The helium and carbon isotope systematics of a continental geothermal system: results from monitoring studies at Long Valley caldera (California, USA). Chem. Geol. 127 (4), 269–295.
Holland, G., Ballentine, C.J., 2006. Seawater subduction controls the heavy noble gas composition of the mantle. Nature 441 (7090), 186–191.
Inostroza, M., Tassi, F., Aguilera, F., Sepúlveda, J.P., Capecchiacci, F., Venturi, S., Capasso, G., 2020. Geochemistry of gas and water discharge from the magmatic-hydrothermal system of Guallatiri volcano, northern Chile. Bull. Volcanol. 82, 1–16.
Kallmeyer, J., Pockalny, R., Adhikari, R.R., Smith, D.C., D'Hondt, S., 2012. Global distribution of microbial abundance and biomass in subseafloor sediment. Proceed. National Acad. Sci. 109 (40), 16213–16216.
Kay, S.M., Ramos, V.A., Dickinson, W.R., 2009. Backbone of the Americas: Shallow subduction, Plateau uplift, and Ridge and Terrane Collision, Vol. 204. Geological Society of America.
Kunz, J., Staudacher, T., Allegre, C.J., 1998. Plutonium-fission xenon found in Earth's mantle. Science 280 (5365), 877–880.
Labidi, J., Barry, P.H., Bekaert, D.V., Broadley, M.W., Marty, B., Giunta, T., Warr, O., Sherwood Lollar, B., Fischer, T.P., Avice, G., Caracausi, A., 2020. Hydrothermal 15N15N abundances constrain the origins of mantle nitrogen. Nature 580 (7803), 367–371.
Labidi, J., Young, E.D., Fischer, T.P., Barry, P.H., Ballentine, C.J., de Moor, J.M., 2021. Recycling of nitrogen and light noble gases in the Central American subduction zone: constraints from 15N15N. Earth Planet. Sci. Lett. 571, 117112.
Lages, J., Rizzo, A.L., Aiuppa, A., Robidoux, P., Aguilar Contreras, R., Apaza Choquehuayta, F.E. and Masías Alvarez, P.J., 2021. Crustal controls on light noble gas isotope variability along the Andean Volcanic Arc. *uri: issn: 2410339X*.
Magnabosco, C., Lin, L.H., Dong, H., Bomberg, M., Ghiorse, W., Stan-Lotter, H., Pedersen, K., Kieft, T.L., Van Heerden, E., Onstott, T.C., 2018. The biomass and biodiversity of the continental subsurface. Nat. Geosci. 11 (10), 707–717.
Marty, B., Contamine, D., Bekaert, D.V., Lastes, A., Pik, R., Labidi, J., Young, E.D., Broadley, M.W., Barry, P.H., Byrne, D.J., Seltzer, A.M., 2024. Uncovering the Xenon Isotope Composition of Continental Rift magmas: Insight from Analysis of Geothermal Gases At Homa Hills. EPSL, Kenya. In Review.
Matthews, S.J., Marquillas, R.A., Kemp, A.J., Grange, F.K., Gardeweg, M.C., 1996. Active skarn formation beneath Lascar Volcano, northern Chile: a petrographic and geochemical study of xenoliths in eruption products. J. Metamorphic Geol. 14 (4), 509–530.
McGlashan, N., Brown, L., Kay, S., 2008. Crustal thickness in the central Andes from teleseismically recorded depth phase precursors. Geophys. J. Int. 175 (3), 1013–1022.
Mook, W.G., Van Der Plicht, J., 1999. Reporting 14C activities and concentrations. Radiocarbon 41 (3), 227–239.
Newell, D.L., Jessup, M.J., Hilton, D.R., Shaw, C.A., Hughes, C.A., 2015. Mantle-derived helium in hot springs of the Cordillera Blanca, Peru: implications for mantle-to-crust fluid transfer in a flat-slab subduction setting. Chem. Geol. 417, 200–209.
Orcutt, B.N., Edwards, K.J., 2014. Life in the ocean crust: lessons from subseafloor laboratories. In: Developments in Marine Geology, 7. Elsevier, pp. 175–196.
Ozima, M., Podosek, F.A., 2002. Noble Gas Geochemistry. Cambridge University Press.
Perkins, J.P., Ward, K.M., de Silva, S.L., Zandt, G., Beck, S.L., Finnegan, N.J., 2016. Surface uplift in the Central Andes driven by growth of the Altiplano Puna Magma Body. Nat. Commun. 7 (1), 13185.
Porcelli, D., Ballentine, C.J., 2002. Models for distribution of terrestrial noble gases and evolution of the atmosphere. Rev. Mineral. Geochem. 47 (1), 411–480.
Profeta, L., Ducea, M.N., Chapman, J.B., Paterson, S.R., Gonzales, S.M.H., Kirsch, M., Petrescu, L., DeCelles, P.G., 2015. Quantifying crustal thickness over time in magmatic arcs. Sci. Rep. 5 (1), 17786.
Quade, J., Dettinger, M.P., Carrapa, B., DeCelles, P., Murray, K.E., Huntington, K.W., Cartwright, A., Canavan, R.R., Gehrels, G., Clementz, M., 2015. The growth of the central Andes, 22 S–26 S.
Ray, M.C., Hilton, D.R., Muñoz, J., Fischer, T.P., Shaw, A.M., 2009. The effects of volatile recycling, degassing and crustal contamination on the helium and carbon geochemistry of hydrothermal fluids from the Southern Volcanic Zone of Chile. Chem. Geol. 266 (1–2), 38–49.
Rogers, T.J., Buongiorno, J., Jessen, G.L., Schrenk, M.O., Fordyce, J.A., de Moor, J.M., Ramírez, C.J., Barry, P.H., Yücel, M., Selci, M., Cordone, A., 2023. Chemolithoautotroph distributions across the subsurface of a convergent margin. ISME J. 17 (1), 140–150.
Salisbury, M.J., 2011. Convergent Margin Magmatism in the Central Andes and Its Near Antipodes in Western Indonesia: Spatiotemporal and Geochemical Considerations. Oregon State University.
Sano, Y., Marty, B., 1995. Origin of carbon in fumarolic gas from island arcs. Chem. Geol. 119 (1–4), 265–274.
Seltzer, A.M., Bekaert, D.V., 2022. A unified method for measuring noble gas isotope ratios in air, water, and volcanic gases via dynamic mass spectrometry. Int. J. Mass spectrom. 478, 116873.
Stern, C.R., 2004. Active Andean volcanism: its geologic and tectonic setting. Revista Geológica de Chile 31 (2), 161–206.
Stuiver, M., Polach, H.A., 1977. Discussion reporting of 14C data. Radiocarbon 19 (3), 355–363.
Summit, M., Baross, J.A., 2001. A novel microbial habitat in the mid-ocean ridge subseafloor. Proceed. National Acad. Sci. 98 (5), 2158–2163.
Syracuse, E.M., Abers, G.A., 2006. Global compilation of variations in slab depth beneath arc volcanoes and implications. Geochem., Geophys., Geosystems 7 (5).
Tassi, E.L., Pedron, F., Barbafieri, M., 2011. Evaluating the absorption of boron by plants—A potential tool to remediate contaminated sediments from Cecina River Basin in Italy. Water, Air, & Soil Pollution 216, 275–287.
Ward, K.M., Zandt, G., Beck, S.L., Christensen, D.H., McFarlin, H., 2014. Seismic imaging of the magmatic underpinnings beneath the Altiplano-Puna volcanic complex from the joint inversion of surface wave dispersion and receiver functions. Earth Planet. Sci. Lett. 404, 43–53.
Xu, Y., Li, X., Luo, M., Xiao, W., Fang, J., Rashid, H., Peng, Y., Li, W., Wenzhöfer, F., Rowden, A.A., Glud, R.N., 2021. Distribution, source, and burial of sedimentary organic carbon in Kermadec and Atacama Trenches. Journal of Geophysical Research: Biogeosciences 126 (5) e2020JG006189.
Young, E.D., Rumble III, D., Freedman, P., Mills, M., 2016. A large-radius high-mass-resolution multiple-collector isotope ratio mass spectrometer for analysis of rare isotopologues of O2, N2, CH4 and other gases. Int. J. Mass spectrom. 401, 1–10.
Yeung, L.Y., Li, S., Kohl, I.E., Haslun, J.A., Ostrom, N.E., Hu, H., Fischer, T.P., Schauble, E.A., Young, E.D., 2017. Extreme enrichment in atmospheric 15N15N. Sci. Adv. 3 (11), eaao6741.

Check for updates

DATA NOTE

PRA Melting-ICE Project: Svalbard 2022 Expeditions Report

[version 1; peer review: awaiting peer review]

Francesco Montemagno[1], Martina Cascone[1], Carlo Cardellini[2,3], Jacopo Pasotti[1], Elena Manini[4], Elisa Baldrighi[4], Enrico Maiero[5,6], Delia Segato[5,7,8], Riccardo Cerrato[9,10], Mauro Mazzola[11], Massimiliano Vardè[5,8], Angelina Cordone[1], Stefano Caliro[12], Iain Rudnik[13], Margaret Cramm[14], James Bradley[15,16], Donato Giovannelli[1,4,17-19]

[1]Department of Biology, University of Naples Federico II, Naples, Campania, Italy
[2]Department of Physic and Geology, University of Perugia, Perugia, Italy
[3]Italian National Institute of Geophysics and Volcanology, INGV, section of Bologna, Bologna, Italy
[4]Institute for Marine Biological Resources and Biotechnologies, Italian National Research Council, CNR-IRBIM, Ancona, Italy
[5]Department of Environmental Sciences, Informatics and Statistics, Ca' Foscari University of Venice, Venice, Italy
[6]National Institute of Oceanography and Applied Geophysics, OGS, Trieste, Italy
[7]European Commission, Joint Research Centre, JRC, Ispra, Italy
[8]Institute of Polar Sciences, Italian National Research Council, CNR-ISP, Venice, Italy
[9]Institute of Atmospheric Pollution Research, Italian National Research Council, CNR-IIA, Firenze, Italy
[10]Department of Earth Science, University of Pisa, Pisa, Italy
[11]Institute of Polar Sciences, Italian National Research Council, CNR-ISP, Bologna, Italy
[12]Italian National Institute of Geophysics and Volcanology, INGV, Naples, Italy
[13]British Antarctic Survey, High Cross, Madingley Road, Cambridge, UK
[14]School of Geography, Queen Mary University of London, Mile End Road, London, UK
[15]Aix Marseille Univ, Université de Toulon, CNRS, IRD, MIO, Marseille, France
[16]School of Biological and Behavioural Sciences, Queen Mary University of London, London, England, UK
[17]Marine Chemistry and Geochemistry Department, Woods Hole Oceanographic Institution, Woods Hole, Massachusetts, USA
[18]Earth-Life Science Institute, ELSI, Tokyo Institute of Technology, Tokyo, Japan
[19]Department of Marine and Coastal Science, Rutgers University New Brunswick, New Brunswick, New Jersey, USA

v1 **First published:** 04 Dec 2024, **4**:257
https://doi.org/10.12688/openreseurope.17772.1
Latest published: 04 Dec 2024, **4**:257
https://doi.org/10.12688/openreseurope.17772.1

Abstract

Arctic regions are among the fastest warming areas of the planet. Increasing average temperatures over the last five decades have deepened the thawing of the upper-most layer of permafrost across the Arctic, which contains significant amounts of organic carbon. The progressive deepening of seasonal thawing releases carbon that is used by active microorganisms which also produce greenhouse gases, potentially onsetting a positive feedback on global warming. Despite their importance in controlling organic matter degradation and greenhouse gas fluxes to the atmosphere, there is a lack of data on activity and dynamics of microbial communities in High Arctic soils in response to seasonal thaw. This report describes three specific

Open Peer Review

Approval Status *AWAITING PEER REVIEW*

Any reports and responses or comments on the article can be found at the end of the article.

expeditions performed on the Svalbard archipelago, carried out within the framework of the PRA (Italian Arctic Research Program) project Melting-ICE, performed between February and October 2022, reporting site characteristics and samples collected. The project aims to investigate the diversity and activity of active layer microbial communities across a full season thaw cycle, correlating microbial diversity with gas fluxes and composition. During these expeditions, a total of eight different sites were selected to investigate the microbiology and geochemistry of soils, as well as to estimate the gas fluxes from the soil to the atmosphere. The data collected in the field, combined with the results obtained in the laboratory, will provide a snapshot of the seasonal activity of the microbial communities present in the permafrost's active layer. The three campaigns will provide data to estimate the impact of permafrost melting on the carbon cycle and the role of microorganisms in the release of greenhouse gases.

Plain language summary

The "Melting-ICE" project examines how the Arctic, particularly the Svalbard archipelago, is responding to rapid climate changes. Located in the Arctic Ocean between latitudes 74°N and 81°N, this group of islands is undergoing faster temperature rises and glacier retreats than many other parts of the world. Approximately 60% of the archipelago is covered with glaciers, and the non-glaciated areas contain permafrost a permanently frozen ground that can be extremely deep. As the region warms, this permafrost is thawing, releasing carbon and greenhouse gases (such as CO2 and methane) that had been trapped in the ice for thousands of years. These gases contribute to the greenhouse effect, further accelerating global warming. A key role in this process is played by microbial communities in the soil, which consume the released carbon and produce greenhouse gases. The project conducted three scientific expeditions to the Ny-Ålesund area in Svalbard from winter to autumn 2022 to study how microbial activity varies with the seasons and its impacts on greenhouse gas emissions. Through field experiments and laboratory analysis, researchers gathered data to better understand how changes in permafrost affect the carbon cycle and greenhouse gas release. These studies are crucial for predicting and managing the effects of climate changes in the Arctic and globally.

Keywords

Expedition report, Permafrost, Arctic, Ny-Ålesund, Climate change, Microbiology, Greenhouse gasses

This article is included in the European Research Council (ERC) gateway.

This article is included in the Horizon 2020 gateway.

Corresponding author: Donato Giovannelli (donato.giovannelli@unina.it)

Author roles: Montemagno F: Data Curation, Formal Analysis, Investigation, Methodology, Project Administration, Resources, Visualization, Writing – Original Draft Preparation, Writing – Review & Editing; **Cascone M**: Data Curation, Investigation, Writing – Review & Editing; **Cardellini C**: Conceptualization, Data Curation, Funding Acquisition, Investigation, Methodology, Project Administration, Resources, Supervision, Writing – Original Draft Preparation, Writing – Review & Editing; **Pasotti J**: Investigation, Writing – Review & Editing; **Manini E**: Funding Acquisition, Methodology, Project Administration, Supervision, Writing – Review & Editing; **Baldrighi E**: Methodology, Writing – Original Draft Preparation; **Maiero E**: Investigation, Resources, Writing – Review & Editing; **Segato D**: Investigation, Resources, Writing – Review & Editing; **Cerrato R**: Investigation, Resources, Writing – Review & Editing; **Mazzola M**: Project Administration, Resources, Writing – Review & Editing; **Vardè M**: Investigation, Writing – Review & Editing; **Cordone A**: Conceptualization, Project Administration, Supervision, Writing – Review & Editing; **Caliro S**: Conceptualization, Data Curation, Methodology, Resources, Writing – Review & Editing; **Rudnik I**: Investigation, Resources, Writing – Review & Editing; **Cramm M**: Investigation, Writing – Review & Editing; **Bradley J**: Conceptualization, Funding Acquisition, Investigation, Project Administration, Resources, Supervision, Writing – Review & Editing; **Giovannelli D**: Conceptualization, Data Curation, Funding Acquisition, Investigation, Methodology, Project Administration, Resources, Supervision, Visualization, Writing – Original Draft Preparation, Writing – Review & Editing

Competing interests: No competing interests were disclosed.

Grant information: This work has received support from the European Research Council (ERC) under the European Union's Horizon 2020 research and innovation program [grant number 948972-COEVOLVE-ERC-2020-STG]. This work was supported by funding from the Italian Ministry of University and Research (MUR) through the Italian Arctic Research Program "Programma Ricerche in Artico (PRA)", project PRA2021-0014 "Impact of climate change-induced permafrost and ice melting on the biodiversity and ecosystem functioning of Arctic environments (Melting-ICE)". This work also received financial support from the NERC Arctic Research Station Access Scheme. JAB also acknowledges support from the CNRS Chaires de Professeur Junior (CPJ).
The funders had no role in study design, data collection and analysis, decision to publish, or preparation of the manuscript.

Copyright: © 2024 Montemagno F *et al*. This is an open access article distributed under the terms of the Creative Commons Attribution License, which permits unrestricted use, distribution, and reproduction in any medium, provided the original work is properly cited.

How to cite this article: Montemagno F, Cascone M, Cardellini C *et al.* **PRA Melting-ICE Project: Svalbard 2022 Expeditions Report [version 1; peer review: awaiting peer review]** Open Research Europe 2024, **4**:257 https://doi.org/10.12688/openreseurope.17772.1

First published: 04 Dec 2024, **4**:257 https://doi.org/10.12688/openreseurope.17772.1

Introduction

The Arctic is warming faster than any other region on the planet (Graversen *et al.*, 2008) and has experienced extreme positive temperature anomalies constantly increasing in the last three decades (Graversen *et al.*, 2008; Walsh, 2014). As a result, the Arctic has lost significant amounts of summer ice cover and permafrost (Graversen *et al.*, 2008; Serreze & Barry, 2011; Tepes *et al.*, 2021). In the last few decades, permafrost temperatures have risen across the Arctic (Smith *et al.*, 2022), and the Global Terrestrial Observing System (GTOS) has identified permafrost as one of six cryospheric indicators of global climate change (Streletskiy *et al.*, 2017). Permafrost thaw has liberated organic carbon, nutrient and trace elements that have been trapped for hundreds to many thousands of years in a frozen state, stimulating microbial activity and increasing the flux of CO_2, N_2O, and CH_4 to the atmosphere (Hayes *et al.*, 2014). While these processes have been extensively studied in soils during the summer months (e.g. Jansson & Taş, 2014; Sipes *et al.*, 2022), the activity of microbial communities and the associated greenhouse gas fluxes during the winter have received comparatively little attention (Graham *et al.*, 2012; Nikrad *et al.*, 2016; Schostag *et al.*, 2015; Vigneron *et al.*, 2019), and data on full seasonal patterns of microbial activity and carbon cycling are scarce. Additionally, the direct coupling between carbon and nutrient utilization by soil microbial communities with the exports to the marine ecosystems, and how these can significantly alter the biogeochemical balance of the area, are significantly less understood (Walvoord & Striegl, 2007).

The response of the Arctic ecosystems to increased melting events is mediated by the microbial community response to these events (Graham *et al.*, 2012). Processes such as respiration, fermentation, methanogenesis, and methane oxidation, together with the efficiency of carbon transfer to higher trophic levels, significantly influence the ultimate fate of the newly released carbon and nutrients (Jansson & Taş, 2014). Characterizing the microbial communities and soil gas fluxes across seasons is of paramount importance to better constrain the response of Arctic soils to ongoing climate change (Graham *et al.*, 2012). While the quality and quantity of carbon released during the summer (and winter) melting events is a strong control on microbial activity (Miner *et al.*, 2022), the release of nutrients and trace elements might place additional constraints on the microbial community response, potentially influencing the type of metabolic processes that are active (Giovannelli, 2023).

The Svalbard archipelago, located in the Arctic Ocean between 74 °N and 81 °N, is highly glaciated and it is experiencing rapid increases in temperature and glacial retreat, making it a model system for future changes to the rest of the Arctic (Martín-Moreno *et al.*, 2017). Approximately 60 % of the archipelago surface is covered by glaciers, leaving a periglacial area where about 25,000 km^2 is covered by permafrost making Svalbard the largest permafrost area in Europe. The archipelago has a continuous permafrost layer that reaches up to 100 m depth in coastal areas and greater than 500 m in mountainous areas. Svalbard permafrost, also known as "warm permafrost", is particularly sensitive to climate change, since its temperature is close to 0 °C (Humlum *et al.*, 2003; Isaksen *et al.*, 2007; Keating *et al.*, 2018). Mountain topography also has a role in making Svalbard permafrost more sensitive to climate change, as variables like altitude, slope, and snow cover can cause changes in the ground temperature and affect the permafrost thickness. Temperatures in the area have steadily increased to about ~3 °C above the seasonal mean, and winter snow cover has been rapidly declining (Isaksen *et al.*, 2007; Vickers *et al.*, 2021). The increasing temperatures have resulted in longer and deeper permafrost thawing events, increasing greenhouse gas emissions in the area. While extensively studied during the summer months, a handful of studies have investigated the soil microbial communities during the winter months in Svalbard (Loganathachetti *et al.*, 2022; Schostag *et al.*, 2015).

The project Melting-ICE was designed to provide an integrated view of the active layers of microbial communities during the winter, summer and autumn seasons while spanning the land-to-sea transition. The project will generate data on the microbial diversity in the active layer, together with quantitative estimates of greenhouse gas fluxes and isotopic signatures. Three independent field expeditions have been conducted to compare the fluxes and microbial diversity during the Arctic winter with the conditions present at the beginning of the summer melt season and the beginning of Autumn freeze events. This report describes the three expeditions to the Ny-Ålesund area, on the island of Spitsbergen, Svalbard archipelago, Norway.

The expedition team and logistics

The project team is composed of a team of interdisciplinary scientists spanning the microbiology, biogeochemistry, microbial ecology and gas geochemistry fields. The expedition was hosted by the Italian "Dirigibile Italia" Arctic Station managed by the Institute of Polar Sciences of the Italian National Research Council and the UK Arctic Research Station, both located in Ny-Ålesund, which provided logistic support. The field science party was responsible for the sample collection and the field measurements. Three sampling expeditions were performed, in February 2022, June 2022 and September 2022, coinciding with a full active layer thaw cycle.

During the winter expedition (i.e., February 2022), given the extremely low temperatures, drilling operations and gas flux measurements were particularly challenging. The Field Science Party performed sampling operations for 17 days with windchill temperatures down to -38 °C (air temperature of -28 °C). Sampling operations were suspended for two days during bad weather conditions when windchill temperatures reached as low as -44 °C. Recovery of intact core samples was difficult due to the fast freezing of the core within the core drill barrel during operation, and only a few intact cores were recovered. For the rest of the locations, coring was performed in sections and the recovery was limited to loose material dislodged from the core barrel. Gas flux

measurements were limited by battery life at low temperatures, in spite of the isolation and heat sources placed in proximity of the instruments. The Onshore Science Party was responsible for supporting the logistics and preparation of the expedition as well as collaborating on sample processing and analysis.

The second 10 days expedition, performed in June, allowed the collection of sediment and fluid samples from the 6 sites originally chosen during the first campaign, and from an additional 7th site. Air temperature ranged between 5 and 8 °C and snow cover was absent. Soils were soaked with meltwater. The 7 days of fieldwork originally planned were reduced to 6 due to the presence of several polar bears nearby the BY4 and BY5 sites (Figure 1).

The fall sampling expedition was carried out at the end of September. Air temperature ranged between 2 and 5 °C, and snow cover was absent. Soil was mostly dry. During this third field expedition, all 7 sites were sampled. (Table 8)

Field Science Party composition: Francesco Montemagno, Martina Cascone, Carlo Cardellini (CoI of the project), James Bradley, Margaret Cramm, Jacopo Pasotti, Enrico Maiero, Delia Segato, Riccardo Cerrato (Italian Acting Station Leader), Massimiliano Vardè, Ian Rudkin, Donato Giovannelli (Expedition Leader and PI of the project).

Support Science Party composition: Elena Manini (CoI of the project), Elisa Baldrighi, Mauro Mazzola, Angelina Cordone (CoI of the project), Stefano Caliro.

Geological and environmental settings

The sampling was performed in the Ny-Ålesund (Svalbard) area (Figure 1) that is located on the Brøggeralvøya on the SW shore of Kongsfjorden, in the northwestern part of Spitsbergen, Svalbard. The area sits on a plateau, surrounded by three main mountains, Zeppelinfjellet (556 m a.s.l.), Berteltoppen (785 m a.s.l.), and Scheteligfjellet (719 m a.s.l.) and by the glacial valleys of Austre-Vestre Brøggerbreen, Vestre Lovénbreen and Midtre Lovénbreen. The Paleocene sandstone, shales, conglomerates, and coal-rich sequence is overlaid by sedimentary rocks from the Middle Carboniferous-Early Triassic (Figure 2) (Van Everdingen, 1981). The bedrock sequences that include conglomerate, sandstone, dolomite, shale, chert, and limestone are involved in a NE-verging thrust fault and NNE-SSW high-angle faults, with closely spaced joints and fractures systems (Cianfarra & Salvini, 2016). The

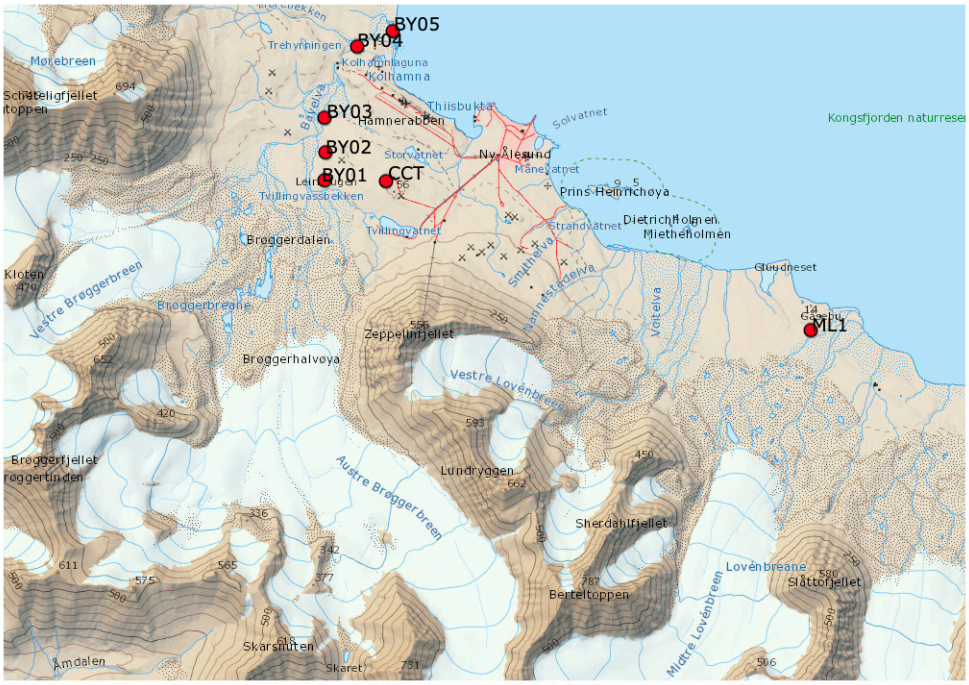

Figure 1. Map of the sampled area with the location of the sampling sites (red dots) and the position of the Ny-Ålesund International Research Station (https://nyalesundresearch.no/). The topographic map was obtained from the Norwegian Polar Institute (https://toposvalbard.npolar.no/).

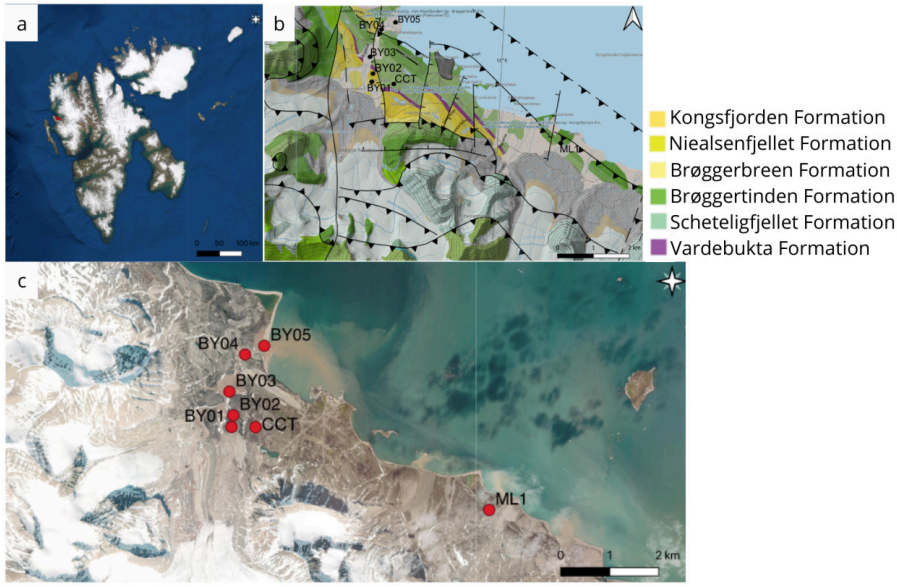

Figure 2. (**a**) Satellite image of Svalbard archipelago, where the sampling took place (**b**) Geological context of the sampling area around Ny-Ålesund, Svalbard. The map was obtained from the site Svalbard Kartet (https://geokart.npolar.no/Html5Viewer/index.html?viewer=Svalbardkartet) (**c**) Satellite image of the Ny-Ålesund area. The sampling sites are reported with the red dots. This panel was created using Google Maps for image (**a**) and (**c**), and QGIS (https://www.qgis.org/en/site/index.html) for image (**b**).

area is also interested by conspicuous moraine deposits and glacier forefield deposits, as Ny-Ålesund is surrounded by a large number of large ice streams, Kongsvegen, Kronebreen, Kongsbreen and Conwaybreen, and glaciers, like Austre Brøggerbreen, Vestre Brøggerbreen, Lovénbreen, Pedersbreen, Botnbreen and Midtre Lovénbreen. The Austre-Vestre Brøggerbreen and Vestre Lovénbreen glaciers melt waters converge in the Bayelva river, discharging directly in the Kingsfjord just NW of Ny-Ålesund.

The Bayelva river is collated in two major glacier valleys that result from the recession of the Brøggerbreen during the present interglacial period (Sadiq *et al.*, 2022). The sampling sites were either placed within moraine deposits or meltwater sedimentary deposits. A sixth site was sampled south-east of Ny-Ålesund, in the forefield of the polythermal valley glacier Midtre Lovénbreen, in an area more representative of the arctic tundra and external to the moraine fields, and close to a temporary year-round monitoring observatory (Cimpoiasu *et al.*, 2024a; Cimpoiasu *et al.*, 2024b). A permanent permafrost monitoring site has been active in proximity of site BY01 since 1998, reporting a yearly average temperature of -2.8 °C (Boike *et al.*, 2018). The area is also monitored by the Italian eddy-covariance system hosted at the "Amundsen-Nobile Climate Change Tower" located eastward of BY01 and in close proximity to site CCT (Figure 1). The average temperature in the region in January ranges between -17.0 and -3.8 °C, while the mean July temperature ranges from 4.6 to 6.9 °C (Maturilli *et al.*, 2012).

Sampling methods

Sediment collection and handling

The sampling was carried out along a transect that flanks the Bayelva river, with the exception of a site located in the forefield of the Midtre Lovénbreen glacier. (Table 1) The exact location of each site was decided in the field during the winter, and at times several attempts were made digging snow pits with the aim of finding areas of soil with minimal rock cover to allow for easy drilling of the permafrost. At each location a snowpit of about 2×3 m was dug to allow at least two people to work inside. The thickness of the snow removed to create the snowpit was recorded, and varied between 19 and 105 cm per site, although in some attempts up to 185 cm of snow were removed. Permafrost depth was also recorded at each site (Table 2).

Coring of the permafrost was performed using a portable driller (Shaw Drill Sondaj, https://backpackdrill.com) equipped with a 41 mm diameter core barrel and a diamond drill bit. At each site three independent boreholes were drilled (Figure 3, Table 3). The presence of rocks at depth prevented complete recovery of all the cores. Once the core was extracted

Table 1. Site coordinates and soil temperatures.

				Soil temperature			
SiteID	Site name	Latitude (°N)	Longitude (°E)	Expedition 1 @ 2 cm (°C)	Expedition 2 @ 2 cm (°C)	Expedition 3 @ 2 cm (°C)	Notes
BY1	Bayelva 1	78.92102	11.83289	-1.6	7.8	4.3	Bayelva permafrost observatory (Boike *et al.*, 2018)
BY2	Bayelva 2	78.92315	11.83403	-3.4	5.8	4.9	
BY3	Bayelva 3	78.92743	11.82908	-5.4	7.7	4.9	
BY3A	Bayelva 3	78.92683	11.82886	NA	10.7	5.2	
BY4	Bayelva 4	78.93416	11.84456	-2.8	9.2	2.7	
BY5	Bayelva 5	78.93651	11.85860	-6.5	7.7	2.2	
ML1	Midtre Lovénbreen 1	78.90833	12.08157	-2.4	8	3.6	ST. 3 form J Bradley (QMUL, UK)
CCT	Climate ChangeTower	78.921367	11.865867	NA	8.1	5	

Table 2. Average depths of the active layer in the three expeditions for each site.

		Active layer depth (cm)		
SiteID	Site name	Expedition 1	Expedition 2	Expedition 3
BY1	Bayelva 1	0	30	35
BY2	Bayelva 2	0	20	26
BY3	Bayelva 3	0	5	20
BY3A	Bayelva 3	NA	20	23
BY4	Bayelva 4	0	25	27
BY5	Bayelva 5	0	15	31
ML1	Midtre Lovénbreen 1	0	35	33
CCT	Climate ChangeTower	NA	40	40

from the ground, the low external temperature immediately froze the material, often preventing the recovery of the intact core. Hot water was used to warm the external surface of the core barrel to allow core recovery (Figure 4). The cores were extracted by placing it on a sterile housing for photographic documentation and length measurements and then transferred into sterile Whirl-Pak sample bags. Either continuous intact cores or multiple core sections were recovered from each borehole. Cores were preserved frozen at -20 °C and returned to the laboratory for further analysis.

During the summer, we revisited the sampling sites previously surveyed in winter, and added one additional location (Table 1). Utilizing shovels and hand tools, we excavated rectangular soil pits, consistently digging from one side to maintain an intact wall. This approach aimed to facilitate soil sampling without the risk of disturbance or mixing. The excavated pits, ranging from 20 to 40 cm in depth, provided a stratified profile for comprehensive analysis (Table 4 and Table 5). At various depths within the excavated pits, sediment samples were collected and subsequently preserved in Whirl-Pak

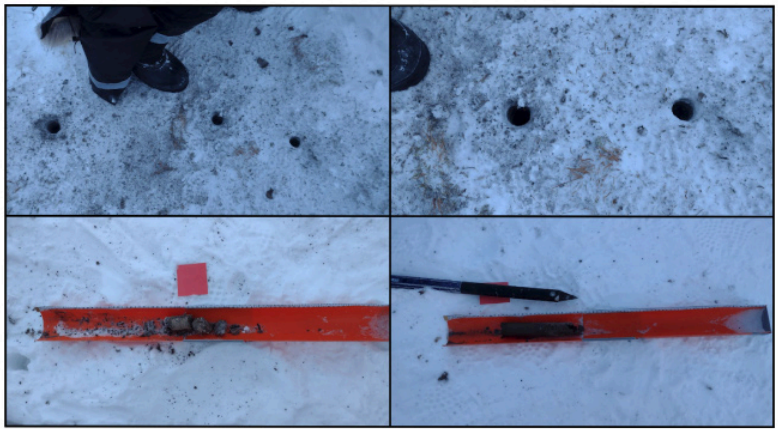

Figure 3. Panel showing snow pit and core operations. Photograph taken by author FM for this publication.

Table 3. List of boreholes and recovered cores in the first expedition, February 2022.

SiteID	Site name	CollectionID	Borehole	Drill depth (cm)	Core Recovery (%)
BY1	Bayelva 1	BY1220225	a	0–19	79
BY1	Bayelva 1	BY1220225	b	0–12	20
BY1	Bayelva 1	BY1220225	b	12–20	50
BY1	Bayelva 1	BY1220225	c	0–19	68
BY2	Bayelva 2	BY2220227	a	0–14	71
BY2	Bayelva 2	BY2220227	a	14–25	145*
BY2	Bayelva 2	BY2220227	b	0–14	121*
BY2	Bayelva 2	BY2220227	c	0–17.5	91
BY3	Bayelva 3	BY3220227	a	0–14	46
BY3	Bayelva 3	BY3220227	a	14–19	140*
BY3	Bayelva 3	BY3220227	b	0–13	NA
BY3	Bayelva 3	BY3220227	c	0–24	NA
BY3	Bayelva 3	BY3220227	c	24–32	175**
BY4	Bayelva 4	BY4220228	a	0–15	87
BY4	Bayelva 4	BY4220228	a	15–21	83
BY4	Bayelva 4	BY4220228	b	0–11	54
BY4	Bayelva 4	BY4220228	c	0–15	57
BY5	Bayelva 5	BY5220228	a	0–10	NA
BY5	Bayelva 5	BY5220228	a	10–23.5	111**
ML1	Midtre Lovénbreen 1	ML122031	a	0–17.5	NA
ML1	Midtre Lovénbreen 1	ML122031	a	17.5–22	NA

SiteID	Site name	CollectionID	Borehole	Drill depth (cm)	Core Recovery (%)
ML1	Midtre Lovénbreen 1	ML122031	a	22–27	130**
ML1	Midtre Lovénbreen 1	ML122031	b	0–11	NA
ML1	Midtre Lovénbreen 1	ML122031	b	11–18	157**
ML1	Midtre Lovénbreen 1	ML122031	c	0–7.3	NA

*Core expansion likely due to freezing upon retrieval and presence of unconsolidated layers

**Core recovery is overestimated due to collection of fragments from the drilling of the above section

Figure 4. Given the low air temperatures, the cores were freezing inside the barrel expanding and hindering easy recovery. Hot water was used to warm the external surface of the core barrel to allow for core extrusion. Photograph taken by a member of the first expedition JP for this publication.

Table 4. List of sites and sampled depths in the second expedition, June 2022.

SiteID	Site name	CollectionID	Depths sampled (cm)
BY1	Bayelva 1	BY1220614	0–5 / 10–15 / 20–30
BY2	Bayelva 2	BY2220614	0–5 / 10–15 / 20–25
BY3	Bayelva 3	BY3220614	0–5
BY3A	Bayelva 3	BY3A220614	0–5 / 10–15 / 20
BY4	Bayelva 4	BY4220619	0–5 / 10–15 / 20–25
BY5	Bayelva 5	BY5220619	0–5 / 10–15
ML1	Midtre Lovénbreen 1	ML1220615	0–5 / 10–15 / 20–30 / 30–40
CCT	Climate Change Tower	CCT220618	0–5 / 10–15 / 20–30 / 30–35

bags (Figure 5). All sampled soils are classified as Gelisoil (IUSS Working Group WRB, 2022).

Gas flux measurements

The diffuse gas flux from the soil surface, and at some sites from the snow surface, was measured using the accumulation chamber method (Chiodini *et al.*, 1998). Three different instrumentations were used. For the first expedition: 1) an in house built instrument by the University of Perugia, equipped with a LI-COR LI-820 Infra-Red detector (IR) for CO_2 set in a range from 0 to 5,000 ppm, connected with an accumulation chamber of ~2.8 L volume; 2) a West System© instrument, equipped with a LI-COR 820 IR for CO_2 set in a range from 0 to 20,000 ppm, with a Tunable Diode Laser Absorption Spectroscopy (TDLAS) detector for CH_4 and an electrochemical sensor for H_2S, connected with an accumulation chamber of ~2.8 L volume. For the second and the third expedition: 1) an in house built instrument by the University of Perugia, equipped with a LI-COR LI-820 Infra-Red detector (IR) for CO_2 set in a range from 0 to 5,000 ppm, connected with an accumulation chamber of ~2.8 L volume; 2) a Thearen © instrument, equipped with a LI-COR 830 IR for CO_2 set in a range from 0 to 20,000 ppm and a Tunable Diode Laser Absorption Spectroscopy (TDLAS) detector for CH_4 connected with an accumulation chamber of ~3.6 L volume. For the first survey the gas flux measurements from the permafrost surface were carried out after removing the layer of snow and ice present above the permafrost, which was instead left undisturbed. Measurements were performed at the sites of permafrost coring and nearby the Italian Arctic station "Dirigibile Italia", for comparison and instrumentation testing.

Gas samples collection

In the first expedition interstitial gas was sampled from the boreholes using a dedicated sampling probe (Figure 6a). The probe is made by an external body of plastic materials containing a stainless-steel capillary of about 3 mm of diameter. The probe is equipped with a series of 4 silicone gaskets at 2 cm from the bottom and every 15 cm, to allow the fitting of the probe to the drilled hole and preventing/limiting air contamination. The gas was collected in both 20 mL glass vials and pre-evacuated vacutainer for laboratory analyses of its chemical composition and of the isotopic composition of the carbon of CO_2. The gas was collected after purging the line using a syringe connected to a 3-way valve (Figure 6b). In the other two expeditions where coring was not performed, a stainless steel probe of 5 mm of diameter was used to reach the

Table 5. List of sites and sampled depths in the third expedition, September 2022.

SiteID	Site name	CollectionID	Depths sampled (cm)
BY1	Bayelva 1	BY1220930	0–5 / 10–15 / 20–25 / 30–35
BY2	Bayelva 2	BY220930	0–5 / 10–15 / 20–26
BY3	Bayelva 3	BY3220930	0–5 / 10–15 / 20
BY3A	Bayelva 3	BY3A220930	0–5 / 10–15 / 20–23
BY4	Bayelva 4	BY422103	0–5 / 10–15 / 20–27
BY5	Bayelva 5	BY422103	0–5 / 10–15 / 20–25 / 30–31
ML1	Midtre Lovénbreen 1	ML122101	0–5 / 10–15 / 20–25 / 30–35 / 40
CCT	Climate Change Tower	CCT220930	0–5 / 10–15 / 20–25 / 30–33

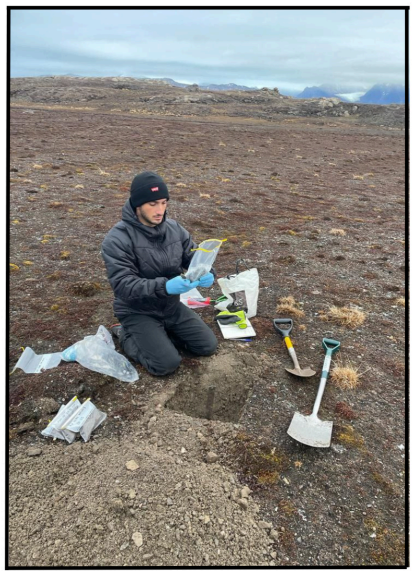

Figure 5. During the second and third expedition, the soil was collected and placed into a Whirl-Pak bag. Photograph taken by a member of third expedition MC for this publication.

desired depth in the soil and, in addition to vacutainer and glass vials, Tedlar and multi-layer foil gas sampling bags of 1 L were used to collect soil gas (Table 6, Table 7 and Table 8).

To characterize the isotopic composition of the carbon of CO_2 released by the permafrost surface, the gas accumulating in the accumulation chamber was sampled using two pre-evacuated vacutainers, one taken at the begin of the measurement and the other after some time, i.e., at higher CO_2 concentration. The time lapse between the two samples depends on the CO_2 flux, in order to ensure a significant difference in CO_2 concentration between the two samples (Chiodini *et al.*, 2008).

Sites and samples log

Details on the sampling locations are given in Table 1 and the underlying data (Montemagno *et al.*, 2024). The complete list of boreholes, pit and recovered cores and gas samples retrieved on the different expeditions are reported in Table 3, Table 4, Table 5 and Table 6. Soil in the selected areas consisted mainly of silty-clay with interspersed stones of various nature. Soil density was previously reported in this area with values of 1.70×10^3 kg m^{-3} and porosities varying from 0.36 to 0.5 (Roth & Boike, 2001).

Site 1 - Bayelva 1 (BY1)

The Bayelva 1 site (78.921000 °N, 11.832895 °E) is located in close proximity to the German Alfred Wegener Institute for Polar and Marine Research and the French Polar Institute Paul-Émile Victor (AWIPEV) Bayelva Permafrost monitoring site (Roth & Boike, 2001). The location is on the top of a moraine hill on the right bank of the Bayelva river.

The first sampling was performed during the winter season on February 24th 2022. At the time of this sampling, the site was covered by 60–70 cm of snow containing a few frozen layers on the top half of the snow cover. A snow pit of 2×2 m was dug to access the soil surface. The surface CO_2 and CH_4 fluxes were measured as described in the field protocols on the undisturbed surface of the permafrost. Additional measurements were made after removing the musk cover. Gas samples from the accumulation chamber were sampled at one site inside the pit. On February 24th 2022 we were unable to drill due to a malfunction of the portable core drill. On February 25th 2022 we returned to the site and successfully completed the sampling. The snow pit was cleaned up before starting drilling operations. The obtained cores were mainly composed of

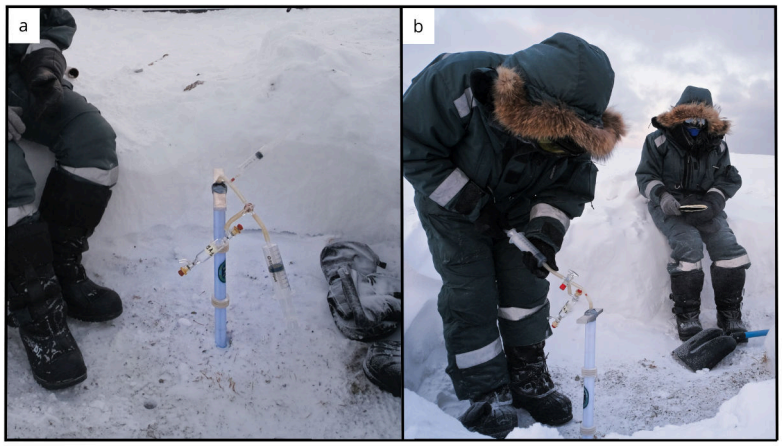

Figure 6. Permafrost borehole gas sampling apparatus. (**a**) Detailed view of gas sampling probe designed for the project. Inside the plastic body is placed a 1/8 inch stainless steel capillary. (**b**) the sampling probe inserted into a borehole during gas sampling operations. Photographs taken by a member of the first expedition JP for this publication.

Table 6. List of collected gas samples for the first expedition, February 2022.

SiteID	Site name	CollectionID	Borehole	Depth (cm)	AC sample	Glass vial	Vacutainer	Notes
BY1	Bayelva 1	F1A			x		x	
BY1	Bayelva 1	F1B			x		x	
BY1	Bayelva 1	BY1A	a	19		x		
BY1	Bayelva 1	BY1B	a	19		x		
BY1	Bayelva 1	BY1A	a	19			x	
BY1	Bayelva 1	BY1B	a	19			x	
BY2	Bayelva 2	BY2A1	a	25			x	
BY2	Bayelva 2	BY2A1	a	25		x		
BY2	Bayelva 2	BY2A2	b	14			x	
BY2	Bayelva 2	BY2A2	b	14		x		
BY2	Bayelva 2	BY2F10			x			
BY2	Bayelva 2	BY2F11			x			
BY2	Bayelva 2	BY2F12			x			bad sample
BY2	Bayelva 2	BY2F13			x			
BY2	Bayelva 2	BY2F14			x			
BY3	Bayelva 3	BY3A1					x	
BY3	Bayelva 3	BY3A1				x		
BY3	Bayelva 3	BY3F10	a	19	x			
BY3	Bayelva 3	BY3F11	a	19	x			
BY4	Bayelva 4	BY4A1	a	21		x		

SiteID	Site name	CollectionID	Borehole	Depth (cm)	AC sample	Glass vial	Vacutainer	Notes
BY4	Bayelva 4	BY4A2	a	21		x		
BY4	Bayelva 4	BY4A1	a	21			x	
BY4	Bayelva 4	BY4A1-B	a	21			x	
BY4	Bayelva 4	BY4F1			x			
BY4	Bayelva 4	BY4F4			x			
BY5	Bayelva 5	BY5A1	a	23.5			x	
BY5	Bayelva 5	BY5A1-B	a	23.5			x	
BY5	Bayelva 5	BY5A2	a	23.5			x	
BY5	Bayelva 5	BY5A1	a	23.5		x		
BY5	Bayelva 5	BY5A1-B	a	23.5		x		
BY5	Bayelva 5	BY5F1			x		x	On the snow
BY5	Bayelva 5	BY5F3			x		x	On the snow
BY5	Bayelva 5	BY5F4			x		x	On the snow
BY5	Bayelva 5	BY5F10			x		x	
BY5	Bayelva 5	BY5F11			x		x	
ML1	Midtre Lovénbreen 1	J3F1			x		x	No Flux measure
ML1	Midtre Lovénbreen 1	J3F2			x		x	No Flux measure
ML1	Midtre Lovénbreen 1	J3F3			x		x	No Flux measure
ML1	Midtre Lovénbreen 1	J3F4			x		x	No Flux measure
ML1	Midtre Lovénbreen 1	J3F6			x		x	No Flux measure
ML1	Midtre Lovénbreen 1	J3F7			x		x	No Flux measure
ML1	Midtre Lovénbreen 1	J3F8			x		x	No Flux measure
ML1	Midtre Lovénbreen 1	ML1A-1	a	17.5		x		
ML1	Midtre Lovénbreen 1	ML1A-1A	a	17.5			x	
ML1	Midtre Lovénbreen 1	ML1A-1B	a	17.5			x	
ML1	Midtre Lovénbreen 1	ML1A-2	a	22.0		x		
ML1	Midtre Lovénbreen 1	ML1A-2A	a	22			x	
ML1	Midtre Lovénbreen 1	ML1A-3A	a	27		x		
ML1	Midtre Lovénbreen 1	ML1A-3B	a	27		x		
ML1	Midtre Lovénbreen 1	ML1A-3A	a	27			x	

SiteID	Site name	CollectionID	Borehole	Depth (cm)	AC sample	Glass vial	Vacutainer	Notes
ML1	Midtre Lovénbreen 1	ML1A-3B	a	27			x	
ML1	Midtre Lovénbreen 1	ML1F10			x		x	
ML1	Midtre Lovénbreen 1	ML1F11			x		x	
ML1	Midtre Lovénbreen 1	ML1F12			x		x	
ML1	Midtre Lovénbreen 1	ML1F13			x		x	
BASE	Base 3	BASEF1			x			Ny-Ålesund base
BASE	Base 3	BASEF2			x			Ny-Ålesund base

Table 7. List of collected gas samples for the second expedition, June 2022.

SiteID	Site name	CollectionID	Depth (cm)	AC sample	Glass vial	Vacutainer	Gas bag	Notes
BY1		BY1B	30		x	x		water @40 cm
BY1	Bayelva 1	BY1B1	30			x		water @40 cm
BY1	Bayelva 1	BY1B2	30			x		water @40 cm
BY1	Bayelva 1	BY1A1	20				x	water @40 cm
BY1	Bayelva 1	BY1B	30				x	water @40 cm
BY1	Bayelva 1	BY1F1		x		x		
BY1	Bayelva 1	BY1F3		x		x		
BY1	Bayelva 1	BY1F5		x		x		
BY1	Bayelva 1	BY1F2		x		x		
BY1	Bayelva 1	BY1F4		x		x		
BY1	Bayelva 1	BY1F6		x		x		
BY2	Bayelva 2	BY2A1	20			x		
BY2	Bayelva 2	BY2A2	20			x		
BY2	Bayelva 2	BY2	20				x	
BY3A	Bayelva 3A	BY3A1	20			x		wet soil
BY3A	Bayelva 3A	BY3A2	40			x		wet soil
BY3A	Bayelva 3A	BY3AF1		x		x		wet soil
BY3A	Bayelva 3A	BY3AF3		x		x		wet soil
BY3A	Bayelva 3A	BY3AF2		x		x		wet soil
BY3A	Bayelva 3A	BY3AF4		x		x		
BY4	Bayelva 4	BY4A1	40			x		
BY4	Bayelva 4	BY4A2	40			x		

SiteID	Site name	CollectionID	Depth (cm)	AC sample	Glass vial	Vacutainer	Gas bag	Notes
BY4	Bayelva 4	BY4A	40		x		x	
BY4	Bayelva 4	BY4B1	20			x		
BY4	Bayelva 4	BY4B2	20			x		
BY4	Bayelva 4	BY4B3	20			x		
BY4	Bayelva 4	BY4B	20		x		x	
BY4	Bayelva 4	BY4F1		x		x		
BY4	Bayelva 4	BY4F2		x		x		
BY4	Bayelva 4	BY4F3		x		x		
BY4	Bayelva 4	BY4F4		x		x		
BY5	Bayelva 4	BY5A	40			x		
BY5	Bayelva 4	BY5B	40			x		
BY5	Bayelva 4	BY5	40		x		x	
BY5	Bayelva 4	BY5F		x				
BY5	Bayelva 4	BY5F11		x				
ML1	Midtre Lovénbreen 1	ML1A1	30			x		water @>30cm
ML1	Midtre Lovénbreen 1	ML1A2	30			x		water @>30cm
ML1	Midtre Lovénbreen 1	ML1A1	30		x		x	water @>30cm
ML1	Midtre Lovénbreen 1	ML1F1		x				
ML1	Midtre Lovénbreen 1	ML1F2		x				
ML1	Midtre Lovénbreen 1	ML1F3		x				
M1L	Midtre Lovénbreen 1	ML1F4		x				
CCT	Climate Change Tower	CCT1A1	40			x		
CCT	Climate Change Tower	CCT1A2	40			x		
CCT	Climate Change Tower	CCT1A	40		x		x	
CCT	Climate Change Tower	CCT1B1	20			x		
CCT	Climate Change Tower	CCT1B2	20			x		
CCT	Climate Change Tower	CCT1B	20		x		x	
CCT	Climate Change Tower	CCT1F1		x				
CCT	Climate Change Tower	CCT1F2		x				

fine-grained particles (silt and small rock debris). A total of 3 boreholes were drilled (Table 3), with recoveries ranging from 20 % to 79 %. Soil gasses were sampled from borehole *a*, at the bottom, to assess the composition and isotopic signature of CO_2. On March 5th 2022 surface CO_2 and CH_4 flux measurements were performed over the snow at several points in the area of the snow pit.

On the 14th of June 2022, we started performing the second sampling. Due to the warmer temperatures, the absence of snow allowed us to choose the best spot near the site sampled in February. We made a soil pit of 40×45 cm (Figure 7a) with a depth of 30 cm using a shovel; the surface soil temperature was 7.8 °C (Table 1). The site was characterized by clayey soil. We took samples of soil at 3 different depths (Table 4). In this season the soil was saturated with meltwater, and liquid water was present in the soil pit. For this reason, we collected, together with the usual samples, water samples. We took three sterivex filters (0.22 µm) after having filtered 360 mL of water for each one of them. We also collected two

Table 8. **List of collected gas samples for the third expedition, October 2022.**

SiteID	Site name	CollectionID	Depth (cm)	AC sample	Glass vial	Vacutainer	Gas bag	Notes
BY1		BY1A	40			x		
BY1		BY1A	40			x		
BY1		BY1A	40		x		x	
BY1		BY1B	20			x		
BY1		BY1B	20			x		
BY1		BY1B	20		x		x	
BY1		F7		x				
BY1		F8		x				
BY1		F9		x				
BY1		F10		x				
BY1		F11		x				
BY1		F12		x				
BY2		BY2A	20			x		water @40 cm
BY2		BY2B	20			x		water @40 cm
BY2		BY2A	20		x		x	water @40 cm
BY2		F13		x				
BY2		F14		x				
BY2		F15		x				
BY2		F16		x				
BY3A		BY3AA	40			x		
BY3A		BY3AA	40			x		
BY3A		BY3AA1	40			x		
BY3A		BY3AA2	40			x		
BY3A		BY3AA	40		x		x	
BY3A		BY3AB	20			x		
BY3A		BY3AB	20			x		
BY3A		BY3AB	20		x		x	
BY3A		F17		x				
BY3A		F18		x				
BY3A		F19		x				
BY3A		F20		x				
BY4		BY4A1	40			x		
BY4		BY4A2	40			x		
BY4		BY4A	40		x		x	
BY4		BY4B1	20			x		
BY4		BY4B2	20			x		
BY4		BY4B	20		x		x	
BY4		F21		x				
BY4		F22		x				

SiteID	Site name	CollectionID	Depth (cm)	AC sample	Glass vial	Vacutainer	Gas bag	Notes
BY4		F23		x				
BY4		F24		x				
BY4		F25		x				
BY4		F26		x				
BY5		BY5A1	40			x		
BY5		BY5A2	40			x		
BY5		BY5A	40		x		x	
BY5		BY5B1	20			x		
BY5		BY5B2	20			x		
BY5		BY5B	20		x		x	
CCT		CCT1A	40			x		
CCT		CCT1A	40		x		x	
CCT		CCT1B	20			x		
CCT		CCT1B	20		x		x	
CCT		F1		x				
CCT		F2		x				
CCT		F3		x				
CCT		F4		x				
CCT		F5		x				
CCT		F6		x				
ML		ML1A1	40			x		
ML		ML1A2	40			x		
ML		ML1A	40		x		x	
ML		ML1B1	20			x		
ML		ML1B2	20			x		
ML		ML1B	20		x		x	
ML		FML1		x				
ML		FML2		x				
ML		FML3		x				
ML		FML4		x				
ML		FML5		x				
ML		FML6		x				
SUN2		SUN2A	40			x		
SUN2		SUN2A	40				x	
SUN2		SUN2B	20			x		
SUN2		F1SUN		x				
SUN2		F2SUN		x				
SUN2		F3SUN		x				
SUN2		F4SUN		x				

Figure 7. Site BY1 (**a**) in June, after digging 30 cm of soil. In (**b**) September we reach 35 cm of depth. Obviously without snow it was an easier sampling. Photographs taken by a member of the second expedition FM for this publication.

50 mL falcons of filtered water and a 10 mL vial. Soil gas samples were collected using the stainless steel probe inserted into the soil next to the pit. Soil CO_2 and CH_4 flux measurements were performed at several points in the area of the pit. At several locations around the pit gas samples from the accumulation chamber were also collected. During the sampling of this site on the second expedition, we also collected approximately 1 kg of sediment near our soil pit to conduct a microcosm experiment to track the release of greenhouse gasses by the microbial community.

The third and last sampling was performed on the 30th of September 2022. At this time, there was no liquid water in the area and the tundra was mostly dry. We collected soil samples at three depths (Table 5). The soil was still thawed, and we proceeded as the second sampling, avoiding the use of the drill. Soil gas samples were collected using the stainless steel probe inserted into the soil next to the sediment sampling point. Soil CO_2 and CH_4 flux measurements were measured at several locations in the area of the sampling point. At several locations, gas samples from the accumulation chamber were also collected.

Site 2 - Bayelva 2 (BY2)

The Bayelva 2 site (78.92315 °N, 11.83403 °E) is located 232 m northward from Bayelva 1 site, and it is the second site of a transect that follows the Bayelva river and goes from the main river watershed to the sea. The site is located on a flat area on the right bank of the Bayelva river and is surrounded by two main moraine hills (Kolhaugen and Leirhaugen) (Figure 8a). At the time of sampling, the site was covered by 80–90 cm of snow containing a few frozen layers on the top half of the snow cover. On February 27th 2022 a snow pit of 2×2 m was dug, and a total of 3 boreholes were drilled (Table 3). The obtained cores were mainly composed of fine-grained particles (silt and small rock debris), with recoveries ranging from 71 % to 145 %. Soil gasses were sampled from boreholes *a* and *b* inserting the probe up to the hole bottom. The surface CO_2 and CH_4 fluxes were measured as described before inside the pit and at one location gas samples from the accumulation chamber were sampled. CO_2 and CH_4 fluxes measurements from the snow surface were performed on March 5th 2022.

We sampled the BY2 site for the second time on June 14th 2022 (Table 2). We made a 35×40 cm pit that had a surface temperature of 5.8 °C and was 25 cm in depth (Figure 8b). We collected samples at three depths (Table 4). During this time of the year, we did not find snow and the sediment we collected was gravelly.

On 30th September 2022 during the third expedition we took the same number of samples in this site (Figure 8c, Table 3 and Table 5). The surface temperature was 4.9 °C.

In both the second and third expedition soil gas samples were collected using the stainless steel probe inserted into the soil in the proximity to the soil pit, and soil CO_2 and CH_4 flux measurements were performed in the area of the pit and gas samples from the accumulation chamber were collected at several flux measuring points (Table 6, Table 7 and Table 8)

Site 3 - Bayelva 3 (BY3)

The Bayelva 3 site (78.92743 °N, 11.82908 °E) is located 492 m northward from the previous site, Bayelva 2, following the transect direction towards the sea. The site is located in the floodplain area of the Bayelva river (Figure 9a). At the time of sampling, the site was covered by 100–105 cm of snow

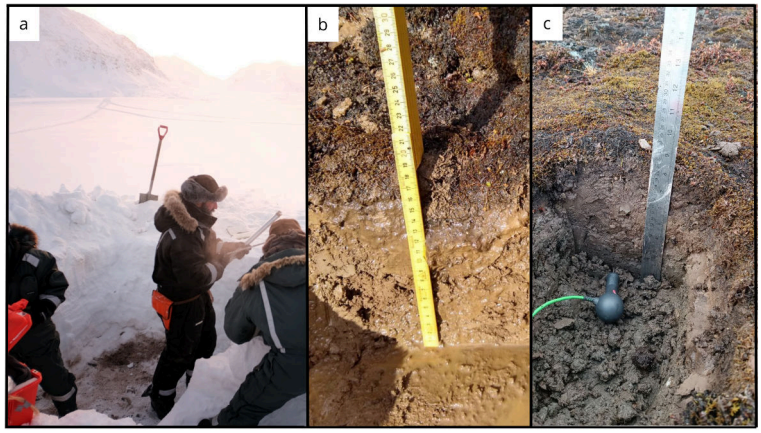

Figure 8. (**a**) Midday at the site Bayelva BY2 before starting the gas flux measurements during the first expedition. (**b**) In the second expedition we observed that the area of our site was covered with rocks, and the terrain was saturated with water. (**c**) In September, there was significantly less water and we were able to excavate to a greater depth. Photographs taken by members of the first expedition JP and FM for this publication.

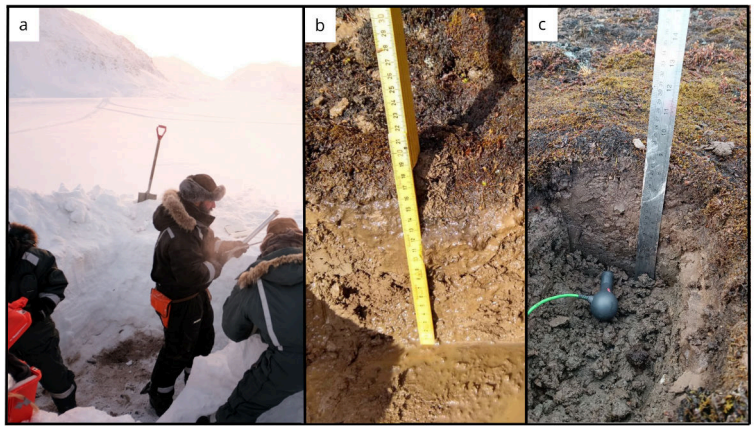

Figure 9. (**a**) Core extrusion operations at site Bayelva BY3 in February. (**b**) In June, the site BY3 was located close to the river banks and, as a result, the soil was filled with sand and water. To address this issue, we relocated BY3 (BY3A) to sample the soil. In September (**c**) samples were collected from both sites (BY3 and BY3A). Photographs taken by members of the first expedition JP and FM for this publication.

containing a few frozen layers on the top half of the snow cover. A 2×2 m snow pit was dug on February 27th 2022. Three boreholes were drilled (Table 2), with recoveries ranging from 46 % to 175 %. The obtained cores were mainly composed of fine-grained particles (silt and small rock debris).

Soil gasses were sampled from the borehole *a* bottom. The surface CO_2 and CH_4 fluxes were measured as described before leaving the permafrost undisturbed and at one location gas samples from the accumulation chamber were collected. The surface CO_2 and CH_4 fluxes measurements from the snow surface were performed on March 5th 2022.

We sampled this site for the second time on 14th June 2022. Once on site, we observed that the melt river flowed very close to the original BY3 location and the soil was rich in

water. We sampled a single depth at this location characterized by silt and sand and relocated for sampling on the river embankment where we made a second pit BY3A (78.926336 °N, 11.826033 °E) (Figure 9b). From this 40×45 cm pit we took samples from three depths. We also sampled river waters for microbiological and geochemical analyses. Near the BY3A site, we also collected approximately 1 kg of sediment during the second expedition, as we did near BY1 during the same expedition.

On 30th September 2022 we repeated the sampling for the third time (Figure 9c). We took soil samples at one depth in BY3 and at three depths in BY3A, and we also collected fluid samples from the river. We also took three sterivex filters (0.22 µm) after having filtered 360 mL of water for each one of them.

In June and September 2022 soil gas sampling, CO_2 flux and CH_4 flux measurements were performed at BY3A and its surrounding. Soil gas samples were collected using the stainless steel probe inserted into the soil. Gas samples from the accumulation chamber were collected at several flux measuring points.

Site 4 - Bayelva 4 (BY4)

The Bayelva 4 site (78.93435 °N, 11.84205 °E) is located 825 m NNE from the previous site, Bayelva 3, and it is located on the riverbank of the Bayelva, close to the river's delta. This site was sampled on February 28th 2022. At the time of sampling, the site was covered by 19 cm of snow, without any frozen layer, and a 2×2 m snow pit was dug. Before reaching this site, two other sites were inspected, but rock and ice layers did not allow for drilling. Moving closer to the riverbank allowed us to find a better spot for the drilling. The surface CO_2 and CH_4 fluxes were measured as described before leaving the permafrost undisturbed. Three boreholes were drilled (Table 3), with recoveries ranging from 54 % to 87 %. Soil gasses were sampled from borehole *a* to assess both composition and isotopic signature. The obtained cores were mainly composed of fine grained particles (silt and small rock debris). The surface CO_2 and CH_4 fluxes measurements from the snow surface were performed on March 5th 2022.

The second sampling of this site, during the summer campaign, was programmed on the 16th June 2022. The presence of polar bears nearby the site made us postpone the sampling up to the 19th June 2022. The surface soil temperature was 9.2 °C and we took three soil samples from the 40×40 cm soil pit. During the third expedition, we collected three soil samples from different depths on October 3th 2022 (Figure 10). River water at this site was sampled during the September expedition for microbiological and geochemical analyses. River water temperature was 1.7 °C. We took three sterivex filters (0.22 µm) after having filtered 180 mL of water for each one of them.

Figure 10. The BY4 site during the last expedition, 27 cm of depth was reached (Table 4). Photograph taken by members of the third expedition FM for this publication.

In June and October 2022 campaigns soil gas samples were collected using the stainless steel probe inserted into the soil, CO_2 flux and CH_4 flux measurements were performed at several points and gas samples from the accumulation chamber were collected at several flux measuring points.

Site 5 - Bayelva 5 (BY5)

The Bayelva 5 site (78.93613 °N, 11.85982 °E) is located 434 m ENE from the previous site, Bayelva 4, and it is located in the Bayelva river's delta. At the time of sampling, the site was covered by 48.5 cm of snow and 20 cm of ice. The site was sampled on February 28th 2022, and a 1×1 m snow pit was dug. The surface CO_2 and CH_4 fluxes were measured as described before, leaving the permafrost undisturbed. In this site, because of the large amount of rocks and ice, we were able to drill a single borehole (Table 3), with a recovery of 111 %. Soil gasses were sampled from the borehole to assess both composition and isotopic signature. The obtained core was mainly composed of fine grained particles (silt and small rock debris). The snow surface CO_2 and CH_4 flux measurements were repeated on March 5th 2022.

In the summer BY5 was sampled on June 19th 2022 in a location closest to the sea and in close proximity with the winter site. We collected soil samples at two depths and sampled water in the proximity of the soil pit. Soil surface temperature was 7.7 °C.

On the third expedition in September 2022 we sampled four different depths in the BY5 site and we also sampled the water river that had a temperature of 1.7 °C. The sampled location was approximately 30 m away from the previous location

due to a change in the river course compared to June 2022 (Figure 11).

In June and September 2022 sampling campaigns soil gas samples were collected using the stainless steel probe inserted into the soil, CO_2 flux and CH_4 flux measurements were performed at several points and gas samples from the accumulation chamber were collected at several flux measuring points.

Site 6 - Midtre Lovénbreen 1 (ML1)

The Midtre Lovénbreen 1 site (78.90833 °N, 12.08157 °E) is located in a plain in front of the glacier Midtre Lovénbreen between the two main melt channels. This site was chosen as more representative of tundra soils and devoid of moraine deposits, unlike previous sites where rocks were often found. The ML1 site was sampled two times in the first expedition, the first on March 1st 2022 and the second on March 3rd 2022. On the first day of sampling a 2×2 m snow pit was dug and three boreholes were drilled (Table 3), with recoveries ranging from 130 % to 157 %. The obtained cores were mainly composed of fine grained particles (silt and small rock debris). Soil gasses were sampled from borehole *a* to assess both composition and isotopic signature. During the first day, radio silence imposed for the Ny-Ålesund area due to ongoing radiometric measurements at the local station did not allow for the use of the bluetooth device for the measurement of CO_2, CH_4 and H_2S fluxes. On the second sampling, two 1×1 m snow pits were dug to measure the surface CO_2, CH_4 and H_2S fluxes leaving the permafrost undisturbed.

Figure 11. The BY5 site during the September expedition (Table 4). Photograph taken by members of the third expedition FM for this publication.

During the second expedition in June we sampled soil at four different depths and sampled water from a pool near our site (Figure 12a). The soil surface temperature was 8 °C.

Water was absent during the third expedition and soil samples were collected at five different depths (Figure 12b). The soil surface temperature was 4.3 °C.

In June and September 2022 sampling campaigns soil gas samples were collected using the stainless steel probe inserted into the soil, CO_2 flux and CH_4 flux measurements were performed at several points and gas samples from the accumulation chamber were collected at several flux measuring points.

Site 7 - Climate Change Tower (CCT)

The CCT site (78.921367 °N 11.865867 °E) is in close proximity to the Climate Change Tower (CCT). The location is on the top of a moraine hill, overlooking the Bayelva river valley and the Bayelva permafrost observatory. This site was added during the June expedition due to the presence of polar bears near Bayelva sites BY4 and BY5. In the first sampling activity of this site, during the June expedition, we made a hole of 35 cm depth (Figure 13a). We took samples from four

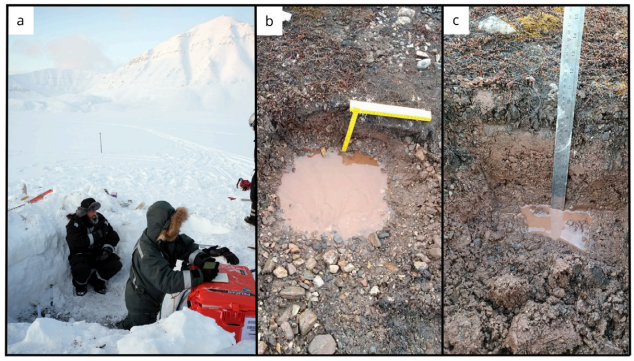

Figure 12. (**a**) In June, the soil exhibited a high moisture content, as evidenced by the imagery from site ML1. (**b**) However, by September, the water content had significantly decreased. (**c**) During our most recent expedition, we were able to locate the boreholes created using the drilling equipment during the winter season. Flare gun used for scale. Photographs taken by a member of the second and third expedition FM for this publication.

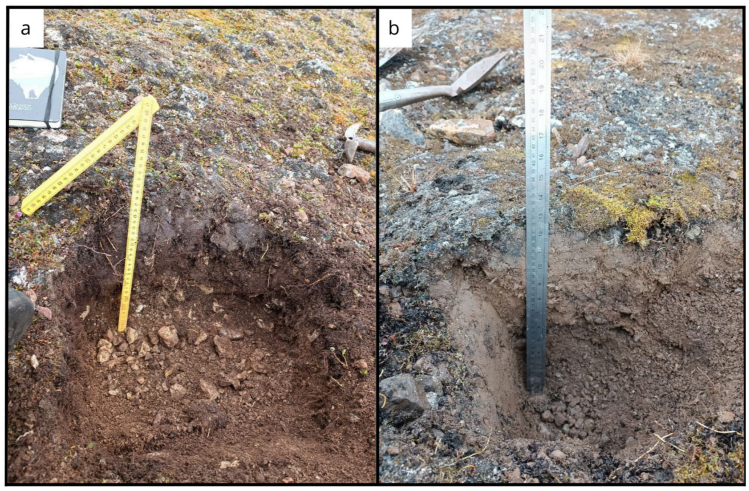

Figure 13. Site CCT near the Climate Change Tower in (**a**) October and (**b**) June. Photographs taken by a member of the second and third expedition FM for this publication.

different depths. In the third expedition instead, we reached 33 cm of depth (Figure 13b) and collected samples at four different depths.

Conclusion

The three expeditions collected coupled gas geochemistry, soil geochemistry and microbiological samples from 7 sites representative of the different conditions found in the area around Ny-Ålesund, Svalbard. The data obtained will present a clear picture of the coupling between microbiological and gas geochemistry during the seasonal melting cycle of the active layer. These data, coupled with the results of the incubation experiments carried out during the second expedition, represent a significant opportunity to characterize in detail the geo-microbiological response to active layer thaw in the high arctic.

Data and software availability

No data have been produced for this study. The expedition site and metadata have been uploaded to the CoEvolve Database (www.coevolvedb.org) and are available through the GitHub repository https://github.com/giovannellilab/PRA_MeltingICE and made available with Zenodo: giovannellilab/PRA_MeltingICE: Data behind the PRA expedition report, under DOI https://doi.org/10.5281/zenodo.10969986 (Montemagno *et al.*, 2024).

This project contains the following underlying data:

- Giovannellilab-PRA_MeltingICE-61b6c16
- PRA_MeltingICE_table1.csv
- PRA_MeltingICE_table2.csv
- PRA_MeltingICE_table3.csv
- PRA_MeltingICE_table4.csv
- PRA_MeltingICE_table5.csv
- PRA_MeltingICE_table6.csv
- PRA_MeltingICE_table7.csv
- PRA_MeltingICE_table8.csv
- README.md

Data is available under the terms of the Creative Commons Attribution 4.0 International

Author contributions

All authors contributed equally to this paper.

Acknowledgements

The authors wish to acknowledge the support of the Institute of Polar Science of the Italian National Research Council (CNR-ISP) and the CNR "Dirigibile Italia" Italian Arctic Station in Ny-Ålesund, Svalbard, for logistic support. The author also acknowledged the UK Arctic Research Station in Ny-Ålesund, Svalbard, for logistic support during the third expedition.

References

Boike J, Juszak I, Lange S, *et al.*: **A 20–year record (1998–2017) of permafrost, active layer and meteorological conditions at a high Arctic permafrost research site (Bayelva, Spitsbergen).** *Earth Syst Sci Data.* 2018; **10**(1): 355–390.
Publisher Full Text

Chiodini G, Caliro S, Cardellini C, *et al.*: **Carbon isotopic composition of soil CO_2 efflux, a powerful method to discriminate different sources feeding soil CO_2 degassing in volcanic-hydrothermal areas.** *Earth Planet Sci Lett.* 2008; **274**(3–4): 372–379.
Publisher Full Text

Chiodini G, Cioni R, Guidi M, *et al.*: **Soil CO_2 ¯ux measurements in volcanic and geothermal areas**. *Appl Geochem.* 1998; **13**(5): 543–552.
Publisher Full Text

Cianfarra P, Salvini F: **Quantification of fracturing within fault damage zones affecting Late Proterozoic carbonates in Svalbard.** *Rendiconti Lincei.* 2016; **27**(Suppl 1): 229–241.
Publisher Full Text

Cimpoiasu MO, Kuras O, Harrison H, *et al.*: **Characterization of a deglaciated sediment chronosequence in the high arctic using near-surface geoelectrical monitoring methods.** *Permafr Periglac Process.* 2024a; **35**(2): 157–171.
Publisher Full Text

Cimpoiasu MO, Kuras O, Harrison H, *et al.*: **High-resolution 4D ERT monitoring of recently deglaciated sediments undergoing freeze-thaw transitions in the High Arctic**. 2024b.
Publisher Full Text

Giovannelli D: **Trace metal availability and the evolution of biogeochemistry.** *Nat Rev Earth Environ.* 2023; **4**: 597–598.
Publisher Full Text

Graham DE, Wallenstein MD, Vishnivetskaya TA, *et al.*: **Microbes in thawing permafrost: the unknown variable in the climate change equation.** *ISME J.* 2012; **6**(4): 709–712.
PubMed Abstract | Publisher Full Text | Free Full Text

Graversen RG, Mauritsen T, Tjernström M, *et al.*: **Vertical structure of recent Arctic warming.** *Nature.* 2008; **451**(7174): 53–56.
PubMed Abstract | Publisher Full Text

Hayes DJ, Kicklighter DW, McGuire AD, *et al.*: **The impacts of recent permafrost thaw on land–atmosphere greenhouse gas exchange.** *Environ Res Lett.* 2014; **9**: 045005.
Publisher Full Text

Humlum O, Instanes A, Sollid JL: **Permafrost in Svalbard: a review of research history, climatic background and engineering challenges.** *Polar Res.* 2003; **22**(2): 191–215.
Publisher Full Text

Isaksen K, Benestad RE, Harris C, *et al.*: **Recent extreme near-surface permafrost temperatures on Svalbard in relation to future climate scenarios.** *Geophys Res Lett.* 2007; **34**(17).
Publisher Full Text

IUSS Working Group WRB: **World Reference Base for Soil Resources. International soil classification system for naming soils and creating legends for soil maps.** 4th Edn. Vienna, Austria: International Union of Soil Sciences (IUSS), 2022.
Reference Source

Jansson JK, Taş N: **The microbial ecology of permafrost.** *Nat Rev Microbiol.* 2014; **12**(6): 414–425.
PubMed Abstract | Publisher Full Text

Keating K, Binley A, Bense V, *et al.*: **Combined geophysical measurements provide evidence for unfrozen water in permafrost in the Adventdalen valley in Svalbard.** *Geophys Res Lett.* 2018; **45**(15): 7606–7614.
Publisher Full Text

Loganathachetti DS, Venkatachalam S, Jabir T, *et al.*: **Total nitrogen influence bacterial community structure of active layer permafrost across summer and winter seasons in Ny-Ålesund, Svalbard.** *World J Microbiol Biotechnol.* 2022; **38**(2): 28.
PubMed Abstract | Publisher Full Text

Martín-Moreno R, Allende Álvarez F, Hagen JO: **'Little Ice Age' glacier extent and subsequent retreat in Svalbard archipelago.** *Holocene.* 2017; **27**(9): 1379–1390.
Publisher Full Text

Maturilli M, Herber A, König-Langlo G: **Climatology and time series of surface meteorology in Ny-Ålesund, Svalbard.** *Earth Syst Sci Data.* 2012; **5**(2): 1057–1076.
Publisher Full Text

Miner KR, Turetsky MR, Malina E, *et al.*: **Permafrost carbon emissions in a changing Arctic.** *Nat Rev Earth Environ.* 2022; **3**: 55–67.
Publisher Full Text

Montemagno F, Giovannelli D, Corso D: **giovannellilab/PRA_MeltingICE: data behind the PRA expedition report (v2.0).** *Zenodo.* Dataset. 2024.
http://www.doi.org/10.5281/zenodo.12743100

Nikrad MP, Kerkhof LJ, Häggblom MM: **The subzero microbiome: microbial activity in frozen and thawing soils.** *FEMS Microbiol Ecol.* 2016; **92**(6): fiw081.
PubMed Abstract | Publisher Full Text

Roth K, Boike J: **Quantifying the thermal dynamics of a permafrost site near Ny-Ålesund, Svalbard.** *Water Resour Res.* 2001; **37**(12): 2901–2914.
Publisher Full Text

Sadiq M, Dutta S, Kumar P, *et al.*: **Ice dynamics of Vestre Brøggerbreen glaciers, Ny-Ålesund, Svalbard, Arctic.** *J Earth Syst Sci.* 2022; **131**(1): 1–15.
Publisher Full Text

Schostag M, Stibal M, Jacobsen CS, *et al.*: **Distinct summer and winter bacterial communities in the active layer of Svalbard permafrost revealed by DNA- and RNA-based analyses.** *Front Microbiol.* 2015; **6**: 399.
PubMed Abstract | Publisher Full Text | Free Full Text

Serreze MC, Barry RG: **Processes and impacts of Arctic amplification: a research synthesis.** *Glob Planet Change.* 2011; **77**(1–2): 85–96.
Publisher Full Text

Sipes K, Paul R, Fine A, *et al.*: **Permafrost active layer microbes from Ny Ålesund, Svalbard (79°N) show Autotrophic and Heterotrophic Metabolisms with diverse carbon-degrading enzymes.** *Front Microbiol.* 2022; **12**: 757812.
PubMed Abstract | Publisher Full Text | Free Full Text

Smith SL, O'Neill HB, Isaksen K, *et al.*: **The changing thermal state of permafrost.** *Nat Rev Earth Environ.* 2022; **3**: 10–23.
Publisher Full Text

Streletskiy D, Biskaborn BK, Smith S, *et al.*: **Strategy and implementation plan 2016–2020 for the Global Terrestrial Network for Permafrost (GTN-P)**. 2017.
Reference Source

Tepes P, Gourmelen N, Nienow P, *et al.*: **Changes in elevation and mass of Arctic glaciers and ice caps, 2010–2017.** *Remote Sens Environ.* 2021; **261**: 112481.
Publisher Full Text

Van Everdingen RO: **Glossary_of_Permafrost_and_Ground-Ice_IPA_ 2005.pdf**. 1981; (Accessed June 18, 2022).
Reference Source

Vickers H, Malnes E, van Pelt WJJ, *et al.*: **A compilation of snow cover datasets for Svalbard: a multi-sensor, multi-model study.** *Remote Sens.* 2021; **13**(10): 2002.
Publisher Full Text

Vigneron A, Lovejoy C, Cruaud P, *et al.*: **Contrasting winter versus summer microbial communities and metabolic functions in a Permafrost Thaw Lake.** *Front Microbiol.* 2019; **10**: 1656.
Publisher Full Text

Walsh JE: **Intensified warming of the Arctic: causes and impacts on middle latitudes.** *Glob Planet Change.* 2014; **117**: 52–63.
Publisher Full Text

Walvoord MA, Striegl RG: **Increased groundwater to stream discharge from permafrost thawing in the Yukon River basin: potential impacts on lateral export of carbon and nitrogen.** *Geophys Res Lett.* 2007; **34**(12).
Publisher Full Text

microorganisms

MDPI

Review

Unveiling the Bioleaching Versatility of *Acidithiobacillus ferrooxidans*

Luca Tonietti [1,2,3,4,*], Mattia Esposito [3], Martina Cascone [3], Bernardo Barosa [3], Stefano Fiscale [1,2], Maria Teresa Muscari Tomajoli [1,2], Tomasa Sbaffi [5], Rosa Santomartino [6], Giovanni Covone [4,7], Angelina Cordone [3], Alessandra Rotundi [1,8] and Donato Giovannelli [3,9,10,11,12,*]

[1] Department of Science and Technology, University Parthenope, 80143 Naples, Italy; stefano.fiscale001@studenti.uniparthenope.it (S.F.); mariateresa.muscaritomajoli001@studenti.uniparthenope.it (M.T.M.T.); alessandra.rotundi@uniparthenope.it (A.R.)
[2] International PhD Programme/UNESCO Chair "Environment, Resources and Sustainable Development", 80143 Naples, Italy
[3] Department of Biology, University Federico II, 80126 Naples, Italy; mattiaesposito253@gmail.com (M.E.); martina.cascone1995@gmail.com (M.C.); bernard.barosa@gmail.com (B.B.); angelina.cordone77@gmail.com (A.C.)
[4] INAF-OAC, Osservatorio Astronomico di Capodimonte, 80137 Naples, Italy; giovanni.covone@unina.it
[5] Molecular Ecology Group (MEG), National Research Council of Italy—Water Research Institute (CNR-IRSA), 28922 Verbania, Italy; tomasa.sbaffi@gmail.com
[6] UK Centre for Astrobiology, School of Physics and Astronomy, University of Edinburgh, Edinburgh EH8 9YL, UK; rosa.santomartino@ed.ac.uk
[7] Department of Physics, University of Naples Federico II, 80126 Naples, Italy
[8] INAF-IAPS, Istituto di Astrofisica e Planetologia Spaziali, 00133 Rome, Italy
[9] National Research Council, Institute of Marine Biological Resources and Biotechnologies, CNR-IRBIM, 60125 Ancona, Italy
[10] Department of Marine and Coastal Science, Rutgers University, New Brunswick, NJ 08901, USA
[11] Marine Chemistry & Geochemistry Department, Woods Hole Oceanographic Institution, Falmouth, MA 02543, USA
[12] Earth-Life Science Institute, ELSI, Tokyo Institute of Technology, Tokyo 152-8550, Japan
* Correspondence: luca.tonietti001@studenti.uniparthenope.it (L.T.); donato.giovannelli@unina.it (D.G.)

check for updates

Citation: Tonietti, L.; Esposito, M.; Cascone, M.; Barosa, B.; Fiscale, S.; Muscari Tomajoli, M.T.; Sbaffi, T.; Santomartino, R.; Covone, G.; Cordone, A.; et al. Unveiling the Bioleaching Versatility of *Acidithiobacillus ferrooxidans*. *Microorganisms* **2024**, *12*, 2407. https://doi.org/10.3390/microorganisms12122407

Academic Editor: Shoushuai Feng

Received: 29 October 2024
Revised: 20 November 2024
Accepted: 21 November 2024
Published: 23 November 2024

Copyright: © 2024 by the authors. Licensee MDPI, Basel, Switzerland. This article is an open access article distributed under the terms and conditions of the Creative Commons Attribution (CC BY) license (https://creativecommons.org/licenses/by/4.0/).

Abstract: *Acidithiobacillus ferrooxidans* is a Gram-negative bacterium that thrives in extreme acidic conditions. It has emerged as a key player in biomining and bioleaching technologies thanks to its unique ability to mobilize a wide spectrum of elements, such as Li, P, V, Cr, Fe, Ni, Cu, Zn, Ga, As, Mo, W, Pb, U, and its role in ferrous iron oxidation and reduction. *A. ferrooxidans* catalyzes the extraction of elements by generating iron (III) ions in oxic conditions, which are able to react with metal sulfides. This review explores the bacterium's versatility in metal and elemental mobilization, with a focus on the mechanisms involved, encompassing its role in the recovery of industrially relevant elements from ores. The application of biomining technologies leveraging the bacterium's natural capabilities not only enhances element recovery efficiency, but also reduces reliance on conventional energy-intensive methods, aligning with the global trend towards more sustainable mining practices. However, its use in biometallurgical applications poses environmental issues through its effect on the pH levels in bioleaching systems, which produce acid mine drainage in rivers and lakes adjacent to mines. This dual effect underscores its potential to shape the future of responsible mining practices, including potentially in space, and highlights the importance of monitoring acidic releases in the environment.

Keywords: *Acidithiobacillus ferrooxidans*; acidophiles; biomining; bioleaching; biorecovery; chemical elements

1. Introduction

Extreme acidophilic microorganisms, which thrive in highly acidic conditions with a pH below 2.5 [1], are of particular importance in the biometallurgy context because they facilitate the mobilization of a diverse array of elements, including transition metals. This is

achieved as a result of a spectrum of reactions involving various elements from the periodic table, through a process known as bioleaching [2–5]. Extremophiles are optimal microorganisms for developing mining applications on Earth [6–8], as well as in space [9–11]. For instance, as shown by Cockell et al. (2020), the extremophilic *Cupriavidus metallidurans* and the mesophilic *Sphingomonas desiccabilis*, through experiments with simulated Mars and Earth gravity on the International Space Station (ISS), have demonstrated key biomining capabilities of economically fundamental elements in space [9]. On the other hand, Tonietti et al. (2023) recently reported a shift in focus to acidophiles as the future avenue of space biomining, with *Acidithiobacillus ferrooxidans* being the prime candidate [11].

The Acidithiobacillaceae family, part of the Gammaproteobacteria class, encompasses acidophilic bacteria adept at surviving in extremely acidic environments [12]. These chemolithoautotrophs derive energy through the oxidation of inorganic compounds and fix carbon dioxide as their carbon source, significantly contributing to the biogeochemical cycling of sulfur and iron [13]. *A. ferrooxidans* and other members of the Acidithiobacillaceae family are widely acknowledged for their ability to mobilize a variety of elements, including metals and metalloids, amidst extreme conditions [12,14]. Their metabolism harnesses inorganic energy sources, such as Fe^{2+}, H_2S, S^0, and molecular hydrogen, to sustain their metabolic activities [15] (Figure 1A).

Among the Acidithiobacillaceae, *A. ferrooxidans* (formerly known as *Thiobacillus ferrooxidans*) is notably well studied. This Gram-negative, rod-shaped gammaproteobacterium is renowned for its ability to oxidize ferrous iron to ferric iron and different reduced forms of sulfur compounds to sulfate. This organism was first isolated from the acidic water and sediments of a coal mine drainage in 1947. It was identified due to its ability to oxidize ferrous iron and sulfur compounds, leading to the production of acid which contributes to the acidic condition of the mine drainage environment. *A. ferrooxidans* thrives in highly acidic environments, typically within a pH range of 1.5 to 2.5. Its genome encodes enzymes critical for iron and sulfur oxidation, as well as mechanisms for adapting to acidic conditions [12]. The metabolism of the organism can be divided into different sections starting from the outer membrane, in which the process of iron oxidation occurs thanks to the presence of a specific electron transfer cytochrome c protein known as Cyc2. Many other different electron transfer molecules are used, such as the cytochrome c4, the cytochrome c552, the bc1 complex, and the cytochrome aa3 oxidase. All of these systems are part of the electron transport chain (ETC), in which electrons from Fe^{2+} are transferred to the inner membrane where the ETC is located. Within the oxidation of iron, *A. ferrooxidans* is also able to oxidize reduced sulfur compounds such as elemental sulfur, thiosulfate, and tetrathionate through different enzymes, e.g., the sox system (soxAX, soxB, soxCD, and soxYZ), sulfide oxidoreductase (SQR), and sulfur dioxygenase (SDO). Being an autotroph, the carbon source is the carbon dioxide (CO_2), which can be used through the Calvin–Benson–Bassham cycle (CBB). Ecologically, Acidithiobacillaceae are predominantly found in environments such as acid mine drainage, sulfuric hot springs, and sulfide mineral deposits [16]. They are key players in biomining, facilitating the extraction of metals from ores through bioleaching. *A. ferrooxidans* is frequently associated with mine tailings and acidic drainage waters, contributing significantly to the oxidation of pyrite and other sulfide minerals [17], playing a crucial role in the formation and maintenance of acidic conditions. In these environments, *A. ferrooxidans* coexists with other hyperacidophiles, including other *Acidithiobacillus* species and members of the archaeal genera such as *Ferroglobus* and *Thermoplasma* [18]. Specifically, *A. ferrooxidans* has several adaptations to survive in these kinds of environments, such as acid-resistant proteins that are adapted to function optimally at low pH, the presence of proton pumps and antiporters to expel protons and maintain internal pH homeostasis, e.g., the presence of genes coding for K^+/H^+ transporting ATPase and the Na^+/H^+ antiporter gene, and the ability to produce biofilms on the mineral surface, providing a micro-environment that can help in pH regulation and nutrient acquisition [5].

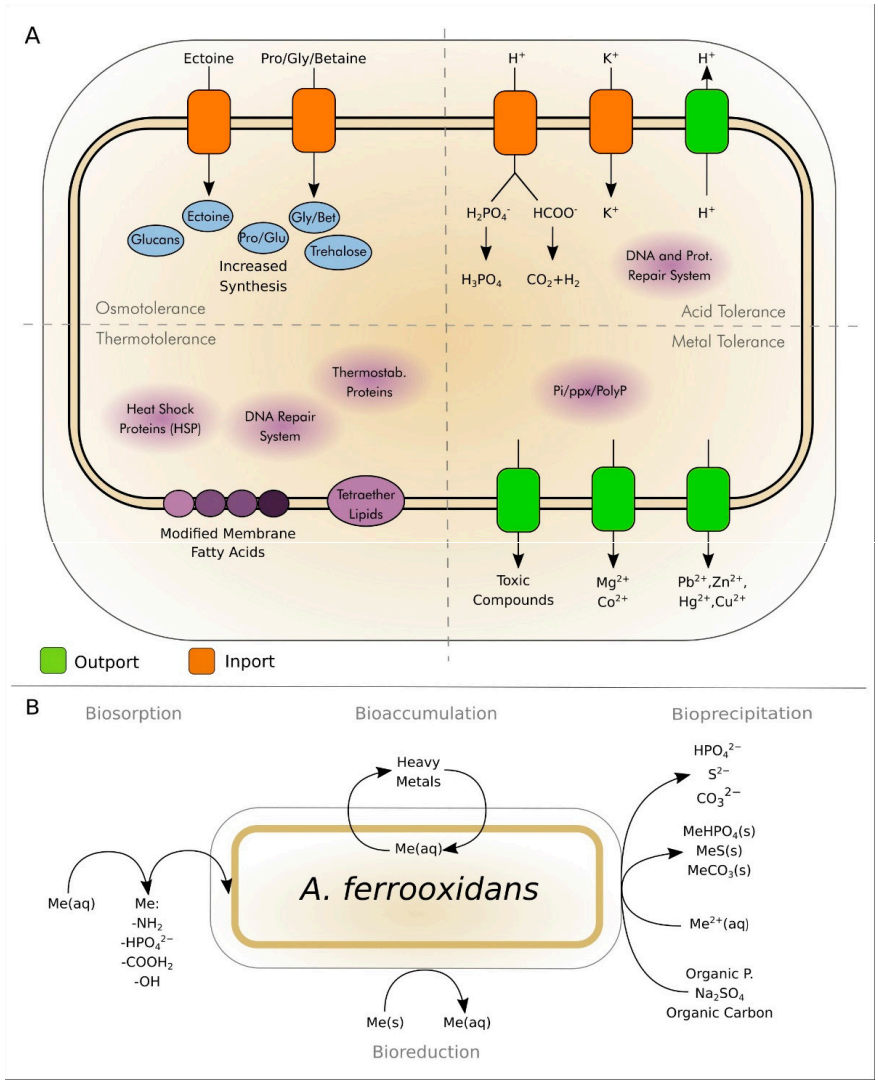

Figure 1. General mechanisms for acidophile tolerances and immobilization of metals from the environment. (**A**) In the upper left, osmotolerance with proteins and transporters. In the upper right, acid tolerance highlighting membrane transport proteins and the principal mechanisms involving proton transport. In the lower left, thermotolerance is displayed, and in the lower right, tolerance to heavy metals such as Pb, Zn, and Hg is illustrated. The main processes of metal immobilization found in acidophilic organisms such as *A. ferrooxidans*. (**B**) Clockwise from the top, bioaccumulation involves the internalization of heavy metals into the cell as aquo-ions, followed by bioprecipitation where hydrated metals are precipitated into their respective hydrogen phosphate, sulfide, and carbonate forms. Bioreduction entails the precipitation of soluble metals as solid metals through redox processes. Finally, biosorption processes involve the absorption of soluble metals by the cell in the form of solids, such as phosphates, or in compatible molecules, e.g., amines, organic acids, or hydroxides.

The metabolic activities of these microorganisms are pivotal in bioleaching and biorecovery processes. *A. ferrooxidans*, along with its consortia partners, leads to the generation of sulfuric acid. This acid production is essential in the leaching of heavy metals from

mine tailings, contributing to the environmental impact observed in mining areas [19,20]. The interactions between *A. ferrooxidans* and other hyperacidophiles in these consortia are complex and involve synergistic relationships that enhance the overall efficiency of mineral oxidation and acid production. Thanks to these kinds of processes, *A. ferrooxidans* is able to derive energy by oxidizing inorganic compounds that release electrons which can be transferred through the ETC, creating a proton motive force that drives the ATP synthesis.

2. General Bioleaching Process

A. ferrooxidans thrives in either aerobic or anaerobic conditions. Under aerobic conditions, Fe^{2+} and/or reduced sulfur compounds in the ores undergo oxidation, resulting in the formation of Fe^{3+} and sulfuric acid (H_2SO_4) [17]. In aerobic conditions (Figure 2A), the redox coupled reactions of *A. ferrooxidans*'s metabolism can be summarized from Equation (1) to Equation (5):

$$4Fe^{2+} + O_2 + 4H^+ \rightarrow 4Fe^{3+} + 2H_2O \quad (1)$$

$$2H_2 + O_2 \rightarrow 2H_2O \quad (2)$$

$$S^{2-} + 2H_2O + 2O_2 \rightarrow {SO_4}^{2-} + 4H^+ \quad (3)$$

$$2CO_2 + O_2 + 4H^+ \rightarrow 2HCOOH + 2H_2O \quad (4)$$

$$2NADH + O_2 + 2H^+ \rightarrow 2NAD^+ + 2H_2O \quad (5)$$

All of the above-mentioned reactions show the oxidation of different elements, e.g., Fe, H, S, CO_2, and NADH coupled with the reduction of oxygen to produce water. The resultant oxidation products, Fe^{3+} and H_2SO_4 (Equations (1) and (3)), engage in chemical interactions with metal sulfide minerals and native metals within ores, leading to the dissolution and/or production of metal cations and the elimination of sulfur [21,22].

The conversion of sulfur/sulfide to sulfuric acid (Equation (3)) culminates in the formation of an intensely acidified medium, due to the production of H_2SO_4 [23]. This process facilitates the abiotic and biotic leaching of sulfides in mines, leading to the acidification of waters and the generation of acid mine drainage [24]. Moreover, oxidation and reduction processes can also be found in immobilization and mobilization processes (Figure 1B).

In the absence of oxygen (Figure 2A), *A. ferrooxidans* undergoes anaerobic growth, performing the reductive dissolution of ferric iron (Fe^{3+}) oxy-hydroxide through the oxidation of elemental sulfur (S^0 to ${S_2O_3}^{2-}$). This reaction assumes pivotal significance in the "Ferredox" process, exemplified by the extraction of nickel from lateritic ores [25,26]. The major coupled reactions involved in the anaerobic metabolism can be summarized as follows [12,21]:

$$2Fe^{3+} + H_2 \rightarrow 2Fe^{2+} + 2H^+ \quad (6)$$

$$S^0 + H_2 \rightarrow S^{2-} + 2H^+ \quad (7)$$

$$2Fe^{3+} + NADH \rightarrow 2Fe^{2+} + NAD^+ + H^+ \quad (8)$$

$$4Fe^{3+}\ 2S^0 + 2H_2O \rightarrow 4Fe^{2+} + {S_2O_3}^{2-} + 4H^+ \quad (9)$$

$$2Fe^{3+} + CO_2 + 2H^+ \rightarrow 2Fe^{2+} + HCOOH \quad (10)$$

In natural environments, sulfide minerals undergo abiotic oxidation by the presence of O_2 or chemical oxidants together with water or moist air [27]. Microorganisms instead utilize Fe^{2+} and sulfur for metabolic processes, leading to the formation of Fe^{3+} and sulfate ions. This metabolic activity results in a higher concentration of these ions, subsequently intensifying the dissolution of sulfide minerals and augmenting the volume of acidic water [28]. A quintessential illustration of this bioleaching phenomenon is the process involving chalcopyrite ($CuFeS_2$) microbial-mediated dissolution (Equation (11)) [29]:

$$CuFeS_2 + 2Fe_2(SO_4)_3 \rightarrow CuSO_4 + 5FeSO_4 + 2S^0 \quad (11)$$

which is driven by the following abiotic reactions (Equations (12)–(14)):

$$CuFeS_2 + 2H_2O + 3O_2 \rightarrow Cu^{2+} + Fe^{2+} + 2H_2SO_4 \quad (12)$$

$$CuFeS_2 + H_2SO_4 \rightarrow Cu^{2+} + FeSO_4 + 2H^+ + 2S^0 \quad (13)$$

$$CuFeS_2 + 4H^+ + O_2 \rightarrow Cu^{2+} + Fe^{2+} + 2H_2O + 2S^0 \quad (14)$$

In the presence of *A. ferrooxidans*, the $FeSO_4$ produced by the abiotic reaction (Equation (13)) is oxidized at the expenses of oxygen in $Fe_2(SO_4)_3$ by the microbe metabolism (Equation (15)), releasing further acidity that supports the overall reaction.

$$3FeSO_4 + H_2SO_4 + 0.5O_2 \rightarrow Fe_2(SO_4)_3 + FeSO_4 + H_2O \quad (15)$$

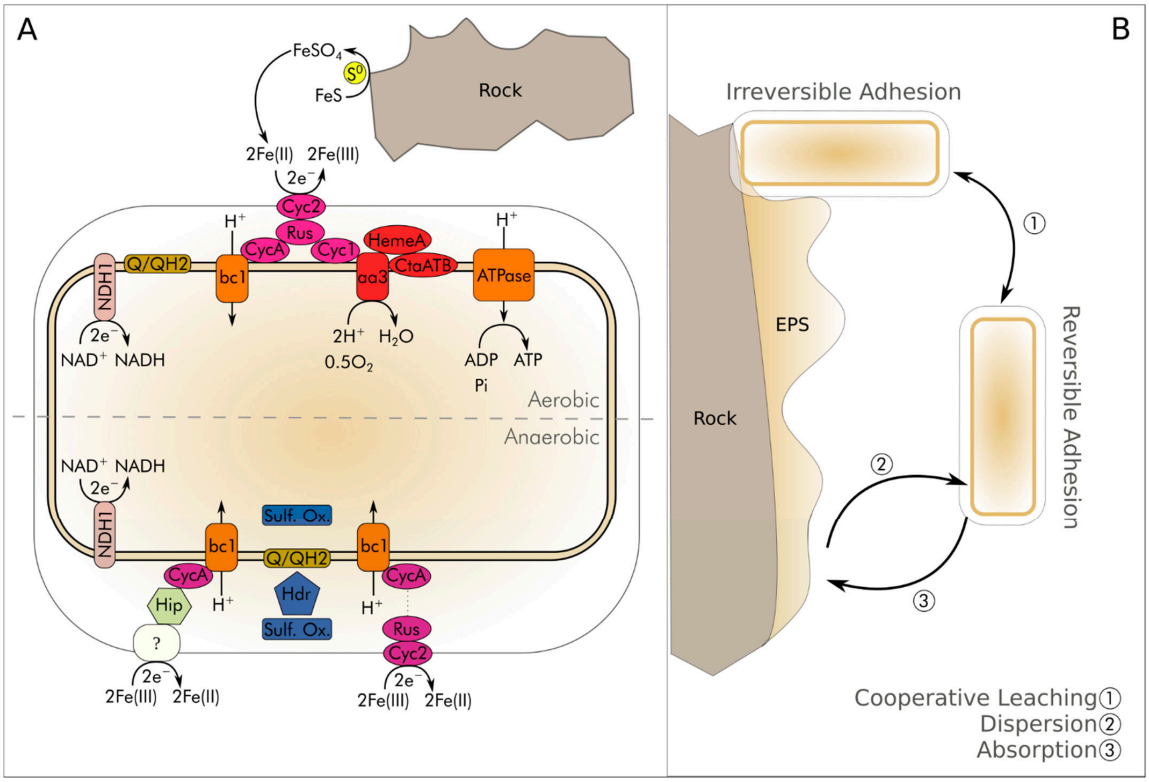

Figure 2. Mobilization mechanisms for *A. ferrooxidans*. (**A**) Aerobic and anaerobic protein pathway for iron oxidation and reduction. Under aerobic conditions, the transition from Fe(II) to Fe(III) occurs through hydrogen oxidation, NAD^+ reduction, ATP production, and sulfur oxidation. In anaerobic conditions, the electron transport chain is mostly understood, except for an unidentified protein (?) responsible for the transformation of Fe(III) to Fe(II). (**B**) Planktonic and sessile cells permanently or non-permanently attached to the substrate. In the case of planktonic or floating cells, leaching occurs in the space between the rock and the organism via a series of redox reactions, while in the case of sessile cells, adherence to the substrate occurs due to extracellular polymeric substance (EPS) production, and leaching is termed direct or contact leaching. Rocks are generally sulfides, but not exclusively. Bioleaching can also be cooperative, wherein sessile and planktonic cells collaborate in metal mobilization between the acidic medium, substrate, and cells. Cell attachment to the substrate can be irreversible if EPS has already been produced, or reversible if not yet produced, and the process by which cells can adhere or detach from the substrate is termed absorption or dispersion.

The resultant primary sulfur product in the process of metal sulfide dissolution is related to the specific sulfide mineral being subjected to bioleaching, subsequently undergoing chemical or biological transformations into elemental sulfur and sulfate [30]. Disulfides, such as FeS_2, MoS_2, and WS_2, can undergo oxidation through thiosulfate ($S_2O_3^{2-}$) as the principal intermediate of the reaction [31]. Only Fe^{3+} ions, arising from the microbial oxidation of Fe^{2+}, serve as oxidative agents for solubilization. The oxidation of $S_2O_3^{2-}$ leads to the formation of SO_4^{2-}, with elemental S^0 generated as a by-product. This elucidates why exclusively Fe^{2+}-oxidizing bacteria possess the capability to oxidize these specific metal sulfides. Two main mechanisms contribute to the enhancement of metal leaching from mineral ores by microbial activity: direct and indirect action [31]. Direct action can be summarized as in Equations (16) and (17) (M is a bivalent metal):

$$MS + H_2SO_4 + 0.5O_2 \rightarrow MSO_4 + S^0 + H_2O \quad (16)$$

$$S^0 + 1.5O_2 + H_2O \rightarrow H_2SO_4 \quad (17)$$

while indirect action uses Fe^{3+} as an oxidizing agent; microbes regenerate Fe^{3+} from Fe^{2+} (Equations (18) and (19)):

$$MS + 2Fe^{3+} \rightarrow M^{2+} + 2Fe^{2+} + S^0 \quad (18)$$

$$2Fe^{2+} + 0.5O_2 + 2H^+ \rightarrow 2Fe^{3+} + H_2O \quad (19)$$

The leaching of mineral sulfides in natural ecosystems is probably a combination of both direct and indirect mechanisms (Figure 2B) [32].

Bacteria, in the bioleaching of sulfide ores, can be momentarily or permanently connected to the mineral substrate, forming a biofilm which often plays a key role in the extraction process (Figure 2B) [33,34]. Extra-polymeric substances (EPSs) facilitate the adhesion of bacteria to metal sulfides, offering a survival advantage in adverse environments [35]. The adsorption affinity of *A. ferrooxidans* can be strengthened by hydrophilic substrates. This indicates that the geobiological affinity of the organism derives from the properties of the different substrates [36]. EPSs render apolar surfaces more polar, facilitating water infiltration through rocks and minerals. The EPSs primarily comprise neutral sugars and lipids, releasing H^+ and Fe^{3+} ions [35]. The EPSs concentrate Fe^{3+} ions complexed with glucuronic acid at the mineral surface [37]. To summarize, in the direct mechanism (contact mechanism), *A. ferrooxidans* directly oxidizes the sulfide minerals or native metals, utilizing its enzymatic pathways to convert metal sulfides into soluble metal ions, e.g., sulfates. This process is facilitated by the bacteria's ability to create EPSs. In the indirect mechanism (non-contact mechanism), *A. ferrooxidans* oxidizes ferrous iron to ferric iron from the environment and not directly from the mineral substrate. The ferric iron then acts as an oxidizing agent, attacking and solubilizing the sulfide minerals indirectly. This dual approach enhances the efficiency of bioleaching, making it a valuable method for metal extraction from environmental alkali cations and sulfate ions (Equation (20)):

$$3Fe^{3+} + 2SO_4^{2-} + 6H_2O + M^+ \rightarrow MFe_3(SO_4)_2(OH)_6 + 6H^+ \quad (20)$$

where M = K^+, Na^+, or NH_4^+. The precipitation of Jarosite (Equation (20)) is responsible for the passivation of certain minerals. The formation of a secondary mineral layer on the mineral surface serves as a diffusion barrier for reactant and product fluxes [38]. The principal contribution of *A. ferrooxidans* to metal extraction arises from its ability to convert insoluble sulfides into corresponding soluble sulfur–metal compounds [30].

A. ferrooxidans has potential applications in biorecovery, e.g., addressing challenges associated with abiotic acid mine drainage (AMD) production at mining sites and recovering heavy metals and other elements from contaminated sites [39]. Its efficacy in the removal of various metals from contaminated sources has been actively explored at the laboratory scale [40,41]. A mercury-resistant strain of *A. ferrooxidans* facilitated the recovery

of mercury compounds from sediments and polluted fluids [42]. *A. ferrooxidans* has been employed in the bioremediation and biorecovery of Cr^{6+} and Cr^{3+} from electroplating waste [43]. The bacterium also plays a crucial role in arsenic bioremediation, leveraging its resistance mechanisms conferred by genes on its chromosome to participate in arsenic precipitation [44]. Regarding electronic waste (E-waste), the sulfuric acid produced by chemolithotrophic organisms, including *A. ferrooxidans*, serves as a leaching agent [45], increasing the acidity of the system and causing possible further releases of fundamental industrial chemical elements, e.g., lithium, into solution [46]. Due to this ability, the metals can be recovered with a feedback mechanism in which the acidity is increased, causing further acidification of the AMDs. This, on one hand, increases the risk of environmental damage, but on the other allows the recovery of toxic metals in confined systems.

Chemical Elements Mobilized by A. ferrooxidans

Biomining and bioleaching are arising as some of the best tools in the context of In Situ Resource Utilization (ISRU) for space exploration, particularly utilizing extremophiles, e.g., *A. ferrooxidans*, or heterotrophic/chemolithoautotrophic organisms, e.g., *S. desiccabilis*, *B. subtilis*, or *C. metallidurans*. Bioleaching has been proposed as a technique for extracting valuable resources from regolith on Solar System bodies [10]. Regolith, a crucial in situ resource, contains elements such as oxygen, water, and trace metals that can help life-supporting devices and fuel production [47]. Bioleaching is a promising approach for extracting metals from regolith with a two-fold advantage for the space missions: (1) minimizing their cost, limiting the need for resources; (2) mitigating their logistical complexities [9,10]. Bioleaching in ISRU operations can contribute to optimizing the selection of landing sites in the frame of human planetary exploration and infrastructure development in space [48]. Biomining and bioleaching processes coupled with biosensors for space applications and new space technologies will be future methods to perform mineral extraction procedures on planets, asteroids, and moons [49–51]. All the techniques that have been proposed to be applied in space will need to rely on resources taken from the Earth, such as oxygen supply, nutrients, and chemicals to support microbial growth. Some of these can be obtained directly from the minerals present on other planetary bodies, while others must be brought from our planet.

Biomining and bioleaching present different ways to maximize economic performance in the mining industry. In the case of polymetallic ore, the achieved recoveries of metals are the following, Cu 90%, Au 90%, Ag 80%, Zn 72%, and Pb 90%, and the values per Net Present Value (NPV) and the Internal Rate of Return (IRR) are USD 21.927 million and 12.55%, respectively. Moreover, a report made by Credence Research (www.credenceresearch.com), an industry involved in data analysis in the changing global industry landscape, has shown that during the economic challenges of the pandemic (COVID-19), biomining showed revenues of USD 1500 million in 2020. Additionally, the projection for the future of biohydrometallurgical processes is promising, with a Compound Annual Growth Rate (CAGR) of over 13%. This trajectory positions biomining and bioleaching processes to reach an estimated value of USD 3600 million by 2027.

A. ferrooxidans is capable of mobilizing or affecting the mobilization of many different elements in the periodic table (Table 1), utilizing biochemical strategies depending on the specific element and the mineral/ore involved. The aim of this review is to report a comprehensive and updated list of elements which are mobilized by *A. ferrooxidans*, including its biochemical leaching mechanisms, and highlighting applications and limitations (Table 2).

Table 1. List of main elements, minerals, chemical compositions, and chemical reactions involved in bioleaching processes through *A. ferrooxidans*.

Element	Mineral	Chemical Formula	Reactions
Li	Lepidolite	$KLi_2Al(Si_4O_{10})(F,OH)_2$	$3Li_2O*2K_2O*5Al_2O_3*10SiO_2*2SiF_4 + 20H_2SO_4 \rightarrow 3Li_2SO_4 + 2K_2SO_4 + 5Al_2(SO_4)_3 + 11SiO_2 + H_2SiF_6 + 18H_2O + 2HF$
P	P-Sludge	$Ca_3(PO)_4$	$3H_2SO_4 + Ca_3(PO_4)_2 \rightarrow 2H_3PO_4 + 3CaSO_4$
V	V-Ti-Magnetite and Vanadates	(V,Ti),$Fe^{2+}Fe^{3+}{}_2O_4$ and V_2O_3	$V_2O_3 + 2Fe^{3+} + 2H^+ \rightarrow 2VO^{2+} + 2Fe^{2+} + H_2O$ $VO_2 + Fe^{3+} \rightarrow VO_2{}^+ + Fe^{2+}$ $10VO_2 + 10Fe^{3+} + 8H_2O \rightarrow HV_{10}O_{25}{}^{5-} + 10Fe^{2+} + 15H^+$
Cr	Cr-Slug	$Ca_3Al_2(H_4O_4, CrO_4)_3$	$Cr^{6+} + 3Fe^{2+} \rightarrow Cr^{3+} + 3Fe^{3+}$
Ni	Ni-Sludge	Ni^0	$Fe_2(SO_4)_3 + Ni^0 \rightarrow Ni^{2+} + SO_4{}^{2-} + 2FeSO_4$
Cu	Chalcopyrite	$CuFeS_2$	$CuFeS_2 + 2Fe_2(SO_4)_3 \rightarrow CuSO_4 + 5FeSO_4 + 2S^0$ $CuFeS_2 + 2H_2O + 3O_2 \rightarrow Cu^{2+} + Fe^{2+} + 2H_2SO_4$ $CuFeS_2 + H_2SO_4 \rightarrow Cu^{2+} + FeSO_4 + 2H^+ + 2S^0$ $CuFeS_2 + 4H^+ + O_2 \rightarrow Cu^{2+} + Fe^{2+} + 2H_2O + 2S0$ $3FeSO_4 + H_2SO_4 + 0.5O_2 \rightarrow Fe_2(SO_4)_3 + FeSO_4 + H_2O$
As	Realgar	As_2S_2 or alpha As_4S_4	$4Fe^{2+} + O_2 + 4H^+ \rightarrow 4Fe^{3+} + 2H_2O$ $As_2S_2 + 6Fe^{3+} \rightarrow 2As^{3+} + 2S^0 + 6Fe^{2+}$ $H_3AsO_3 + H_2O \rightarrow H_3AsO_4 + 2H^+ + 2e^-$ $H_3AsO_4 + Fe^{3+} \rightarrow FeAsO_4 + 3H^+$ $As_2S_2 + 14H_2O \rightarrow 2H_3AsO_3 + 2HSO_4{}^- + 20H^+ + 18e^-$
Mo	Mo Sulfide	MoS_2	$4MoS_2 + 4Fe^{3+} + 16H_2O \rightarrow 4MoO_4{}^{2-} + 4Fe^{2+} + 32H^+ + 8S^0$
W	Tungstate Salts	$WO_4{}^{2-}$	$H_2SO_4 + FeWO_4 \rightarrow FeSO_4 + H_2WO_4$
Au	Au Ores	Au^0	$4Au^0 + 8NaCN + 2H_2O + O_2 \rightarrow 4NaAu(CN)_2 + 4NaOH$
Hg	Cinnabar	HgS	$HgS + 2Fe^{3+} \rightarrow Hg^{2+} + 2Fe^{2+} + S^0$ $2HgS + 4Fe^{3+} + 1.5O_2 + 2H_2O \rightarrow 2Hg^{2+} + 4Fe^{2+} + 2H_2SO_4$
U	U Oxide	UO_2	$U^{(IV)}O_2 + 2Fe^{3+} \rightarrow U^{(VI)}O_2{}^{2+} + 2Fe^{2+}$

Table 2. Selected bioleached elements by *A. ferrooxidans*. A = *Acidithiobacillus ferrooxidans*, B = other organisms, and C = consortia. 1. According to the literature, the estimated copper extraction through biohydrometallurgy is about 30% worldwide. For the other metals, there are no clear data in the literature. * All the biomining experiments made in space refer to microgravity conditions on the ISS or simulated environments. d—estimates according to British Geological Survey.

Element	Main Alloys	Application Fields	Metal Printing	Electronics	Extraction Yield (ktons/year) [d]	Biomining on Earth	Biomining in Space *	Biorecovery	References
Ti	Alpha/BetaTi alloys	Aerospace, Construction, Automobile	Yes	Major (hardware)	6300	Yes (A)	No	Yes (A,B,C)	[52]
V	Ferrovanadium	Structural, Fusion Reactor	No	Minor (semiconductors)	81	Yes (A)	Yes (B)	Yes (A,B,C)	[9,10,53–56]
Cr	FeCr, Stainless steel	Automobile, High Temperature	Yes	Minor (anticorrosive coating)	38,600	Yes (A)	No	Yes (A,B,C)	[43,57–59]
Fe	Steel, Inox	Construction, Automobile, Aerospace,	Yes	Major (solder)	3,040,000	Yes (A,B,C)	Yes (B)	Yes (A,B,C)	[9,10,22]
Ni	NiCrFe	Medical, Aerospace, Energy, Isolators, Automotive, Cables	Yes	Minor (plating agent)	2700	Yes (A)	Yes (B)	Yes (A,B,C)	[9,10,60]

Table 2. *Cont.*

Element	Main Alloys	Application Fields	Metal Printing	Electronics	Extraction Yield (ktons/year) [d]	Biomining on Earth	Biomining in Space *	Biorecovery	References
Cu	Brass, Bronze	Construction, Marine, Automotive, Medical, Aerospace	Yes	Major (cables)	20,700	Yes (A,B,C) 1	Yes (B)	Yes (A,B,C)	[9,10,61]
Ga	GaAlZn alloys	Semiconductors, Diodes, Circuits	No	Major (diodes)	0.380	Yes (A)	No	No	[62,63]
As	As Bronze	Automobile, Ammunition	No	Minor (batteries)	NA	Yes (A,B,C)	No	Yes (A,B,C)	[44,64]
W	W,Ni,Cu and W,Ni,Fe alloys	Aerospace, Medical, Automobile	Yes	Minor (light bulbs)	91.5	Yes (A)	No	Yes (A,B,C)	[65–67]
Au	AuPt alloys	Increasing Corrosion Resistance	No	Major (connector)	3.3	Yes (A)	No	No	[68–71]
Pb	PbCu, alloys	Automobile, Ammunition, Batteries	No	Major (solder)	4700	Yes (A,C)	No	Yes (A,B,C)	[72,73]
U	Mulberry	Increasing Corrosion Resistance	No	None	53	Yes (A)	No	Yes (A,B,C)	[74–76]

3. Alkali Metals: Lithium

The alkali metals (Group 1 of the periodic table) constitute a highly reactive group of elements: lithium, sodium, potassium, rubidium, cesium, and francium. These metals share common characteristics: low melting points, high reactivity with water, tendency to form ionic compounds, and ability to readily donate electrons, leading to the formation of alkali metal cations with a + 1 charge [77]. Regarding bioleaching processes performed by the acidophile *A. ferrooxidans*, only lithium can be actively leached.

Being the lightest alkali metal, and due to its distinctive electrochemical reactivity, lithium finds extensive applications in metallurgy, aerospace, ceramics, battery technology, and fuel cells [78]. The utilization of Li-ion batteries for powering portable devices and electric vehicles has led to an escalating demand for lithium [79]. Naturally occurring sources of lithium include lake brines, pegmatites ore bodies, and sedimentary rocks, with over 80% of the current global production being derived from brines [80]. Developing technologies capable of extracting lithium from solid ores holds significant importance in addressing future lithium demand [81].

In comparison to brine extraction, the process of obtaining lithium from rocky sources is notably more intricate. This procedure encompasses a series of distinct operations, including roasting rocks in sulfate or carbonate environments to render lithium into water-soluble species [82].

One of the primary industrial minerals for lithium extraction is spodumene ($LiAlSi_2O_6$), a Li-bearing pyroxene found in pegmatites, i.e., coarse-grained igneous rocks rich in lithium, with a relatively low occurrence of other metals. Lepidolite ($3Li_2O*2K_2O*5Al_2O_3*10SiO_2*2SiF_4$), a form of pegmatite, member of the mica group, represents the most abundant lithium ore, with a distribution far surpassing that of Li-brines [83]. The Li_2O content in lepidolite ranges from 3.0% to 7.7% by weight (1.39–3.58% Li), comparatively lower than that of spodumene, 6–8% by weight as shown by Sedlakova-Kadukova et al. (2020). Lepidolite exploitation in industrial processes is constrained by the elevated costs associated with lithium recovery from the mineral, necessitating high concentrations of acid in purification procedures [84]. The adoption of alternative technology has gained importance due to its potential for cost reduction, heightened efficiency, and environmentally sustainable processing [85]. A bio-extraction approach utilizing a consortium of different bacterial strains—namely, *A. ferrooxidans*, *A. thiooxidans*, as well as the heterotrophic fungus *Aspergillus niger* and yeast *Rhodotorula mucilaginosa*—has been investigated [86]. These microorganisms play

integral roles in processes such as the bio-weathering of rocks, mobilization of metals from minerals, metal precipitation, and deposition [87]. For this reason, they have been extensively employed in biohydrometallurgical practices.

The mechanisms underlying lepidolite bioleaching by bacteria remain undisclosed. Nevertheless, it has been observed that, apart from H^+ ions, no other substance contributes to the dissolution of Li^+ ions. This implies that the dissolution of lithium in lepidolite is facilitated by acidic conditions [86,88]. Presumably, the primary reaction involved in the bioleaching of mixed alkali metals can be expressed through Equation (21), in which the metal oxide is converted into a soluble sulfate.

$$M_2O + H_2SO_4 \rightarrow M_2SO_4 + H_2O \quad (21)$$

where M presents alkali metals. Metals inside the mineral can be dissolved to form the sulfate counterpart, resulting in lepidolite dissolution [86]. The reaction of lepidolite bioleaching in sulfuric acid produced by bacteria can be seen in Equation (22):

$$3Li_2O{*}2K_2O{*}5Al_2O_3{*}10SiO_2{*}2SiF_4 + 20H_2SO_4 \rightarrow 3Li_2SO_4 + 2K_2SO_4 + 5Al_2(SO_4)_3 + 11SiO_2 + H_2SiF_6 + 18H_2O + 2HF \quad (22)$$

In bacterial involvement, the composition of the medium emerged as the predominant factor influencing lithium bioleaching. The authors of [89] report that, within a nutrient-rich medium tailored for acidophilic chemoautotrophic acidithiobacilli, featuring essential energy sources in the form of ferrous ions and elemental sulfur, no lithium bioleaching was observed throughout the entire duration of the process. Conversely, in a medium with restricted nutrient content and limited energy sources, comprising solely sulfuric acid and elemental sulfur, the presence of Li^+ ions was discernible within a matter of days. This suggests that bacteria, essential for lithium bioleaching from lepidolite, as no lithium was detected in abiotic control samples, may have been compelled to directly utilize nutrients vital for their sustenance from the leached material. Lithium extraction, achieved through bacterial intervention, necessitates at least 22 days to occur [86].

4. Non-Metals: Phosphorus

Non-metals encompass a variety of elements critical for chemical reactions and biological processes [90]. Non-metals, characterized by their lack of metallic luster, malleability and conductivity, such as oxygen, nitrogen, and carbon, are included in compounds essential for life, i.e., water, proteins, and DNA [91]. They contribute significantly to the Earth's atmosphere, with oxygen being a crucial component for sustaining aerobic life [90]. Phosphorus (P) is the only non-metal of industrial interest bioleached by *A. ferrooxidans*, which can actually metabolize other non-metal elements such as carbon, nitrogen, and sulfur.

Phosphorus (P), a crucial plant nutrient, has attained increasing importance as a natural resource, given its finite supply [92]. The leaching of phosphorus into superficial waters poses a significant environmental challenge. Sewage sludge represents a substantial reservoir of phosphorus and, considering its substantial quantities generated globally daily, projections indicate a surge production attributable to population growth [93]. The disposal of such large volumes of sewage sludge raises substantial environmental apprehensions. Its application on agricultural land emerges as an attractive option, offering nutrient recycling and augmentation of soil organic content [94]. However, this approach confronts several constraints, as sludge (1) harbors numerous pathogens, (2) may contain elevated levels of heavy metals, and (3) is bulky and has associated transport costs, which pose logistical challenges [95].

Phosphorus recovery from sewage sludge in the form of phosphoric acid is facilitated by the use of sulfuric acid. Nevertheless, the process entails the costly steps of sludge drying and the utilization of significant quantities of commercial acid [96]. Active phosphorus extraction from P-sludge, deriving from the metabolic activities of acidophiles, is well connected with environmental recovery challenges, linking bioleaching and biore-

covery. The bioleaching of rock phosphate employing acid-generating microorganisms has been extensively investigated [97,98]. The biochemical approach offers distinct advantages regarding eco-friendly approaches and biorecovery techniques [99]. The development of a biochemical process for phosphorus recovery from sludge is a highly advantageous endeavor.

A. ferrooxidans and *A. thiooxidans* present viable candidates for the recovery and bioleaching of P-rich sludge [100]. These microorganisms possess the capability to generate sulfuric acid through the oxidation of reduced sulfur compounds, allowing for the establishment of an acidic pH level, potentially below 1. This produced sulfuric acid serves to solubilize the phosphorus content. *A. thiooxidans* demonstrates the capacity to recover 94% of phosphorus from rock phosphate, while *A. ferrooxidans* can be employed to solubilize phosphorus from desiccated sewage sludge [101]. The chemical reactions governing the leaching of phosphorus from the sludge are delineated by Equations (23) and (24):

$$3H_2SO_4 + Ca_3(PO_4)_2 \rightarrow 2H_3PO_4 + 3CaSO_4 \quad (23)$$

$$3H_2SO_4 + 2FePO_4 \rightarrow 2H_3PO_4 + Fe_2(SO_4)_3 \quad (24)$$

The process takes circa 63 days to recover 92% of the phosphorus from the sludge. The extracted phosphoric acid can be used for different purposes, including the production of ammonium phosphate [101]. Being a technique based on microorganisms and not on expensive industrial processes, the operation is time-consuming but allows the recovery of phosphorus from wastes.

5. Transition Metals

Transition metals exhibit distinctive electronic configurations, with partially filled d-orbitals contributing to their characteristic properties. Their ability to form stable coordination complexes makes them essential in fields such as catalysis, where they play a crucial role in accelerating chemical reactions [102]. Transition metals are known to be fundamental to many organisms; in microbes, they drive the global biogeochemical cycling of elements [103,104]. Today, 25% of the total transition metals can be mobilized by *A. ferrooxidans*.

5.1. Vanadium

Vanadium (V) represents a prototypical redox-sensitive transition metal widely employed in industries, including metallurgy, manufacturing, and petroleum refining [105]. Vanadium serves as a catalytic agent in denitrification processes, acting as a metallic cofactor within enzymes responsible for catalyzing such reactions [106]. Vanadium redox batteries present a further potential application in addressing the escalating global energy demand [107].

A significant proportion of the world's vanadium production stems from slags generated during steelmaking operations employing V-titanium magnetite [108]. Conventional methods for vanadium extraction are marked by high costs and inefficiencies, accompanied by pronounced environmental challenges, encompassing alkali melting, chloridizing roasting, acid leaching, water leaching, and deposition [109]. Bioleaching has been successfully employed for the solubilization of vanadium from solid waste sources, including spent refinery catalysts and oil-fired ash [110], and thus, its integration with established processes holds considerable promise. Successful bioleaching of vanadium through heterotrophic organisms has been demonstrated in microgravity conditions aboard the International Space Station (ISS) [111]. The incorporation of vanadium into steel enhances critical attributes such as hardness, tensile strength, and fatigue resistance, thereby elevating overall performance. Therefore, vanadium holds a key role in future space exploration by its possible use in the manufacturing of rovers, pressurized buildings, superconducting materials, batteries, and alloys for nuclear reactors. Being sufficient on Earth for the next few decades or centuries, it would be fundamental to find a way to extract it locally on other

planetary bodies to reduce the environmental and economic cost associated with space transportation [111].

Minerals conducive to vanadium extraction encompass V-titanium magnetite ((V, Ti),$Fe^{2+}Fe^{3+}{}_2O_4$), maghemite (a specific variant of magnetite characterized by a low Fe^{2+} concentration), bixbyte (containing vanadium along with $(Mn, Fe)_2O_3$)), vanadium oxide, and jacobsite, typically $(Mn, Mg)Fe_2O_4$ [52]. A prominent participant in the interaction with these mineral types for vanadium extraction is *A. ferrooxidans*, catalyzing the conversion of Fe^{2+} to Fe^{3+} under acidic conditions (Equation (19)); following the oxidation of iron, the resulting Fe^{3+} can be used to oxidize vanadium in Equations (25)–(27) [112,113]:

$$V_2O_3 + 2Fe^{3+} + 2H^+ \rightarrow 2VO^{2+} + 2Fe^{2+} + H_2O \quad (25)$$

$$VO_2 + Fe^{3+} \rightarrow VO_2{}^+ + Fe^{2+} \quad (26)$$

$$10VO_2 + 10Fe^{3+} + 8H_2O \rightarrow HV_{10}O_{25}{}^{5-} + 10Fe^{2+} + 15H^+ \quad (27)$$

Presumably, V^{5+} represents the predominant speciation in the leachate. Vanadium manifests three principal valence states in natural aqueous solutions, with V^{5+} prevailing as the most prevalent form in oxidizing environments [114]. V^{5+} can be readily retrieved from the leachate through NH_4Cl precipitation [115]. In summary, *A. ferrooxidans* proves highly effective in the recovery of vanadium from both raw minerals and intermediate materials utilized in vanadium extraction processes. The average recovery efficiency is estimated to be approximately 30% [113].

5.2. Chromium

Chromium (Cr) slags represent a category of hazardous waste characterized by the prevailing toxicity of Cr^{6+}. This hexavalent chromium species possesses a robust oxidizing potential toward living cells and has been associated with gene mutations and carcinogenic effects in animal studies (Sharma et al., 2022 [57]). In specific chromium slag compositions, such as $Ca_3Al_2(H_4O_4, CrO_4)_3$ and $Ca_4Al_2(OH)_{12}(CrO_4)_3{*}26H_2O$, approximately 20–25% of the total mass is constituted by hexavalent chromium [58]. Chromium salts are extensively employed in the leather industry for tanning processes, a treatment that safeguards leather against various environmental stressors, including microbial degradation and moisture [116]. An estimated 90% of tanneries employ chromium salts as a principal tanning agent. Chromium exhibits limited biodegradability and tends to accumulate within biological organisms, resulting in severe health ailments. Disposal methods for tannery sludge encompass incineration, solidification, landfills, and ocean dumping, with the last two facing mounting scrutiny in numerous countries due to environmental considerations [59].

The recovery of chromium from sludge can be facilitated through the action of sulfur- and iron-oxidizing bacteria. This microbiological approach enables the ready solubilization of metals via the oxidation of metal sulfides into soluble sulfates, or through acid dissolution employing sulfuric acid [117]. Subsequently, released chromium can be efficiently removed. Chromium is naturally occurring in minerals such as the Cr-bearing phase of goethite $Fe^{3+}O(OH)$, or in limonite deposits [118]. The liberation of chromium from sludge or rocks is contingent upon redox processes. The indirect activity of *A. ferrooxidans* mediates the oxidation of iron from Fe^{2+} to Fe^{3+}, thereby facilitating the reduction of Cr^{6+} to the less toxic and water-insoluble Cr^{3+} species, increasing biorecovery processes [119]. In this process, Fe^{2+}, reduced sulfur, and organic matter constitute the principal sources of electrons. These electrons released by the oxidation of iron through indirect mechanisms carried out by *A. ferrooxidans* are able to reduce the chromium in solution, leaving it free to be recovered in industrial processes. The reduced Fe^{2+} can serve as a reducing agent for Cr^{6+}. The Fe^{3+} formed in the oxidation of Fe^{2+} is capable of accepting electrons from Cr^{6+}, thereby reducing chromium. The Fe^{3+} can be further reduced back to Fe^{2+} by the microbial

activity or other reducing agents present in the environment, maintaining a cycle that can continuously facilitate the reduction of Cr^{6+}.

$$Cr^{6+} + 3Fe^{2+} \rightarrow Cr^{3+} + 3Fe^{3+} \quad (28)$$

The reduction of chromium under experimental conditions [120] is a process that iron-oxidizing bacteria, such as *A. ferrooxidans*, *A. thiooxidans*, and *P. putida*, can mediate.

5.3. Iron

Iron (Fe) is a fundamental element in various industrial processes, serving as a critical component in the production of steel, alloys, and numerous other materials essential for modern infrastructure. The demand for iron in industry underscores the significance of efficient extraction methods. Iron is also fundamental in household applications, e.g., refrigerators, stoves, washing machines, and packaging [121].

A. ferrooxidans exhibits the ability to oxidize ferrous iron to ferric iron, a process crucial for the solubilization of iron minerals in ore deposits. This metabolic proficiency includes iron oxidases, cytochromes, and electron transport chains within the bacterial cell. The unique redox chemistry of *A. ferrooxidans* enables it to thrive in highly acidic environments, where conventional mining operations are impractical [22]. The oxidation of ferrous iron by *A. ferrooxidans* can be seen in Equation (19).

The use of *A. ferrooxidans* in iron biomining from pyrite and iron sulfides, such as bornite (Cu_5FeS_5), offers several significant environmental advantages. Unlike traditional mining practices, which often result in extensive environmental degradation and habitat destruction, biomining is a less-impacting process [122]. By harnessing the metabolic capabilities of *A. ferrooxidans*, the extraction of iron from ore deposits can be achieved with minimal disturbance to surrounding ecosystems in a controlled environment. The reduction in chemical reagents and energy consumption associated with biomining contributes to lower carbon emissions compared to conventional mining techniques [39].

The application of *A. ferrooxidans* in iron biomining holds immense potential for the mining industry. With advancements in biotechnology and microbial engineering, there is a growing opportunity to optimize the efficiency and scalability of this process [123]. Ongoing research efforts are focused on expanding the repertoire of biomining microorganisms, potentially unlocking new niches for the extraction of valuable metals from diverse mineral resources [14].

The unique metabolic capabilities of *A. ferrooxidans* in iron biomining hold promise for extraterrestrial applications. In space exploration, the availability of essential resources such as iron is of paramount importance for construction, habitat development, and various technological endeavors. Leveraging *A. ferrooxidans* in biomining processes could facilitate the sustainable extraction of iron from planetary bodies, reducing reliance on resource-intensive transportation from Earth [11].

5.4. Nickel

Nickel (Ni) plays a prominent role in the manufacturing of electronic devices, which are subject to heightened demand driven by planned obsolescence and rapid market penetration. This results in a substantial accumulation of electronic waste (E-waste), which constitutes a vital reservoir of metals relevant for industry and rare elements [124]. Printed circuit boards (PCBs) account for approximately 3% of the total E-waste mass [125]. PCBs encompass notable quantities of Cu (10–20%), Ni (1–3%), Fe (1–4%), and Pb (1–5%), as well as precious metals (0.3–0.4%) including Au, Ag, and Pt, rendering them a valuable secondary metal resource [126]. Metal recovery from E-waste stands as a more sustainable and resource-efficient endeavor in terms of energy utilization, environmental protection, and overall sustainable resource management [125]. While hydrometallurgical and pyrometallurgical processes present notable drawbacks, e.g., concentrated acidic effluents, high energy consumption and big volumes of hazardous waste, [127,128], bioleaching contributes to the conservation of non-renewable energy [129].

Nickel and its compounds exert detrimental effects on the human heart and liver [130]. Coupling nickel's hazards with its high demand in the electronics industry, bioleaching emerges as a promising method for its recovery from waste sources. In oxygen-rich environments and under acidic conditions, *A. ferrooxidans* through the oxidation of iron (Equation (19)) is able to produce Fe^{3+}, which can be used in nickel oxidation [60].

In this manner, Ni^0 present in E-waste undergoes oxidation through ferric ions, which are subsequently reduced to ferrous ions as in Equation (29):

$$Fe_2(SO_4)_3 + M^0 \rightarrow M^{2+} + {SO_4}^{2-} + 2FeSO_4 \quad M[Cu, Ni, Ga] \tag{29}$$

In this specific case, M is nickel. The ferrous ions are oxidized back to ferric ions through *A. ferrooxidans* activity: a recurrent iron cycle is instituted within the nickel bioleaching process, whose efficiency depends on pH adjustment (88.9% with pH adjustment vs. 92.1% without it) [131]. Arshadi and Yaghmaei (2020) demonstrated the generation of jarosite and goethite, [60] see Equation (20).

5.5. Copper

Copper (Cu), a vital element in various industries, including electronics, construction, and transportation, necessitates efficient extraction methods to meet global demands. It is a fundamental material for electrical wiring, power transmission, and electronic components due to its superior conductivity, making it essential for powering homes, industries, and electronic devices [61]. Copper is also widely employed in plumbing, roofing, and architectural elements. Its corrosion resistance and durability make it a preferred choice for water pipes, roofing materials, and decorative features in buildings. Copper is used in transportation and the automotive industry and intensely in industrial machinery and equipment [132]. The presence of Fe^{2+} acts as an electron donor in this redox process, enabling the sustenance of *A. ferrooxidans* in highly acidic environments [133]. The bioleaching of copper minerals, e.g., chalcopyrite, can be represented by Equations (11)–(14) (see also Table 1). By harnessing the metabolic capabilities of *A. ferrooxidans*, the extraction of copper can be achieved with reduced ecological impact. The decreased dependence on harsh chemical reagents and energy-consuming methods results in a smaller environmental footprint relative to traditional mining techniques [134].

Biohydrometallurgy processes, including bioleaching, account for approximately 20–25% of the world's copper production [135]. These processes involve the microbial oxidation of sulfide minerals, converting insoluble metal sulfides into soluble metal sulfates according to Equation (11). This approach is particularly efficient for low-grade ores, which are economically unfeasible to process using traditional methods. Traditional methods, such as smelting, require high energy input and produce significant environmental pollution. In contrast, bioleaching operates at ambient temperatures and pressures, utilizing natural microbial processes to extract metals with minimal environmental disruption [136].

The efficiency of bioleaching in low-grade ore deposits makes it an invaluable tool for mining operations. These deposits, often overlooked due to their low metal content, become viable sources of copper through bioleaching. This not only maximizes the utilization of available resources but also minimizes waste and environmental impact, aligning with sustainable mining practices [137]. Consequently, bioleaching with *A. ferrooxidans* represents a cost-effective, environmentally friendly alternative to conventional methods, contributing significantly to the global supply of copper.

Copper can also be extracted from many different minerals such as chalcocite (Cu_2S) and covellite (CuS), with a total copper recoveries of 65–80%, and from enargite (Cu_3AsS_4), with a recovery rate between 7.3 and 27.1%. Furthermore, the addition of particular cations to the reaction e.g., Ag^+, Hg^{2+}, Bi^{2+}, Cu^{2+}, and Co^{2+}, can decrease the time required for the bioleaching process. They reported that the majority of studies are focused on Ag^+ in copper-bearing ore and chalcopyrite leaching. The addition of Ag^+, at a catalytic concentration, led to the formation of a thin layer of silver sulfide (Ag_2S) on the mineral surface, minimizing passivation throughout the process and enhancing electron

transfer to the oxidant. The chemical reactions behind this process can be seen from Equations (30)–(32):

$$CuFeS_2 + 4Ag^+ \rightarrow Cu^{2+} + Fe^{2+} + 2Ag_2S \quad (30)$$

$$2Ag_2S + 4Fe^{3+} \rightarrow 4Ag^+ + 4Fe^{2+} + 2S^0 \quad (31)$$

$$CuFeS_2 + 4Fe^{3+} \rightarrow Cu^{2+} + 5Fe^{2+} + 2S^0 \quad (32)$$

Elemental silver can also be formed as in Equation (33):

$$CuFeS_2 + 4Ag^+ \rightarrow Cu^{2+} + Fe^{2+} + 4Ag^0 + 2S^0 \quad (33)$$

The main role of *A. ferrooxidans* in this process is the conversion of Fe^{2+} to Fe^{3+}, which is capable of oxidizing the Ag_2S layer.

In general, the addition of 7.1 g of Ag^+ per Kg of minerals to the reaction led to a final yield of recovery of 89.3% of Cu compared to the traditional one of 28% without a catalyst. Similar results can be also obtained for Hg^{2+} (80% recovery after addition of the cation compared to 25% without), and Bi^{2+} (90% vs. 80% recovery ratio) [61,132–137].

5.6. Zinc

Zinc (Zn) is a critical element in the galvanizing, cosmetic, die-casting, and manufacturing sectors. With a global production exceeding 8×10^6 tons, zinc is primarily extracted utilizing sulfide ores through hydro-metallurgical processes (roasting, leaching, and electrowinning), with the leaching kinetics playing a key role in the smelting procedure [138]. Zinc sulfide ores, especially sphalerite (ZnFe)S, are suitable and useful sources for Zn extraction as they are easily separated and concentrated by flotation from waste rocks [139]. Due to the increasing demand for zinc and Zn compounds, new zinc sources, e.g., low-grade oxide ores, have been considered.

The leaching of zinc ores with sulfuric acid has been investigated [140]. The zinc general chemical mobilization from ores can be summarized following Equation (16), in which M can be substituted by zinc.

Fowler and Crundwell (1998) experimentally disentangled two *A. ferrooxidans* zinc extraction mechanisms, direct and indirect, demonstrating that the indirect mechanism plays a central role in the leaching of zinc sulfide [141].

5.7. Molybdenum

Molybdenum (Mo) is an important element in sectors such as metallurgy, aerospace, and electronics [142]. Molybdenum is known for its exceptional heat resistance and high melting point, making it a crucial component in alloys that withstand extreme temperatures. Its ability to facilitate electron transfer makes it indispensable in electronics and electrical applications. Molybdenum finds extensive use in the production of steel and other alloys, contributing to enhanced strength and corrosion resistance [143]. Given its increasing demand, efforts have been made for the recovery of molybdenum from waste sources, contributing to sustainable resource management [144]. Bioleaching presents a promising avenue for molybdenum recovery: *A. ferrooxidans* has shown potential in solubilizing molybdenum from various sources, offering advantages in terms of safety, environmental sustainability, and energy efficiency [145].

Molybdenum is oxidized from Mo^{4+} to Mo^{6+} through the activity of *A. ferrooxidans* (Equation (34)). The ferrous ions released from Equation (34) are further oxidized to ferric ions, establishing a recurring iron cycle within the process. The soluble molybdenum can then be readily extracted, contributing to the efficient recovery of molybdenum from waste materials [145].

$$4MoS_2 + 4Fe^{3+} + 16H_2O \rightarrow 4MoO_4{}^{2-} + 4Fe^{2+} + 32H^+ + 8S^0 \quad (34)$$

This reaction leads to the dissolution of molybdenum sulfide minerals, releasing molybdenum ions (MoO_4^{2-}) into the solution [146]. *A. ferrooxidans* contributes to the precipitation and immobilization of molybdenum through biomineralization processes [145]. Under appropriate conditions, molybdenum ions in solution can react with other elements to form various Mo-containing minerals. For example, the reaction between molybdenum ions and calcium ions (Ca^{2+}) can lead to the formation of calcium molybdate $CaMoO_4$ [147].

5.8. Tungsten

Among others metal ions (iron, copper, nickel, zinc, and molybdenum) tungsten (W) serves as an essential component of various metalloenzymes, playing pivotal roles in biological processes [104]. Some bacteria have evolved the capability to synthesize metal-binding proteins, facilitating the storage of these crucial metal ions within the cell [148]. Tungsten exhibits multiple oxidation states (e.g., W^{6+}, W^{4+}, W^{2+}, and W^0), with limited knowledge regarding its speciation in natural environments. Wolframite—$(Fe,Mn)WO_4$—an iron, manganese, and tungstate mineral, alongside scheelite ($CaWO_4$), represents a primary source of tungsten ore [65]. Wolframite undergoes instability in acidic and oxidizable conditions, leading to the formation of H_2WO_4 as the prevalent secondary tungsten mineral [66]. In acidic and reducing environments, the dominant tungsten species are W^{4+} and metallic W^0. The leaching process of wolframite is a two-step reaction (Equations (35) and (36)), occurring after the oxidation of sulfides and necessitating interaction with the product of the first step of the reaction, H_2SO_4 [67].

$$H_2SO_4 + FeWO_4 \rightarrow FeSO_4 + H_2WO_4 \quad (35)$$

$$H_2SO_4 + MnWO_4 \rightarrow MnSO_4 + H_2WO_4 \quad (36)$$

The activity of acidophiles can result in the release of natural organic compounds, which have the potential to significantly enhance the mobility of tungsten in the environment [149]. These organic compounds can co-precipitate with ferrihydrite, $Fe(OH)_3$, across a wide pH range (from 4 to 11), potentially interfering with the interaction between soluble tungstate oxyanions (WO_4^{2-}) and ferrihydrite [150]. The activity of acidophiles plays a pivotal role in the decomposition of wolframite and the mobilization of tungsten in mining waste environments [151]. During the initial stages of wolframite weathering under acidic conditions, free tungstate ions may bind with various cations, giving rise to a diverse array of secondary tungsten minerals, e.g., gallium-rich tungstate and sanmartinite $(Zn,Fe)WO_4$ [152]. This phenomenon could potentially restrict the availability of tungsten in the environment.

The activity of *A. ferrooxidans* and acidophilic organisms holds significant potential for bioleaching tungsten minerals, primarily wolframite. The efficiency of this process is highly contingent on the microbial composition of the environment and the specific speciation of tungsten, which is thermodynamically influenced by the in situ redox state and other environmental variables [66].

5.9. Gold

Gold (Au) has played a key role in the development of human civilization, as the basis for decorative, ceremonial, and religious artifacts. Due to the physical and chemical properties of gold, such as its ability to not chemisorb oxygen, or the fact that it does not corrode, makes it an excellent catalyst. It is widely used in industrial applications by both homogeneous and heterogeneous gold catalysis [153]. The recovery of gold from rock mostly relies on the cyanidation process, Equation (37):

$$4Au^0 + 8NaCN + 2H_2O + O_2 \rightarrow 4NaAu(CN)_2 + 4NaOH \quad (37)$$

The use of cyanide for the dissolution of gold poses harsh environmental risks while bioleaching for gold recovery reveals promising avenues for more sustainable prac-

tices. Cyanide-producing bacteria autonomously convert cyanide to the less toxic form B-cyanoalanine [154]. *A. ferrooxidans* in the bioleaching of gold is part of the indirect method towards the elimination of interfering metal sulfides from ores containing precious metals. In gold ores, minute gold particles are encapsulated or tightly bound within a sulfide mineral, typically pyrite, arsenopyrite, or a combination of both [68]. To achieve satisfactory gold recovery, it is important to first oxidize the sulfide minerals prior to subjecting the ore to cyanide treatment for gold dissolution [69,155].

5.10. Mercury

Mercury (Hg) is produced globally, with the European contribution led by the Spanish mining industry. The Americas and Asia, particularly Kyrgyzstan, Russia, and China, also play significant roles in mercury extraction [156]. The 20th century saw a spike in global production, driven by industrial use, especially in the chlor-alkali industry, where mercury cells are used for electrolysis [157,158]. Beyond industry, mercury has been used in dentistry for over a century, with dental amalgam making up a significant portion of its usage in the USA and Sweden. Despite alternatives and known environmental impacts, international efforts against Hg in dental amalgam are lacking [158].

Cinnabar (HgS) has a long history of use as a natural pigment and in medicine and preservation for thousands of years [159]. The dissolution of cinnabar was found to be closely related to iron concentration, particularly influenced by ferric iron generated by *A. ferrooxidans* [160]. Although natural oxidation of cinnabar is limited [161], ferric iron catalyzes the reaction as in Equation (38):

$$HgS + 2Fe^{3+} \rightarrow Hg^{2+} + 2Fe^{2+} + S^0 \quad (38)$$

During prolonged reactor operation with immobilized cells, it has been observed that a significant number of cells emerge into the liquid medium; this process has been explained by the adhesion of *A. ferrooxidans* on sulfur particles, with it becoming hydrophilic [162]. Thermodynamically, the free energy of adhesion is determined by interfacial tensions between bacteria, liquid, and sulfur phases [163]. Hydrophobic secretion by *A. ferrooxidans* enhances contact and adhesion [164]. The adhered sulfur particles are further oxidized by *A. ferrooxidans* (Equation (17)). This reaction inhibited ferric iron hydrolyzation [165], maintaining oxidant (ferric iron) concentration [166]. Substituting this into the cinnabar oxidation equation in Equation (39) yields the following:

$$2HgS + 4Fe^{3+} + 1.5O_2 + 2H_2O \rightarrow 2Hg^{2+} + 4Fe^{2+} + 2H_2SO_4 \quad (39)$$

A. ferrooxidans rapidly oxidizes ferrous iron. The oxidation process led to a reduction in H^+ concentration, thereby aiding in the dissolution of cinnabar. The detected change in surface area pre- and post-bioleaching suggested a smoother particle surface prior to the reaction, which subsequently became more fragmented. This transformation was attributed to the indirect catalytic effect of ferric iron produced by *A. ferrooxidans* and the direct oxidation function that supplied energy for the growth of the bacteria [162]. By utilizing *A. ferrooxidans*, the toxic cinnabar can be broken down, reducing its environmental impact and recovering the mercury present in it.

6. Post-Transition Metals

Beyond the classical distinction between metals and nonmetals, a diverse group known as post-transition metals comprise elements found between the transition and metalloid regions. Post-transition metals, including aluminum and gallium, showcase a diversity of properties, encompassing malleability, conductivity, and varied oxidation states [167]. Their presence in alloys, combined with their unique reactivity patterns, makes them essential in the manufacturing of diverse materials, from lightweight alloys to corrosion-resistant coatings [168].

6.1. Gallium

The demand for Gallium (Ga) is projected to undergo rapid escalation from 2014 to 2050 [62,169] due to development of light-emitting diodes (LEDs) [63]. Bioleaching presents distinct advantages for Gallium recovery, characterized by its enhanced safety, environmental friendliness, and energy-efficient processes, enabling the leaching of metals even at relatively low concentrations. An adapted strain of *A. ferrooxidans* demonstrated the capacity to leach approximately 60% of the gallium content from powdered LEDs [170]. The efficacy of *A. ferrooxidans* for augmenting gallium bioleaching from LED powder establishes a suitable path for gallium recovery from LED waste [171]. The general bioleaching process can be summarized following Equation (29), in which M is gallium.

6.2. Lead

Lead (Pb) holds a long history of human use dating back many centuries. Its malleability and resistance to corrosion have made it a valuable metal for various applications, including pipes and paints, since the time of the Romans [172]. Lead found application e.g., in lead glazes for pottery and insecticides, despite being recognized for its carcinogenic properties; it is still utilized in the production of car batteries, pigments, ammunition, cable sheathing, radiation shielding, and soldering [72]. The primary mineral source of lead is galena (PbS), which is processed through roasting [173], and among others is Anglesite ($PbSO_4$) [174]. Bioleaching using *A. ferrooxidans* and *A. thiooxidans* is a noteworthy alternative to conventional roasting and smelting processes for lead extraction [73]. The precipitation of Pb^{2+}, released by galena as lead sulfate, concurs with elemental sulfur and sulfides undergoing oxidation by *A. ferrooxidans*, resulting in $SO_4{}^{2-}$ [175], as can seen from Equations (40)–(45):

$$PbS + H_2SO_4 + 0.5O_2 \rightarrow PbSO_4 + H_2O + S^0 \quad (40)$$

$$2S^0 + 2H_2O + 3O_2 \rightarrow 2SO_4{}^{2-} + 4H^+ \quad (41)$$

$$PbS + 2Fe^{3+} \rightarrow Pb^{2+} + 2Fe^{2+} + S^0 \quad (42)$$

$$Pb^{2+} + SO_4{}^{2-} \rightarrow PbSO_4 \quad (43)$$

$$PbS + H_2SO_4 \rightarrow PbSO_4 + H_2S \quad (44)$$

$$2H_2S + O_2 \rightarrow 2S^0 + 2H_2O \quad (45)$$

A. ferrooxidans and microbial consortia can facilitate the biorecovery of lead through various mechanisms such as the ones shown in Equations (40)–(45) and through biosorption, bioaccumulation, and biomineralization, effectively reducing the toxicity and mobility of lead in contaminated environments.

7. Metalloids: Arsenic

Arsenic (As) exhibits a pervasive presence, ranking 20th in abundance within the Earth's crust, 14th in seawater, and emerging as the 12th most prevalent element within the human body [64]. Since its initial discovery, As has found diverse applications encompassing medicine, agriculture, metallurgy, and even as a potent poisonous substance for various organisms [176]. Arsenic is a known toxicant; nevertheless (1) it holds therapeutic potential as a frontline chemotherapeutic agent against specific hematopoietic cancers [177]; (2) some prokaryotes thrive and endure elevated As concentrations [178]. Among the mineral deposits, sulfide mineral realgar (alpha-As_4S_4) stands out due to its notably high arsenic content [179].

Among metalloids, arsenic is efficiently mobilized by *A. ferrooxidans*, which exhibits resilience to arsenic concentrations in the gram per liter range—an amount considered poisonous for numerous organisms. The catalytic conversion of Fe^{2+} to Fe^{3+} in an acidic solution instigates the generation of cationic As, as illustrated from Equations (46)–(50) [180]:

$$4Fe^{2+} + O_2 + 4H^+ \rightarrow 4Fe^{3+} + 2H_2O \quad (46)$$

$$As_2S_2 + 6Fe^{3+} \rightarrow 2As^{3+} + 2S^0 + 6Fe^{2+} \quad (47)$$

$$H_3AsO_3 + H_2O \rightarrow H_3AsO_4 + 2H^+ + 2e^- \quad (48)$$

$$H_3AsO_4 + Fe^{3+} \rightarrow FeAsO_4 + 3H^+ \quad (49)$$

In the presence of *A. ferrooxidans*:

$$As_2S_2 + 14H_2O \rightarrow 2H_3AsO_3 + 2HSO_4^- + 20H^+ + 18e^- \quad (50)$$

Bioleaching of arsenic and precipitation and oxidation of arsenite or reduction to arsenate are some valid processes involved in biorecovery activities and in treating contaminated environments such as AMDs, industrial wastewater, and polluted soils.

8. Actinides: Uranium

Uranium (U) is the only known actinide to be mobilized by *A. ferrooxidans*. The actinides, or actinide series, elements with atomic numbers ranging from 89 to 103, are situated beneath the lanthanide series. From uranium to lawrencium, each actinide brings its own set of intriguing features, making the study of this series crucial for understanding nuclear reactions, reactor design, and the behavior of radioactive materials [181].

Uranium finds applications in nuclear energy generation, the production of uranium oxide (U_3O_8), the formulation of anti-corrosive alloys, and coloring agents for glass and porcelain [74]. The conventional extraction of uranium relies on a process that utilizes acids as leaching agents [75]. Extracting uranium from low-grade ores through chemical leaching is often economically unfeasible [182]. In contrast, bioleaching is recognized for its economic viability and environmental compatibility [183]. *A. ferrooxidans* stands out in bioleaching for uranium extraction, leveraging its indirect oxidation capabilities as in Equation (51) [76,184]:

$$U^{(IV)}O_2 + 2Fe^{3+} \rightarrow U^{(VI)}O_2^{2+} + 2Fe^{2+} \quad (51)$$

Uranium exhibits limited solubility in an aqueous medium when it is in the +4 oxidation state. However, within an acidic environment, the ferric ion facilitates the oxidation of U^{4+} to U^{6+}, a form that readily dissolves. In a complementary reaction to the oxidation of U^{4+}, the ferric ion undergoes reduction to become the ferrous ion. Under the influence of *A. ferrooxidans* oxidation function, it is subsequently re-oxidized back to the ferric state. This enables it to once again engage in the oxidation of uranium [76]. Particularly, *A. ferrooxidans* sp. FJ2 is able to extract uranium by modulating the operon gene rus by 100% in 13 days [76]. The expression of some operons such as rus and petI, both involved in iron oxidation, are enhanced in the presence of radioactive minerals and after gamma-irradiation. Moreover, after exposure to gamma-rays, it was shown that this type of radiation does not affect the pH or the electrochemical parameters of the whole reaction, but increases the expression of all the genes encoded by the aforementioned operons without significant changes in uranium extraction rate [76].

9. Conclusions

A. ferrooxidans stands as a cornerstone in trace element bioleaching and in the biomining and biorecovery industry (Figure 3) [185]. Its specialized metabolic pathways, particularly in the oxidation of ferrous iron and sulfur compounds, combined with its ability to thrive and contribute to hyperacidic conditions, empower the efficient solubilization of diverse valuable trace elements from mineral deposits [12]. This microorganism has demonstrated remarkable proficiency in boosting metal (including alkali and transition metals, Figure 2) recovery rates, revolutionizing conventional mining methodologies. Its use significantly reduces the environmental footprint of mining operations, representing a critical step towards sustainable and eco-friendly mining practices [185]. This underscores

the transformative potential of *A. ferrooxidans* in the journey toward sustainability [14], increasing our ability to recover critical metals from low-grade ore deposits, recycle E-wastes, and bioremediate contaminated sites.

Peering into the future, the application of *A. ferrooxidans* holds exciting prospects in space exploration. Its unique adaptability and capacity to facilitate metal extraction on Earth represents a groundbreaking future opportunity for resource utilization on other planetary bodies. By mitigating the challenges of resource transport from our home planet, the use of *A. ferrooxidans* may support future space missions, catalyzing the extraction of key elements for the development of extraterrestrial habitats and advancing technological frontiers [11].

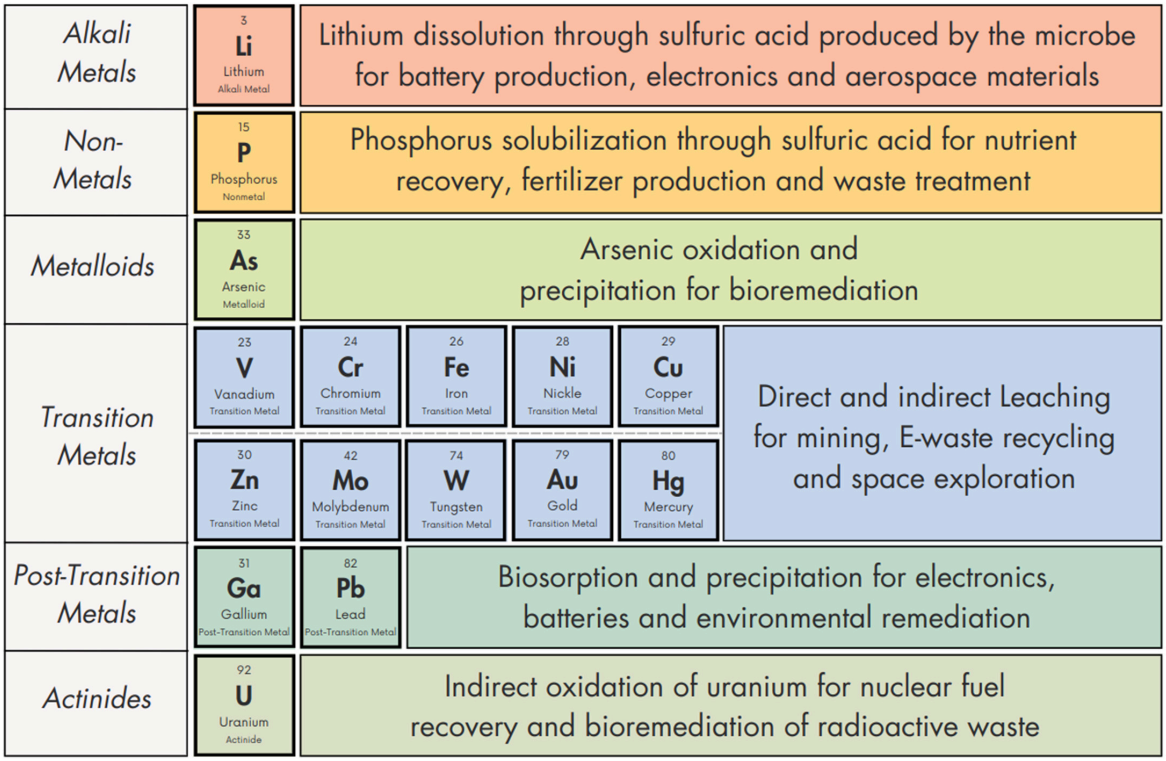

Figure 3. Periodic table of *A. ferrooxidans*-mobilized elements with main involved processes in elemental extraction techniques divided by chemical group. The periodic table of *A. ferrooxidans* is presented in bold.

One major concern with bioleaching and biomining is the production of acid mine drainage, a process that leads to significant environmental challenges [39]. However, bioleaching operations can be carefully controlled and optimized to minimize contamination risks and mitigate environmental impacts. Strategies such as monitoring pH, optimizing microbial consortia, and designing contained bioreactors or controlled leaching systems ensure that bioleaching processes can be sustainable. To counteract these negative impacts, it can be useful to employ biorecovery strategies, e.g., the usage of either naturally occurring or deliberately introduced microorganisms to consume and break down environmental pollutants, which are considered essential [186]. The effectiveness of biomining relies on the intricate interactions among the microbial communities involved. A deep comprehension of these interactions is strictly related to the effective management and optimization of the microbial consortia to enhance biomining efficiency [187], since the majority of current

biomining activities use naturally occurring microbial populations [188]. It is worth noting that the dangers associated with the discharge of the bioremediating microorganisms into the surrounding environment to counteract acid mine drainage production are considered minimal, because these organisms are already present in the ecosystem [189,190]. As a consequence, while bioleaching and biomining present forward-thinking solutions for extracting metals, it is important to address their environmental repercussions and ensure sustainable resource recovery, aligning with the objectives of a circular economy [14].

The application of bioleaching to E-waste holds significant potential for enhancing social development and bolstering the economies of developing nations. The utilization of mesophilic and acidophilic/hyperacidophilic bacteria, particularly *A. ferrooxidans*, represents a substantial stride towards advancing base metal recovery both on Earth and potentially in extraterrestrial environments, e.g., planets (Mars), moons (Moon, Enceladus, Europa), and asteroids (Lutetia, Kleopatra). As we delve deeper into the intricacies of microbial-driven biomining processes, it is imperative to acknowledge the multifaceted contributions of *A. ferrooxidans*. From bolstering metal recovery rates on Earth to potentially revolutionizing resource extraction in space, this remarkable bacterium exemplifies the transformative potential of biotechnology in mining and beyond. With ongoing research and technological advancements, we are poised to further harness the capabilities of *A. ferrooxidans*, propelling us toward a future marked by sustainability, innovation, and abundant resources.

Author Contributions: Conceptualization, L.T., A.R. and D.G.; methodology, L.T. and M.E.; validation, L.T., A.R. and D.G.; formal analysis, L.T., M.E., M.C., and B.B.; investigation, L.T. and M.E.; resources, L.T.; data curation, L.T.; writing—original draft preparation, L.T., M.E., M.C. and B.B.; writing—review and editing, L.T., M.E., M.C., B.B., S.F., M.T.M.T., T.S., R.S., G.C., A.C., A.R. and D.G.; visualization, L.T. and D.G.; supervision, A.R., D.G., and G.C.; project administration, A.R. and D.G.; funding acquisition, A.R. and D.G. All authors have read and agreed to the published version of the manuscript.

Funding: This work has been conducted thanks to the following funding: the PhD program PON "Ricerca e Innovazione" 2014–2020, DM n. 1061 (10 August 2021) and n. 1233 (30 July 2020) by the Ministero dell'Università e della Ricerca (MUR); the ASI-INAF agreements I/024/12/0 and 2020-4-HH.0, by the Italian Space Agency (ASI). This work was supported by funding from the European Research Council (ERC) under the European Union's Horizon 2020 research and innovation program (Grant Agreement No. 948972—COEVOLVE—ERC-2020-STG).

Data Availability Statement: No new data were created.

Acknowledgments: We thank MUR (Ministero dell'Università e della Ricerca) for the PhD program PON "Ricerca e Innovazione" 2014–2020, DM n.1061 (10 August 2021) and n. 1233 (30 July 2020).

Conflicts of Interest: The authors declare no conflicts of interest.

References

1. Merino, N.; Aronson, H.S.; Bojanova, D.P.; Feyhl-Buska, J.; Wong, M.L.; Zhang, S.; Giovannelli, D. Living at the Extremes: Extremophiles and the Limits of Life in a Planetary Context. *Front. Microbiol.* **2019**, *10*, 780. [CrossRef] [PubMed]
2. Bosecker, K. Bioleaching: Metal solubilization by microorganisms. *FEMS Microbiol. Rev.* **1997**, *20*, 591–604. [CrossRef]
3. Ilyas, S.; Anwar, M.A.; Niazi, S.B.; Ghauri, M.A. Bioleaching of metals from electronic scrap by moderately thermophilic acidophilic bacteria. *Hydrometallurgy* **2007**, *88*, 180–188. [CrossRef]
4. Navarro, C.A.; von Bernath, D.; Jerez, C.A. Heavy metal resistance strategies of acidophilic bacteria and their acquisition: Importance for biomining and bioremediation. *Biol. Res.* **2013**, *46*, 363–371. [CrossRef]
5. Zhao, F.; Wang, S. Chapter 7—Bioleaching of Electronic Waste Using Extreme Acidophiles. In *Electronic Waste Management and Treatment Technology*; Prasad, M.N.V., Vithanage, M., Eds.; Butterworth-Heinemann: Oxford, UK, 2019; pp. 153–174.
6. Niehaus, F.; Bertoldo, C.; Kähler, M.; Antranikian, G. Extremophiles as a source of novel enzymes for industrial application. *Appl. Microbiol. Biotechnol.* **1999**, *51*, 711–729. [CrossRef]
7. Watling, H.R.; Shiers, D.W.; Collinson, D.M. Extremophiles in Mineral Sulphide Heaps: Some Bacterial Responses to Variable Temperature, Acidity and Solution Composition. *Microorganisms* **2015**, *3*, 364–390. [CrossRef] [PubMed]
8. Giovanella, P.; Vieira, G.A.; Otero, I.V.R.; Pellizzer, E.P.; Fontes, B.d.J.; Sette, L.D. Metal and organic pollutants bioremediation by extremophile microorganisms. *J. Hazard. Mater.* **2020**, *382*, 121024. [CrossRef]

9. Cockell, C.S.; Santomartino, R.; Finster, K.; Waajen, A.C.; Eades, L.J.; Moeller, R.; Rettberg, P.; Fuchs, F.M.; Van Houdt, R.V.; Leys, N.; et al. Space station biomining experiment demonstrates rare earth element extraction in microgravity and Mars gravity. *Nat. Commun.* **2020**, *11*, 5523. [CrossRef] [PubMed]
10. Santomartino, R.; Zea, L.; Cockell, C.S. The smallest space miners: Principles of space biomining. *Extremophiles* **2022**, *26*, 7. [CrossRef]
11. Tonietti, L.; Barosa, B.; Pioltelli, E.; Giovannelli, D.; Covone, G.; Di Donato, P.; Cordone, A.; Inno, L.; Magliano, C.; Fiscale, S.; et al. Exploring the Development of Astrobiology Scientific Research through Bibliometric Network Analysis: A Focus on Biomining and Bioleaching. *Minerals* **2023**, *13*, 797. [CrossRef]
12. Valdés, J.; Pedroso, I.; Quatrini, R.; Dodson, R.J.; Tettelin, H.; BlakeII, R.; Eisen, J.A.; Holmes, D.S. *Acidithiobacillus ferrooxidans* metabolism: From genome sequence to industrial applications. *BMC Genom.* **2008**, *9*, 597. [CrossRef] [PubMed]
13. Wang, R.; Lin, J.-Q.; Liu, X.-M.; Pang, X.; Zhang, C.-J.; Yang, C.-L.; Gao, X.-Y.; Lin, C.-M.; Li, Y.-Q.; Li, Y.; et al. Sulfur Oxidation in the Acidophilic Autotrophic *Acidithiobacillus* spp. *Front. Microbiol.* **2019**, *9*, 3290. [CrossRef] [PubMed]
14. Kaksonen, A.H.; Petersen, J. The Future of Biomining: Towards Sustainability in a Metal-Demanding World. In *Biomining Technologies: Extracting and Recovering Metals from Ores and Wastes*; Johnson, D.B., Bryan, C.G., Schlömann, M., Roberto, F.F., Eds.; Springer International Publishing: Cham, Switzerland, 2023; pp. 295–314.
15. Ibáñez, A.; Garrido-Chamorro, S.; Coque, J.J.R.; Barreiro, C. From Genes to Bioleaching: Unraveling Sulfur Metabolism in *Acidithiobacillus* Genus. *Genes* **2023**, *14*, 1772. [CrossRef] [PubMed]
16. Baker, B.J.; Banfield, J.F. Microbial communities in acid mine drainage. *FEMS Microbiol. Ecol.* **2003**, *44*, 139–152. [CrossRef] [PubMed]
17. Pedersen, T.F. Shouldn't We Be Putting Our Sulphide-Rich Mine Tailings in the Ocean or in Lakes Rather than on Land? In *Waters in Peril*; Bendell-Young, L., Gallaugher, P., Eds.; Springer: Boston, MA, USA, 2001; pp. 151–162.
18. Hafenbradl, D.; Keller, M.; Dirmeier, R.; Rachel, R.; Rossnagel, P.; Burggraf, S.; Huber, H.; Stetter, K.O. *Ferroglobus placidus* gen. nov., sp. nov., A novel hyperthermophilic archaeum that oxidizes Fe^{2+} at neutral pH under anoxic conditions. *Arch. Microbiol.* **1996**, *166*, 308–314. [CrossRef] [PubMed]
19. Nguyen, V.K.; Lee, J.-U. Effect of sulfur concentration on microbial removal of arsenic and heavy metals from mine tailings using mixed culture of *Acidithiobacillus* spp. *J. Geochem. Explor.* **2015**, *148*, 241–248. [CrossRef]
20. Bruscella, P.; Appia-Ayme, C.; Levicán, G.; Ratouchniak, J.; Jedlicki, E.; Holmes, D.; & Bonnefoy, V. Differential expression of two bc1 complexes in the strict acidophilic chemolithoautotrophic bacterium Acidithiobacillus ferrooxidans suggests a model for their respective roles in iron or sulfur oxidation. *Microbiology* **2007**, *153 Pt 1*, 102–110. [CrossRef]
21. Quatrini, R.; Appia-Ayme, C.; Denis, Y.; Ratouchniak, J.; Veloso, F.; Valdes, J.; Lefimil, C.; Silver, S.; Roberto, F.; Orellana, O.; et al. Insights into the iron and sulfur energetic metabolism of *Acidithiobacillus ferrooxidans* by microarray transcriptome profiling. *Hydrometallurgy* **2006**, *83*, 263–272. [CrossRef]
22. Zhan, Y.; Yang, M.; Zhang, S.; Zhao, D.; Duan, J.; Wang, W.; Yan, L. Iron and sulfur oxidation pathways of *Acidithiobacillus ferrooxidans*. *World J. Microbiol. Biotechnol.* **2019**, *35*, 60. [CrossRef]
23. Liu, H.-L.; Lan, Y. Optimal production of sulphuric acid by *Thiobacillus thiooxidans* using response surface methodology. *Process. Biochem.* **2004**, *39*, 1953–1961. [CrossRef]
24. Fortin, D.; Davis, B.; Southam, G.; Beveridge, T.J. Biogeochemical phenomena induced by bacteria within sulfidic mine tailings. *J. Ind. Microbiol.* **1995**, *14*, 178–185. [CrossRef]
25. Pronk, J.T.; de Bruyn, J.C.; Bos, P.; Kuenen, J.G. Anaerobic Growth of *Thiobacillus ferrooxidans*. *Appl. Environ. Microbiol.* **1992**, *58*, 2227–2230. [CrossRef] [PubMed]
26. Plessis, C.A.D.; Slabbert, W.; Hallberg, K.B.; Johnson, D.B. Ferredox: A biohydrometallurgical processing concept for limonitic nickel laterites. *Hydrometallurgy* **2011**, *109*, 221–229. [CrossRef]
27. Akcil, A.; Koldas, S. Acid Mine Drainage (AMD): Causes, treatment and case studies. *J. Clean. Prod.* **2006**, *14*, 1139–1145. [CrossRef]
28. González-Paz, J.R.; del Carmen Monterrubio, M.; Ordaz, A.; García-Peña, E.I.; Guerrero-Barajas, C. Influence of Fe^{2+} and Fe^{3+} on the Performance and Microbial Community Composition of a MFC Inoculated with Sulfate-Reducing Sludge and Acetate as Electron Donor. *J. Chem.* **2022**, *2022*, e5685178. [CrossRef]
29. Córdoba, E.M.; Muñoz, J.A.; Blázquez, M.L.; González, F.; Ballester, A. Leaching of chalcopyrite with ferric ion. Part I: General aspects. *Hydrometallurgy* **2008**, *93*, 81–87. [CrossRef]
30. Vera, M.; Schippers, A.; Hedrich, S.; Sand, W. Progress in bioleaching: Fundamentals and mechanisms of microbial metal sulfide oxidation–part A. *Appl. Microbiol. Biotechnol.* **2022**, *106*, 6933–6952. [CrossRef]
31. Sand, W.; Gehrke, T.; Jozsa, P.-G.; Schippers, A. (Bio)chemistry of bacterial leaching—Direct vs. indirect bioleaching. *Hydrometallurgy* **2001**, *59*, 159–175. [CrossRef]
32. Suzuki, I. Microbial leaching of metals from sulfide minerals. *Biotechnol. Adv.* **2001**, *19*, 119–132. [CrossRef]
33. Van Gerven, T.; Moors, J.; Dutré, V.; Vandecasteele, C. Effect of CO_2 on leaching from a cement-stabilized MSWI fly ash. *Cem. Concr. Res.* **2004**, *34*, 1103–1109. [CrossRef]
34. Liu, Y.; Fang, J.; Liu, S.; An, X.; Kang, Y.; Wang, L. Effect of Different CO_2 Treatments on the Metal Leaching in Steel Slag Binders. *Front. Energy Res.* **2021**, *9*, 765519. [CrossRef]

35. Vu, B.; Chen, M.; Crawford, R.J.; Ivanova, E.P. Bacterial Extracellular Polysaccharides Involved in Biofilm Formation. *Molecules* **2009**, *14*, 2535–2554. [CrossRef] [PubMed]
36. Tan, S.N.; Chen, M. Early stage adsorption behaviour of *Acidithiobacillus ferrooxidans* on minerals I: An experimental approach. *Hydrometallurgy* **2012**, *119*, 87–94. [CrossRef]
37. Maluckov, B. The Catalytic Role of *Acidithiobacillus Ferrooxidans* for Metals Extraction from Mining-Metallurgical Resource. *Biodivers. Int. J.* **2017**, *1*, 1–12. [CrossRef]
38. Nazari, B.; Jorjani, E.; Hani, H.; Manafi, Z.; Riahi, A. Formation of jarosite and its effect on important ions for *Acidithiobacillus ferrooxidans* bacteria. *Trans. Nonferrous Met. Soc. China* **2014**, *24*, 1152–1160. [CrossRef]
39. Jerez, C.A. Biomining of metals: How to access and exploit natural resource sustainably. *Microb. Biotechnol.* **2017**, *10*, 1191–1193. [CrossRef]
40. Metal Removal by Acidithiobacillus ferrooxidans Through Cells and Extra-Cellular Culture Supernatant in Biomachining-ScienceDirect. Available online: https://www.sciencedirect.com/science/article/pii/S1755581712000181 (accessed on 20 March 2024).
41. Cai, G.; Ebrahimi, M.; Zheng, G.; Kaksonen, A.H.; Morris, C.; O'Hara, I.M.; Zhang, Z. Effect of ferrous iron loading on dewaterability, heavy metal removal and bacterial community of digested sludge by *Acidithiobacillus ferrooxidans*. *J. Environ. Manag.* **2021**, *295*, 113114. [CrossRef] [PubMed]
42. Takeuchi, F.; Sugio, T. Volatilization and recovery of mercury from mercury-polluted soils and wastewaters using mercury-resistant *Acidithiobacillus ferrooxidans* strains SUG 2-2 and MON-1. *Environ. Sci. Int. J. Environ. Physiol. Toxicol.* **2006**, *13*, 305–316.
43. Cabrera, G.; Viera, M.; Gómez, J.M.; Cantero, D.; Donati, E. Bacterial removal of chromium (VI) and (III) in a continuous system. *Biodegradation* **2007**, *18*, 505–513. [CrossRef]
44. Camm, G.S.; Glass, H.J.; Bryce, D.W.; Butcher, A.R. Characterisation of a mining-related arsenic-contaminated site. Cornwall, UK. *J. Geochem. Explor.* **2004**, *82*, 1–15. [CrossRef]
45. Adetunji, A.I.; Oberholster, P.J.; Erasmus, M. Bioleaching of Metals from E-Waste Using Microorganisms: A Review. *Minerals* **2023**, *13*, 828. [CrossRef]
46. Hubau, A.; Bryan, C.G. Metal Recovery from E-wastes. In *Biomining Technologies: Extracting and Recovering Metals from Ores and Wastes*; Johnson, D.B., Bryan, C.G., Schlömann, M., Roberto, F.F., Eds.; Springer International Publishing: Cham, Switzerland, 2023; pp. 239–259.
47. Hadler, K.; Martin, D.J.P.; Carpenter, J.; Cilliers, J.J.; Morse, A.; Starr, S.; Rasera, J.N.; Seweryn, K.; Reiss, P.; Meurisse, A. A universal framework for Space Resource Utilisation (SRU). *Planet. Space Sci.* **2020**, *182*, 104811. [CrossRef]
48. Gumulya, Y.; Zea, L.; Kaksonen, A.H. In situ resource utilisation: The potential for space biomining. *Miner. Eng.* **2022**, *176*, 107288. [CrossRef]
49. Cinti, S.; Singh, S.; Covone, G.; Tonietti, L.; Ricciardelli, A.; Cordone, A.; Iacono, R.; Mazzoli, A.; Moracci, M.; Rotundi, A.; et al. Reviewing the state of biosensors and lab-on-a- chip technologies: Opportunities for extreme environments and space exploration. *Front. Microbiol.* **2023**, *14*, 1215529. [CrossRef] [PubMed]
50. Della Corte, V.; Ferretti, S.; Piccirillo, A.M.; Zakharov, V.; Di Paolo, F.; Rotundi, A.; Ammannito, E.; Amoroso, M.; Bertini, I.; Di Donato, P.; et al. DISC-the dust impact sensor and counter on-board Comet Interceptor: Characterization of the dust coma of a dynamically new comet. *Adv. Space Res.* **2023**, *71*, 3457–3467. [CrossRef]
51. Magliano, C.; Covone, G.; Dobal, R.; Cacciapuoti, L.; Tonietti, L.; Giacalone, S.; Vines, J.I.; Inno, L.; Jenkins, J.S.; Lissauer, J.J.; et al. A systematic validation of hot Neptunes in TESS data. *Mon. Not. R. Astron. Soc.* **2023**, *519*, 1562–1577. [CrossRef]
52. Peng, Z.; Wang, Z.; Han, Z.; Zhu, Y.; Li, Y.; Xie, K. Vanadium–Titanium Magnetite Concentrate, Calcium–Magnesium Composite Roasting and Sulfuric Acid Leaching for Vanadium Extraction from Pellets. *Metals* **2023**, *13*, 1135. [CrossRef]
53. Hao, L.; Zhang, B.; Feng, C.; Zhang, Z.; Lei, Z.; Shimizu, K.; Cao, X.; Liu, H.; Liu, H. Microbial vanadium (V) reduction in groundwater with different soils from vanadium ore mining areas. *Chemosphere* **2018**, *202*, 272–279. [CrossRef]
54. Shi, C.; Cui, Y.; Lu, J.; Zhang, B. Sulfur-based autotrophic biosystem for efficient vanadium (V) and chromium (VI) reductions in groundwater. *Chem. Eng. J.* **2020**, *395*, 124972. [CrossRef]
55. Tambat, V.S.; Patel, A.K.; Chen, C.-W.; Raj, T.; Chang, J.-S.; Singhania, R.R.; Dong, C.-D. A sustainable vanadium bioremediation strategy from aqueous media by two potential green microalgae. *Environ. Pollut.* **2023**, *323*, 121247. [CrossRef]
56. Zhang, B.; Zhang, H.; He, J.; Zhou, S.; Dong, H.; Rinklebe, J.; Ok, Y.S. Vanadium in the Environment: Biogeochemistry and Bioremediation. *Environ. Sci. Technol.* **2023**, *57*, 14770–14786. [CrossRef] [PubMed]
57. Sharma, P.; Singh, S.P.; Parakh, S.K.; Tong, Y.W. Health hazards of hexavalent chromium (Cr (VI)) and its microbial reduction. *Bioengineered* **2022**, *13*, 4923–4938. [CrossRef] [PubMed]
58. Liu, S.; Chen, L.; Gao, Y. Hexavalent Chromium Leaching Influenced Factors in the Weathering Chrome Slag. *Procedia Environ. Sci.* **2013**, *18*, 783–787. [CrossRef]
59. Garg, S.K.; Tripathi, M.; Srinath, T. Strategies for chromium bioremediation of tannery effluent. *Rev. Environ. Contam. Toxicol.* **2012**, *217*, 75–140. [PubMed]
60. Arshadi, M.; Yaghmaei, S. Advances in bioleaching of copper and nickel from electronic waste using *Acidithiobacillus ferrooxidans*: Evaluating daily pH adjustment. *Chem. Pap.* **2020**, *74*, 2211–2227. [CrossRef]

61. Li, B.; Li, H.; Dong, Z.; Lu, Y.; Liu, N.; Hao, X. The global copper material trade network and risk evaluation: A industry chain perspective. *Resour. Policy* **2021**, *74*, 102275. [CrossRef]
62. Lu, F.; Xiao, T.; Lin, J.; Ning, Z.; Long, Q.; Xiao, L.; Huang, F.; Wang, W.; Xiao, Q.; Lan, X.; et al. Resources and extraction of gallium: A review. *Hydrometallurgy* **2017**, *174*, 105–115. [CrossRef]
63. DenBaars, S.P.; Feezell, D.; Kelchner, K.; Pimputkar, S.; Pan, C.-C.; Yen, C.-C.; Tanaka, S.; Zhao, Y.; Pfaff, N.; Farrell, R.; et al. Development of gallium-nitride-based light-emitting diodes (LEDs) and laser diodes for energy-efficient lighting and displays. *Acta Mater.* **2013**, *61*, 945–951. [CrossRef]
64. Mandal, B.K.; Suzuki, K.T. Arsenic round the world: A review. *Talanta* **2002**, *58*, 201–235. [CrossRef]
65. Boury, C.; Green, S.R.; Allanore, A. Production of Metallic Tungsten and Tungsten Carbide from Natural Wolframite and Scheelite via Sulfide Chemistry. *Met. Mater. Trans. B* **2023**, *54*, 3270–3287. [CrossRef]
66. Han, Z.; Levett, A.; Edraki, M.; Jones, M.W.M.; Howard, D.; Southam, G. Accelerating bioleaching of tungsten mining wastes using indigenous acidophilic bacteria. *J. Hazard. Mater.* **2023**, *454*, 131490. [CrossRef] [PubMed]
67. Hällström, L.; Alakangas, L.; Martinsson, O. Scheelite weathering and tungsten (W) mobility in historical oxidic-sulfidic skarn tailings at Yxsjöberg, Sweden. *Environ. Sci. Pollut. Res.* **2020**, *27*, 6180–6192. [CrossRef] [PubMed]
68. El-Midany, A. Gold recovery from sulphide minerals: A bioprocessing approach. *Afinidad-Barc.* **2012**, *68*, 62–68.
69. Medina, D.; Anderson, C.G. A Review of the Cyanidation Treatment of Copper-Gold Ores and Concentrates. *Metals* **2020**, *10*, 897. [CrossRef]
70. Sen, C. Bioleaching of Gold: An alternative green mining technology for 21st century. *Microbiol. World* **2015**, *3*, 11–20.
71. Işıldar, A.; van de Vossenberg, J.; Rene, E.R.; van Hullebusch, E.D.; Lens, P.N.L. Two-step bioleaching of copper and gold from discarded printed circuit boards (PCB). *Waste Manag.* **2016**, *57*, 149–157. [CrossRef] [PubMed]
72. Flora, G.; Gupta, D.; Tiwari, A. Toxicity of lead: A review with recent updates. *Interdiscip. Toxicol.* **2012**, *5*, 47–58. [CrossRef]
73. Kamoldeen, A. Bioleaching of Lead from Nigerian Anglesite Ore by *Acidithiobacillus ferrooxidans*. *Trends Appl. Sci. Res.* **2012**, *8*, 5591–5598.
74. Chen, L.; Liu, J.; Zhang, W.; Zhou, J.; Luo, D.; Li, Z. Uranium (U) source, speciation, uptake, toxicity and bioremediation strategies in soil-plant system: A review. *J. Hazard. Mater.* **2021**, *413*, 125319. [CrossRef]
75. Costine, A.; Nikoloski, A.N.; Costa, M.D.; Chong, K.F.; Hackl, R. Uranium extraction from a pure natural brannerite mineral by acidic ferric sulphate leaching. *Miner. Eng.* **2013**, *53*, 84–90. [CrossRef]
76. Pal, S.; Pradhan, D.; Das, T.; Sukla, L.B.; Chaudhury, G.R. Bioleaching of low-grade uranium ore using *Acidithiobacillus ferrooxidans*. *Indian J. Microbiol.* **2010**, *50*, 70–75. [CrossRef] [PubMed]
77. Dye, J.L. The alkali metals: 200 years of surprises. *Philos. Trans. R. Soc. A Math. Phys. Eng. Sci.* **2015**, *373*, 20140174. [CrossRef] [PubMed]
78. Garcia, L.V.; Ho, Y.-C.; Thant, M.M.M.; Han, D.S.; Lim, J.W. Lithium in a Sustainable Circular Economy: A Comprehensive Review. *Processes* **2023**, *11*, 418. [CrossRef]
79. Wang, T.-W.; Liu, T.; Sun, H. Direct recycling for advancing sustainable battery solutions. *Mater. Today Energy* **2023**, *38*, 101434. [CrossRef]
80. Ding, T.; Zheng, M.; Peng, S.; Lin, Y.; Zhang, X.; Li, M. Lithium extraction from salt lakes with different hydrochemical types in the Tibet Plateau. *Geosci. Front.* **2023**, *14*, 101485. [CrossRef]
81. Vikström, H.; Davidsson, S.; Höök, M. Lithium availability and future production outlooks. *Appl. Energy* **2013**, *110*, 252–266. [CrossRef]
82. Marcinov, V.; Klimko, J.; Takáčová, Z.; Pirošková, J.; Miškufová, A.; Sommerfeld, M.; Dertmann, C.; Friedrich, B.; Orac, D. Lithium Production and Recovery Methods: Overview of Lithium Losses. *Metals* **2023**, *13*, 1213. [CrossRef]
83. Szlugaj, J.; Radwanek-Bąk, B. Lithium sources and their current use. *Gospod. Surowcami Miner.-Miner. Resour. Manag.* **2022**, *38*, 61–87.
84. Guo, H.; Kuang, G.; Wan, H.; Yang, Y.; Yu, H.; Wang, H. Enhanced acid treatment to extract lithium from lepidolite with a fluorine-based chemical method. *Hydrometallurgy* **2019**, *183*, 9–19. [CrossRef]
85. Moazzam, P.; Boroumand, Y.; Rabiei, P.; Baghbaderani, S.S.; Mokarian, P.; Mohagheghian, F. Lithium bioleaching: An emerging approach for the recovery of Li from spent lithium ion batteries. *Chemosphere* **2021**, *277*, 130196. [CrossRef]
86. Sedlakova-Kadukova, J.; Marcincakova, R.; Luptakova, A.; Vojtko, M.; Fujda, M.; Pristas, P. Comparison of three different bioleaching systems for Li recovery from lepidolite. *Sci. Rep.* **2020**, *10*, 14594. [CrossRef] [PubMed]
87. Biswal, B.K.; Balasubramanian, R. Recovery of valuable metals from spent lithium-ion batteries using microbial agents for bioleaching: A review. *Front. Microbiol.* **2023**, *14*, 1197081. [CrossRef] [PubMed]
88. Xin, B.; Zhang, D.; Zhang, X.; Xia, Y.; Wu, F.; Chen, S.; Li, L. Bioleaching mechanism of Co and Li from spent lithium-ion battery by the mixed culture of acidophilic sulfur-oxidizing and iron-oxidizing bacteria. *Bioresour. Technol.* **2009**, *100*, 6163–6169. [CrossRef] [PubMed]
89. Mishra, D.; Kim, D.-J.; Ralph, D.E.; Ahn, J.-G.; Rhee, Y.-H. Bioleaching of metals from spent lithium ion secondary batteries using *Acidithiobacillus ferrooxidans*. *Waste Manag.* **2008**, *28*, 333–338. [CrossRef]
90. Yao, B.; Kuznetsov, V.L.; Xiao, T.; Slocombe, D.R.; Rao, C.N.R.; Hensel, F.; Edwards, P.P. Metals and non-metals in the periodic table. *Philos. Trans. R. Soc. A Math. Phys. Eng. Sci.* **2020**, *378*, 20200213. [CrossRef]

91. Jomova, K.; Makova, M.; Alomar, S.Y.; Alwasel, S.H.; Nepovimova, E.; Kuca, K.; Rhodes, C.J.; Valko, M. Essential metals in health and disease. *Chem. Interactions* **2022**, *367*, 110173. [CrossRef] [PubMed]
92. El Wali, M.; Golroudbary, S.R.; Kraslawski, A. Circular economy for phosphorus supply chain and its impact on social sustainable development goals. *Sci. Total. Environ.* **2021**, *777*, 146060. [CrossRef]
93. Daneshgar, S.; Buttafava, A.; Callegari, A.; Capodaglio, A.G. Simulations and Laboratory Tests for Assessing Phosphorus Recovery Efficiency from Sewage Sludge. *Resources* **2018**, *7*, 54. [CrossRef]
94. Mabrouk, O.; Hamdi, H.; Sayadi, S.; Al-Ghouti, M.A.; Abu-Dieyeh, M.H.; Zouari, N. Reuse of Sludge as Organic Soil Amendment: Insights into the Current Situation and Potential Challenges. *Sustainability* **2023**, *15*, 6773. [CrossRef]
95. Tytła, M. Assessment of Heavy Metal Pollution and Potential Ecological Risk in Sewage Sludge from Municipal Wastewater Treatment Plant Located in the Most Industrialized Region in Poland—Case Study. *Int. J. Environ. Res. Public Health* **2019**, *16*, 2430. [CrossRef]
96. Jama-Rodzeńska, A.; Sowiński, J.; Koziel, J.A.; Białowiec, A. Phosphorus Recovery from Sewage Sludge Ash Based on Cradle-to-Cradle Approach—Mini-Review. *Minerals* **2021**, *11*, 985. [CrossRef]
97. Priha, O.; Sarlin, T.; Blomberg, P.; Wendling, L.; Mäkinen, J.; Arnold, M.; Kinnunen, P. Bioleaching phosphorus from fluorapatites with acidophilic bacteria. *Hydrometallurgy* **2014**, *150*, 269–275. [CrossRef]
98. Calle-Castañeda, S.M.; Márquez-Godoy, M.A.; Hernández-Ortiz, J.P. Phosphorus recovery from high concentrations of low-grade phosphate rocks using the biogenic acid produced by the acidophilic bacteria *Acidithiobacillus thiooxidans*. *Miner. Eng.* **2018**, *115*, 97–105. [CrossRef]
99. Chi, R.; Xiao, C.; Gao, H. Bioleaching of phosphorus from rock phosphate containing pyrites by *Acidithiobacillus ferrooxidans*. *Miner. Eng.* **2006**, *19*, 979–981. [CrossRef]
100. Cortés, M.P.; Acuña, V.; Travisany, D.; Siegel, A.; Maass, A.; Latorre, M. Integration of Biological Networks for *Acidithiobacillus thiooxidans* Describes a Modular Gene Regulatory Organization of Bioleaching Pathways. *Front. Mol. Biosci.* **2020**, *6*, 155. [CrossRef] [PubMed]
101. Pradhan, S.K.; Heinonen-Tanski, H.; Veijalainen, A.-M.; Peräniemi, S.; Torvinen, E. Phosphorus Recovery from Sewage Sludge Using Acidithiobacilli. *Int. J. Environ. Res. Public. Health* **2021**, *18*, 7135. [CrossRef] [PubMed]
102. Durrant, M.C. Transition Metal Chemistry; past, present and future. *Transit. Met. Chem.* **2019**, *44*, 1–3. [CrossRef]
103. Giovannelli, D. Trace metal availability and the evolution of biogeochemistry. *Nat. Rev. Earth Environ.* **2023**, *4*, 597–598. [CrossRef]
104. Mele, B.H.; Monticelli, M.; Leone, S.; Bastoni, D.; Barosa, B.; Cascone, M.; Migliaccio, F.; Montemagno, F.; Ricciardelli, A.; Tonietti, L.; et al. Oxidoreductases and metal cofactors in the functioning of the earth. *Essays Biochem.* **2023**, *67*, 653–670.
105. White, D.; Levy, L. Vanadium: Environmental Hazard or Environmental Opportunity? A Perspective on Some Key Research Needs. *Environ. Sci. Process. Impacts* **2021**, *23*, 527–534. [CrossRef]
106. Yang, B.; He, J.; Zhang, G.; Guo, J. (Eds.) Chapter 15—Vanadium catalysts. In *Vanadium*; Elsevier: Amsterdam, The Netherlands, 2021; pp. 415–443.
107. Zhang, C.; Zhang, L.; Ding, Y.; Peng, S.; Guo, X.; Zhao, Y.; He, G.; Yu, G. Progress and prospects of next-generation redox flow batteries. *Energy Storage Mater.* **2018**, *15*, 324–350. [CrossRef]
108. Odebiyi, O.S.; Gao, F.; Du, H.; Liu, B.; Wang, S. Theoretical Modeling and Experimental Evaluation of Vanadium Recovery from Mechanical Activation-Assisted Vanadium Titano-Magnetite Ore $(NH_4)_2C_2O_4$ Leaching. *Min. Met. Explor.* **2023**, *40*, 2505–2517. [CrossRef]
109. He, D.; Feng, Q.; Zhang, G.; Ou, L.; Lu, Y. An environmentally-friendly technology of vanadium extraction from stone coal. *Miner. Eng.* **2007**, *20*, 1184–1186. [CrossRef]
110. Rastegar, O.; Mousavi, S.M.; Shojaosadati, S.; Sarraf-Mamoory, R. Bioleaching of V, Ni, and Cu from residual produced in oil fired furnaces using *Acidithiobacillus ferrooxidans*. *Hydrometallurgy* **2015**, *157*, 50–59. [CrossRef]
111. Cockell, C.S.; Santomartino, R.; Finster, K.; Waajen, A.C.; Nicholson, N.; Loudon, C.-M.; Eades, L.J.; Moeller, R.; Rettberg, P.; Fuchs, F.M.; et al. Microbially-Enhanced Vanadium Mining and Bioremediation Under Micro- and Mars Gravity on the International Space Station. *Front. Microbiol.* **2021**, *12*, 641387. [CrossRef] [PubMed]
112. Bredberg, K.; Karlsson, H.; Holst, O. Reduction of vanadium(V) with *Acidithiobacillus ferrooxidans* and *Acidithiobacillus thiooxidans*. *Bioresour. Technol.* **2004**, *92*, 93–96. [CrossRef]
113. Li, J.; Zhang, B.; Yang, M.; Lin, H. Bioleaching of vanadium by *Acidithiobacillus ferrooxidans* from vanadium-bearing resources: Performance and mechanisms. *J. Hazard. Mater.* **2021**, *416*, 125843. [CrossRef] [PubMed]
114. Shearer, C.K.; McKay, G.; Papike, J.; Karner, J.M. Valence state partitioning of vanadium between olivine-liquid: Estimates of the oxygen fugacity of Y980459 and application to other olivine-phyric Martian basalts. *Am. Miner.* **2006**, *91*, 1657–1663. [CrossRef]
115. Peng, H. A Literature Review on Leaching and Recovery of Vanadium. *J. Environ. Chem. Eng.* **2019**, *7*, 103313. [CrossRef]
116. Zeiner, M.; Rezić, I.; Ujević, D.; Steffan, I. Determination of total chromium in tanned leather samples used in car industry. *Coll. Antropol.* **2011**, *35*, 89–92.
117. Anekwe, I.M.S.; Isa, Y.M. Bioremediation of acid mine drainage—Review. *Alex. Eng. J.* **2023**, *65*, 1047–1075. [CrossRef]
118. Santos, A.L.; Dybowska, A.; Schofield, P.F.; Herrington, R.J.; Cibin, G.; Johnson, D.B. Chromium (VI) Inhibition of Low pH Bioleaching of Limonitic Nickel-Cobalt Ore. *Front. Microbiol.* **2022**, *12*, 802991. [CrossRef] [PubMed]
119. Meruane, G.; Vargas, T. Bacterial oxidation of ferrous iron by *Acidithiobacillus ferrooxidans* in the pH range 2.5–7.0. *Hydrometallurgy* **2003**, *71*, 149–158. [CrossRef]

120. Bolaños-Benítez, V.; Van Hullebusch, E.D.; Lens, P.N.L.; Quantin, C.; Van de Vossenberg, J.; Subramanian, S.; Sivry, Y. (Bio)leaching Behavior of Chromite Tailings. *Minerals* **2018**, *8*, 261. [CrossRef]
121. Teixeira, A.; Tristão, J.; Araujo, M.; Oliveira, L.C.; Moura, F.; Ardisson, J.; Amorim, C.C.; Lago, R.M. Iron: A versatile element to produce materials for environmental applications. *J. Braz. Chem. Soc.* **2012**, *23*, 1579–1593. [CrossRef]
122. Zhang, L.; Qiu, G.; Hu, Y.; Sun, X.; Li, J.; Gu, G. Bioleaching of pyrite by *A. ferrooxidans* and *L. ferriphilum*. *Trans. Nonferrous Met. Soc. China* **2008**, *18*, 1415–1420. [CrossRef]
123. Watling, H. Microbiological Advances in Biohydrometallurgy. *Minerals* **2016**, *6*, 49. [CrossRef]
124. Manikandan, S.; Inbakandan, D.; Nachiyar, C.V.; Namasivayam, S.K.R. Towards sustainable metal recovery from e-waste: A mini review. *Sustain. Chem. Environ.* **2023**, *2*, 100001. [CrossRef]
125. Qiu, R.; Lin, M.; Ruan, J.; Fu, Y.; Hu, J.; Deng, M.; Tang, Y.; Qui, R. Recovering full metallic resources from waste printed circuit boards: A refined review. *J. Clean. Prod.* **2020**, *244*, 118690. [CrossRef]
126. Priya, A.; Hait, S. Extraction of metals from high grade waste printed circuit board by conventional and hybrid bioleaching using *Acidithiobacillus ferrooxidans*. *Hydrometallurgy* **2018**, *177*, 132–139. [CrossRef]
127. Cui, J.; Zhang, L. Metallurgical recovery of metals from electronic waste: A review. *J. Hazard. Mater.* **2008**, *158*, 228–256. [CrossRef] [PubMed]
128. Rossini, G.; Bernardes, A.M. Galvanic sludge metals recovery by pyrometallurgical and hydrometallurgical treatment. *J. Hazard. Mater.* **2006**, *131*, 210–216. [CrossRef] [PubMed]
129. Rendón-Castrillón, L.; Ramírez-Carmona, M.; Ocampo-López, C.; Gómez-Arroyave, L. Bioleaching Techniques for Sustainable Recovery of Metals from Solid Matrices. *Sustainability* **2023**, *15*, 10222. [CrossRef]
130. Genchi, G.; Carocci, A.; Lauria, G.; Sinicropi, M.S.; Catalano, A. Nickel: Human Health and Environmental Toxicology. *Int. J. Environ. Res. Public. Health* **2020**, *17*, 679. [CrossRef] [PubMed]
131. Arshadi, M.; Mousavi, S.M. Multi-objective optimization of heavy metals bioleaching from discarded mobile phone PCBs: Simultaneous Cu and Ni recovery using *Acidithiobacillus ferrooxidans*. *Sep. Purif. Technol.* **2015**, *147*, 210–219. [CrossRef]
132. Seck, G.S.; Hache, E.; Bonnet, C.; Simoën, M.; Carcanague, S. Copper at the crossroads: Assessment of the interactions between low-carbon energy transition and supply limitations. *Resour. Conserv. Recycl.* **2020**, *163*, 105072. [CrossRef]
133. Rawlings, D.E. Characteristics and adaptability of iron- and sulfur-oxidizing microorganisms used for the recovery of metals from minerals and their concentrates. *Microb. Cell Factories* **2005**, *4*, 13. [CrossRef]
134. Lennox, J.; Blaha, T. "Leaching of Copper Ore" by Thiobacillus Ferrooxidans. *Am. Biol. Teach.* **1991**, *53*, 361–368. [CrossRef]
135. Schippers, A.; Hedrich, S.; Vasters, J.; Drobe, M.; Sand, W.; Willscher, S. Biomining: Metal Recovery from Ores with Microorganisms. In *Geobiotechnology I: Metal-Related Issues*; Schippers, A., Glombitza, F., Sand, W., Eds.; Springer: Berlin/Heidelberg, Germany, 2014; pp. 1–47.
136. Villares, M.; Işıldar, A.; Beltran, A.M.; Guinee, J. Applying an ex-ante life cycle perspective to metal recovery from e-waste using bioleaching. *J. Clean. Prod.* **2016**, *129*, 315–328. [CrossRef]
137. Yi, Q.; Wu, S.; Southam, G.; Robertson, L.; You, F.; Liu, Y.; Wang, S.; Saha, N.; Webb, R.; Wykes, J.; et al. Acidophilic Iron- and Sulfur-Oxidizing Bacteria, *Acidithiobacillus ferrooxidans*, Drives Alkaline pH Neutralization and Mineral Weathering in Fe Ore Tailings. *Environ. Sci. Technol.* **2021**, *55*, 8020–8034. [CrossRef]
138. Hussain, S.; Khan, M.; Sheikh, T.M.M.; Mumtaz, M.Z.; Chohan, T.A.; Shamim, S.; Liu, Y. Zinc Essentiality, Toxicity, and Its Bacterial Bioremediation: A Comprehensive Insight. *Front. Microbiol.* **2022**, *13*, 900740. [CrossRef] [PubMed]
139. Picazo-Rodríguez, N.G.; de J, M.; Martínez-Luévanos, A.; Almaguer-Guzmán, I.; Chaidez-Félix, J.; Carrillo-Pedroza, F.R. Direct Acid Leaching of Sphalerite: An Approach Comparative and Kinetics Analysis. *Minerals* **2020**, *10*, 359. [CrossRef]
140. Xu, H.; Wei, C.; Li, C.; Fan, G.; Deng, Z.; Li, M.; Li, X. Sulfuric acid leaching of zinc silicate ore under pressure. *Hydrometallurgy* **2010**, *105*, 186–190. [CrossRef]
141. Fowler, T.A.; Crundwell, F.K. Leaching of Zinc Sulfide by *Thiobacillus ferrooxidans*: Experiments with a Controlled Redox Potential Indicate No Direct Bacterial Mechanism. *Appl. Environ. Microbiol.* **1998**, *64*, 3570–3575. [CrossRef]
142. Oehlerking, F.; Stawovy, M.T.; Ohm, S.; Imandoust, A. Microstructural characterization and mechanical properties of additively manufactured molybdenum and molybdenum alloys. *Int. J. Refract. Met. Hard Mater.* **2022**, *109*, 105971. [CrossRef]
143. Huang, X.-Y.; Hu, D.-W.; Zhao, F.-J. Molybdenum: More than an essential element. *J. Exp. Bot.* **2022**, *73*, 1766–1774. [CrossRef]
144. Xu, G.; Wang, J.; Liu, L.; Wang, Y.; Xiao, H. Negligible emissions and highly efficient recovery of Mo, V, and Al from spent hydroprocessing catalysts through alkaline leaching and solvent extraction. *J. Environ. Chem. Eng.* **2023**, *11*, 111052. [CrossRef]
145. Pistaccio, L.; Curutchet, G.; Donati, E.; Tedesco, P. Analysis of molybdenite bioleaching by *Thiobacillus ferrooxidans* in the absence of iron (II). *Biotechnol. Lett.* **1994**, *16*, 189–194. [CrossRef]
146. Aracena, A.; Azocar, A.; Ibáñez, J.P.; Jerez, O. Mechanism and leaching kinetics of molybdenite concentrate in a hydrogen peroxide-acid system. *Physicochem. Probl. Miner. Process.* **2018**, *55*, 140–152.
147. Wan, H.; Yang, W.; Cao, W.; He, T.; Liu, Y.; Yang, J.; Guo, L.; Peng, Y. The Interaction between Ca^{2+} and Molybdenite Edges and Its Effect on Molybdenum Flotation. *Minerals* **2017**, *7*, 141. [CrossRef]
148. Permyakov, E.A. Metal Binding Proteins. *Encyclopedia* **2021**, *1*, 261–292. [CrossRef]
149. Nguyen, T.H.; Won, S.; Ha, M.-G.; Nguyen, D.D.; Kang, H.Y. Bioleaching for environmental remediation of toxic metals and metalloids: A review on soils, sediments, and mine tailings. *Chemosphere* **2021**, *282*, 131108. [CrossRef] [PubMed]

150. Zelin, X.; Hu, M.; Zhang, H.; Peacock, C.; Liu, X.; Nie, N.; Xue, Q.; Lei, M.; Tie, B. Natural organic matter decreases uptake of W(VI), and reduces W(VI) to W(V), during adsorption to ferrihydrite. *Chem. Geol.* **2020**, *540*, 119567.
151. Han, Z.; Levett, A.; Edraki, M.; Jones, M.; Howard, D.; Southam, G. Microbially Influenced Tungsten Mobilisation and Formation of Secondary Minerals in Wolframite Tailings. *J. Hazard. Mater.* **2023**, *445*, 130508. [CrossRef]
152. Martins, J.I. Leaching Systems of Wolframite and Scheelite: A Thermodynamic Approach. *Miner. Process. Extr. Met. Rev.* **2014**, *35*, 23–43. [CrossRef]
153. Ciriminna, R.; Falletta, E.; Della Pina, C.; Teles, J.H.; Pagliaro, M. Industrial Applications of Gold Catalysis. *Angew. Chem. Int. Ed.* **2016**, *55*, 14210–14217. [CrossRef] [PubMed]
154. Alvillo-Rivera, A.; Garrido-Hoyos, S.; Buitrón, G.; Thangarasu-Sarasvathi, P.; Rosano-Ortega, G. Biological treatment for the degradation of cyanide: A review. *J. Mater. Res. Technol.* **2021**, *12*, 1418–1433. [CrossRef]
155. Wang, J.; Faraji, F.; Ramsay, J.; Ghahreman, A. A review of biocyanidation as a sustainable route for gold recovery from primary and secondary low-grade resources. *J. Clean. Prod.* **2021**, *296*, 126457. [CrossRef]
156. Hylander, L.D.; Meili, M. 500 years of mercury production: Global annual inventory by region until 2000 and associated emissions. *Sci. Total. Environ.* **2003**, *304*, 13–27. [CrossRef]
157. Sznopek, J.L.; Goonan, T.G. *The Materials Flow of Mercury in the Economies of the United States and the World*; Circular/1197; U.S. Geological Survey: Reston, VA, USA, 2000.
158. Hylander, L.D.; Meili, M. The Rise and Fall of Mercury: Converting a Resource to Refuse After 500 Years of Mining and Pollution. *Crit. Rev. Environ. Sci. Technol.* **2005**, *35*, 1–36. [CrossRef]
159. Feng, X. Mercury Pollution in China—An Overview. In *Dynamics of Mercury Pollution on Regional and Global Scales*; Pirrone, N., Mahaffey, K.R., Eds.; Springer: Boston, MA, USA, 2005; pp. 657–678.
160. Schippers, A.; Sand, W. Bacterial Leaching of Metal Sulfides Proceeds by Two Indirect Mechanisms via Thiosulfate or via Polysulfides and Sulfur. *Appl. Environ. Microbiol.* **1999**, *65*, 319–321. [CrossRef] [PubMed]
161. Zhou, X.; Zeng, K.; Wang, Q.; Yang, X.; Wang, K. In vitro studies on dissolved substance of cinnabar: Chemical species and biological properties. *J. Ethnopharmacol.* **2010**, *131*, 196–202. [CrossRef] [PubMed]
162. Wang, Y.J.; Yang, Y.J.; Li, D.P.; Hu, H.F.; Li, H.Y.; He, X.H. Bioxidative dissolution of cinnabar by iron-oxidizing bacteria. *Biochem. Eng. J.* **2013**, *74*, 102–106. [CrossRef]
163. Devasia, P.; Natarajan, K.A. Adhesion of *Acidithiobacillus ferrooxidans* to mineral surfaces. *Int. J. Miner. Process.* **2010**, *94*, 135–139. [CrossRef]
164. Kinzler, K.; Gehrke, T.; Telegdi, J.; Sand, W. Bioleaching—A result of interfacial processes caused by extracellular polymeric substances (EPS). *Hydrometallurgy* **2003**, *71*, 83–88. [CrossRef]
165. Yujian, W.; Xiaojuan, Y.; Wei, T.; Hongyu, L. High-rate ferrous iron oxidation by immobilized *Acidithiobacillus ferrooxidans* with complex of PVA and sodium alginate. *J. Microbiol. Methods* **2007**, *68*, 212–217. [CrossRef] [PubMed]
166. Breed, A.W.; Hansford, G.S. Effect of pH on ferrous-iron oxidation kinetics of *Leptospirillum ferrooxidans* in continuous culture. *Biochem. Eng. J.* **1999**, *3*, 193–201. [CrossRef]
167. Wang, Y.; Zhao, Y.; Ding, X.; Qiao, L. Recent advances in the electrochemistry of layered post-transition metal chalcogenide nanomaterials for hydrogen evolution reaction. *J. Energy Chem.* **2021**, *60*, 451–479. [CrossRef]
168. Tang, S.; He, T.; Yu, H.; Ou, Z.; Ren, Z.; Li, M.; Sheng, W. A novel coating to avoid corrosion effect between eutectic gallium–indium alloy and heat sink metal for X-ray optics cooling. *Rev. Sci. Instrum.* **2022**, *93*, 123102. [CrossRef]
169. Ueberschaar, M.; Otto, S.J.; Rotter, V.S. Challenges for critical raw material recovery from WEEE—The case study of gallium. *Waste Manag.* **2017**, *60*, 534–545. [CrossRef]
170. Pourhossein, F.; Mousavi, S.M. Enhancement of copper, nickel, and gallium recovery from LED waste by adaptation of *Acidithiobacillus ferrooxidans*. *Waste Manag.* **2018**, *79*, 98–108. [CrossRef] [PubMed]
171. Maneesuwannarat, S.; Vangnai, A.S.; Yamashita, M.; Thiravetyan, P. Bioleaching of gallium from gallium arsenide by *Cellulosimicrobium funkei* and its application to semiconductor/electronic wastes. *Process Saf. Environ. Prot.* **2016**, *99*, 80–87. [CrossRef]
172. Ghazi, A.M.; Millette, J.R. 4-Lead. In *Environmental Forensics*; Morrison, R.D., Murphy, B.L., Eds.; Academic Press: Burlington, ON, Canada, 1964; pp. 55–79.
173. Cheriton, L.W.; Gupta, J.P. Building Materials. In *Encyclopedia of Analytical Science*, 2nd ed.; Worsfold, P., Townshend, A., Poole, C., Eds.; Elsevier: Oxford, UK, 2005; pp. 304–314.
174. Grant, R.M. Lead Production. In *Encyclopedia of Materials: Science and Technology*; Buschow, K.H.J., Cahn, R.W., Flemings, M.C., Ilschner, B., Kramer, E.J., Mahajan, S., Veyssiere, P., Eds.; Elsevier: Oxford, UK, 2001; pp. 4439–4442.
175. Jiang, L.; Zhou, H.; Peng, X.; Ding, Z. Bio-oxidation of galena particles by *Acidithiobacillus ferrooxidans*. *Particuology* **2008**, *6*, 99–105. [CrossRef]
176. Páez-Espino, D.; Tamames, J.; de Lorenzo, V.; Cánovas, D. Microbial responses to environmental arsenic. *Biometals Int. J. Role Met. Ions Biol. Biochem. Med.* **2009**, *22*, 117–130. [CrossRef]
177. Liu, J.; Waalkes, M.P. Liver is a Target of Arsenic Carcinogenesis. *Toxicol. Sci.* **2008**, *105*, 24–32. [CrossRef] [PubMed]
178. Zargar, K.; Hoeft, S.; Oremland, R.; Saltikov, C.W. Identification of a Novel Arsenite Oxidase Gene, arxA, in the Haloalkaliphilic, Arsenite-Oxidizing Bacterium *Alkalilimnicola ehrlichii* Strain MLHE-1. *J. Bacteriol.* **2010**, *192*, 3755–3762. [CrossRef]
179. Chen, P.; Xu, R.; Yan, L.; Wu, Z.; Wei, Y.; Zhao, W.; Wang, X.; Xie, Q.; Li, H. Properties of realgar bioleaching using an extremely acidophilic bacterium and its antitumor mechanism as an anticancer agent. *Biol. Res.* **2017**, *50*, 17. [CrossRef]

180. Chen, P.; Yan, L.; Li, H. Optimal parameters for bioleaching of realgar using *Acidithiobacillus ferrooxidans* under different growth conditions and mathematical analysis. *Biocatal. Biotransformation* **2013**, *31*, 33–41. [CrossRef]
181. Allard, B.; Olofsson, U.; Torstenfelt, B. Environmental actinide chemistry. *Inorganica Chim. Acta* **1984**, *94*, 205–221. [CrossRef]
182. Vázquez-Campos, X.; Kinsela, A.S.; Collins, R.N.; Neilan, B.A.; Waite, T.D. Uranium extraction from a low-grade, stockpiled, non-sulfidic ore: Impact of added iron and the native microbial consortia. *Hydrometallurgy* **2017**, *167*, 81–91. [CrossRef]
183. Kaksonen, A.H.; Lakaniemi, A.-M.; Tuovinen, O.H. Acid and ferric sulfate bioleaching of uranium ores: A review. *J. Clean. Prod.* **2020**, *264*, 121586. [CrossRef]
184. Ruiz, L.M.; Castro, M.; Barriga, A.; Jerez, C.A.; Guiliani, N. The extremophile *Acidithiobacillus ferrooxidans* possesses a c-di-GMP signalling pathway that could play a significant role during bioleaching of minerals. *Lett. Appl. Microbiol.* **2012**, *54*, 133–139. [CrossRef] [PubMed]
185. Romero-González, M.; Nwaobi, B.C.; Hufton, J.M.; Gilmour, D.J. Ex-situ Bioremediation of U(VI) from Contaminated Mine Water Using *Acidithiobacillus ferrooxidans* Strains. *Front. Environ. Sci.* **2016**, *4*, 39. [CrossRef]
186. Jerez, C.A. 3.60-Bioleaching and Biomining for the Industrial Recovery of Metals. In *Comprehensive Biotechnology*, 2nd ed.; Moo-Young, M., Ed.; Academic Press: Burlington, ON, Canada, 2011; pp. 717–729.
187. Johnson, D. The Biogeochemistry of Biomining. In *Geomicrobiology: Molecular and Environmental Perspective*; Springer: Dordrecht, Germany, 2010; pp. 401–426.
188. Brune, K.D.; Bayer, T.S. Engineering microbial consortia to enhance biomining and bioremediation. *Front. Microbiol.* **2012**, *3*, 203. [CrossRef] [PubMed]
189. Johnson, D.B.; Hallberg, K.B. Acid mine drainage remediation options: A review. *Sci. Total Environ.* **2005**, *338*, 3–14. [CrossRef]
190. Gomes, H.I.; Funari, V.; Ferrari, R. Bioleaching for resource recovery from low-grade wastes like fly and bottom ashes from municipal incinerators: A SWOT analysis. *Sci. Total. Environ.* **2020**, *715*, 136945. [CrossRef]

Disclaimer/Publisher's Note: The statements, opinions and data contained in all publications are solely those of the individual author(s) and contributor(s) and not of MDPI and/or the editor(s). MDPI and/or the editor(s) disclaim responsibility for any injury to people or property resulting from any ideas, methods, instructions or products referred to in the content.

La borsa di dottorato è stata cofinanziata con risorse del
Programma Operativo Nazionale Ricerca e Innovazione 2014-2020, risorse FSE REACT-EU
Azione IV.4 “Dottorati e contratti di ricerca su tematiche dell’innovazione”
e Azione IV.5 “Dottorati su tematiche Green”